EVAPORATION MEASUREMENT ABOVE VEGETATED SURFACES USING MICROMETEOROLOGICAL TECHNIQUES

by

MJ Savage[1], CS Everson[2] and BR Metelerkamp[1*]

[1]Department of Agronomy, University of Natal
Pietermaritzburg, South Africa

[2]Division of Water, Environment and Forestry Technology, CSIR
Department of Agronomy, University of Natal, Pietermaritzburg, South Africa
[*]Present address: 11A Millhouse Drive, Howick, Auckland, New Zealand

Final report to the Water Research Commission on the project:

"Evaporation measurement above vegetated surfaces using micrometeorological techniques"

WRC Report No: 349/1/97
ISBN No: 1 86845 363 4

Table of contents

Executive summary

1 Motivation

Roberts (1986) contrasted present (1980) and future (2010) water demands for southern Africa for various economic sectors. With a predicted increase of 52.2% in water usage, there is no doubt of the importance of high-rainfall catchments in terms of water capture. One of the most important factors affecting water supply from a catchment is the evaporation from the climax grassland community.

The impact of a large establishment of new commercial forests on agricultural and natural (especially wetland) communities must be assessed. In spite of the importance of evaporation in these different communities, there is very little research being done in southern Africa on the processes and measurement techniques of evaporation.

There have been very few attempts at evaporation measurements in the Drakensberg catchments. Henrici (1943) measured transpiration of grasses in the sour mountain grassveld of the Drakensberg and compared these with the water loss of indigenous forests. As far as could be ascertained, our initial measurements using the Bowen ratio energy balance method for evaporation measurement (BREB) in the Drakensberg catchments was the first in a mountainous region, although recently the adequate performance of the BREB method on a 22° slope has been verified by Nie *et al.* (1992).

Until such time as the available models are tested, there may be a reluctance by decision makers to fully utilise the potential of model calculations. However, evaporation measurements are difficult and usually only lysimetric methods give sufficient accuracy (at great cost). The choice of the experimental site was strongly influenced therefore by the fact that a lysimeter with a drainage system had been constructed for use as a source of absolute measurement as part of another project.

2 Objectives

2.1 Project aims

A. Investigation of Bowen ratio and eddy correlation micrometeorological methods for the measurement of evaporation and comparison with: (a) each other; (b) traditional micrometeorological calculations of evaporation; (c) lysimetric measurements of evaporation.

In the case of most of these techniques, because of the roughness of the terrain, it will be necessary to assess the stability of the atmosphere and obtain a measure of advection.

B. Seasonal measurement of evaporation.

C. Comparative evaporation measurements between different sites.

D. The effect of some management practices (for example, burning and residue placement) on evaporation.

(a) Comparison between Bowen ratio estimates of evaporation for a grassland and a riparian zone community.

(b) Effect of fire on the evaporation of grassland and wetland communities.

(c) Investigation of the eddy correlation technique and comparison with Bowen ratio and lysimetric measurements of evaporation at the same site for a range of weather conditions.

(d) Quantification of surface roughness, turbulence, advection and fetch.

2.2 Background

This project was primarily concerned with the measurement of evaporation using a variety of micrometeorological techniques. This involved checking the function of sensors developed overseas and developing methods for checking collected data. After these methods had been developed, the aim was to use these measurement systems for the routine field measurement of evaporation.

2.3 Investigation of the Bowen ratio micrometeorological methods

2.3.1 Baseline comparisons

Prior to our study, the Bowen ratio method for the measurement of evaporation had not been used in South Africa.

It was our intention to use two Bowen ratio systems adjacent to each other to investigate the quality of evaporation measurements and identify possible errors.

2.3.2 Field measurements of evaporation and sensible heat

We wished to compare the Bowen ratio technique with other evaporation techniques and use it for a variety of surfaces (grassland and vines) and compare our measurements with (i) traditional micrometeorological calculations of evaporation; (ii) lysimetric measurements of evaporation.

2.3.2.1 Alternative methods for evaporation measurement

We investigated whether or not it would be possible to determine sensible heat from measuring air temperature gradients only and not both air temperature and water vapour pressure gradients.

2.3.2.2 Seasonal measurement of evaporation

In the process of testing our techniques, we wished to obtain seasonal measurements of evaporation in Catchment VI of Cathedral Peak.

2.4 Investigation of the eddy correlation micrometeorological methods

2.4.1 Laboratory investigations

Our aim was to identify the factors limiting accurate measurement of evaporation and sensible heat using the eddy correlation technique

2.4.2 Field investigations

We wished to compare the eddy correlation technique with the Bowen ratio technique. We also wanted to use the eddy correlation technique above a variety of surfaces (bare soil, maize, grassland and vines).

2.4.2.1 Placement height investigations

We wished to quantify fetch by measuring sensible heat, using the eddy correlation technique, by varying the measurement to fetch height ratio. This was accomplished by varying the placement height instead of varying the fetch distance.

2.4.2.2 Surface temperature technique for sensible heat measurement

We investigated the possibility of using surface temperature and air temperature measurements in conjunction with profile measurements of wind speed to calculate sensible heat and made comparisons with eddy correlation measurements of the same.

2.4.2.3 Stability quantification

Our aim was to quantify stability using field measurements above a short grassland surface and eddy correlation measurements supplemented by profile measurements of wind speed.

2.5 Calibration considerations

For energy balance techniques, a limiting factor is the accuracy of the net irradiance measurements. We wanted to develop an inexpensive calibration methodology for net radiometers.

3 Results and conclusions

3.1 The logistics of calculating flux densities from raw Bowen ratio data

We detailed accurate expressions for the calculation of so-called "temperature dependent constants" used in energy and mass transfer expressions. Such constants affect the value of the calculated Bowen ratio and the resultant latent and sensible heat energy flux densities.

3.2 The rejection criteria for the exclusion of out-of-range and "bad" or doubtful data

We successfully used rejection criteria based (a) on the accuracy limits of water vapour pressure and air temperature differences between two levels; (b) on the fact that the measured averaged water vapour pressure between the two levels cannot exceed the saturation value corresponding to the measured air temperature. For case (a), if the upper and lower limit inequality is satisfied then there is a high possibility that the Bowen ratio will be very near -1 and therefore the calculated flux will not have numerical meaning. Data fulfilling this inequality are therefore excluded from further processing. The majority of the data during clear days were not rejected, and all datum points rejected were done so justifiably when checked. The method had the additional benefit of calculating condition-sensitive daily totals. It thereby negates the requirement of calculating daylengths and adjusting calculations according to those daylengths. The procedure is sensitive to the times of day when reasonable fluxes occur, rejecting points other than these good data points. This allows an 18-hour-day set of data to be used at all times, so avoiding having to decide when to start and stop data collection for each daylength.

3.3 Error considerations of the Bowen ratio energy balance method

From error analyses, the relative error in evaporation has been found to be most sensitive to net irradiance measurement errors. With accurate net radiometers, most of the error arises from the soil heat flux determinations, even though their contribution relative to net irradiance is small. This is due partly to the accuracy of the net radiometers and to the difficulties encountered with soil heat flux density determinations. The soil heat flux-related errors introduced by contact between soil and sensor, depth positioning and spatial dissimilarity are constant, while those arising from uncertainties in the calculation of the stored heat energy content in the layer above the flux plates (due mainly to changes in soil water content) change with time.

3.4 Evaporation measurement comparisons and advective influences using Bowen ratio, lysimetric and eddy correlation methods

A study in KwaZulu-Natal involving Bowen ratio and eddy correlation aerodynamic measurements, equilibrium and Priestley-Taylor evaporation calculations and lysimetric measurements showed good comparison between Bowen ratio and lysimetric measurements and equilibrium evaporation calculations for the measurement period of the data. Priestley-Taylor evaporation calculations overestimated the evaporation by as much as 20 % compared to the other techniques whereas eddy correlation measurements underestimated the evaporation significantly. The influence of advection on Bowen ratio evaporation measurements, calculated from Bowen ratio and lysimeter data, appeared to be relatively insignificant but variable. The total daily evaporation amounts for two Bowen ratio systems compared favourably with each other, lysimeter evaporation and with equilibrium evaporation, but less so for 20 min intervals.

3.5 Comparisons of vineyard sensible heat measured using eddy correlation and Bowen ratio systems

The placement of an eddy correlation (EC) system, in a wide row system such as in a vineyard with limited fetch, is problematical. Sensible heat measurements in a vineyard were obtained using two EC and four Bowen ratio (BR) systems. We compared EC and BR measurements of sensible heat and evaporation. Sensible heat estimates from the two EC systems agreed with each other when the two EC systems were placed 1 m directly above adjacent N-S canopy rows 3 m apart. There were differences in EC sensible heat for EC systems placed directly above row and between row (above soil) positions. The EC sensible heat directly above the row was much greater than that at the between row position (1.5 m away). We attributed these differences to the lack of air mixing between the above row and between row positions. The standard deviation of the vertical wind speed at the between row position was also much greater than that at the above canopy position. Our measurements demonstrate that sensible heat and the vertical turbulent intensity above the row compared to that between the canopy rows are different. These findings illustrate that due consideration should be given to the lateral placement of sensors for row crops for sites with limited fetch. At the 95 % level of significance, there was no statistical difference between BR and EC sensible heat measurements when the EC systems were placed 1 m directly above adjacent N-S canopy rows. Our data suggests that the BR sensible heat, due to the nature of the BR calculation method, was very sensitive to the measured net irradiance. The EC sensible heat measurements were not sensitive to net irradiance since the EC technique is absolute and independent of net irradiance and soil heat flux density measurement errors.

3.6 Placement height of eddy correlation sensors above a short turfgrass surface

Variation in measured sensible heat flux density F_h with sensor height above short turfgrass during mainly unstable conditions was investigated using the eddy correlation (EC) technique. Our data showed that EC-measured sensible F_h at 0.25 and 0.38 m above the turfgrass were 15 and 10 % lower, respectively, than that at the 1.00-m height. There was no statistical difference in the EC F_h at 0.50, 1.00 and 1.25 m. An analysis of "footprints" showed that at least 90 % of the measured F_h at a height of 0.5 m was from our experimental site, decreasing to less than 70 % at the 1.5-m height. Sensor placement at the 0.5-m height would result in little reduction, as did occur at heights less than 0.50 m, in the covariance between vertical wind speed fluctuation and air temperature fluctuation due to small-sized eddies being contained between the separation distance of the sonic anemometer transducers. We speculate that measurements closer than 0.5 m to the surface differed from those at

1.00 m due to small-sized eddies near the surface being contained between the sonic separation distance and therefore not completely detected by the sonic anemometer.

3.7 Calibration of net radiometers and infra red thermometers

Using a radiator, the net radiometer (long wave) calibration factors were reproducible. Net radiometer (long wave) calibration factors were similar to the manufacturers short wave calibration factor obtained four months previously for new net radiometers. Long wave calibrations over a wide irradiance range were possible. Calibration of infra red thermometers (IRT's) for a wide temperature range was possible. The calibration slope for the same IRT for different calibration runs is reasonably reproducible. Most IRT's overestimated surface temperature for temperatures greater than 25 °C. We recommend calibration of IRT's if surface temperatures greater than 35 °C are recorded.

3.8 The "footprints" of eddy correlation and other micrometeorological measurements

Sensible heat flux density measurements were obtained during mainly unstable atmospheric conditions using the eddy correlation (EC) technique at eight different heights between 0.25 and 2.0 m above a short grassland canopy surface. Calculations based on fetch showed that the lowest four heights were within the equilibrium layer whereas the heights at or greater than 1.25 m were above the equilibrium layer. The greater F_h measurements above the 1.25-m height, compared to the lower heights, were probably from advected F_h from nearby tar roads and buildings. There were no statistical differences between the sensible heat measurements at the 0.5, 1.0 and 1.25 m heights. Measurements of atmospheric stability were obtained by calculating the ratio of height z above surface to the Monin-Obukhov length. Most measurements were obtained under unstable conditions when mixed convection prevailed. Our measurements show that it is possible for EC sensors to be placed as low as 0.50 m above the surface, during unstable periods, without significant difference from the F_h measurements at a height of 1.00 m. Data were obtained with a pan filled with soil placed 0.27 m below the fine wire thermocouple of an EC system placed 1.00 m above surface. These data demonstrated that the reduction in the sensible heat was not due to acoustic reflections from that surface. Possibly, the reduction was due to small-sized eddies near the surface being contained between the sonic separation distance. An analysis of "footprints" showed that, for our unstable conditions, at least 0.96 of the measured F_h at a height of 0.25 m was from our experimental site. This fraction decreased to less than 0.7 at the 2.0-m placement height. Calculations showed that the fetch requirement for micrometeorological measurements above a forest canopy was more stringent than for a grassland canopy.

3.9 Comparison between a surface temperature and eddy correlation method for sensible heat determination above a grassland surface

Aerodynamic techniques for the measurement of evaporation from surfaces have some advantages over conventional methods. Two aerodynamic evaporation (AE) measurement methods including the eddy correlation method (a single level measurement technique), and an infra red surface temperature method (requiring a profile of wind speed) are used. The AE measurements are more portable compared with fixed lysimetric measurements. Hourly or subhourly AE measurements are possible compared to daily measurements for the neutron probe. Aerodynamic measurements need to represent processes at the canopy surface, have fetch limitations and may be affected by advection.

3.10 Measurement of sensible and latent heat using eddy correlation techniques

The KH20 and CA27 sensors of the eddy correlation technique used for the measurement of latent and sensible heat respectively were evaluated under laboratory and field conditions. Our investigations showed that the KH20 hygrometer underestimated the mean water vapour density. We showed that it was possible to apply a correction to this underestimation provided that an accurate humidity sensor was used to simultaneously measure the mean water vapour density.

3.11 Determination and use of a generalized exchange coefficient, K

A method of obtaining a reliable estimate of a generalized exchange coefficient K for any site was found. If used correctly, this method would result in considerable savings in instrumentation and therefore expense. All that would be required to calculate the sensible heat flux density, is a K value and a single differential temperature measurement. From this, in conjunction with an estimate of the available energy, the amount of evaporation could be calculated for the site.

3.12 Seasonal comparisons of total evaporation in a Drakensberg catchment

Evaporation in Catchment VI is a significant fraction of both the energy and water balance. It represents more than 65 % of net radiation over the 39-month period and more than 90 % of the rainfall over the same period. The total evaporation over the 39 months was 3330.7 mm and the rainfall total was 3618.4 mm. The evaporation for a riparian zone, for the month of January 1992, was about 30 % greater than that upslope. Apart from the soil heat, each term of the Bowen ratio equation used to calculate the evaporation contributed to greater evaporation values at the riparian location compared to that upslope. The term that showed the most marked difference between the two sites was the soil heat flux, which decreased evaporation for the riparian location compared with that upslope.

4 Extent to which contract objectives have been met

While many of the elements of the project were more demanding than was originally anticipated, the objectives were satisfactorily achieved. Some additional aspects were investigated that had not been originally planned, and this necessitated more detailed research. In the evaluation of the eddy correlation sensors, particularly the KH20 humidity sensor, it became clear that certain limitations restricted routine use of this equipment. Poor performance of this sensor resulted in a concentration on the CA27 sonic anemometer and fine wire thermocouple. The limitations of the Bowen ratio technique have been thoroughly investigated. The Bowen ratio estimates of evaporation during winter (when the water vapour pressure gradient was small) were not satisfactory and in particular following burning. Measurement comparisons are reported on in Chapter 9. Besides these comparisons, few comparisons were made between different sites due to insufficient equipment (although measurements have been made at Cathedral Peak at different points in a catchment as part of a WRC-funded Division of Water, Environment and Forest Technology, CSIR project). Originally, we had planned to use the Bowen ratio technique to identify fetch limitations. However this was fully investigated by Heilman *et al.* (1989) using the Bowen ratio technique and hence we used the eddy correlation technique to pursue this aspect.

5 Useful contributions in the report

- Thorough investigation of the Bowen ratio technique;
- investigation of the limitations of the eddy correlation technique;
- use of the Bowen ratio and eddy correlation techniques in the following systems: climax grassland sites (Cathedral Peak, Catchment VI), maize canopy (Cedara), grassland site (Pietermaritzburg and College Station), vineyard site (Lamesa), bare soil site (College Station);
- a method for determining the effect of placement height on flux measurements has been published in an international journal;
- a surface temperature method for determining sensible heat for a grassland surface was found adequate;
- a method for calibrating net radiometers (and infra red thermometers) was developed;
- a method for determining sensible and latent heat using a generalized *K* value and air temperature gradients was developed;
- comparative measurements of evaporation between a riparian zone and an upslope zone;
- seasonal comparisons of evaporation for Cathedral Peak Catchment VI;
- four papers published in Agricultural and Forest Meteorology (two in 1994, one in 1995 and one in 1996) on Bowen ratio and eddy correlation measurements of sensible and latent heat for a bare soil surface, mixed grassland surface and a vineyard;
- one paper, on the "footprints" of micrometeorological measurements, was published in the South African Journal of Science;
- numerous (national and one international) conferences were attended and the results of our investigations were presented.

5.1 Project publications and conference presentations

1. Heilman, J.L., K.J. McInnes, R.W. Gesch, R.J. Lascano, and M.J. Savage, 1996. Effects of trellising on the energy balance of a vineyard. Agricultural and Forest Meteorology 81: 79-93.
2. Heilman, J.L., K.J. McInnes, M.J. Savage, R.W. Gesch and R.J. Lascano, 1994. Soil and canopy energy balances in a west Texas vineyard. Agricultural and Forest Meteorology. 71:99-114.
3. McInnes, K.J., Heilman, J.L. and M.J. Savage, 1994. Aerodynamic conductances along a bare ridge-furrow tilled soil surface. Agricultural and Forest Meteorology 68:119-131.
4. Metelerkamp, B.R., 1992. Measuring the [evaporation] loss. Natal University Focus on Water 3, 19.
5. Metelerkamp, B.R., 1993. The use of the Bowen ratio energy balance method over a grassed surface for the determination of total evaporation. M. Sc. Agric. thesis, University of Natal.
6. Metelerkamp, B.R. and M.J. Savage, 1994. A back-calculation method for determining all terms of the Penman Monteith equation using Bowen Ratio measurements II: Feasibilty over a commercial timber crop. Southern African Society for Crop Production, Cedara, Natal. 42.
7. Metelerkamp, B.R. and M.J. Savage, 1994. Reference evaporation in real-time from an automated weather station. Southern African Society for Crop Production, Cedara, Natal.
8. Metelerkamp, B.R., M.J. Savage and C.S. Everson, 1993. Seasonal comparisons of evaporative flux density in a Drakensberg catchment under a biennial veld burning regime. *In* S.A. Lorentz, S.W. Kienzle and M.C. Dent (eds). Proceedings of the Sixth South African National Hydrological Symposium, Volume 1: 35-42.

9. Monnik, K.A. and M.J. Savage, 1993. Eddy correlation estimate of total evaporation over maize. Abstracts of the Tenth Annual Conference of the South African Society of Atmospheric Sciences. P 41.

10. Monnik, K.A. and M.J. Savage, 1994. Eddy correlation estimate of total evaporation over maize. Southern African Society for Crop Production, Cedara, Natal. P 46.

11. Monnik, K.A., M.J. Savage and C.S. Everson, 1995. Comparison of eddy correlation estimates of evaporation with Bowen ratio and equilibrium evaporation. Proceedings of the Southern African Irrigation Symposium, 167-171.

12. Salisbury, F.B. and M.J. Savage, 1996. Energy transfer. *In* F.B. Salisbury (ed) Units, Symbols and Terminology for Plant Physiology: A Reference for Presentation of Research Results in the Plant Sciences, Chapter 7, 65-71. Oxford University Press, Oxford.

13. Savage, M.J., 1996. Basic thermodynamic quantities. *In* F.B. Salisbury (ed) Units, Symbols and Terminology for Plant Physiology: A Reference for Presentation of Research Results in the Plant Sciences, Chapter 4, 45-54. Oxford University Press, Oxford.

14. Savage, M.J., 1990. Aerodynamic Bowen ratio measurements and comparison with equilibrium evaporation used in CERES models. Presentation delivered to the Department of Agronomy as part of a seminar session organized for the Department of Agriculture and Water Supply (to coincide with a visit by Professors Jones and Boote from the University of Florida, USA).

15. Savage, M.J., 1991. Energy and water relations techniques in the soil-plant-atmosphere continuum. Dohne Research Station, Dohne, Cape. Invited seminar.

16. Savage, M.J., 1992a. Evaporation measurement using aerodynamic and sap flow techniques. Department of Agronomy and Soil Science, Washington State University, Pullman, Washington, USA.

17. Savage, M.J., 1992b. Water flux and water potential measurement techniques. Invited seminar delivered to the Department of Horticultural Sciences (cosponsored with Plant Physiology), Texas A & M University, College Station, Texas, USA.

18. Savage, M.J., G.S. Campbell and J.L. Heilman, 1993. Field use aspects and laboratory calibration of net radiometers and infra-red thermometers. Abstracts of the Tenth Annual Conference of the South African Society of Atmospheric Sciences. P 45.

19. Savage, M.J., C.S. Everson and B.R. Metelerkamp, 1990. Determination of evaporation for Catchment VI of the Natal Drakensberg using the Bowen ratio technique. South African Agrometeorology and Remote Sensing Conference, Department of Agriculture and Water Supply, Cathedral Peak, Natal Region. Invited paper presentation.

20. Savage, M.J., C.S. Everson and B.R. Metelerkamp, 1995. Evaporation measurement comparisons and advective influences using Bowen ratio, lysimetric and eddy correlation methods. Proceedings of the Southern African Irrigation Symposium, 160-166.

21. Savage, M.J. and J.L. Heilman, 1993a. Aerodynamic measurement of evaporation. *In* S.A. Lorentz, S.W. Kienzle and M.C. Dent (eds). Proceedings of the Sixth South African National Hydrological Symposium, Volume 1: 63-70.

22. Savage, M.J. and J.L. Heilman, 1993b. Field use aspects and laboratory calibration of net radiometers and infra-red thermometers. South African Society of Atmospheric Sciences, Midrand, Transvaal.

23. Savage, M.J., J.L. Heilman and K.J. McInnes, 1993. Comparison between a surface temperature and eddy correlation method for sensible heat transfer above a grassland surface. Abstracts of the Tenth Annual Conference of the South African Society of Atmospheric Sciences. P. 41.

24. Savage, M.J., J.L. Heilman, K.J. McInnes and R.W. Gesch, 1992. Evaporation and turbulence measurements in a vineyard. Abstracts of the 84 th Agronomy Meetings, Minneapolis, Minnesota. P 22.

25. Savage, M.J., J.L. Heilman, K.J. McInnes and R.W. Gesch, 1993. Evaporation and micrometeorological measurements in a vineyard using the eddy correlation technique. Supplement to Journal of the South African Society for Horticultural Sciences 3, 20.

26. Savage, M.J., J.L. Heilman, K.J. McInnes and R.W. Gesch, 1995. Placement height of eddy correlation sensors above a short grassland surface. Agricultural and Forest Meteorology 74, 195-204.

27. Savage, M.J., J.L. Heilman and K.J. McInnes, 1994. Placement height of eddy correlation sensors for sensible heat measurement and other micrometeorological aspects. Southern African Society for Crop Production, Cedara, Natal. P57.

28. Savage, M.J., K.J. McInnes and J.L. Heilman, 1996. The "footprints" of eddy correlation sensible heat flux density, and other micrometeorological measurements. South African Journal of Science 92, 137-142.

29. Savage, M. J., Metelerkamp, B. R., Everson, C. S.,1994. A back-calculation method for determining all terms of the Penman Monteith equation using Bowen Ratio measurements I: Theory and application. Southern African Society for Crop Production, Cedara, Natal. P 58.

30. Savage, M.J. and K. A. Monnik 1993. Sensible heat transfer in a vineyard. South African Agrometeorology and Remote Sensing Conference, Department of Agriculture and Water Supply, Stellenbosch, Western Cape Region. Invited paper presented by K.A. Monnik. Awarded best paper of the conference.

6 Future research

6.1 General comments

One of the the major limitations to real economic growth of South Africa is water resources. Research in the field of evaporation measurement (and the consequential micrometeorological aspects) needs to be continued for the benefit of all in South Africa. Lack of research interest and funding in this crucial area will impact on, for example, land management controversies such as the use of sugar cane as opposed to afforestation.

6.2 Bowen ratio methodology

Our research has concentrated on energy and water movement exclusively and therefore has ignored the important aspect of plant productivity in terms of the amount of water used. We believe that the Bowen ratio research needs to be extended to research on a Bowen ratio carbon dioxide and water vapour system. This research would allow such a Bowen ratio CO_2 system to determine water use efficiency in real-time. Such a system is already commercially available. Interestingly enough, the method is based on the generalized *K* coefficient research of Chapter 3 (Section 3.7). This important research should continue.

A more user friendly data rejection methodology, than that described in Chapter 3, should be finalised and made available.

Lindroth and Halldin (1990) pointed out the inappropriateness of inferring gradients from difference measurements at only two points above a grassland surface. Given this and the cost of the present Bowen ratio system commonly used, it would be prudent to investigate the manufacture of multi-level (aspirated) wet and dry-bulb psychrometers. In conjunction with the measurement of net irradiance and soil heat flux density, a complete description of the surface energy balance would then be possible.

6.3 Eddy correlation methodology

While a one-dimensional sonic anemometer can yield much information, it is desirable to use a three-dimensional system that is also waterproof. Such a system is commercially available. Measurements in three dimensions theoretically allow both flux measurements and the quantification of turbulence and stability.

Currently, the fast responding KH20 hygrometers have been shown to be inadequate for eddy correlation research. Research on an alternative to these hygrometers should be pursued. It is however possible to use a fast responding infra red gas analyser for the measurement of carbon dioxide and water vapour concentration.

6.4 Effect of surface management on evaporation

The limitations of the techniques for the measurement of evaporation following burning, for example, can be used to develop alternative methodology to measure evaporation (and the surface energy balance) following surface modification. This research should also involve footprint determination.

6.5 Remote sensing

It appears possible to use remote sensing techniques (Chapter 5) for the determination of sensible heat if measures of aerodynamic resistance are also possible. In view of the possibility of "areal" measures of sensible heat, it may then be possible to also calculate surface evaporation from estimates of net irradiance and soil heat flux.

6.6 Technology transfer

It is proposed that a variety of methods be used to transfer some of the technology of the research investigated here: small workshops, conference workshops and e-mail interest groups. A cooperative effort should perhaps be coordinated in some way by the FRD and the WRC. Technology transfer forums should encourage young scientists as much as possible. These processes would quickly permit the transfer of the technology described in this report to historically disadvantaged Universities.

Much of the research described here has already benefited students, researchers and technical staff at the University of Natal, University of the Orange Free State, Texas A & M University and the CSIR. Most of the material has already been presented at local and international conferences (see Section 5.1 of the Executive Summary).

It is envisaged that there will be further publications from this report.

7 Acknowledgements

The research in this report emanated from a project funded by the Water Research Commission entitled:

- "Evaporation measurement above vegetated surfaces using micrometeorological techniques".

The Steering Committee responsible for this project consisted of the following persons:

Dr G.C. Green (Water Research Commission), Chairman;

Dr M.J. Donkin (formerly of the Institute of Commercial Forestry Research);

Mr H. Maaren (Water Research Commission);

Professor R.E. Schulze (Department of Agricultural Engineering, University of Natal);

Professor W.H. van Zyl (formerly of the Department of Agrometeorology, University of the Orange Free State);

Mr D.B. Versfeld (CSIR);

Mr D.J. Huyser (Water Research Commission), Secretary.

The financing of the project by the Water Research Commission and the contribution of the members of the Steering Committee is gratefully acknowledged. The project was only possible with the cooperation of the following:

CSIR for use of facilities at Cathedral Peak;

staff of the Electronic Centre of the University of Natal for their support in the repair and checking of equipment;

Ms Jothi (Jody) Moodley (Agrometeorology) of the Department of Agronomy, University of Natal for the endless list of tasks, including the Plotit graphics editing, that required attention;

Mr Peter N. Dovey (Agrometeorology) of the Department of Agronomy, University of Natal for part of the technical support required for this project;

the staff of CSIR (Cathedral Peak Forestry Research Station) and in particular Ms Karen Hudson and Mr Goodenough Molefe;

financial assistance from the University of Natal, the South African Foundation for Research Development, Texas A & M University and the United States Council for the International Exchange of Scholars for a Fulbright grant to the project leader is gratefully acknowledged;

the cooperation of Drs J.L. Heilman and K.J. McInnes (Department of Soil and Crop Sciences, Texas

A&M University, College Station, Texas, USA) in the work of Chapters 5 (parts), 6, 7 and 8, is gratefully acknowledged;

use of two of the EC systems from Dr W.A. Dugas, Blackland Research Center, Texas Agricultural Experiment Station, Temple, Texas is gratefully acknowledged;

reviewers and the USA Regional Editor of the journal Agricultural and Forest Meteorology and reviewers of the journal South African Journal of Science made many helpful comments on the work of Chapter 8;

Karl Monnik of the Institute of Soil, Climate and Water who assisted with the very early eddy correlation measurements of maize (- see Monnik, Savage and Everson, 1995);

our wives, in particular Meryl A. Savage and Dr Terry M. Everson for their support and encouragement.

"In the beginning God created the heavens and the earth" (Genesis 1:1, The Bible).

8 Information about this report

Initially the XyWrite (III Plus version 3.54 from XyQuest, Billerica, MA, USA) wordprocessing software package was used for entering text for this report. In the draft and final report stages, WordPerfect was used. The final report was generated using the destop publishing program Ventura Publisher version 4.1. Virtually all of the computer graphics was generated using Plotit 3.1 and vesion 3.20e (Scientific Programming Enterprises, Haslett, Michigan). The Plotit graphics were copied to the Windows 3.1 clipboard and pasted individually directly into Ventura frames and saved in the Windows metafile format (wmf). Some of the graphics (for example, all of Figs 1.1, 2.4, 2.5, 2.6 and parts f2.7, 2.8 and 3.19) were generated using CorelDraw! 3.00, revision B from Corel Cooperation and copied to the Windows 3.1 or Windows NT clipboard and pasted directly in Ventura frames. The report was printed using a Hewlett Packard LaserJet 4 printer at the 300 dpi by 300 dpi resolution. Most of the calculations for this report were performed using Quattro Pro (Windows and DOS versions) and Excel (Microsoft Corporation). Most of the calculations of Chapter 9 were performed using Excel (which allowed a year of 20 min data for each Excel worksheet file). The data required to generate the graphics was copied from Quattro Pro or Excel to Plotit using the Windows 3.1/NT clipboard and saved in Plotit as prn files.

A List of figures and plates

Chapter 5

Chapter 9

B List of tables

Chapter 2

Chapter 3

Chapter 5

Chapter 6

Chapter 7

Chapter 8

C List of symbols used

a	regression coefficient	
a	available energy: $a = I_{net} - F_s \; (= L_v F_w + F_h)$	W m^{-2}
$a_{surface}$	absorptivity of the surface	
A	area of rectangular plate	m^2
A	advection heat flux density $A = A_w + A_h$, energy flux density removed from the system ($A > 0$)	W m^{-2}
A_h	sensible heat flux density advected	W m^{-2}
A_w	latent heat flux density advected	W m^{-2}
b	regression coefficient,	
c_p	specific heat capacity of air at constant pressure (≈ 1004 J kg^{-1} K^{-1})	J kg^{-1} K^{-1}
c_{soil}	soil specific heat capacity	J kg^{-1} K^{-1}
c_{dsoil}	specific heat capacity of dry soil	J kg^{-1} K^{-1}
c_w	specific heat capacity of water	J kg^{-1} K^{-1}
C	Bowen's definition of the sum of conductive and convective heat energy flux densities $C = R\,(L_v F_w)$	W m^{-2}
d	radius of circular plate	m
d	zero-plane displacement height	m
de	actual water vapour pressure difference	kPa
dt	time interval	s
dT	actual air temperature difference	°C or K
dT_{soil}	change in soil temperature during the datalogger output interval	°C
dI_{net})	first differential of net irradiance measurement	W m^{-2}
$d\,(L_v F_w)$	first differential of latent heat flux density	W m^{-2}
dz	vertical displacement between measurement positions	m
D	surface roughness element separation	m
D_h	thermal diffusivity of air	m^2 s^{-1}
D_w	water vapour diffusivity	m^2 s^{-1}
e	water vapour pressure at a known height above ground	kPa
e_a	vapour pressure of air	kPa
e_{lower}	water vapour pressure at the lower level of the Bowen ratio system	kPa
$e_s\,(T_s)$	saturated water vapour pressure at the surface temperature	kPa
e_s	saturation water vapour pressure at the measured air temperature $e_s(T_a)$	kPa
e_1	atmospheric water vapour pressure at height z	kPa
e_2	atmospheric water vapour pressure at height z	kPa
e_{upper}	water vapour pressure at the upper level of the Bowen ratio system	kPa
e_w	water vapour pressure of the evaporating surface: usually saturated ($e_w = e_s$)	kPa
$E(e)$	resolution limit of the hygrometer sensor	kPa
$E(T)$	resolution limit of the air temperature sensor	°C
$\bar{f}$	frequency	Hz or s^{-1}

f'	frequency	Hz or s^{-1}
F	view factor of a circular plate	
F_c	carbon dioxide flux density	kg s^{-1} m^{-2}
F_e	flux density of energy contained in the evaporated water	W m^{-2}
F_e	flux density of entity E	various units
F_E	flux density of entity E	various units
$F_{h_{BREB}}$	sensible heat flux density determined with the BREB method	W m^{-2}
$F_{h_{LYS}}$	sensible heat flux density determined lysimetrically	W m^{-2}
F_m	upward flux of momentum at height z ($F_m = -\tau_z$)	Pa
F_h	sensible heat flux density (sometimes H is used)	W m^{-2}
F_s	soil heat flux density ($F_s = G + F_{stored}$)	W m^{-2}
F_{stored}	energy flux density stored in the soil above the soil heat flux plate	W m^{-2}
F_w	water vapour flux density	kg s^{-1} m^{-2}
g	acceleration due to gravity	m s^{-2}
G	plate-measured soil heat flux density	W m^{-2}
h	surface roughness element height	m
h	canopy height	m
h	altitude	km
H	sensible heat flux density	W m^{-2}
I_{net}	net irradiance $I_{net} = I_s - rI_s + L_d - L_u$ (sometimes R_{net} is used)	W m^{-2}
I_s	incoming short wave irradiance	W m^{-2}
IBL	inner or internal boundary layer	
k	von Karman's constant ($k = 0.41$)	
K	general turbulent exchange coefficient	m^2 s^{-1}
K_h	turbulent exchange coefficient for sensible heat transfer	m^2 s^{-1}
K_m	turbulent exchange coefficient for momentum transfer	m^2 s^{-1}
K_q	exchange coefficient for entity q	m^2 s^{-1}
$K_{s,q}$	turbulent exchange coefficient for entity s, q	m^2 s^{-1}
K_w	turbulent exchange coefficient for latent heat transfer (water vapour)	m^2 s^{-1}
K_w	absorption coefficient for water vapour	m^3 g^{-1} mm^{-1}
l	surface roughness element breadth	m
L	Monin-Obukhov length	m
LAI	leaf area index	
LE	latent heat	W m^{-2}
L_d	incoming long wave irradiance	W m^{-2}
L_u	long wave irradiance emitted by the surface to the atmosphere	W m^{-2}
L_v	specific latent heat of vaporization of water	MJ kg^{-1}
$L_v F_w$	evaporation of water (latent heat flux density) - sometimes LE is used	W m^{-2}
$L_v F_{w_{BREB}}$	evaporation (latent heat flux density) determined by the BREB method	W m^{-2}
$L_v F_{w_{equilibrium}}$	equilibrium evaporation	W m^{-2}

$L_v F_{w_{Priestley\text{-}Taylor}}$	Priestley-Taylor evaporation	$W\ m^{-2}$
$L_v F_{w_{reference}}$	reference evaporation	$W\ m^{-2}$
$L_v F_{w_{LYS}}$	evaporation (latent heat flux density) determined lysimetrically	$W\ m^{-2}$
$L_v F_{wo}$	actual evaporation at the canopy surface (equivalent to $L_v F_{w_{LYS}}$)	$W\ m^{-2}$
$L_v F_{wcorrected}$	corrected eddy correlation latent heat flux density	$W\ m^{-2}$
$L_v F_{wuncorrected}$	uncorrected eddy correlation latent heat flux density	$W\ m^{-2}$
M	molar mass	$kg\ mol^{-1}$
M_d	molar mass of dry air	$kg\ mol^{-1}$
M_{soil}	mass of soil	kg
M_w	molar mass of water vapour	$kg\ mol^{-1}$
n	amount of substance	mol
∂	partial derivative	
P	environmental air pressure	kPa
P_o	atmospheric pressure at sea-level	kPa
PBL	atmospheric or planetary boundary layer	
q	specific humidity	$g\ kg^{-1}$
$\overline{q}_{207}$	specific humidity measured using a 207 humidity sensor	$g\ m^{-3}$
$\overline{q}_{KH20}$	specific humidity measured using a KH20 krypton hygrometer sensor	$g\ m^{-3}$
q_{mirror}	absolute humidity measured using a Dew 10 cooled dew point mirror	$g\ m^{-3}$
q'	specific humidity fluctuation	$g\ kg^{-1}$
Q	flux density of the entity q	$s^{-1}\ m^2$
q_{207}	specific humidity measured using a 207 humidity sensor	
q_{KH20}	specific humidity measured using a KH20 krypton hygrometer	
r	reflection coefficient	
r_a	aerodynamic resistance	$s\ m^{-1}$
r_{ah}	aerodynamic resistance for sensible heat	$s\ m^{-1}$
r_{am}	momentum	
r_{av}	aerodynamic resistance for latent heat	$s\ m^{-1}$
r_c	canopy resistance	$s\ m^{-1}$
r_i	isothermal resistance $r_i = \rho\, c_p\, \delta e / [\gamma / (L_v F_w + F_h)]$	$s\ m^{-1}$
r_s	canopy resistance (also referred to as the bulk stomatal resistance)	$s\ m^{-1}$
$r_{surface}$	surface reflection coefficient	
$r_T'\, q'$	cross correlation coefficent of air temperature and specific humidity fluctuation	$W\ m^{-2}$
r_{wt}	cross correlation of vertical wind speed air temperature	$W\ m^{-2}$
r_{we}	cross correlation of vertical wind speed and water vapour pressure	$W\ m^{-2}$
r_{wt}/r_{we}	ratio of correlation coefficients of atmospheric long wave irradiance	$W\ m^{-2}$
rI_s	short wave reflected irradiance	$W\ m^{-2}$
R	Bowen's relationship between conduction and convection to the amount of evaporation	unitless
R	Universal gas constant	$J\ mol^{-1}\ K^{-1}$
Ri	Richardson number: $Ri = \frac{g}{T} \frac{\partial\theta/\partial z}{\partial u^2/\partial z^2}$	unitless

L_d	atmospheric long wave irradiance (atmosphere to surface)	W m^{-2}
R_{net}	net irradiance	W m^{-2}
T	average air temperature	°C
T'	air temperature	°C
$\overline{T}$	average air temperature	°C
$\overline{T}_2$, $\overline{T}_1$	time-averaged air temperatures at heights z_2 and z_1 respectively	°C or K
$\overline{T}_{air}$	average air temperature (of the two sensing levels) over the 20 min time period	°C
T_a	instantaneous air temperature	°C
T_{arm}	reference temperature inside the metal arm of the CA27 sonic anemometer	°C
T_{dp}	dew point temperature	°C
$T_{dplower}$	dew point at the lower level of the Bowen ratio system	°C
$T_{dpupper}$	dew point at the upper level of the Bowen ratio system	°C
T_e	temperature of the evaporating water	°C
T_{plate}	temperature of a cooling plate	°C
T_r	temperature of the replacing water	°C
T_{ref}	reference temperature	°C
T_s	temperature of the surface	°C
T_{soil}	soil temperature	°C
$T_{surface}$	temperature of the plate surface	°C
$T_{surrounds}$	temperature of the surrounds	°C
T_w	temperature of the water surface (or body evaporating water)	°C
T_{air}	air temperature	°C
$T_{surface}$	surface temperature	°C
T_{corr}	corrected infra red temperature	°C
T_{uncorr}	uncorrected infra red temperature	°C
u	horizontal wind speed	m s^{-1}
u_1	wind speed at a height of 1m	m s^{-1}
u_2	wind speed at a height of 2m	m s^{-1}
u_3	wind speed at a height of 3m	m s^{-1}
$\overline{u}_1$	average horizontal wind speed at level 1	m s^{-1}
$\overline{u}_2$	average horizontal wind speed at level 2	m s^{-1}
u_*	friction velocity	m s^{-1}
u_{*1}	friction velocity for canopy 1	m s^{-1}
u_{*2}	friction velocity for canopy 2	m s^{-1}
V	voltage from krypton hygrometer	mV
V_o	voltage from krypton hygrometer corresponding to a specific humidity of 0 g kg^{-1}	mV
V_{207}	the specific humidity measured a 207 humidity sensor but converted to a krypton hygrometer	mV
V_{KH20}	KH20 krypton hygrometer voltage corresponding to specific humidity q	mV
V_{net}	voltage output from a net radiometer	mV

V_{soil}	soil volume	m^3
V_T	measured voltages corresponding to the air temperature measured using the Campbell Scientific eddy correlation system	mV
V_w	measured voltages corresponding to the vertical wind speed measured using the Campbell Scientific eddy correlation system	mV
w'	vertical wind speed	$m\ s^{-1}$
x	fetch	m
x	pathlength of krypton hygrometer	m
x	fetch distance	m
y	distance y-direction	m
z	height above ground	m
z_1	placement height at level 1 above canopy	m
z_2	placement height at level 2 above canopy	m
z_o	roughness length for momentum (– strictly z_{om})	m
z_{o1}	zero plane displacement height above canopy 1	m
z_{o2}	zero plane displacement height above canopy 2	m
z_{oh}	roughness length for sensible heat	m
z_{om}	roughness length for momentum	m
z_{ov}	roughness length for latent heat	m
$z-d$	height above the surface corrected for zero plane displacement	m
α	ratio of latent heat flux density $L_v F_w$ to the available heat flux density $A = L_v F_w + F_h = I_{net} + F_s$. Hence $\alpha = L_v F_w / A = L_v F_w / (L_v F_w + F_h)$	
$\alpha_{equilibrium}$	α under equilibrium conditions (weak flow of humid air over a wet canopy)	
$\alpha_{reference}$	α corresponding to reference evaporation	
β	Bowen ratio	
β	angle between vertical and the line from the sensor to the edge of the circular plate	
β_{breb}	Bowen ratio calculated using the Bowen ratio technique	
β_{LYS}	Bowen ratio calculated using lysimetric measurements.	
δ	thickness of internal boundary layer	m
δe	measured water vapour pressure profile difference	Pa
δ'	thickness of equilibrium sub layer	m
δq	measured specific humidity profile difference	$kg\ kg^{-1}$
δT	measured air temperature profile difference	^oC
Δ	slope of the saturation water vapour pressure *vs* temperature	$Pa\ ^oC$
δz	depth increment	m
δe	finite difference in water vapour pressure	Pa
δT	finite difference in air temperature	^oC
$\delta_{boundary}$	thickness of internal boundary layer	m
$\delta_{equilibrium}$	thickness of equilibrium layer	m
ε	emissivity	
ε_a	atmospheric emissivity	
ε_s	surface emissivity	

ε_{IRT}	IRT emmissivity setting	0.98
$\varepsilon_{surface}$	emissivity of the surface	
γ	psychrometric constant	Pa °C^{-1}
γ_i	incorrect psychrometric constant	Pa °C^{-1}
Γ	dry adiabatic lapse rate	°C m^{-1}
Φ_q	dimensionless stability function for entity q	
Φ_h	dimensionless stability function for sensible heat	
Φ_m	dimensionless stability function for momentum	
Φ_w	dimensionless stability function for latent heat,	
ρ	density	kg m^{-3}
ρ_{air}	air density	kg m^{-3}
ρ_{soil}	soil bulk density	kg m^{-3}
σ	Stefan-Boltzmann constant	W m^{-2}
σ_T/σ_e	ratio of standard deviation of air temperature to that of water vapour pressure,	
τ	Momentum flux density	Pa
τ_o	momentum flux density at the surface	Pa
θ	potential temperature	°C
θ_1	potential temperature at height z_1	°C
θ_2	potential temperature at height z_2	°C
θ_h	eqivalent temperature	°C
θ_m	eass water content	kg kg^{-1}
θ_w	soil water content on a mass basis	kg kg^{-1}
ξ	quantum yield	J kg^{-1}
ζ	dimensionless variable proposed by Monin-Obukhov	

Chapter 1

Introduction

1.1 Abstract

The impact of population pressures on the limited water resources of South Africa justifies the investigation on the measurement of evaporation. The direct measurement of evaporation may provide valuable data for many useful purposes. The physical processes of evaporation and transpiration are discussed as are evaporation measurement techniques. Techniques associated with micrometeorological measurements, such as the Bowen ratio and eddy correlation techniques, are the basis of the work. Aspects such as fetch, which affect evaporation measurements, are introduced. The objectives of the study, together with the project aims are presented. A summary structure of the report, on a chapter-by-chapter basis, is outlined.

1.2 Motivation for this study

A change in the land use pattern of an area, such as a doubling of forest production, would alter water use patterns and the water balance of a catchment. Since evaporation is an important component of the water balance, the direct measurement of evaporation may provide valuable data for many useful purposes. Some of these purposes include:

- validation of daily evaporation models;
- provision of data which may be compared with cruder methods of evaporation calculation;
- provision of important data from which different land use and seasonal effects on evaporation may be investigated;
- provision of important data from which the effect of manipulation of the surface may be investigated;
- provision of actual evaporation data for the independent evaluation of various modelling strategies;
- provision of actual evaporation data for the evaluation of management strategies, such as the doubling of plant production, at the catchment level.

In the process of studying evaporation measurement techniques, using the Bowen ratio and eddy correlation measurement methods, other techniques (such as a surface temperature technique), have been investigated. We have gained experience in the use of many micrometeorological measurement techniques. We have also taken the opportunity of obtaining valuable data that enables the stability of the atmosphere to be determined. A number of micrometeorological parameters have also been determined in this study through the investigation of evaporation measurement.

Life, as we know it, could not exist without water. In the course of evolution, living organisms have become absolutely dependent on water in many ways. Three factors affecting the future progress and development of South Africa must include overpopulation, the impact of Aids and limited water resources. In particular, agriculture, by the year 2010 will have to make do with less water at a far higher price. Certainly, the impact of the Reconstruction and Development Programme on the limited water resources of South Africa needs serious investigation.

1.2.1 United Nations study

The United Nations (UN) has reported recently that the world's population is set to increase from 5.7 billion to a staggering 10 billion by the middle of the next century. Global figures however conceal the diverging fortunes of different regions. Africa's population growth of 2.9 % a year is the highest in the world, easily outstripping Asian and Latin American growth of less than 2 %. The UN report flags a long list of economic, social and environmental concerns that follow from its projections. It warns that population growth will place huge strains on the supply of natural resources such as forests, fish and clean air. The UN report points out that the improvement in food production has been unevenly distributed; in Africa during the past decade, food decreased by 5 % while the population increased by a third. The UN report concludes that while production should be sufficient to meet all needs for the foreseeable future, poverty translates global adequacy into national and local shortages. Water, as much as food, may prove an increasing source of friction between countries and regions, the UN suggests. Rapidly industrializing countries such as China are facing intense demand for water supplies from industry as well as from rural populations. The UN warns that developing countries should brace themselves for huge internal migrations as surplus rural labour moves to the towns to look for work. The report estimates that 1.3 billion people will be added to the workforces of Asia, Africa and Latin America between 1995 and 2020. It adds that cities are likely to contain half the world's population by the end of the century.

1.2.2 Crop production

In terms of crop production, agriculture will have to concentrate on production at a higher water use efficiency against the background of a decreasing agricultural land area. While the aspect of water use efficiency is not addressed directly in this report, it is a natural continuation to this subject of study. Given an increase in population, water resources are not going to become more available at the same rate. Population pressures also degrade the quality of water, making it less available for useful agricultural, industrial, municipal and other purposes.

1.2.3 The physical processes of evaporation and transpiration

Evaporation is defined as the physical process whereby a liquid or a solid substance is transformed to the gaseous state. In meteorology, evaporation is usually restricted to the change of liquid to gas/vapour without change in temperature while sublimation is used to describe the change from solid to gas. The liquid that will be considered in this report is water.

The evaporation of water exists everywhere in the hydrological cycle, from raindrops, and from land and water surfaces. When water evaporates from a surface, there is a release of energy from the surface. Thus evaporation is a cooling process. Whilst part of this energy remains latent in the atmosphere, it is again released when water vapour condenses. This is an ongoing process as the average tenure of a water vapour molecule in the atmosphere is about nine days. Thus water vapour is an energy carrier, and energy must be available to cause the water to evaporate. Evaporation is referred to as a latent process. That part of heat energy flow which produces a temperature change is often referred to as sensible heat to distinguish it from latent heat. The word "latent" is derived from the Latin word *lateo* meaning hidden. The reason for the choice of the word "latent" to describe the evaporation process is because there is no temperature rise during the evaporation process even though a cooling effect at the surface is evident. The energy available for evaporation to occur must be available at the evaporating surface. At 30 °C, 1 kg of water will remove 2.43 MJ energy from the evaporating surface if all the water evaporates. The sources of this energy in the hydrological system are:

- sun (solar energy);
- heat energy carried into the area by wind (advected energy);
- heat energy stored in land masses;
- heat energy stored in water.

The most important of these energy sources is solar energy, but advected energy, which includes what is referred to as Berg winds in South Africa, may often be considerable. It does not follow that the amount of water vapour in the atmosphere is always increasing, in the presence of energy. There are occasions when energy is available for evaporation, but because the air is saturated, there is a balance between water evaporating and atmospheric water condensing. In this case then, the relative humidity (*RH*) of the atmosphere is 100 %. It is obvious, therefore, that for evaporation to occur, there must be a source of liquid water (if evaporation occurs from ice, this is termed sublimation), there must be sufficient energy available, and there must be a water vapour pressure difference between the evaporating surface and the atmosphere above the surface. The specific latent heat of vaporization, L_v (MJ kg^{-1}), is the heat energy per unit mass needed to change a substance from the liquid to the vapour phase without changing its' temperature. The quantity L_v is temperature dependent. Thus at lower temperatures more energy per unit mass is required to evaporate the water.

1.2.4 Evaporation measurement techniques

The scientific study of evaporation and transpiration processes dates to the time of Aristotle who concluded in the fourth century BC that "wind is more influential in evaporation than the Sun." Today, the hydrologic approach for estimating total evaporation (evaporation plus transpiration) is widely used. Often, this is the most practical approach. The disadvantages in this approach (Slatyer 1967) are the low level of measurement accuracy and the difficulties of determining total evaporation during rainy periods. Even with careful measurements, it is difficult to detect soil water changes with an accuracy better than ± 2 mm of water. Furthermore, the errors associated with the water balance approach invalidate it for estimating daily total evaporation.

Over an extensive uniform stand of level vegetation, fluxes of momentum, heat energy, water vapour and carbon dioxide are constant with height in the lowest parts of the turbulent boundary layer, roughly corresponding to the lowest 15 %. Bulk rates of exchange between the canopy and the air flowing over it can be determined by measuring vertical fluxes in this part of the boundary layer.

1.2.4.1 Fetch

Simply, fetch is the distance of traverse across a uniformly rough surface (Fig. 1.1). A maize crop may be regarded as a typical rough surface. If we wish to measure evaporation above a maize crop then due consideration must be given to the fetch. Adequate fetch would ensure that the evaporation from the maize is being measured and not the evaporation from areas adjacent to the maize.

1.2.4.2 Lysimetry

Lysimeters are large containers, filled with soil, water and other chemicals and whole plants, which can be weighed at regular time intervals. These devices allow the water loss from such containers to be measured for very short time intervals and longer (- minutes to days or longer). The main component of water loss is due to transpiration through plants and evaporation from the exposed soil surface. Lysimeters are regarded as the standard for evaporation measurement. However, lysimetric techniques

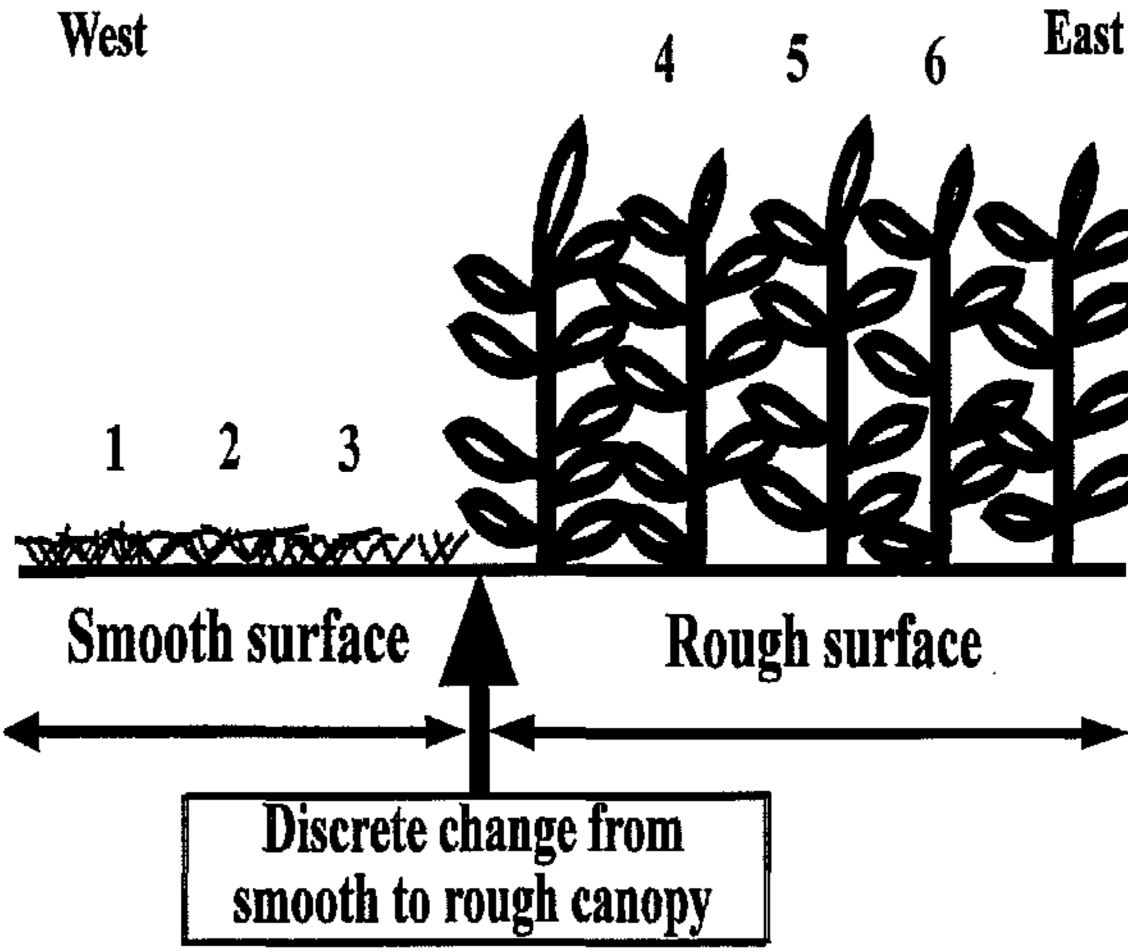

Fig. 1.1 Change in surface roughness on moving from the field depicted on the left (a short grassland canopy) to a 1-m tall maize canopy on the right. The various wind directions would determine the position of sensors (at points 1, 2 or 3 and 4, 5 or 6) placed above the respective canopies

are expensive, destructive (in the sense that usually a relatively large volume of disturbed or sometimes undisturbed soil is placed in a container usually of metal construction) and non-portable. These disadvantages serve as a justification for the alternative techniques we used in this study. We do however compare our measurement techniques with the lysimeter technique.

1.2.4.3 Micrometeorological techniques

Three methods of determining fluxes above a uniform stand of vegetation from micrometeorological measurements in the boundary layer were used in this report, one direct and two indirect methods. The direct method, known as "eddy correlation" (Swinbank 1951, Verma *et al.* 1992) requires simultaneous measurement of rapid fluctuations of vertical wind speed (w') and air temperature (T') for the determination of sensible heat. The covariance of these two fluctuations is a direct measure of the sensible heat at the point of measurement. The Bowen ratio method (Bowen 1926), an indirect method of determining fluxes, relies on the measurement of mean air temperatures and water vapour pressures and their gradients in the atmosphere. The second indirect measurement method we used involved the temperature difference measurement between canopy surface and overlying air and the measurement of wind speed. The canopy surface temperature was measured using infrared thermometers.

1.2.4.4 Transpiration

Transpiration may be measured directly using a variety of techniques. One of these, a sap flow technique, forms the basis of WRC project (K348).

If evaporation could be measured using above-canopy surface techniques, they would be more portable than lysimetric techniques. However, such measurement techniques have not been fully researched. The height placement of sensors placed above surfaces, in relation to the *fetch* distance, is important. Fetch may be simply defined as the distance across a uniformly rough surface. The fetch often depends on the wind direction (unless the shape of the uniformly rough surface is circular). To make the discussion more practicable, consider two surfaces, one a short grassland surface next to a 1-m tall maize surface (Fig. 1.1). At the interface between these two surfaces, there is a change in turbulent boundary layer conditions. If one wanted to measure sensible and latent heat above the 1-m canopy, under conditions were there is no dominant wind direction, one would place the above-canopy sensors in the middle of the field of maize (indicated by the 5). If the wind direction was always from the west one would place the sensors at the position marked with a 6. Similarly, if the wind was predominantly from the east, one would place the sensors at position marked 4. These positions would maximize the fetch. Maximizing the fetch ensures that the measured entities emanate from the 1-m canopy and not the shorter or other canopies. For the short grassland surface, one would use positions 1 or 3 depending on whether the wind direction was predominantly from the west or east respectively or position 2 if there is no dominant wind direction.

The complexity of the above-surface measurement techniques becomes evident when one considers that the aim is to estimate sensible and latent heat exchange at the canopy surface under situations where the atmosphere between canopy and measurement point(s) is a non-static fluid. Furthermore, it is through this fluid that various gases and radiation (solar and terrestrial wavelengths) with variable concentration and amounts are transferred and/or transported.

1.2.5 Objectives

1.2.5.1 Original project aims

A. Investigation of Bowen ratio and eddy correlation micrometeorological methods for the measurement of evaporation and comparison with: (a) each other; (b) traditional micrometeorological calculations of evaporation; (c) lysimetric measurements of evaporation.

In the case of most of these techniques, because of the roughness of the terrain, it will be necessary to assess the stability of the atmosphere and obtain a measure of advection.

B. Seasonal measurement of evaporation.

C. Comparative evaporation measurements between different sites.

D. The effect of some management practices (for example, burning and residue placement) on evaporation: (a) comparison between Bowen ratio estimates of evaporation for a grassland and a riparian zone community; (b) effect of fire on the evaporation of grassland and wetland communities; (c) investigation of the eddy correlation technique and comparison with Bowen ratio and lysimetric measurements of evaporation at the same site for a range of weather conditions; (d) quantification of surface roughness, turbulence, advection and fetch.

1.2.5.2 Background

This project was primarily concerned with the measurement of evaporation using a variety of micrometeorological techniques. This involved checking the function of sensors developed overseas and developing methods for checking collected data. After these methods had been developed, the aim was to use these measurement systems for the routine field measurement of evaporation. A detailed breakdown of the objectives of the study is given.

1.2.5.3 Investigation of the Bowen ratio micrometeorological methods

1.2.5.3.1 Baseline comparisons

Prior to our study, the Bowen ratio method for the measurement of evaporation had not been used in South Africa.

Our aim was to use two Bowen ratio systems adjacent to each other to investigate the quality of evaporation measurements and identify possible errors.

1.2.5.3.2 Field measurements of evaporation and sensible heat

We wished to compare the Bowen ratio technique with other evaporation techniques and use it for a variety of surfaces (grassland and vines) and compare our measurements with:

(a) traditional micrometeorological calculations of evaporation;

(b) lysimetric measurements of evaporation.

1.2.5.3.3 Alternative methods for evaporation measurement

We investigated whether or not it would be possible to determine sensible heat from measuring air temperature differences only and not both air temperature and water vapour pressure differences.

1.2.5.3.4 Seasonal measurement of evaporation

In the process of testing our techniques, we wished to obtain seasonal measurements of evaporation in Catchment VI of Cathedral Peak.

1.2.5.4 Investigation of the eddy correlation micrometeorological methods

1.2.5.4.1 Laboratory investigations

Our aim was to identify the factors limiting accurate measurement of evaporation and sensible heat using the eddy correlation technique.

1.2.5.4.2 Field investigations

We wished to compare the eddy correlation technique with the Bowen ratio technique. We also wanted to use the eddy correlation technique above a variety of surfaces (bare soil, maize, grassland and vines).

1.2.5.4.3 Placement height investigations

We wished to quantify fetch by measuring sensible heat, using the eddy correlation technique, by varying the placement height to fetch ratio. This was accomplished by varying the placement height instead of varying the fetch distance.

1.2.5.5 Surface temperature technique for sensible heat measurement

We investigated the possibility of using surface temperature and air temperature measurements in conjunction with wind speed profile measurements to calculate sensible heat and made comparisons with eddy correlation measurements of the same.

1.2.5.6 Stability quantification

Our aim was to quantify stability using field measurements above a short grassland surface and eddy correlation measurements supplemented by profile measurements of wind speed.

1.2.5.7 Calibration considerations

For energy balance techniques, a limiting factor is the accuracy of the net irradiance measurements. We wanted to develop an inexpensive laboratory calibration methodology for net radiometers (and infra red thermometers).

1.3 Structure of the report

There is a List of Symbols and List of Figures and Tables following the Executive Summary. This may prove particularly useful to the reader. The definition of a particular term may not be sufficient in this list so the reader may find a fuller definition in the body of the report.

The main emphasis of this study was on the use of techniques for the measurement of evaporation, with emphasis on the Bowen ratio and eddy correlation techniques. Chapter 2 is a review of the literature with particular emphasis on the Bowen ratio technique. A very brief discussion on the practical considerations of the Bowen ratio and eddy correlation techniques also appear in this chapter. The use of the Bowen ratio and eddy correlation techniques are discussed in Chapters 3, 4 and 5. These chapters therefore represent a major section of the report. Most of the detail of the Bowen ratio technique appears in Chapter 3 and the eddy correlation technique is discussed in Chapter 4.

Chapter 5 describes the use of a variety of techniques for the measurement of evaporation. The evaluation of these techniques included: Bowen ratio, lysimetric, surface temperature and eddy correlation methods and the influence of advection on Bowen ratio measurements.

Chapter 6 describes laboratory methodology for the calibration of net radiometers and infra red thermometers. The net radiometer is an important instrument central to the techniques used in Chapters 3, 4 and 5. The infra red thermometer is used as part of a surface temperature technique for determining sensible heat (Chapter 5).

Chapter 7 applies the Bowen ratio methodology (Chapter 3) and eddy correlation methodology (Chapter 4) to a vineyard.

Chapter 8 considers the placement height of eddy correlation sensors above a short turfgrass surface. This work, has already been published in the international literature. This chapter also considers the so-called "footprints" of measurements at a certain placement height which has been published in the South African literature.

The final chapter, Chapter 9, is an application of the measurement techniques described in this report. We report on seasonal comparisons of total evaporation in a Drakenberg catchment over a three-year period. We conclude in this chapter that the Bowen ratio energy balance method is suitable for the long term monitoring of total evaporation of a grassland surface.

The equipment information cards for the Bowen ratio and eddy correlation techniques are contained in **Appendices 1** and **2** respectively. These appendices contain detailed information on the use and checking of the equipment and would be particularly useful to users of such equipment.

For the convenience of the reader, the first mention of a table or figure is indicated in bold type. The decimal point system has been used throughout and there has been strict adherence to the International System of Units (Savage 1979, Salisbury 1996, Salisbury and Savage 1996).

Chapter 2

Bowen ratio energy balance method

2.1 Abstract

The quantification of the flux and total amount of evaporative water loss from natural and agricultural lands may be accomplished by various means. The Bowen ratio and eddy correlation methods are two methods that can be used in conjunction with sensors attached to a datalogger and computer to provide hourly or sub-hourly evaporation estimates and many other micrometeorological data, both for local irrigation scheduling and monitoring of remote sites. The ratio of sensible to latent heat flux density, defined as the Bowen ratio, is measured as the ratio of the time-averaged vertical air temperature and water vapour pressure differences by differential thermometry and psychrometry respectively. The vertical flux density of water vapour, $L_v F_w$ (W m^{-2}) may be calculated from 20 minute averages of measurements of the Bowen ratio, and of the major components of the energy balance. Excluding stored canopy and biochemical energy and advection, these comprise net irradiance, soil heat flux density and energy flux density stored in the soil. The exclusion of advected energy from the energy balance can lead to underestimations in the calculation of $L_v F_w$ of up to 45 %. Both sensible and latent advection should be quantified and included in the method. The Bowen ratio method is based on the assumption of Similarity Principle between the exchange coefficients for latent and sensible heat which has been found to apply only under certain circumstances. The ongoing controversy over this assumption and the history of modifications to correct for various atmospheric conditions are reviewed.

The eddy correlation is an absolute technique that can be used for the measurement of sensible and latent heat flux density and therefore, theoretically, the other components of the energy balance and the net irradiance need not be determined.

2.2 Introduction

The importance of evaporation, especially in a country such as South Africa, should not be understated. An excellent summary of this importance appears in the publication "Opportunities in the Hydrologic Sciences" (1991, 337 pages, ISBN 0 309 042445, available from: National Academic Press, 2101 Constitution Avenue, N.W. Washington, D C 20418 USA):

"Water vapour has been termed the working fluid of the atmospheric heat engine as through evaporation and condensation it drives atmospheric and oceanic circulations and thereby redistributes solar energy. The overall planetary temperature is influenced strongly by water vapour as it is the primary greenhouse gas. Through fluvial erosion and sedimentation, water, together with tectonics, shapes the land surface. Water is the universal solvent and the medium in which most changes of matter take place, and hence it is the agent of element cycling and is also essential for life. Large investments have been made in water resources management to provide the levels of potability and availability of water currently expected in developed countries, yet relatively little has been invested in the basic science underlying water's other roles in the planetary mechanisms. In the modern scientific establishment, however, although hydrologic science, has a natural place as a geoscience alongside atmospheric, ocean, and solid earth sciences, its niche is vacant. This is so because until now there has not been a practical need to build a comprehensive understanding of the global water cycle. The whole process has been driven by narrowly focused issues of engineering hydrology, and so the patches of small-scale application-related scientific knowledge have not merged into the coherent whole needed to understand water's function on a more global scale.

It is for these reasons that all hydrological studies, be they ground, surface or atmospherically based, should be seen and carried out taking cognizance of all the related disciplines. If this is done, then studies based on catchment-size scales may be extrapolated to a much larger scale by identifying the range of area to which the results are applicable, or may be adapted."

Accurate hourly absolute estimations of water loss by evaporation are required in both irrigated agricultural areas and natural ecosystems for irrigation scheduling and hydrological monitoring respectively.

The loss of water in the gaseous phase is a large component of the water loss from an area and may be estimated by measuring, *inter alia*, the flux density of water vapour by various means. Meteorological methods have the advantage over lysimetry and large scale hydrological modelling in that they are non-destructive, continuous, mobile and rely less on empirical factors. They also are capable of measuring evaporation for periods from as short as 12 minutes upwards, in areas from field to sub-regional size. Although initial costs are quite large, accuracy is high and a wealth of data are collected. The measurements usually need only be supplemented by one or two instruments to supply data as a complete meteorological station.

The Bowen Ratio Energy Balance method, abbreviated BREB, is another meteorological method that has been employed for the quantification of evaporation over vegetated surfaces. It has traditionally been employed as a research tool over flat and only moderately hilly (Garratt 1984), extensive crop surfaces to determine crop responses to various treatments, most commonly water stress. Currently work is being undertaken to test a more practicable and remote application in the KwaZulu-Natal Drakensberg catchments. The site has slope and weather conditions not previously reported on in the literature, and thus new ground is being broken in these respects. The BREB method is also commonly tested and used over uniform crops such as wheat, soybean and sometimes row crops such as maize, but less often over natural grasslands such as the climax veld of the Drakensberg catchments.

2.3 Surface radiation and energy balance exchange

Energy flux density available at the earth's surface is mainly sensible F_h (results in temperature change with no phase change of water) or latent $L_v F_w$ (results in a phase change of water usually from liquid to vapour with no temperature change). Managers of farms or ecosystems are attempting to, wittingly or unwittingly, alter these energy terms. Bowen (1926) realized the relative significance of the terms and considered the ratio $F_h/L_v F_w$ to be important for partitioning the energy balance into its various components. This ratio is, now more commonly known as the Bowen ratio β.

Of the other meteorological methods, the profile (or aerodynamic) and the combination methods require various measures of air temperature, resistance to water vapour flow, and surface roughness and other height parameters such as canopy height h. An alternative evaporation measurement technique, the eddy correlation method, may require daily attended operation and equipment that is sensitive, delicate and expensive (Tanner 1963, Sharma 1987).

Advection is usually not routinely accounted for when using the Bowen ratio profile method to calculate sensible and latent heat energy flux densities from a surface. Rosenberg (1969) found that evaporation in spring can exceed net irradiance by up to 80 % and that it was due to strong local and regional advection. Net irradiance is the sum of the incoming short and long wave irradiance, less the short wave reflected and long wave emitted by the surface:

$$I_{net} = I_s - r{\cdot}I_s + L_d - L_u \qquad 2.1$$

(commonly referred to as the radiation balance equation). The available energy flux density in J s^{-1} m^{-2} or in W m^{-2} is the difference between the net irradiance and the amount F_s stored by and entering (or leaving) the soil surface:

$$\text{available energy} = I_{net} - F_s = L_v F_w + F_h + \xi F_c,$$

(net irradiance I_{net} minus soil heat flux density F_s both in W m^{-2}), at a vegetated surface is partitioned into sensible (F_h) and latent ($L_v F_w$) energy flux densities, and photosynthetic flux density ξF_c where ξ is the quantum yield (J kg^{-1}) and F_c is the flux density of carbon dioxide in kg s^{-1} m^{-2}). The sensible heat component with units W m^{-2} is F_h. The vapour flux density (F_w in kg s^{-1} m^{-2}), multiplied by the specific latent heat of vaporization, L_v (in MJ kg^{-1}) is the latent heat flux density, in W m^{-2}. The shortened energy balance equation neglects advection, physically and biochemically (photosynthetically) stored heat flux densities in the canopy as they are considered negligible (Thom 1975):

$$I_{net} = L_v F_w + F_h + F_s \qquad 2.2$$

(commonly referred to as the energy balance equation). The sign convention here is that during the day the net irradiance (Eq. 2.1) is positive with terms on the right hand side of Eq. 2.2 leaving the earth's surface being regarded as positive. This convention has been used throughout in this work. The alternative convention requires that terms leaving the surface are negative and that :

$$I_{net} + L_v F_w + F_h + F_s = 0. \qquad 2.3$$

This sign convention results in negative latent and sensible heat values under normal daytime conditions.

Under non-advective conditions, the amount of evaporation is strongly correlated to the amount of available energy, and the available energy differs only in small amounts from the net irradiance. Questionable results from the application of the Bowen ratio method are very often ascribed to insufficiently accurate instrumentation. Bertela (1989) points out that most authors are merely aware of the problems introduced by advection, but attach more importance to the accuracy of measurements. He used the unpublished data of Pampoloni and Paloscia (1985) to show examples of occasions when the Bowen ratio failed due to advective energy inputs and showed a method to identify and quantify these.

2.4 Introduction to stability parameters

The effect of the stability of the atmosphere on the turbulence encountered in the region of the entity fluxes needs to be characterized.

2.4.1 The Richardson number

One measure of atmospheric stability is the Richardson number (*Ri*), given by:

$$Ri = \frac{g}{\overline{T}} \frac{\frac{\partial\theta}{\partial z}}{\frac{\partial^2 u}{\partial z^2}} \approx \frac{g}{\overline{T}} \frac{(\theta_2 - \theta_1)(z_2 - z_1)}{(\overline{u}_2 - \overline{u}_1)^2} \approx \frac{g}{\overline{T}} \frac{d\overline{T}\,dz}{(du)^2} \qquad 2.4$$

where g is the acceleration due to gravity (m s^{-2}), $\overline{T}$ is the average air temperature between the two levels (K), θ is the potential temperature (K), and u is the wind speed in the predominant direction of flow (m s^{-1}). For the first few meters above ground, an air temperature gradient dT/dz may be substituted for the potential temperature gradient $d\theta/dz$ (Rosenberg 1974).

The Richardson number is a dimensionless measure of the intensity of mixing (turbulence), and provides a simple criterion for the existence or non-existence thereof in a stably stratified environment. A large positive value of $Ri > 0.25$ is indicative of weak and decaying turbulence and that the environment is tending towards a stable condition.

Since the Richardson number is a non-dimensional ratio describing conditions in the surface layer over uniform terrain, it can, according to Monin-Obukhov Similarity theory, be equated directly to $z/\mathcal{L}$ (defined in following section) in unstable air (Panofsky and Dutton 1984). The properties of $z/\mathcal{L}$ are described in **Table 2.1**. It is however influenced by height, and thus other indices, such as the Monin-Obukhov length and related parameters are preferable (Arya 1988).

2.4.2 The Monin-Obukhov length

In stratified turbulent flow any dimensionless characteristic is determined by: the height $z - d$, the shear stress at the surface τ_o, the air density ρ_a, and the production rate of turbulent energy resulting from the work of buoyancy forces. These four quantities can be expressed in terms of the three basic dimensions of time, length and mass, combined into one dimensionless variable, ζ (pronounced zeta) proposed by Monin and Obukhov (1954),

Table 2.1 Qualitative interpretation of $z/\mathcal{L}$ and therefore of *Ri* (after Panofsky and Dutton 1984)

$z/\mathcal{L}$	Description
Strongly negative	Heat convection dominant
Negative but small	Mechanical turbulence dominant
Zero	Purely mechanical turbulence
Slightly positive	Mechanical turbulence slightly damped by temperature stratification
Strongly positive	Mechanical turbulence severely reduced by temperature stratification

$$\zeta = (z-d)/\mathcal{L}$$

where $\mathcal{L}$ is Obukhov's (1946) stability length (Brutsaert 1982) or "buoyancy length scale", defined by its originator Obukhov (1946) as "the characteristic height (scale) of the sublayer of dynamic turbulence".

The relevance of this is that, in magnitude, $\mathcal{L}$ represents the thickness of the layer of dynamic influence near the surface in which shear or friction effects are always important. On strongly convective (windless free-convective) days, $\mathcal{L} \approx -10$ m (*i.e.* small and negative), $\mathcal{L} \approx -100$ m on windy days, and approaches infinity with purely mechanical turbulence (Brutsaert 1982). At night, or with downward heat flux, $\mathcal{L}$ is positive, and when turbulence ceases, $\zeta \rightarrow 0$.

Closest to the surface (*i.e.* $z < |\mathcal{L}|$) shear effects dominate, and buoyancy effects are insignificant, whereas the latter dominates when $z > |\mathcal{L}|$. Thus the ratio $(z-d)/\mathcal{L}$ is important in assessing the relative importance of buoyancy versus shear effects in the stratified surface layer, similar to the *Ri* number, to which it can be related (Panofsky and Dutton 1974). Under stable conditions, $(z-d)/\mathcal{L}$ varies linearly with height showing the increasing importance of buoyancy above the surface (Arya 1988).

The differential form of the wind profile equation can be written in generalized form as (Brutsaert 1982):

$$\frac{\partial u}{\partial z} = \frac{u_*}{k\,(z-d)} \cdot \Phi_m \qquad 2.5$$

where $\partial u/\partial z$ is horizontal wind speed gradient in the vertical direction, u_* is the friction velocity (m s^{-1}), and k is von Karman's constant ($k = 0.41$) and Φ_m is a dimensionless stability function for momentum with a value larger or smaller than unity in stable and unstable conditions respectively. The height above ground z, and d, the zero-plane displacement height, are both in metres.

The dependence of $\Phi_{m,h,w,q}$ on stability is generally expressed as a function of terms that depend on the ratio of the production of energy by buoyancy forces to the dissipation of energy by mechanical turbulence. The subscripts $_{m,\,h,\,w}$ and $_q$ refer to momentum, sensible heat, latent heat and any entity q respectively. The Richardson number *Ri* (Eq. 2.4), and the Monin-Obukhov parameter ζ are generally used.

The dependence of Φ on stability is a unique function of ζ (eg. Dyer 1974):

$$\Phi_m\,(\zeta) = \frac{k\,(z-d)}{u_*}\frac{\partial u}{\partial z}$$

or

$$\Phi_h\,(\zeta) = k\,u_*\,\frac{(z-d)}{F_h}\,\rho_a\,c_p\,\frac{\partial \theta}{\partial z}$$

where F_h is the sensible heat flux density, ρ_a (abbreviated ρ) is the density of air, c_p is the specific heat capacity of dry (unsaturated) air and $\partial\theta/\partial z$ is the potential temperature gradient.

From flux gradient relationships

$$\tau = \rho\,u_*^2 = \rho\,K_m\,\frac{\partial u}{\partial z}$$

(where τ is the momentum flux density or shearing stress), and the wind profile equation (Eq. 2.5), it can be shown that:

$$K_m = k\,u_*\,(z-d)\cdot\Phi_m^{-1}, \qquad 2.6$$

and

$$K_h = k\,u_*\,(z-d)\cdot\Phi_h^{-1}, \qquad 2.7$$

$$K_w = k\,u_*\,(z-d)\cdot\Phi_w^{-1}, \qquad 2.8$$

and

$$K_q = k\,u_*\,(z-d)\cdot\Phi_q^{-1}. \qquad 2.9$$

Wind speed profiles consisting of at least three measurement heights are required to determine these functions.

The conclusion reached by Verma *et al.* (1978) was that the underestimation of evaporation under regional advection was a result of Φ_w differing from Φ_h under stable conditions.

The Richardson number *Ri* has the advantage that it contains only gradients which can be measured experimentally. However, it varies with elevation. The Monin-Obukhov theory seems daunting due to the number of hard-to-visualize [dimensionless] variables, and is less easily measured, but is independent of height, and can be used to correct flux-gradient equations.

2.5 Description of various micrometeorological methods, excluding Bowen ratio, of evaporation measurement

2.5.1 Aerodynamic and energy balance methods

Traditionally, research into turbulent transport in the lower atmosphere has been confined to studies of the vertical fluxes of momentum, sensible heat, and water vapour over a horizontally-uniform flat area. The simplifications gained by applying these conditions have been so attractive that they have led to the assumption of a constant flux layer (see Section 2.11) in which the transport of the components mentioned varies so little with height that the height variation can be ignored (Haugen *et al.* 1971). Although such conditions rarely if ever exist, much theory is still based on these premises, and data is assumed to have conformed to the logical expectations (Haugen *et al.* 1971). Denmead (1984) was of the opinion that:

"micrometeorological approaches to quantifying processes which influence evaporation have not been very fruitful because of their reliance on flux-gradient.relationships."

In defense of using the flux-gradient approach for evaporation measurements, the alternatives all have their weaknesses: chamber systems cannot mimic the natural environment; heat pulse and radioactive isotope tracer techniques avoid environmental problems but require knowledge of the plant's leaf area index, the pathway water takes in the stem and the planting density. Combination methods whilst avoiding surface measurements, require many difficult measurements and a large sample number. The water balance approach is used on a much larger, catchment-sized scale, and is thus not capable of even a "daily-total" time scale.

As the BREB method is a micrometeorological method which falls into both the aerodynamic and energy balance techniques, these two separate types will be discussed first.

2.5.1.1 Aerodynamic methods

The pure aerodynamic methods require the determination of a turbulent transfer coefficient for the entity (the eddy diffusivity mentioned above), as well as the vertical gradient of the entity. The turbulent transfer coefficient for water vapour, K_w, is usually related to that for momentum, K_m, which can be derived from measurements of the mean vertical gradients of wind speed. To allow for departures from a 1:1 relationship between the two coefficients, a dimensionless empirical factor Φ_w related to the atmospheric stability is used, *i.e.*

$$K_w = \Phi_w K_m$$

so that

$$L_v F_w = \frac{\rho\, c_p}{\gamma} K_m \frac{\partial e}{\partial z} \Phi_w$$

where Φ_w is smaller than, equal to or greater than unity for stable, neutral and unstable conditions respectively (Arya 1988) (Section 2.4.2).

An alternative aerodynamic method based on the correlation of eddies carrying water vapour and sensible heat, the eddy correlation (EC) method, has "promised real progress" (Denmead 1984), but our experience has shown for unattended use, the method has failed to deliver to date mainly due to instrumentation problems.

2.5.1.2 Energy balance methods

The energy balance methods require the measurement or estimation of all the terms in the energy balance equation but one, the latent heat flux density $L_v F_w$. This is calculated as the balance between net irradiance and sensible heat flux density plus the soil heat flux density. Soil heat flux density may be measured or assumed zero over longer time periods, while the heat flux density stored in the canopy (physically and biochemically) is usually assumed negligible in the short term, especially in short canopies such as grasses. The sensible heat flux density is measured directly by one of the aerodynamic methods, and the remainder of the energy flux density must be the latent heat. Thus, $L_v F_w$ is being indirectly determined with an energy balance method, but an aerodynamic (or eddy correlation) method has been used to measure F_h. It makes more sense, therefore, to combine the two types of method more completely and avoid several of the problems associated with the aerodynamic and energy balance techniques when used alone.

2.5.2 Combination methods

2.5.2.1 The Bowen ratio energy balance method

The BREB method combines the aerodynamic and energy balance methods to determine how the available energy is partitioned. Measurements of the profile gradients of air temperature and water vapour pressure are combined with a measurement of the amount of available energy flux density to quantify the two unknown flux densities, while the two [unknown] exchange coefficients are assumed equal, and their ratio therefore unity. These methods require a greater degree of accuracy in the measurement of the gradients. The dependence on the accurate measurement of the available energy flux density term, although large, is not increased compared to energy balance methods alone.

2.5.2.2 The Penman-Monteith equation method

For completeness the Penman-Monteith equation is briefly discussed (described by Monteith 1965 and

Thom 1975 and based on Penman 1948). By definition:

$$\alpha = \frac{L_v F_w}{L_v F_w + F_h}$$

or from Eq. 2.2

$$\alpha = \frac{L_v F_w}{I_{net} - F_s}. \qquad 2.10$$

The term α represents the fraction of evaporation (that is, latent heat energy flux density) relative to the total available energy flux density $I_{net} - F_s$ ($= L_v F_w + F_h$) (*cf.* Eq. 2.2).

The Penman-Monteith equation for the determination of canopy evaporation is derived from a different combination of the aerodynamic flux and energy balance methods, and has been represented by Thom (1975) in fundamental form as:

$$\alpha = \frac{\Delta r_a + \gamma r_i}{\Delta r_a + \gamma (r_a + r_s)}. \qquad 2.11$$

The resistance r_s is the canopy resistance (s m^{-1}) (also referred to as the bulk stomatal resistance) and r_a (s m^{-1}) is the aerodynamic resistance. The resistance $r_i = \rho\, c_p\, \delta e / [\gamma\, (L_v F_w + F_h)]$ is referred to as the isothermal resistance (s m^{-1}) where δe is the water vapour pressure deficit (Pa): $\delta e = e_s - e$ where e_s is the saturation water vapour pressure at the measured air temperature at a known height above ground, and e is the water vapour pressure at the same height.

The temperature-dependent constants Δ and γ of the Penman-Monteith equation are usually represented on the psychrometric chart by the magnitude of the slope of the saturation water vapour pressure *vs* temperature curve and the slope of the wet bulb temperature line of the psychrometric chart, respectively (both terms having units Pa K^{-1}).

Unlike net irradiance, it is not practical to measure aerodynamic and surface resistances continually or even on a daily basis. The "fundamental equation" (Eq. 2.11) in this form can be applied to various sets of environmental conditions for which certain of the types of resistances may be assumed negligibly small compared to the others (Thom 1975).

2.5.2.3 The "equilibrium conditions" case

The "equilibrium" condition is defined by Slatyer and McIlroy (1967) as that created by air that has been in contact with a wet surface over a very long fetch, so that it may tend to become vapour saturated. Under these conditions, they reasoned the only large resistance is r_a, when compared to r_i and r_s reducing Eq. 2.11 to:

$$\alpha_{equilibrium} = \frac{\Delta}{\Delta + \gamma}. \qquad 2.12$$

The significance of this dependence of $\alpha_{equilibrium}$ solely on temperature means that at air temperatures 6, 18 and 26 °C, $\alpha_{equilibrium}$ has the value 0.50, 0.67 and 0.75 respectively. Thus, the fraction of the available energy partitioned into evaporation is found by simply substituting $\alpha_{equilibrium}$ from Eq. 2.12 into Eq. 2.10 and solving for $L_v F_{w\ equilibrium}$:

$$L_v F_{w\ equilibrium} = \frac{\Delta}{\Delta + \gamma} \cdot (I_{net} - F_s). \qquad 2.13$$

This is the ideal set of circumstances as, in order to calculate an evaporative flux, no resistances need to be measured. Unfortunately the method can only be used to compare equilibrium- and BREB-determined evaporation values when "equilibrium" conditions exist, *i.e.* during the calm and wet periods (humid atmosphere and wet canopy) of any year, and not during the more crucial and dry periods which are difficult to measure. As a measurement tool it is therefore not much use outside of the rainy season in southern Africa.

Priestley and Taylor (1972) found that actual evaporation from oceans, bare soil and vegetation was about 26 % greater than $L_v F_{w\ equilibrium}$:

$$L_v F_{w\ Priestley\text{-}Taylor} = 1.26\, L_v F_{w\ equilibrium} = 1.26 \frac{\Delta}{\Delta + \gamma} \cdot (I_{net} - F_s). \qquad 2.14$$

This estimate of the actual evaporation has been shown to be reliable for humid regions but has not been tested in arid and semi-arid regions such as are found in southern Africa.

2.6 Bowen ratio theory

Bowen (1926) was the first to attempt to show that "the process of evaporation and diffusion of water vapour from any water surface into the air above it is exactly similar to that of the conduction or "diffusion"of specific heat energy from the water surface into that same body of air". Bowen expanded on work by Cummings (1925) on evaporation from lakes to take into account factors previously ignored, namely conduction and convection. By relating conduction and convection to the amount of evaporation by a factor "R" in his original paper, Bowen (1926), included these important parameters in an indirect way:

$$C = R \cdot L_v F_w$$

where he defined C as conduction and convective heat energy flux density, both in W m^{-2}. Conduction implies heat transfer through a solid, and convection that through the fluid, air, above that solid providing the heat. Bowen's definition of advection as used here is contrary to the modern definition of heat energy introduced by horizontal differences in air temperature and water vapour pressure. Water vapour flux density $L_v F_w$ is defined more fully below in Eq. 2.16. The factor R is a function of vapour pressure and air temperature gradients between the evaporating surface and the bulk air respectively, and the psychrometric constant as follows:

$$R = 46\ [(T_w - T_a)/(e_w - e_a)]\ P/P_o$$

where T_w and T_a are the temperature of the water surface (or body evaporating water), and air (°C), e_w and e_a are the water vapour pressures of the evaporating surface (usually saturated), and the air above it (Pa) respectively. The atmospheric pressure at sea-level is P_o, while P is the environmental pressure (in Pa). The factor 46 is the temperature-dependent psychrometric "constant" taking the density and specific heat capacity of air, as well as the latent heat of vaporization into account, and has units Pa K^{-1}.

This method uses surface measurement of temperature to calculate the saturated water vapour pressure at the surface. These are used with measurements at a point away from the surface to calculate the factor R. The surface temperature of water is easy to measure, and the air is saturated at the surface. With vegetation, a representative surface leaf temperature is extremely difficult to measure, and the exchange of latent energy across this interface far more complex than from the simple and flat water surface. For this reason the single layer measurement Penman-Monteith, and double layer Bowen ratio methods were developed, both of which have no directly measured surface variables.

According to Fick's Law, the flux density of any entity is equal to the product of an exchange coefficient and the entity concentration gradient. In general:

$$Q = K_q\,[\partial(\rho_{air}\,\overline{q})/\partial z] \qquad 2.15$$

where Q is the flux density of q ($s^{-1}\ m^{-2}$), ρ_{air} is the density of the medium (moist air is approximately 1.12 kg m^{-3}), K_q is the turbulent exchange coefficient ($m^2\ s^{-1}$), and $\partial\overline{q}/\partial z$ is the mean concentration gradient of the quantity q over the time period of measurement. This general equation can be modified to describe the flux density of any particular entity such as those involved in the energy exchange at a surface.

According to Fick's Law of Diffusion, the latent heat energy flux density $L_v F_w$ (W m^{-2}) is given in finite difference form by:

$$L_v F_w = (\rho_{air}\,c_p/\gamma)\,K_w\,\delta\overline{e}/\delta z = (\rho_{air}\,c_p/\gamma)\,K_w\,(\overline{e}_2 - \overline{e}_1)/(z_2 - z_1) \qquad 2.16$$

where ρ_{air} is the air density, c_p the specific heat capacity of dry air at constant pressure, γ the psychrometric constant (66 Pa K^{-1} at sea level), K_w the exchange coefficient for latent heat transfer, and $\overline{e}_2$ and $\overline{e}_1$ the time-averaged water vapour pressures at heights z_2 and z_1 respectively. In this report, d is taken as the actual finite difference of the term following. The term δ is taken to be an approximation of the difference of the term to follow (see Notation list). Hence, for example, δe is an approximation of de. Indeed, δe is referred to as a finite difference approximation of de.

Similarly, the sensible heat energy flux density F_h is given in finite difference form by:

$$F_h = (\rho\,c_p\,K_h)\,(\overline{T}_2 - \overline{T}_1)/(z_2 - z_1) \qquad 2.17$$

where K_h is the exchange coefficient for sensible heat transfer ($m^2\ s^{-1}$), $\overline{T}_2$ and $\overline{T}_1$ are the time-averaged air temperatures at heights z_2 and z_1 respectively.

Following Bowen (1926), we consider the ratio β:

$$\beta = F_h/L_v F_w = (\gamma\,K_h/K_w)\,(\overline{T}_2 - \overline{T}_1)/(\overline{e}_2 - \overline{e}_1).$$

Hence β can be determined from a measurement of air temperature and water vapour pressure at two levels in the atmosphere. Ignoring photosynthesis and advection, the surface energy balance is given by:

$$I_{net} = L_v F_w + F_h + F_s \qquad 2.2$$

where I_{net} is the net irradiance and F_s is the soil heat flux density. Combining the latter two expressions:

$$L_v F_w = (I_{net} - F_s)/(1 + \beta) \qquad 2.18$$

$$\text{and } F_h = \beta\,(I_{net} - F_s)/(1 + \beta) \qquad 2.19$$

$$\text{where } \beta = \gamma\,(\overline{T}_2 - \overline{T}_1)/(\overline{e}_2 - \overline{e}_1). \qquad 2.20$$

if it is assumed that $K_h = K_w$. The equality of these two exchange coefficients,

$$K_h = K_w, \qquad 2.21$$

is often referred to as the Similarity Principle.

The available energy $I_{net} - F_s$, (net irradiance I_{net} minus soil heat flux density F_s both in W m^{-2}), at a vegetated surface is partitioned into sensible (F_h) and latent ($L_v F_w$) energy flux densities. The sensible heat component with units W m^{-2} is, from Fick's Law (Eq. 2.15):

$$F_h = \rho\, c_p\, K_h\, (\partial\overline{T}/\partial z) \qquad 2.22$$

and F_w, the vapour flux density in kg s^{-1} m^{-2}), multiplied by the specific latent heat of vaporization, L_v (in MJ kg^{-1}), to yield the latent heat flux density, in W m^{-2}:

$$L_v F_w = (\rho_a\, c_p\, K_w/\gamma)\cdot(\partial\overline{e}/\partial z) \qquad 2.23$$

where ρ_a is the air density, c_p is the specific heat capacity of air at constant pressure, approximately 1004 J kg^{-1} K^{-1}, K_h is the turbulent exchange coefficient for sensible heat transfer (m^2 s^{-1}), K_w is the turbulent exchange coefficient for latent heat transfer (m^2 s^{-1}), γ is the psychrometric constant (approximately 66 Pa K^{-1}), representing the magnitude of the slope of the wet-bulb temperature line on the psychrometric chart, $\overline{T}$ is the mean air temperature over the sampling period (°C or K), $\overline{e}$ is the mean water vapour pressure (Pa), δz is the vertical displacement between measurement positions, taken in finite difference form as Δz (m), yielding vertical differences $\Delta\overline{T}$ and $\Delta\overline{e}$ over Δz where $\Delta\overline{T}$ is the change in mean air temperature due to an increase in the energy content of air per unit volume, by an amount ΔE. The sensible heat concentration gradient per unit volume $\partial\overline{T}/\partial z$ (more correctly $\Delta\overline{T}/\Delta z$), is defined to be the change in energy content of air per unit volume per unit vertical distance: $\Delta E/\Delta z = \rho_{air}\, c_p\, \Delta\overline{T}/\Delta z$.

The ratio of the sensible to latent heat flux density was defined by Bowen (1926), and has since been known as the Bowen ratio:

$$\beta = F_h/L_v F_w \qquad 2.24$$

or in full:

$$\beta = [(\rho\, c_p\, K_h)\cdot\partial\overline{T}/\partial z]/[(\rho\, c_p\, K_w)/\gamma)\cdot\partial\overline{e}/\partial z]$$

which may be simplified, by taking finite differences as representing the concentration gradients (Panofsky 1965), to:

$$\beta = \gamma\,(K_h/K_w)\,[(\overline{T}_2 - \overline{T}_1)/(\overline{e}_2 - \overline{e}_1)] \qquad 2.25$$

where the subscripts 2 and 1 refer to the upper and lower levels respectively, and where these air temperatures and water vapour pressures are actually time averaged values, $\overline{T}_2$, $\overline{T}_1$, $\overline{e}_2$ and $\overline{e}_1$.

Generally, the exchange coefficients K_h and K_w are unknown. However, Rider (1954) showed that their ratio is not too far from unity. Hence, assuming this principle, the Similarity Principle (see Section 2.7.3), the Bowen ratio equation is further simplified to:

$$\beta = F_h/L_v F_w = \gamma\,[(\overline{T}_2 - \overline{T}_1)/(\overline{e}_2 - \overline{e}_1)]. \qquad 2.20$$

The sign of β depends upon the direction of the two fluxes, since any energy gains by the surface are considered positive whilst losses are negative. Typical daily summer β values lie between 0 and 2 but may far exceed 2 in winter. The magnitude of β depends upon the proportion of the available energy directed into evaporation and sensible heat transfer. The value of β is thus seasonal due to the larger sensible component in winter, while in summer the availability of water results in the majority of the heat being lost by the latent heat exchange in the evaporative process. The flux density of $L_v F_w$ is strongly correlated to the available energy except under conditions of advective increases or when lower night time temperatures increase canopy resistance (Rosenberg 1969).

The latent heat flux density $L_v F_w$ may be obtained by combining Eq. 2.20 and the shortened[1] energy balance equation:

$$I_{net} = L_v F_w + F_h + F_s \quad 2.2$$

and rearranging into the form $L_v F_w = (I_{net} - F_s)/(1 + \beta)$ 2.18

where I_{net} is the net irradiance, and F_s (or S) is the soil heat flux density both in (W m^{-2}). Tanner and Pelton (1960) found that changes in I_{net} and F_s are strongly coupled, and from this base (in conjunction with surface temperature and a water balance), less accurate but larger scale estimates of evaporation can be made.

2.7 Assessment of the assumptions in the Bowen ratio technique

2.7.1 The use of the shortened energy budget equation

Heat stored in the plant is of relative consequence only when the energy budget is very small (Tanner 1960a). Biochemically consumed energy is also considered negligible, and these two amounts are thus not included in the energy balance calculation (Thom 1975).

2.7.2 The use of finite differences as a measure of entity gradients

Finite differences are taken as being an adequate indication of gradients in air temperature and water vapour pressure (Panofsky 1965):

$$(\partial\bar{T}/\partial z)/(\partial\bar{e}/\partial z) \approx \Delta\bar{T}/\Delta\bar{e}$$

for small Δz for small values of $dz \approx 1$ to 3 m. Because of this, and the prohibitive expense of measuring at more than two heights, the procedure is accepted as standard practice in flux-gradient based techniques.

When measurements are made over rough surfaces where gradients are small or at heights of more than a few metres over any vegetated surface, it is important to allow for the decrease in air temperature with height that arises from adiabatic expansion and subsequent cooling when a parcel rises (Brutsaert 1982). That is, the dry adiabatic lapse rate

$$\Gamma = -(\partial T/\partial z) = -g/c_p \approx -1°\mathrm{C}/100\ \mathrm{m}.$$

All air temperatures in vertically-oriented gradient measurements should be replaced by potential temperature $\theta = T - \Gamma$, and temperature gradients dT/dz by $d\theta/dz = (dT/dz) - \Gamma$. The correction is unnecessary only in a neutral atmosphere (in which case θ is constant with height), however, with measurements taken over the order of 1 m the amount is insignificant and may be ignored (Brutsaert 1982).

1 The shortened energy balance equation neglects advection, physically and biochemically (photosynthetically) stored heat in the canopy as they are considered negligible (Thom 1975) (Section 2.3)

2.7.3 The assumption of Similarity

Under conditions of neutral atmospheric stability, it has commonly been assumed that the exchange coefficients for momentum, sensible heat and water vapour are the same (Rider and Robinson 1951, Rider 1954, Tanner 1963, Dyer 1967 and Swinbank and Dyer 1967). The justification for this assumption is that all the processes involved occur across and through the same interface and have to do with the same set of vapours in the same atmospheric layer presumably moving in the same direction. This is not always the case. Under unstable conditions K_h exceeds K_w because there is preferential upward transport of heat (Monteith 1963). Measurements (reviewed by Dyer 1974) supported the view that $K_h = K_w = K_q$ in unstable conditions. Dyer (1974) inferred that $K_m = K_h = K_w$, but that there were few measurements to confirm his assumption.

At high levels of evaporative flux, values of β are small, and an assumption of equality of K_h and K_w when the two are not markedly different will not lead to serious error in the estimate of $L_v F_w$. When the surface is dry and $L_v F_w$ small, β values are large and a given departure of K_h/K_w from unity can lead to almost as large errors in the estimate of $L_v F_w$ (Denmead and McIlroy 1970). Pasquill (1949) showed theoretically that under stable conditions $K_h = K_w$, while under unstable conditions $K_h \geq K_w$, with $K_h = 2K_w$ at $Ri = 0.1$. The Richardson number (Ri):

$$Ri = (g/\overline{T})\,(\partial\theta/\partial z)/(\partial u/\partial z)^2,$$

where g is the acceleration due to gravity (m s^{-2}), $\overline{T}$ is the average air temperature between the two levels (K), and θ the potential temperature (K), the others as previously defined, is one measure of atmospheric stability. The Richardson number is however, influenced by height and thus other indices such as the Monin-Obukhov length and related parameters are preferable. Rider and Robinson (1951) also accepted $K_h = K_w$ but added that this stood irrespective of height, while Rider (1954) accepted the same irrespective of conditions. He calculated the ratio of K_h/K_w with 51 profile measurements to be 1.14 ± 0.06. Thus when the assumption of Similarity is applied it evidently results in the underestimation of the Bowen ratio resulting in overestimated sensible and underestimated latent heat flux density components (Motha *et al.* 1979b). Rider (1954) further noted that corrections to this equality are required for unstable atmospheric conditions.

Tanner (1963) found from his literature review that K_h/K_w was believed to be less than unity for inversion conditions and greater than unity for the lapse case. He further found that most workers (at that time) believed the error in assuming $K_h = K_w$ (= K_m) is negligible if $-0.03 < Ri < 0.03$, where K_m is the transfer coefficient for momentum. Tanner concurred with this by stating that K_h/K_w is most likely to approach unity when winds are strong and friction contributes much more to the turbulence than buoyancy (that is the Richardson number is therefore small). The error is further reduced by measuring close to the surface where frictional effects are most pronounced. Pruitt and Aston (1963) agreed that $K_h = K_w$ under unstable conditions, but proposed that the ratio K_h/K_w lay between 1.2 and 1.3 for $Ri = 0$ and between 2 and 3 in very stable conditions.

Dyer (1967) and Swinbank and Dyer (1967) concluded that the transfer mechanisms for heat and water vapour transfer were identical, and therefore that $K_h = K_w$ under lapse conditions. Webb (1970) and Oke (1970) showed that under nocturnal inversion conditions, because air temperature and water vapour pressure fluctuations were highly correlated in stable conditions, $K_h = K_w$, although Swinbank and Dyer (1967) observed the same under unstable conditions. Webb (1970) also defined the critical Ri value at which the change from neutral to stable conditions occurs as $Ri = 0.2$. These conclusions were all reached without consideration of sensible heat advection and were drawn, presumably, not under potential evaporation, or at least relatively high and unrestricted evaporative conditions. Potential evaporation is defined as the evaporation that would occur from a continuously moist surface with regional characteristics but with an area so small that the fluxes of heat and water vapour have no significant effect on the evaporability of the over passing air (Morton 1971). The evaluation of atmospheric exchange coefficients should be made under conditions that do not confound the measurements. A limited supply of water will decrease the absolute flux density of the entity under consideration, yet its K value will not have changed. This is because the exchange coefficients (or eddy diffusivities), are only dependent on the aerodynamic resistance, eddy size and turbulence or flow properties. Further, they show no apparent dependence on molecular properties such as the mass density and temperature, as predicted in simple molecular diffusivity theory (Arya 1988). Another limitation of present eddy diffusivity theory is that down-gradient transport is absent in for example, a convective mixed layer where the potential temperature gradient becomes zero. This would imply infinite or even zero values of K_h indicating that K theory becomes invalid in this case. Thus the development of a molecular basis can go no further, and an alternative approach needs to be applied. Denmead and McIlroy (1970) found that $K_h = K_w$ in the range $-0.026 \leq Ri \leq 0.001$ in unstable conditions, close to the ground for wheat under non-potential evaporation conditions. They further found no significant variation in the ratio K_h/K_w under differing stabilities. Campbell (1973) concluded that $K_h = K_w = 1$ for the stable range which he defined as $0 < Ri < 0.5$. In the strongly stable case, ($Ri \approx 0.5$), $K_h > K_w$ and applying the assumption $K_h = K_w$ will lead to an error of some 10 % in β and at least as much in $L_v F_w$. For the stable range ($-2.5 < Ri < 0.05$), Campbell (1973) found that the ratio is close enough to unity to cause errors of less than 10 % in $L_v F_w$. He concluded by urging the development of a non-empirical stability-dependent correction factor to account for the assumption's inaccuracies when used on the Bowen ratio energy balance method under dry conditions.

Over forest canopies the roughness lengths are large, and workers have reported that the dimensionless functions, especially those for heat and momentum, are different from those obtained over surfaces of low roughness, (*eg.* Thom 1975, Denmead and Bradley 1985). The lack of Similarity has been found by Grip *et al.* (1979), amongst others, to be the cause of poor results using the BREB method above forests. Not observing an adequate height to fetch ratio is more likely to have been the problem, since the fetch requirement is much greater with the high measuring positions above tall forests.

Munro (1985) found that over forests K_h differs from K_w in a manner consistent with the radiatively controlled variation in zero-plane displacement d (or source) of sensible heat. They proposed a modification of the influence functions ($\Phi_{h,w}$) to include surface effects, as well as stability effects, thereby correcting for different surface influences, zero-plane displacements and combinations of the two. The results showed that although some radiatively-induced changes in the source of sensible heat were possible, this was no reason to abandon or modify the BREB technique over forests as traditionally employed. **Table 2.2** summarizes the Similarity Principle controversy historically.

2.8 The assumption of *Similarity* as affected by advection

Due to the inadequate performance of the Bowen ratio method in semi-arid conditions, Blad and Rosenberg (1974) questioned the use of the assumption of Similarity under advective conditions. They concluded that the principal reason for the underestimation of $L_v F_w$ under advective conditions is the erroneous assumption of Similarity. They proposed that increasing the value of K_h/K_w to between 1.2

Table 2.2 History of the limits of the Similarity Principle according to stability conditions and the Richardson number Ri

Authors/s	Conditions for which: $K_h = K_w$	$K_h > K_w$	Comments and conditions
Pasquill (1949)	Stable	Unstable	$\|K_h\| = 2\,\|K_w\|$; $Ri = 0.1$
Rider and Robinson (1951)	Stable	Unstable	Irrespective of height
Rider (1954)	Stable	Unstable	$K_h/K_w = 1.14 \pm 0.06$
Tanner (1963)	Strong wind		
Pruitt and Aston (1963)	Unstable	$K_h/K_w = 1.25$; $Ri = 0$ and very stable	
Dyer (1967)	Lapse conditions		
Dyer and Swinbank (1967)	Lapse and unstable conditions		
Webb (1970)	Nocturnal inversion conditions		Neutral to stable change at $Ri = 0.2$
Oke (1970)	Nocturnal inversion conditions		
Denmead and McIlroy (1970)	$-0.026 \le Ri \le 0.001$ (unstable)	Found no variation under differing stabilities	Close to ground and non-potential evaporation conditions
Campbell (1973)	All except stable range	$0 \le Ri \le 0.5$ (stable range)	

and 1.5 would be enough to correct for periods of moderately intense temperature inversions, but noted that additional studies under very stable daytime sensible heat advection conditions were required.

Based on his theoretical analysis, Warhaft (1976), indicated that K_h/K_w may depart from unity when the gradients of air temperature and water vapour pressure are opposite in direction, or when $r_{T'q'}$ (the cross correlation coefficient of the temperature and humidity fluctuation), is small. Some experimental data gave qualitative support to this, but he noted that further measurements under varying conditions of stability were required.

Under advective conditions the sensible heat is directed towards the crop or surface, as defined by the temperature difference between canopy and overlying air. The crop then attempts to compensate by increasing the evaporative flux to repartition the heat load from sensible to latent. It is possible that the increased load of advected heat to the plant may inhibit normal, pre-loaded, evaporative cooling as a stress-delaying mechanism. This may be in addition to the fact that the plant may already have been at peak vapour flux, either determined physiologically or, (not considered in the above cases), due to soil water restrictions, and thus incapable of an increase. The latent heat flux density may then appear to remain the same and the sensible heat flux density to be increasing, when in fact the latent flux density decreases marginally. This is to be expected as energy balance must be satisfied in the short term. The exchange of sensible heat will then appear to be more efficient due to the increase in magnitude and not due to a larger sensible heat exchange coefficient. From the absolute magnitude of the flux density components and their directions, Motha *et al.* (1979b), showed that the latent flux density actually does decrease as the positive sensible flux density (to the surface) begins to increase (Fig. 2.1).

Differences in flux densities do not necessarily imply changes in their respective exchange coefficients. Since the exchange coefficients are essentially determined by the stability state of the atmosphere, implying that they are dependent on the wind and turbulence regimes, estimations of K_h/K_w should only be done under potential evaporation conditions. This will exclude any plant resistance or other evaporative inhibitions from the measurements. It will also maximize the flux density and ease the task of taking the fine measurements required to measure exchange coefficients. Whether these potential flux densities are maintained under conditions of strong sensible heat advection for long enough to complete measurements is questionable. It is therefore important to state their objectives clearly and under what conditions their conclusions apply. Both Verma *et al.* (1978) and Motha *et al.* (1979b) showed that K_h over alfalfa under conditions of sensible heat advection was generally greater than K_w. Verma *et al.* (1978) were the first to publish coefficients for the regression of the ratio K_h/K_w on various parameters. They found a strong correlation with $\Delta T/\Delta e$ which is negative under advective conditions, as the downwards sensible heat is opposite in direction to the latent heat under these conditions. Regression on $L_v F_{w\,LYS}/(I_{net} - F_s)$ yielded no distinct relationship although some correlation was reported. The lysimetrically determined latent heat flux density $L_v F_{w\,LYS}$ becomes smaller under advective conditions.

Brakke *et al.* (1978) used the empirical correction derived by Verma *et al.* (1978) to calculate a modified Bowen ratio (see below), and corrected flux density, $L_v F_{w\,MREB}$ (the modified Bowen ratio energy balance estimate of latent heat flux density), to closely estimate $L_v F_{w\,LYS}$ along the 1:1 line, except for occasions of very high latent heat flux density (Fig 2.2). These high flux density periods

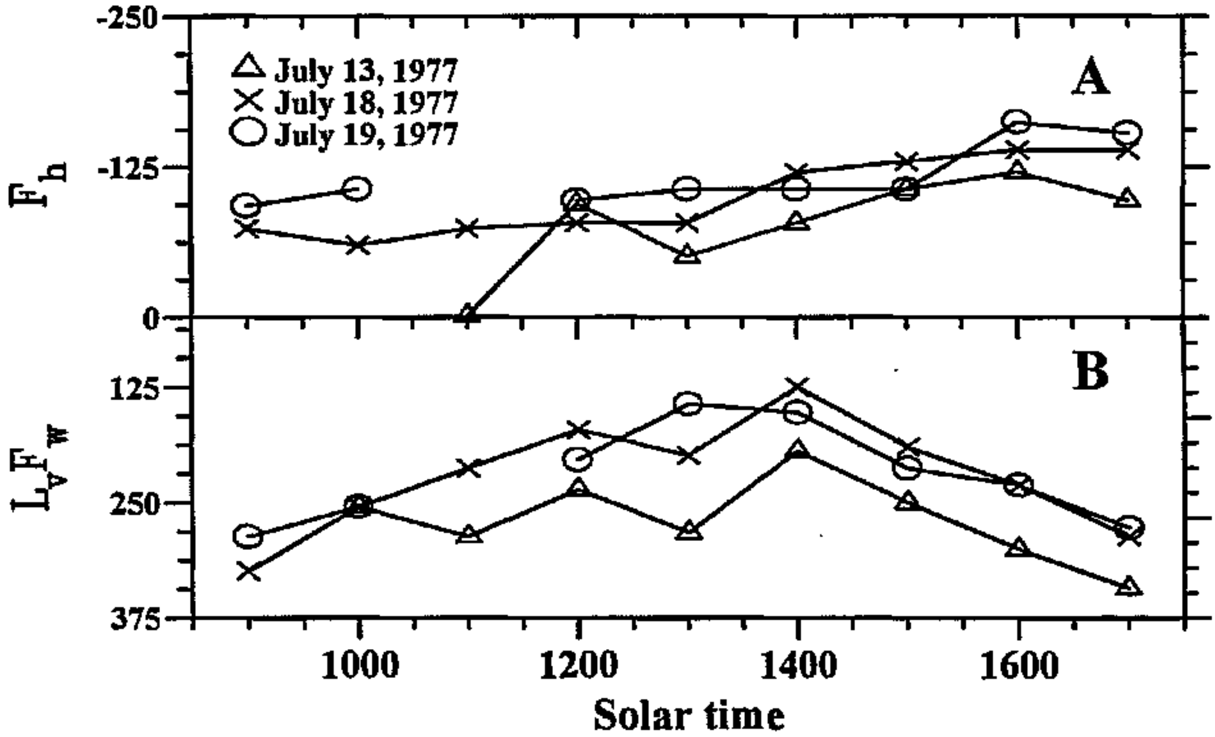

Fig 2.1 Daily patterns of sensible heat flux, (A), and water vapour flux, (B), over a well-watered alfalfa crop as a function of time of day for July 13, 18 and 19, 1977 (after Motha *et al.* 1979b)

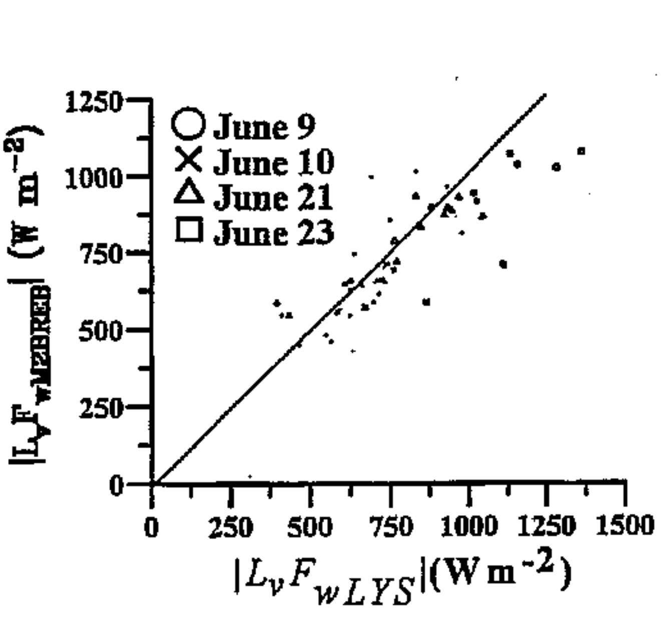

Fig. 2.2 The absolute value of $L_v F_w$ estimated by the M2BREB ("modified modified" Bowen ratio energy balance) method compared with $|L_v F_w|$ measured lysimetrically (after Brakke *et al.* 1978)

ostensibly occur most commonly under strongly advective conditions for which the adjustment does not cater. A more detailed and quantitative measure of atmospheric conditions is therefore required.

For -0.8 °C kPa^{-1} $\leq (\Delta T/\Delta e) \leq -0.1$ °C kPa^{-1}, a quadratic equation in $\Delta T/\Delta e$ was used to calculate K_h/K_w:

$$K_h/K_w = 2.95 + 3.72\,(\Delta T/\Delta e) + 1.72\,(\Delta T/\Delta e)^2$$

and thus the modified Bowen ratio formula is:

$$\beta(MBREB) = \gamma\,[2.95 + 3.72\,(\Delta T/\Delta e) + 1.72\,(\Delta T/\Delta e)^2]\,(\Delta T/\Delta e)$$

and is used to calculate the "modified modified" $L_v F_w(M2BREB)$ amount.

Eddy correlation techniques involving latent heat and sensible heat flux densities measurements provide an alternate method for the determination of the coefficients which Motha *et al.* (1979b) used under conditions of strong regional advection. Their results were in agreement with the results obtained above using the Bowen ratio energy balance method, but corrections were not reported. The diurnal variation in the ratio K_h/K_w from three day's measurement showed an increase in sensible heat flux density. The intensity of sensible heat flux density advected was gauged by the magnitude and direction of the heat flux density. In the afternoon, (although with a concurrent decrease in net irradiance), there was an increase in the K_h/K_w ratio, up to approximately 3. This implies that K_h increases with respect to K_w under such advective conditions and that either the transport of sensible heat flux density is enhanced, the transport of latent heat is inhibited, or a combination of the two occurs. Motha *et al.* (1979b) also examined the components of K_h and K_w and concluded that the sensible components increased with respect to latent components, indicating that sensible heat flux density transfer is more efficient than latent heat transfer, as indicated by the ratio of the correlation coefficients (r_{wT}/r_{we}), and the ratio of the standard deviations (σ_T/σ_e). Again, the magnitude of the latent flux may have been inhibited here, and conclusions about the size of exchange coefficients should not be drawn except under potential evaporation conditions.

2.9 Measurement of the exchange coefficients

The measurement of K_h and K_w is accomplished either by direct comparison with lysimetric measurements, or indirectly, with eddy correlation measurements.

2.9.1 Lysimetric comparisons

The most direct method of testing the validity of the assumption of Similarity (and of checking any system that measures latent heat flux density), is by direct comparison with a lysimeter. Denmead ad McIlroy (1970) measured I_{net} and F_s directly, and the latent heat flux density by lysimetry ($L_v F_w(LYS)$), while F_h was calculated as the remainder of the sum in the energy balance equation (from Eq. 2.3). The lysimeter Bowen ratio value β_{LYS} was then calculated from these results and compared with β_{BR} values from gradient measurements done in the normal way. The points conformed well to the assumption $K_h = K_w$ (Fig. 2.3), in spite of some apparently random scatter. A wide range of stabilities was considered with no significant variation in β_{LYS}/β_{BR} and no dependence on the stability conditions. With no outside interference such as advective inputs or other dissimilarities between he two systems, a 1:1 ratio between β_{LYS} and β_{BR} was found implying equality between K_h and K_w.

Pasquill (1949) using a similar procedure, found that$K_h \approx K_w$, but this may well have been due to the size and nature of his mini-lysimeters (Denmead and McIlroy 1970), but also most probably due to sensible heat advective conditions as these results suggest.

Verma *et al.* (1978) evaluated the exchange coefficients under advective conditions taking

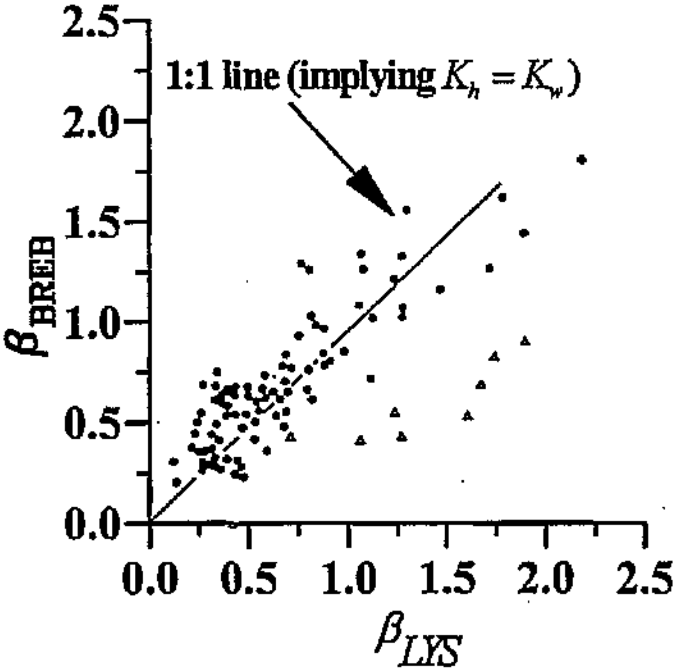

Fig. 2.3 Comparison of β_{BR} and β_{LYS} Dots are for data obtained by Denmead and McIlroy's. Triangles represent data from Pasquill (1949) (after Denmead and McIlroy 1970)

advection flux density A into account in the fuller energy budget equation:

$$I_{net} = L_v F_w + F_h + F_s + A_w + A_h. \qquad 2.26$$

where $A = A_w + A_h$ is the sum of advection latent and sensible heat flux density. Hence K_h and K_w may be computed from Eqs 2.22 and 2.23 using $L_v F_{w\,LYS}$ as the actual $L_v F_w$ value, thereby obtaining a correction factor for advection in the form of the K_h/K_w ratio.

2.9.2 Eddy correlation measurements

The K_h and K_w ratios were computed by Motha *et al.* (1979b) by substituting the turbulent flux densities of sensible heat and latent heat determined using the eddy correlation technique:

$$F_h = \rho\, c_p \overline{w'T'} \qquad 2.27$$

$$\text{and } L_v F_w = L_v \overline{w'q'} \qquad 2.28$$

and gradients of air temperature and vapour pressure (as represented by Bowen ratio-measured finite differences) in Eqs 2.16 and 2.17. In Eqs 2.27 and 2.28, w', T' and q' are respectively the fluctuation in vertical wind speed, air temperature and absolute humidity. The term $w'T'$, for example, is the covariance between w' and T'. The conclusions that Motha *et al.* (1979b) drew agreed qualitatively with those of others that K_h exceeded K_w under strongly advective conditions but they gave no quantitative adjustment.

The advantage of the eddy correlation technique is that it is, theoretically, an absolute technique and therefore the other components of the energy balance need not be determined. The eddy correlation is a very useful technique in that it also allows for the measurement of other flux densities such as the flux density of carbon dioxide, ammonia etc. if fast responding sensors for the measurement of the concentration of carbon dioxide, ammonia, etc. are available.

2.10 Limitations of the Bowen ratio system

2.10.1 Theoretical limitations

Due to the formulation of the theory, the calculation of $L_v F_w$ tends to infinity as the Bowen ratio approaches −1. This may be seen by examining the $(1 + \beta)$ denominator, which may not be zero, in Eq. 2.18. A value of $\beta \rightarrow -1$ (and hence $F_h/L_v F_w = -1$ or $F_h = -L_v F_w$ or $F_h + L_v F_w = 0$ (*cf.* Eq. 2.3)) occurs in the early morning and late afternoon periods when the available energy approaches zero due to the decrease in net irradiance I_{net}. Rainfall events during the day have the same effect but at these times the latent heat flux density is low, and so these periods may be, and commonly are, ignored. When β is between −1.25 and −0.75, the heat flux densities are assumed negligible and are therefore neither calculated nor included in daily total calculations (Tanner 1960). Proof of the small flux densities at these times is the small difference between the measured net radiant flux (that is, integrated net irradiance) and the flux totals calculated for any day.

Condensation of dew on sensors, (thermocouples, air intakes and net radiometer), precludes any meaningful measurement of negative or positive flux densities: that is, evaporation and condensation respectively. This is because the air temperature thermocouples will be measuring the wet bulb temperature and the air around both the Bowen ratio equipment air intakes will be approaching saturation water vapour pressure.

2.10.2 Practical limitations

The measured differential in water vapour pressure and air temperature across the vertical distance chosen must, of necessity, be larger than the resolution of the individual sensors for meaningful results. If the difference approaches the resolution, the measured differences tend towards zero and random "experimental error" values occur. Towards the drier periods this implies that the displacement between the measuring arms must be increased to stay above these resolution limits. This measured difference should be used as one of the criteria for rejection of periods of calculations of β, $L_v F_w$ and F_h.

The condensation of dew on to the sensors prevents reasonable measurement often until 10h00 when it has all evaporated, and after dew-fall as early as 16h00. After rain-events similar limitations apply. The loss of data at these low fluxes due to the atmospheric conditions after rain is not as serious as the morning losses of data. This is because the average cloudless morning latent heat flux density should usually far exceed the inter- and post-rain evaporative flux densities, which represent mainly the evaporation of the most recent precipitation. The evaporation of intercepted water is important however, as it reduces soil evaporation.

2.10.3 Boundary layer limitations

The principle of profile-based theories according to Brutsaert (1982), requires a uniform upwind fetch of some 50 to 100 m at the least for measurements to be taken up to 1 m above ground. This implies that to take all wind directions into account, the measurements must be done in the center of an area of uniform cover large enough to allow the development of an internal boundary up to the measurement height. The internal boundary layer is defined by Brutsaert (1982) as the region of the atmosphere affected by a step change in the surface conditions.

During periods of low β values (when the latent heat flux density approaches [radiative] ground heating), fetch requirements decrease from the often quoted overly pessimistic values of 100:1 to as low as 20:1 (Heilman *et al.* 1989). Heilman *et al.* (1989) also concluded that the Bowen ratio and its variability increased with measurement height, and that, for Bermuda grass, significant boundary-layer adjustment occurred within the first 15 m of fetch. **Table 2.3** summarizes the history of the maximum placement height to fetch distance ratio.

The measurement of water vapour pressure and air temperature gradients must be done in the transition zone of the internal boundary layer (**Fig. 2.4**), in order to correctly assess the respective fluxes. The transition zone ends where the effects of the surface are no longer felt. The vertical profiles of water vapour content, wind speed and air temperature approach a new equilibrium with the active surface. Only once the boundary layer stops growing upward has the air layer become representative of the new surface. It is only here that horizontal gradients have disappeared and the flow of air reverts to a non-advective profile (Rosenberg 1974, Oke 1978, Brutsaert 1982). The height of this fairly indistinct level sets the limit to the maximum gradient-sensor height. The extent of the uniform upwind fetch and the type of surface change (rough to smooth *vs* smooth to rough, and moist to dry etc.) will determine the thickness of the internal boundary layer. Measurement of the extent of the boundary layer is difficult as it fluctuates depending on both the atmospheric stability conditions and the stage of crop growth, (*via* the influence of z_o, where $z_o \approx 0.13 \times h$ where h is the canopy height). Perhaps due to this fact, an intermediate layer, the inertial sublayer, has also been defined (Raupach and Legg 1984), and further confounds an absolute definition of the outer limit of the boundary layer (Fig. 2.4).

Table 2.3 Height to fetch ratios used in different aerodynamic measurement experiments

Author/s	Height:fetch	Comments and conditions
Elliot (1958)	Height = 0.75 fetch$^{0.8}$	For fetch greater than 10 m
Priestley (1959)	1/20	Inadequate
Lettau (1959)	1/50	
Brooks (1961)	1/100 (and greater)	Add 8 times obstacle height to fetch
Dyer (1963)	0.5/70 (fetch = 140 m)	These height:fetch
	1/170 (fetch = 170 m)	ratios are
	2/420 (fetch = 210 m)	for a 90 % profile
	5/1350 (fetch = 270 m)	adjustment
	1/330 (fetch = 330 m)	Add 2.5 times obstacle height to fetch for a 95 % adjustment
Panofsky and Townsend (1964)	1/10	
Dyer (1965)	1/200	
Rosenberg *et al.* (1983)	1/100	Adequate for most measurements
Heilman *et al.* (1989)	1/20	Periods with larger β values will require larger fetch

The internal equilibrium sublayer is the lower portion of the boundary layer which has once again come into water vapour pressure, air temperature and momentum equilibrium with the surface (Fig. 2.4), defined by Brutsaert (1982) as the region where the momentum flux density is within 10 % of the value at the surface. The roughness of the surface governs the thickness of the internal equilibrium sublayer and, thus, the lowest height setting of the lower measuring arm for adequate horizontal spatial homogeneity. More accurately, the minimum sensor height is governed by the vertical amplitude of the surface roughness. As a rule of thumb, five times the roughness structure may be used as the lowest measuring height (where horizontal patchiness of air temperature and humidity are smaller than the sample height) (Tanner 1963, Brutsaert 1982). The measurement of the roughness structure or elements is taken from z_o to the top of the average structure extending above z_o (Brutsaert 1982). Garratt's (1978) data indicated a minimum level of three to five times the roughness elements. Consequently, the minimum level should be set conservatively high to decrease the margin for error. This recommendation will however need to be viewed against the available fetch should this be limited. Brutsaert (1982) does caution that for forests 10 m or more tall, the height requirement of Garratt (1978) for Similarity may be prohibitive. Brutsaert (1982) quotes personal communications with C. B. Tanner (1976) that indicate that Bowen ratio measurements taken too close to the top of the canopy may cause serious errors in the application of the method over forests. To avoid the error, Brutsaert (1982) recommended the measurement of air temperature and water vapour pressure at more than two levels to test the Similarity and the constancy of the Bowen ratio with altitude.

Tall row crops will increase the height of both the lower and upper arm settings considerably, and therefore the boundary layer considerations set the limit to the type of vegetation over which the Bowen ratio can successfully be employed.

Due to the attenuating nature of the water vapour pressure and air temperature gradients, the points at which gradient differences are measured must be as close to the ground as possible, with the greatest possible displacement between the two points, the limits being set by the above two constraints.

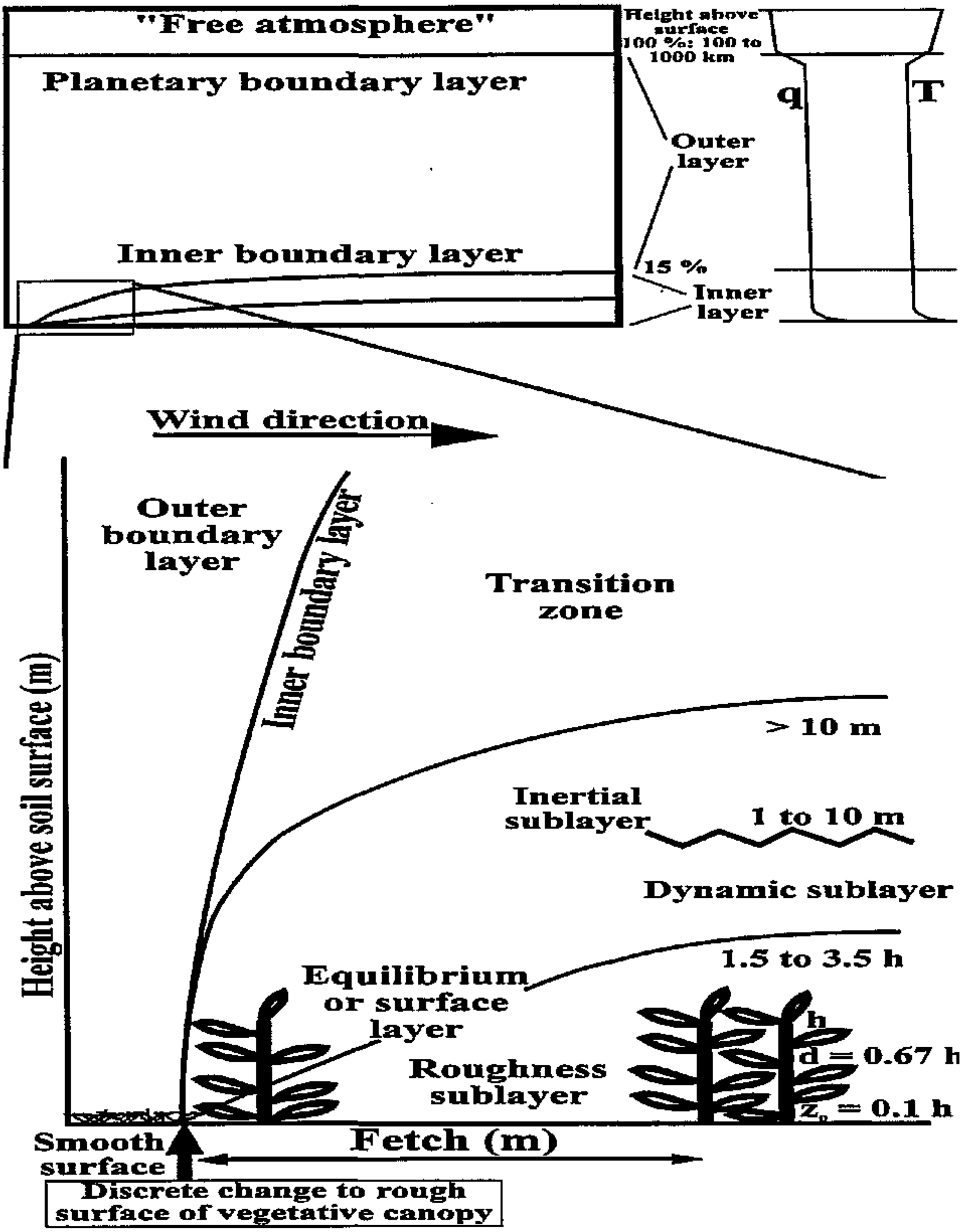

Fig. 2.4 Diagrammatic representation of the two-dimensional internal boundary layer problem (after Rosenberg 1974, Oke 1978, Brutsaert 1982, Raupach and Legg 1984 and Heilman *et al.* 1989). Notation: d is the zero-plane displacement (the mean height of momentum absorption by the rough surface) (Thom 1972), h is the mean canopy height and therefore the roughness-element height, and z_o is the roughness length. Also shown are typical macro-scale profiles of air temperature T and specific humidity q. The inner layer is characterized by strong gradients, the convective mixed layer by the lack thereof, and the top of the PBL by a step

The thickness of the internal boundary layer δ, may be calculated using the Munro and Oke (1975) equation for stable conditions:

$$\delta = x^{0.8} z_o^{0.2} \qquad 2.29$$

where x is the fetch (m) and z_o is the momentum roughness length of the surface (m). Instability will increase boundary layer thickness (Heilman *et al.* 1989).

2.11 A description of atmospheric conditions and the planetary boundary layer

2.11.1 Introduction

In **laminar** boundary layers, the transfer of momentum, mass and sensible heat is determined by the vertical atmospheric concentration gradient profiles, as well as by diffusivities associated with *molecular* agitation. Laminar conditions are, however, almost always displaced by a **turbulent** boundary layer found above vegetated surfaces during the sunlight hours. In turbulent transfer theory, the same transfer principles are thought to apply, but the diffusivities are associated with *turbulent eddies* (which are larger by many orders of magnitude) (*eg.* Arya 1988).

The terminology in the literature pertaining to the various atmospheric layers is extremely ambiguous, and needs some general clarification. The **atmospheric** or **planetary boundary layer** (PBL) is that layer of air in the immediate vicinity of the earth's surface in which significant exchanges of momentum, heat and mass occur (*eg.* Arya 1988). Sharp variations in the properties of flow of variables such as wind velocity, air temperature and mass concentration also occur in the boundary layer. The PBL extends upwards to a fairly sharp boundary between the irregular, turbulent motions within, and the considerably smooth laminar flow of the free atmosphere above the PBL to a height of the order of 10^3 m varying from 100 to 2000 m (Elliot 1958, Brutsaert 1982 (Fig. 2.4), Arya 1988).

Of more interest to micrometeorologists is the **inner** or **internal boundary layer** IBL which is defined by Brutsaert (1982) as the region of the atmosphere affected by a step change in the surface conditions. In other words, it is the height up to which a disturbance (a step change in surface cover) has been propagated (see Fig. 2.4), and is thus the appropriate layer in which to perform micrometeorological measurements. It may extend from 1 m (in extremely stable nocturnal inversion conditions) to 500 m (in convective, unstable conditions).

Most work on boundary layer theory deals with wind speed (or momentum) profiles as these are more easily measured than the entities of heat and water vapour which are then commonly assumed to follow the same rules.

Measurement of the extent of the IBL is difficult as it fluctuates depending on the atmospheric stability conditions, the fetch and the stage of crop growth (*via* the influence of the momentum roughness length of the surface, z_o, where $z_o \approx 0.13\ h$, where h is the canopy height) (Brutsaert 1982). The depth of the turbulent boundary layer, δ, is however mainly related to the extent of the uniform upwind fetch. The thickness of the internal boundary layer δ is dictated by wind speed profiles or momentum transfer considerations, and oftentimes the subscript m notation is used (much as the roughness length z_o should strictly be denoted z_{om}). The depth or extent of the inner layer, then, may be calculated using the Munro and Oke (1975) power equation (Eq. 2.29) for stable conditions.

This equation was developed for neutral stability, but its use under unstable conditions would be expected to *increase* boundary layer thickness (Munro and Oke 1975, Heilman *et al.* 1989). The momentum roughness length may be obtained from wind speed profiles, or from the approximation $z_o \approx 0.13\,h$ (Tanner and Pelton 1960) (**Table 2.4**).

Using these values in Eq. 2.28, with a range of fetches, we note that the boundary layer thickness is most dependent on the fetch and only slightly dependent on the roughness of the cover, as is evident from **Table 2.5**. The IBL makes up about 15 % of the total atmospheric boundary layer ABL, but of this 15 %, most is made up of a **transition zone**[2]. This layer is in the process of reaching complete equilibrium with the characteristics of the new surface over which it is now flowing.

Air flowing from smooth-to-rough surfaces must decelerate from the ground upwards due to the increased shear stress caused by the greater surface roughness (as indicated by the roughness length z_o), and the wind speed profile therefore deviates from the logarithmic wind speed profile.

The lowest portion of the transition zone which has become fully adjusted is termed the **equilibrium sublayer** (δ'), which implies that the wind speed profile is now fully logarithmic (Munro and Oke 1975). This layer which has come into water vapour, air temperature and momentum equilibrium with the new surface over which it is flowing (Fig. 2.4) has been defined by Brutsaert (1982) as the fully turbulent region where the turbulent fluxes do not change appreciably from their value at the surface, *i.e.* the momentum flux density is within 10 % of the value at the surface.

The extent of this equilibrium sublayer has been found to be approximately 10 and 5 % for air

Table 2.4 Typical values of roughness length z_o for canopy heights h between 8 and 1540 mm calculated using $z_o \approx 0.13\,h$

Canopy height h	(mm)	8	20	50	100	200	500	770	1540
Roughness length z_o	(mm)	1.0	2.6	6.5	13	26	65	100	200

Table 2.5 The extent of the IBL (δ), in the body of the table, as a function of fetch (x) and surface roughness z_o calculated using Eq. 2.29

	Roughness length z_o (mm)							
Fetch x (m)	1.0	2.6	6.5	13	26	65	100	200
5	0.9	1.1	1.3	1.5	1.7	2.1	2.3	2.6
15	2.2	2.7	3.2	3.7	4.2	5.1	5.5	6.3
30	3.8	4.6	5.5	6.4	7.3	8.8	9.6	11.0
70	7.5	9.1	10.9	12.6	14.4	17.3	18.9	21.7
300	24.1	29.2	35.0	40.2	46.2	55.5	60.5	69.5
5000	228.7	276.8	332.5	381.9	438.7	526.9	574.3	659.8

2 In the transition zone the shear stress is expected to vary with height, which is in contrast to early theories which assumed equilibrium in the transition zone, thereby leading to the misnomer for this layer - the equilibrium sublayer

flowing from relatively smooth-to-rough and rough-to-smooth transitions respectively (Brutsaert 1982), and is thus estimated from:

$$\delta' = 0.1 \cdot x^{0.8} z_o^{\ 0.2}. \qquad 2.30$$

The major portion of the equilibrium layer is the upmost **inertial sublayer** where an assumption of constant stress is not too far from the truth, for the first few tens of meters (Brutsaert 1982). Flux-gradient type (K-theory) models that are based on assumptions of constant shear and require measurements to be made within this layer. Brutsaert (1982) pointed out that constant shear and stress imply that the wind speed profile has adjusted to be fully logarithmic, and the flux densities are therefore nearly constant with height. However, it has been found possible to successfully formulate Similarity hypotheses without this constant stress assumption (Brutsaert 1982), thereby strengthening the argument in favour of the assumption of Similarity used in the BREB method.

In the lower portion of the inertial sublayer under non-neutral conditions, is found the **dynamic sublayer** in which water vapour and sensible heat may be considered passive admixtures, and so do not affect (and are not affected by) the flow of air and momentum. Under neutral conditions, the whole equilibrium sublayer takes on these characteristics. It follows that for other than neutral conditions, in the majority of the equilibrium layer, the movement of water vapour and sensible heat are actively strengthened or suppressed depending on the atmospheric conditions. Instability leads to eddies which are larger in their vertical than their horizontal dimension. This aids buoyancy, compared to stable conditions where vertical movements are damped by the opposite set of circumstances (*eg*. Thom 1972).

In the upper portion of the inertial sublayer, the surface-defined scales of surface roughness element height h, breadth l, and separation D, are not dynamically significant, and so the friction velocity u_* (which scales the constant momentum flux density), and the element height itself are the only factors which control the flow (*eg*. Thom 1972).

Very close to the roughness elements of the surface, the turbulence structure is influenced by the wakes generated by the elements, establishing a **roughness sublayer** (Raupach and Legg 1984) as illustrated diagrammatically in Fig. 2.4. This roughness sublayer is influenced by factors such as the distribution and structure of foliage elements and the spacing between plants (thus no simple expression for an exchange coefficient for any entity K_q is possible without including h, l and D).

It is well known (Corsin 1974) that gradient-diffusion models such as are applied in the BREB method can only be justified when the length scale of the turbulence is much smaller than the length scale over which mean gradients must change appreciably. In inhomogeneous turbulence such as is found in this layer, these two length scales are of the same order (Tennekes and Lumley 1972), so measurements should not be taken within this layer. In the literature, the roughness sublayer has also been termed the canopy, interfacial, viscous or internal equilibrium sublayer. The roughness sublayer is the lower portion of the boundary layer where the viscosity and the molecular nature of K_h and K_w must be taken into account. Over a rough surface it extends to a height of approximately 1.5 to 3.5 h (Brutsaert 1982).

The description of the boundary layer affected by the surface conditions may best be illustrated by schematic representations of the profiles of wind speed, air temperature and water vapour pressure. The wind speed profile before and after a rough-to-smooth change in surface roughness caused by taller

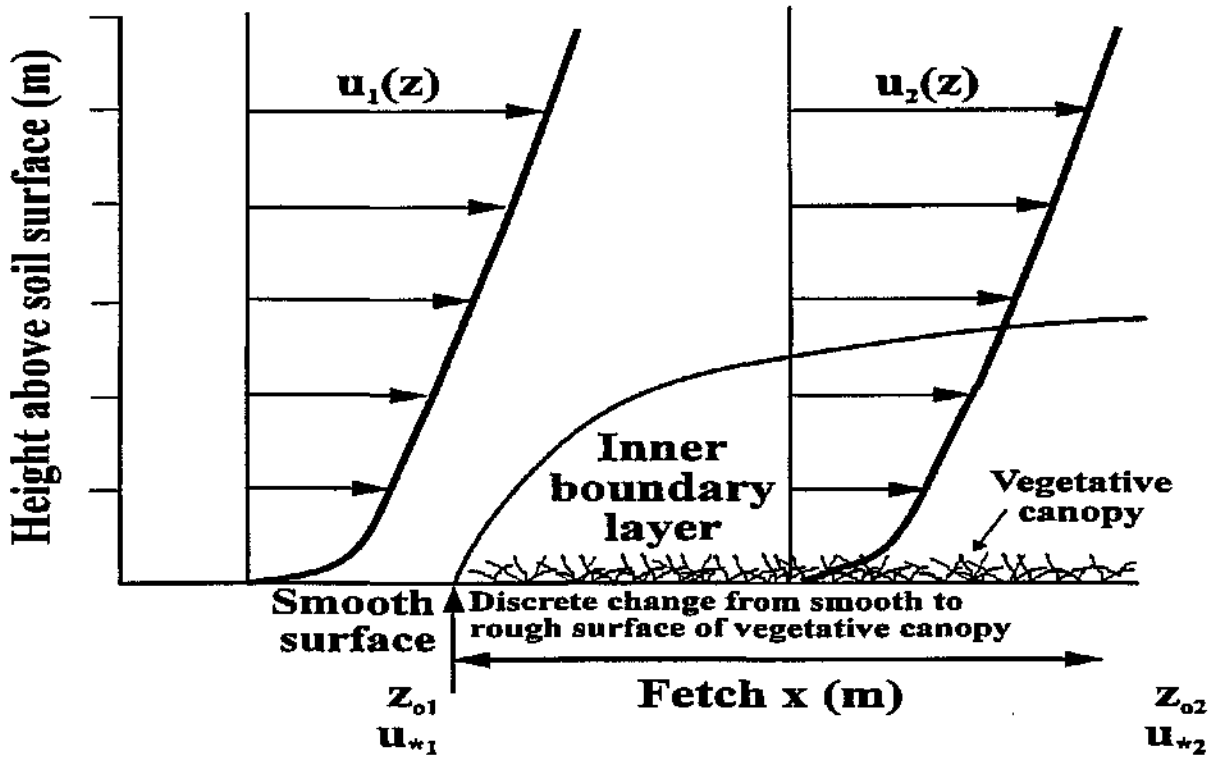

Fig. 2.5 Schematic showing the development of the inner boundary layer and the associated modification of the wind speed profile after a step change in surface roughness. The wind speed is a function of height as well as of the friction velocity, u_{*1} and u_{*2}, and of the surface roughness z_{01} and z_{02} which change with the variations in surface roughness (after Arya 1988)

vegetation is shown (Fig. 2.5). The wind speed over the smooth surface (u_1) is a function of the roughness height z_{01} and friction velocity u_{*1} that describe that surface (as well as height above ground). The modified flow (u_2) is a function of the modified parameters z_{02} and u_{*2} (as well as height above ground).

The profiles of air temperature (T) and water vapour pressure (e) as a function of fetch over a dry to wet change in surface cover, as well as of height are shown (Fig. 2.6). The profiles at positions 2 and 3 show the inadequacy of measurement of profiles with insufficient time to adjust to the new conditions. Only at the greatest fetch distance (extreme right of Fig. 2.6) would gradient measurements have become representative of the profile.

2.11.2 Boundary layer limitations on the placement of sensors

Campbell (1973) pointed out that Bowen's ratio was that of the ratio of *turbulent* sensible and latent heat fluxes and the measurements must therefore be carried out only in the turbulent region of the PBL. Campbell (1973) further noted that the atmosphere is laminar close to the surface for varying thicknesses, and this may differentially affect the transfer of heat or water vapour. Thus, if the laminar layer is thin, little difference will be evident, but under windless free-convection conditions, the growth of this layer may selectively hinder transport.

Since the roughness characteristic of the surface governs the thickness of the internal equilibrium sublayer, it establishes the lowest height setting of the lowest measuring sensor used in aerodynamically based studies to obtain adequate horizontal spatial homogeneity. The minimum sensor height is governed by the vertical amplitude of surface roughness, with the implication that the rougher

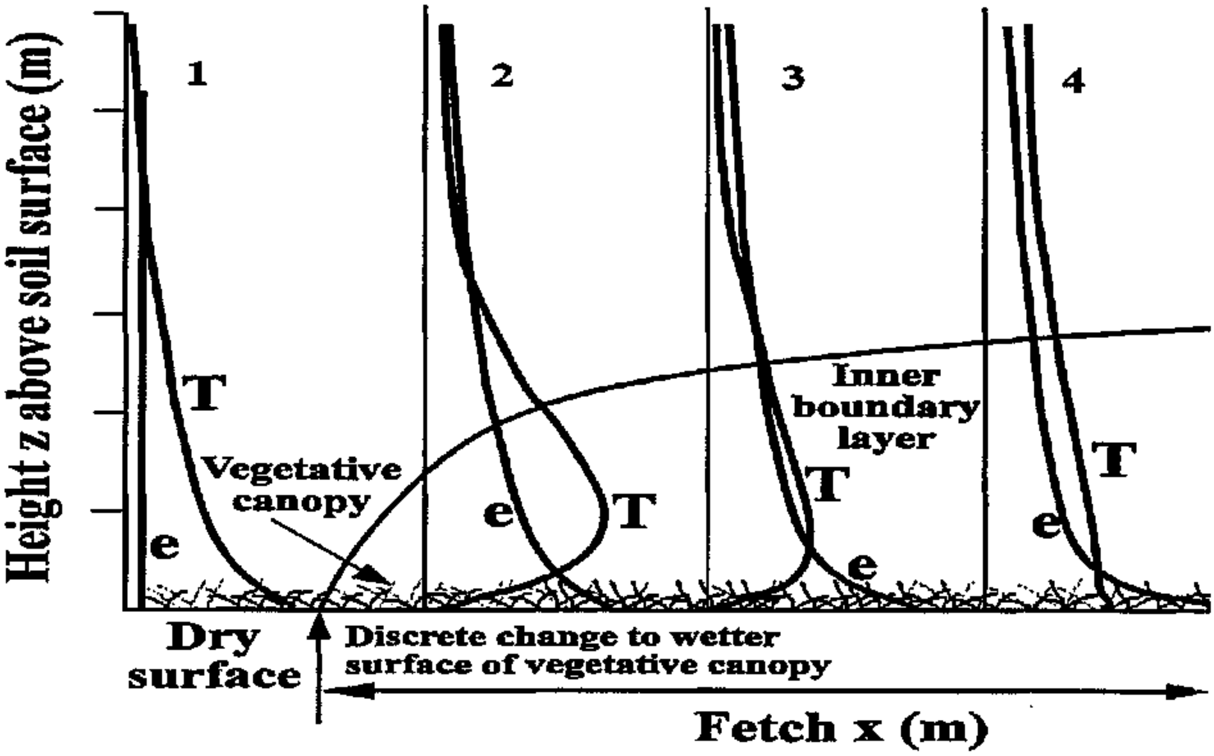

Fig. 2.6 Schematic showing the adjustment of atmospheric water vapour pressure (*e*) and air temperature (*T*) profiles as air passes over a discrete change in surface conditions. The vertical scale is greatly expanded compared to the horizontal (after Webb 1965)

the surface the further removed from the surface the sensors must be. As mentioned previously, as a rule of thumb, five times the roughness structure[3] may be used as the lowest measuring height (where horizontal patchiness of air temperature and water vapour pressure measurements are smaller than the sample height) (Tanner 1963, Brutsaert 1982). Garratt's (1978) data indicated a minimum level of three to five times the roughness element height. Consequently the minimum level should be set conservatively *high* to decrease the risk of error. Under limited fetch conditions, most workers have however used a minimum level that is much lower than that suggested by Garrat (1978).

The principle of profile-based theories, according to Brutsaert (1982), requires a uniform upwind fetch of some 50 to 100 m at the least for measurements to be taken up to 1 m above ground. This implies that to take all wind directions into account, the measurements must be done in the center of an area of uniform cover large enough to allow the development of an internal boundary up to the measurement height (Fig. 1.1). Furthermore, it is required that wind over the fetch has come into equilibrium with the evaporating surface and is thus representative of the energy flux density conditions at the point of measurement. A further prerequisite is that the sensors are placed within that boundary layer, and in the "safe" region of the atmosphere as indicated in Fig. 2.7. Thus, it would seem that although it is desirable to measure exclusively within the equilibrium sublayer, conditions within the *entire* internal boundary layer are suitable for flux-gradient measurements.

3 The measurement of the roughness structure or elements is taken from z_0 to the top of the average structure extending above z_0 (Brutsaert 1982)

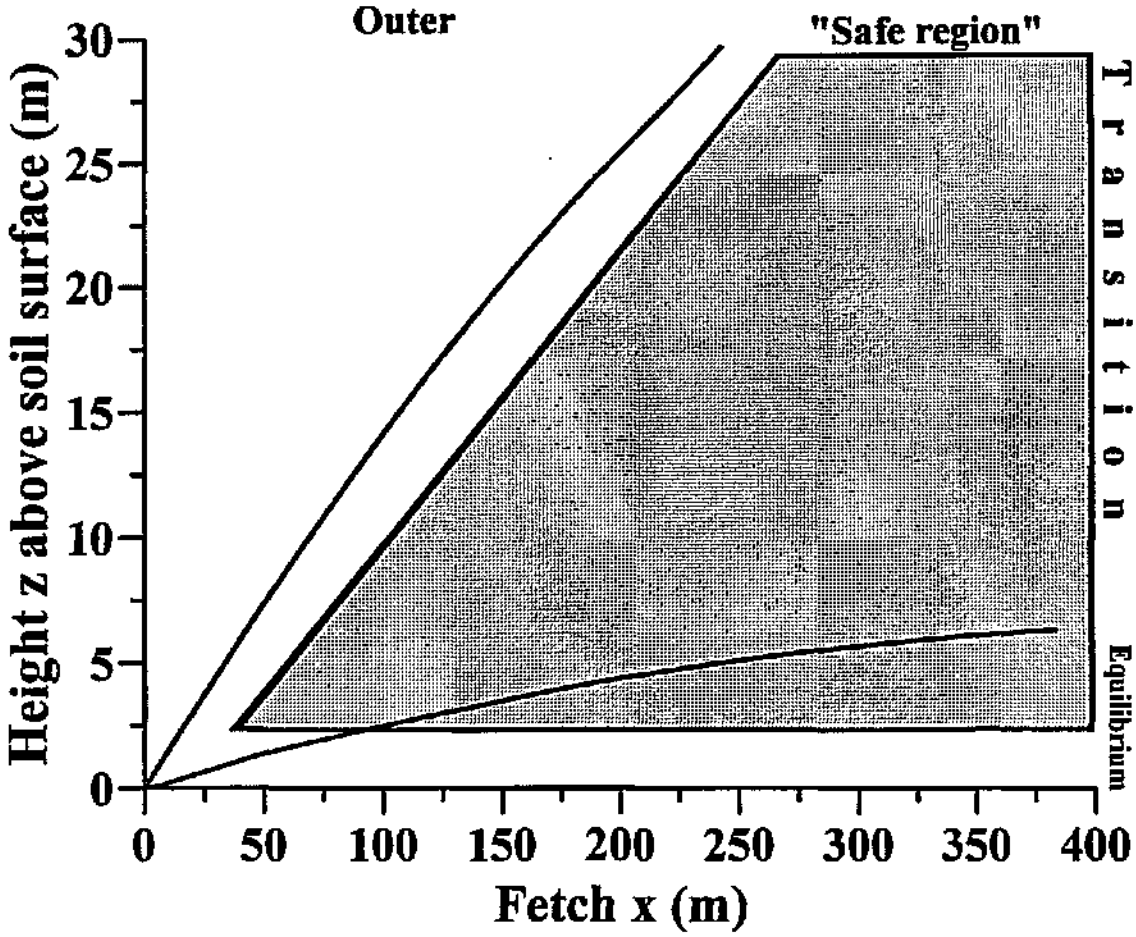

Fig. 2.7 Diagrammatic representation of the "safe region" for flux-gradient measurements

During periods of low β values (when the evaporative energy flux approaches [radiative] ground heating – which implies no advection), fetch requirements decrease from the often-quoted overly-pessimistic values of 100:1 to as low as 20:1 (Heilman *et al.* 1989). They also concluded that for Bermuda grass, significant boundary-layer adjustment occurred within the first 15 m of fetch. Table 2.3 summarizes the history of the maximum height:fetch ratio, which shows the trend towards shorter fetch requirements for a given height.

Heilman *et al.* (1989) published an extremely useful paper on the effect of height placement of sensors and fetch requirements on Bowen ratio measurements. Their calculations indicated that the Bowen ratio method may be less sensitive to imperfect fetch than other techniques when the Bowen ratio is small, and confirmed the conclusions drawn by Yeh and Brutsaert (1971). Selirio (1975) had verified this by finding no significant difference in Bowen ratio values measured at different levels above a corn-field (as long as these measurements were within the equilibrium sublayer[4]). Heilman *et al.* (1989) however also found that the Bowen ratio and its variability increased with measurement height, but the measurement heights were starting to extend above the internal layer (no pair of sensors were placed entirely within the equilibrium sublayer, yet adequate results were obtained (**Fig. 2.8**)).

4 Whether their "equilibrium layer" refers to the internal layer or not is unclear

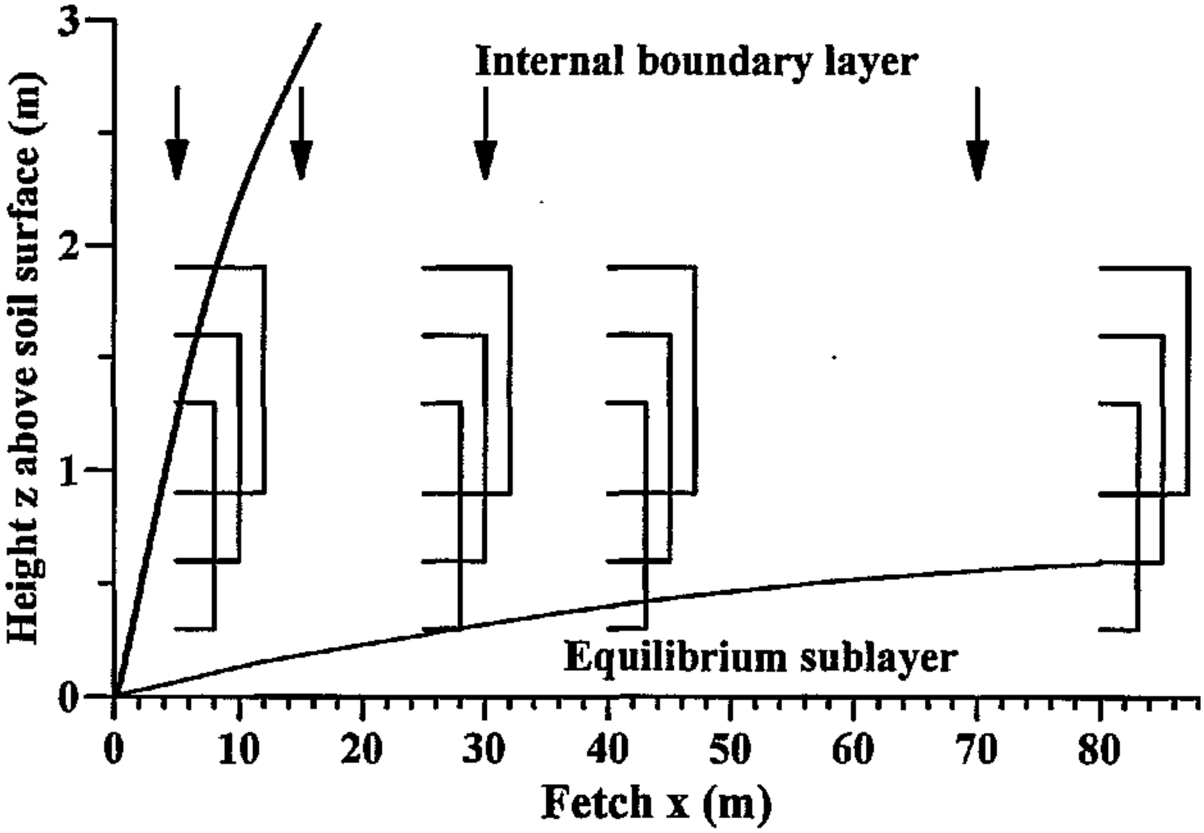

Fig. 2.8 Diagrammatic representation of the three height positions of the psychrometer sensor pairs on three different dates relative to the equilibrium and internal layers (after Heilman *et al.* 1989). The arrows represent the four fetch distances 5, 15, 30 and 70 m

2.11.3 Conclusion

A conflict exists between measuring flux-profile variables too close to the surface and too far from the surface. Unfortunately, no visible phenomenon exists to give a clue as to what level is too low or too high, and even if one did exist, it would vary continuously according to atmospheric conditions. The measurements required to ascertain these heights will require equipment often of greater complexity than that of the experimental equipment. When flux-profile equipment is set up, then, these height considerations are often not given the attention they deserve, and intuitive guesses at the levels have to be made.

In summary, sensors for flux-profile measurements cannot be set too low for fear of introducing "local-effects" thereby not satisfying the assumption of homogeneity of cover. At the same time, the sensors cannot be too far removed from the surface or else they will be out of the region affected by the surface conditions. These points are, in fact, the satisfaction of the fetch requirement expressed in another way.

The problem therefore remains, that due to the attenuating nature of the water vapour pressure and air temperature gradients, the points at which gradient differences are measured must be as close to the ground as possible. In order to measure the very slightest gradient, and to increase precision, the greatest possible displacement between the two points is required. The topmost sensors must therefore be as high as is practical, the limits for these requirements being set by the above two constraints.

Sharma (1987) pointed out that measurement heights close to ground are desirable since this minimizes both advection, and the effect of buoyancy on the exchange coefficients (Eqs 2.6 to 2.9).

Taller vegetation, especially forests, above which gradients are smaller, will therefore substantially increase the height requirements of the measuring sensors. These requirements may thus limit the successful use of the method to shorter crops, or, to taller vegetation with very large areas of common cover and thus extensive fetch.

2.12 Measurement and error considerations

We have used both Bowen ratio and eddy correlation measurement techniques above a variety of vegetated surfaces: grassland, vineyard and bare soil surfaces. These measurements are reported in Chapters 3 to 9.

2.12.1 Introduction

It is possible under conditions of only large scale advection to successfully measure evaporation with a Bowen ratio energy budget system (Fritschen 1965). Areas with different cover and wetness régimes upwind will introduce local advection effects not accounted for in the conventional Bowen ratio method. Hanks *et al.* (1971) noted underestimation errors as large as 45 % from measurements over small areas of irrigated crop in semi-arid regions. Evidently the vertical flux divergence which occurs under advective conditions is not small enough to ignore (Dyer and Crawford 1965), and therefore Bowen ratio estimates need to be augmented by an assessment of advection by measurements of wind speed and horizontal gradients of air temperature and water vapour pressure. Lang (1973) has suggested that it may be possible to determine a single height at which to measure these parameters so as to be most representative of the horizontal advective gradients, and thus the advective contribution. He stresses, however, that lysimetric calibration is necessary for any advection corrections, and especially in the determination and use of a single representative height.

Tanner (1963) noted the importance of horizontal spatial sampling to avoid the affects of surface inhomogeneities which can affect measurements and thereby their calculations of the ratio K_h/K_w. Sampling by sensors physically travelling on a horizontal arm has been used in the past, but is not popular due to mechanical complexity. More recently the accepted strategy for adequate spatial sampling has been the placement of sensors far enough above the surface or canopy to be in the region where turbulent mixing occurs. This height is limited by the fetch-height constraint (Section 2.7.2) and since under stable conditions errors due to thermal stratification increase with height, an additional limitation is imposed.

The error introduced by using the Similarity Principle will always underestimate $L_v F_w$, and therefore overestimate F_h, as during advective periods it is the sensible heat exchange coefficient that becomes greater than the latent, and thus should increase the "constant" multiplier $\gamma\,(K_h/K_w)$ in Eq. 2.25. At high levels of latent heat flux density, values of β are small, and an assumption of equality between K_h and K_w when the two are not markedly different will not lead to serious error in the estimate of $L_v F_w$. When the surface is dry and $L_v F_w$ small, β values are large and a given departure of K_h/K_w from unity can lead to almost as large errors in the estimate of $L_v F_w$. Corrections to the assumption of Similarity are therefore required for nearly all sites (Denmead and McIlroy 1970). It is evident from Eq. 2.20 that the sensitivity of β is directly related to the measured differences; a one percent error in a measurement results in a one percent error in β, although if both the differences are under-estimated, the error cancels somewhat. The size of the error therefore, is directly proportional to the size of β, under any particular constant energy balance régime.

Bertela (1989) found situations in which the application of the Bowen ratio energy balance method has resulted in inconsistent flux density partitioning between sensible and latent heat. From the unpublished Bowen ratio data of Pampoloni and Paloscia (1985) he isolated examples of periods in the calculation of flux partitioning which were physically impossible when analyzed according to his method. The periods he used however, were of dubious merit as he chose early morning or late afternoon times when the Bowen ratio is likely to fail anyway due to the available energy flux density approaching zero. When the BREB method does fail due to neglecting advection these solutions must be discarded, as they must be at the times when β approaches -1. Whether the neglect of the advection term from measurements is permissible cannot be decided until the effect is quantified, and hence measurement of advection should always accompany the collection of data for use in the BREB determination of flux partitioning.

Nocturnal evaporation of up to 20 % of the daily total can occur in alfalfa fields due to strong temperature inversions in spring (Rosenberg 1969), and omitting these periods can significantly decrease calculated totals. No values for nocturnal grassland evaporation could be found in the literature.

2.12.2 Practical considerations of the Bowen ratio technique

The Bowen ratio energy balance technique requires familiarity with a number of different sensors (**Fig. 2.9**, **Plate 2.1**): fine-wire thermocouples (**Fig. 2.10**) for the measurement of the air temperature difference at two vertical points above the canopy, a dew point hygrometer for the measurement of the water vapour pressure difference (Fig. **2.11**), a net radiometer for the measurement of the above-canopy net irradiance (Fig. 2.9), soil heat flux plates for the measurement of soil heat flux density at the plate position and soil thermocouples for the measurement of the soil heat flux density stored above the plate position (**Figs 2.12, 2.13**). All of these sensors are connected to a microprocessor controlled datalogger. The entire system is powered by at least one battery (at least 75 A h capacity is desirable) that is charged from a solar panel. *For sensors that require power, it is advisable to use separate batteries for the datalogger(s) and sensor(s) with the negative terminal of each battery connected. This procedure of providing one ground line for the system will eliminate common mode range problems.* The Bowen ratio information card, describing sensor wiring details and containing a listing of the Campbell Scientific Inc. 21X datalogger program (modified to switch off measurements at night) proved valuable when visiting the research sites (Appendix 1).

The net irradiance and soil heat flux density errors contribute to the overall error in $L_v F_w$, and are independent of the size of β. From error analyses, the relative error in $L_v F_w$ has been found to be most sensitive to errors in I_{net}. With accurate net radiometers most of the error arises from the soil heat flux density determinations even though their contribution relative to net irradiance is small. This is due partly to the accuracy of the net radiometers and to the difficulties encountered with soil heat flux density determinations. The soil heat flux-related errors introduced by contact between soil and plate, depth positioning and spatial dissimilarity are constant, while those arising from uncertainties in the calculation of the stored heat energy content in the layer above the flux plates (due mainly to changes in soil water content), change with time.

If the separation distance dz between the thermocouples is known (Fig. 2.10), then the air temperature gradient dT/dz may be calculated. Typically, the distance between the thermocouples is 1 m. The symbols for earth, high (Hi) and low (Lo) indicate that these wires are connected to the earth, analogue high and analogue low channels of the datalogger. The block connectors (Fig. 2.10) reduce

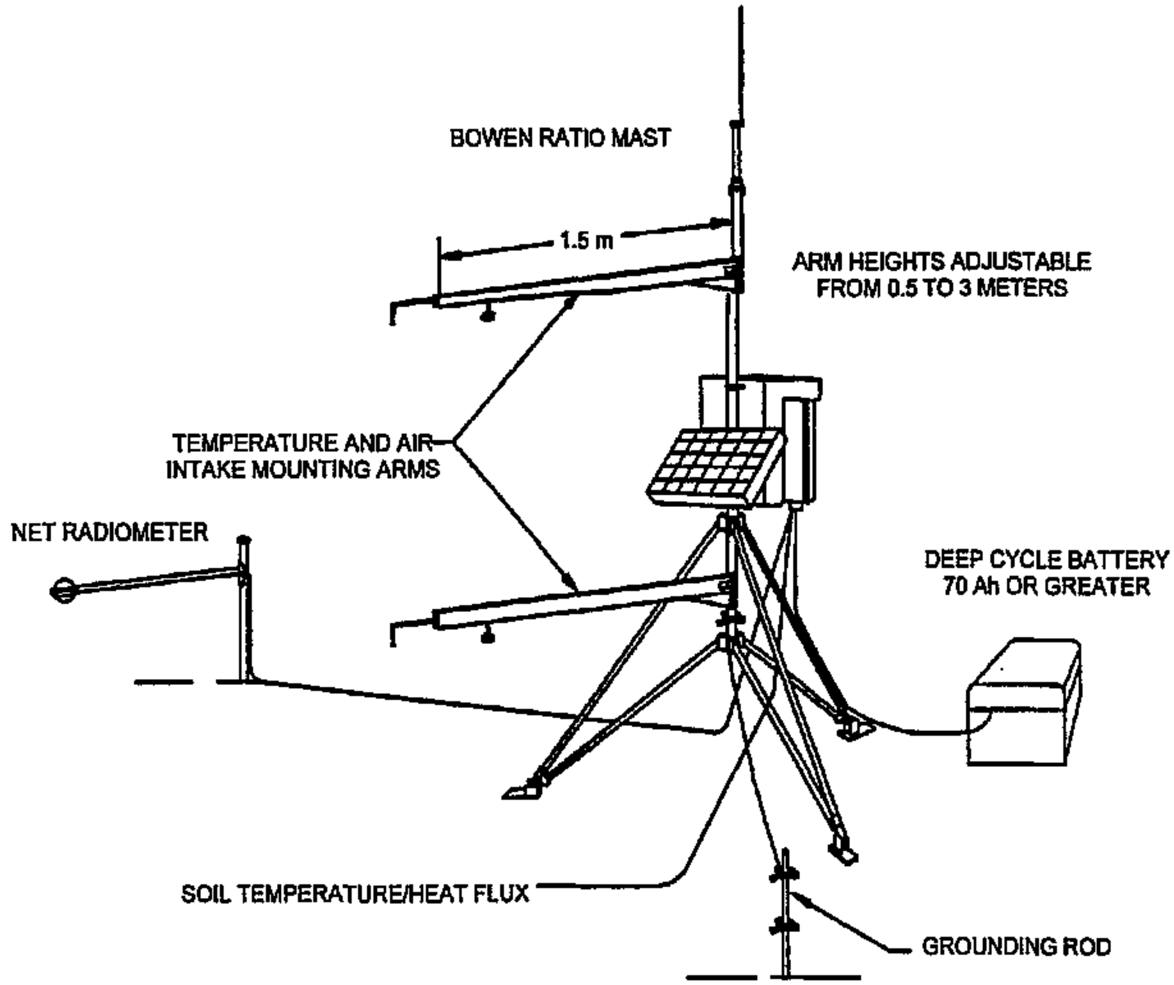

Fig. 2.9 Diagrammatic representation (not to scale) of the Bowen ratio system used. The thermocouples used for the measurement of air temperature are at the end of the intake mounting arms. Also shown is the lightning rod and grounding rod, the net radiometer for the measurement of net irradiance I_{net}, the solar panel and the housing for the datalogger and the cooled dew point mirror, flow meters and solenoids (taken from Campbell Scientific Inc. documentation)

the conduction of heat energy (mainly from absorbed solar irradiance) to the point of temperature measurement. At both the upper and lower temperature measurement levels, the thermocouples are each connected in parallel. This configuration allows for continued air temperature measurement even if one of the thermocouples are damaged. Ideally, for greatest measurement accuracy, the upper and lower thermocouples should be radiatively similar. Spider webs and the like can invalidate measurements. Differential radiative heating of the thermocouples due to dissimilarity between the two thermocouples, (due perhaps to spider's web or other deposits of dirt on one sensor and not on the other), especially at the peak radiative load directly after a cloud pass, can increase the measured temperature difference. This results in a smaller Bowen ratio and thus an overestimated $L_v F_w$.

The theory illustrates that measurement of I_{net}, F_s, and $\overline{T}$ and $\overline{e}$ at two heights are required for estimating $L_v F_w$ and F_h (Eqs 2.18 to 2.20). Atmospheric pressure should also be known but may be estimated from altitude and the atmospheric pressure at a nearby site: a 4 % change in atmospheric pressure results in about a 4 % change in $L_v F_w$. The main assumptions are that the exchange coefficients are equal and that advection is negligible.

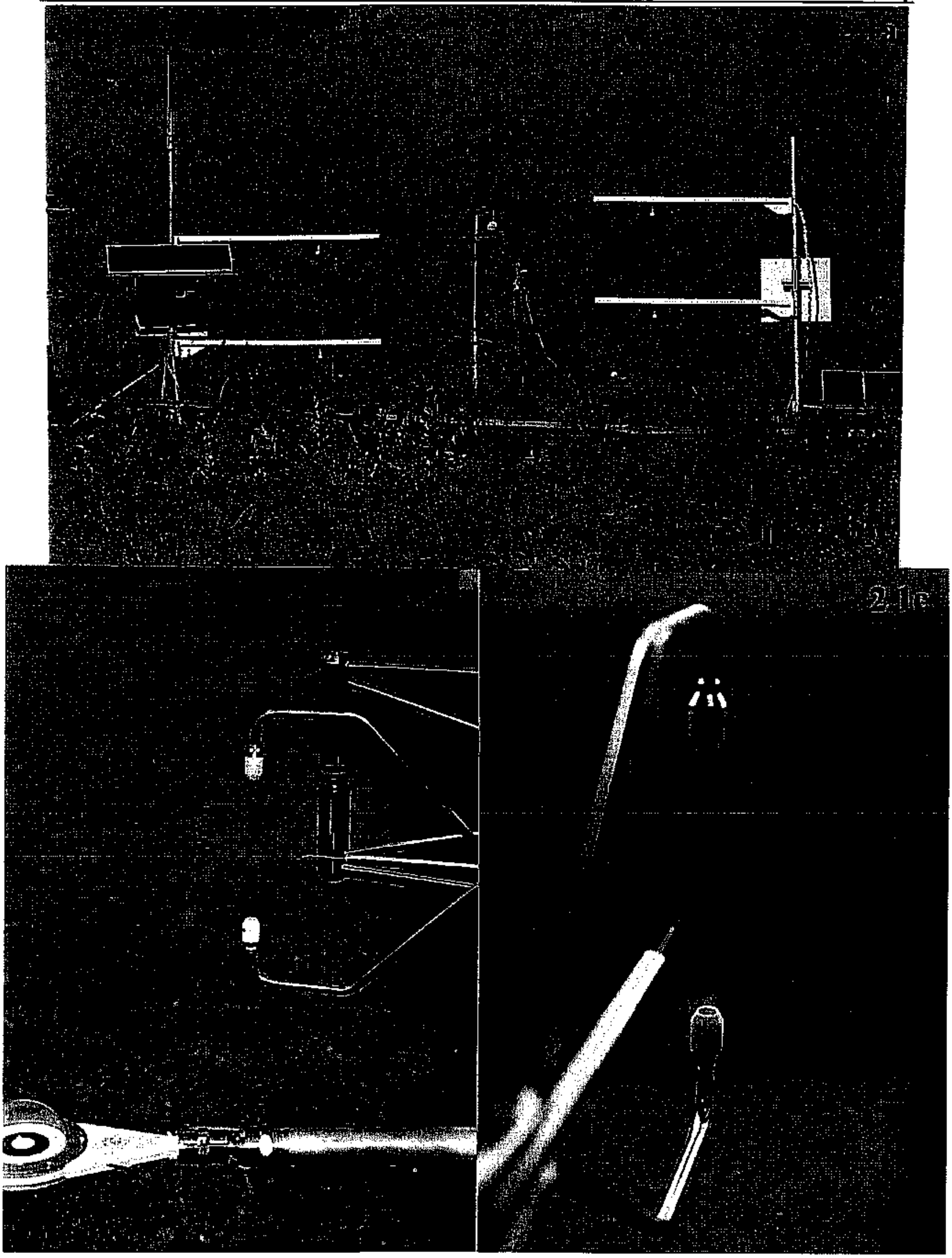

Plate 2.1a Two sets of Bowen ratio equipment located in Cathedral Peak Catchment VI. At the end of each of the two horizontal arms is a fine wire thermocouple for air temperature measurement. For water vapour pressure measurement, air is drawn through a cup containing a filter; 1 b eddy correlation equipment. The KH20 krypton hygrometer (extreme right), the CA27 one-dimensional sonic anemometer (third from right), the fine wire thermocouple and a net radiometer (extreme left); 1c Eddy correlation equipment. CA27 one-dimensional sonic anemometer arms (upper and lower portions) and the fine wire thermocouple (middle)

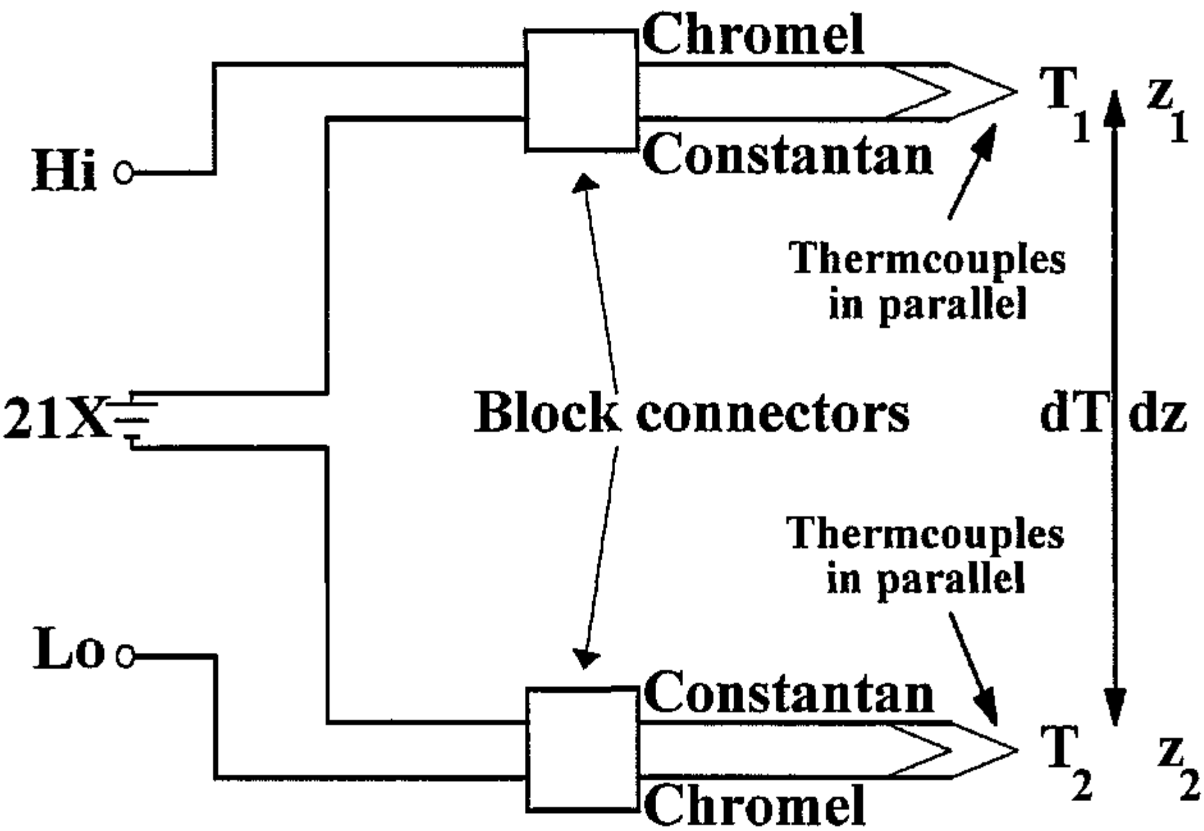

Fig. 2.10 Diagrammatic representation (not to scale) of a pair of Bowen ratio (chromel-constantan) thermocouples used to measure the air temperature difference dT (°C) at two points (typically dz = 1 m) above canopies (adapted from Campbell Scientific Inc. documentation)

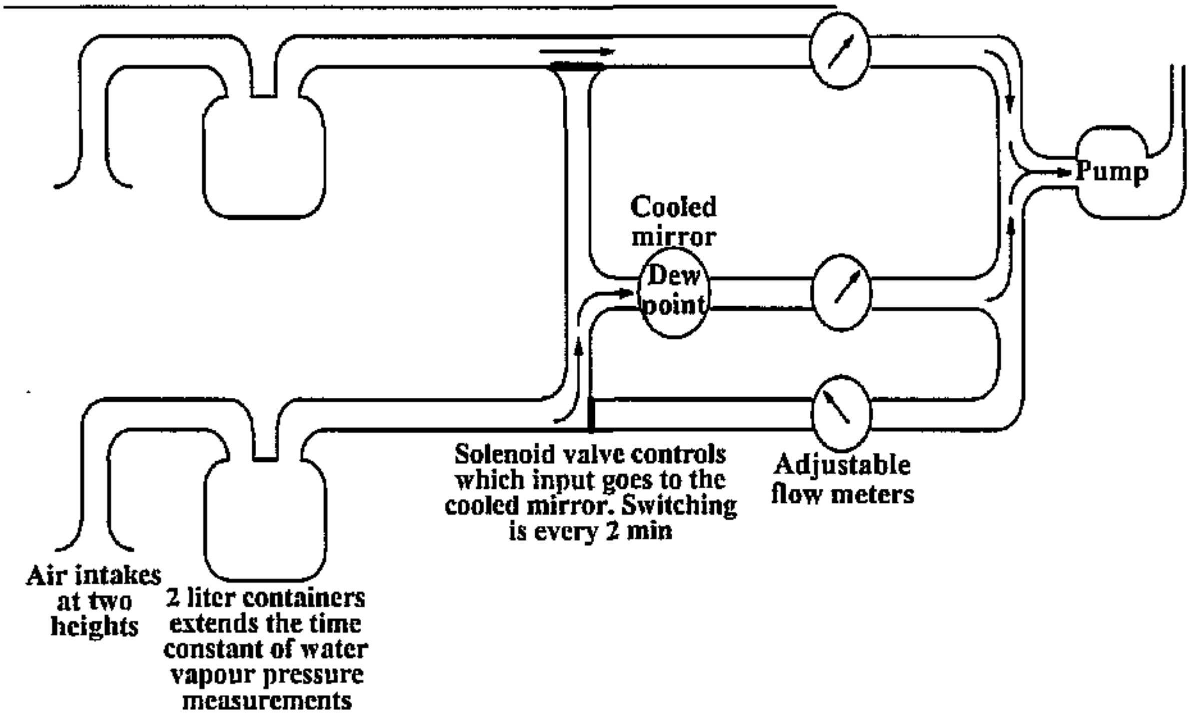

Fig. 2.11 Diagrammatic representation (not to scale) of the Bowen ratio water vapour pressure measurement system. Datalogger-controlled solenoid valves, switched every 2 min, pass air from one of two levels to a single cooled dew point mirror. Typically, the two intakes are 1 m apart (adapted from Campbell Scientific Inc. documentation)

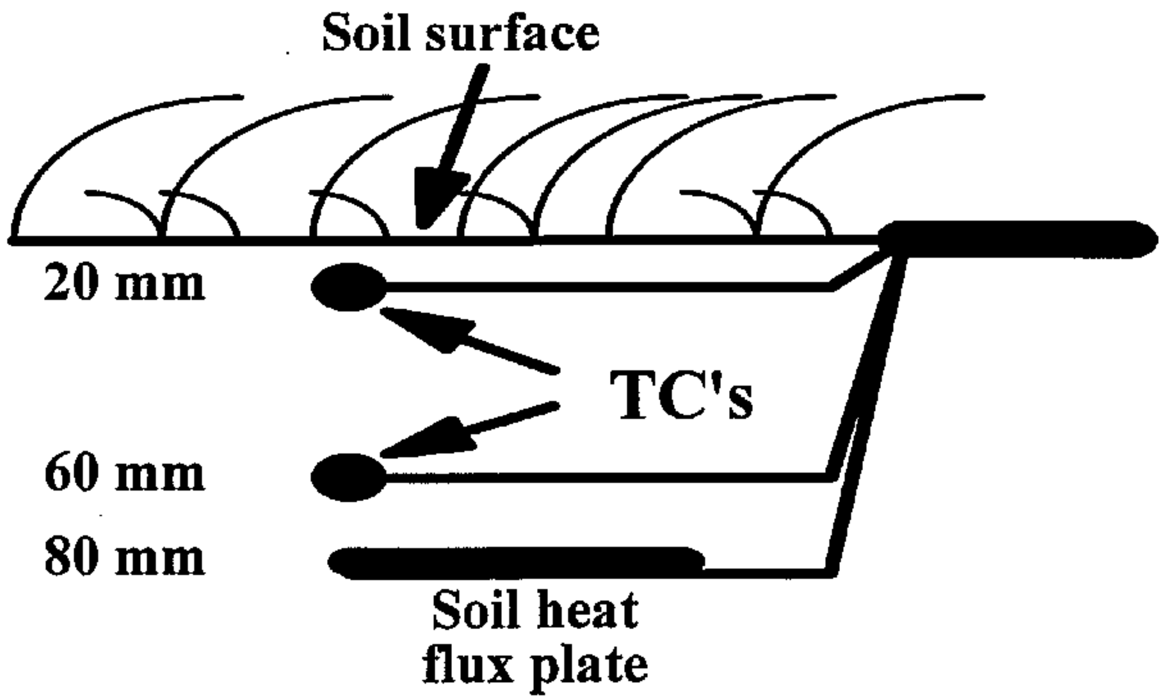

Fig. 2.12 Diagrammatic representation of the placement of a soil heat flux plate and soil thermocouples for the measurement of $F_{soil} = G + F_{stored}$ and the change in soil temperature dT_{soil} over the time interval between consecutive datalogger data outputs (typically 20 min)

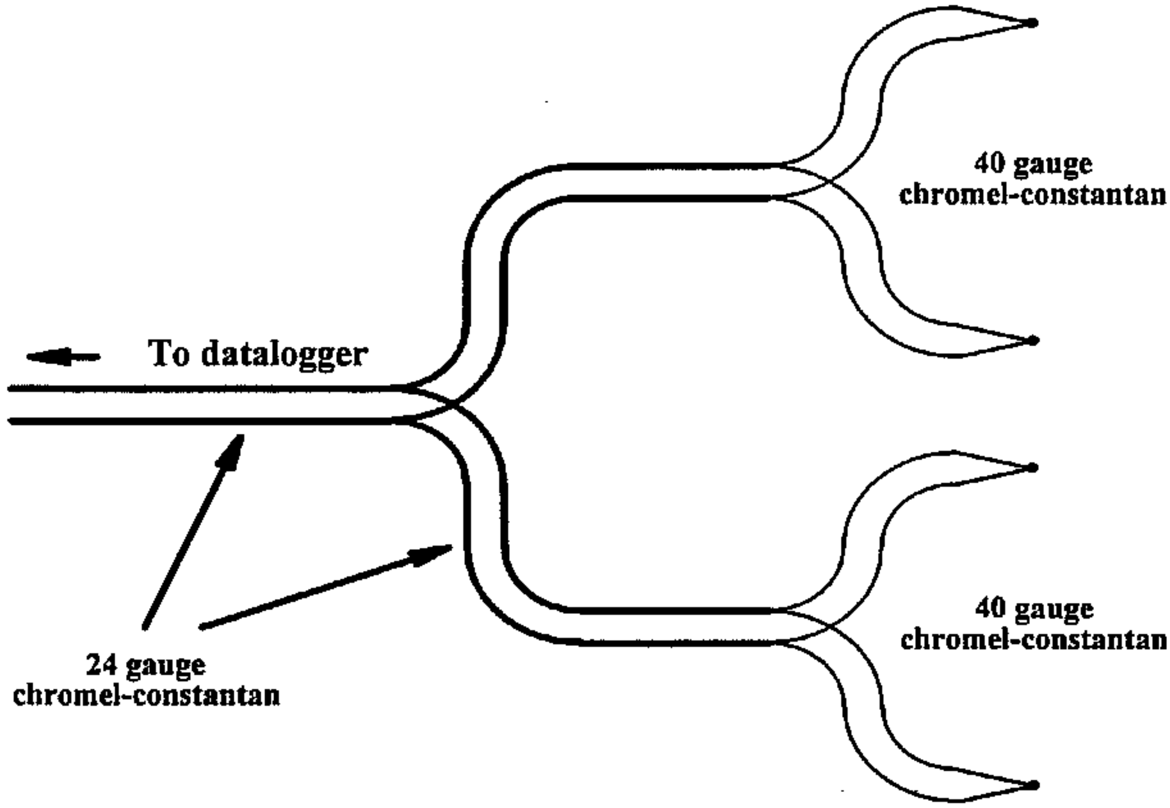

Fig. 2.13 Diagrammatic representation (not to scale) of spatial averaging thermocouples for measuring the soil temperature difference at two points 100 mm apart in soil. This measurement allows the soil heat flux density above the soil heat flux plates to be determined

2.12.2.1 Net irradiance I_{net}

A net radiometer needs weekly attention. The net radiometer domes should be checked for dirt and punctures. If the domes have a "milky white" appearance, they should be replaced and, ideally, the net radiometer recalibrated at the same time. The sensor should be recalibrated at least twice a year. Net irradiance measurements I_{net} are fundamental to the Bowen ratio technique, as the defining equations illustrate.

2.12.2.2 Water vapour pressure e measurements

Accurate water vapour pressure measurements with a resolution of ± 10 Pa are possible using cooled dew point mirror sensors with a resolution of ± 0.003 °C. The limitation of the commercially-available Dew-10 is the 0.05 °C sensor stability. Some workers have used two sensors (expensive and sensor difference errors can occur), or an oscillating boom-type arrangement to minimize the cost and reduce errors. More commonly though, only one sensor is used with air being sucked from the one height and then from the other.

2.12.2.3 Air temperature T measurement

Chromel-constantan thermocouples (TCs) (25 or 75 μm diameter) are used. We have used the 75 μm diameter TCs. Radiation shielding may be unnecessary if the sensors are exposed to the same radiant energy heating. It is a good idea to have two TC's at each height in parallel and thus average the measured temperatures. Also, if one sensor is damaged, the system will continue functioning. Sensors need to be checked frequently for cleanliness and symmetry between the two levels.

2.12.2.4 Soil heat flux density F_s

Soil heat flux plates, if placed too close to the surface, disrupt energy and mass flow in soil. It is therefore better to bury them at a typical depth of 80 mm and use thermocouples to estimate the heat energy flux density stored above the plate (F_{stored}) that should be added to the amount G sensed by the plate at a depth of 80 mm (Fig. 2.12) (technique attributed to Tanner 1960):

$$F_s = G + F_{stored} \qquad 2.31$$

where

$$F_{stored} = \text{stored energy/(area × time)} = M_{soil}\, dT_{soil}\, c_{soil}/\text{(area × time)} = \rho_{soil} V_{soil}\, dT_{soil}\, c_{soil}/\text{(area × time)}$$

$$= \rho_{soil} \Delta z\, dT_{soil}\, c_{soil}/dt \qquad 2.32$$

where ρ_{soil} is the bulk density of the soil, and the soil depth Δz = 0.08 m. The term dT_{soil} is the change in soil temperature during the datalogger output interval between the 20 and 60 mm soil positions (Fig. 2.12), c_{soil} is the specific heat capacity of the soil and dt is the time interval between consecutive datalogger output storage (typically 1200 s). The specific heat capacity of the soil is calculated as the specific heat capacity of dry soil plus that of water using:

$$c_{soil} = c_{dsoil} + \theta_w\, c_w \qquad 2.33$$

where c_{dsoil} is the dry soil specific heat capacity, θ_m is the soil water content (mass basis in kg water per kg soil) and c_w = 4190 J kg^{-1} °C^{-1}, the specific heat capacity of water.

The disadvantage of this method is that one needs to know the soil water content, soil bulk density and the specific heat capacity of dry soil. Frequent destructive sampling to determine the soil water content is a disadvantage of this procedure. In view of soil spatial variability, it may be advisable to measure soil heat flux density F_s at a number of points and average these measurements using datalogger techniques. Unless otherwise specified, two measurement points are routinely used.

2.12.2.5 Soil temperature

This measurement is above the soil heat flux plate in order to calculate the stored soil heat energy above the plate. Typically the probes horizontally in soil at depths of 20 and 60 mm below the soil surface. The probes have been wired to average these two measurements (Figs 2.12, 2.13) but occupy only one datalogger channel.

2.12.2.6 Sensor height and separation

For short grassland canopies, most workers have used a separation distance of 1 m with the lower arm being at a height of 0.5 m above the canopy surface. Under conditions of low water vapour pressure differences between the two measurement positions (Fig. 2.9), it may be necessary to increase the separation distance to 1.5 or 210 m. For a given fetch, there often has to be a compromise between the lower arm distance as well as the separation distance. These distances may have to be changed depending on the measured water vapour pressure and air temperature differences and canopy height.

2.12.3 Practical considerations of the eddy correlation technique

The eddy correlation technique is regarded by many as an absolute technique in that sensible and latent heat flux densities are calculated directly and independently. For the determination of latent heat flux density, the technique relies on the covariance between the vertical wind speed and absolute humidity fluctuations. For these determinations, net irradiance I_{net} and soil heat flux density F_s are not required. However, it is possible to cross-check eddy correlation measurements by such I_{net} and F_s measurements and ensuring that the energy balance is valid (Eq. 2.3). Vertical wind speed fluctuation is measured using a sonic anemometer (Plate 2.1b), the absolute humidity measured using a krypton hygrometer and the air temperature fluctuations measured using a fine wire thermocouple (**Fig. 2.14**). These sensors are expensive compared to the sensors used in the Bowen ratio technique. The eddy correlation sensors are fast responding sensors (usually allowing ten measurements per second). Furthermore, the eddy correlation sensors do require more intensive use of microprocessors or computers for the determination of the fluxes. Unlike the Bowen ratio technique which requires the measurement of air temperature and water vapour pressure at two levels in the atmosphere, the eddy correlation technique requires measurements at one level only. It would appear that the technique has similar fetch requirements to the Bowen ratio technique; this aspect is discussed in Chapter 8. The eddy correlation information card, describing sensor wiring details and containing a listing of the 21X datalogger program proved valuable when visiting the research sites (Appendix 2). Sensor error checking details are described in Chapter 4 and in Appendix 2 in more detail.

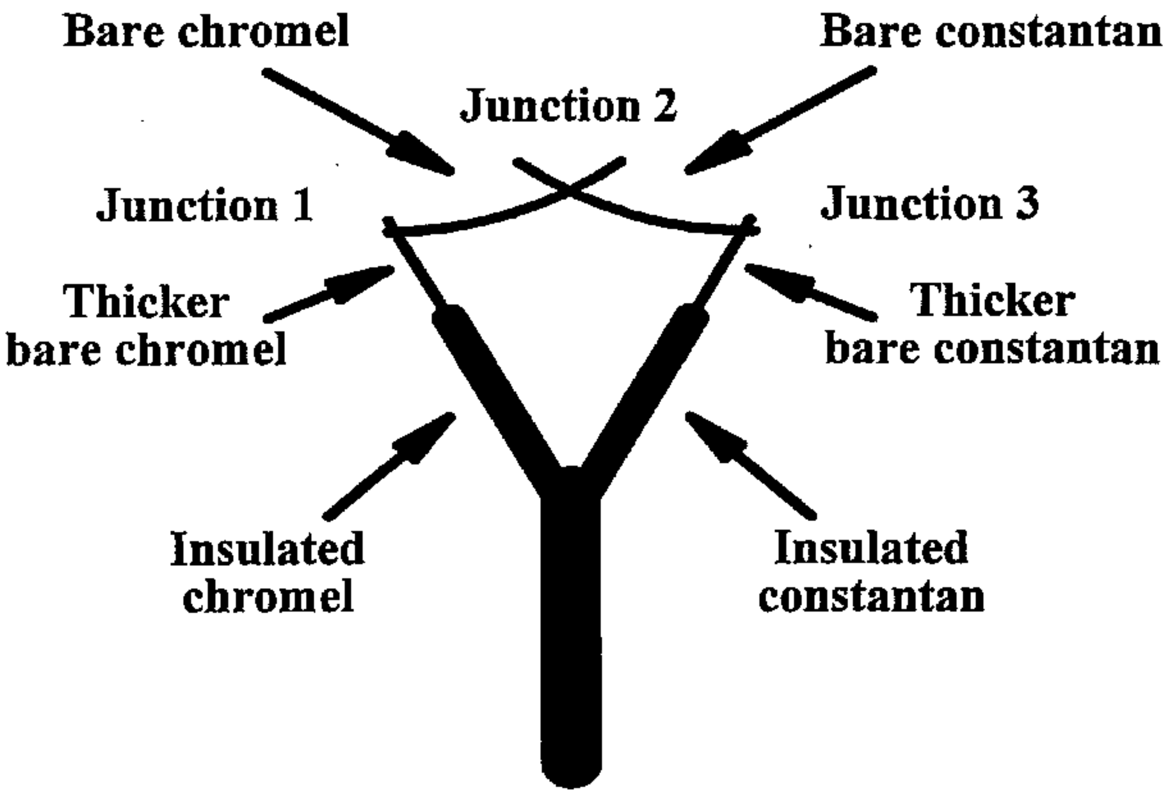

Fig. 2.14 Diagrammatic representation (not to scale) of the Campbell Scientific CA27 fine-wire chromel-constantan thermocouple used as part of the eddy correlation system for the measurement of air temperature fluctuations

Chapter 3

The logistics of calculating flux densities from Bowen ratio data

3.1 Abstract

A theoretical basis is used to specify the so-called "temperature dependent constants" needed to calculate Bowen ratio latent and sensible heat flux densities. One of these constants, the psychrometric constant γ, determines the value of the Bowen ratio, latent heat and sensible heat flux densities. These constants may also be temperature, water vapour and atmospheric pressure dependent. The effect of not accounting for the temperature, water vapour pressure and atmospheric pressure dependence of the constants is not insignificant. The error in the Bowen ratio due to not correcting the psychrometric constant for these factors is related to the ratio of the uncorrected to the actual psychrometric constant. This error can range between -2 and 16 % for air temperature between 0 and 40 °C and water vapour pressure varying from 0 to 2.0 kPa. The error in not correcting the "temperature" dependent constants on sensible heat results in an underestimation by between 8 % and 5 % for air temperature varying between 0 and 40 °C and water vapour between 0 and 2.0 kPa. Latent heat is overestimated by between 0 and 6 %. The error magnitudes are not insignificant and may be larger than evaporation measurements between different research sites. The errors may be avoided using the equations developed in this chapter.

The logistics of calculating sensible and latent heat flux density from measurements of net irradiance, soil heat flux density and the measurement of time-averaged air temperature and water vapour pressure differences are discussed. Criteria for the rejection of "bad" data corresponding to the Bowen ratio tending to -1 are presented. An error analysis showed that the major contributor to total error in latent heat is the error in the measurement of the water vapour pressure gradient. When evaporation rates are high, the relative accuracy in latent heat is good, even with a poorly measured Bowen ratio β. When β becomes large and evaporation less, the absolute error is smaller due simply to the smaller values, but the relative error increases. Some practical error aspects of the Bowen ratio technique are discussed.

The most limiting factor in the routine use of the Bowen ratio system in remote sites is that of the electronic bias of the dew point mirror system. Our experience has shown that, for accurate measurements, the system needs to be checked and the electronic bias adjusted approximately every four days.

From Bowen ratio data we calculated a generalized exchange coefficient K. For the time period of the experiment, we obtained an average of 0.239 $m^2\ s^{-1}$. We proposed a back-calculation method that enabled latent and sensible heat flux densities to be calculated from *a priori* knowledge of K and measurement of the air temperature gradient (for sensible heat) and water vapour pressure gradient (for latent heat). A "standard deviation" method, based on measuring the ratio of the standard deviation in air temperature and water vapour pressure (over a 20-minute period say) is discussed. The method does require equally responsive air temperature and water vapour pressure sensors. The advantage of the method is that measurements at one atmospheric level only are required.

3.2 Theory

3.2.1 Introduction

This section is concerned primarily with accurate expressions for the calculation of so-called "temperature dependent constants" used in energy and mass transfer expressions. Such constants affect the value of the calculated Bowen ratio and the resultant latent and sensible heat energy flux densities. Furthermore, we will show that the rejection criteria of Bowen ratio data is based on the so-called psychrometric constant γ. Hence a full understanding of γ is important.

3.2.2 Acceleration due to gravity

Atmospheric pressure and air density depends on the acceleration of gravity. The acceleration of gravity (m s^{-2}) is in turn dependent on latitude φ (in degrees) and altitude h (m). Values of the acceleration of gravity have been published by Weast (1989) for various latitudes. A quadratic equation in latitude φ was fitted to the tabled data of Weast (1989) and an altitude correction (h in m above sea-level) applied. The equations obtained, with g in m s^{-2} and h in m, are:

$$g = 9.779890 + 0.00014155\,\varphi + 1.00545\times10^{-5}\,\varphi^2 - 0.3086\,h/1000000 \qquad 3.1$$

for latitudes between 0 and 45° and

$$g = 9.738225 + 0.0019533\,\varphi - 1.00423\times10^{-5}\,\varphi^2 - 0.3086\,h/1000000 \qquad 3.2$$

for latitudes between 45 and 90°. The analysis of variance tables for some of these calculations are shown (Table 3.1). For Cathedral Peak, for example, $\varphi \approx 29.4833°$ and h = 1935 m so that g = 9.79221 m s^{-2}. For Pietermaritzburg, $\varphi \approx 29.5833°$, h = 684 m and g = 9.79267 m s^{-2}.

3.2.3 Density of air and total atmospheric pressure[5]

This section deals mainly with the affect that altitude, air temperature and water vapour pressure have on the density of air and atmospheric pressure. Below an altitude of about 750 m, the corrections may be insignificant but in the case of Cathedral Peak, the corrections are necessary. The density of air ρ refers to the total density of air. Ignoring the contribution that carbon dioxide makes to the total density ρ of air, $\rho = \rho_w + \rho_d$ where the density of water vapour is $\rho_w = M_w\,e/R\,T$, the density of dry air $\rho_d = M_d\,(P-e)/R\,T$, and M_w the molecular mass of water, M_d the molecular mass of dry air, e the water vapour pressure (Pa), P the atmospheric pressure (Pa), R = 8.31451 J mol^{-1} K^{-1} the Universal gas constant and T (K) is the air temperature. Assuming that the atmospheric pressure P at an altitude h is that at sea-level less the pressure due to the overlying air of depth h, so that

$$P = P_o - \rho\,g\,h, \qquad 3.3$$

we have:

$$\rho = M_w\,e/R\,T + M_d\,(P_o - \rho\,g\,h - e)/R\,T.$$

Rearranging, $\rho\,R\,T = M_w\,e + M_d P_o - M_d\,\rho\,g\,h - M_d\,e$ or: $\rho\,(R\,T + M_d\,g\,h) = -e\,(M_d - M_w) + M_d P_o$

5 If the atmospheric pressure is in kPa, then the altitude should be in km. If the pressure is in Pa, the altitude should be in m

Table 3.1 Analysis of variance data for the calculation of the acceleration of gravity for a given latitude

		Regression Output: 0 to 45 degrees
Constant		9.779890
Std Error of Y Estimate		0.0002579
R Squared		0.99910
Number of Observations		22
Degrees of Freedom		19
X Coefficient(s)	1.4155E-04	1.005454E-05
Std Err of Coef.	1.7802E-05	3.61887E-07
		Regression Output: 45 to 90 degrees
Constant		9.738225
Std Err of Y Estimate		2.628657E-04
R Squared		0.99908
No. of Observations		22
Degrees of Freedom		19
X Coefficient(s)	1.9533E-03	-1.00423E-05
Std Err of Coefficient	4.8995E-05	3.68798E-07

and hence

$$\rho = [-e\,(M_d - M_w) + M_d P_o]/[RT + M_d\, g\, h]. \qquad 3.4$$

If e is in kPa, then the molecular masses M_d and M_w must be in g mol^{-1} and h in km. If e is in Pa, then M_d and M_w must be in kg mol^{-1} and h in m. Since M_d = 0.028964 kg mol^{-1}, M_w = 0.01801534 kg mol^{-1}, R = 8.31451 J K^{-1} mol^{-1} (Weast 1989), g = 9.79221 m s^{-2} for Cathedral Peak and P_o = 101325 Pa:

$$\rho = [-0.01094866\, e + 2934.7773]/[8.31451 \cdot (T_d + 273.15) + 0.28362157\, h] \qquad 3.5$$

where ρ is in kg m^{-3}, e in Pa, T_d is the air temperature in °C and h = 1935 m. The density of air ρ is therefore atmospheric water vapour pressure, air temperature and altitude dependent. If the corrections for the acceleration of gravity are applied (Eqs 3.1 or 3.2), then ρ is also dependent on latitude. A density of air of 1.211 kg m^{-3} corresponds to that at a relative humidity of 50 %, 20 °C and 101325 Pa atmospheric pressure (that is, at sea-level) (Kaye and Laby 1986). The value of 1.12 kg m^{-3} given by Fritschen and Gay (1979) on their page 17 presumably should be 1.21 kg m^{-3}. A comparison of our ρ calculations with those from Kaye and Laby (1986) show excellent agreement (**Table 3.2**). The density of air is more sensitive to air temperature changes than to water vapour pressure changes (**Fig. 3.1**). Our calculations have been checked against those (for a relative humidity of 50 % for atmospheric pressure varying between 80000 and 106000 Pa) presented by Kaye and Laby (1986). The differences between their and our calculations are shown (Table 3.2). For Cathedral Peak (h = 1935 m), ρ = 0.9656

Table 3.2 Comparison of the density of air (ρ, kg m^{-3}) values calculated using Eq. 3.5 as a function of atmospheric pressure (first row of each air temperature set) and that presented by Kaye and Laby (1986, p 18) shown on the second temperature row and indicated by K&L. The Kaye and Laby (1986) value accounts for the contribution that carbon dioxide makes to the total density of air. The atmospheric pressure (kPa) is indicated in the top row of the table and the water vapour pressure (kPa) is shown in the second column. The relative humidity is taken as 50 %. The third row for each temperature set represents the percentage difference between the two calculations relative to the Kaye and Laby (1986) tabled value

T	e	80	81	82	83	84	85	86	87	88	89	90	91	92	93	94	95	96	97	98	99	100	101	102
6	.3054	0.997	1.009	1.022	1.034	1.047	1.059	1.072	1.084	1.097	1.109	1.122	1.134	1.147	1.159	1.172	1.184	1.197	1.209	1.222	1.234	1.246	1.259	1.271
6	K&L	0.997	1.009	1.022	1.034	1.046	1.059	1.071	1.084	1.096	1.109	1.121	1.134	1.146	1.159	1.171	1.184	1.196	1.209	1.221	1.234	1.246	1.259	1.271
		0.01	-0.04	0.01	-0.03	-0.08	-0.03	-0.07	-0.02	-0.07	-0.02	-0.06	-0.02	-0.06	-0.01	-0.05	-0.01	-0.05	-0.00	-0.04	-0.00	-0.04	0.00	-0.04
8	.4675	0.989	1.001	1.014	1.026	1.039	1.051	1.063	1.076	1.088	1.101	1.113	1.125	1.138	1.150	1.163	1.175	1.187	1.200	1.212	1.224	1.237	1.249	1.262
8	K&L	0.989	1.002	1.014	1.026	1.039	1.051	1.064	1.076	1.088	1.101	1.113	1.126	1.138	1.150	1.163	1.175	1.188	1.200	1.212	1.225	1.237	1.250	1.262
		-0.01	0.06	0.02	-0.02	0.04	-0.00	0.06	0.02	-0.02	0.04	0.00	0.06	0.02	-0.01	0.04	0.01	0.06	0.03	-0.01	0.04	0.01	0.06	0.03
10	.5364	0.982	0.994	1.006	1.019	1.031	1.043	1.056	1.068	1.080	1.092	1.105	1.117	1.129	1.142	1.154	1.166	1.179	1.191	1.203	1.216	1.228	1.240	1.252
10	K&L	0.982	0.994	1.006	1.019	1.031	1.043	1.056	1.068	1.080	1.093	1.105	1.117	1.129	1.142	1.154	1.166	1.179	1.191	1.203	1.216	1.228	1.240	1.253
		0.03	-0.00	-0.04	0.03	0.00	-0.03	0.04	0.01	-0.02	0.05	0.02	-0.01	-0.03	0.03	0.00	-0.02	0.03	0.01	-0.02	0.04	0.02	-0.01	0.05
12	.6140	0.975	0.987	0.999	1.011	1.023	1.036	1.048	1.060	1.072	1.084	1.097	1.109	1.121	1.133	1.146	1.158	1.170	1.182	1.194	1.207	1.219	1.231	1.243
12	K&L	0.974	0.987	0.999	1.011	1.023	1.036	1.048	1.060	1.072	1.084	1.097	1.109	1.121	1.133	1.146	1.158	1.170	1.182	1.195	1.207	1.219	1.231	1.243
		-0.05	0.03	0.01	-0.02	-0.04	0.04	0.02	-0.00	-0.02	-0.04	0.03	0.01	-0.01	-0.03	0.04	0.02	0.00	-0.02	0.05	0.03	0.01	-0.00	-0.02
14	.7013	0.967	0.979	0.992	1.004	1.016	1.028	1.040	1.052	1.064	1.076	1.089	1.101	1.113	1.125	1.137	1.149	1.161	1.174	1.186	1.198	1.210	1.222	1.234
14	K&L	0.967	0.979	0.991	1.004	1.016	1.028	1.040	1.052	1.064	1.076	1.089	1.101	1.113	1.125	1.137	1.149	1.161	1.174	1.186	1.198	1.210	1.222	1.234
		-0.03	-0.05	-0.06	0.03	0.02	0.00	-0.01	-0.02	-0.03	-0.05	0.03	0.02	0.01	-0.00	-0.01	-0.03	-0.04	0.04	0.03	0.02	0.00	-0.01	-0.02
16	.7993	0.960	0.972	0.984	0.996	1.008	1.020	1.032	1.045	1.057	1.069	1.081	1.093	1.105	1.117	1.129	1.141	1.153	1.165	1.177	1.189	1.201	1.213	1.225
16	K&L	0.960	0.972	0.984	0.996	1.008	1.020	1.032	1.044	1.056	1.068	1.081	1.093	1.105	1.117	1.129	1.141	1.153	1.165	1.177	1.189	1.201	1.213	1.225
		-0.02	-0.02	-0.03	-0.03	-0.04	-0.04	-0.04	-0.05	-0.05	-0.06	0.03	0.03	0.02	0.02	0.01	0.01	0.01	0.00	-0.00	-0.01	-0.01	-0.01	-0.02
18	.9091	0.953	0.965	0.977	0.989	1.001	1.013	1.025	1.037	1.049	1.061	1.073	1.085	1.097	1.109	1.121	1.133	1.145	1.156	1.168	1.180	1.192	1.204	1.216
18	K&L	0.953	0.965	0.977	0.989	1.001	1.013	1.025	1.037	1.049	1.061	1.073	1.085	1.096	1.108	1.120	1.132	1.144	1.156	1.168	1.180	1.192	1.204	1.216
		-0.01	-0.01	-0.00	0.00	0.01	0.01	0.01	0.02	0.02	0.02	0.02	0.03	-0.06	-0.06	-0.05	-0.05	-0.05	-0.04	-0.04	-0.04	-0.03	-0.03	-0.03
20	1.0320	0.946	0.958	0.970	0.982	0.994	1.005	1.017	1.029	1.041	1.053	1.065	1.077	1.089	1.101	1.112	1.124	1.136	1.148	1.160	1.172	1.184	1.196	1.207
20	K&L	0.946	0.958	0.969	0.981	0.993	1.005	1.017	1.029	1.041	1.053	1.065	1.076	1.088	1.100	1.112	1.124	1.136	1.148	1.160	1.172	1.184	1.195	1.207
		-0.00	0.01	-0.08	-0.07	-0.06	-0.04	-0.03	-0.02	-0.01	0.00	0.01	-0.07	-0.06	-0.05	-0.04	-0.02	-0.01	-0.00	0.01	0.02	0.03	-0.05	-0.04
22	1.1691	0.939	0.951	0.963	0.974	0.986	0.998	1.010	1.022	1.033	1.045	1.057	1.069	1.081	1.092	1.104	1.116	1.128	1.140	1.151	1.163	1.175	1.187	1.199
22	K&L	0.939	0.950	0.962	0.974	0.986	0.998	1.009	1.021	1.033	1.045	1.057	1.068	1.080	1.092	1.104	1.116	1.128	1.139	1.151	1.163	1.175	1.187	1.198
		-0.00	-0.09	-0.06	-0.04	-0.02	-0.00	-0.08	-0.06	-0.04	-0.02	-0.00	-0.08	-0.06	-0.04	-0.02	-0.00	0.01	-0.06	-0.04	-0.02	-0.01	0.01	-0.06
24	1.3219	0.932	0.944	0.955	0.967	0.979	0.991	1.002	1.014	1.026	1.038	1.049	1.061	1.073	1.084	1.096	1.108	1.120	1.131	1.143	1.155	1.166	1.178	1.190
24	K&L	0.931	0.943	0.955	0.967	0.978	0.990	1.002	1.014	1.025	1.037	1.049	1.061	1.072	1.084	1.096	1.107	1.119	1.131	1.143	1.154	1.166	1.178	1.190
		-0.11	-0.08	-0.05	-0.02	-0.09	-0.06	-0.04	-0.01	-0.08	-0.05	-0.02	0.00	-0.06	-0.04	-0.01	-0.08	-0.05	-0.03	-0.00	-0.07	-0.04	-0.02	0.01
26	1.4919	0.925	0.937	0.948	0.960	0.972	0.983	0.995	1.007	1.018	1.030	1.041	1.053	1.065	1.076	1.088	1.100	1.111	1.123	1.135	1.146	1.158	1.170	1.181
26	K&L	0.924	0.936	0.948	0.959	0.971	0.983	0.994	1.006	1.018	1.029	1.041	1.053	1.064	1.076	1.088	1.099	1.111	1.122	1.134	1.146	1.157	1.169	1.181
		-0.11	-0.07	-0.03	-0.10	-0.06	-0.03	-0.09	-0.05	-0.02	-0.08	-0.05	-0.01	-0.07	-0.04	-0.01	-0.06	-0.03	-0.09	-0.06	-0.02	-0.08	-0.05	-0.02
28	1.6806	0.918	0.930	0.941	0.953	0.964	0.976	0.987	0.999	1.011	1.022	1.034	1.045	1.057	1.068	1.080	1.092	1.103	1.115	1.126	1.138	1.149	1.161	1.173
28	K&L	0.917	0.929	0.941	0.952	0.964	0.975	0.987	0.998	1.010	1.022	1.033	1.045	1.056	1.068	1.079	1.091	1.103	1.114	1.126	1.137	1.149	1.160	1.172
		-0.12	-0.07	-0.02	-0.08	-0.04	-0.09	-0.05	-0.10	-0.06	-0.02	-0.07	-0.03	-0.08	-0.04	-0.09	-0.05	-0.01	-0.06	-0.03	-0.08	-0.04	-0.09	-0.05
30	1.8898	.911	0.923	0.934	0.946	0.957	0.969	0.980	0.992	1.003	1.015	1.026	1.038	1.049	1.060	1.072	1.083	1.095	1.106	1.118	1.129	1.141	1.152	1.164
30	K&L	.910	0.922	0.933	0.945	0.956	0.968	0.979	0.991	1.002	1.014	1.025	1.037	1.048	1.060	1.071	1.083	1.094	1.106	1.117	1.129	1.140	1.152	1.163
		-0.12	-0.04	-0.12	-0.06	-0.11	-0.06	-0.11	-0.05	-0.10	-0.05	-0.10	-0.05	-0.10	-0.05	-0.09	-0.04	-0.09	-0.04	-0.08	-0.04	-0.08	-0.04	-0.08

kg m^{-3} for T = 25 °C, RH = 50 %. For Pietermaritzburg (h = 684 m), ρ = 1.0915 kg m^{-3} for T = 25 °C and RH = 50 % if the correction for elevation is applied to gravity (Eq. 3.1).

3.2.4 The psychrometric constant and Δ, the slope of the saturation water vapour pressure *vs* temperature relationship

3.2.4.1 Introduction

The psychrometric constant γ (kPa K^{-1}) and the slope of the saturation water vapour pressure e_s (Table 3.3) *vs* temperature T relationship ($\Delta = de_s/dT$) are as fundamental in energy and mass exchange considerations as other constants such as the Universal gas constant. The psychrometric constant is the basis of the psychrometric chart (Fig. 3.2). At sea-level pressure and an air temperature of 0 °C, the

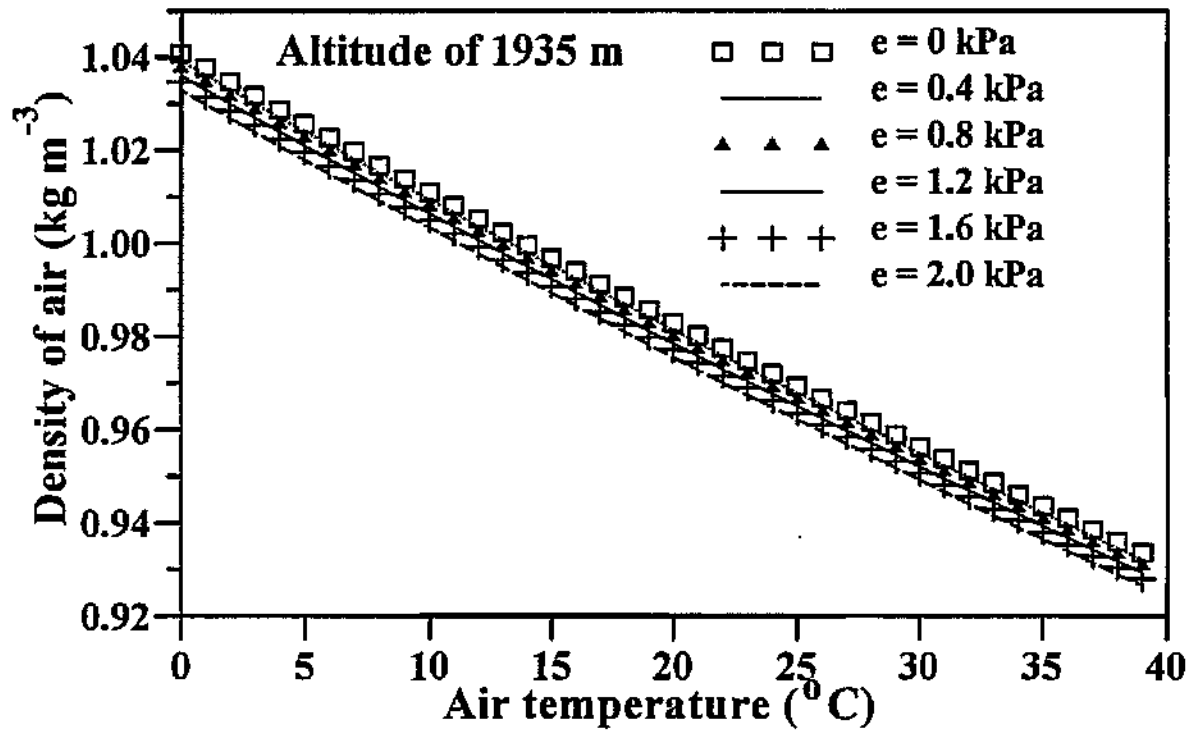

Fig. 3.1 The variation of the density of air (kg m^{-3}) as a function of air temperature and water vapour pressure for an altitude of 1935 m

psychrometric constant is 0.0655 kPa K^{-1} increasing to 0.0668 kPa K^{-1} at 20 °C for an aspirated and unfrozen wet bulb (see Section 3.2.4.6). These values differ slightly from those in Table 6.3 of Fritschen and Gay (1979) as they assumed that the specific heat capacity of air c_p = 1.004 kJ kg^{-1} K^{-1} and did not correct for temperature. They also used an atmospheric pressure of 100 kPa and assumed that $\varepsilon = M_w/M_d =$ 0.622.

The psychrometric constant is dependent on quantities that are in turn dependent on air temperature, acceleration of gravity, etc. It is our aim to specify this dependence exactly.

3.2.4.2 Psychrometric constant and the psychrometric chart

The saturation water vapour pressure e_s (kPa) as a function of the dry bulb temperature T_d (°C) is familiar to many from the psychrometric chart. However, the psychrometric constant is unfamiliar in relation to the psychrometric chart (Fig. 3.2). Simply, the psychrometric constant is the slope magnitude of the wet bulb temperature lines of the psychrometric chart (in units kPa K^{-1}). The water vapour pressure is defined by

Table 3.3 The saturation water vapour pressure of water e_s (kPa) as a function of the dry-bulb temperature (T_d, °C): $e_s = 0.6108 \exp[(17.2694\, T_d)/(237.3 + T_d)]$

T(°C)	0	10	20	25	30	40	50	60	70	80	90	100
e_s (kPa)	0.611	1.228	2.338	3.168	4.243	7.375	123.35	19.930	31.211	47.516	70.504	102.194

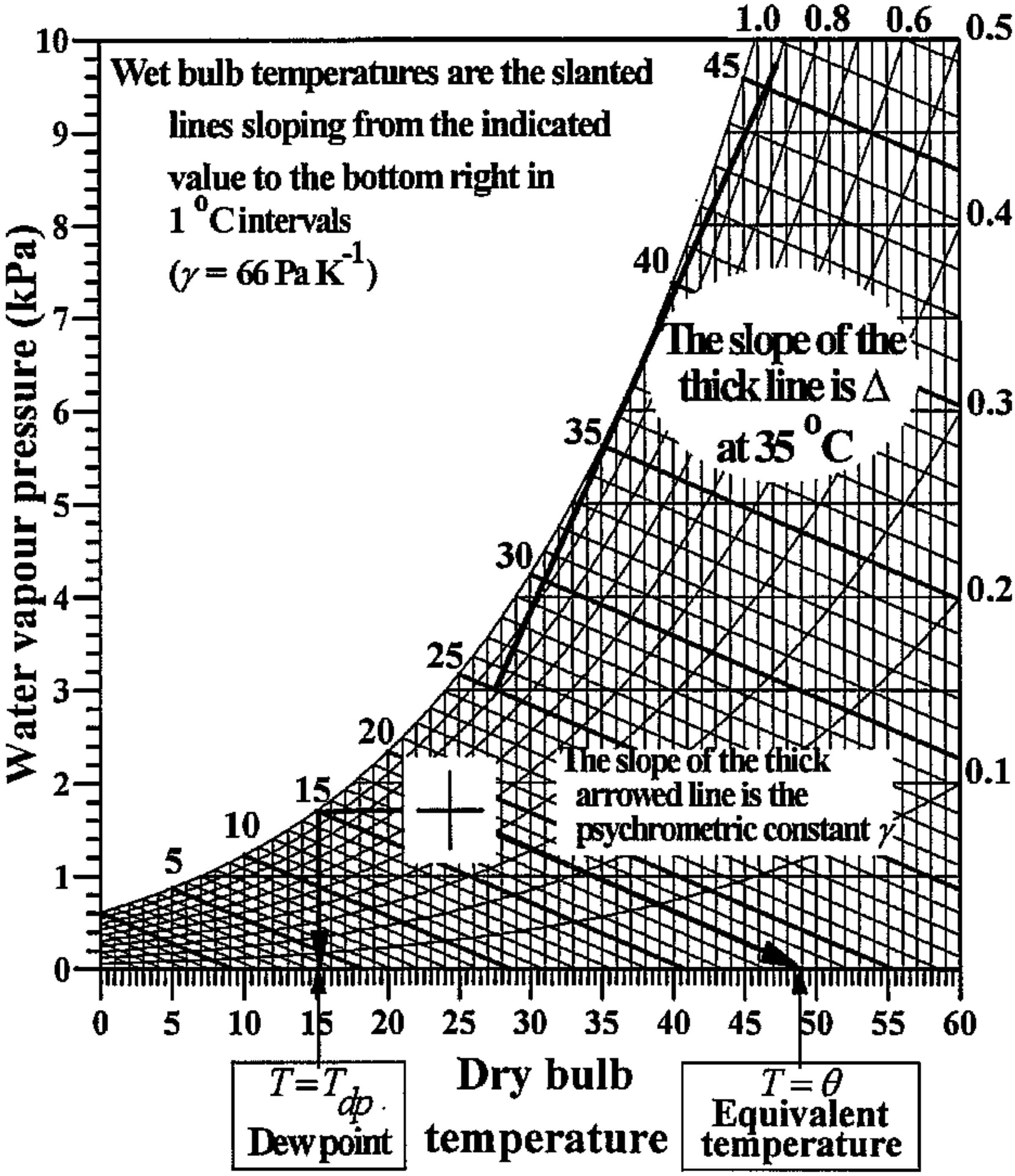

Fig. 3.2 The psychrometric chart. On the right, increasing upwards, is shown the fractional relative humidity (0.1, 0.2, etc.) corresponding to the upward curves as the dry bulb temperature increases. The point marked with a large + sign is defined either by a dry and wet bulb temperature pair or a dry and dew point temperature. The equivalent temperature $\theta = T + e/\gamma$ is the dry bulb temperature at the end of the arrow (the slope of the arrow being the psychrometric constant) taken from the + point. In this case, θ = 48.8 °C. The dew point is determined by starting at +, decreasing the temperature until saturation without changing the water vapour pressure (that is, a horizontal decrease in the dry bulb temperature until intersection with the curve corresponding to a fractional relative humidity of 1.0). In this case, T_{dp} = 15 °C. The slope of the saturation water vapour pressure $\Delta = de_s/dT$ is shown for a dry bulb temperature of 35 °C

$$e = A - B = e_s(T_w) - B, \tag{3.6}$$

where A is the saturation water vapour pressure at the wet bulb temperature T_w,

$$B = \gamma\,(T_d - T_w)\cdot(1 + 0.00115T_w), \tag{3.7}$$

$$\gamma = c_p\,P/\varepsilon\,L_v, \tag{3.8}$$

T_w is the wet bulb temperature, $e_s(T_w)$ the saturation water vapour pressure (kPa) at the wet bulb temperature, $\varepsilon = M_w/M_d \approx$ 0.01801534 kg mol^{-1}/0.028964 kg mol^{-1} $\approx$ 0.6219807 the ratio of the molecular mass of water to that of dry air, c_p is the specific heat capacity of air at constant pressure (often assumed to be 1.004 kJ kg^{-1} K^{-1}) and where L_v is the specific latent heat of vapourization. Actual expressions for c_p and L_v will be presented later. Hence $B = A - e$ and $\partial B/\partial T_d$ expresses the slope magnitude of the wet bulb temperature line. But, $B = \gamma\,(T_d - T_w)\cdot(1 + 0.00115T_w)$ with the result that $\partial B/\partial T_d \approx \gamma$. More exactly the slope magnitude of the wet bulb temperature line is given by $\partial B/\partial T_d = \gamma \cdot (1 + 0.00115\,T_w)$.

3.2.4.3 Correction of the psychrometric constant for atmospheric pressure

It is to be expected that the evaporation of water from a surface is atmospheric pressure dependent. To correct for atmospheric pressures other than sea-level pressure we use the following familiar relationship:

$$\gamma\ (\text{at pressure } P) = \gamma\ (\text{at sea-level pressure } P_o) \times P/P_o = \gamma_o \times P/P_o. \tag{3.9}$$

If accuracy is not imperative, and if atmospheric pressure P is not known, then it is assumed that the density of air is 1.211 kg m^{-3}. Hence,

$$P\ (\text{kPa}) = 101.325 - 1.211 \times 9.80665 \times h = 101.325 - 11.87585 \times h$$

where h (km) is the altitude of the site at which the wet and dry bulb temperature measurements were obtained. However, if greater accuracy for atmospheric pressure P is required, then the following more rigorous calculation method may be applied:

the pressure P (kPa) at altitude h (km) above sea-level is given by

$$P = P_o - \rho\,g\,h \tag{3.3}$$

where P_o is the sea-level pressure (= 101.325k Pa) and ρ is the air density (kg m^{-3}) calculated using Eq. 3.5, and g the acceleration of gravity (m s^{-2}) calculated using Eq. 3.1 or 3.2. The variation of atmospheric pressure P with air temperature and water vapour pressure is shown (Fig. 3.3).

The following subroutine, using the theory developed (written in QuickBasic IV) may be used to estimate the air pressure from a sample pair of wet and dry bulb temperatures. The subroutine assumes that the psychrometric constant is fixed at 0.066 kPa °C^{-1} and that the site elevation has been specified previously. The method starts with an atmospheric pressure P = 101.325 kPa (sea level pressure). A rough estimate of the water vapour pressure e and air density ρ are calculated, and then used to calculate a better estimate of the atmospheric pressure P. This process is repeated until the atmospheric pressure is estimated to within 0.001 kPa:

```
'T is the dry bulb temperature
CLS
```

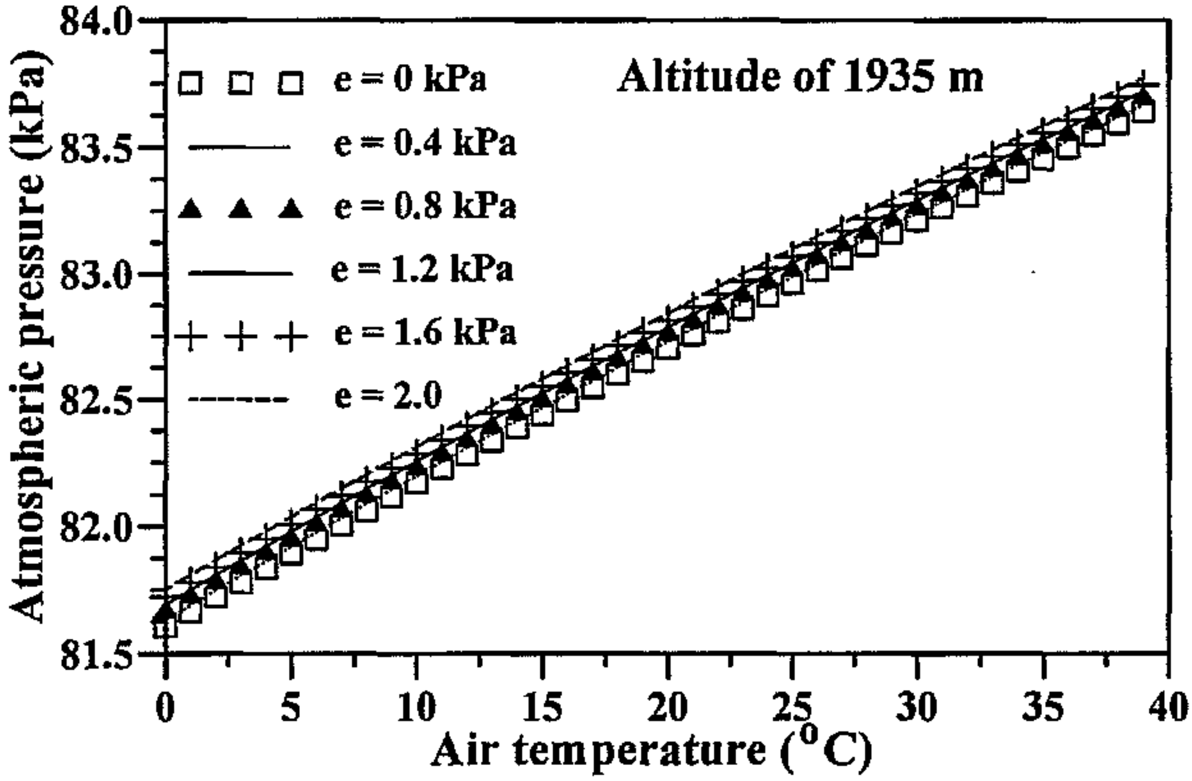

Fig. 3.3 The variation of atmospheric pressure (kPa) as a function of air temperature (°C) and water vapour pressure (kPa) for an altitude of 1935 m

```
Md = .028964
Mw = .01801534
R = 8.31451
gr = 9.79221
P = 0
newP = 101.325
WHILE (ABS(newP - P) > .001 OR ABS(oldE - e) > .001)
   oldE = e
   P = newP
     es = .61078 * EXP(17.2693882# * T1 / (237.3 + T1))
     G = 0.066
     e = es - G * (P / 101.325) * (T - T1) * (1 + .00115 * T1)
   ELSE
     e = .61078 * EXP(17.2693882# * T1 / (237.3 + T1))
   END IF
      IF e < 0 THEN CALL Writer(ToFile, "VAPOUR PRESSURE IS NEGATIVE;
POSSIBLY TOO DRY", 0, -1)
   d = (101.325 * Md - (Md - Mw) * e) / (R * (273.15 + T) + Md * gr * h)
   newP = 101.325 - d * gr * h
WEND
P = newP / 1000
RETURN
```

3.2.4.4 Specific latent heat of vapourization

The specific latent heat of vapourization decreases with increase in air temperature as a decreased amount of energy is required to evaporate water at higher air temperatures. This expectation is expressed in the relationship

$$L_v\,(\text{kJ kg}^{-1}) = 2500.95 - 2.36679\,T_{air}\,(^{\circ}\text{C}) \qquad 3.10$$

where T_{air} is the air temperature. The values for L_v (kJ kg^{-1}) compare with those of Fritschen and Gay (1979, Table 6.3).

3.2.4.5 Specific heat capacity of moist air at constant pressure

In many of the equations describing surface exchange processes, the specific heat capacity of the overlying air is a factor that appears in the numerator of equations describing the sensible and latent heat flux densities. According to List (1951, p 339), the specific heat capacity of air (J kg^{-1} K^{-1}) at constant pressure is defined by:

$$c_p = 1000\,[7\!/\!2\,(R/M_d) + (4\,R/M_d)\,(r/\varepsilon) + \delta c_p] = 1000\,[7\!/\!2\,(R/M_d) + (4\,R/M_d)\cdot e/(P-e) + \delta c_p] \qquad 3.11$$

where r is the mixing ratio ($r = \varepsilon\, e/(P-e)$) for a water vapour pressure e (kPa) at atmospheric pressure P (kPa) and $\varepsilon \approx 0.6219807$, M_d is the molecular mass of dry air and δc_p is the isobaric specific heat capacity residual of moist air (List 1951). Simplifying,

$$c_p = 1004.722587 + 1148.254385\cdot e/(P-e) + \delta c_p \qquad 3.12$$

where δc_p is dependent on atmospheric pressure, air temperature and the fractional relative humidity. A useful relationship, determined by examination of the δc_p data presented by List (1951) is:

$$\delta c_p = 1.256\,(1 + T_{air}/40)\cdot[1 + (e/e_s)]. \qquad 3.13$$

For $e = 2$ kPa, $T_{air} = 25$ °C (and hence $e_s = 3.168$ kPa) and $P = 85$ kPa, $r \approx 0.015$ kg kg^{-1} with the result that $c_p = (1004.72 + 27.67 + \delta c_p)$ J kg^{-1} K^{-1} = (1032.39 + 3.33) J kg^{-1} K^{-1} = 1035.72 J kg^{-1} K^{-1}. The variation in the specific heat capacity shows little temperature dependence but c_p does have a greater water vapour pressure dependence (**Fig. 3.4**).

3.2.4.6 Psychrometric constant

The psychrometric equation provides a relationship between water vapour pressure and wet and dry bulb temperatures. The heat energy flux transferred from air to the wet bulb is equivalent to the heat energy lost from a mass of air m_1 cooled from temperature T_{air} to temperature T_w. This heat will evaporate enough water to cause a mass of air m_2 to saturate at temperature T_w. Formally, the psychrometric constant γ is defined as:

$$\gamma = P\,c_p/(\varepsilon\,L_v). \qquad 3.8$$

Besides ventilation rate, the psychrometric constant is temperature dependent, atmospheric pressure dependent and water vapour pressure dependent. The term "aspirated" implies that the ventilation velocity exceeds about 3 m s^{-1} (Fritschen and Gay 1979, p 130). Non-aspirated psychrometers are usually assumed to have a natural ventilation of about 1 m s^{-1} (Unwin 1980, p 73). We have assumed that the ventilation rate for the Bowen ratio equipment exceeds 3 m s^{-1} so that the mass ratio m_1/m_2 is unity. Using the relationships for atmospheric pressure P (Eq. 3.3) and the density of air (Eqs 3.4 for air density and 3.5, 3.12 and 3.13 for specific heat capacity of air c_p (Eqs 3.12 and 3.13) and the latent heat

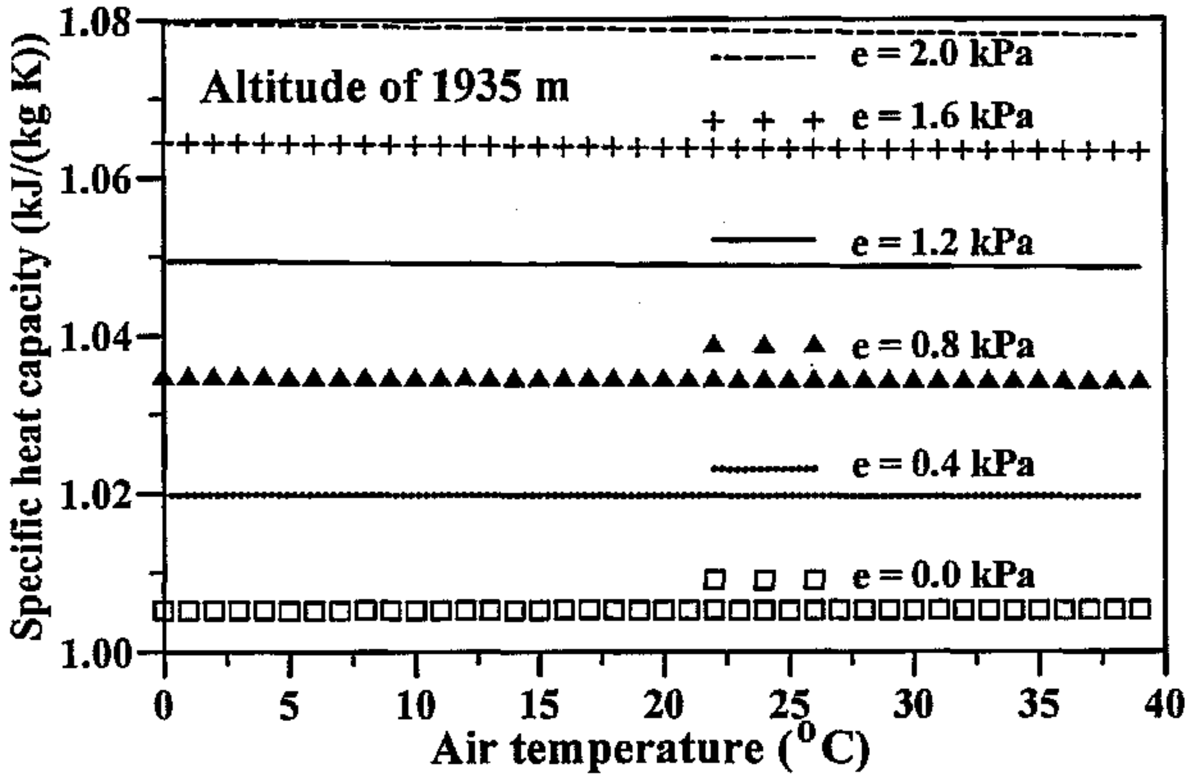

Fig. 3.4 The variation of the specific heat capacity of air at constant pressure (kJ kg^{-1} K^{-1}) as a function of air temperature and water vapour pressure for an altitude of 1935 m

of vaporization L_v (Eq. 3.10), the overall dependence of the psychrometric constant on air temperature and water vapour pressure is shown (for an altitude of 1935 m, latitude of 29.4833 °S with resultant acceleration of gravity of 9.79221 m s^{-2}) (Fig. 3.5). Also shown is the error in assuming a fixed psychrometric constant of 53.45 Pa K^{-1} (corresponding to an atmospheric pressure of 81.3 kPa, c_p = 1010 J kg^{-1} K^{-1}, ε = 0.622 and L_v = 2470 kJ kg^{-1} (Fig. 3.5, right hand y axis).

At an atmospheric pressure of 100 kPa, the psychrometric constant is 59.4 Pa K^{-1} for an aspirated and frozen wet bulb, 79.9 Pa K^{-1} for a non-aspirated and unfrozen wet bulb, and 72.0 Pa K^{-1} for a non-aspirated and frozen wet bulb (Unwin 1980, p 73).

3.2.4.7 Ratio of Δ to psychrometric constant

The $\Delta = de_s/dT$ (where e_s is the saturation water vapour pressure at temperature T) to γ ratio is as fundamental in energy and mass exchange considerations as other constants such as the Universal gas constant. The saturation water vapour pressure e_s (kPa) as a function of the dry bulb temperature T_d (°C) is familiar to many from the psychrometric chart and is given mathematically by:

$$e_s = 0.6108 \cdot \exp\,[17.2694\, T_d/(237.3 + T_d)] \qquad 3.14$$

(Table 3.3), or as a power series in T_d:

$$e_s = 0.61055 + 4.4769 \times 10^{-2}\, T_d^2 + 1.378 \times 10^{-3}\, T_d^3 + 2.2 \times 10^{-7}\, T_d^4 + 3.2 \times 10^{-9}\, T_d^5. \qquad 3.14a$$

Using Eq. 3.14, the slope of the saturation water vapour pressure e_s (kPa) *vs* temperature curve, de_s/dT_d in kPa K^{-1} is given by:

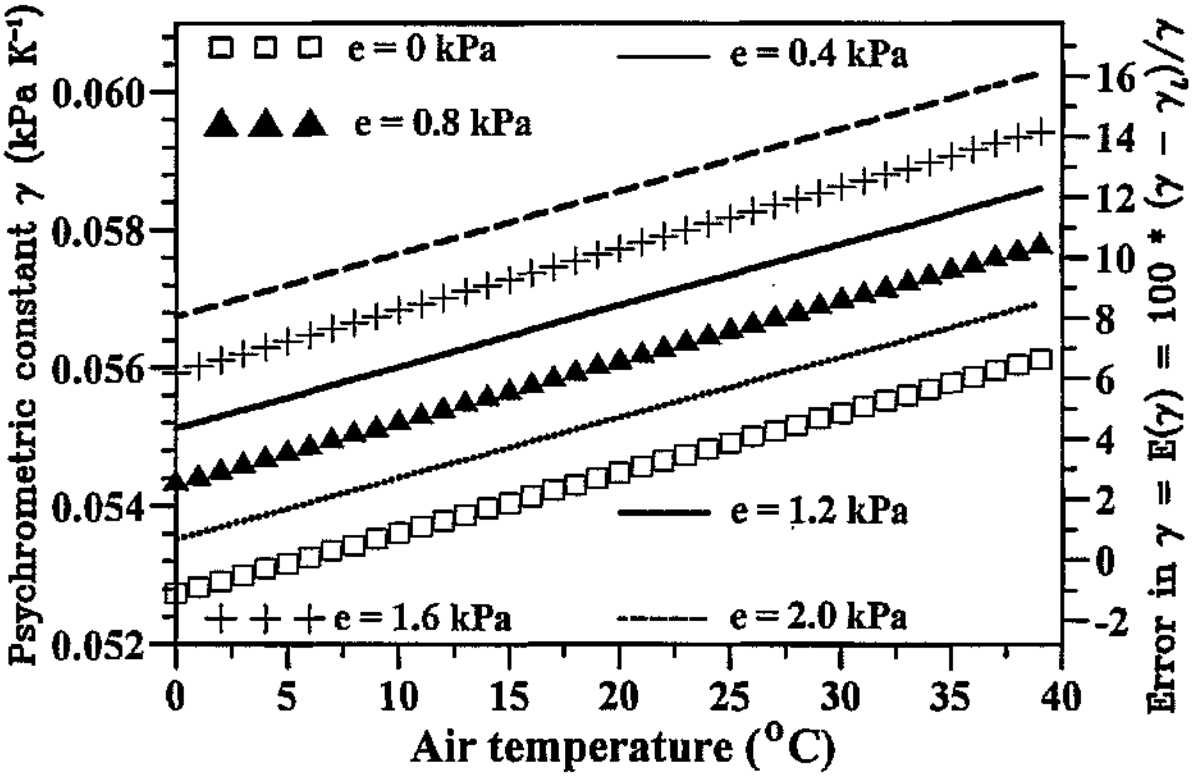

Fig. 3.5 The variation of the psychrometric constant γ (kPa K^{-1}) (left hand y axis) and the relative error in assuming a fixed and incorrect psychrometric constant of $\gamma_i = 0.05345$ kPa K^{-1} compared to the actual psychrometric constant γ (kPa K^{-1}) (right hand y axis) as a function of air temperature and water vapour pressure for an altitude of 1935 m

$$\Delta = de_s/dT_d = (d/dT)\ \{0.6108 \cdot \exp[17.2694 \cdot T_d/(237.3 + T_d)]\}$$

$$\text{or } \Delta = 4098.02862 \cdot e_s/(237.3 + T_d)^2. \qquad 3.15$$

Substituting T_d = 6, 18 and 26 °C into these equations, yields e_s = 0.93510, 2.06390 and 3.36124 kPa and $\Delta = de_s/dT_d$ = 0.064736, 0.129766 and 0.198689 kPa K^{-1} for the respective temperatures. For $P = P_o$ = 101.325 kPa and e = 0 kPa, $\gamma = \gamma_i = P_o c_p/(L_v \varepsilon)$ = 0.065914, 0.066700 and 0.067235 kPa K^{-1} and $\Delta/\gamma \approx$ 1.0, 2.0 and 3.0 at 6, 18 and 26 °C respectively.

3.2.4.8 Equilibrium evaporation

Equilibrium evaporation is defined to exist when there is weak flow of humid air over an irrigated crop. For such conditions, the vapour pressure deficit $\delta e = e_s(T_{air}) - e$ of the atmosphere is small, the wind speed is low and the stomatal resistance of the crop is small. These conditions result in the three resistances in the Penman-Monteith equation (Eq. 2.11), r_i, r_s and r_a, being small, small and large, respectively. Hence, neglecting the former two resistances in comparison to the third in the Penman-Monteith equation for α (the ratio of latent heat energy flux density to the sum of latent and sensible heat energy flux density Eq. 2.11), we get:

$$\alpha_{equilibrium} = \Delta/(\Delta + \gamma) = (\Delta/\gamma)/[(\Delta/\gamma) + 1] \qquad 3.16$$

(Fig. 3.6) where $\Delta/\gamma \approx$ 1, 2, and 3 at 6, 18 and 26 °C respectively. Hence: $\alpha_{equilibrium} \approx$ 0.5, 0.67 and 0.75 at 6, 18 and 26 °C. Since α is the ratio of latent heat energy flux density to the sum of latent and

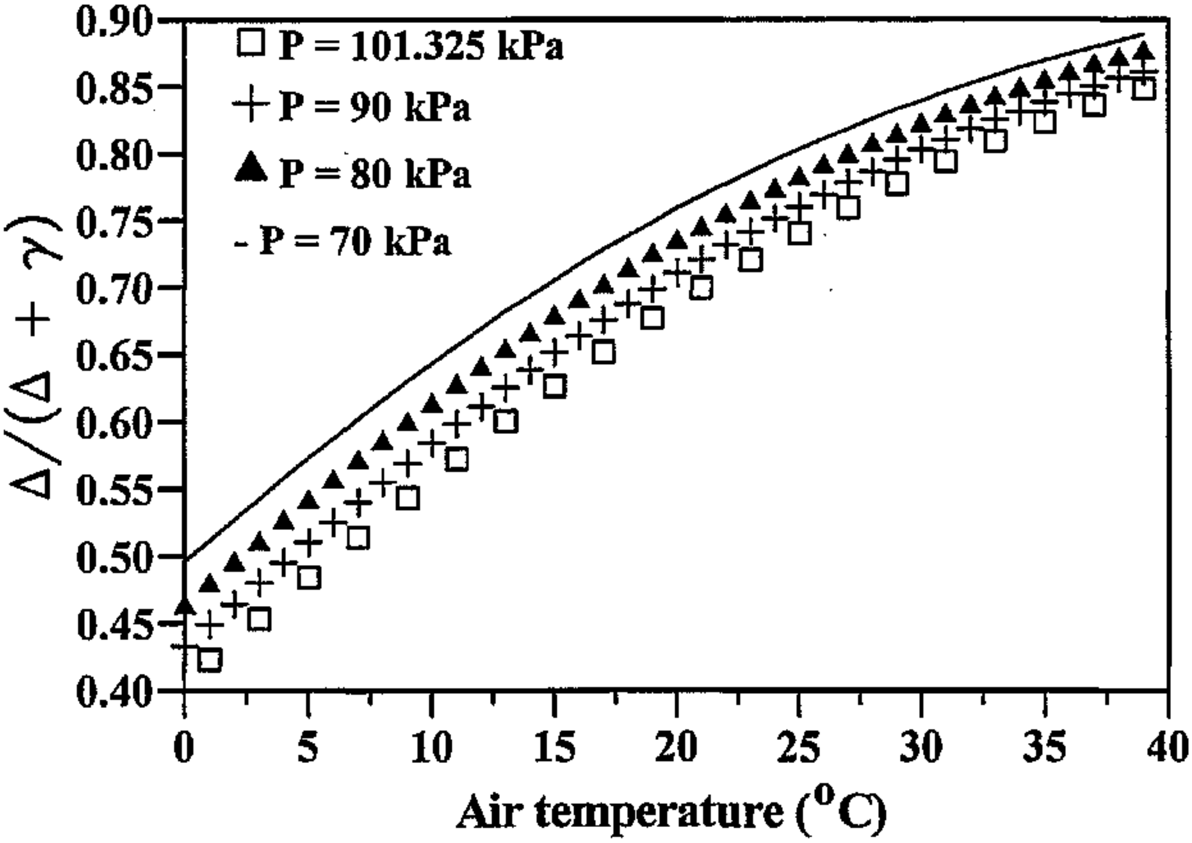

Fig. 3.6 The variation of the ratio $\Delta/(\Delta+\gamma)$ as a function of air temperature and atmospheric pressure

sensible heat energy flux density:

$$(L_v F_w)_{equilibrium} = [\Delta/(\Delta+\gamma)]\cdot(I_{net} - F_s). \qquad 3.17$$

An accurate relationship for $\Delta/(\Delta+\gamma)$, for a pressure of 100 kPa, is given by:

$$\Delta/(\Delta+\gamma) = 0.413188419 + 0.0157973\, T_{air} - 0.00011506\, T^2_{air}. \qquad 3.18$$

A less accurate relationship is expressed by:

$$\Delta/(\Delta+\gamma) = 0.416065 + 0.012345\, T_{air}. \qquad 3.19$$

It is however necessary to account for the atmospheric pressure dependence by using γ in Eqs 3.16 and 3.17 (Fig. 3.6) where γ is calculated from Eq. 3.8. In spite of the increased complexity of calculating the psychrometric constant γ using Eq. 3.8 (and in turn invoking Eqs 3.3 for atmospheric pressure P, 3.4 and 3.5 for air density ρ, 3.12 and 3.13 for specific heat capacity c_p and 3.10 for specific latent heat of vapourization L_v), this calculation method was preferred.

3.2.5 Calculation of water vapour pressure deficit, relative humidity, absolute humidity, dew point temperature, mixing ratio, specific humidity, mole fraction of water vapour and equivalent temperature

3.2.5.1 Introduction

Many terms have been used for expressing the "humidity" of an atmosphere. This situation has probably arisen because no single quantity has been found suitable for all purposes. It is therefore necessary to be aware of the terms used, how they are calculated and how to interconvert from one calculated term to another.

3.2.5.2 *Vapour pressure deficit and relative humidity*

The water vapour pressure deficit δe (kPa) is defined as $e_s - e$ (kPa) and the relative humidity (%) as $100 \times e/e_s$ where e_s is defined by Eq. 3.14 or 3.14a. The water vapour pressure is calculated using Eqs 3.6, 3.7 and 3.8 for the corresponding psychrometric constant.

Once the vapour pressure e and saturation vapour pressure e_s are calculated, it is a simple matter to calculate their difference or their ratio. Note that both relative humidity and the water vapour pressure deficit are not unique functions of dry bulb temperature in that a greater vapour pressure deficit or relative humidity does not imply a greater water vapour pressure unless the dry bulb temperatures are identical. Hence, it is not correct to compare relative humidity or water vapour pressure deficit for different sites and then to draw conclusions based on the differences between them; conclusions should be based on water vapour pressure or vapour density comparisons.

3.2.5.3 *Absolute humidity*

The calculation of the density of water vapour or the absolute humidity ρ_w is based upon the ideal gas law applied to water vapour: $e\,V = n\,R\,T$ where e (Pa) is the water vapour pressure for a given volume V (m^3) and temperature T (K) and n (mol) is the amount of substance ($= M/M_w$ where M is the mass of water vapour). Hence:

$$e = M\,R\,T/(M_w\,V) = (M/V)\cdot R\,T/M_w = \rho_w\,R\,T/M_w$$

where ρ_w is the density of water vapour (kg m^{-3}), commonly referred to as the absolute humidity. Hence

$$\rho_w = M_w\,e/RT = M_w\,e/[R\,(T_d + 273.15)] = 2.166735\times10^{-3}\cdot e/(T_d + 273.15) \qquad 3.20$$

where T_d (°C) is the dry bulb temperature.

3.2.5.4 *Dew point temperature*

As mentioned previously, the dew point temperature T_{dp} (°C) is uniquely determined by the atmospheric water vapour pressure e (Pa) (Fig. 3.2). Since the dew point temperature is the temperature at which condensation occurs without the addition of water vapour, an expression for the dew point may be obtained by substituting e for e_s and T_d for T_{dp} in Eq. 3.14 and then solving for T_{dp}:

$$T_{dp} = -273.16 + [273.16 - 2.0765067\cdot\ln(e/610.8)]/[1 - 0.0579059\cdot\ln(e/610.8)]. \qquad 3.21$$

3.2.5.5 *Mixing ratio*

In a system containing dry air and water vapour, the mixing ratio r is the ratio of the mass of water vapour to the mass of dry air in kg kg^{-1}. Since the water vapour has a pressure e and the dry air a pressure of $P - e$, it can be easily shown, using the ideal gas law, that:

$$r = (M_w/M_d)\,[e/(P - e)] = \varepsilon\,[e/(P - e)]. \qquad 3.22$$

The mixing ratio r is therefore calculated from the water vapour pressure e and the atmospheric pressure P. If the water vapour pressure is insignificant in comparison to the atmospheric pressure P, then:

$$r \approx \varepsilon\, e/P. \tag{3.22a}$$

3.2.5.6 Specific humidity

In a system containing dry air and water vapour, the specific humidity q is the ratio of the mass of water vapour to the mass of air (that is, dry air and water vapour) in kg kg^{-1}. For a given water vapour pressure e and atmospheric pressure P, it can be shown, using the ideal gas law that:

$$q = \varepsilon\, e/[P + e\,(1 - \varepsilon)] = 0.6219807\, e/(P + 0.37802\, e). \tag{3.23}$$

It is therefore a simple matter to calculate the specific humidity q given the water vapour pressure e and the atmospheric pressure P. If the water vapour pressure is insignificant compared to the atmospheric pressure P, then:

$$q \approx \varepsilon\, e/P \approx r. \tag{3.23a}$$

However, there is greater error in this equation in neglecting e compared to neglecting e in the corresponding expression for r.

3.2.5.7 Mole fraction of water vapour

The so-called mole fraction[6] of water vapour, symbol w (mmol mol^{-1}) is simply the ratio of the partial water vapour pressure to the total atmospheric pressure:

$$w = 1000\, e/P \tag{3.23b}$$

where the factor of 1000 is to account for the mmol mol^{-1} = 10^{-3} mol mol^{-1} unit used. Using the Universal gas equation, one may show that

$$w = 1000\, \rho_w/\rho$$

where ρ_w is the density of water vapour (Eq. 3.20) and ρ is the total density of air (Eq. 3.4). A direct measure of the mole fraction of water vapour (and carbon dioxide) is obtained using infra-red gas analysers (as in the case of the LI-COR 6262).

3.2.5.8 Equivalent temperature

Equivalent temperature θ (K) is defined by:

$$\theta = T + e/\gamma \tag{3.24}$$

where T (K) = T_d (°C) + 273.15 and e (kPa) is the water vapour pressure. The intersection between wet and dry bulb temperatures of the psychrometric chart defines the water vapour pressure e (Fig. 3.2). From calculus, and noting that the wet bulb line is a straight line with slope γ (Eq. 3.8), we know that the slope of a line is defined by dy/dx so that $dx = dy/slope$. In other words, e/γ represents the increase in the dry bulb temperature T if all the water vapour condensed at constant pressure, the latent heat released being used to heat the air and increase T by e/γ to the equivalent temperature $\theta = T + e/\gamma$ (Fig. 3.2). So the equivalent temperature θ is the intersection of the wet bulb temperature line with the x-axis

6 This term does not comply with the SI system in that more correctly it should be referred to as the amount of substance fraction since the mol is the SI unit for the amount of substance

(corresponding to $e = 0$ kPa). The elegance of the equivalent temperature θ is that it allows e to be treated as a temperature (by dividing by γ) and combined with the dry bulb temperature (expressed in K) and then the two treated as one temperature entity θ. Expressions involving the equivalent temperature θ will be used to reject Bowen ratio data. The quantities equivalent temperature θ, psychrometric constant γ and $\Delta = de_s/dT_d$, are depicted in Fig. 3.2.

3.2.6 Derivation of the data rejection criteria equation

The Bowen ratio method of calculating the latent heat flux density $L_v F_w$ (Eq. 2.18) cannot be used when the Bowen ratio β approaches -1.

Following Ohmura (1982), we derive expressions for the objective rejection of Bowen ratio data associated with the Bowen ratio β approaching -1. We will then show a much more elegant method of obtaining the same result but in terms of the equivalent temperature θ (Eq. 3.24, Fig. 3.2). Ohmura (1982) used specific humidity q (Eq. 3.23) instead of water vapour pressure, definings the Bowen ratio using $\beta = \gamma\, \delta T/\delta q$ where δT is the measured air temperature difference between levels z_2 and z_1 and δq is the corresponding measured specific humidity difference.

Suppose that δT and δe are the respective measured profile air temperature and water vapour pressure differences. If the resolution limits of the air temperature and hygrometer sensors is $E(T)$ and $E(e)$ respectively, then the true profile air temperature difference dT must fall between the two limits:

$$\delta T - 2\,E(T) < dT < \delta T + 2\,E(T) \qquad 3.25$$

and that for the profile water vapour pressure difference being given by:

$$\delta e - 2\,E(e) < de < \delta e + 2\,E(e). \qquad 3.26$$

Converting Eqs 3.25 and 3.26 into similar units (K) by multiplying Eq. 3.25 by c_p and Eq. 3.26 by $\varepsilon\, L_v/P$ and adding yields:

$$c_p[\delta T - 2E(T)] + (\varepsilon L_v/P)[\delta e - 2E(e)] < c_p dT + (\varepsilon L_v/P)\, de < c_p\,[\delta T + 2E(T)] + (\varepsilon L_v/P)[\delta e + E(e)]. \qquad 3.27$$

When the Bowen ratio $\beta = \gamma\, dT/de = (c_p\, P/\varepsilon\, L_v)\cdot dT/de$ equals -1, $c_p\, dT + L_v\, dq = 0$ in terms of specific humidity q or $c_p\, dT + (\varepsilon\, L_v/P)\, de = 0$ in terms of water vapour pressure e. [By considering what is referred to as a pseudoadiabatic[7] process at constant pressure (a process used in meteorology), Byers (1974) shows that $c_p\, dT + L_v\, dq = 0$. Hence, since $\beta = -1$ is equivalent to $c_p\, dT + L_v\, dq = 0$, the conditions under which $\beta = -1$ are pseudoadiabatic and isobaric.]

Dividing Eq. 3.27 through by c_p and subtracting δT from all terms yields:

7 The adiabatic process is defined as one in which no heat energy is added or removed

$$(\varepsilon L_v/c_p P)\,[\delta e - 2\,E(e)] - 2\,E(T) < -\delta T < (\varepsilon L_v/c_p P)\,[\delta e + 2\,E(e)] + 2\,E(T)$$

$$\text{or } -(\varepsilon L_v/c_p P)\,[\delta e + 2\,E(e)] - 2\,E(T) < \delta T < -(\varepsilon L_v/c_p P)\,[\delta e - 2\,E(e)] + 2\,E(T)$$

$$\text{or } -(1/\gamma)\,[\delta e + 2\,E(e)] - 2\,E(T) < \delta T < -(1/\gamma)[\delta e - 2\,E(e)] + 2\,E(T)$$

$$\text{or } -2\,E(e)/\gamma - 2\,E(T) < \delta\, e/\gamma + \delta T < E(e)/\gamma + 2\,E(T) < 2\,E(e)/\gamma + 2\,E(T)$$

$$\text{or } -2\,E(\theta) < \delta e/\gamma + \delta T < 2\,E(\theta). \qquad 3.28$$

where $\delta e/\gamma + \delta T = \delta\theta$.

There is a much more elegant method of deriving Eq. 3.28 that has not been previously considered. Consider the profile difference in the equivalent temperature $\theta = T + e/\gamma$ where $d\theta = dT + de/\gamma$ is the true profile equivalent temperature difference. We assume that the difference between the measured profile equivalent temperature difference $\delta\theta$ and the true profile equivalent temperature difference $d\theta$ is less than twice the resolution limit in equivalent temperature $E(\theta)$:

$$|\delta\theta - d\theta| < 2\,E(\theta) \qquad 3.29$$

$$\text{where } E(\theta) = E(T) + E(e)/\gamma. \qquad 3.30$$

It can easily be shown that if $\beta = \gamma\, dT/de = -1$, then

$$d\theta = 0. \qquad 3.31$$

This condition implies that the equivalent temperature is the same at both levels in the atmosphere. Substituting $d\theta = 0$ into Eq. 3.29 and expanding, we get:

$$-2\,E(\theta) < \delta\theta < 2\,E(\theta)$$

where the measured profile equivalent temperature difference $\delta\theta = \delta T + \delta e/\gamma$.

Hence:

$$-2\,E(\theta) < \delta T + \delta e/\gamma < 2\,E(\theta)$$

or the limits of the measured profile temperature difference being defined by:

$$-\delta e/\gamma - 2\,E(\theta) < \delta T < -\delta e/\gamma + 2\,E(\theta). \qquad 3.32$$

These expressions will be employed as data rejection criteria.

3.3 Data collection, handling and processing

3.3.1 Introduction

The calculation of flux densities of sensible and latent heat from the Bowen ratio data requires several steps of processing. These steps include developing and writing the data manipulation parameter files, error-checking and verifying the data and the calculations, and finally, documenting the procedure. A number of decisions in terms of the periods for which data, and what variable, would be included and excluded had to be taken prior to intensive data processing.

The datalogger used in the measurement of Bowen ratio data was programmed to periodically save its final memory storage to tape in 512 final storage location units. A Bowen ratio information card

(Appendix 1) was used to facilitate instrumentation checks during field visits Initially, weekly visits to the site were frequent enough to download final memory to computer disk with some overlap of the data from the previous download. Thus the tape storage was used as a back up only. But when additional sensors, and measurements, particularly standard deviation outputs were added to final storage memory requirements, tape dumps were more frequent due to the increased amount of data. Considerable gaps occurred in the data downloaded weekly to computer disk using TELCOM (as discussed by Mottram *et al.* 1991) although it was all saved to tape. It thus became more efficient to extract the data from tape alone, rather than try to "patch in" the missing data periods from tape.

The raw data were extracted from cassette tape with the Campbell Scientific[8] PC208 TAPE software and the PC201 card inserted in an IBM compatible Personal Computer and connections designed specifically for data transfer. The data were then merged into large input files for use in the PC208 software: SPLIT (version 4.4, last update received in early 1991). These files were then temporarily saved onto computer virtual memory disk to facilitate processing. The SPLIT parameter files request the following information and are of the form:

```
Name/s of input DATA FILE(s):
Name of OUTPUT FILE to generate:
START reading in :
STOP reading in :
SELECT element #(s) in :
COPY from :
HEADING for report:
VARIABLE names:
```

The 'OUTPUT FILE' may be followed by switches to control the format of the output file and the method of reporting blank, missing and out-of-range data. The 'START reading in' and 'STOP reading in' lines can be set to begin and end data processing at the required points. The 'COPY from' line can be used to select out certain periods such as times of day while the 'SELECT element #(s) in' line is where processing takes place. Boolean algebra can be incorporated into most of the lines so as to be able to accomplish all the required tasks. 'HEADING for report' and 'VARIABLE names' are used to facilitate identification of the columns as they move up the screen during processing.

As a check on both the value of any variable and its correct placement in the selection procedure, ranges of allowable values were set in the 'SELECT element #(s) in' line. These ranges were set to defined limits, just greater than the probable, allowable and expected values. As an extra check, these range-checks were carried out at more than one stage (**Table 3.4**). In the calculation of daily totals, a simple algorithm was developed to check the integrity and continuity of each day's data. The day (DAY) and time of day (TOD) columns were used so that if any data periods were missing or extra, a number other than the integer pertaining to the correct Day would be reported. Any out of range measurements (±6999 for low resolution voltage measurements and ±9999 for high resolution), were

8 The PC201 card and TAPE program as well as the PC208 suite of software (which includes TELCOM, SPLIT and TERM) are marketed commercially by Campbell Scientific Inc. The mention of proprietary products here and elsewhere is for convenience of the reader and does not imply endorsement or otherwise by the Water Research Commission, the University of Natal, the FRD or the CSIR (Environmentek)

Table 3.4 The ranges of the various parameters used in the SPLIT parameter files were set to their defined limits, just greater than the probable, allowable and expected values. As an extra check, these range-checks were carried out at more than one stage

Variable Name	Allowable Range	Units	Pass
D	1..366		0 2 4 5
TOD	0500..1900	100 h + min	0 2
TOD	0600..1800	100 h + min	4
TOD	1000..1600	100 h + min	5
T_{lower}	-20..50	°C	0 2 4
$T_{diff} = T_{lower} - T_{upper}$	-5..5	°C	0 2
e_{lower}	0.01..5	kPa	0 2
e_{upper}	0.01..5	kPa	0 2
$e_{lower} - e_{upper}$	-5..5	kPa	2
I_{net}	-50..1200	W m^{-2}	0 2
SHF1 and 2	-50..100	W m^{-2}	0 2
G	-200..200	W m^{-2}	4
dT_s	-2..3	°C	0 2
θ_m	0.1..0.99	kg kg^{-1}	2
I_s^*	0..1400	W m^{-2}	2 4
Wind speed	0..10	m s^{-1}	2 4
Wind direction	0..360		2 4
Precipitation	0..50	mm	2 4
K_h, K_w**	0..5	m^2 s^{-1}	4
β	-20..25		5
Equilibrium $(L_v F_w)_{equilibrium}$	-500..1200	W m^{-2}	3 4
$L_v F_w$	-500..1000	W m^{-2}	4
F_h	-400..800	W m^{-2}	4

*A maximum of 1400 W m^{-2} for solar irradiance is to allow for such values when partly cloudy conditions result in direct and significant scattered irradiance

**The exchange coefficients cannot be negative unless countergradient flux densities occur also blanked during the course of processing. This proved to be the appropriate stage to add a 'SELECT element #(s) in' condition to select only data from 05h00 to 18h00 inclusive and thus save on processing time and computer disk space.

3.3.2 Description of split parameter files

3.3.2.1 Pass 0

The first pass using the software SPLIT uses a parameter file designed to collate the two arrays (the output of tables one and two of the datalogger), and output them to a file consisting of single arrays. As the logger outputs to final storage from both datalogger program tables 1 and 2 under normal conditions, the data is output into two consecutive arrays each with its own identifier preceded by '1' or '2', and then a figure indicating the program number in which the output flag occurred, eg. 110 and 217 (110 for program table 1 and tenth program step and 217 for program table 2 and 17 th program step). When changes are made to the datalogger program, these output array identifiers automatically change. To avoid missing any periods of data when selecting arrays, due to the value of the identifier, ranges of 100..199 and 200..299 were used in the "COPY from" line of the parameter file. An output from datalogger program table 3 of the logger only occurs when the battery voltage decreases below the minimum of 11.75 V when a report of the date and time of the system shutdown is output. After alleviation of early battery and solar-panel problems with an overnight power-saving time-switch, few such events recurred. We used 40 W solar panels to minimize the number of battery interchanges and voltage drops.

3.3.2.2 Pass 1

Pass 1 utilizes the time-synchronization capacity of SPLIT to combine the raw Bowen ratio data with soil water content data and weather data. Overlapping files were correctly merged, and Day and TOD identifiers placed where periods of missing data or files occurred. A complete, uninterrupted array is ensured with this facility. Soil water content θ_m samples taken up to twice a week and interpolations between points, taking precipitation events into account, were made. In the preparation of the θ_m data, it is calculated in and exported from a spreadsheet by printing to a file. This file must first be edited to remove blanks and separate data points by commas before it can be read in by SPLIT as SPLIT requires all the input files in one pass to have the same format. This was most easily accomplished using an ASCII wordprocessor such as Xywrite. The weather data were treated in a similar manner in its preparation.

3.3.2.3 Pass 2

This step was only used where correction of the raw data were required such as a few occasions of incorrect calibration factors (mainly for the net radiometers). This involved a simple multiplication of one variable between the 'START reading in' and 'STOP reading in' conditions. For example the calibration factor for the UNP net radiometer used in the datalogger program was, for a short period incorrectly entered as 11.89 W m^{-2} mV^{-1}, instead of the correct value of 11.4 W m^{-2} mV^{-1}. A correction factor (11.4/11.89 = 0.9588) was used to correct this error. In this regard, for net radiometers, it is advisable to use the −500 to 500 mV with the datalogger voltage resolution set to high in order to prevent out-of-range voltages. This range will encompass all season net irradiances.

The output of this step can theoretically replace the raw data, as nothing has been lost, but the overlaps have been eliminated, the corrections have been made and the data in large files complete with the measured mass soil water content θ_m and weather data ready for processing.

3.3.2.4 Pass 3

In Pass 3 the output files of Pass 2 are used to efficiently and accurately calculate the Bowen ratio and shortened energy balance components including the amount of evaporation in W m^{-2}. Initially, Pass 3 required the specification of the θ_m measured in the soil layer 20 to 60 mm. This meant that for each period of constant water content, individual runs were required resulting in a large number of small output files, each corresponding to the short periods for which the water content was assumed to hold. The periods were usually 3 to 4 days or however infrequently the water content was measured, but the inclusion of 20 minute calculated θ_m values in Pass 1 circumvented this problem.

Failure to take account of the water vapour pressure, atmospheric pressure and air temperature dependence of the psychrometric constant, γ, can cause considerable error in the calculation of the Bowen ratio (some of the dependence reported by Revfeim and Jordan 1976) as shown by Fig. 3.5. These errors are large if the water vapour pressure deficit is large. The dependency of the psychrometric constant γ on air temperature and altitude and therefore atmospheric pressure and water vapour pressure was incorporated by calculating γ for each 20 min period (using Eq. 3.8). The actual psychrometric "constant" $\gamma = c_p P / \varepsilon L_v$ was used where ε is the ratio of the molecular mass of water to that of dry air = M_w/M_d = 0.01801534 kg mol^{-1}/0.028964 kg mol^{-1} = 0.6219807. The specific heat capacity of air at constant pressure, c_p (kJ kg^{-1} K^{-1}) was corrected for water vapour pressure e and atmospheric pressure P which in turn is dependent on altitude, latitude and air temperature using Eqs 3.12 and 3.13.

For an altitude of 1.935 km and an air temperature of 20 °C, c_p varies from 1000 to 1100 J kg^{-1} K^{-1} with e varying from 0 to 2.5 kPa. These values are −1 to 8.1 % different from the value most often quoted for sea-level ambient temperatures of 1.01 kJ kg^{-1} K^{-1} (Fig. 3.4).

To increase the accuracy of the value of the specific latent heat of vaporization of water (L_v) by including the dependency on air temperature, Eq. 3.10 was used. At 20 °C this yields a value of 2453.61 kJ kg^{-1}. The psychrometric constant at 20 °C for an altitude of 1935 m varies from 46.5 to 48.5 Pa K^{-1} as e varies from 0 to 2.0 kPa (a less than 5 % difference). However, with the water vapour pressure varying between 0 and 2.0 kPa and air temperature between 0 and 40 °C, the psychrometric constant varies from 44.8 to 50 Pa K^{-1} (a 11.6 % difference) which then corresponds to a 11.6 % difference in the Bowen ratio $\beta = \gamma\, \delta e / \delta T$. These sorts of error magnitudes could not be ignored, necessitating correction of the so-called "constants" for altitude, air temperature and water vapour pressure.

3.3.2.4.1 Calculation of equilibrium evaporation

The equilibrium evaporation $(L_v F_w)_{equilibrium}$ (designated *EQ* in the SPLIT parameter pass files) amount was calculated using the independent air temperature T_{air} from the weather data, but using the Bowen ratio net irradiance and soil heat flux density measurements.

Priestley and Taylor (1972) found that actual evaporation from oceans, bare soil and vegetation was about 26 % greater than $(L_v F_w)_{equilibrium}$:

$$(L_v F_w)_{Priestley\text{–}Taylor} = 1.26\, (L_v F_w)_{equilibrium} = 1.26\, [\Delta/(\gamma + \Delta)]\cdot(I_{net} - F_s). \qquad 3.33$$

The above corrections and calculations required the extraction of the lower water vapour pressure

e_{low}, and the lower air temperature T_{low} from the raw data. The Pass 0, 1 and 2 parameter files were modified to carry the lower air temperature, water vapour pressure and the various "constants" through each pass to allow for calculation of the adjusted constants and equilibrium evaporation amounts for each 20 min time period.

3.3.2.4.2 The rejection criteria for the exclusion of out-of-range and "bad" or doubtful data

Values of the Bowen ratio β near sunrise and sunset often approached −1 due to F_h downward approaching the upward $L_v F_w$ as the net irradiance diminishes and the available energy approached zero. The result is that the calculated value of $L_v F_w$ first approaches infinity and then becomes undefined as the denominator of:

$$L_v F_w = (I_{net} - F_s)/(1 + \beta), \qquad 3.34$$

$$\text{namely } 1 + \beta \to 0.$$

Interestingly, $1 + \beta \to 0$ implies a constant equivalent temperature $\theta = T + e/\gamma$ at the two levels (Eq. 3.31). Results calculated from data within the range $-1.25 \le \beta \le -0.75$ should be carefully screened and those that are spurious should be rejected. This process is tedious and subjective when carried out manually. A further consideration at this stage is whether the resolution of the sensors has been exceeded. When the vapour pressure difference decreases below the 0.01 kPa dew point mirror sensor resolution of the system, the data for that time is considered inconclusive and should be rejected. Similarly, if the air temperature difference decreases below the fine wire thermocouple sensor resolution of 0.001 °C then these periods are not suitable for processing. All of the above criteria were combined in a method used by Ohmura (1982) which we applied for the routine checking of all the data used in Pass 3. The resolution thresholds ($\delta T = T_2 - T_1$ and $\delta e = e_2 - e_1$), incorporated into the method have particular relevance to dry periods when β is large, and even the smallest errors in either cause gross errors in $L_v F_w$ (Angus and Watts 1984). The method sets limits to the value that the profile air temperature difference $\delta T = T_2 - T_1$ can assume with respect to the value of the profile water vapour pressure difference $\delta e = e_2 - e_1$ and the instrumental resolution of both these sensors. The argument stems from the mathematical idiosyncrasy that occurs when the Bowen ratio is in the region of −1 with the available energy $L_v F_w + F_h = I_{net} - F_s \to 0$. At these times, usually in the early morning and evening periods, evaporation is generally low (except under berg or foehn advective conditions). Under these conditions physically inconsistent, and therefore extremely inaccurate and impossibly large positive and negative fluxes are calculated. Simply disregarding Bowen ratio (β) values between arbitrarily chosen values of −1.25 and −0.75 will to some extent remedy the problem. However, the more sensitive and dynamic approach proposed by Ohmura (1982) decreases the amount of data previously excluded unnecessarily, and prevents any rogue values escaping detection.

For this purpose, an upper and lower limit to the value that $\delta T = T_2 - T_1$ can hold before β will be likely to be in the region of −1 is calculated (as per the derivation of Eq. 3.32).

The saturation value of the water vapour pressure e_s at the temperature recorded for that time period is also found.

3.3.2.4.3 The calculation of the exchange coefficients for sensible and latent heat energy

Exchange coefficients for the sensible and latent heat fluxes (K_h and K_w) were calculated using the measured gradients in temperature and humidity and flux densities in sensible and latent heat. The constants of air density, specific heat capacity and psychrometric constant were calculated as far as possible according to the environmental information available for each 20 min interval between 10h00 and 16h00. Identical K values are calculated from both of the constituent equations:

$$K = K_h = F_h/(\rho\, c_p) = K_w = L_v\, F_w\, \gamma/(\rho\, c_p) \quad 3.35$$

(where $K = K_h = K_w$ as calculated by this method). Once they were verified to be identical, only one was calculated.

3.3.2.5 Setting rejection tags

The output of Pass 3 was imported into a standardized Quattro Pro (version 3.02, 3.01 or higher) spreadsheet where the lower and upper limits were compared against the $\delta T = T_2 - T_1$ value and a rejection tag set. The water vapour pressure e was similarly compared to the saturation value e_s corresponding to the average of the two fine wire thermocouple temperatures for that time period and another rejection tag set if the absurd condition $e > e_s[(T_1 + T_2)/2]$ was found to be true. These two tags further were compared and a third tag set to indicate whether none, one or both (and then which) rejection criterion was responsible for that rejection. Finally, the data now with the three tags was exported from the spreadsheet for use in Pass 4. If the data were to be rejected, the first of the two tags exported would be equated to the numeric value 9999, and 1 if accepted.

3.3.2.6 Pass 4

In order to calculate daily totals, averages and standard deviations of the variables for differing durations, SPLIT required the separation of data into files with common durations. Thus all those variables to be totalled for the entire day were selected out. All the variables were multiplied by the first rejection tag (1 or 9999), this would ensure that all the variables were out of range if they were to be rejected, and not affect those that were accepted.

3.3.2.7 Pass 5

The variables that required longer morning periods to stabilize before averaging or integration could be performed on them, such as the Bowen ratio and the exchange coefficients, were selected out in this step. The interval from 10h00 to 16h00 was chosen, and the variables were, as in the previous pass, multiplied by the rejection tags of 9999.

3.3.2.8 Pass 6

The "F option" in SPLIT, when utilized in the 'STOP reading in' line, triggers vertical processing on selected elements as used in this step. Totals, averages, maxima, minima, standard deviations and other scientific functions may be performed on the elements. The calculation of daily totals of net irradiance I_{net}, solar irradiance I_s, $L_v F_w$ and F_h are easily performed using the appropriate constants to attain the required total daily units of either MJ m^{-2} or mm (of water).

3.3.2.9 Pass 7

The time-series processing is again used to calculate the daily values, and is triggered at the end of the short-day, that is at 16h00.

3.3.2.10 Pass 8

In the final stage of processing the time-synchronization facility was again used to recombine the two sets of daily totals into one array.

3.4 The sensitivity of Bowen ratio calculations to the variables soil water content θ_m and the psychrometric constant

3.4.1 Soil water content

The role of soil water content on the surface energy balance is *via* the calculation of the soil heat flux density $F_s = G + S$ where G is the measured soil heat flux density at a depth of 80 mm and S is the above-plate stored heat flux density (Fig. 2.12, Eqs 2.31 to 2.33).

The effect of changing the water content on the ultimate calculation of $L_v F_w$ was examined for a set of data with parameter files differing only in the soil water content parameter. This was changed from the actual value (for a particular period) of 66.8 % to 61.8 % and 56.8 %, representing decreases of 5 and 10 %. The error resultant from using too low a soil water content tends to be an underestimation in $L_v F_w$ and consequent overestimation of F_h, while the opposite is true when too high a water content is used. The results showed that for Day 95 to 100 (1990 data), the 5 % change resulted in less than 1 % error in $L_v F_w$, while the 10 % decrease introduced an error of up to 8 W m^{-2} in the day time $L_v F_w$ values of around 300 to 450 W m^{-2} range. This translates to a worst case error of 3 %. As this is the worst-case scenario in the driest part of the year, the wetter periods of the year are expected to be less sensitive to water content-introduced errors as sensible heat flux density becomes a relatively less important constituent of the energy balance. This viewpoint was supported by Spittlehouse and Black (1980) in their evaluation of the Bowen ratio method under various conditions (*cf.* their Table 2, p. 109). The Bowen ratio, β, was found to decrease below unity towards summer, and thus the contribution of sensible heat flux density decreased in the wet season. This is due to both a greater availability of water to consume the available energy and to the more completely closed canopy resulting in less soil heating. Thus the estimations made of θ_m between measurement periods are justified, and a new θ_m need really only be used after more than a 5 % change was measured.

3.4.2 Effect of not correcting the psychrometric constant for atmospheric pressure, air temperature and water vapour pressure

The effect of using an incorrect atmospheric pressure, which is a component of the psychrometric constant γ (Eq. 3.8), was assessed with a similar sensitivity analysis. Using too high a value underestimated the amount of evaporation since atmospheric pressure P is in the numerator of the equation defining β, and is thus in the denominator of the equation used to calculate $L_v F_w$. The error in assuming a fixed psychrometric constant only corrected for atmospheric pressure (Fig. 3.5), as advocated by Tanner *et al.* (1987) will result in a 19 to 8 % underestimate in β.

What is the effect of assuming an incorrect and fixed psychrometric constant of $\gamma_i = 0.05345$ kPa K^{-1} on the calculations of latent and sensible heat flux density? If $L_v F_w$ is the correct latent heat flux density and $(L_v F_w)_i$ is the calculated value corresponding to the incorrect and fixed psychrometric constant γ_i, then from Eq. 3.34: $I_{net} - F_s = L_v F_w (1 + \beta) = (L_v F_w)_i (1 + \beta_i)$ or

$$L_v F_w = (L_v F_w)_i (1 + \beta_i)/(1 + \beta) \qquad 3.36$$

where β_i corresponds to the Bowen ratio for γ_i. However, from the defining equation for the Bowen ratio:

$$\beta = \gamma \cdot \delta T / \delta e \tag{3.37}$$

$$\text{we see that } \beta_i / \beta = \gamma_i / \gamma$$

$$\text{so that } \beta_i = \beta\, \gamma_i / \gamma. \tag{3.38}$$

Defining the error shown on the y-axis of Fig. 3.5 as $E(\gamma)$, we have

$$\gamma_i / \gamma = (1 - E(\gamma))/100. \tag{3.39}$$

Substituting Eq. 3.39 into 3.38 and the combination into Eq. 3.36, we get:

$$(L_v F_w)_i = L_v F_w \cdot [1 + (1 - E(\gamma))/100]/(1 + \beta). \tag{3.40}$$

Similarly:

$$(F_h)_i = F_h \cdot (1 + 1/\beta)/\{1 + 1/[(1 - E(\gamma)/100) \cdot \beta]\}. \tag{3.41}$$

The ratios $(L_v F_w)_i / L_v F_w$ and $(F_h)_i / F_h$ for Eqs 3.40 and 3.41 respectively are shown as a function of air temperature for various water vapour pressures (**Figs 3.7 to 3.12**). The $(L_v F_w)_i / L_v F_w$ ratio increases with increasing air temperature, Bowen ratio and water vapour pressure (Figs 3.7 to 3.9), corresponding to an overestimation of the actual latent heat flux density $L_v F_w$. By contrast, $(F_h)_i / F_h$ ratio is less than unity and increases in air temperature and water vapour pressure causes the ratio to decrease (Figs 3.10 to 3.12). Increases in the Bowen ratio β causes this ratio to increase towards unity. While the magnitudes of the errors are lower than the errors in γ, they are of a magnitude that necessitate correction particularly so at the higher air temperatures.

3.4.3 Further comments on data rejection

3.4.3.1 Rejection of profile air temperature and water vapour pressure

The inequality specified by Eqs 3.27 or 3.32 defines our rejection procedure where we assume that $E(T) = 0.001$ K and $E(e) = 0.01$ kPa so that $E(\theta) = 0.001 + 0.01/\gamma$ (Eq. 3.30). If the inequality is satisfied then there is a high possibility that the Bowen ratio will be very near -1 and therefore the calculated flux densities will not have numerical meaning. Data fulfilling this inequality should be excluded from evaluation. An intensive examination of data from Cathedral Peak Catchment VI for days between 200 and 218, 1990 showed that the majority of the data during the day were not rejected (**Figs 3.13 to 3.16**) and all rejected datum points had been done so justifiably when checked. The method had the additional benefit of calculating a real daily total thus negating the requirement of calculating daylength and adjusting calculations according to that daylength. The other measured parameters of this period of study are also shown (**Figs 3.17 and 3.18**).

After initial implementation and success with the inequality as a rejection criterion, it was decided that data points not satisfying the inequality on the lower side had to be those when dT was large and negative. This set of circumstances is indicative of inversion conditions, which occur under either nocturnal condensation (dew-fall) or periods of horizontal heat advection. The nocturnal latent energy gains (dew) are not included in daily total evaporation calculations, but advection can nearly double a windless day's water loss. Including such times is of obvious importance. Fortunately, during the nocturnal inversions, the vapour pressure gradient is very small, and the region of rejection small. However, during advective inversions, the magnitude of the water vapour pressure gradient is uncertain and therefore the temperature difference values may not fall inside the rejection limits. Due to these

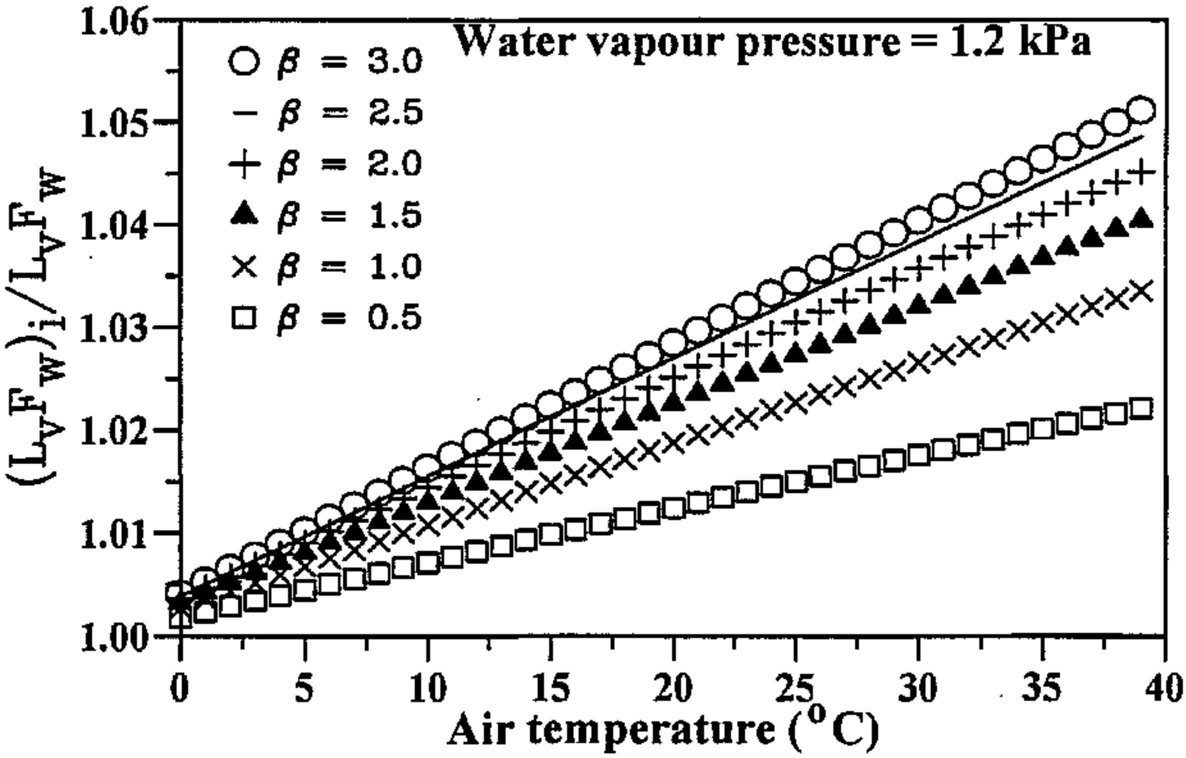

Fig. 3.7 The variation in the ratio $(L_v F_w)_i / L_v F_w$ (Eq. 3.40) as a function of air temperature and actual Bowen ratio β for a water vapour pressure of 1.2 kPa for an altitude of 1935 m; $(L_v F_w)_i$ corresponds to $\gamma_i = 53.45$ Pa K^{-1}

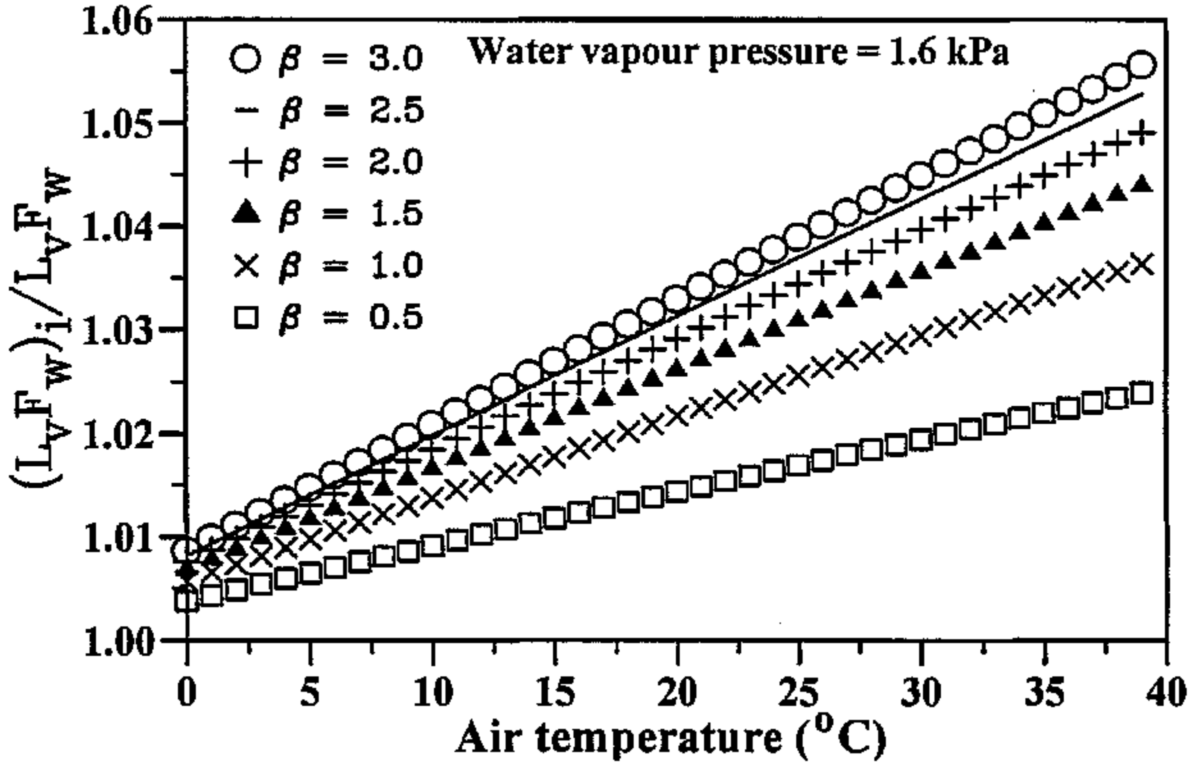

Fig. 3.8 The variation in the ratio $(L_v F_w)_i / L_v F_w$ (Eq. 3.40) as a function of air temperature and actual Bowen ratio β for a water vapour pressure of 1.6 kPa for an altitude of 1935 m; $(L_v F_w)_i$ corresponds to $\gamma_i = 53.45$ Pa K^{-1}

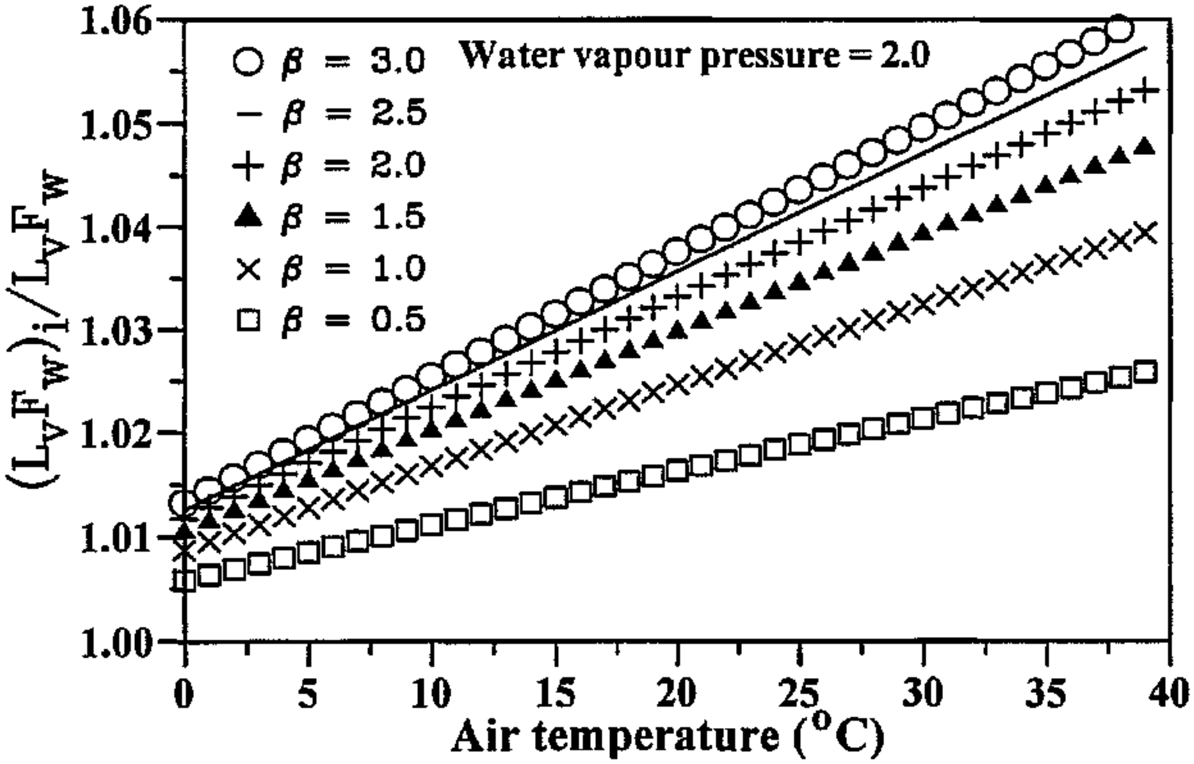

Fig. 3.9 The variation in the ratio $(L_v F_w)_i / L_v F_w$ (Eq. 3.40) as a function of air temperature and actual Bowen ratio β for a water vapour pressure of 2.0 kPa for an altitude of 1935 m; $(L_v F_w)_i$ corresponds to $\gamma_i = 53.45$ Pa K^{-1}

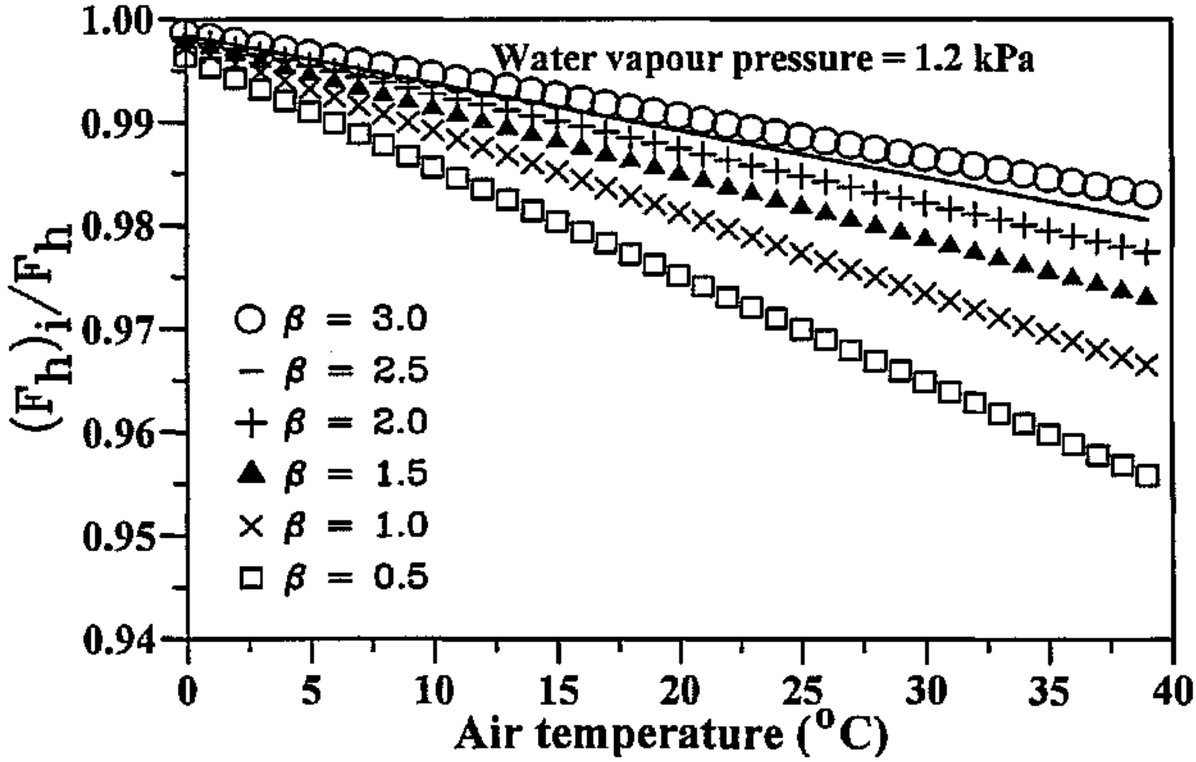

Fig. 3.10 The variation in the ratio $(F_h)_i / F_h$ (Eq. 3.41) as a function of air temperature and actual Bowen ratio β for a water vapour pressure of 1.2 kPa for an altitude of 1935 m; $(F_h)_i$ corresponds to γ_i = 53.45 Pa K^{-1}

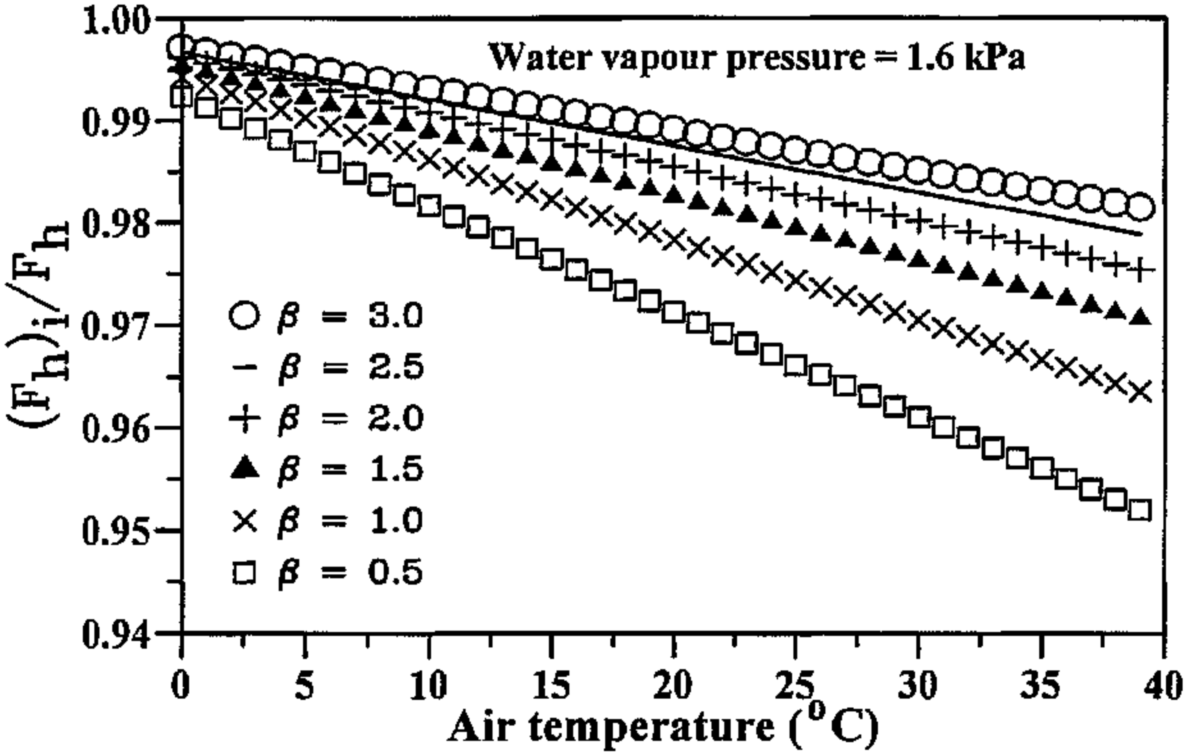

Fig. 3.11 The variation in the ratio $(F_h)_i/F_h$ (Eq. 3.41) as a function of air temperature and actual Bowen ratio β for a water vapour pressure of 1.6 kPa for an altitude of 1935 m; $(F_h)_i$ corresponds to γ_i = 53.45 Pa K^{-1}

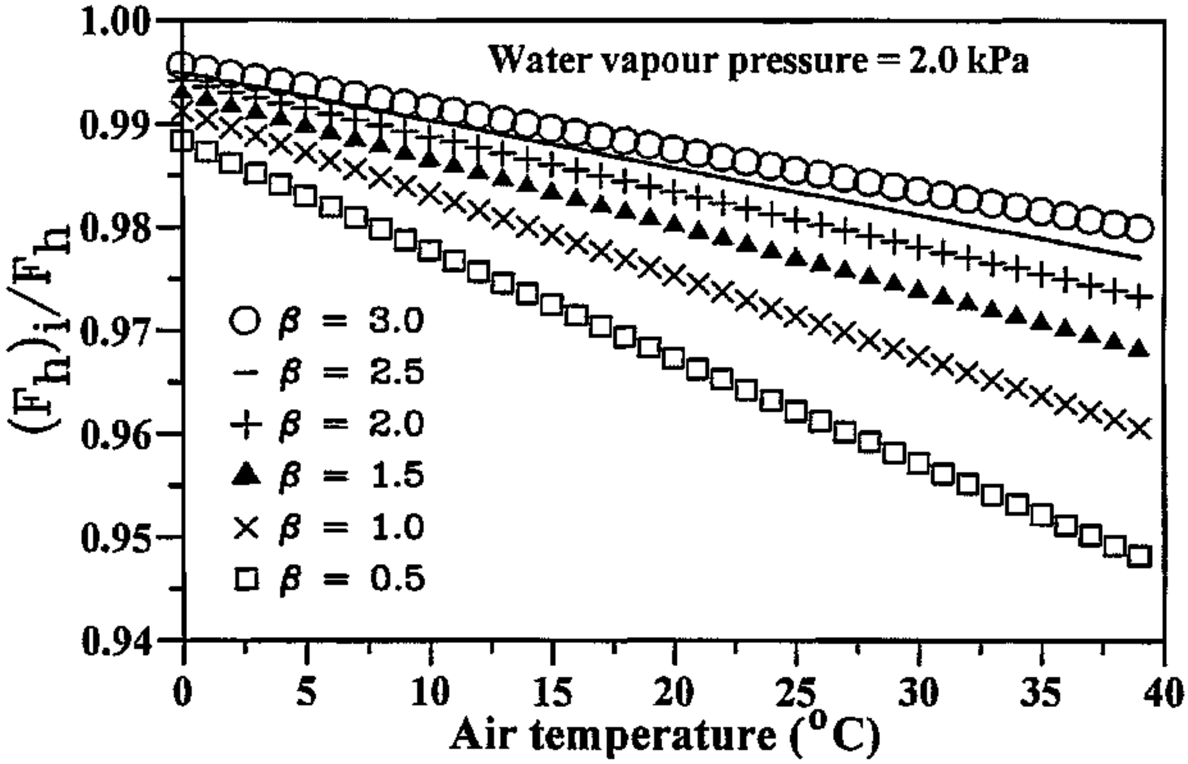

Fig. 3.12 The variation in the ratio $(F_h)_i/F_h$ (Eq. 3.41) as a function of air temperature and actual Bowen ratio β for a water vapour pressure of 2.0 kPa for an altitude of 1935 m; $(F_h)_i$ corresponds to γ_i = 53.45 Pa K^{-1}

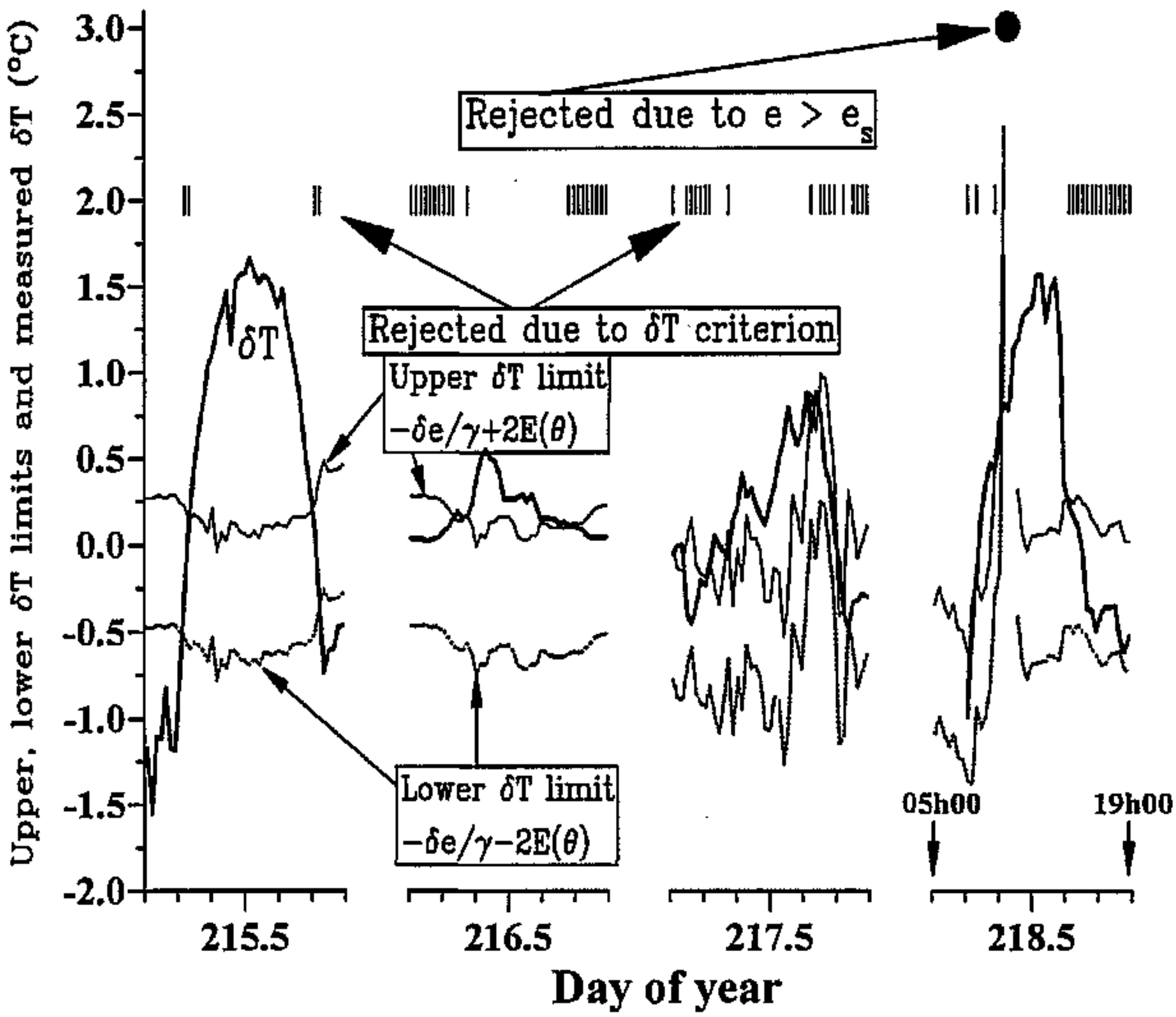

Fig. 3.13 The 20 min variation in δT (K) as a function of day (215 to 218, 1990) for Cathedral Peak Catchment VI for the times 05h00 to 19h00 (each small tick interval is 140 min). The horizontal line corresponding to δT = 3.0 K indicates rejection tags for the absurd condition $e > e_s\ [(T_1 + T_2)/2]$ (usually corresponding to dewfall or rainfall wetting the fine wire thermocouples completely) and the line corresponding to δT = 2.0 K indicates rejection tags for the condition expressed in Eq. 3.32 (viz., that the Bowen ratio β is around −1). The upper limit curve is defined by $\delta T = -\delta e/\gamma + 2\,E(\theta)$ and the lower by $\delta T = -\delta e/\gamma - 2\,E(\theta)$. Rejection of air temperature and water vapour pressure data occurs if δT is within the lower and upper limit

uncertainties, we stipulated the upper limit:

$\delta T < -\delta e/\gamma + 2\,[E(T) + E(e)/\gamma)]$ of the Eq. 3.32 inequality as the rejection criterion.

3.4.3.2 Rejection of single level water vapour pressures and air temperatures

We have noted that under dew or rainfall conditions, with the likelihood that the thermocouples are covered with water and possibly at the wet bulb temperature (see the psychrometric equation defined by Eqs 3.6 to 3.8), the measured water vapour pressure from the dew point mirror system can be greater than the saturation water vapour pressure corresponding to the temperature of the fine-wire thermocouple. If the fine wire thermocouple is measuring the wet bulb temperature $e_s\,(T_w)$ then since $T_w \le T_{air}$, $e_s\,(T_w) \le e_s\,(T_{air})$ allows for the easy automatic rejection of single level water vapour pressures

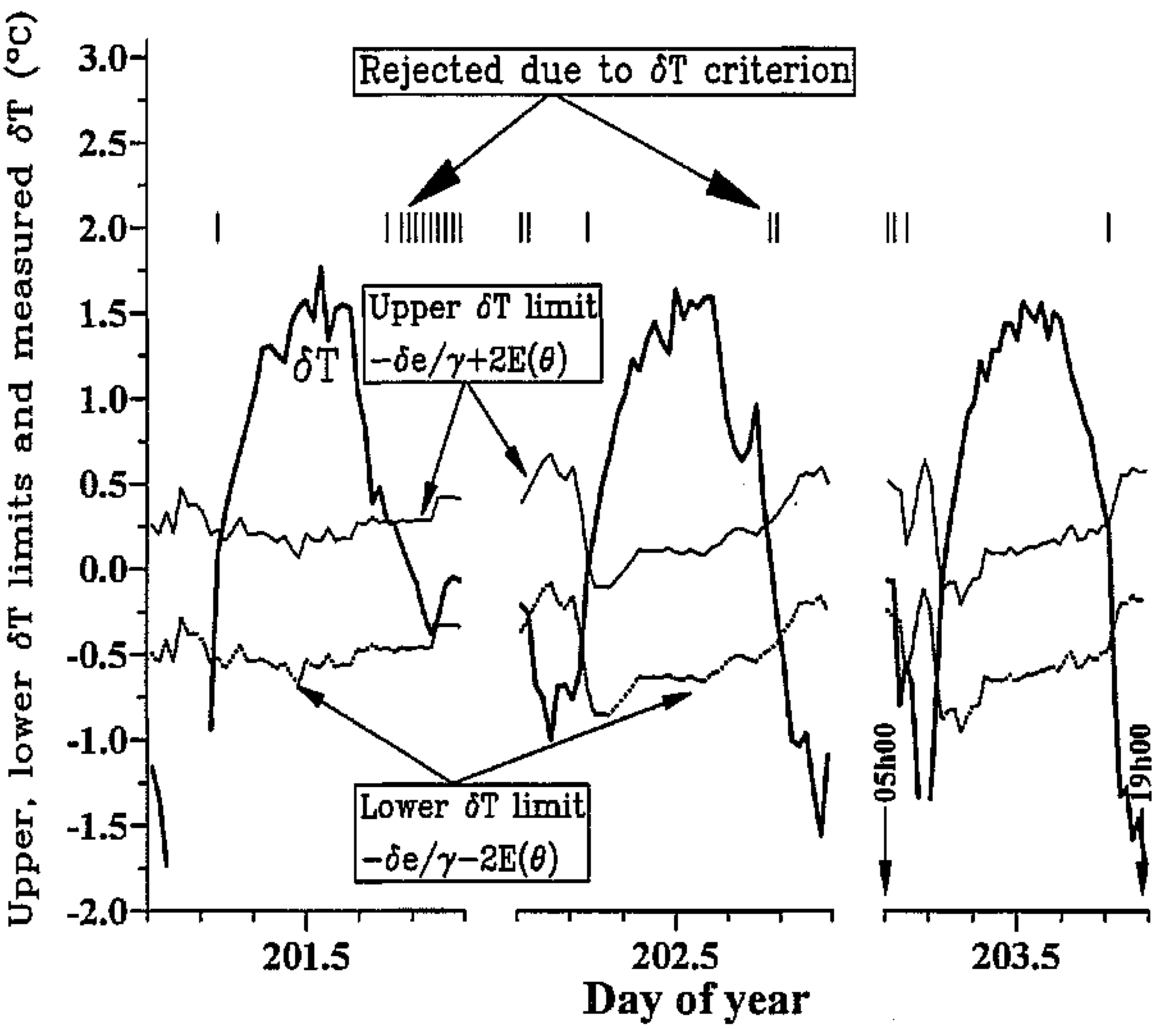

Fig. 3.14 The 20 min variation in δT (K) as a function of day (201 to 203, 1990) for Cathedral Peak Catchment VI for the times 05h00 to 19h00 (each small tick interval is 140 min).. The horizontal line corresponding to $\delta T = 2.0$ K indicates rejection tags for the condition expressed in Eq. 3.32 (viz., that the Bowen ratio β is around -1, usually at early morning and late afternoon times). The upper limit curve is defined by $\delta T = -\delta e/\gamma + 2\,E(\theta)$ and the lower by $\delta T = -\delta e/\gamma - 2\,E(\theta)$. Rejection of air temperature and water vapour pressure data occurs if δT is within the lower and upper limit

and air temperatures. A water vapour preesure e greater than $e_s\,(T_{air})$ when the air is unsaturated at that time indicates a problem with the bias setting of the cooled dewpoint mirror. This situation is referred to as the $e > e_s$ condition in Figs 3.13 to 3.16. The times when the data needs to be excluded, according to these criteria, is infrequent but it is necessary to apply the exclusion criteria (Figs 3.13 to 3.16 but more especially 3.13 and 3.15). The output data of pass 3 were imported to the spreadsheet and tagged with a 1 if $e \le e_s\,(T_{air})$ and 9999 (that is, out of range data) if $e > e_s\,(T_{air})$, exported to a comma-delineated file, with a Pass 5 SPLIT run used to multiply the $e > e_s\,(T_{air})$ vapour pressures and air temperatures by the zero tag to erase the rejected data.

Early on in our evaporation measurement investigation, a loose hose to the dew point mirror of the one Bowen ratio system caused water vapour pressures e to be greater than $e_s\,(T_{air})$. The above

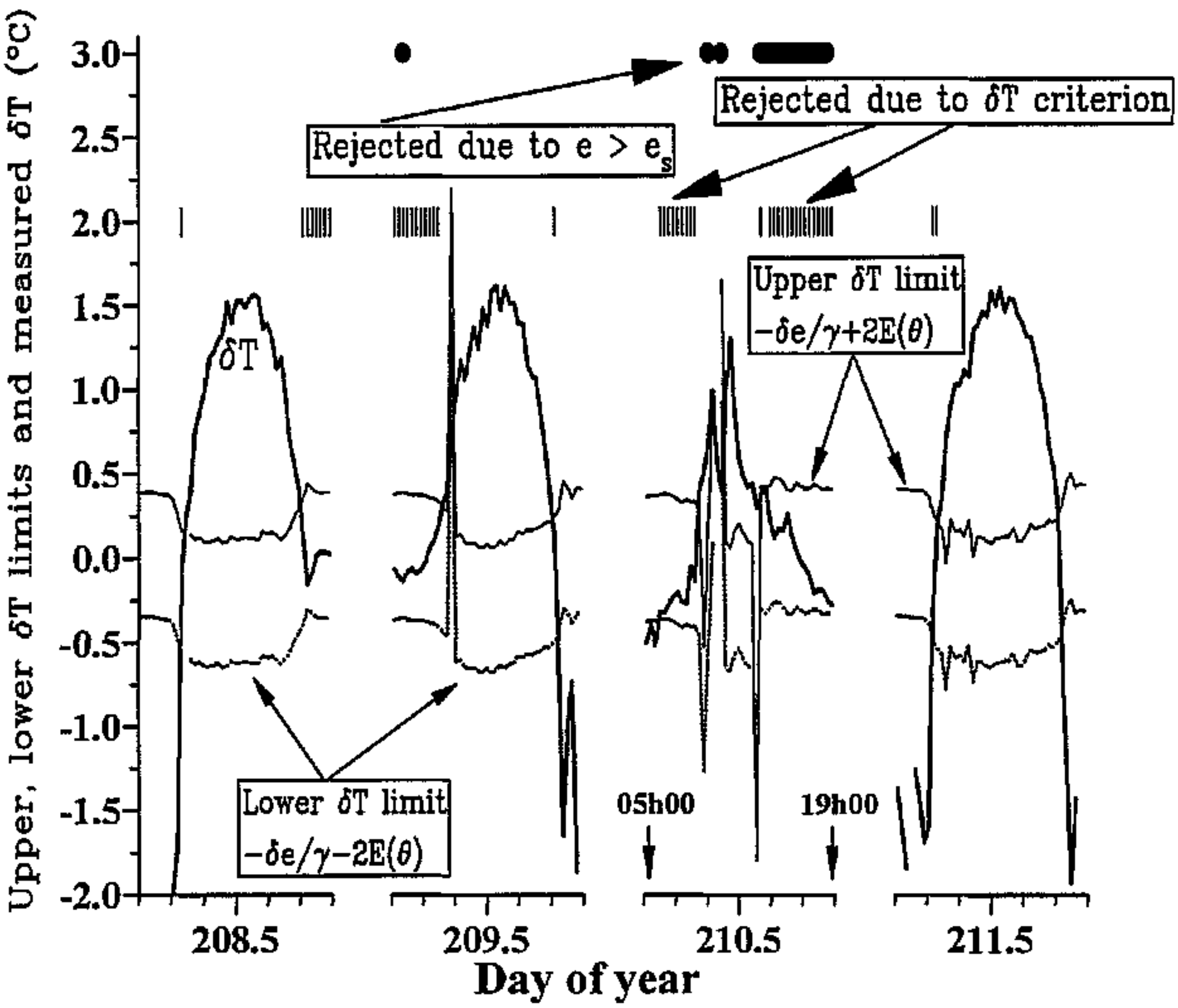

Fig. 3.15 The 20 min variation in δT (K) as a function of day (208 to 211, 1990) for Cathedral Peak Catchment VI for the times 05h00 to 19h00 (each small tick interval is 140 min).. The horizontal line corresponding to δT = 3.0 K indicates rejection tags for the absurd condition $e > e_s$ $[(T_1 + T_2)/2]$ (usually corresponding to dewfall or rainfall wetting the fine wire thermocouples completely). Note the large number of tags for this condition, due to a rainfall event on day 210. The horizontal line corresponding to δT = 2.0 K indicates rejection tags for the condition expressed in Eq. 3.32 (viz., that the Bowen ratio β is around −1). The upper limit curve is defined by $\delta T = -\delta e/\gamma + 2\,E(\theta)$ and the lower by $\delta T = -\delta e/\gamma - 2\,E(\theta)$. Rejection of air temperature and water vapour pressure data occurs if δT is within the lower and upper limit

procedures would have assisted in an earlier identification of the loose hose problem. On another occasion, the electronic bias of the dew point mirror one of the systems and later the other system was being set too infrequently with the result that water continually condensed on the mirror. The system therefore indicated a T_{dp} too high with $e > e_s$ (T_{air}). Again the SPLIT procedures would have assisted in an earlier identification of the incorrect electronic bias setting.

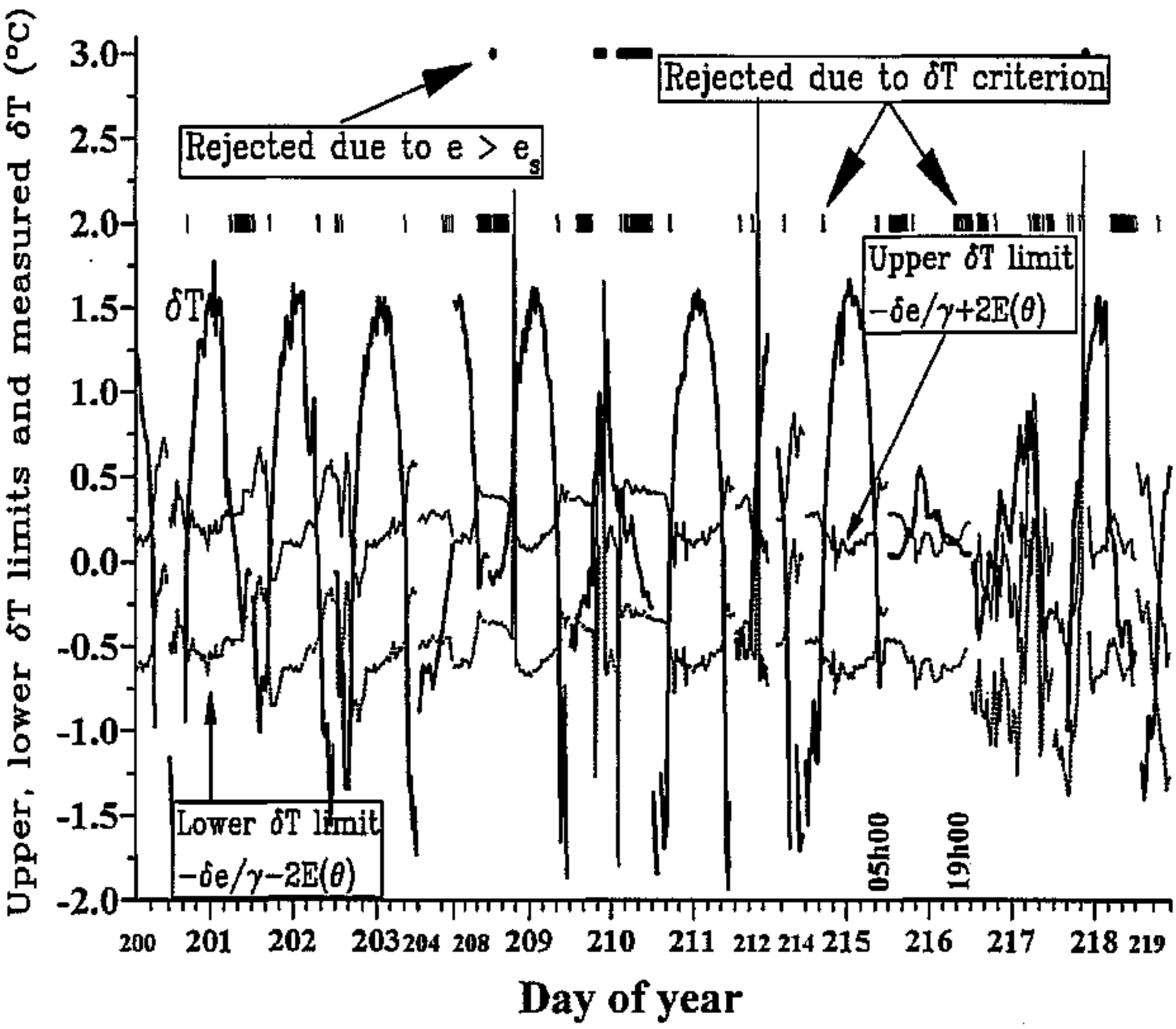

Fig. 3.16 The 20 min variation in δT (K) as a function of day for all days of the period investigated thoroughly (200 to 218, 1990) for Cathedral Peak Catchment VI for the times 05h00 to 19h00 (except for days with incomplete data indicated by a corresponding day number in a smaller typeface). Each day indication corresponds to midday. Each small tick interval is 140 min. The horizontal line corresponding to $\delta T = 3.0$ K indicates rejection tags for the absurd condition $e > e_s\,[(T_1 + T_2)/2]$ (corresponding to dewfall or rainfall wetting the thermocouples). Note the large number of tags, due to a rainfall event, on day 210. The horizontal line corresponding to $\delta T = 2.0$ K indicates rejection tags for Eq. 3.32. The upper limit curve is defined by $\delta T = -\delta e/\gamma + 2\,E(\theta)$ and the lower by $\delta T = -\delta e/\gamma - 2\,E(\theta)$. Rejection of air temperature and water vapour pressure data occurs if δT is within the lower and upper limit

3.5 Data analysis

3.5.1 The use of spreadsheet

Initially, before daily totals were calculated with SPLIT, the QPro spreadsheet was used to manually compute the required numeric data. Firstly, the 20 min output files were organized into manageable sizes of two week periods and imported into a standardized spreadsheet for inspection, modification and storage. Deviations from the expected diurnal patterns showed up clearly in graphic form when a fine enough time scale- usually weekly, was used. Seasonal trends were, however more difficult to

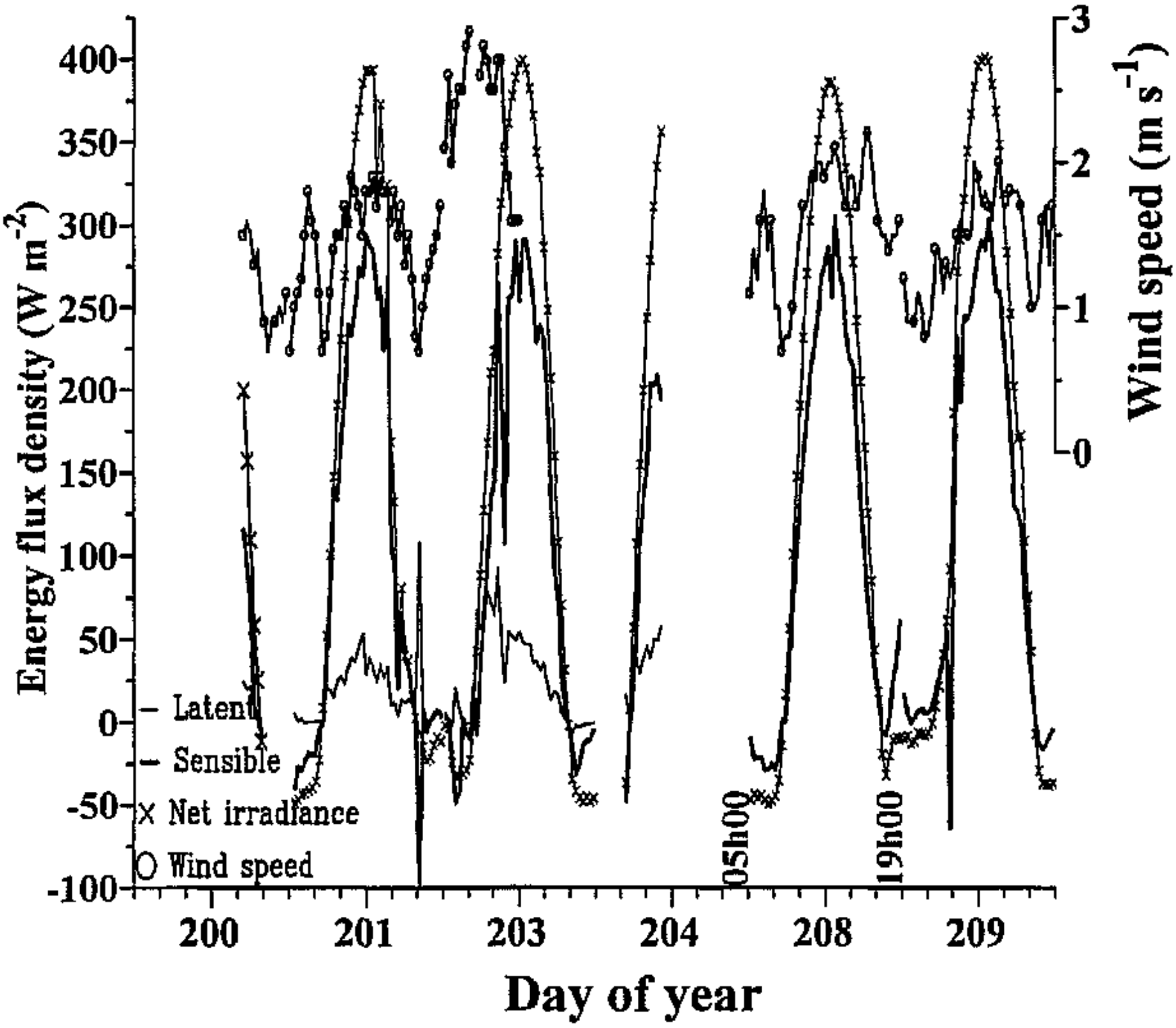

Fig. 3.17 The 20 min variation in some of the components (net irradiance, latent heat flux density and sensible heat flux density) of the shortened energy balance (left hand y-axis, W m^{-2}) as a function of day for day 200 to 209, 1990 for Cathedral Peak Catchment VI for the times 05h00 to 19h00. Each day indication corresponds to midday. Each small tick interval is 140 min. The right-hand y-axis indicates the wind speed (m s^{-1}). Since the sensible heat flux density F_h is quite stable from day to day around 250 W m^{-2} and the latent heat flux density $L_v F_w$ around 50 W m^{-2} with a resultant Bowen ratio of about 5 for this dry time of the year

arrive at, as the size limitations of the spreadsheet meant that only one or two variables could be collected at a time for the required number of days. The calculation of daily totals and averages in the spreadsheet was extremely time-consuming, cumbersome and prone to the introduction of errors. After six months of data analysis, this method of data analysis was abandoned in preference to the use of SPLIT. Spreadsheets were thus used only once daily totals had been produced with the above SPLIT processing procedure. In this form, the entire data set with all the variables for more than a year could easily be contained and manipulated in a spreadsheet.

3.5.2 Detailed documentation on the parameter files

3.5.2.1 Capture of parameter files from computer screen

Bowen ratio parameter files were captured from a VGA personal computer screen (under DOS 5.0)

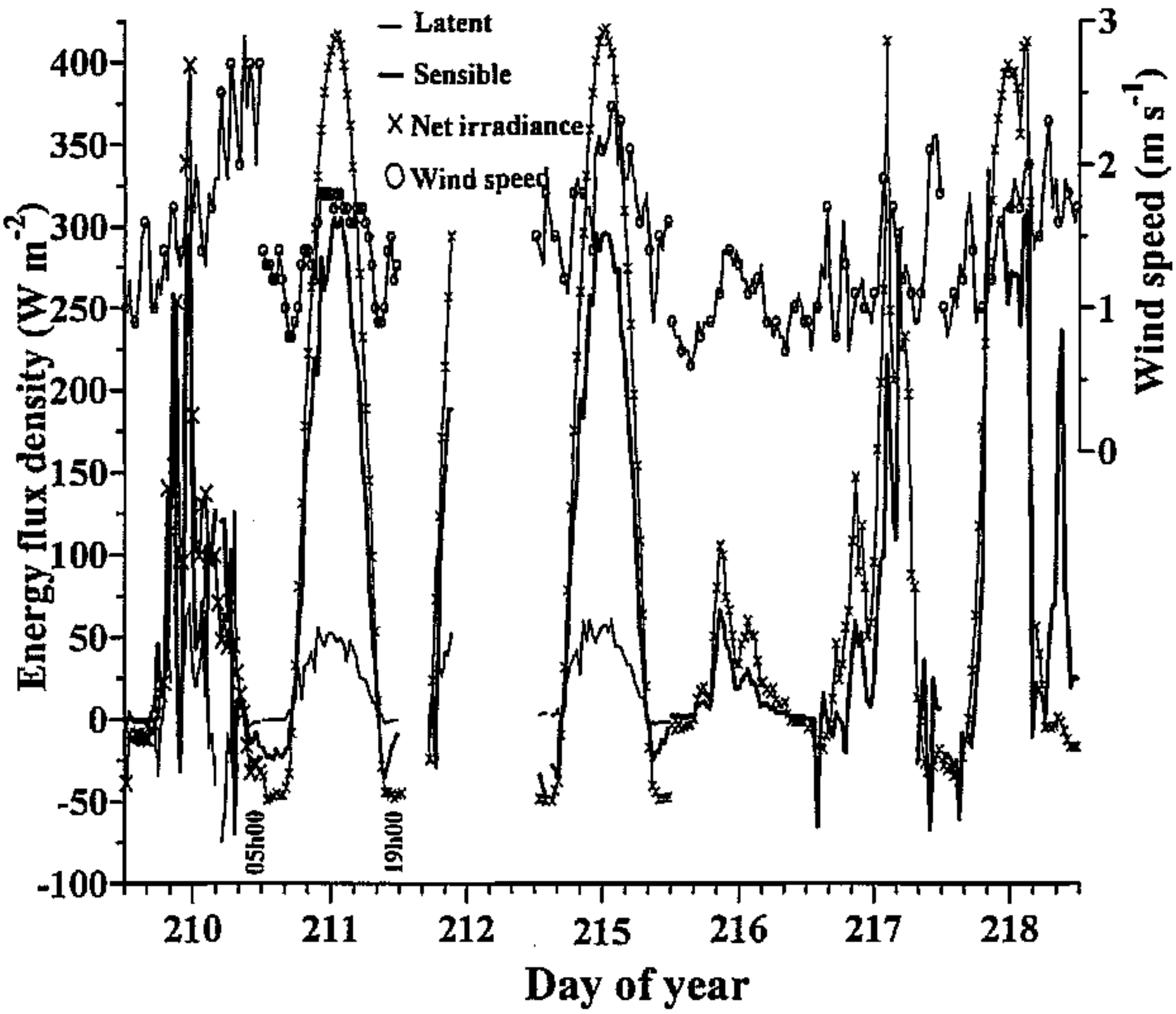

Fig. 3.18 The 20 min variation in some of the components (net irradiance, latent heat flux density and sensible heat flux density) of the shortened energy balance (left hand y-axis, W m^{-2}) as a function of day for day 210 to 218, 1990 for Cathedral Peak Catchment VI for the times 05h00 to 19h00. Each day indication corresponds to midday. Each small tick interval is 140 min. The right-hand y-axis indicates the wind speed (m s^{-1}). Since the sensible heat flux density F_h is quite stable from day to day around 250 W m^{-2} and the latent heat flux density $L_v F_w$ around 50 W m^{-2} with a resultant Bowen ratio of about 5 for this dry time of the year

using the program HiJaak version 2.02 from Inset Systems. The procedure for this is briefly described. From within the HiJaak subdirectory (hj2) and from the DOS command line execute

loadrpm

followed by the enter key. Then run the Campbell Split program in the normal fashion. Call up the parameter file to be captured. When it is viewed on the screen, capture the screen image by pressing ALT CTRL (hold the ALT key down and then press the CTRL key). Move the down arrow key to Quick Capture and press the enter key. The user is prompted by a file name (usually scm0.igf where the igf format is the internal format used by HiJaak). Press the up arrow key to and the enter key to specify Initial Application to get back to Split. Then move the cursor further down to capture the rest of the Split parameter file (if not already complete) or choose another parameter file to be screen captured.

When the second screen is captured (repeating much the same procedure described previously), the file name will automatically change to scrn1.igf. All the igf files are placed in the hj2 subdirectory. To remove the rpm memory resident program, from the DOS command line, type freerpm followed by the enter key.

Once all the parameter files have been captured, exit from Split and then execute hj to convert the *.igf files captured from screen to *.txt files. The files can then be imported into a text editor, merged, edited, and then printed out for record keeping purposes and for use in editing the parameter files.

3.5.2.2 Pass 0

Pass 0 was used in SPLIT on the raw data files to collate the two line array into one line arrays. The Pass 0 file is listed as:

PASS 0: Parameter file name pass0.par

```
F1=Help  F2=Commands            Insert is On   Param file is pass0.PAR
____________________________________________________________

   Name(s) of input DATA FILES(s): 00.PRN,00.PRN
  Name of OUTPUT FILE to generate: 00.PS1 /[""] /0
       START reading in 00.PRN:
          START reading in :
        STOP reading in 00.PRN:
           STOP reading in :
           COPY from 00.PRN: 1[100..199] AND 3[0500..1900]
              COPY from : 1[200..299] AND 3[0500..1900]
  SELECT element #(s) in 00.PRN: 2[1..366],3[0500..1900],5[-20..50],6[-5.
                   .5],8[0.01..5],10[0.01..5]
       SELECT element #(s) in : 4[-50..1200],5[-50..100],6[-50..100],8[-
                   2..3]
          HEADING for report: COMBINATION OF ARRAYS 1xx AND 2xx INTO A
                   SINGLE ARRAY
  HEADINGS for 00.PRN, col. # 1: DOY
              column # 2: TOD
              column # 3: Tlo
              column # 4: Tdiff
              column # 5: eLo
              column # 6: eHi
      HEADINGS for , col. # 7: Rn
              column # 8: SHF1
              column # 9: SHF2
              column # 10: dTs
```

3.5.2.3 Pass 1

After Pass 0 the data is in arrays in the order:

1: DAY; 2: TOD; 3: T_{lower}; 4:$T_{diff} = T_{lower} - T_{upper}$; 5: e_{lower}; 6: e_{upper}; 7: $I_{net} = R_{net}$; 8: SHF1 = $F_{soil\,1}$; 9: SHF2 = $F_{soil\,2}$; 10: dT_s.

The combination of water content data, the relevant weather data and the independent gradients from the other BR system into the data arrays was accomplished with the parameter file name pass1new.parnew.

```
F1=Help  F2=Commands            Insert is On   Param file is pass1new.PAR

     Name(s) of input DATA FILES(s): 00.PS1,00.PS1,SWCORECT.PRN,072303W0.PRN,
                         00COLIN.PS1
    Name of OUTPUT FILE to generate: 00.PS2 /[""] /0
       START reading in 00.PS1: 1[71]:2[1500]
          START reading in : 1[71]:2[1500]
          START reading in : 1[71]:2[1500]
          START reading in : 1[71]:2[1500]
          START reading in : 1[71]:2[1500]
       STOP reading in 00.PS1:
          STOP reading in :
          STOP reading in :
          STOP reading in :
          STOP reading in :
          COPY from 00.PS1: 1[1] and 2[20]
             COPY from : 1[1] AND 2[20]
             COPY from : 1[1] and 2[20]
             COPY from : 1[1] AND 2[20]
             COPY from : 1[1] AND 2[20]
     SELECT element #(s) in 00.PS1: D=(-.0109491*5*1000.+.0289644*101325.)/(
                         8.31451*(3+273.15)+0.0289644*9.79221*193
                         5.),EA=(5+6)/2.,P=101.325-((9.79221*1935
                         .)/1000.)*D,ES=0.6108*EXP(17.2694*((2.*3
                         -4)/2.)/(237.3+(2.*3-4)/2.))
       SELECT element #(s) in : EA=(5+6)/2.,CP1=1.004722587+1.148254385*
                         EA/(P-EA),DCP=.001256*(1.+25./40.)*(1.+(
                         EA/ES)),CP2=CP1+DCP,LV=2500.95-2.36679*(
                         (2.*3-4)/2.),G=CP2*P/(LV*.6219807),LL=-(
                         (5-6)/G)-2.*((.01/G)+.001),RL=-((5-6)/G)
                         +2.*((.01/G)+.001),D,P,CP2,ES,LV,G,LL,RL
                         ,1..10
       SELECT element #(s) in : 1..3
       SELECT element #(s) in : 1,2,3,5..8
       SELECT element #(s) in : 1,2,4..6
          HEADING for report: TIME SYNCHED RAW DATA WITH WATER CONTENT
```

```
HEADINGS for , col. # 1: D
            column # 2: P
            column # 3: CP2
            column # 4: ES
            column # 5: LV
            column # 6: G
            column # 7: LL
            column # 8: RL
            column # 9: DOY
           column # 10: TOD
           column # 11: Tlo
           column # 12: Tdiff
           column # 13: ELO
           column # 14: EHI
           column # 15: Rnet
           column # 16: SHF1
           column # 17: SHF2
           column # 18: dTs
HEADINGS for , col. # 19: DOYWC
           column # 20: TODWC
           column # 21: WC
HEADINGS for , col. # 22: DOYW
           column # 23: TODW
           column # 24: Tair
           column # 25: Is
           column # 26: Wspeed
           column # 27: Wdir
           column # 28: Ppt.
HEADINGS for , col. # 29: DOYC
           column # 30: TODC
           column # 31: TdiffC
           column # 32: eLoC
           column # 33: eHiC
```

3.5.2.4 Pass 2

To correct any factors or other data, parameter file name pass2new.par was used.

```
Edit  Run  Save  Quit  Load new parameter file

 . Name(s) of input DATA FILES(s): 00.PS2
  Name of OUTPUT FILE to generate: 00.PS3 /[""] /0
       START reading in 00.PS2: 9[71]
```

```
        STOP reading in 00.PS2:
            COPY from 00.PS2: 10[0500..1900]
    SELECT element #(s) in 00.PS2: 1..8,9[1..366],10[0500..1900],11[-20..50
                    ],12[-5..5],13[0.01..5],14[0.01..5],15[-
                    50..1200],16[-50..100],17[-50..100],18[-
                    2..3],21[.1..0.99],24[-20..50],25[0..120
                    0],26[0..10],27[0..360],28[0..50],29..33

          HEADING for report: CORRECTED INET etc.
    HEADINGS for 00.PS2, col. # 1: D
                column # 2: P
                column # 3: CP
                column # 4: ES
                column # 5: L
                column # 6: G
                column # 7: LL
                column # 8: RL
                column # 9: DOY
               column # 10: TOD
               column # 11: Tlo
               column # 12: Tdiff
               column # 13: eLO
               column # 14: eHI
               column # 15: Rnet
               column # 16: SHF1
               column # 17: SHF2
               column # 18: dTs
               column # 19: WC
               column # 20: Tair
```

3.5.2.5 Pass 3

The main calculations are accomplished in pass 3 parameter file name pass3new.par.

```
------------------------------------------------------------------------

Edit  Run  Save  Quit  Load new parameter file

   Name of OUTPUT FILE to generate: 00.PS3,00.PS3,00.PS3,00.ps3
       START reading in 00.PS3: 00.TSS /["] /0
           START reading in :
           START reading in :
           START reading in :
        STOP reading in 00.PS3:
            STOP reading in :
            STOP reading in :
```

```
          STOP reading in :
          COPY from 00.PS3:
             COPY from :
             COPY from :
             COPY from :
    SELECT element #(s) in 00.PS3:
       SELECT element #(s) in : DA=1,P=2,CP=3,ES=4,LV=5,GAM=6,LL=7,RL=8,
                    DE=13-14,W=.5
       SELECT element #(s) in : B=P*CP*12/(.6219807*LV*DE),F=SPAAVG(16,1
                    7),S=18/1200.*.1*860.*(837.+W*4190.),GS=
                    F+S,LE=(15-GS)/(1.+B),H=15-GS-LE,KH=H/(D
                    A*CP*1000.*12),KW=(LE*GAM)/(DA*CP*1000.*
                    DE),9,10,15,GS,B,LE,H,F,S,12,DE,KH,KW
       SELECT element #(s) in : EM=0.413188419+0.0157973*11-0.00011506*1
                    1*11,EF=EM[.42..1],EQ=EF*(15-GS),EQ[-500
                    ..1200],19..24,LL,RL,ES,13,14,DA,CP,GAM
       SELECT element #(s) in : DEL=4098.02862*ES/((237.3+11)*(237.3+11)
                    ),ALP=DEL/(DEL+GAM),ED=ALP*(15-GS),ED,25
                    ..29
         HEADING for report: BR OUTPUT: DOY,TOD,RN,G,BR,LE,H,F,S,DT,D
                    E,KH,KW,Eqm,WC,Tair,Is,Wspd,Wdir,Ppt.
       HEADINGS for , col. # 1: DOY
             column # 2: TOD
             column # 3: RN
             column # 4: G
             column # 5: BR
             column # 6: LE
             column # 7: H
             column # 8: F
             column # 9: S
             column # 10: DT
             column # 11: DE
             column # 12: KH
             column # 13: KW
       HEADINGS for , col. # 14: EQM
             column # 15: WC
             column # 16: Tair
             column # 17: Is
             column # 18: Wspd
             column # 19: Wdir
             column # 20: Ppt
             column # 21: Wdir
             column # 22: LL
```

```
            column # 23: es
            column # 24: eLo
            column # 25: eHi
            column # 26: da
            column # 27: cp
            column # 28: gam
    HEADINGS for , col. # 29: ED
            column # 30: DOYC
            column # 31: TODC
            column # 32: TdiffC
            column # 33: eLoC
            column # 34: eHiC
```

3.5.2.6 Pass 4

The output of pass 3 was imported to the spreadsheet TAGIMPRT.WQ1 and then printed to a file as ALLMGRAD.PS4. Pass 4 and 5 were then used to separate the variables to be processed over differing times of day and to multiply the variables by TAGM to either accept or reject the datum point:

PASS 4: Parameter file name pass4new.par

```
Edit  Run  Save  Quit  Load new parameter file

   Name(s) of input DATA FILES(s): 00.ps4
  Name of OUTPUT FILE to generate: 00.pS5 /[""] /0
      START reading in 00.ps4: 3[72]:4[0600]
       STOP reading in 00.ps4:
          COPY from 00.ps4: 3[1] AND 4[20]
   SELECT element #(s) in 00.ps4: 3[1..366],4[0600..1800],1,2,5[-50..1200]
                     ,6[-200..200],LE=7,B=1*LE,B[-500..1000],
                     H=8,D=1*H,D[-400..800],EQM=9,F=1*EQM,F[-
                     500..1200],18[-20..50],19[0..1000],20[0.
                     .10],21[0..360],22[0..50],K=14,G=1*K,G[-
                     2..5]
         HEADING for report: Series to be totalled from 0600 to 1800
                     WITH LE, H, EQM and K BLANKED WHEN TAGGED
    HEADINGS for 00.ps4, col. # 1: DOY
             column # 2: TOD
             column # 3: TAGM
             column # 4: TAG
             column # 5: RN
             column # 6: G
             column # 7: LE
             column # 8: H
             column # 9: Eqm
```

column # 10: Tair
column # 11: Is
column # 12: Wspeed
column # 13: Wdir
column # 14: Ppt.
column # 15: Kh

The output of this pass was taken to spreadsheet for examination of K values, calculations using K and gradients, and daily totals in $L_v F_w$ and H.

3.5.2.7 Pass 5

PASS 5: Parameter file name pass5new.par

```
Edit  Run  Save  Quit  Load new parameter file

  Name(s) of input DATA FILES(s): 00.ps4
  Name of OUTPUT FILE to generate: 00.pS6 /[""] /0
      START reading in 00.ps4:
       STOP reading in 00.ps4:
          COPY from 00.ps4: 4[1000..1600]
  SELECT element #(s) in 00.ps4: 3[1..366],4[1000..1600],7[-20..25],12[-2
                   ..5],13[-2..5],1,2,BRALL=7,BRTAG=1*BRALL
                   ,BRTAG[-20..25],KHALL=12,KHTAG=1*KHALL,K
                   HTAG[-2..5],KWALL=13,KWTAG=1*KWALL,KWTAG
                   [-2..5]
        HEADING for report: Series to be totalled from 1000 to 1600
  HEADINGS for 00.ps4, col. # 1: DOY
              column # 2: TOD
              column # 3: BRALL
              column # 4: KhALL
              column # 5: KwALL
              column # 6: TAGM
              column # 7: TAG
              column # 8: BRTAG
              column # 9: KhTAG
              column # 10: KwTAG
```

3.5.2.8 Pass 6

PASS 6: Parameter file name pass6new.par

```
Edit  Run  Save  Quit  Load new parameter file

  Name(s) of input DATA FILES(s): 00.PS5
  Name of OUTPUT FILE to generate: 00.pS7/[""]/0
      START reading in 00.PS5:
```

```
        STOP reading in 00.PS5: F,2[1600]
           COPY from 00.PS5:
    SELECT element #(s) in 00.PS5: MIN(1),max(1)-min(1)+avg(1)+min(2)-500.+
                    total(2)-51040.,max(2),min(2),TOTAL(5)*0
                    .0012,TOTAL(7)*12./24700.,TOTAL(7)*0.001
                    2,TOTAL(8)*0.0012,TOTAL(9)*0.0012,TOTAL(
                    11)*0.0012,max(12),AVG(12),AVG(13),MAX(1
                    0),MIN(10),AVG(10),TOTAL(14),COUNT(7),BL
                    ANKS(7)
         HEADING for report: DAILY TOTALS 19H00 WITH TAGGED DATA REJE
                    CTED
    HEADINGS for 00.PS5, col. # 1: DOY
                column # 2: DOYchk
                column # 3: maxTOD
                column # 4: minTOD
                column # 5: InMJ.d
                column # 6: LEmm.d
                column # 7: LEMJ.d
                column # 8: H MJ.d
                column # 9: EqLEMJ
               column # 10: IsMJda
               column # 11: maxWsp
               column # 12: avgWsp
               column # 13: avgWd
               column # 14: maxTa
               column # 15: minTa
               column # 16: avgTa
               column # 17: totPpt
               column # 18: COUNT
               column # 19: BLANKS
```

3.5.2.9 Pass 7

PASS 7: Parameter file name pass7new.par

```
Edit  Run  Save  Quit  Load new parameter file


    Name(s) of input DATA FILES(s): ALL.PS6
   Name of OUTPUT FILE to generate: ALL.pS8/[""]/0
       START reading in ALL.PS6:
        STOP reading in ALL.PS6: F,2[1600]
           COPY from ALL.PS6:
    SELECT element #(s) in ALL.PS6: max(1)-min(1)+avg(1)+min(2)-1000.+total(
                    2)-24460.,max(2),min(2),AVG(3..5),SD(3..
```

```
                    5),MAX(7),AVG(8.10),SD(8..10),COUNT(6),B
                    LANKS(6)
          HEADING for report: DAILY TOTALS 16H00
   HEADINGS for ALL.PS6, col. # 1: DOY
                column # 2: DOYchk
                column # 3: maxTOD
                column # 4: minTOD
                column # 5: avgBRA
                column # 6: avgKhA
                column # 7: avgKwA
                column # 8: sdBRA
                column # 9: sdKhA
               column # 10: sdKwA
               column # 11: maxTAG
               column # 12: avgKhT
               column # 13: avgKwT
               column # 14: sdKhT
               column # 15: sdKwT
               column # 16: count
```

PASS 8: Parameter file name pass8new.par

```
Edit  Run  Save  Quit  Load new parameter file

   Name(s) of input DATA FILES(s): ALL.ps7,ALL.ps8
  Name of OUTPUT FILE to generate: ALL.ps9 /[""] /0
       START reading in ALL.ps7: 1[200],1[1..366]:
           START reading in : 1[200],1[1..366]:
        STOP reading in ALL.ps7:
            STOP reading in :
           COPY from ALL.ps7: 1[1]
               COPY from : 1[1]
   SELECT element #(s) in ALL.ps7: 1..19
       SELECT element #(s) in : 1..17
          HEADING for report: ALL DAILY TOTALS
   HEADINGS for ALL.ps7, col. # 1: DOY
                column # 2: DOYchk
                column # 3: maxTOD
                column # 4: minTOD
                column # 5: InMJ.d
                column # 6: LEmm.d
                column # 7: LEMJ.d
                column # 8: H MJ.d
                column # 9: EqLEMJ
```

column # 10: IsMJda
column # 11: maxWsp
column # 12: avgWsp
column # 13: avgWd
column # 14: maxTa
column # 15: minTa
column # 16: avgTa
column # 17: totPpt
column # 18: COUNT
column # 19: BLANKS
HEADINGS for , col. # 20: DOY
column # 21: DOYchk
column # 22: maxTOD
column # 23: minTOD
column # 24: avgBRA
column # 25: avgKhA
column # 26: avgKwA
column # 27: sdBRA
column # 28: sdKhA
column # 29: sdKwA
column # 30: maxTAG
column # 31: avgKhT
column # 32: avgKwT
column # 33: sdKhT
column # 34: sdKwT
column # 35: count
column # 36: blanks

3.5.3 Allowable ranges for output variables

The allowable range or ranges of each variable are tabled (Table 3.4) along with the pass number or numbers in which they occur. These ranges were used to exclude erroneous data.

3.5.4 Discussion on the use of the rejection criteria

The rejection criteria are summarised by the following sets of conditions, with identifying tags generated in the spreadsheet TAGIMPRT.WQ1 according to class of rejection in **Table 3.5**. The identifying tags were used in order to be able to identify the cause of rejection.

Data points not rejected are tagged "1". Vapour pressures above saturation or too close to each other are rejected and tagged "2" (the "WVP" criteria) and rejected on one of these two sets of grounds. If the upper and lower limit inequality (lower limit condition of Eq. 3.32) (tagged "3") is satisfied then there is a high possibility that the Bowen ratio will be very near −1 and therefore the calculated flux will not have numerical meaning. Data fulfilling this inequality are therefore excluded from further processing. The majority of the data during clear days were not rejected, and all datum points rejected were done so justifiably when checked. The method had the additional benefit of calculating condition-sensitive daily totals. It thereby negates the requirement of calculating daylengths and adjusting calculations according to those daylengths. The procedure is sensitive to the times of day

Table 3.5 Summary of rejection conditions and associated rejection tag identifiers

Condition	Tag
No rejection	1
e_{lower} or $e_{upper} > (e_s + 0.01)$ or $\|e_{lower} - e_{upper}\| < 0.01$ kPa (*ie.* $\|T_{dp\ lower} - T_{dp\ upper}\| < 0.003°C$)	2
Lower Limit $< \delta T <$ Upper Limit	3
Both of the above (2 and 3)	4

when reasonable fluxes occur, rejecting points other than these good data points. This allows an 18-hour-day set of data to be used at all times, so avoiding having to decide when to start and stop data collection for each daylength.

Initially both the Upper Limit (UL) and Lower Limit (LL) for δT were used as rejection criteria. It was found that the periods where δT decreased below LL were those in the very early morning and late evening (before and after morning and evening periods when $\beta \rightarrow -1$ respectively). These periods are often already rejected by the "WVP" criteria (case 2 in Table 3.5). A relatively small number of points not already rejected by the WVP criteria were rejected by the UL criterion. The reason for this is that at these times I_{net} is negative. Those that are not rejected by negative I_{net}, but occur during the morning and evening periods, are often rejected by the water vapour pressure criteria, since at these times, δe values approach the resolution of the sensor (and to a lesser extent, approach their saturation value).

The water vapour pressure (WVP) criterion is made up of two components; the resolution limit check, and the check on each value with respect to its saturation value. Because only the former check is included in the UL check, the WVP criterion is required in the data rejection procedure.

Due to these arguments, only the upper inequality was used as the rejection criterion (upper limit condition of Eq. 3.32):

$$\delta T < -\delta e/\gamma + 2E(\theta) \qquad 3.42$$

The additional points rejected by using only the upper rejection criterion were found to be occasional large spurious points within the other rejection limits, as well as a few small values close to morning and evening times in which the classes of rejection have been separated out). These points, however, had already mostly been rejected by the WVP and negative I_{net} criteria. Comparisons of daily totals using both and then only the upper criterion, show that the disadvantage of rejecting the [good] low data points in the morning and evening are over-shadowed by the disadvantage of not rejecting the far fewer, but much larger, [bad] spurious data points that also occurred, but that had escaped rejection by the other criteria (Table 3.6).

From Table 3.6 the benefits of applying these rejection criteria are evidenced by the contribution that large spurious values make to the evaporation totals for each of four chosen days. Two days were chosen to show "good" conditions (Day 4 and 16), and two examples of "poor" conditions (Day 2 and 31), when irradiance levels were low and/or variable. There was a small amount of precipitation on the mornings of Day 4 and 31.

Table 3.6 Comparison of daily total evaporation (mm day^{-1}) calculated with differing sets of rejection criteria for Day 2, 4, 16 and 31, 1992 (Cathedral Peak, CVI)

Rejection criterion type	Day 2	Day 4	Day 16	Day 31
No rejection criteria[1]	-3.37	2.63	10.80	3.20
Split range limits only[2]	2.16	2.65	6.74	2.07
"WVP" limits[3]	1.65	2.24	6.63	1.60
LL < δT < UL[34]	0.41	2.14	6.23	0.70
δT < UL[345]	0.41	2.14	6.23	0.70

Notes:

1 Other than missing data caused by division by zero when $\beta \rightarrow -1$

2 The [from..to] range limits as listed in Table 3.4

3 As well as the Split range limits which apply over and above this

4 With the use of this criterion, a significant reduction in daily total evaporation occurred on day 2 and 31 as a result of the large spurious negative and positive daytime evaporation values not rejected by the above criteria

5 No change was observed when only the UL was used because the few additional points rejected were very low values

Based on the above discussion, it was decided to reject all data periods when δT decreased below *both* the UL and the LL in the procedure used. Whether this is entirely justified under all conditions requires some clarification. For δT to decrease below the LL requires a large negative air temperature gradient (a strong inversion), as well as δe close to zero, or positive if δT is not large. This set of circumstances is indicative of inversion conditions, which occur under either nocturnal condensation (dew-fall) or periods of positive horizontal heat advection. The nocturnal latent energy gains (dew) cannot be included in daily total evaporation calculations, but advection can nearly double a windless day's water loss. Dew-fall renders both the air intake levels saturated, thereby making water vapour pressure gradient determinations and flux calculations impossible. Wet thermocouples will measure the wet bulb temperature, preventing the measurement of air temperature gradients. It follows that including the latter is of obvious importance. Under advective conditions, wind speeds are high enough to ensure a completely mixed or convective boundary layer. If the Bowen ratio sensors are high enough above the surface to be out of any low-level inversion caused by advection, then this effect should not confound evaporation measurements by causing the data to be rejected. A local source of energy additional to the available energy (as defined by the assumption that excludes advection), will increase the flux densities flowing upwards from the surface. However, they will not be perceived by sensors above the low-level inversion, and so introduce an error due to advection. Some way of obtaining measurements of the advective energy input must therefore be found to avoid this error.

3.6 Error considerations of the Bowen ratio energy balance method

3.6.1 Introduction and literature review

Several workers have dealt almost exclusively with error-related aspects of the BREB method, most notably Fritschen (1965), Fuchs and Tanner (1970), Sinclair *et al.* (1975), and Angus and Watts (1984).

Other workers have concentrated on the positioning of the Bowen ratio sensors. For example, Heilman *et al.* (1989) found that the Bowen ratio and its variability increased with measurement height. The measurement heights were starting to extend above the internal layer, yet adequate results were obtained.

The high precision of Bowen ratio measured fluxes was confirmed by Revfeim and Jordan (1976), while absolute accuracy was affirmed by Nie *et al.* (1992) (during the 1987 FIFE[9] intercomparison of surface flux measuring systems).

Tanner (1963) noted the importance of horizontal spatial sampling to avoid the effects of surface inhomogeneities which can affect measurements and thereby also calculations of the ratio K_h/K_w. The practice of sampling by using sensors which travel physically on a horizontal arm has been used in the past, but is mechanically more complex. More recently the accepted strategy for adequate spatial sampling has been the placement of sensors far enough above the surface or canopy to be in the region where greater turbulent mixing occurs. Further from the evaporating surface, however, the profile gradients are smaller and thus more difficult to measure. Closer to the surface, the gradients are larger in magnitude (and thus easier to measure), but the problem of patchiness of cover overshadows the benefits (Tanner 1960). The choice of heights is limited by the fetch-height constraints and because under stable conditions, errors due to thermal stratification increase with height, an additional profile-limitation is imposed (Rao *et al.* 1974). Fortunately such stable conditions are infrequent and, in any event, result in minimal water losses.

Black (1973) found that the performance of the BREB method improved when the height difference between the sensors was increased, although this was probably due to changes in fetch, and increased magnitudes of the measured δT and δe relative to the measurement error (Munro 1985).

From the literature, it seems that during advective periods it is the sensible heat exchange coefficient that becomes greater than the latent, and thus should increase the "constant" multiplier K_h/K_w of Eq. 3.13. The error introduced by applying the assumption of Similarity will result in an underestimation of $L_v F_w$, and therefore an overestimation of F_h. Verma *et al.* (1978) confirmed this for regionally advective conditions over grass.

At high levels of evaporative flux, values of β are small, and an assumption of equality between K_h and K_w when the two are not markedly different will not lead to serious error in the estimation of $L_v F_w$. However, when the surface is dry and $L_v F_w$ small, β values are large and a given departure of K_h/K_w from unity can lead to almost as large errors in the estimate of $L_v F_w$. Corrections to the assumption of Similarity are therefore required for nearly all sites (Denmead and McIlroy 1970). It is evident from Eq. 3.15 that the sensitivity of β is directly related to the measured gradients; a one percent error in a measurement results in a one percent error in β, although if both the gradients are under- (or, less likely: over-) estimated, the error cancels somewhat. The size of the error therefore, is directly proportional to the size of β, under any particular constant energy balance régime.

Angus and Watts (1984) stressed the dependence of the absolute error in β on the size of β. They assumed a constant and independent error of approximately ±4 % in the determination of available

9 The First ISLSCP (International Satellite Land Surface Climatology Project) Field Experiment, or FIFE, was one of the most complex interdisciplinary research efforts undertaken in Earth Science

energy which is added to the error from β. Under high evaporation conditions at or near the potential rate ($-0.2 < \beta < 0.2$), errors of up to 30 % in β produce errors of less than 5 % in $L_v F_w$ (9 % when added to the available energy error). However under extremely dry conditions, the high value of β causes a need for increasingly precise psychrometric measurements in order to maintain error levels accuracies (T_{dp} to within ±0.0013 °C). Such accuracy levels were considered to be an order of magnitude greater than could be expected from most Bowen ratio equipment at the time.

Pruitt *et al.* (1987) pointed out that under calm, cool or humid conditions, evaporation is insignificant. However the resultant large evaporative flux densities which usually occur when β approaches −1 under highly advective conditions, cannot be measured. Whether the neglection of the advection term from measurements is permissible cannot be decided until the effect is quantified, and hence measurement of advection should always accompany the collection of data for use in the BREB determination of flux partitioning. By meeting the aforementioned fetch requirements, the effects of any local advection should be assuaged and not affect evaporation measurements. This again emphasizes the requirements of measuring within the correct boundary layer, and therefore of placing sensors in areas of ample size and uniform cover. When the BREB method does fail due to the neglection of advection, these solutions must be discarded, as they must be at the times when $\beta \rightarrow -1$.

Webb (1965) and Angus and Watts (1984) discussed an interesting phenomenon relating to advection. This was previously reported by Dyer and Crawford (1965) working at the same site and time of year. They found that although a uniform boundary layer had been established, this was no guarantee of the same in profiles of diffusing entities such as energy or gases. Angus and Watts (1984) further found advective periods where, under fairly strong radiative conditions, low-level temperature inversions occurred. These would confound the inference of profiles at normal heights used for Bowen ratio measurements, since the sensors would be above and thus not detect the inversion. The sources and sinks of sensible and latent heat would not be the same, the fluxes may well be in opposite directions, and consequently the assumption of Similarity would no longer hold. With a displaced source of heat (Fig. 3.19), meaningful flux measurements would not be possible.

Panofsky (1965) notes that a two-point gradient measurement can be used as an estimate of that gradient. This would introduce considerable error under the above conditions. Normally, however, the error introduced by this approximation is not significant at the heights of measurements commonly used in the BREB method.

Nocturnal evaporation of up to 20 % of the daily total can occur in alfalfa fields due to strong temperature inversions in spring (Rosenberg 1969a), and omitting these periods can significantly decrease calculated totals. Abdel-Aziz *et al.* (1964) and van Bavel (1967) also reported measurable nocturnal evaporation over alfalfa.

3.6.2 The error associated with the psychrometric and other "constants"

Revfeim and Jordan (1976) noted that failure to take temperature and pressure corrections into account when calculating the psychrometric constant could cause considerable errors if the wet bulb depression were large. The psychrometric constant is required when using psychrometry to determine water vapour pressure (WVP) gradients.

Angus and Watts (1984) considered errors introduced in the determination of Δ and γ an order of magnitude smaller than those from gradient measurements, and CSI's documentation (Anon 1991) supplied with the Bowen ratio equipment merely suggested static values for most of the dynamic

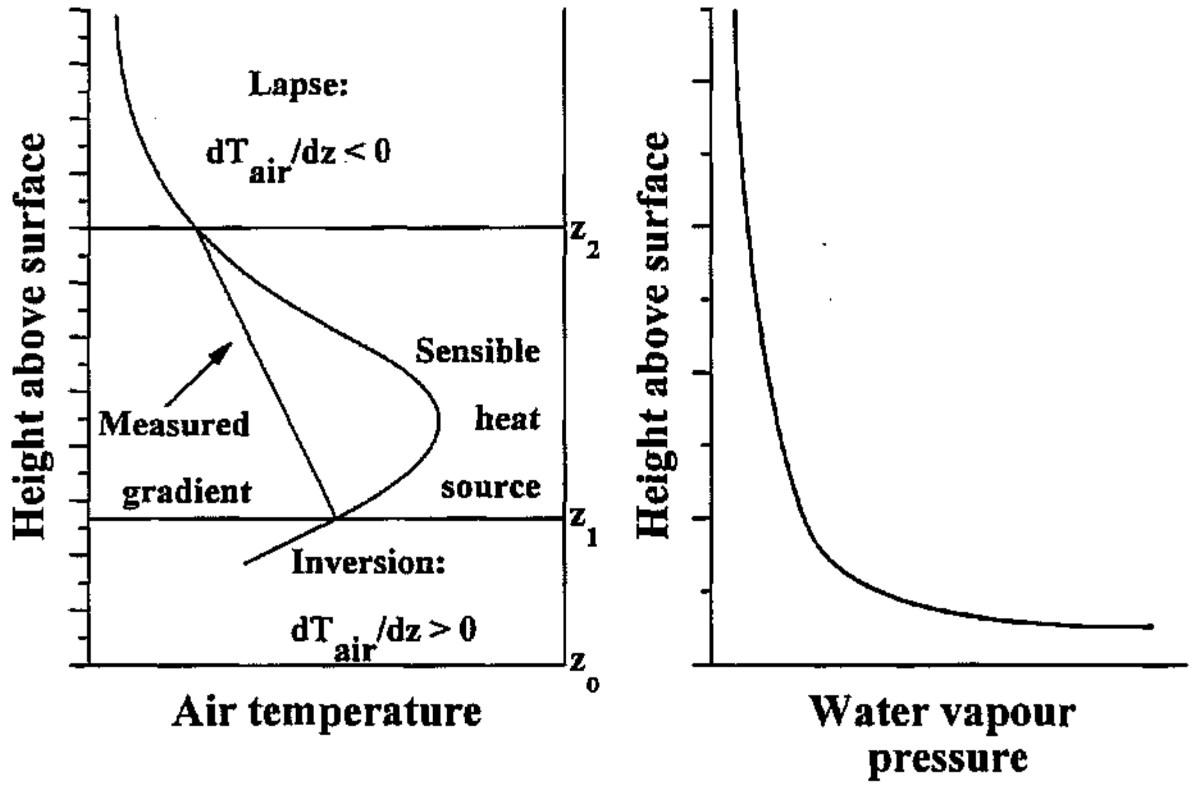

Fig. 3.19 Diagrammatic representation of (left), a low-level temperature inversion found under early morning advective conditions. This demonstrates periods when flux-gradient measurements cannot yield rational results. On right, a typical water vapour pressure profile (after Angus and Watts 1984, Lang *et al.* 1983)

"constants". A detailed analysis of the effects of using arbitrary static values as opposed to calculated values was done (Savage *et al.* 1991). Their results were convincingly in favour of using corrected values. During data processing, therefore, the variables were calculated for each time interval to correct for the environmental conditions as closely as possible. The implementation of the corrections was discussed in the section concerning data processing (Section 3.5).

3.6.3 Estimation of the error in $L_v F_w$

Intra-systematic error estimation of the Bowen ratio method has been thoroughly reviewed by Tanner (1960), Fuchs and Tanner (1970), Sinclair *et al.* (1975), Revheim and Jordan (1976), and others. The representative opinion at that time, reached by Sinclair *et al.* (1975) was that latent flux densities can be estimated to within 10 %.

The error may be assessed as the sum of the individual error-introducing components as per standard methods (see for example Fuchs and Tanner 1970, Angus and Watts 1984), as follows:

If $z = f(x)$ then $\overline{z} = \overline{f(x)}$, and $\sigma(z) = [f'(x)]^2\,\sigma(x)$

where f' denotes the first partial derivative, and if $z = f(x, y, p, q)$, then

$$\sigma(z) = [(\partial z/\partial x)^2(\sigma x)^2 + (\partial z/\partial y)^2(\sigma y)^2 + (\partial z/\partial p)^2(\sigma p)^2 + (\partial z/\partial q)^2(\sigma q)^2\,]^{0.5}$$

It follows that if

$$\sigma(L_v F_w) = [\sigma\ (component\ 1)^2 + \sigma\ (component\ 2)^2 + \sigma\ (component\ 3)^2 + ..]^{\ 0.5}$$

then the equation used to calculate the unknown for which we wish to calculate the relative error:

$$L_v F_w = (I_{net} - F_s)/(1 + \beta) = (I_{net} - F_s)\cdot(1 + \beta)^{-1}$$

may be expanded to:

$$\sigma\,(L_v F_w) = [\,(\frac{\partial L_v F_w}{\partial I_{net}})^2\cdot\sigma\, I_{net}{}^2 + (\frac{\partial L_v F_w}{\partial F_s})^2\cdot\sigma\, F_s{}^2 + (\frac{\partial L_v F_w}{\partial dT})^2\cdot\sigma\, dT^2 + (\frac{\partial L_v F_w}{\partial de})^2\cdot\sigma\, de^2\,]^{\ 0.5} \qquad 3.43$$

where F_s is made up of the plate-measured soil heat flux density G and the heat stored in the soil F_{stored} (Eq. 2.31). The latter is calculated from soil temperature T_{soil}, bulk density ρ_{soil} (kg m^{-3}), gravimetric soil water content θ_m and specific heat capacity c_{soil} (J kg^{-1} K^{-1}); and its error may be estimated from:

$$\sigma\,(F_{stored}) = [\,(\frac{\partial F_{stored}}{\partial \rho_{soil}})^2\cdot\sigma\,\rho_{soil}{}^2 + (\frac{\partial F_{stored}}{\partial \theta_m})^2\cdot\sigma\,\theta_m{}^2 + (\frac{\partial F_{stored}}{\partial c_{soil}})^2\cdot\sigma\, c_{soil}{}^2\,]^{\ 0.5}$$

but is taken as a combined 20 % of F_s (Angus and Watts 1984).

On differentiation, the components are simplified to:

$$\partial L_v F_w/\partial I_{net} = 1/(1+\beta)$$

$$\partial L_v F_w/\partial F_s = -1/(1+\beta)$$

$$\partial L_v F_w/\partial dT = -L_v F_w\cdot\gamma/[(1+\beta)\cdot de]$$

$$\partial L_v F_w/\partial de = L_v F_w\cdot 2\beta/[(1+\beta)\cdot de].$$

Simplifying by substituting these expressions into Eq. 3.43 yields:

$$\sigma\,(L_v F_w) = [(1+\beta))^2\cdot\sigma I_{net}^2 + (-1/(1+\beta))^2\cdot\sigma F_s^2 +$$
$$[-L_v F_w\,\gamma/(1+\beta)\,de]^2\cdot\sigma\, dT^2 + [L_v F_w\,2\,\beta/(1+\beta)\,de]^2\cdot\sigma\, de^2]^{0.5}. \qquad 3.44$$

The error in the determination of $L_v F_w$ may be estimated for each time of day, and will vary according to the prevailing conditions since some are more conducive to accurate measurement than others. Strong profile gradients in conjunction with an ample supply of water and radiative energy will result in low absolute and relative errors. The relative error increases with lower evaporative fluxes under drier conditions (due to relative errors in β becoming larger) because the difficulty of measuring small gradients in water vapour pressure increase (Angus and Watts 1984). The absolute error however, is largest when fluxes are large, and smallest when conditions are dry, simply because the latent heat flux density itself is small (Angus and Watts 1984).

Angus and Watts (1984) disregarded the error in the psychrometric constant as they found it was a factor smaller than those in the wet bulb temperature determination. Since the values used in our data processing were corrected for local conditions, our error is expected to be even less, and so does not enter into the equation.

The error in the determination of the available energy $I_{net} - F_s$ enters independently of the Bowen ratio determination, and can be estimated from the accuracy of calibration of the instruments (Angus and Watts 1984). Although no calibration error was quoted in the net radiometer's documentation, the high quality of the unit used warranted using the same value of 2.5 % of I_{net} used by Angus and Watts (1984). Similarly, for the soil heat flux, an overall 20 % of the F_s value was used to take into account spatial variability and sampling problems inherent with these sensors, as well as errors in the determination of stored heat energy from the change in soil temperature, the soil's bulk density and the specific heat capacities of soil and water.

Values for $\sigma(\delta T)$ and $\sigma(\delta e)$ were taken as twice the resolution of the respective sensor. The values used were: $\sigma(\delta T) \approx 0.012$ °C; $\sigma(\delta e) \approx 0.02$ kPa; $\sigma(I_{net}) \approx 0.025\, I_{net}$ and $\sigma(F_s) \approx 0.2\, F_s$. Typical daytime values for the following were used:

$I_{net} = 400$ W m^{-2}, $F_s = -10$ W m^{-2},

$\delta T = 0.08$ °C, $\delta e = 0.15$ kPa

then $\beta = 0.5993$

and $L_v F_w = 256.5$ W m^{-2}.

The error in I_{net}, $\sigma(I_{net}) = 0.025 \times 400$ W m^{-2} = 10 W m^{-2}, and in F_s, $\sigma(F_s) = 0.2 \times -10$ W m^{-2} = -2 W m^{-2}.

This yields $\sigma(L_v F_w) = 25.62$ W m^{-2} or some **10 %** of the evaporative flux density (Eq. 3.43).

As discussed by Angus and Watts (1984), the absolute error in the latent heat flux density increases with dry conditions, when β is larger and the water vapour pressure gradient small. Under these conditions, the water vapour pressure gradient is the major contributor to the total error, which stresses the importance of accurate water vapour pressure determinations as well as the lack of systematic error. When conditions are wet, β is small due to the large δe value and correspondingly small δT value, and the level of confidence in the evaporative flux is dependent mainly on the level of irradiance.

In summary, when evaporation rates are high, relative accuracy in the latent heat flux density is good, even with a poorly measured β. When β becomes large and evaporation less, absolute error is smaller due simply to the smaller values, but relative error increases.

To illustrate these points, $L_v F_w$ for the four days are presented in **Fig. 3.20** along with the calculated absolute error. The latter is represented by the height of the vertical bars. Periods where the relative error is greater than 30 % are annotated at the top of the figure along with an indication of which data periods had been rejected by the data rejection process. The periods with low relative error occur on "good" high flux, high radiation load days when β is small and rejections few. On the "poor" days, relative errors increase since evaporative fluxes drop way down, although spurious large values have been rejected from the data set. The net irradiance levels, Bowen ratio and gradient values are presented (**Figs 3.21** and **3.22**) to gain a fuller understanding of conditions on the days. The Bowen ratio is most indicative of likely error levels, as a stable low value (Day 4 and 16) means high flux levels with low relative error. A low positive β value results from δT and δe differences as occurred on these two days (Fig. 3.21 and 3.22). But where variable and large β levels occur (Day 2 and 31) mainly due to inconsistent water vapour pressure gradients, fluxes are low and prone to rejection of spurious values as well as large relative errors.

3.6.4 Practical aspects

Far fewer papers dealt in detail with the practical aspects of error avoidance. A notable exception to this was a paper by Lindroth and Halldin (1990) assessing gradient measurements above forests. They pointed out the inappropriateness of inferring gradients from difference measurements at only two points over low vegetation, since the gradients were far larger (an order of magnitude), and less linear

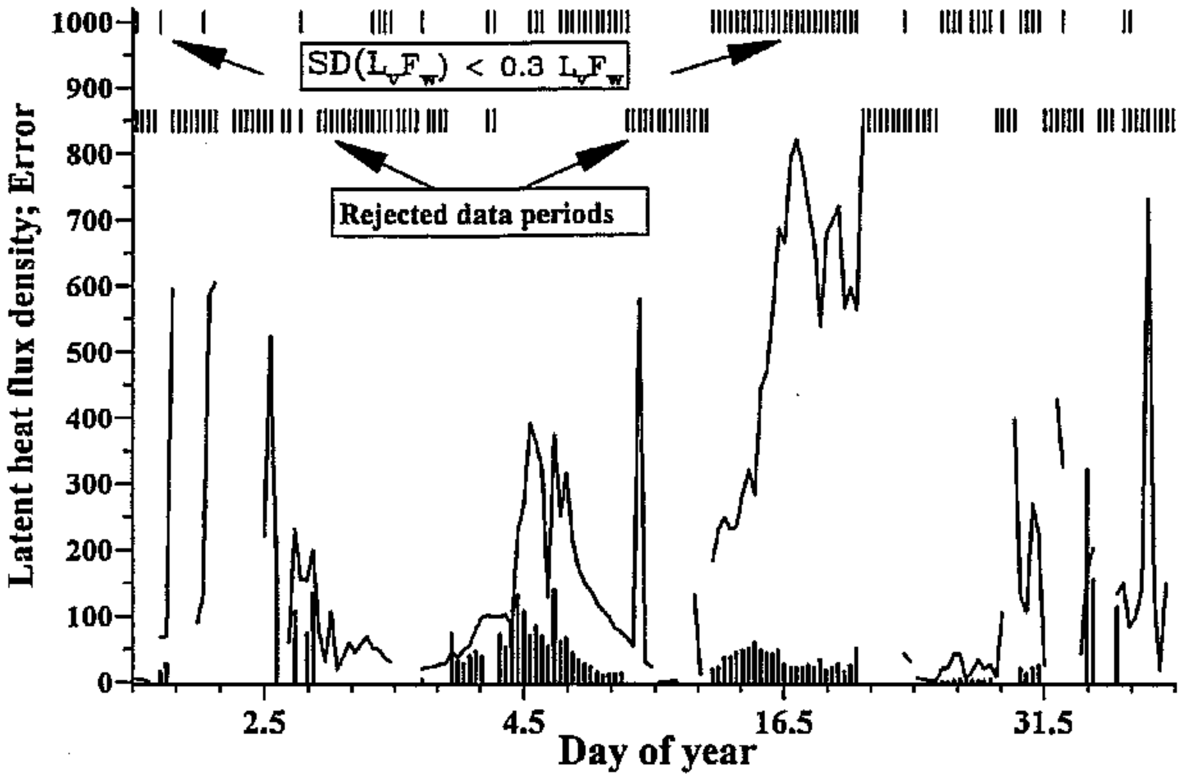

Fig. 3.20 Latent heat flux density (—) and its relative error level (bar graph) for four days. The periods where the error is less than 30% of the flux are annotated above, as well as those periods which are rejected (|). Day of year indication, 2.5 for example, corresponds to midday for Day 2

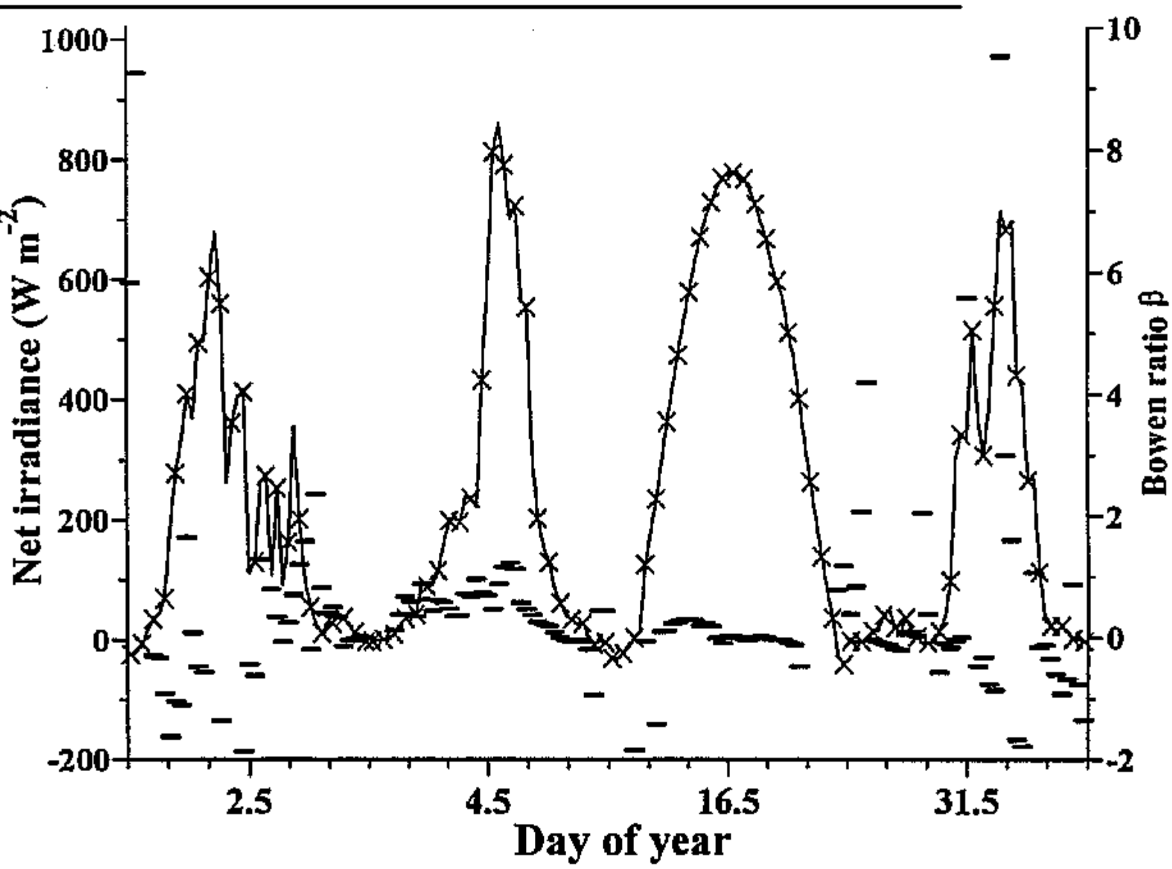

Fig. 3.21 Variation of net irradiance (x) and Bowen ratio (–) for the four days

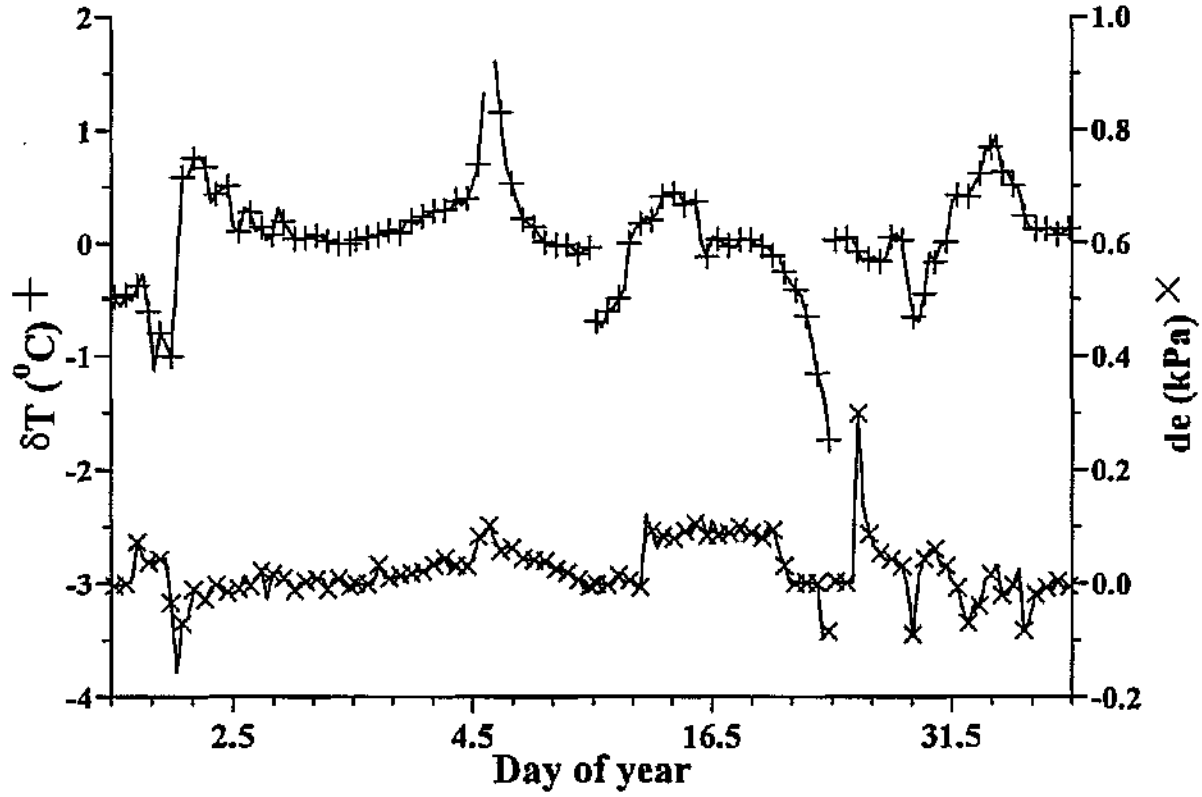

Fig. 3.22 Value of air temperature (+, left hand y axis) and water vapour pressure (x, right hand y axis) differences for the four days

that those over forest canopies.

From experience obtained using the Bowen ratio equipment, it was found that seemingly unimportant aspects required a lot of attention, and evidence of a problem was only found a lot later when examination of the data was possible during processing. In other words, frequent and early examination of current data can prevent months of collection of useless data.

From error analyses, the relative error in $L_v F_w$ has been found to be most sensitive to I_{net} measurement errors. With accurate net radiometers, most of the error arises from the soil heat flux density determinations, even though their contribution relative to net irradiance is small due to the small magnitude of the former. This is due partly to the accuracy of the net radiometers and to the difficulties encountered with soil heat flux density determinations. The important aspect of the calibration of the net radiometer is discussed in Chapter 6. The soil heat flux-related errors introduced by soil:probe contact, depth positioning and spatial dissimilarity are constant, while those arising from uncertainties in the calculation of the stored heat energy content in the layer above the flux plates (due mainly to changes in soil water content) change with time. Our experience has shown that soil heat flux density F_s (Figs 2.12, 2.13; Eqs 2.31 to 2.33) to be a variable component of the energy balance (Eqs 2.2 or 2.3). It is therefore advisable to measure soil heat flux density F_s (and soil temperature T_{soil}) at at least two different positions. The sensors can be connected in parallel so as to conserve the number of datalogger channels required. In the case of short canopies, soil heat flux density may be an important of the energy balance and it is worth the effort to obtain reliable measurements using the procedures suggested here.

Differential radiative heating of the fine wire thermocouples due to dissimilarity, (resulting from perhaps a spider's web or other deposits of dirt on one sensor and not on the other), especially at the peak radiative load directly after a cloud pass, can increase the measured temperature difference. This results in a smaller Bowen ratio and thus an overestimated $L_v F_w$. Morning dew will evaporate from the net radiometer and thermocouples much faster than from the air intakes, where it has a tendency to collect. Thus the vapour pressure difference will be small, β too large, and $L_v F_w$ underestimated. Care is needed to ensure that sudden spurts of vegetation growth (particularly following summer rains) do not damage the lower thermocouple or change the height of the lower sensor in relation to the canopy.

The slope of the surface needs some consideration in terms of affecting the measurement methodology of both horizontal and vertical gradients. Slopes induce air-flow up or down depending on time of day, and are thus rarely windless. Sampling of atmospheric gradients above a surface in the presence of wind should surely be done perpendicular to that surface, or a degree of representativeness will be lost. Slopes of up to 10° require a cosine correction that results in a reduction of less than 3 %, and thus correction is only necessary with quite large slopes.

Any increase in elevation could affect site comparisons due to pressure, and therefore, temperature changes, but would probably have an insignificant and undetectable effect on calculations with changes in altitude of tens of meters.

Our experience has been that the Bowen ratio system cannot be regarded as one that can be used to measure sensible and latent heat flux densities at remote sites unless it is possible to visit the site at at least weekly intervals. Besides the possibility of thermocouple damage and the need to change the filters, the most limiting factor was the need to set the bias of the dew point mirror system and clean the mirror at time intervals of probably less than a week. It is possible with an improved design in the electronics of the dew point mirror, that the time period of a week could be increased substantially.

The filters needed checking at each visit and replaced if necessary. During the burning season, the filters needed replacement more frequently because of increased dust and ash in the atmosphere. The net radiometer domes need to be replaced every six months and the sensor requires calibration once or twice a year. The manufacturers[10] recommend return of the instruments to them for recalibration every six months. A calibration method to alleviate the problems and costs associated with instrument return are described in Chapter 6.

The early pumps used with the Bowen ratio system used motors that were not brushless and had a life of about a year. The newer pumps are brushless and probably have a life time exceeding a year.

We recommend that the entire Bowen ratio system be returned to the laboratory every six months for a complete service and bench check of the sensors, datalogger, pump and mirror system. The user is advised to have available a standard sensor for the measurement of water vapour pressure and temperature. The datalogger requires checking against a standard voltage source, as recommended by the suppliers. It is also advisable that some of the sensors be checked in the field whenever possible (against an Assmann psychrometer, for example).

It is advisable to keep an extra supply of filters, thermocouples and net radiometer domes. In

10 The authors have the manufacturers' addresses for all components of the system. These could be supplied on request

addition, the user should have an extra pump available. These items should be taken to the field at each visit to avoid the inconvenience of extra travel.

Data stored should be properly identified, including a year identifier. Each research site, should be allocated a unique data storage area identifier. This is accomplished by the use of program instruction 80 (store area) when using the Campbell Scientific dataloggers. Together with the year identifier, the final storage identifier can assist the user in determining exactly the nature of the data. If the final storage identifier is altered every 1 January, there is no need to also attach the year identifier. This method would reduce the size of the data files.

3.7 Determination and use of a generalized exchange coefficient, K

3.7.1 Introduction

If a method of obtaining a reliable estimate of a generalized exchange coefficient K for any site could be found, considerable savings in instrumentation and therefore expense could be made. All that would be required to calculate the sensible heat flux density, is a K value and a single differential temperature. From this, in conjunction with an estimate of the available energy, the amount of evaporation could be calculated for the site.

The main assumption of the BREB method is the "assumption of Similarity" where the turbulent exchange coefficients for latent and sensible heat are assumed equal: ($K = K_w = K_h$) (Rider and Robinson 1951, Rider 1954, Tanner 1963, Dyer 1967 and, Swinbank and Dyer 1967). It is assumed that the ratio of the exchange coefficients (or eddy diffusivities) for the two types of energy fluxes considered is not significantly different from unity under the conditions for which the method applies. Therefore only one K value is required – the assumed (common) K value.

The original purpose of the study was to calculate and assess the temporal stability of the assumed K value. From this the applicability of the assumed Similarity between the two exchange coefficients could be assessed. In addition, the periods for which a uniform and relatively stable K value resulted could be found. From this, in turn, it could be assessed at what times of the day and under what conditions the Bowen ratio method can more confidently be applied.

Our aim was therefore to calculate the value and stability of the exchange coefficient under various atmospheric conditions, using a back-calculation method, without any measurements other than those for the Bowen ratio. We thereby also wished to determine the applicability of the assumption of Similarity. A revised aim became to postulate whether such a K value could be used site-specifically to calculate sensible and latent heat flux densities from a two point-differential air temperature measurement alone.

3.7.2 The "back-calculation" method of obtaining K values

The value of the exchange coefficient may be calculated directly from the governing diabatic profile equations[11] (Fuchs and Tanner 1967). This method requires *a priori* wind speed profile measurements and an assessment of the dependency of some of the parameters in the equations on atmospheric stability conditions by means of further measurements. It was therefore not attempted.

11 The transfer coefficient with the diabatic influence accounted for is given by Sellers (1965)

The value of the exchange coefficient can also be calculated indirectly either from simultaneous lysimetric and Bowen ratio measurements of heat flux density (Verma *et al.* 1978), or from simultaneous Bowen ratio and eddy correlation measurements at one site (Motha *et al.* 1979b) as discussed in Chapter 2. Rearranging the Bowen ratio and energy balance equations and substituting *lysimetrically* determined values for the flux densities would yield the best estimate of the unknown K. A single Bowen ratio system was used in the calculation of K.

The assumption of similarity between the two exchange coefficients ($K_h = K_w$) means that individual values for both of the exchange coefficients are not required (due to the assumption that the two diffusivities are equal and therefore cancel). Thus a common K value may be found using Bowen ratio measurements alone, and is, due to the formulation of the Bowen ratio, identical in value whether calculated from the sensible or latent heat flux density amount.

From the simplified energy balance equation: $I_{net} = L_v F_w + F_h + F_s$ and the simplified Bowen ratio: $\beta = \gamma\, \delta T/\delta e$, the unknowns $L_v F_w$ and F_h can be calculated from:

$$L_v F_w = \frac{I_{net} - F_s}{1+\beta} \text{ and } F_h = \frac{I_{net} - F_s}{1+(1/\beta)}.$$

The back calculation method can reveal the value of K ($= K_h = K_w$):

$$K_h = [F_h/\rho_a c_p]\, \delta z/\delta T \qquad 3.45$$

$$\text{and } K_w = [L_v F_w \gamma/\rho_a c_p]\, \delta z/\delta e. \qquad 3.46$$

If the calculated K value is now used in conjunction with the gradient measurements from another Bowen ratio system (or other independent source) to calculate the flux densities, a comparison of the results without any auto-self correlation is possible.

3.7.3 Results and discussion

3.7.3.1 The back-calculation method of obtaining K

It should be noted that an independent method of calculating (or preferably directly measuring) K is required to be able to simultaneously check the accuracy and precision of the method before it is applied. The method of calculation and the lack of a completely independent data set preclude the drawing of definite and quantitative conclusions and the comparisons made all contain a degree of auto-selfcorrelation. However, gradients used to calculate K were obtained from one set of Bowen ratio apparatus and those to check the dependency of K from another set adjacent to the first.

Confidence in the applicability of the assumption of Similarity between exchange coefficients will be greater if the back-calculated value of K does not vary considerably from one measurement period to the next. That is, if its covariance is low, then the assumption of Similarity is acceptable. But if the value of the calculated K varies considerably from one 20 min period to the next, then the likelihood that the two exchange coefficients are not similar is greater.

The exchange coefficient K during cloudless "normal" days was found to reach a fairly even and stable plateau of around 0.2 to 0.3 $m^2\ s^{-1}$ for the period 10h00 to 16h00 (Fig. 3.23). At later times, the value decreased consistently slowly towards zero at sunset, temporarily becoming negative but remaining just above zero until the next sunrise. Large spurious spikes occurred at the expected times due to the available energy approaching zero in the early morning and evening. The results were consistent with the values reported by Motha *et al.* (1979b) and Verma *et al.* (1978), although they reported a larger range of values, (0.1 to 0.7 $m^2 s^{-1}$) and larger maximum values, probably since their studies were carried out under advective conditions. The values reported by Fuchs and Tanner (1967) were much lower than was found, but their work was done over bare soil with the result that the latent heat flux density was much lower than that of the sensible component, indicating a lower midday common exchange coefficient of between 0.10 and 0.15 $m^2 s^{-1}$, possibly due to the effect of lack of vegetative cover. Fritschen *et al.* (1985) found that the value of the eddy diffusivity increased with plant height, surface roughness and instability, and reported midday values of 0.08, 0.8 and 8 $m^2 s^{-1}$ for alfalfa (0.5 to 0.8 m), saltcedar (2 to 6 m) and Douglas fir (30 m).

Night-time assessments of K were originally thought not possible due to the failure of the Bowen ratio technique at these times (when the available energy approaches zero). From the measurements however, an extremely stable value of 0.01 to 0.02 $m^2 s^{-1}$ was found after the rejection of data around sunrise and sunset time. Although the contribution that nocturnal evaporation makes is small, a continuous, 24 hour calculation of fluxes seems possible with the proposed method.

Analysis of the dependence of K on δT and δe showed that even though these were the "independent" variables used to calculate K (*via* the Bowen ratio-determined flux densities), they alone were not responsible for the trends observed (data not shown).

The ratio $\delta T/\delta e$ which constitutes the dynamic part of the Bowen ratio proved to account for much of the dependence. The dependence on wind speed (and therefore approximately on stability), was somewhat less. The net irradiance also had some effect on K, mainly by virtue of the fact that large

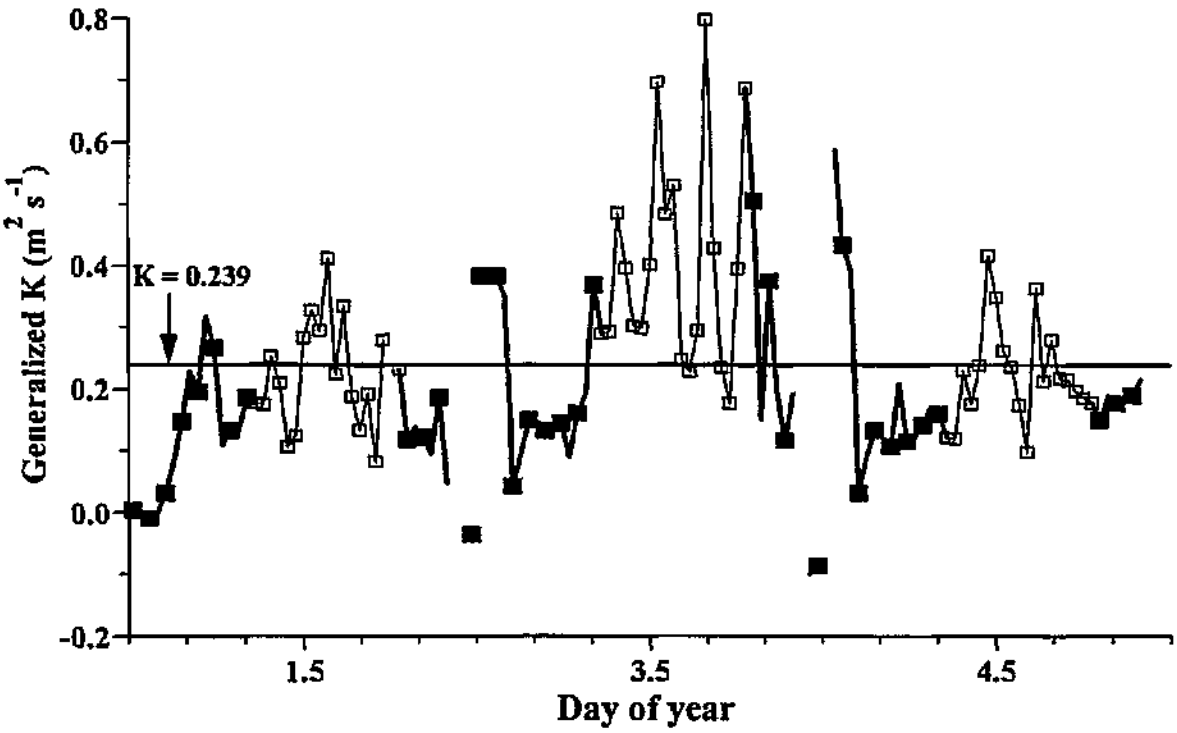

Fig. 3.23 Diurnal trend of a generalized K on three typical days in 1992. The "long" day (06h00 to 18h00 thin horizontal line -□-) and "short" day -■- (10h00 to 16h00 thick horizontal line) means are similar at this time of year. The overall mean for several month's data $K = 0.239\ m^2 s^{-1}$ is presented. The trend was consistent throughout the year, both in shape and value, and was comparable with similar trends found by Motha *et al.* 1979b

fluxes are primarily caused by large positive net irradiances. Less variability is encountered under high flux conditions with the result that the calculated value of K is more stable between measurement periods.

The mean and standard error of K over a typical period (Table 3.7) illustrates these points, and suggests that only "normal" cloudless days with large fluxes be used in the calculation of a representative K value for a site. The comparison of BREB-determined F_h values to results calculated with the average K value of 15 days (Table 3.8) and the independent temperature gradients were within 2 % over the period, even though the 20 minute predictions were somewhat lagged. The $L_v F_w$ comparison was generally within 5 %.

In the normal BREB formulation, all the energy balance components other than the latent and sensible heat flux densities must be measured, as well as gradients in *both* air temperature and water vapour pressure. But with the back-calculation method once a K value has been found for a site, only net irradiance and soil heat flux densities, and *either* of the gradients are required to find *both* F_h and $L_v F_w$.

A number of instrumental alternatives are thus possible:

- 1. measure $\delta T/\delta z$ and $\delta e/\delta z$ and hence calculate F_h and $L_v F_w$ (along with prior knowledge of K).
- 2. measure I_{net}, F_s and $\delta e/\delta z$ (from which $L_v F_w$ could be calculated from *a priori* knowledge of K, then F_h is calculated from the balance of the available energy: $F_h = I_{net} - L_v F_w - F_s$, or,
- 3. measure net irradiance, I_{net}, F_h, and $\delta T/\delta z$ from which F_h could be calculated from *a priori* knowledge of K: then $L_v F_w$ is calculated from the balance of the available energy using the equation $L_v F_w = I_{net} - F_h - F_s$.

Method 1 is essentially equivalent to the standard Bowen ratio method and as no instrumental savings are made, is the most accurate after the conventional BREB method. Method 2 requires the more

Table 3.7 Mean, standard error and covariance (CV) of K over a typical 15 day period

Day (1991)	$\bar{K}$ (m^2 s^{-1})	$\sigma(K)$ (m^2 s^{-1})	CV (%)
121	0.231	0.045	19.5
122	0.242	0.058	23.8
123	0.248	0.062	24.9
124	0.239	0.070	29.0
125	0.219	0.059	26.7
126	0.220	0.047	21.4
127	0.225	0.055	24.6
128	0.203	0.048	23.8
129	0.210	0.075	35.8
130	0.349	0.088	25.3
131	*****	*****	****
132	0.270	0.0551	204.0
133	0.267	0.056	21.0
134	0.219	0.084	38.5
135	0.239	0.149	85.9

Table 3.8 Comparison of $L_v F_w$ and F_h calculated with the conventional BREB method and the back-calculated K-method (MJ m^{-2}) (using independent δT values and $K = 0.239$ m^2 s^{-1})

Day	$L_v F_w$			F_h		
	BREB	K and δe	Difference	BREB	K and δT	Difference
121	5.17	4.45	0.72	5.21	5.17	0.04
122	4.28	4.53	-0.25	4.73	3.40	1.33
123	5.93	4.20	1.73	3.49	4.16	-0.67
124	4.10	1.18	2.92	5.34	5.38	-0.04
125	4.93	0.25	4.68	4.65	4.43	0.22
126	5.22	0.67	4.55	4.36	4.96	-0.60
127	5.22	0.35	4.87	4.12	3.82	0.30
128	4.85	0.31	4.54	4.29	4.91	-0.62
129	3.84	-0.34	4.18	3.61	3.66	-0.05
130	0.40	-0.40	0.80	1.33	0.57	0.76
131	2.49	-0.55	3.04	-2.72	4.36	-7.08
132	1.51	-1.78	3.29	2.32	0.89	1.43
133	4.48	0.12	4.36	5.64	4.69	0.95
134	4.33	0.56	3.77			
135	6.12	0.68	5.44	2.27	2.55	-0.28

difficult and expensive measurement of vapour pressure gradients but circumvents air temperature gradient measurement. The third choice represents the optimal saving in instrumentation, expertise, expense and upkeep, without sacrificing accuracy.

For the most accurate calculations of $L_v F_w$ and F_h once a time averaged K value has been found, the use of temperature gradients rather than the vapour pressure gradients is recommended. This is due to the good agreement obtained between sensible heat flux densities calculated in this way, and those sensible heat flux densities obtained as the result of the independent Bowen ratio method. The K method greatly underestimated the latent heat flux calculated with vapour pressure gradients on most days. This was perhaps due to underestimated daily evaporation totals due to the inclusion of large negative spurious data points after dark, (to which temperature gradient-determined daily totals are less susceptible). The latent component can then be more accurately calculated from the available energy, and thus has the additional (and over-riding) benefit of negating the requirement for a humidity sensor.

No discernible seasonal trend in K was found, which corroborates the conclusion that the K values obtained are correct, as the parameters from which K were calculated (Eqs 3.45 and 3.46) are seasonal. This study was carried out prior to the development of the intensive data rejection processes described in Section 3.2.6 but the conclusions remain unaltered.

3.7.3.2 A standard deviation method of obtaining β

An interesting alternative to the Bowen ratio technique is based on the assumption that air temperature and water vapour pressure fluctuations associated with the eddies that carry fluxes vertically are almost perfectly correlated (Swinbank and Dyer 1967, McBean and Miyake 1972). Hence, assuming that the exchange coefficients for sensible heat and latent heat flux density transfer are equal (Eq. 2.21), one may conclude:

$$\beta = \gamma\, \delta T/\delta e \approx \gamma\, \sigma_T/\sigma_e \qquad 3.47$$

where σ_T and σ_e are the standard deviations of the air temperature and water vapour pressure fluctuations (Kanemasu *et al.* 1979). However, Kanemasu *et al.* (1979) caution that the air temperature and water vapour pressure measurements must be performed by sensors that have the same time response. This is not the case for the sensors that have been used in the current study. The LI-COR LI6262 CO_2/H_2O infra red gas analyzer would enable the Bowen ratio to be determined using Eq. 3.47. The attraction of this approach is that the calculation of sensible and latent heat flux density may then be obtained using measurements at one atmospheric level only. The "standard deviation" method then is similar in approach to the eddy correlation method. Further research is required on this method.

3.7.4 Conclusions

A trend in the value of K was found that agreed well with the sparse literature available on this subject (Fuchs and Tanner 1967, Verma *et al.* 1978, Motha *et al.* 1979b and Fritschen *et al.* 1985). An overall average for K was 0.239 $m^2\,s^{-1}$(for L_vF_w greater than 200 W m^{-2}). More importantly, the lack of variability between measurement time intervals showed that the value of K_h/K_w is not changing markedly from one measurement period to another. This implies that the ratio is close to unity and the assumption is valid.

The requirements for long-term continuous monitoring of evaporative and sensible heat fluxes from one site may, by the proposed method be significantly reduced. An initial period spanning at least a set of seasons should be used to find a representative value of K for further use at the site. The instrumental requirements would be decreased to a two-point temperature gradient measurement and sensors to determine the available energy. One set of thermocouples, a net radiometer and soil heat flux plates, or some simpler estimate of available energy, are all that is required.

Since the measurements made for the calculation of the Bowen ratio can be used to determine the size and variability of K, this back-calculation method can routinely be carried out as part of the processing of Bowen ratio data. This enables an assessment of the conditions under which the Similarity Principle may be applied and thus the Bowen ratio method is acceptable.

Periods were found when the variability in K indicated that the assumption of similarity probably does not hold and should not be applied. These periods were found to be usually in the early morning and therefore these were most likely the stable periods of the day. At these times either the Bowen ratio results should be rejected or the ratio of the exchange coefficients adjusted in some way to account for the discrepancy. Data are probably rejected at many of these times by the other data rejection criteria. Days with low radiation loads and low wind speeds contributed to more varied K values temporally, due to the low values of F_h and L_vF_w and this could have somewhat confounded the drawing of such conclusions.

3.8 General conclusions

The effect of not accounting for the temperature, water vapour pressure and atmospheric pressure dependence of the so-called "temperature dependent" constants is not insignificant. The error in the Bowen ratio due to not correcting the psychrometric constant for these factors is related to the ratio of the uncorrected to the actual psychrometric constant. The errors may be avoided using the equations developed in this chapter.

The logistics of calculating sensible and latent heat flux density from measurements of net irradiance, soil heat flux density and the measurement of time-averaged air temperature and water vapour pressure differences are discussed. Criteria are required for the rejection of "bad" data corresponding to the Bowen ratio tending to -1. The major contributor to total error in latent heat is the error in the measurement of the water vapour pressure gradient. When evaporation rates are high, the relative accuracy in latent heat is good, even with a poorly measured Bowen ratio β. When β becomes large and evaporation less, the absolute error is smaller due simply to the smaller values, but the relative error increases.

Improvements in the Bowen ratio equipment we used should be devoted to improving the stability of the dew point mirror system.

Chapter 4

Measurement of sensible and latent heat using eddy correlation techniques

4.1 Abstract

The theory associated with the use of a krypton hygrometer, fine wire thermocouple and one-dimensional sonic anemometer for the eddy correlation measurement of latent and sensible heat is presented. The theory is modified for the case where the KH20 krypton hygrometer does not accurately measure the average water vapour density $\overline{q}$. This theory requires that $\overline{q}$ is known or measured accurately for the determination of latent heat flux density. The practical use, including sensor checking and datalogger aspects, of the eddy correlation equipment is presented. We showed that a single quadratic calibration equation can be used to compute vapour density using the KH20 hygrometer. Initial experimentation involved the use of a KH20 hygrometer and a PC207 relative humidity sensor in the laboratory. These measurements demonstrate that the KH20 hygrometer cannot be relied upon to yield a correct average vapour density. We showed that cleaning of the windows of the KH20 with a damp cloth did not decrease the deviation between $\overline{q}_{KH20}$ and $\overline{q}_{207}$. We showed that exposure of the KH20 hygrometer to a varying wind speed did not significantly alter $\overline{q}_{KH20}$. However exposing the source tube of the KH20 to a temperature different to that of the detector tube significantly altered $\overline{q}_{KH20}$. A field experiment confirmed that the underestimation in eddy correlation latent heat (measured using the KH20 hygrometer) compared to Bowen ratio measurements was due to the underestimation in the actual water vapour density. We obtained eddy correlation latent heat flux density measurements, that compared with Bowen ratio measurements, by adjusting $\overline{q}_{KH20}$ to $\overline{q}_{207}$ measured by a 207 relative humidity sensor.

4.2 Introduction

The advantage of eddy correlation techniques for the determination of sensible F_h and latent heat flux densities $L_v F_w$, is that the techniques are absolute. Commercially available eddy correlation equipment, have been available for some time. Data from an eddy correlation system may be checked by confirming that net irradiance I_{net}, measured using a net radiometer, satisfies the equation $I_{net} = L_v F_w + F_h + F_s$ for a short time period where F_s is the soil heat flux density, where physical storage, biochemical storage and advection heat flux density have been ignored. This check must be satisfied for each such time period. Alternatively, the latent heat amount measured using an eddy correlation system is often compared with lysimetric or Bowen ratio estimates. Problems surrounding the use of eddy correlation equipment, highlighted by Duell and Nork (1985) and Kizer, Elliott and Stone (1990), involve the integrity of the KH20 krypton hygrometer. In these cases, only a sonic anemometer and a fine wire thermocouple were used (enabling the sensible heat flux density F_h to be determined) with the latent heat amount $L_v F_w$ being calculated from $I_{net} - F_h - F_s$. This chapter concentrates on the use and problems associated with the krypton hygrometer as part of the eddy correlation system.

4.3 Theory

From the continuity equation for a compressible and homogenous medium,

$$\partial\,(\overline{w\,\rho_a})/\partial z = 0.$$

Integrating between the surface $z = 0$ and the measurement height z, we get

$$(\overline{w\,\rho_a})_z - (\overline{w\,\rho_a})_o = 0$$

where the subscripts refer to measurement height and canopy surface respectively. Since $\overline{w} = 0$ at the surface, we get that the time-averaged vertical flux density of dry air (kg s^{-1} m^{-2}) at the measurement height (- the first term of the above equation) is zero. Removing reference to the measurement height, we have:

$$w\,\bar{\rho}_a = 0 \qquad 4.1$$

where the bar indicates the time average (over 10 min, say). The instantaneous vertical wind speed can be written as a mean value $\overline{w}$ and a fluctuation w':

$$w = \overline{w} + w'.$$

Similarly, the instantaneous air density may be expressed as a mean value $\overline{\rho_a}$ and a fluctuation ρ_a':

$$\rho_a = \overline{\rho_a} + \rho_a'$$

Hence

$$\overline{(\overline{w} + w')(\overline{\rho_a} + \rho_a')} = 0$$

Expanding, and noting that, by definition the mean of a fluctuation is zero so that

$$\overline{w'} = \overline{\rho_a'} = 0,$$

we get:

$$\overline{w'\,\rho_a'} = -\overline{\rho_a}\,\overline{w}. \qquad 4.2$$

Hence

$$\overline{w} = 0$$

only if

$$\overline{w'\,\rho_a'} = 0.$$

The flux density F_E of an entity E, over a specified time period, is given by:

$$F_E = \overline{w\,\rho_a\,E} = \overline{(\overline{w} + w')\cdot(\overline{\rho_a} + \rho_a')\cdot(\bar{E} + E')}.$$

Hence

$$\begin{aligned}
F_E &= \overline{(\overline{w} + \overline{w})\cdot(\overline{\rho_a} + \rho_a')\cdot(\bar{E} + E')} = (\overline{w}\,\overline{\rho_a} + w'\,\overline{\rho_a} + \overline{w}\,\rho_a' + w'\,\rho_a')\cdot\overline{(\bar{E} + E')} \\
&= \overline{(\overline{w}\,\rho_a)\,\bar{E} + w'\,\rho_a'\,\bar{E} + w'\,\rho_a\,E' + \overline{w}\,\rho_a'\,E' + (w'\,\rho_a')\,E'} \\
&= \overline{(\overline{w}\,\rho_a)\,\bar{E}} + \overline{w'\,\rho_a'\,\bar{E}} + \overline{w'\,\rho_a\,E'} + \overline{\overline{w}\,\rho_a'\,E'} + \overline{(w'\,\rho_a')\,E'}
\end{aligned}$$

since

$$\overline{w'\,\rho_a\,\overline{E}} = \overline{\overline{w}\,\rho_a{}'\,\overline{E}} = \overline{\overline{w}\,\overline{\rho_a}\,E'} = 0 \text{ as } \overline{w'}.$$

Hence since

$$\overline{w'\,\rho_a{}'} = -\overline{\rho_a}\,\overline{w}$$

(Eq. 4.2),

$$F_E = \overline{w\,\rho_a\,E} = \overline{(\overline{w}\,\rho_a)\,\overline{E}} - \overline{(\overline{w}\,\rho_a)\,\overline{E}} + \overline{w'\,\rho_a\,E'} + \overline{\overline{w}\,\rho_a{}'\,E'} - \overline{(\overline{w}\,\rho_a)\,E'}.$$

By comparison $\overline{w}\,\overline{\rho_a{}'\,E'}$ is insignificant compared to $\overline{\rho_a}\,\overline{w'\,E'}$ and since

$$\overline{E'} = 0, \text{ we get:}$$

$$F_E = \overline{w\,\rho_a\,E} = \overline{w'\,\rho_a\,E'} = \overline{\rho_a}\,\overline{w'\,E'} = \text{covariance } (w, E).$$

The only assumptions in this derivation are that

$$\overline{w\,\rho_a} = 0$$

and that

$$\overline{w}\,\overline{\rho_a{}'\,E'}$$

is significantly less than $\overline{\rho_a}\,\overline{w'\,E'}$. Note that it has not been necessary to assume that $\overline{w} = 0$. Our sonic anemometer measurements of the average vertical wind speed above flat and sloped terrain (maize and grassland canopies) show that $\overline{w}$ is not always zero.

For latent heat flux density,

$$L_v\,F_w = L_v \cdot [\text{covariance } (w, q)] = L_v\,\overline{w'\,q'} \qquad 4.3$$

and for sensible heat flux density

$$F_h = \rho\,c_p \cdot [(\text{covariance } w, T)] = \rho\,c_p\,\overline{w'\,T'}, \qquad 4.4$$

where w, q, ρ, T are, respectively, the vertical wind speed, absolute humidity, air density and air temperature and c_p is the specific heat capacity of dry air at constant pressure.

For a krypton hygrometer, a Beer's law relationship is used to describe the attenuation of the 123.6 nm krypton line by water vapour. For a narrow range in vapour density:

$$V/V_o = \exp\,(-q\,x\,K_w) \qquad 4.5$$

$$\text{or } \ln V = \ln V_o - q\,x\,K_w \qquad 4.6$$

where V is the measured voltage corresponding to a given water vapour density q (g m^{-3}), V_o is the voltage corresponding to $q = 0$ g m^{-3}, x is the pathlength between the source and detector tubes of the sensor (mm) and K_w is the absorption coefficient for water vapour (m^3 g^{-1} mm^{-1}). The term $-x\,K_w$ is the slope of the calibration relationship (ln V *vs* q). The slope of this relationship is negative (for absorption) so that $x\,K_w$ is positive.

From statistical theory, $\sigma_q = [-1/(x\,K_w\,\overline{V})] \cdot \sigma_V$. Also, the standard deviation of q, SD(q) = $[-1/(x\,K_w\,\overline{V})] \cdot$ SD(V). Using finite differences, we have that the fluctuation in a quantity q' (where in this case, q' is the fluctuation in the water vapour density), defined by $q' = q - \overline{q}$, is approximately dq.

Hence:

$$q' \approx dq = dV \cdot (dq/dV) \approx V' \cdot (dq/dV). \tag{4.7}$$

Combining Eqs 4.3 and 4.7, the mean latent heat flux density over a defined time period is given by:

$$L_v F_w = L_v \overline{w' q'} = L_v \overline{w' V'} \cdot (dq/dV)_{V = \overline{V}}. \tag{4.8}$$

Combining Eqs 4.5 and 4.5, we have that

$$q' = V' \cdot [-1/(x K_w \overline{V})]. \tag{4.9}$$

$$L_v F_w = L_v \overline{w' V'} \cdot [-1/(x K_w \overline{V})]. \tag{4.10}$$

Calibration data supplied by Campbell Scientific, the manufacturers of the KH20 krypton hygrometer sensor show that a plot of ln V *vs* q is linear for a narrow range in vapour density. We propose a quadratic relationship between q and ln V over the whole range in vapour density. Hence,

$$[dq/dV]_{V = \overline{V}} = (b + 2\,a \cdot \ln \overline{V})/\overline{V} \tag{4.11}$$

where a and b are regression constants obtained from the KH20 krypton hygrometer calibration data. Based on this theory, a more accurate expression for the calculation of $L_v F_w$ is given by:

$$L_v F_w = L_v \overline{w' V'} \cdot (b + 2\,a \ln \overline{V})/\overline{V}. \tag{4.12}$$

The krypton hygrometer must accurately sense the fluctuation V' and $\overline{V}$ corresponding to q' and $\overline{q}$, respectively (Eq. 4.10). What if the KH20 hygrometer cannot be relied upon for absolute measurements of vapour density q but is however reasonably accurate for measurements corresponding to the fluctuation in water vapour density q'? We propose that if this is the case, then $\overline{V} = \overline{V}_{KH20}$ be replaced by $\overline{V}_{207}$ which corresponds to that of a 207 or Vaisala relative humidity sensor in close proximity to the KH20 sensor. Hence, using the Beer's law relationship between q and ln V, we get

$$\begin{aligned} (L_v F_w)_{corrected} &= (\overline{V}_{207}/\overline{V}_{KH20}) \cdot L_v \overline{w' V'} / [-1/(x K_w \overline{V}_{KH20})] \\ &= (\overline{V}_{207}/\overline{V}_{KH20}) \cdot (L_v F_w)_{uncorrected} = \exp\,[x K_w (q_{KH20} - q_{207})] \cdot (L_v F_w)_{uncorrected}. \end{aligned} \tag{4.13}$$

Although not entirely necessary, this procedure would be more convenient if the ratio $(\overline{V}_{KH20}/\overline{V}_{207})$ were constant.

The expression for sensible heat flux density is:

$$F_h = \rho\, c_p \overline{w' T'}, \tag{4.14}$$

where T' is the fluctuation in air temperature. Unlike the latent heat expression, the sensible heat expression does not involve an absolute measurement term.

4.4 Materials and methods

4.4.1 Sensor checking details

A simple check program was used for the fine wire thermocouple. We checked our sensors in the laboratory prior to field use. There are a number of checks that one could routinely perform on the sensors. At the back of the sonic anemometer arm there is a green military connector. We connected a wire between the A position of the connector and 1H (first high analogue connecting channel) of the

21X and another wire between the H position of the military connector and 1L of the 21X. The following program, in Edlog format, was entered into a 21X datalogger:

```
*   1      Table 1 Programs

 01: 0.1   s Execution Interval

01: P17    Panel Temperature
 01: 1     Loc :

02: P14    Thermocouple Temp (DIFF)
 01: 1     Rep
 02: 11    5 mV fast Range
 03: 1     IN Chan
 04: 2     Type E (Chromel-Constantan)
 05: 1     Ref Temp Loc
 06: 2     Loc :
 07: 1     Mult
 08: 0.0   Offset

03: P      End Table 1
```

Compiling the program by pressing *0 on the datalogger and *6 A A resulted in the actual temperature of the fine wire thermocouple (not the temperature fluctuations) being displayed on the 21X display. When placed in a laboratory, the temperature of the fine wire thermocouple should be fairly close to the datalogger panel temperature. A fine wire thermocouple temperature of -99999 indicates an open circuit and therefore a damaged thermocouple or a loose wire.

4.4.2 Field measurements

Fluctuations in wind speed w' (m s^{-1}), air temperature T' (K) and water vapour density q' (g m^{-3}) were measured using a CA27 sonic anemometer (Plate 2.1), a 127 fine wire chromel-constantan thermocouple (Fig. 2.15), a KH20 krypton hygrometer (Plate 2.1) and a 21X datalogger all of which are available from Campbell Scientific. The datalogger program enabled the determination of $\overline{w'q'}$ and $\overline{w'T'}$. Two 207 relative humidity sensors were used to measure the average water vapour density $\overline{q}$ (g m^{-3}) and average air temperature $\overline{T}$ (K) in close proximity to the KH20 sensor. Measurements were performed at 10 Hz for the fast response sensors and 1 Hz for all other sensors. A REBS Q*6 net radiometer was used to measure net irradiance I_{net} (W m^{-2}) and to check for closure (*viz.* that $I_{net} = L_v F_w + F_h + F_s$). Two Middleton soil heat flux plates were placed at a depth of 80 mm and the heat flux density stored above the plate calculated from soil specific heat capacity and soil temperature range with F_s being defined as the sum of the two. Soil temperature was measured using a pair of chromel-constantan thermocouples, one placed at a depth of 20 mm and the other at a depth of 60 mm. For the maize experiment, the one sensor was placed in the interrow and the other in the row.

A field comparison between mean specific humidity $\overline{q}$ measured using a cooled dew point mirror (Eastern Electric) used as part of a Bowen ratio system, a 207 relative humidity sensor and a KH20 krypton hygrometer was performed.

4.4.3 Laboratory measurements

For the laboratory measurements, an ultraviolet lamp was used to more easily control the duration and direction of exposure of the KH20 sensor to wavelengths less than 400 nm. A fan and a Casella air meter were used to create and measure various horizontal wind speeds in the vicinity of the KH20 hygrometer.

4.4.4 Datalogger programming

The limitation of the use of a Campbell Scientific 21X datalogger for eddy correlation measurements is that the datalogger execution time may be too long for the sensor measurement time. Typically, we used a measurement time of 0.1-s (corresponding to a frequency of 10 Hz). Therefore, it was essential to keep the datalogger program execution time to a minimum. The following parameters (described in Chapter 3) were calculated prior to measurements:

$$\rho \approx 2934.7773/[8.31451(T_d + 273.15) + 0.28362157\, h)]$$

(based on Eq. 3.5) where T_d is the average air temperature in °C and h is the altitude in m and

$$c_p = 1.0047226 + 1.148254 \times e/P$$

(Eq. 3.13) where e is an average water vapour pressure (in kPa) and P is the atmospheric pressure (kPa). Routinely, we used the following values: T_d = 25 °C and e/P = 0.01.

Since $F_h = \rho\, c_p \cdot$(covariance w, T) (Eq. 4.4) and since the multiplier for the vertical wind speed sensor is 0.001 m s^{-1} mV and that for the air temperature sensor is 0.004 °C mV^{-1}, we have:

$$F_h = \rho\, c_p \cdot 0.001 \times 0.004 \cdot [\text{covariance } (V_w, V_T)].$$

where V_w and V_T are the measured voltages (in mV) corresponding to the vertical wind speed and air temperature measured using the Campbell Scientific eddy correlation system.

For Pietermaritzburg, $\rho\, c_p \approx 1136$ J °C^{-1} m^{-3} (at 25 °C and RH = 50 %), then

$$F_h = 0.0048 \cdot [\text{covariance } (V_w, V_T)]$$

$$\text{or } F_h = 0.06742 \times 0.06742 \cdot [\text{covariance } (V_w, V_T). \qquad 4.15$$

The advantage of writing the sensible heat flux density in this form (Eq. 4.15) is that in the datalogger program for the determination of sensible heat flux density, the identical multiplier of 0.06742 (which should be entered as .06742 in the logger) can be used for both vertical wind speed and air temperature sensors. Therefore, both sensors can be monitored using a single voltage (single-ended) instruction with the multiplier of 0.06742. With this option, the execution time for the eddy correlation program for two eddy correlation systems is 134.7 ms with the output flag low and 143.1 ms for the output flag high. The execution time for a similar eddy correlation program for one eddy correlation system is 90.4 ms with the output flag low and 95.2 ms for the output flag high. These times would be increased by 76 ms for the two-system eddy correlation program if the single voltage instruction were not used and increased by 38 ms for a single-system program. Generally, one may therefore use an execution time of 0.1 s, corresponding to 10 Hz measurements if a single EC system is used. An execution time of 0.2 s, corresponding to 5 Hz measurements, may be used for a two-system eddy correlation system.

For Cathedral Peak Catchment VI, the constant in Eq. 4.4 should be replaced by 0.06335; for Lamesa, Texas, it should be 0.0666 and for College Station, Texas it should be 0.0.06953. A program that we used, consisting of six program statements, for one eddy correlation system connected to a single Campbell Scientific 21X is listed. The sensor connections are given in Appendix 2.

```
*  1          Table 1 Programs
 01: 0.2  s   Execution Interval

01:  P1       Volt (SE)
 01: 2        Reps
 02: 15       5000 mV fast Range
 03: 1        IN Chan
 04: 1        Loc :
 05: .06742   Mult 0.001 m/(s mV); 0.004 °C/mV; 1136 = ρ cp; Multiplier is the square root of 0.001 *
0.004 * 1136.3 to yield Fh in W m-2
 06: 0.0      Offset

02:  P92      If time is
 01: 0        minutes into a
 02: 5        minute interval
 03: 10       Set flag 0 (output)

03:  P62      CV/CR (OSX-0)
 01: 2        No. of Input Values
 02: 2        No. of Means
 03: 00       No. of Variances
 04: 00       No. of Std. Dev.
 05: 1        No. of Covariances
 06: 00       No. of Correlations
 07: 900      Samples per Average: Make this 900 for four subinterval averages during a 12 min
period
 08: 1        First Sample Loc
 09: 3        Loc :

04:  P77      Real Time
 01: 1110     Year, Day,Hour-Minute

05:  P70      Sample
 01: 3        Reps
 02: 3        Loc

06:  P71      Average
 01: 3        Reps
 02: 6        Loc

07:  P        End Table 1
```

4.5 Results and discussion

4.5.1 Calibration

Replicated calibration data, supplied by the manufacturers for the KH20 krypton hygrometer, were pooled and a single quadratic equation obtained:

$$q = 40.92762 - 0.5084 \ln V - 0.5833 [\ln V]^2, \quad 4.16$$

($r^2 = 0.999358$, 27 degrees of freedom, $S_{y,x} = 0.144597$ g m^{-3}) was fitted for vapour densities between 2 and 20 g m^{-3} (Fig. 4.1). The difference in dq/dV, evaluated at the mean $\bar{V}$ (see Eqs 4.8 and 4.10), using $[dq/dV]_{V=\bar{V}} = -1/(x K_w \bar{V})$ and $[dq/dV]_{V=\bar{V}} = (b + 2a \ln \bar{V})/\bar{V}$, exceeded 12 % for $q < 2$ g m^{-3} and -18 % for $q > 20$ g m^{-3} with no difference if $q \approx 10$ g m^{-3}. These large percentage differences justify the use of the quadratic relationship. However, to keep datalogger computation to a minimum, the quadratic equation was only applied after data collection using a computer.

4.5.2 Laboratory evaluation of sensor performance

After a period of 38 h in the dark, the KH20 mean vapour density measurements (10 min average) compared with that measured using a 207 relative humidity sensor (Fig. 4.2). Scaling of the KH20 windows, due to the 123.6 nm wavelength does not therefore affect measurement accuracy in the dark. After 38 h, under isothermal and dark conditions, the coefficient of variation of the KH20 vapour density measurements are less than 0.9 % compared to less than 0.1 % for the 207 sensor. However, after 38 h, the 207 and KH20 mean vapour densities deviated with the latter becoming greater. After removal of both sensors from the dark to low laboratory lighting conditions, the mean vapour densities

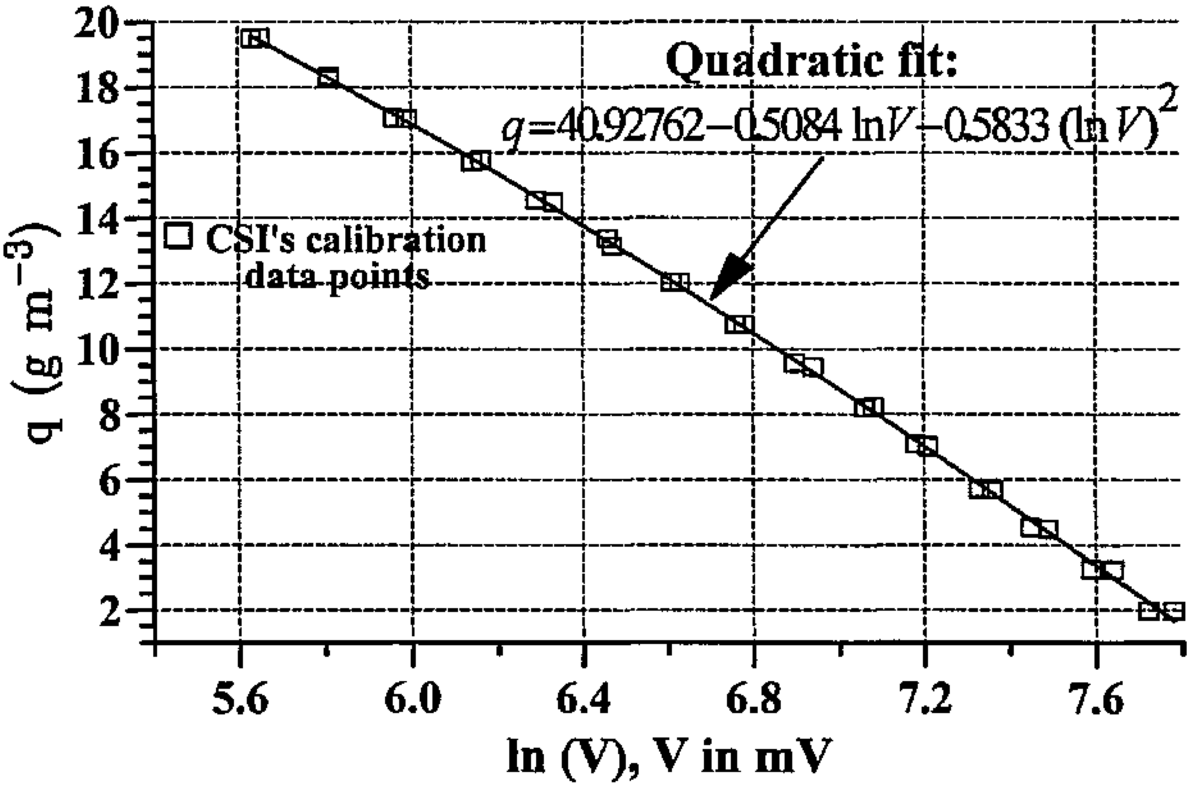

Fig. 4.1 Calibration data for a KH20 krypton hygrometer: absolute humidity q (g m^{-3}) as a function of ln V where V in mV is the krypton KH20 hygrometer voltage. Also shown is the quadratic relationship that applies to the entire water vapour density range

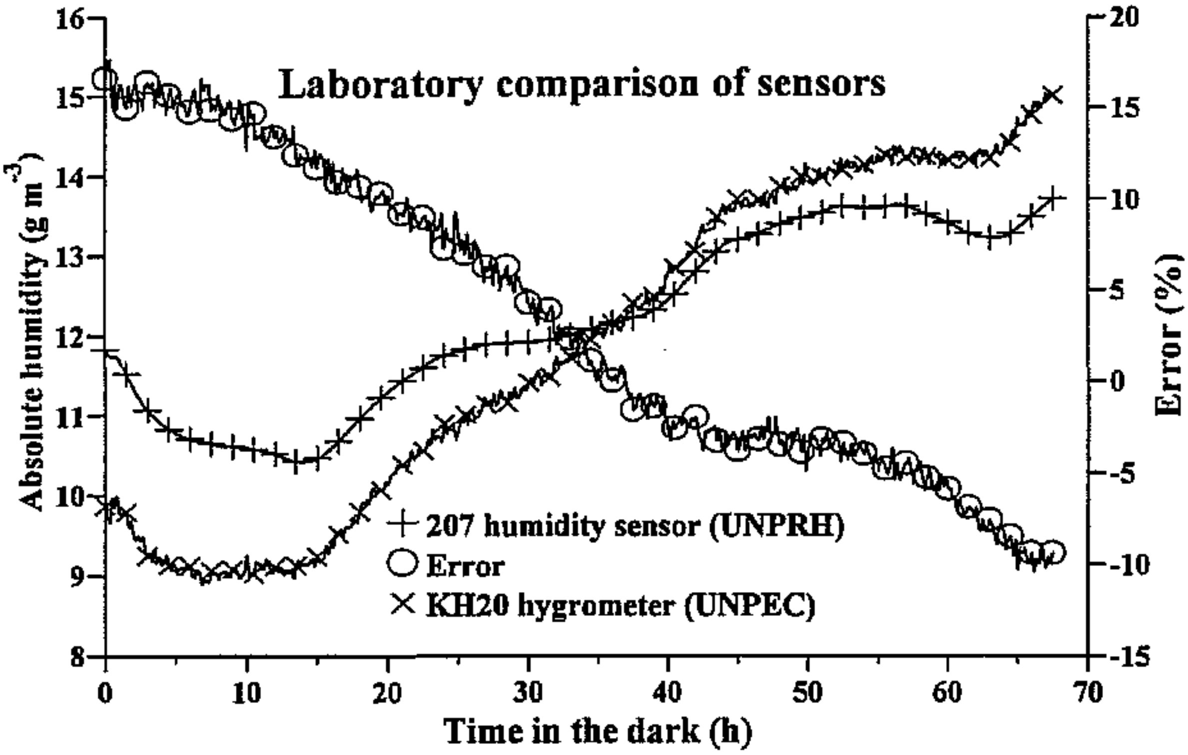

Fig. 4.2 The variation in the mean water vapour density q (g m^{-3}) using the eddy correlation KH20 sensor and the 207 humidity probe. Both sensors were maintained under dark and isothermal conditions for the full 70 hours of this experiment. The percentage error, assuming the 207 mean vapour density is correct, is shown on the right hand y axis

measured by the two sensors deviated with the KH20 vapour density decreasing below that of the 207 probe. These measurements show conclusively that the KH20 cannot be trusted to measure mean values of vapour density. Kizer *et al.* (1990) claim that the KH20 hygrometer sensor becomes encrusted with an unidentified deposit, due to some reaction of the air with the radiation, that is easily removed by wiping the windows with damp cotton. However, wiping the windows with a damp cloth did not decrease the deviation between the mean vapour densities measured using the KH20 and the 207 relative humidity sensor.

When the KH20 source tube was subjected to a temperature different from that of the detector tube, the average vapour density displayed by the datalogger increased. Holding the source tube (increasing its temperature by more than 10 °C) almost doubled the measured average vapour density. The experiments with the ultraviolet lamp were inconclusive as the switching on of the lamp also resulted in a temperature difference between the two tubes of the KH20 hygrometer. The experiments indicated that thermal insulation of the detector and source tubes is necessary.

Tanner (1984) pointed to one possible cause of error in a portable eddy correlation system: that the underestimation of latent heat flux density was perhaps the result of air flow constriction between the hygrometer source and sensor tubes. We tested this supposition by exposing the KH20 hygrometer to variable horizontal wind speeds, in the laboratory, using a non-oscillating fan (speed settings varying from 0 to 3). The wind speed was changed randomly every 2 min with the mean vapour density measured every 0.1 s but averaged over the 2 min period using a KH20 hygrometer. We could find no significant effect of wind speed on the mean vapour density in spite of a slowly varying mean value vapour density (Fig. 4.3).

4.5.3 Field evaluation of sensor performance

The underestimation of latent heat flux density using eddy correlation (using the KH20 sensor) is, in our opinion, due to the underestimation in the mean vapour density measured. In this experiment, water vapour density was measured using a KH20 hygrometer, a 207 relative humidity probe and a cooled dew point mirror system (as part of a Bowen ratio system). For the 207 vapour density calculations, the temperature used was that measured using the 207 temperature sensor. No corrections were made in the calculation of vapour density using the 207 probe or the cooled dew point mirror. The vapour density $q_{KH20} << q_{207}$ and $q_{207} \approx q_{mirror}$ (Fig. 4.4). The KH20 hygrometer was cleaned every hour and therefore the underestimation could not have been due to the encrustation on the window surface of the hygrometer, unless the encrustation occurs within an hour. The underestimation is quite consistent, implying that a uniform correction may be possible. The underestimation has been observed under field conditions and in the laboratory under relatively low lighting (Fig. 4.4). An underestimation in $\overline{q}$ would result in an overestimation in $\overline{V}$ (see Eq. 4.6, with $V = \overline{V}$ and $q = \overline{q}$) with a consequent underestimation in $L_v F_w$ (Eqs 4.8 and 4.10).

Tanner *et al.* (1985) found a reduction in the standard deviation of w', as measured using a sonic anemometer, with reducing temperature. We insulated our sonic anemometer to reduce any possible temperature influence on vertical wind speed. For a maize canopy, with a very slight increase in air temperature (as measured using the temperature sensor of a 207 relative humidity sensor), we measured large reductions in the standard deviation of w'.

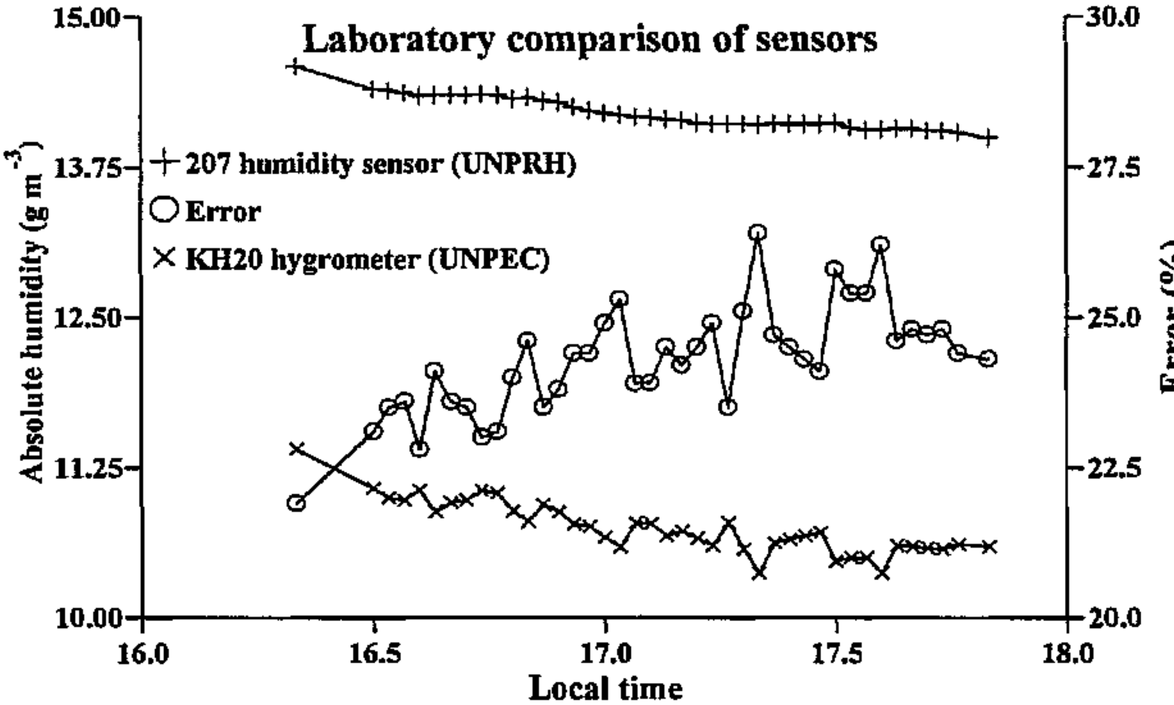

Fig. 4.3 The variation in the mean water vapour density q (g m^{-3}) using the eddy correlation KH20 sensor and the 207 humidity probe. Both sensors were maintained under variable and random wind speeds from a non-oscillating fan (speeds randomly varied between 0 and 3) under low laboratory lighting conditions. The percentage error, assuming the 207 mean vapour density is correct, is shown on the right hand y axis

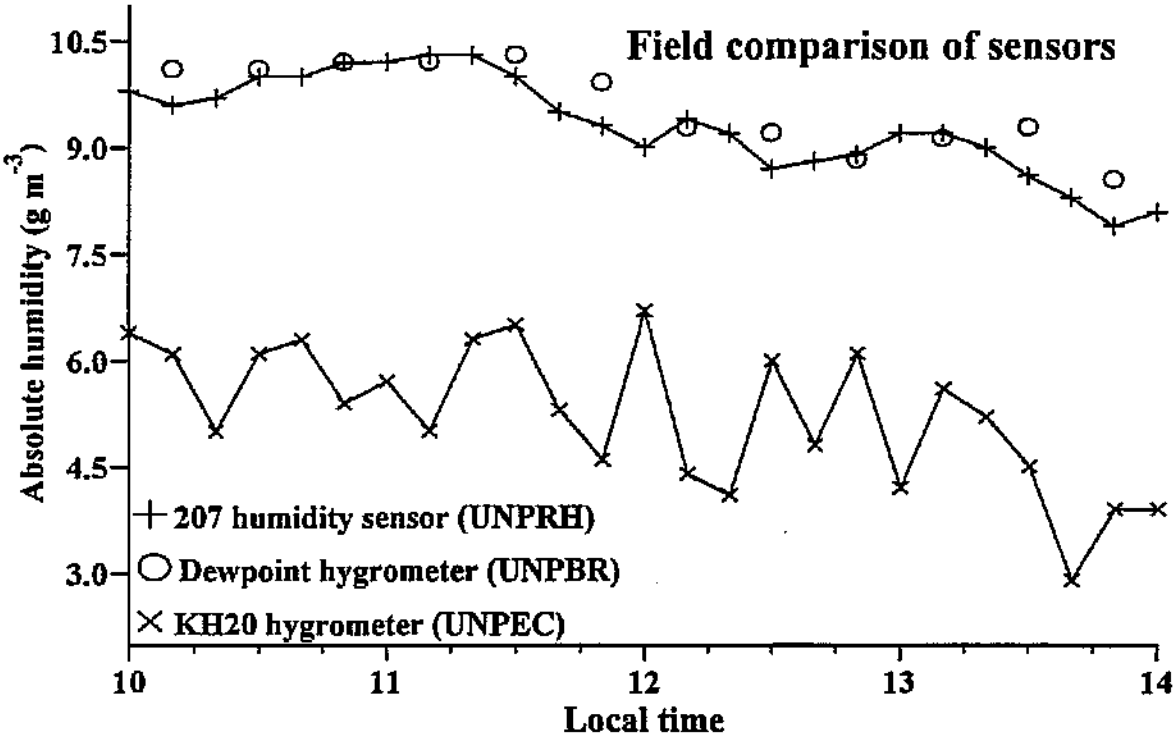

Fig. 4.4 The variation in the mean water vapour density $\overline{q}$ (g m^{-3}) using the eddy correlation KH20 sensor, a Bowen ratio dew point hygrometer and a 207 humidity probe. All sensors were maintained under variable and random wind speeds under field conditions (Cathedral Peak CVI) under cloudless conditions

4.6 Conclusions

Procedures for the laboratory checking of the eddy correlation sensors are presented. A single eddy correlation system may be attached to a 21X datalogger operating at 0.1 s (10 Hz). If two eddy correlation systems are attached, the measurement time should be 0.2 s (equivalent to a frequency of 5 Hz). Laboratory and field measurements demonstrated that the KH20 krypton hygrometer cannot be trusted to measure mean values of water vapour density. Generally, the sensor underestimates the mean water vapour density. Wiping the windows of the KH20 sensor with a damp cloth did not decrease the deviation between the mean vapour densities measured using the KH20 and the 207 relative humidity sensor. An underestimation in $\overline{q}$ would result in an underestimation in $L_v F_w$. The KH20 krypton hygrometer can be used for eddy correlation determination of latent heat flux density provided that the mean vapour density $\overline{q}$ is measured with another more accurate and reliable method. We found the 207 relative humidity sensor adequate for this purpose.

Chapter 5

Comparison of evaporation measurements and role of advective influences using Bowen ratio, lysimetric, surface temperature and eddy correlation methods[12]

5.1 Abstract

A study in KwaZulu-Natal (Cathedral Peak Catchment VI) involving Bowen ratio and eddy correlation aerodynamic measurements, equilibrium and Priestley-Taylor evaporation calculations and lysimetric measurements showed good comparison between Bowen ratio and lysimetric measurements and equilibrium evaporation calculations for the measurement period of the data. Priestley-Taylor evaporation calculations overestimated the evaporation by as much as 20 % compared to the data from the other techniques whereas eddy correlation measurements underestimated the evaporation significantly. The influence of advection on Bowen ratio evaporation measurements, calculated from Bowen ratio and lysimeter data, appeared to be relatively insignificant but variable. The total daily evaporation amounts for two Bowen ratio systems compared favourably with each other, lysimeter evaporation and with equilibrium evaporation, but less so for 20 min intervals. Methodology for the determination of aerodynamic, isothermal and canopy resistances are presented. For the data period selected, canopy resistance was typically less than 100 s m^{-1} during the middle part of the day with a canopy resistance to aerodynamic resistance ratio of about 0.5. The aerodynamic resistance was typically about 200 s m^{-1}. Eddy correlation latent heat flux density measurements above maize and above a mixed grassland community showed poor comparisons between equilibrium evaporation and Bowen ratio and eddy correlation latent heat flux density respectively. In another study above a turf grass surface, a surface temperature technique involving the measurement of the surface temperature to air temperature difference as well as a profile of wind speed, was used. Using this surface temperature method for calculating sensible heat flux density, agreement was obtained with eddy correlation measurements, even for a 12-min time-scale. An estimate of the friction velocity used in the surface temperature method was calculated from the wind speed at one level. The surface temperature method is significantly cheaper than eddy correlation and Bowen ratio techniques if friction velocity may be calculated from wind speed measurement at one level.

5.2 Introduction

In irrigated agriculture, information on total evaporation is important in selecting cropping strategies, designing irrigation systems and irrigation scheduling. Methods for evaporation measurement include soil based, plant (heat pulse, sap flow, porometry) and aerodynamic techniques. Aerodynamic measurements have the following advantages over the other methods mentioned: 1. measurement of leaf area index (*LAI*) is not necessary; 2. the techniques are portable compared to fixed lysimetric measurements; and 3. hourly or sub-hourly measurements are possible compared to the daily measurements obtained using the neutron probe.

However, aerodynamic measurements of sensible and latent heat flux density at the canopy surface,

12 Based on the paper by Savage *et al.* (1995a)

have fetch limitations (Heilman *et al.* 1989) and may be affected by advection (Lang 1973, Blad *et al.* 1977, Brakke *et al.* 1978, Bertela 1989). Furthermore, certain assumptions, that may be necessary for the theoretical development of a measurement system, may not actually apply.

In this study, evaporation was measured above a mixed grassland community and a maize crop at various locations in KwaZulu-Natal using Bowen ratio (Tanner 1960, Tanner and Fuchs 1969, Tanner *et al.* 1987) and eddy correlation techniques (Swinbank 1951, Tanner *et al.* 1985). These measurements, which appear to be the first reporting of such measurements for KwaZulu-Natal, were supplemented with lysimeter measurements, equilibrium evaporation and Priestley and Taylor (1972) evaporation estimates of actual evaporation. From the data collected, we were able to determine the influence of advection on the Bowen ratio evaporation measurements. In addition, measurements were performed above a turf grass surface using a surface temperature technique.

5.3 Theoretical considerations

When considering sensor height placement, advection and fetch influences on measurements above a vegetated surface, there are a few constraints that exist in the case of aerodynamic methods: vertical distance between sensors should allow the detection of large enough profile differences in the measured parameter; sensors placed above a vegetated surface for the purpose of monitoring sensible F_h and latent heat flux densities $L_v F_w$ at the canopy surface, need to be placed at a height z within the boundary layer for which both flux densities are constant with vertical height; and the measurement height for Bowen ratio and eddy correlation sensors is critical (Pasquill 1972).

5.3.1 Bowen ratio theory

According to Fick's Law of Diffusion, the latent heat energy flux density $L_v F_w$ (W m^{-2}) is given, in finite-difference form, by:

$$L_v F_w = (\rho c_p / \gamma) K_w (\bar{e}_2 - \bar{e}_1)/(z_2 - z_1) \qquad 5.1$$

where ρ is the air density (kg m^{-3}), c_p the specific heat capacity of dry air (J kg^{-1} K^{-1}) at constant pressure, γ the psychrometric constant (66 Pa K^{-1} at sea level), K_w the exchange coefficient (m^2 s^{-1}) for latent heat transfer, and $\bar{e}_2$ and $\bar{e}_1$ the time-averaged water vapour pressures (Pa) at heights z_2 and z_1 (m) respectively. The sign convention used here for latent heat and other flux density terms (except for the net irradiance I_{net}) is that an amount leaving the surface is positive and that being received is negative. The psychrometric constant γ (at atmospheric pressure p) may be calculated from γ_o, the psychrometric constant at sea-level atmospheric pressure p_o ($\approx$ 100 kPa):

$$\gamma \text{ (at atmospheric pressure } p) = \gamma \text{ (at sea-level pressure } p_o) \times p/p_o. \qquad 5.2$$

Similarly, the sensible heat energy flux density F_h (W m^{-2}) is given, in finite difference form, by:

$$F_h = (\rho c_p K_h)(\bar{T}_2 - \bar{T}_1)/(z_2 - z_1) \qquad 5.3$$

where K_h is the exchange coefficient for sensible heat energy transfer (m^2 s^{-1}) and $\bar{T}_2$ and $\bar{T}_1$ are the time-averaged air temperatures at heights z_2 and z_1 respectively.

Following Bowen (1926), we consider the Bowen ratio β (Chapter 3):

$$\beta = F_h/L_v F_w = (\gamma K_h/K_w)(\bar{T}_2 - \bar{T}_1)/(\bar{e}_2 - \bar{e}_1). \tag{5.4}$$

Generally, the exchange coefficients K_h and K_w are unknown. Rider (1954) showed that K_h/K_w is close to unity under a variety of conditions. Similarity holds when convective conditions are fully forced, that is, for which the Richardson number Ri satisfies the condition: $-0.01 \le Ri \le 0.01$ (Thom 1975). It is now generally accepted that the Similarity Principle holds good under neutral conditions, as opposed to stable or unstable conditions (Dyer 1974). Assuming this principle holds, then substituting $K_h/K_w = 1$ into Eq. 5.4, we get:

$$\beta = F_h/L_v F_w = \gamma(\bar{T}_2 - \bar{T}_1)/(\bar{e}_2 - \bar{e}_1). \tag{5.5}$$

Hence the Bowen ratio β can be determined from a measurement of air temperature and water vapour pressure at two levels (above canopy surface) in the atmosphere. The aerodynamic approach used thus far only enables the $F_h/L_v F_w$ ratio to be determined but not the individual flux density terms. To do this, we need to invoke the surface energy balance. Assuming that photosynthetic and physical heat energy storage amounts in the canopy are small and neglecting advection, the surface energy balance is given by:

$$I_{net} = L_v F_w + F_h + F_s \tag{5.6}$$

where I_{net} is the net irradiance above the canopy and F_s is the soil heat flux density. Substituting $F_h = \beta L_v F_w$ (from Eq. 5.5) into Eq. 5.6 and solving for $L_v F_w$, we get:

$$L_v F_w = (I_{net} - F_s)/(1 + \beta) \tag{5.7}$$

where $L_v F_w$ is indeterminate if $\beta = -1$ (that is, $F_h = -L_v F_w$ or, in other words, F_h and $L_v F_w$ are equal in magnitude but opposite in direction). Similarly, since $F_h = \beta L_v F_w$ (from Eq. 5.5), and using Eq. 5.7, we get:

$$F_h = \beta (I_{net} - F_s)/(1 + \beta). \tag{5.8}$$

If advection heat flux density A is not negligible, then Eq. 5.6 becomes:

$$I_{net} = (L_v F_w)_{BR} + (F_h)_{BR} + F_s + A_w + A_h \tag{5.9}$$

where the subscript BR indicates measurements using the Bowen ratio technique, $A = A_w + A_h$ is the energy flux density removed from the system ($A > 0$ W m^{-2}) or advected horizontally into the system ($A < 0$ W m^{-2}), and A_w and A_h represent the latent and sensible heat flux densities advected, respectively. It can be shown that, approximately:

$$A = (1 + \beta)\cdot A_w = (1 + \beta)\cdot[(L_v F_w)_o - (L_v F_w)_{BR}] \tag{5.10}$$

where $(L_v F_w)_o$ is the actual evaporation flux density at the canopy surface (Savage *et al.*, in preparation).

5.3.2 Lysimetric measurements

Evaporation measurements least affected by advection, theoretically, are lysimeter latent heat flux density measurements $(L_v F_w)_o$ and calculated lysimeter sensible heat flux density $(F_h)_o$ values where the latter is given by:

$$(F_h)_o = I_{net} - (L_v F_w)_o - F_s. \tag{5.11}$$

These values, $(L_v F_w)_o$ and $(F_h)_o$, are advection free for at the lysimeter surface, wind speed $\bar{V} = 0$ m s^{-1} so that advection flux density $A = 0$ W m^{-2}. The Bowen ratio method for the determination of $(L_v F_w)_{BR}$ and $(F_h)_{BR}$, which includes advective effects, may be compared with the respective $(L_v F_w)_o$ (using Eq. 5.10) and $(F_h)_o$ lysimeter values, the latter calculated from Eq. 5.11.

5.3.3 Equilibrium evaporation

The Penman-Monteith equation for the determination of canopy evaporation has been represented by (Thom 1975):

$$\alpha = L_v F_w / (I_{net} - F_s) \tag{5.12}$$

where

$$\alpha = [\Delta\, r_a + \gamma\, r_i] / [\Delta\, r_a + \gamma\, (r_a + r_s)]. \tag{5.13}$$

The term α represents the fraction of evaporation (that is, latent heat energy flux density) relative to the total available energy flux density $I_{net} - F_s = L_v F_w + F_h$ (Eq. 5.6). The so-called isothermal or quasi resistance r_i (s m^{-1}) (Thom 1975) is given by:

$$r_i = \rho\, c_p\, \delta e / [\gamma\, (L_v F_w + F_h)] = \rho\, c_p\, \delta e / [\gamma\, (I_{net} - F_s)] \tag{5.14}$$

where δe is the saturation water vapour pressure deficit (Pa): $\delta e = e_s - e$ where e_s is the saturation water vapour pressure at the measured air temperature and e is the water vapour pressure at a known height above ground. The resistance r_s is the bulk stomatal resistance (s m^{-1}) (also referred to as the canopy resistance r_c) and r_a (s m^{-1}) is the aerodynamic resistance.

The temperature dependent constants Δ and γ of the Penman-Monteith equation (Eq. 5.13) are usually represented on the psychrometric chart, by the magnitude of the slope of the saturation water vapour pressure *vs* temperature curve and the slope of the wet bulb temperature line of the psychrometric chart, respectively (both terms having units Pa K^{-1}). Air temperature affects evaporation *via* the relative magnitude of the temperature dependent constants Δ and γ:

$$\Delta/\gamma = 0.69347 + 0.043314\, \bar{T} + 0.00104 \bar{T}^2 + 2.725 \times 10^{-5}\, \bar{T}^3 \tag{5.15}$$

where $\bar{T}$ is the average air temperature in °C and γ is at 100 kPa.

The equilibrium condition is defined as that caused by a weak flow of humid air over an irrigated crop. Weak flow implies that r_a is large, humid air implies r_i is small compared to r_a and an irrigated crop implies that r_c is small compared to r_a. So the only large resistance is r_a, when compared to r_i and r_c. Hence, given these conditions, Eq. 5.13 reduces to:

$$\alpha_{equilibrium} = \Delta / (\Delta + \gamma). \tag{5.16}$$

At air temperatures 6, 18 and 26 °C, $\alpha_{equilibrium}$ has the value 0.50, 0.67 and 0.75 respectively (Fig. 3.6). Substituting $\alpha_{equilibrium}$ from Eq. 5.16 into Eq. 5.12 and solving for $(L_v F_w)_{equilibrium}$, we get:

$$(L_v F_w)_{equilibrium} = [\Delta / (\Delta + \gamma)] \cdot (I_{net} - F_s). \tag{5.17}$$

Priestley and Taylor (1972) found that actual evaporation from oceans, bare soil and vegetation was about 26 % greater than $(L_v F_w)_{equilibrium}$:

$$(L_v F_w)_{Priestley-Taylor} = 1.26\,(L_v F_w)_{equilibrium} = 1.26\,[\Delta/(\Delta+\gamma)]\cdot(I_{net} - F_s). \qquad 5.18$$

The Priestley-Taylor estimate of the actual evaporation $L_v F_w$ has been shown to be reliable for humid regions but has not been tested in arid and semi-arid regions such as southern Africa.

5.3.4 Eddy correlation

Ideally, eddy correlation sonic anemometer measurements (Chapter 4) of vertical wind speed fluctuation should be at a height that allows one eddy between the unit's separation distance d. If the sensor is too close to the canopy surface, more than one eddy may be sensed. Also, sonic reflections from vegetation may affect measurements. The first problem underestimates vertical wind speed fluctuation and there may be an overestimate for the second. Theoretically, for a sonic anemometer with source and detector tubes a distance d apart, the minimum operating height for flux density measurements is $6\,\pi\,d$ (Kaimal 1975). The eddy correlation technique (Swinbank 1951) is an absolute technique for the measurement of surface evaporation with sensors placed above the canopy.

5.4 Materials and methods

5.4.1 Bowen ratio measurements and eddy correlation measurements of maize

Two independent Bowen ratio systems were used to determine surface evaporation, the sensors of the systems being placed about 1 m apart. The research location was Catchment VI of the Cathedral Peak Forestry Research Station, in the foothills of the Drakensberg, Natal, South Africa at 29.00°S, 29.25°E, at an altitude 1935 m and with a predominantly north-facing aspect and average slope of 0.27. It is 0.677 km^2 (68 ha) in area and varies in altitude from 1847 to 2076 m (Schulze, 1975).

Net irradiance and soil heat flux density data were collected using separate sensors connected to separate dataloggers. Two net radiometers (one Middleton and one Fritschen type-), four soil heat flux plates (Middleton type-) and eight soil temperature sensors were used to measure net irradiance I_{net} (W m^{-2}), soil heat flux density F_s (W m^{-2}) and soil temperature T_{soil} (°C) respectively (Fig. 2.9) and used to calculate the Bowen ratio latent heat flux density $L_v F_w$ (W m^{-2}, Eq. 5.5) for each system. Lysimeter data enabled the surface latent heat flux density $(L_v F_w)_o$ to be measured directly. The construction details of the lysimeter are: the surface area of the lysimeter is 1 m^2 and contained 1 m^3 of soil with the design allowing a depth resolution of 0.1 mm. The net radiometers were placed 1.0 m above ground on a north-south axis with the radiometer support on the south side to avoid shading of the ground surface by the supports. The soil heat flux plates were buried at a depth of 80 mm, on a north-south axis together with a liberal length of wire to reduce the influence of heat conduction along the surface exposed wires to the sensor (Fig. 2.12). Four soil temperature sensors (type E thermocouples mounted in tubes and similar in design to other temperature sensors described by Savage 1980) were buried at depths of 20 mm and 60 mm below the soil surface (Fig. 2.12). These sensors were connected in parallel to produce a spatially averaged soil temperature measurement for the two depths for two different positions (Fig. 2.13). Soil water content in the 80 mm layer was gravimetrically measured every week.

In each of the Bowen ratio systems, a single cooled dew point hygrometer was employed to measure the dew point T_{dp} (°C) of air drawn in from 0.8 m or 1.8 m above ground (Figs 2.10, 2.11). For each system, air temperature at 0.8 m and the air temperature difference between 0.8 and 1.8 m was measured using two bare type E thermocouples each with a parallel combination of 76 µm diameter thermocouples. This combination would function even if one of the thermocouples were damaged. However, it is possible that a damaged thermocouple would result in greater measurement error. Since the thermocouples are unshielded from solar irradiance, a single damaged thermocouple at one of the levels may result in different radiation load at that level compared to the other level. This possibility was not investigated in this study.

All sensors were connected to a Campbell 21X datalogger, one datalogger being used for each of the Bowen ratio systems. A frequent measurement period of 1 s for dew point and air temperatures was employed and 10 s for all other sensors. The dew point temperature was averaged for a period of 80 s (after a mirror stabilization time of 20 s first), converted to water vapour pressure and then the datalogger switched a solenoid to sample the other level. Every 20 minutes the datalogger converted an average of the input storage values to final storage. Weekly, the data were transferred to computer and the Bowen ratio energy components calculated for each 20 min period from 08h00 to 18h00. Details of the eddy correlation measurement system was discussed more fully Chapter 4.

Equilibrium evaporation (Eq. 5.17) and Priestley-Taylor evaporation (Eq. 5.18) were calculated using net irradiance and soil heat flux density measurements (from one of the Bowen ratio systems). An independent air temperature (model MCS 174) from a weather station less than 10 m away was used to calculate $\Delta/(\Delta+\gamma)$ (using Eq. 5.15) where $\Delta/(\Delta+\gamma) = (\Delta/\gamma)/[(\Delta/\gamma)+1]$.

Due to the effect of dew, but also because the Bowen ratio $\beta = (F_h)_{BR}/(L_v F_w)_{BR}$ tends to -1 around sunrise and sunset causing $(L_v F_w)_{BR}$ (using Eq. 5.7) to be indeterminate (even in the absence of dew), only measurements between 08h00 and 18h00 were used for comparison with other techniques or calculations. This problem was not experienced with lysimetric or eddy correlation evaporation measurements. However, eddy correlation measurements were never obtained under condensation or dew conditions for fear of damaging the sonic anemometer and krypton hygrometer sensors.

5.4.2 Surface temperature and eddy correlation measurements above turf grass

All of the measurements discussed in this section were performed outside the Agricultural Engineering Workshops at Texas A & M University, College Station, Texas, United States of America (altitude of 100 m, latitude 30° 30′ N and longitude of 96° W) above a 1.6 ha short and flat bermudagrass (*Cynodon dactylon* L.) surface on a Boonville soil series (fine, montmorillonitic, thermic Mollic Albaqualfs) for Days 231 to 283, 1992.

Sensible heat flux density was determined using four EC systems. Fluctuations in vertical wind speed w' and the air temperature T' were measured using a CA27 sonic anemometer and a 127 fine wire (12.5 μm diameter) chromel-constantan thermocouple (available from Campbell Scientific, Logan, Utah, USA) (Fig. 2.15). The 127 thermocouple allows a temperature difference measurement but not an absolute temperature measurement. Alterations to the sensors included insulating the reference thermojunction of the 127 thermocouple and the metal arm containing the reference junction due to the fact that the response time of this junction could vary (Biltoft 1991, pers. comm.). We used extra insulation to increase the time response of the reference junction.

Air temperature at a height of 1 m above canopy was measured using five 50 μm copper-constantan thermocouples. The temperatures were averaged to produce one 12-minute air temperature average. Canopy temperatures were measured with 4° field-of-view infra red radiometers (Model 4000A, Everest Interscience, Tustin, CA). Three infra red radiometers at a height of 1.8 m above the canopy surface and at a view angle of 45° from the horizontal were pointed at the canopy surface to obtain an average canopy surface temperature.

Corrections (typically less than 1 °C) to surface temperatures (Jackson, 1982) were made for surface emissivity (ε_s) and atmospheric long-wave radiation (R_l, W m^{-2}) by

$$T_{corr} = [(\varepsilon_{irt}\,\sigma\,T^4_{uncorr} - (1-\varepsilon_s)\,0.38R_1)/(\varepsilon_s\,\sigma)]^{0.25} \qquad 5.19$$

where T_{corr} is the corrected temperature (K), T_{uncorr} is the measured (uncorrected) surface temperature (K), ε_{irt} is the IRT emissivity setting (0.98), σ is the Stefan-Boltzmann constant (5.673 × 10^{-8} W m^{-2} K^{-4}), and 0.38 is the estimated fraction of the full spectrum contained in the 8 to 14 µm IRT bandpass (Idso, 1971). Surface emissivity ε_s was taken as 0.975 (Lorentz, 1968; Brutsaert, 1982, Table 6.5). The atmospheric long wave irradiance R_l was calculated from $R_l = \varepsilon_a\,\sigma\,T_a^4$ where ε_a is the atmospheric emissivity and T_a is the air temperature (K). As skies were generally clear during the experiment, ε_a was estimated from (Idso and Jackson 1969):

$$\varepsilon_a = 1 - 0.261\,\exp\,[-0.000777\,(273 - T_a)^2]. \qquad 5.20$$

The calibration of the infra red thermometers is discussed in Chapter 6.

Wind profile data were used to determine the friction velocity u_* (m s^{-1}) for each 12-minute period as follows. The average wind speed was measured at 0.25, 0.5, 1.0, 1.25 and 1.5 heights z above canopy surface using model 12102 direct current three-cup anemometers (R M Young, Traverse City, Michigan) for each 12-minute interval.

The slope of plots of $\bar{u}$ as a function of ln (z) were equated to u_*/k (Thom 1975) where k is von Karman's constant ($k \approx 0.41$) from which u_* was calculated:

$$u = (u_*/k)\cdot\ln\,[(z-d)/z_o]. \qquad 5.21$$

The flux density of momentum τ (Pa) is defined by $\tau = \rho\,u_*^2$ 5.22

$$\text{where } \tau = \rho u(z)/r_{am}. \qquad 5.23$$

Combining these two equations we obtain an expression for the aerodynamic resistance for momentum:

$$r_{am} = u(z)/u_*^2. \qquad 5.24$$

5.5 Results and discussion

5.5.1 Bowen ratio estimates

The data of Fig. 5.1 indicate that $(L_v F_w)_{BR}$ comparisons between the two systems were good (Table 5.1). Hence either:

- both systems compare but are not accurately indicating the actual surface evaporation;
- or both systems compare but do accurately indicate the actual surface evaporation.

The slight bias in 20 min latent heat flux density $(L_v F_w)_{BR}$ values (Fig. 5.1, Table 5.1) and hence in sensible heat flux density F_h (data not shown) between the two systems is mainly due to the net irradiance differences between the two net radiometers (Fig. 5.2). However, these differences do not explain some of the scatter of the data (Table 5.1) of Fig. 5.1. The response of both systems to the changing microclimate is excellent (Fig. 5.3), the response being indicated by a change in evaporation

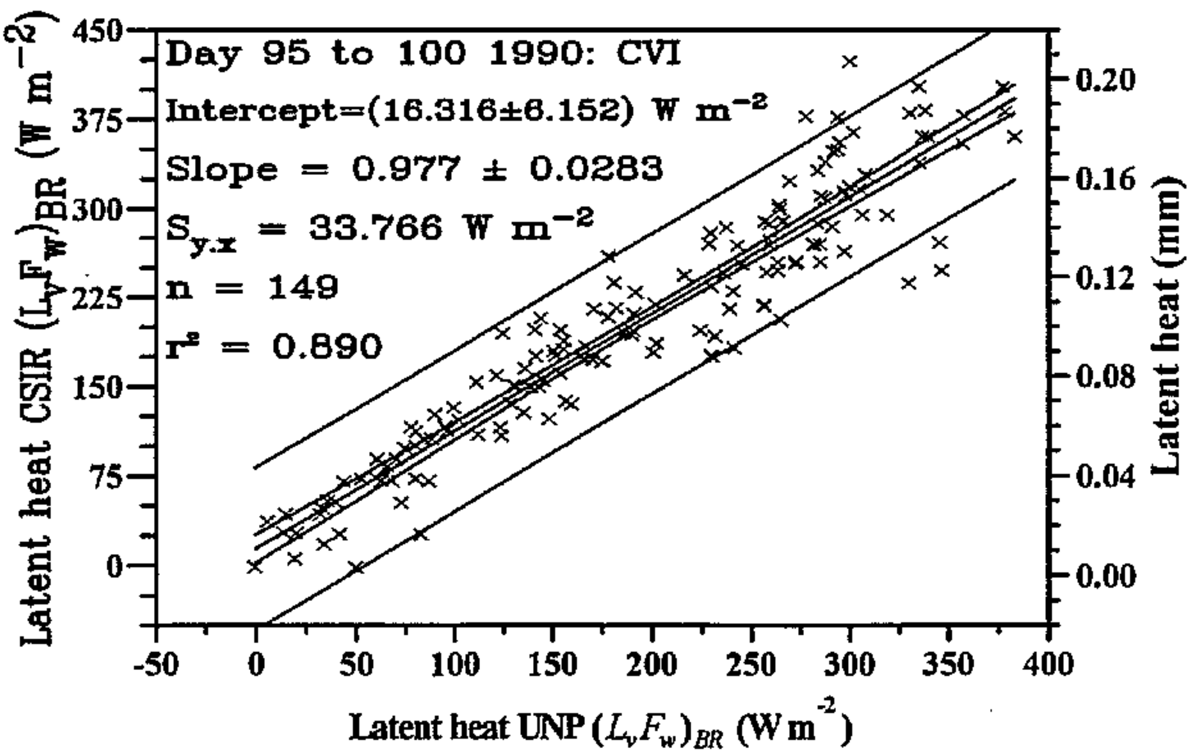

Fig. 5.1 Comparison between latent heat flux density $(L_v F_w)_{BR}$ (W m^{-2}, Eq. 5.7) (left hand y-axis) or in mm (right hand y-axis) for Day 95 to 100 inclusive (1990) for the 20 min data between 08h00 and 18h00 for UNP and CSIR Bowen ratio systems. The narrow confidence belts are for the mean and the wide for a single predicted value

$(L_v F_w)_{BR}$ to a sudden change in net irradiance I_{net}. The Bowen ratio technique is critically dependent on net irradiance measurements. It is therefore essential that the net radiometers being used are calibrated frequently. This aspect is discussed in detail in Chapter 6.

While there is some variability in the 20 min Bowen ratio $(L_v F_w)_{BR}$ data between the two systems, these differences are negated when calculating daily total evaporation (Table 5.2); the maximum percentage difference between the two systems for the five-day period was less than 8 % but the percentage differences averaged less than 3 %. The energy balance components are as expected for this time of year with latent heat flux density being the greatest component (Table 5.2). For these days (Table 5.2), so-called potential or reference evaporation is about 12 % greater than the Bowen ratio estimate of evaporation.

5.5.2 Eddy correlation evaporation

Unlike the Bowen ratio and lysimetric techniques, the eddy correlation is an absolute technique not requiring the use of the energy balance (Eq. 5.6) for the determination of $L_v F_w$ and F_h. However, the technique appears to underestimate evaporation when compared to the Bowen ratio and equilibrium estimates of actual evaporation (Table 5.1). The reasons for this underestimation was discussed in Chapter 4. The eddy correlation estimate of sensible heat flux density is discussed in Section 5.5.9.

5.5.3 Lysimeter evaporation

Bowen ratio evaporation estimates compare favourably with lysimetric estimates (Fig. 5.4, left hand y-axis in W m^{-2}, the right hand axis being in mm), indicating that both techniques are measuring actual

Table 5.1 Statistical data[1] associated with the 20 min comparisons between evaporation estimates $(L_v F_w)_{BR}$ (Eq. 5.7) from two Bowen ratio systems (W m^{-2}, Eq. 5.7), between equilibrium evaporation heat flux density $(L_v F_w)_{equilibrium}$ and UNP Bowen ratio evaporation (Day 95 to 100 inclusive, 1990), between lysimeter evaporation heat flux density $(L_v F_w)_o$ and Bowen ratio evaporation (Day 11 to 14, 1991) between eddy correlation and UNP Bowen ratio evaporation and between equilibrium and eddy correlation evaporation for the 08h00 to 18h00 time period. During this daylight hours, rainfree conditions prevailed. Also included are some of the statistics from the surface temperature technique (Section 5.5.9)

Site and statistical information	CSIR Bowen *vs* UNP Bowen	Equilibrium *vs* UNP Bowen	CSIR Bowen *vs* lysimeter	Eddy correlation *vs* UNP Bowen	Equilibrium *vs* eddy correlation	Surface temperature technique *vs* eddy correlation
Day of year, year	95 to 100, 1990	95 to 100, 1990	12 to 14, 1991	42 to 43, 1991	332 and 355, 1990	152, 156 to 159, 1992
Site	Cathedral Peak CVI	Cathedral Peak CVI	Cathedral Peak CVI	Cathedral Peak CVI	Cedara	College Station, Texas
Surface	Mixed grassland	Mixed grassland	Mixed grassland	Mixed grassland	Maize	Turfgrass
Slope	0.977	1.150[3]	0.911	0.449[3]	1.4558[3]	0.9606
SE_{slope}	0.0283	0.0203	0.0467	0.1410	0.2151	0.0428
Intercept (W m^{-2})	16.315[2]	-23.201[2]	54.592[2]	65.280	46.883	7.603
$SE_{intercept}$ (W m^{-2})	6.152	4.253	20.671	58.883	55.809	
Number of data points	149	158	75	26	60	543
r^2	0.890	0.954	0.839	0.297	0.441	0.895
S_{yx} (W m^{-2})	33.766	25.892	56.348	52.465	146.3	25.75
100 * root mean square systematic error/total mean square error	37.8	26.4	32.8	65.0	31.3	5.4
100 * root mean square unsystematic error/total mean square error	62.2	73.6	67.2	35.0	68.7	94.6
Total root mean square error (W m^{-2})	258.60	385.30	424.17	208.7	280.7	615.9

[1]In each case, the technique mentioned first has been used to generate the dependent evaporation data set and the second technique used to generate the independent evaporation data set

[2]We reject the null hypothesis that the intercept is 0 W m^{-2}, at the 95 % level of statistical significance

[3]We reject the null hypothesis that the slope is 1, at the 95 % level of statistical significance

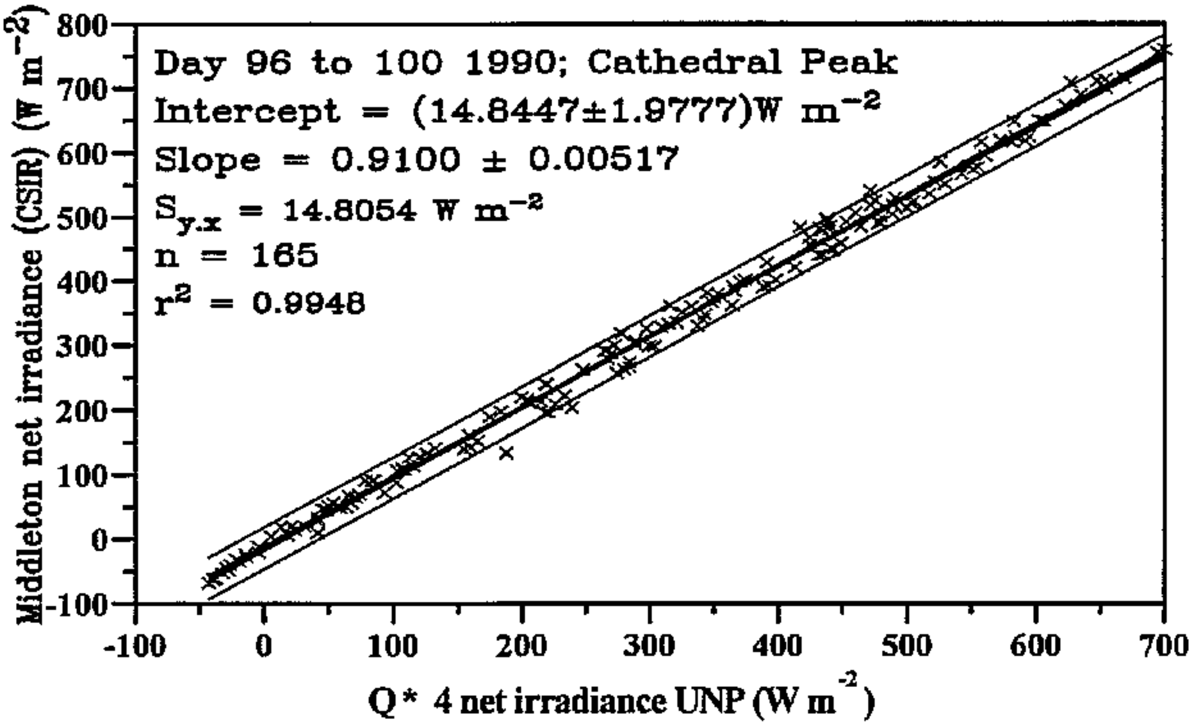

Fig. 5.2 Comparison of the Q*4 net radiometer (x-axis) with the Middleton net radiometer net irradiance I_{net} (W m^{-2}) for 20 min data (Day 95 to 100 inclusive) indicate a consistent bias. The narrow confidence belts are for the mean and the wide for a single predicted value

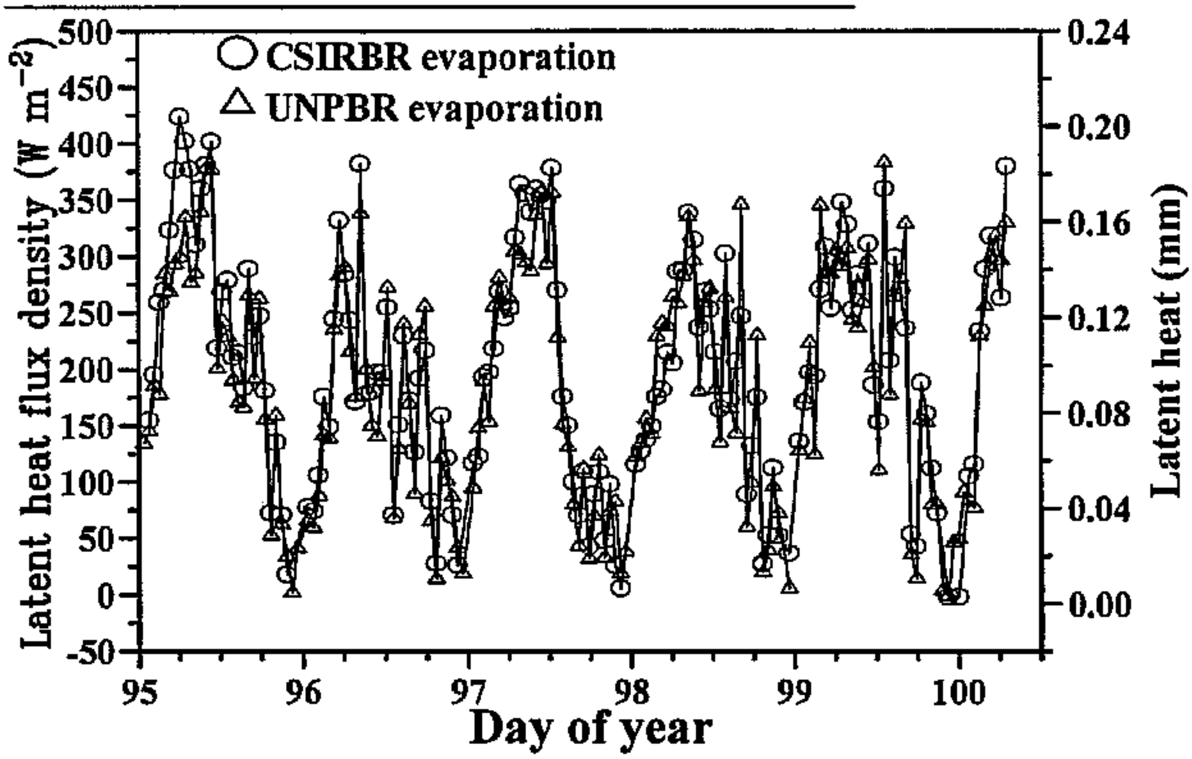

Fig. 5.3 Diurnal variation in Bowen ratio $(L_v F_w)_{BR}$ (W m^{-2}, Eq. 5.7) latent heat flux densities for the UNPBR and CSIRBR systems and equilibrium evaporation $(L_v F_w)_{equilibrium}$ (Eq. 5.18), for Day 95 to 100 inclusive (1990) for 20 min data between the times 08h00 and 18h00. The Day (of year) indication on the x-axis indicates the first measurement time for that day (08h00)

Table 5.2 Total daily estimates of the surface energy balance[1] (MJ m^{-2}) and evaporation (mm) using two Bowen ratio systems and wind speed and solar irradiance data for eight days (Day 93 to 100 inclusive) in April 1990 for the 08h00 to 18h00 time period for Cathedral Peak Catchment VI. The net irradiance (integrated for the day), marked with the double vertical line should be equal to the sum of the energy balance components (marked with a thick vertical line). The days chosen were rainfree during the daylight hours

System/method	Total daily evaporation (mm) for various days								Six day total (Days 95 to 100) (mm)
	93	94	95	96	97	98	99	100[2]	
Bowen ratio UNP (mm)	3.2	1.3	3.2	2.4	2.8	2.7	3.0	1.0	15.0
Bowen ratio CSIR (mm)			3.4	2.4	2.9	2.6	2.9	1.1	15.3

	Total daily value of the indicated term for various days								Eight day total (mm or MJ m^{-2})
	93	94	95	96	97	98	99	100	
$(L_v F_w)_{equilibrium}$ (mm)	3.3	1.0	3.3	2.3	2.7	3.0	2.8	1.3	19.7
$(L_v F_w)_{equilibrium}$ (MJ m^{-2})	8.16	2.57	8.02	5.58	6.57	7.46	6.90	3.26	48.54
$(L_v F_w)_{reference}$ (mm)	3.9	1.6	4.5	2.6	3.2	3.3	3.6	1.7	24.2
$(L_v F_w)_{reference}$ (MJ m^{-2})	9.52	3.97	10.99	6.46	7.80	8.14	8.75	4.12	59.74
Solar irradiance (MJ m^{-2})	19.44	7.29	16.06	13.46	17.42	17.97	15.83	18.12	116.74
I_{net} (MJ m^{-2})	12.43	3.30	11.68	7.69	9.35	10.84	9.20	4.38	68.86
$L_v F_w$ (MJ m^{-2})	8.03	3.13	8.01	5.99	7.04	6.90	7.69	3.52	56.81
F_h (MJ m^{-2})	4.03	0.54	3.04	1.84	2.06	3.59	1.53	0.89	11.25
F_s (MJ m^{-2})	0.30	-0.53	0.63	-0.14	0.25	0.35	-0.02	-0.03	0.81

[1]All values in MJ m^{-2} were calculated to three decimals and rounded off to two decimals; all values in mm were calculated to two decimals and rounded off to one decimal

[2]Incomplete day

surface evaporation (Table 5.1). Since the lysimeter is less affected by advection influences, it appears that advection is not playing a role to the extent that the Bowen ratio estimates are in error. As was the case with the two Bowen ratio systems, the response of both the lysimeter and Bowen ratio systems to the changing microclimate is good (Fig. 5.4).

5.5.4 Equilibrium evaporation

Equilibrium evaporation compares favourably with Bowen ratio estimates of evaporation for Cathedral Peak, Catchment VI (Figs 5.3, 5.5 and Table 5.2). It therefore appears that the equilibrium evaporation formulation accurately estimates actual evaporation for this time of year for a natural grassland surface. The diurnal variation in Bowen ratio latent heat flux density and equilibrium evaporation is depicted in Fig. 5.6 for Day 93 (1990). The in-phase variation is indicative of the influence of net irradiance on all three evaporation calculations. Typically, "reference evaporation" is the greatest of all three. For this day, equilibrium exceeds the Bowen ratio estimate of evaporation (Table 5.2, Fig. 5.6).

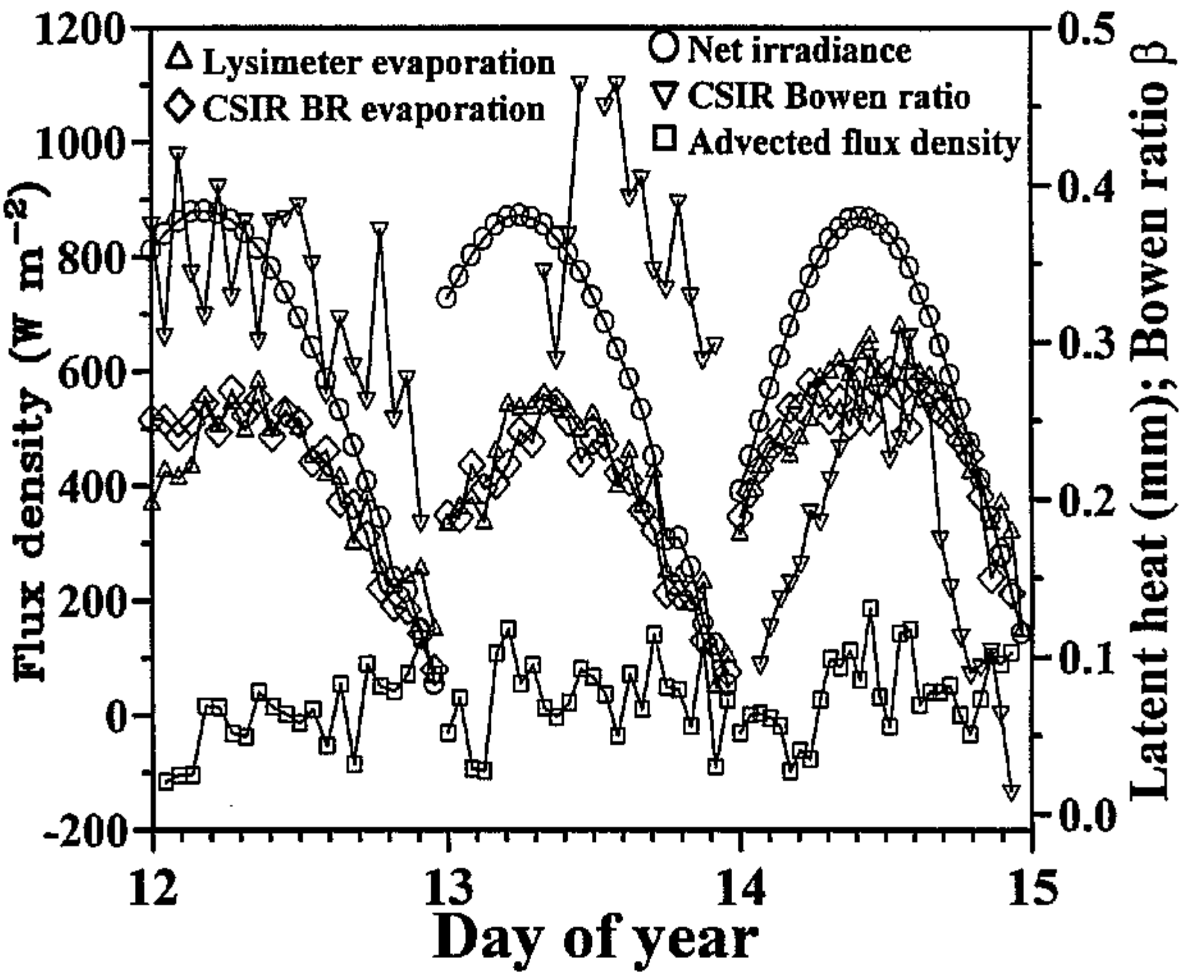

Fig. 5.4 Diurnal variation in net irradiance I_{net} (W m^{-2}, left hand y-axis; mm, right hand y-axis), advection heat flux density A (W m^{-2}), lysimeter evaporation flux density $(L_v F_w)_o$ (W m^{-2}, left hand y-axis; mm, right hand y-axis), Bowen ratio $(L_v F_w)_{BR}$ (Eq. 5.7) latent heat flux densities (W m^{-2}, left hand y-axis; mm, right hand y-axis), and the Bowen ratio β (Eq. 5.5, right hand y-axis only) for Day 12 to 14 (1991) inclusive for 20 min data between the times 08h00 and 18h00. The Day indication on the x-axis corresponds to the first measurement time for that day (08h00)

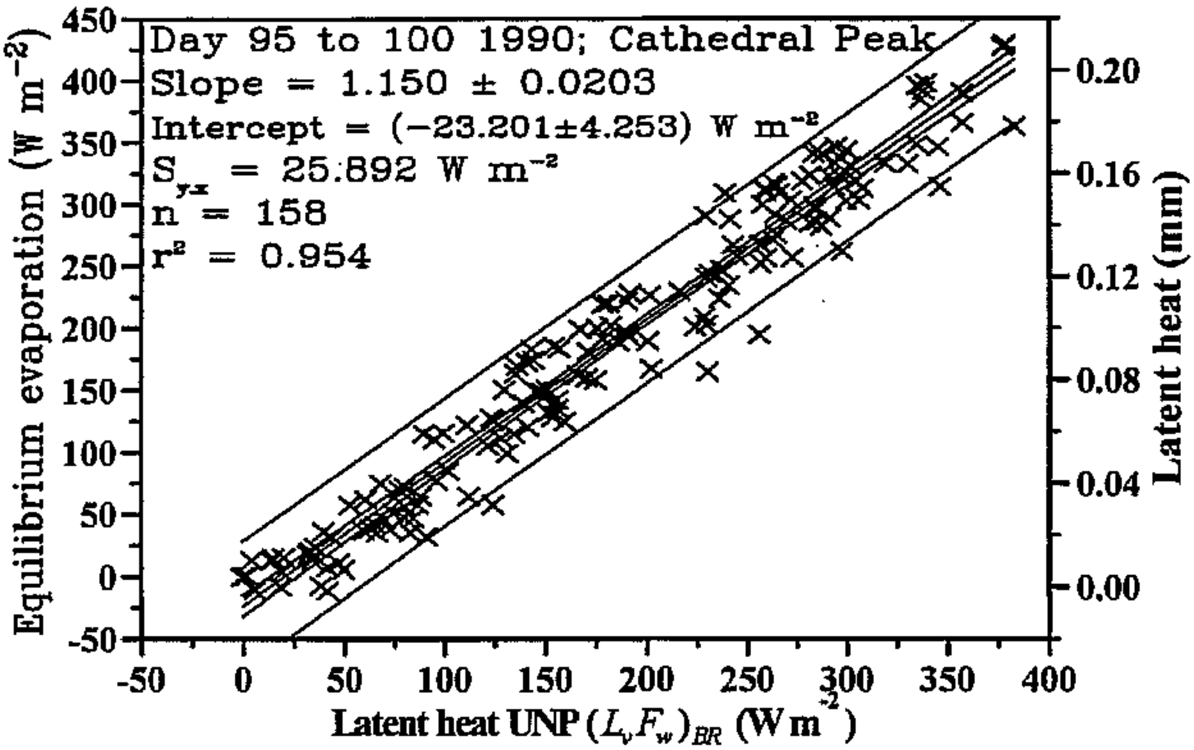

Fig. 5.5 Comparison between latent heat flux density $(L_v F_w)_{BR}$ (W m^{-2}, Eq. 5.7) for Day 95 to 100 inclusive (1990) for the 20 min data between 08h00 and 18h00 for the UNP Bowen ratio system and equilibrium evaporation flux density $(L_v F_w)_{equilibrium}$ (Eq. 5.16, left hand y-axis in W m^{-2} or right hand y-axis in mm. The narrow confidence belts are for the mean and the wide for a single predicted value

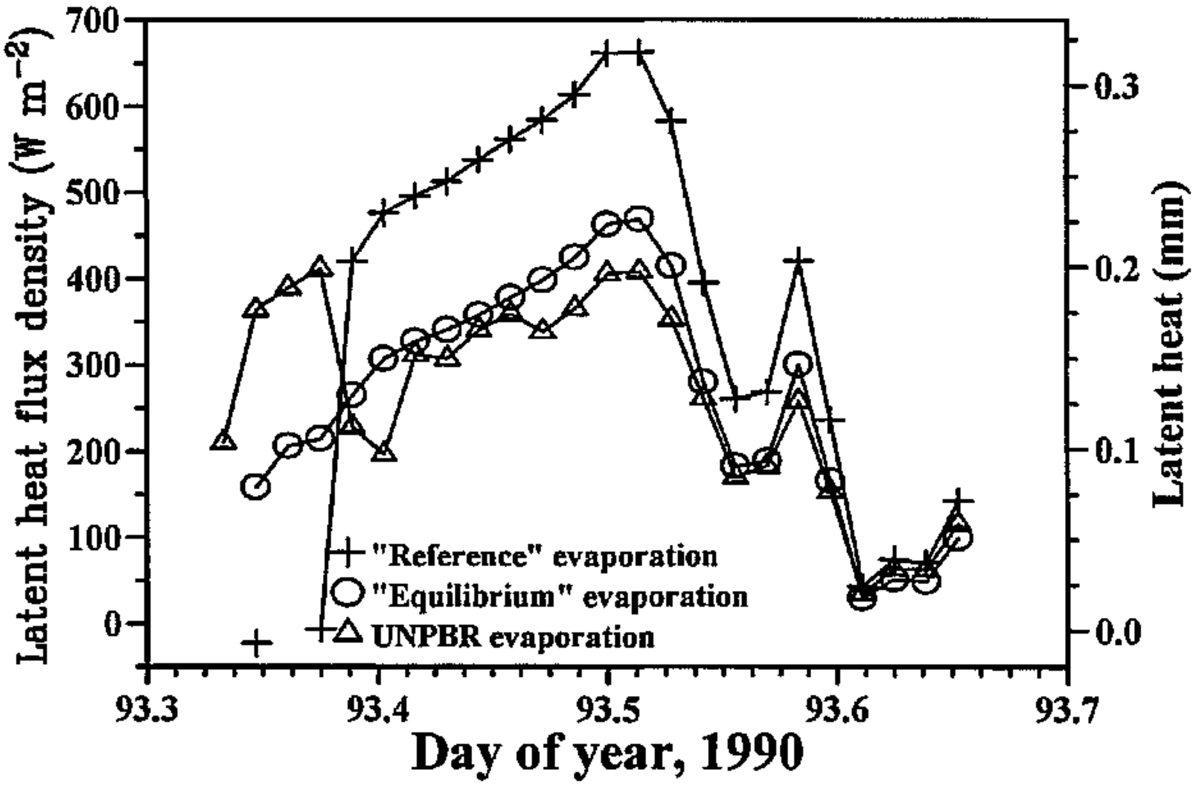

Fig. 5.6 The diurnal variation in reference evaporation, equilibrium and Bowen ratio evaporation for Day 93, 1990. The evaporation totals are 3.9 mm, 3.3 mm and 3.2 mm respectively (Table 5.2)

5.5.5 Effect of advection on Bowen ratio evaporation measurements

Evidence of advection has been obtained by comparing latent heat flux density $L_v F_w$ and $I_{net} - F_s$: if $L_v F_w > I_{net} - F_s$, then sensible heat flux density F_h has been drawn from the air and consumed in evaporation (Rosenberg *et al.* 1983). This inequality implies a negative Bowen ratio β (- see Eq. 5.7). We have never noticed a negative β value for our data sets (except during dew and rainfall events) and therefore have had to use other methods for determining the significance or otherwise of advection. The role of advection was investigated by comparing Bowen ratio evaporation with equilibrium and lysimeter evaporation. From the definition of equilibrium evaporation (viz., weak flow of humid air over a wet (that is actively transpiring) canopy, it is clear that if Bowen ratio estimates are significantly larger than equilibrium evaporation then:

- advection is significant;
- or the canopy cannot be considered to be green and transpiring.

The Bowen ratio estimates of evaporation compared favourably with equilibrium evaporation (Fig. 5.3, Table 5.1) except for times in winter when the canopy was extremely dry, with Bowen ratio estimates significantly less than equilibrium evaporation (Savage *et al.*, in preparation). This evidence indicates then that advection seldom played a role and that the Bowen ratio estimates indicated actual evaporation.

Interestingly enough, it appeared that equilibrium evaporation compared favourably with Bowen ratio evaporation estimates for values when the Bowen ratio β was less than 1 (at times of the year when the canopy was relatively wet). The differences between equilibrium evaporation and Bowen ratio evaporation increased as the Bowen ratio exceeded 1.

For eight days in April, the comparison of either of the two Bowen ratio evaporation estimates (Fig. 5.1) with equilibrium evaporation (Fig. 5.3) is very good for 20 min intervals, daily periods and for the eight day total time scales (Table 5.2) indicating that advection was not playing a significant role.

Assuming no error in lysimeter and Bowen ratio evaporation measurements, the advection flux density A (W m^{-2}) was calculated (Eq. 5.10) for three consecutive days for which Bowen ratio and lysimeter data were available (Fig. 5.4). For Day 13 and 14 (**Table 5.3**), $A > 0$ W m^{-2} indicating heat energy was being removed by advection during these times but for Day 12, A was generally negative indicating heat energy was being advected into the area. For this three day period, the magnitude of A never exceeded 203 W m^{-2} (Table 5.3). The data shown in Table 5.3 further indicate that the role of

Table 5.3 Mean $\bar{A}$, standard deviation SD_A, maximum and minimum of the 20 min advection heat flux density A values (W m^{-2}, Eq. 5.11) for three consecutive days (Day 12, 13 and 14, 1991) for the 08h00 to 18h00 time period for Cathedral Peak Catchment VI

Day of year	$\bar{A}$ (W m^{-2})	SD_A (W m^{-2})	Maximum A (W m^{-2})	Minimum A (W m^{-2})
12	-6	78	133	-203
13	32	68	150	-97
14	35	69	187	-97

advection is small for this three day period. However, it is clear from Fig. 5.4 and the standard deviation of A compared to the mean $\bar{A}$ (Table 5.3), that advective influences are variable. The Bowen ratio (right hand y-axis of Fig. 5.4), between the midday hours, averaged between 0.3 and 0.4, indicating high evaporation conditions.

5.5.6 Resistance estimates

For a reference crop, Smith (1991) gives a standard value of 70 s m^{-1} for the canopy resistance r_c. He also gives the relation:

$$r_a = 208/u_2 \tag{5.25}$$

where u_2 is the wind speed at a height of 2 m above the soil surface. For wind speed measured at 3 m, the relation is $r_a = 226/u_3$ assuming that the log wind profile relationship is valid (Eq. 5.21). Applying Eq. 5.21 and 5.24 with $z = 2$ m, $d = 0.67\ h$, $z_o = 0.1\ h$ and $h = 55$ mm and assuming that $r_{am} = r_a$, yields $r_a = 206$ s m^{-1}. So the use of Eq. 5.25 implies a canopy height of 55 mm. McInnes *et al.* (1994) found that $r_a = 1000/(0.55 + 9.8\ u^{0.5})$ for a bare ridge-furrow tilled soil surface.

The three resistances in the Penman-Monteith equation (Eq. 5.13) were calculated from Bowen ratio and wind speed data (Fig. 5.7). The aerodynamic resistance r_a (s m^{-1}) was calculated as:

$$r_a = 303.78/u_1 \tag{5.26}$$

(Section 5.5.9) for a short turf grass surface where u_1 is the mean horizontal wind speed (s m^{-1}) at a height of 1 m during a 20-min period. The isothermal resistance r_i (also referred to as the quasi-resistance) was calculated from the water vapour pressure deficit and the available energy flux density (Eq. 5.14). The canopy resistance r_c was back-calculated using the Penman-Monteith equation and knowledge of all terms (including the measured Bowen ratio latent heat flux density) except the canopy resistance. The ratio of canopy to aerodynamic resistance, r_c/r_a at midday is about 0.5 (Fig. 5.7). This is in contrast to the ratio 50 for forests quoted by Monteith and Unsworth (1990). In their review of other work, they show that dry forests have a daily minimum canopy resistance of 100 to 150 s m^{-1}. Hence, for the ratio of 50, the aerodynamic resistance was 2 to 3 s m^{-1} compared to our typical values of 200 s m^{-1}. The dramatic change in r_a for forests compared to grassland is due to the fact that r_a is a reciprocal function of wind speed which increases logarithmically with height (Eq. 5.21). Monteith and Unsworth (1990) give r_c/r_a values for forests as typically 50, and agricultural crops often close to unity. These values compare favourably with our value of 0.5. However, Ripley and Redmann (1976) show canopy resistances for a grassland site of less than 10 s m^{-1}. The shape of the curve for canopy resistance is similar to that published in the literature (Oke 1987, Monteith and Unsworth 1990).

5.5.7 Evaporation ratio

The ratio of Bowen ratio latent heat to so-called reference or potential evaporation (the latter calculated assuming a canopy resistance of 0 s m^{-1}) is shown for Day 93, 1990 (Fig. 5.8). The ratio shown is greater than 0.75 for both days, indicating that the actual evaporation is close to reference evaporation. One may expect that this ratio would vary seasonally.

5.5.8 Priestley-Taylor evaporation

Total daily Priestley-Taylor evaporation (Eq. 5.18) would overestimate Bowen ratio evaporation although correspondence is good. The 1.26 factor used for Priestley-Taylor evaporation would have to

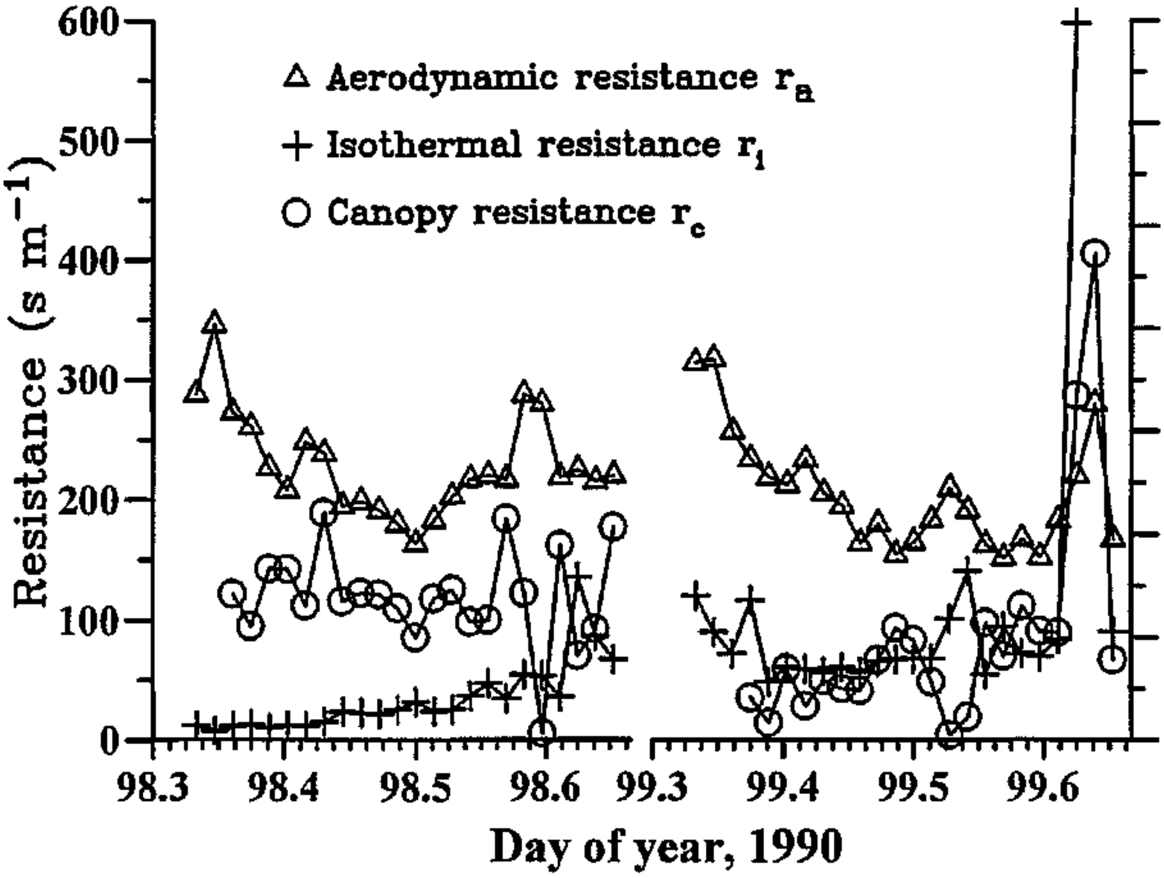

Fig. 5.7 Diurnal variation in the aerodynamic resistance r_a, isothermal resistance r_i and the canopy resistance r_c (s m^{-1}) for Days 98 and 99, 1990. The former resistance, a reciprocal function of the wind speed (Eq. 5.26), is generally the greatest during the daylight hours

be decreased to 1.05 for equality between the two estimates (Table 5.2). Bowen ratio evaporation estimates were closer to equilibrium evaporation (Eq. 5.17) than to Priestley-Taylor (Eq. 5.18) estimates.

5.5.9 Surface temperature and eddy correlation technique comparisons[13]

During this study above a flat, short turf grass surface, winds were generally southerly. Under such conditions, the uniform fetch distance was at least 190 m. Sensible heat measurements were only performed when the wind direction was between SW and ESE. The internal boundary layer thickness $\delta_{boundary}$, at the locations of the eddy correlation measurements was calculated using the Munro and Oke (1975) equation $\delta = x^{0.8} z_o^{0.2}$ where x is the fetch distance (≈ 190 m) and z_o, the surface roughness length (≈ 0.1 × canopy height), varied between 1.5 to 3 mm. Since a rough-to-smooth transition existed at our site, the lowest 5 % of the boundary layer was assumed to be in equilibrium with the surface (Brutsaert 1982). Therefore $\delta_{equilibrium} = 0.05 \times \delta_{boundary}$ with $\delta_{equilibrium}$ varying between about 0.90 and 1.05 m. Calculating z_o as ≈ 0.13 × canopy height yielded an equilibrium layer thickness of 0.96 to 1.10 m. It is therefore likely that eddy correlation measurements at 1 m were within the equilibrium layer.

13 Based on the paper by Savage *et al.* (1993) and Savage and Heilman (1993)

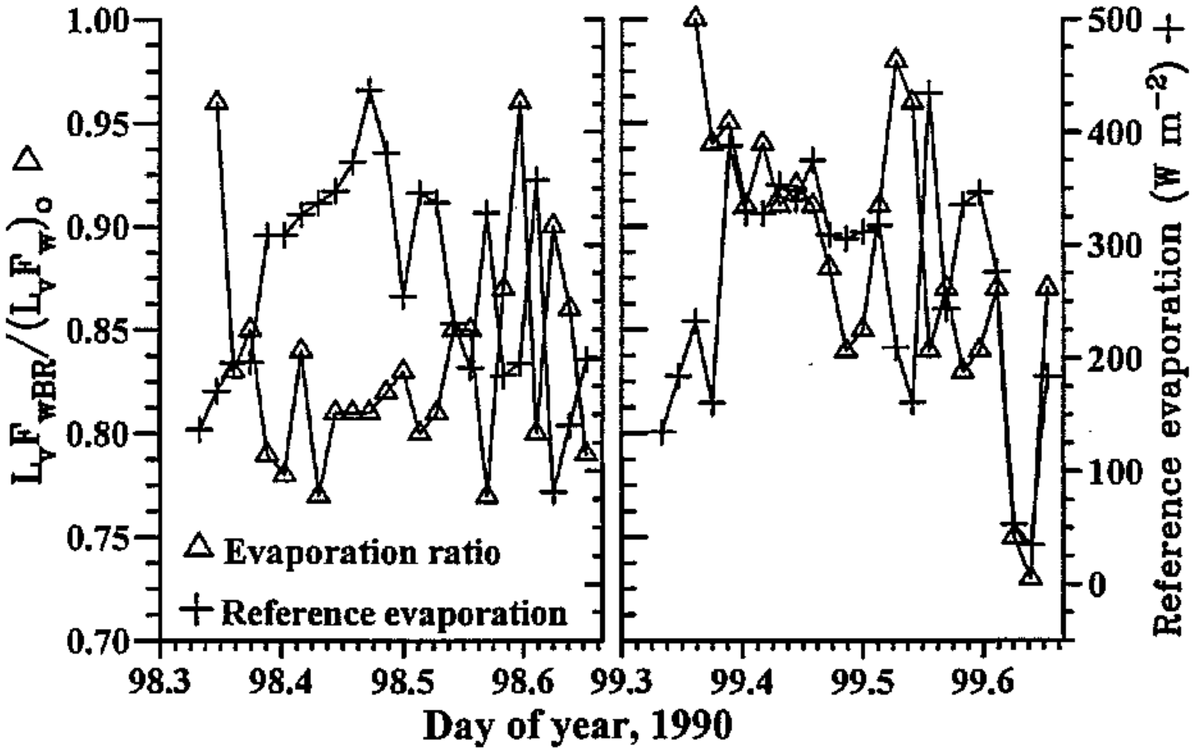

Fig. 5.8 The diurnal variation in the evaporation ratio (left hand y-axes) and reference evaporation (right hand y-axes) for Days 98 and 99 (1990)

In the case of the surface temperature technique, it is important to establish the reliability of the calculated friction velocity u_*. The variation of wind speed with height and local time, which was used to determine the friction velocity u_* (m s^{-1}), is shown in Fig. 5.9[14]. Of note is the increase in wind speed at around 10h00 local time at all heights, typically corresponding to the change in stability conditions to instability. The diurnal variation in the friction velocity u_* (m s^{-1}) and the corresponding statistics (determined for each 12-minute period) r^2 and $S_{y.x}$ (m s^{-1}) of the u *vs* ln $(z-d)$ relation for Day 249 is also shown (Fig. 5.10). As expected, the friction velocity also increased at around 10h00 when there was an increase in wind speed at all heights. The r^2 and S_{yx} values of the u *vs* ln $(z-d)$ relationship correspondingly decreased and increased respectively at about the same time (Fig. 5.10). The logarithmic relationship ln $(z-d)$ *vs* u is shown (Fig. 5.11) for selected times on Day 249. The regression lines show the good linear relation. It would appear that the method used to determine the friction velocity u_* is a robust one and that therefore the friction velocity data so obtained are reliable. There were however times when the wind speed was low and the relationships shown in Fig. 5.11 were less reliable. In such cases, stable conditions usually prevailed. The other disadvantage is that the stall speed of three-cup anemometers may be as high as 0.5 m s^{-1}. A wind speed of this magnitude would mean that events may be excluded from the calculation of sensible heat flux density using the surface temperature technique.

14 A three dimensional (fishnet projection) of the local time, placement height and wind speed data triplet set was generated using a bivariate interpolation of wind speed (Fig. 5.9)

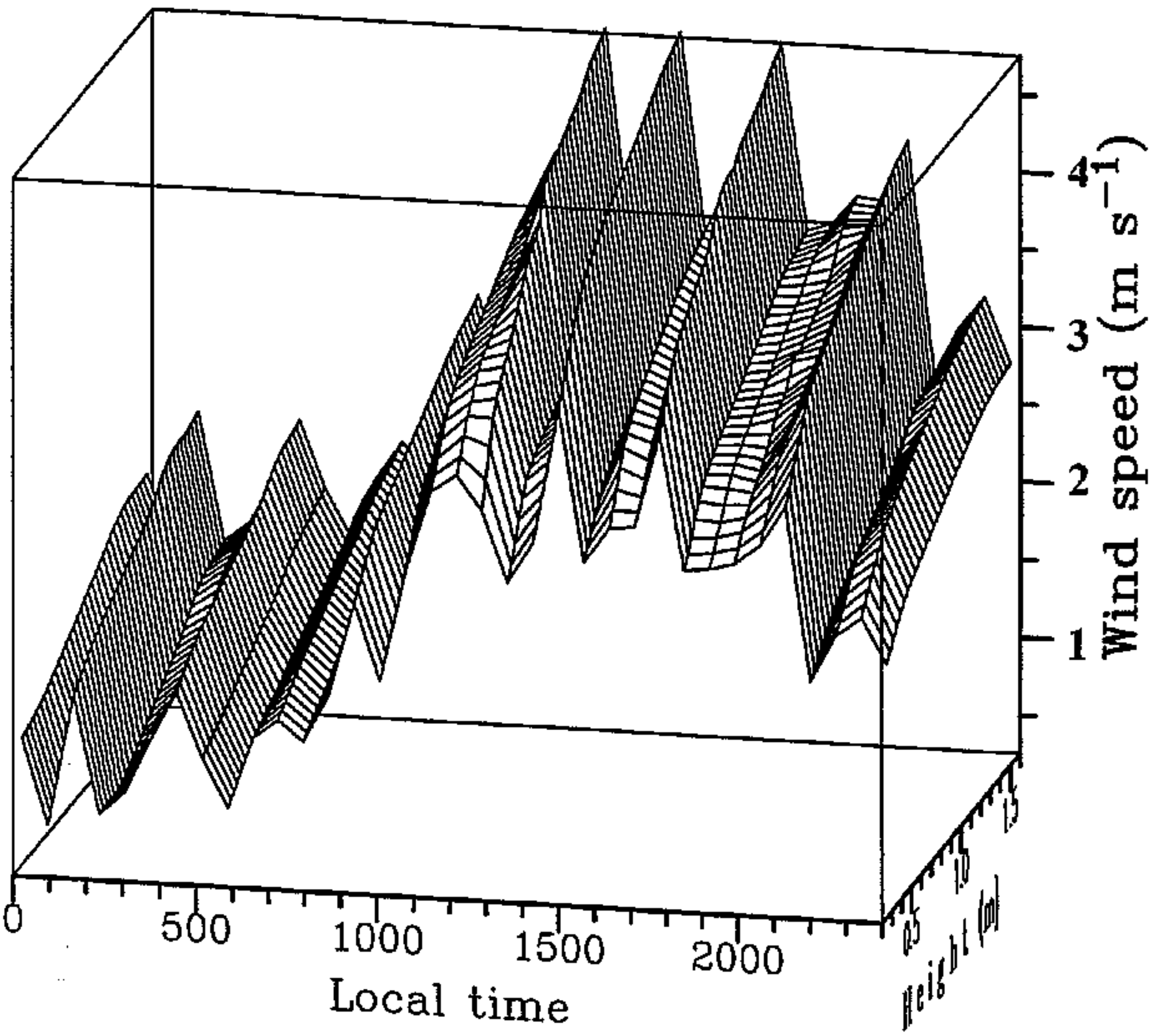

Fig. 5.9 The diurnal variation in wind speed u (m s^{-1}) as a function of local time (Day 249, 1992) and placement height z

We used three infra red radiometers to measure canopy temperature T_o. Air temperature T_z was measured, using five fine-wire thermocouples, at a single height (1 m in our case). The three canopy temperature and five air temperature measurements were averaged for each 12-minute period. These measurements allowed the calculation of sensible heat F_h from:

$$F_h = \rho\, c_p\, (T_o - T_z)/r_{ah} \qquad 5.27$$

where ρ ($\approx$1.17 kg m^{-3}) is the air density, $c_p \approx$ 1056 J kg^{-1} K^{-1}, and r_{ah} (s m^{-1}) is the aerodynamic resistance to sensible heat transfer. Since the canopy temperature T_o and air temperature T_z are known, it remains to determine an expression for the aerodynamic resistance r_{ah}. Considering the flux density of momentum τ (Pa), we write:

$$\tau = \rho\, u_*^2 = \rho\, u(z)/r_{am}$$

(Thom 1975) where u_* is the friction velocity (diurnal plot shown in Fig. 5.10), and r_{am} the aerodynamic resistance for momentum transfer. Assuming Similarity between r_{am} and r_{ah}, we have:

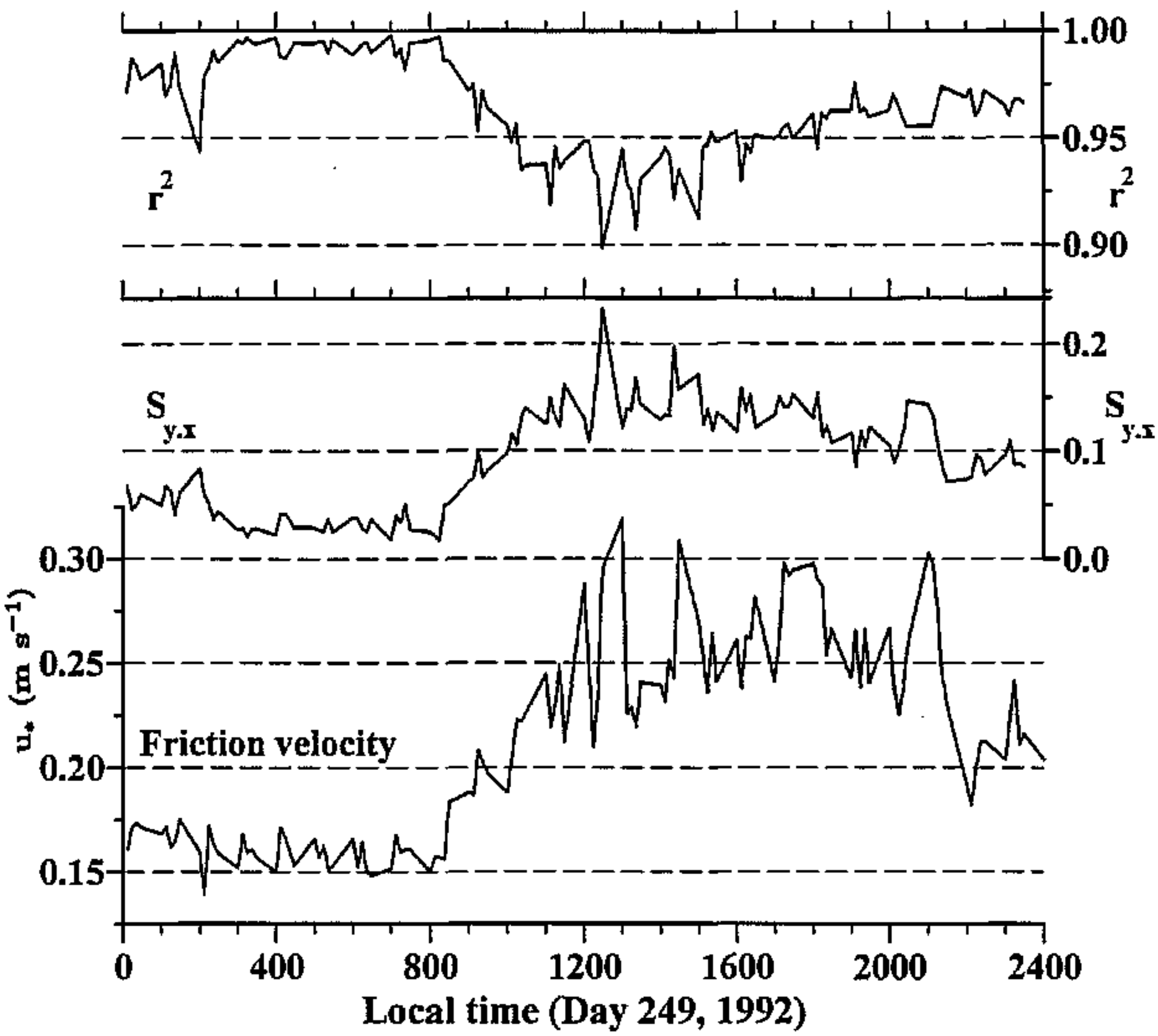

Fig. 5.10 The diurnal variation in friction velocity u_* (m s^{-1}) and statistical parameters r^2 (top curve) and $S_{y.x}$ (m s^{-1}) of the u vs $\ln(z-d)$ relationship for Day 249, 1992

$$r_{ah} = u(z)/u_*^2 = r_{am} = r_a. \qquad 5.28$$

We have already shown the reliability in the friction velocity calculation (Fig. 5.11). The wind speed at the 1-m height and the friction velocity u_* calculated from the wind profile data was used (Eq. 5.28, Fig. 5.11) to calculate r_a. The sensible heat F_h was then calculated using:

$$F_h = \rho\, c_p\, (T_o - T_z)/r_a. \qquad 5.29$$

These calculations were compared with eddy correlation sensible heat measurements (Figs 5.12, 5.13). Each point represents a 12-min measurement. The wide limits of Fig. 5.12 are the 95 % confidence limits for an estimated individual y value and the narrower limits are the 95 % confidence limits for the population mean. Also shown is the regression line. Good agreement between the two estimates of sensible heat (Figs 5.12, 5.13) suggests that the indirect surface temperature method could be used as an alternative to the direct eddy correlation method, at least for "smooth" surfaces. The surface temperature method is much less costly than either the Bowen ratio or eddy correlation methods. A drawback of the surface temperature method lies in the determination of the friction velocity u_*. However, a regression of friction velocity u_* as a function of the wind speed u at the 1-m height (Fig.

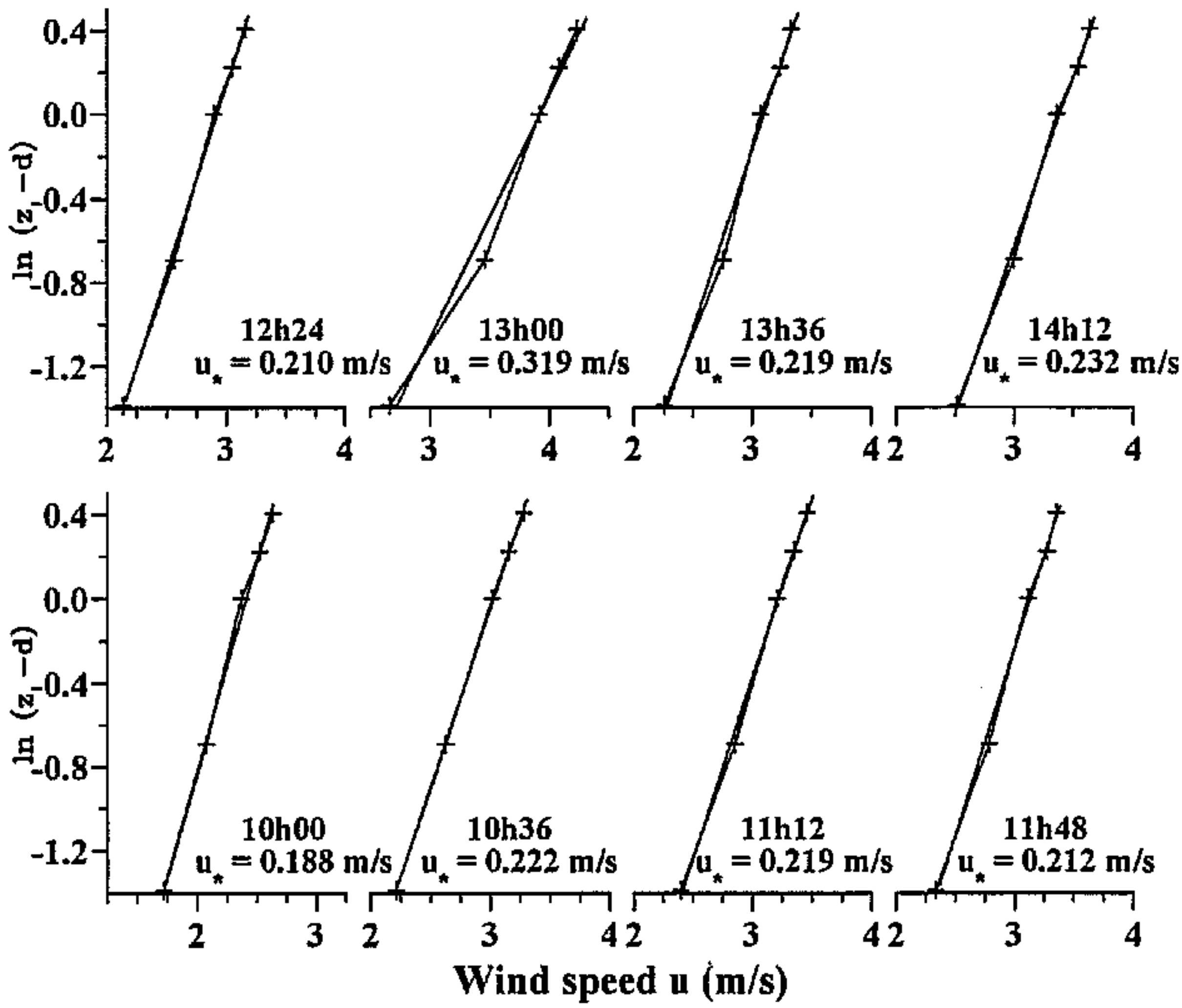

Fig. 5.11 The ln $(z - d)$ vs u relationship for selected times for Day 249, 1992 (data points and regression line are shown as well as the corresponding friction velocity u_* values). The scales on both x and y axes are identical although the x axis scale has, whenever necessary, being displaced to encompass the prevailing wind speeds. The slope for each time is equal to k/u_* (Eq. 5.21)

5.14) shows that friction velocity may be calculated from the wind speed at one level. The relationship $u_* = 0.05717\ u$ obtained allows the aerodynamic resistance r_a using Eq. 5.28:

$$r_a = 303.78/u. \tag{5.30}$$

This relation was used in Section 5.5.6. (Eq. 5.26). Using the logarithmic wind profile equation (Eq. 5.21), this relationship corresponds to a short canopy with a height of 8 mm. By contrast, the relation recommended by Smith (1991), Eq. 5.25, for 2-m wind speed measurements corresponds to a canopy height of 55 mm. The effect of atmospheric stability on these relations needs to be considered but this has not been dealt with here.

Thus, the minimum instrumentation requirements for measurement of sensible heat flux density are an infra red thermometer, anemometer and air temperature sensor. If a net radiometer and soil heat flux plates and soil temperature sensors are also used, it is possible to calculate the latent heat flux density.

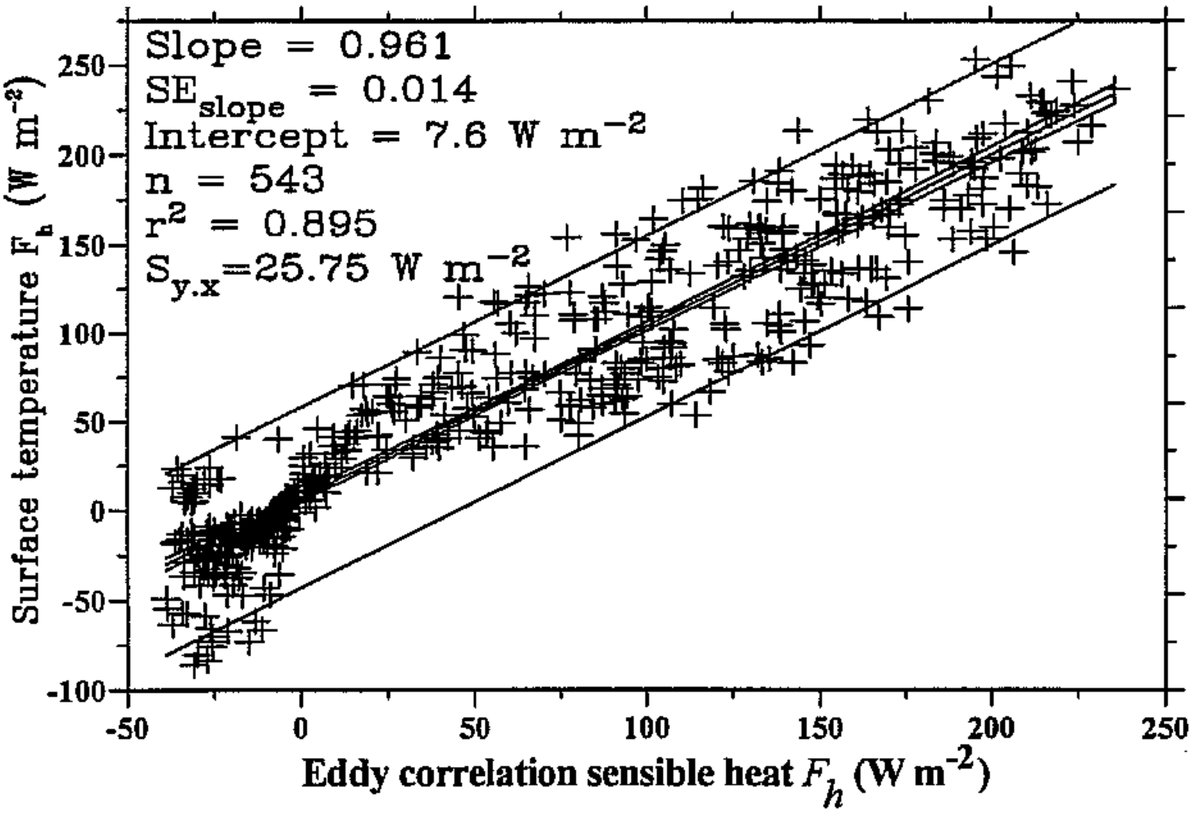

Fig. 5.12 Regression of the surface temperature method of indirect sensible heat flux density determination against sensible heat flux density measured using eddy correlation system #1147EC for Day 152 and 156 to 159, 1992. Each data point is a 12-min measurement

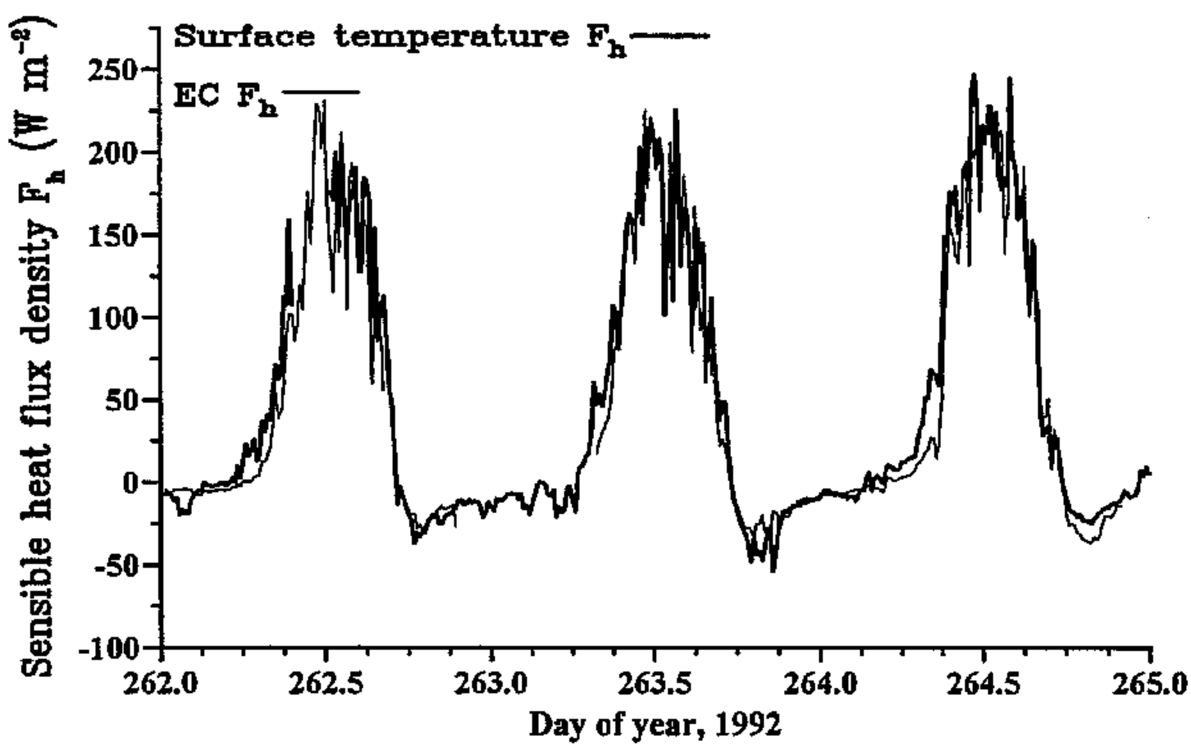

Fig. 5.13 Diurnal variation in sensible heat flux density for Days 262 to 264 inclusive using the indirect surface temperature sensible heat flux density determination against sensible heat flux density measured using eddy correlation system #1147EC. Each data point is a 12-min measurement

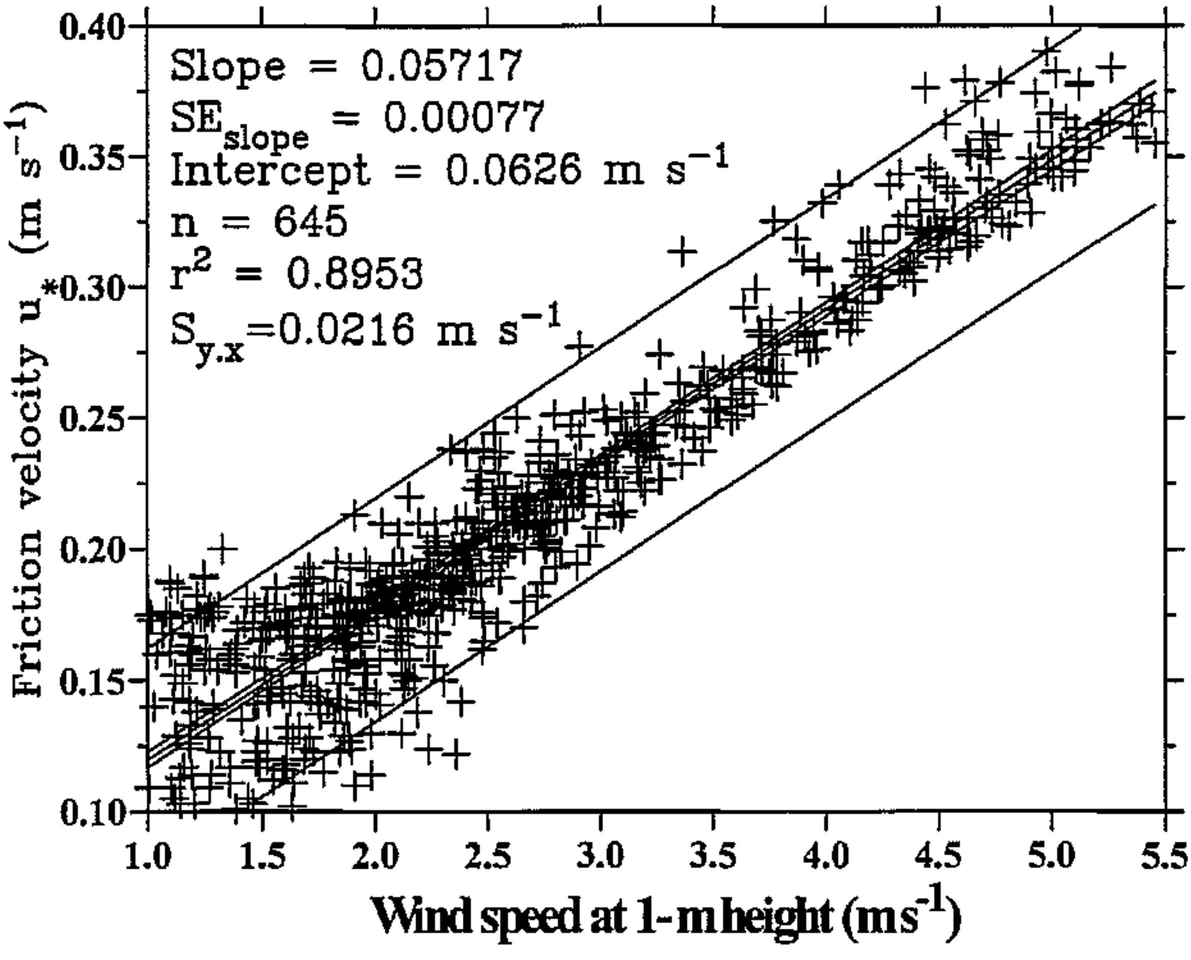

Fig. 5.14 The regression of the friction velocity u_* (m s^{-1}) obtained from the wind profile data as a function of the measured wind speed at a height of 1 m. Each data point is a 12-min measurement

5.6 Conclusion

Bowen ratio evaporation (daily total) compares adequately with equilibrium and lysimeter evaporation indicating a lack of advective influences for our data set of April 1990. The Bowen ratio technique has proved to be a reliable technique for measuring evaporation requiring routine maintenance two to five times per month. The eddy correlation technique appears to significantly underestimate evaporation, for reasons discussed in Chapter 4. Bowen ratio, lysimetric and equilibrium estimates of evaporation were found to compare favourably during the summer rainfall periods. During drier periods, the equilibrium estimate of evaporation overestimated compared to the other techniques. While 20 min evaporation estimates for the techniques (excluding eddy correlation and Priestley-Taylor evaporation) were reasonably comparable, daily totals were very good. Advection flux density estimates were shown to be relatively small and variable (for 20 min periods). This aspect requires more attention and data. Our research paves the way to a more routine use of the more portable Bowen ratio technique for the estimation of actual evaporation.

Diurnal estimates in the evaporation ratio, reference and equilibrium evaporation, appeared to be as expected. The aerodynamic resistance r_a was greater than the isothermal resistance r_i and the canopy resistance r_c. The calculated values were consistent with those found in the literature.

Using a surface temperature method for calculating sensible heat flux density agreement was obtained with the eddy correlation measurement even for a 12-min time-scale. It appeared as if an estimate of the friction velocity used in the surface temperature method may be calculated from the wind speed at one level. Real-time and continuous sensible heat measurements were possible using the EC technique but not with the surface temperature method. The surface temperature method is significantly cheaper than eddy correlation and Bowen ratio techniques if friction velocity may be calculated from wind speed measurement at one level.

Chapter 6

Calibration of net radiometers and infrared thermometers

6.1 Abstract

Net radiometers are an essential part of energy balance investigations. The manufacturers' calibration factor is usually used with the measured net radiometer voltage to obtain the net irradiance. This involves a field or a short wave laboratory calibration using an expensive standard radiometer. The use of an incorrect calibration factor for net irradiance measurement has been noted as a problem in energy balance investigations. The aim of this work was to describe an accurate and inexpensive laboratory method for the long wave calibration of a net radiometer. Our method also allowed for the simultaneous calibration of a number of infrared thermometers (radiometric thermometers). The experimental method for calibrating net radiometers or IRT's involved the use of a radiator. The radiator was painted matt black. At five locations 24-gauge copper-constantan thermocouples were pushed through from the radiator bottom to top. The 5-mm tip of each thermocouple was bent to form an "L" shape and then soldered on to the radiator surface. The radiator was connected to a heater stirrer device with water circulated between the two. The temperature of the heater stirrer was increased to 70 °C. A single net radiometer was placed in a darkened room just above the radiator surface. After 5 min equilibration, the heater was switched off but water circulation continued. A datalogger was used to measure the average radiator surface temperature and net irradiance, while the unit cooled, from which the calibration factor was determined. The procedures for IRT calibration were similar. Our net radiometer calibration factors were reproducible and quick to obtain. The calibration factors agreed remarkably well with the manufacturers' short wave calibration performed a few months previously. The calibration relationship for the IRT's was different for different sensors. The IRT's were most accurate at about 20 °C. The magnitude of the difference between actual and measured temperatures increased on either side of 20 °C. We recommend IRT calibration for surface temperatures greater than 35 °C.

6.2 Introduction

Net radiometers are an essential part of energy balance investigations and especially so in the case of Bowen ratio estimates of sensible and latent heat transfers. Invariably, the manufacturers' calibration factor is used with the measured net radiometer voltage to obtain the net irradiance R_{net} (W m^{-2}). Such a calibration usually involves use of an expensive standard radiometer and is thus a short wave calibration only.

In a micrometeorological investigation (Kanemasu *et al.* 1987), the five groups that participated measured a midday net irradiance of between 300 and 530 W m^{-2} - more than a 75 % variation. The large differences in sensible and latent heat flux density values obtained by these investigators, were attributed to the calibration factor in the net irradiance and soil heat flux density measurement. From personal communications, we know that other workers arrived at similar conclusions. Tanner and Greene (1989) found a 16 % difference in daytime net irradiance between different net radiometers using calibration factors supplied by the manufacturers.

The most common method for calibrating net radiometers is the occulting" or "shading technique (Idso 1974). Calibration by this method is accomplished by positioning a net radiometer next to a pyranometer or pyrheliometer standard or sub-standard, and alternately shading and unshading both instruments simultaneously from the direct rays of the sun (Savage 1988). Shading is done using identical, small opaque shields. The change in the net radiometer output between shaded and unshaded conditions can be equated to the known change in short wave irradiance recorded by the pyranometer or pyrheliometer (measurements from the latter being resolved to the plane of the observers' horizon) and thus a calibration factor for the net radiometer found. When the occulting calibration technique is used:

1) the net radiometer should not be positioned too close to the canopy or soil surface since its' shadow may alter the amount of radiation received from the ground;

2) the accuracy of the calibration factor will be no better than that of the radiation standard used to obtain it;

3) the calibration factor obtained is that for the net radiometer's voltage response to short wave irradiance and does not indicate the response to long wave irradiance. The "occult" method assumes no change in the net long wave irradiance during measurements. The only way to check the similarity of the voltage response to short wave or long wave irradiance is to also perform a controlled environment calibration of the net radiometer for long wave irradiance (wavelengths greater than 3 μm) (Idso 1974);

4) the *in situ* "occult" calibration is fraught with the problems of a non-static radiation source causing the shaded and unshaded measurements to be performed at different times;

5) the shaded net radiometer and shaded pyranometer or pyrheliometer measurements using the sensor standard may be subject to error and involve the use of an expensive radiation sensor.

The aim of this work is to describe an accurate and inexpensive method for the long wave calibration of a net radiometer. As a consequence of problems associated with the calibration technique described, we propose a short wave calibration method performed in the laboratory and a calibration method for the simultaneous calibration of multiple infrared thermometers (radiometric thermometers).

Barber and Brown (1978) used a blackbody surface for the calibration of infrared thermometers. The unit could display its surface temperature but no temperature control was possible. Sadler and van Bavel (1982) devised a simple method, modified by Ham (1990), for the calibration of infrared thermometers using a black body calibration chamber. Our method allows for the simultaneous calibration of a number of infrared thermometers whereas the method of Sadler and van Bavel (1982) only allows for single unit calibrations and cannot be used for the calibration of net radiometers. A field technique for the direct separation of the upward (L_u) and downward (L_d) long wave irradiance components of net irradiance R_{net} is presented.

6.3 Theory

Suppose that a net radiometer is placed directly over the centre of a metal circular plate of area A. The view factor F for the circular plate with the distance between the plate and the net radiometer being d is given by:

$$F = 1/\sin \beta^2 = A/(A + \pi d^2). \qquad 6.1$$

where β is the angle between the vertical and the line from the sensor to the edge of the circular plate. However, if a rectangular plate with area A is used, we assume that:

$$r \approx \sqrt{A/\pi}. \tag{6.2}$$

may be used in Eq. 6.1 to calculate F.

The long wave irradiance L_u emitted by a rectangular plate of area A and emissivity $\varepsilon_{surface}$ is therefore:

$$L_u = [A/(A + \pi\, d^2)] \cdot \varepsilon_{surface}\, \sigma\, T^4_{surface} = F \cdot \varepsilon_{surface}\, \sigma\, T^4_{surface}. \tag{6.3}$$

If the plate has a surface temperature $T_{surface}$ (K) and an emissivity $\varepsilon_{surface}$ and an infra red thermometer registers a temperature of T_{irt} (K) for the plate, then:

$$\sigma\, T^4_{irt} = \varepsilon_{surface}\, \sigma\, T^4_{surface} + (1 - r_{surface})\, \sigma\, T^4_{surrounds} \tag{6.4}$$

where $r_{surface}$ is the place surface reflectivity and where the Stefan-Boltzmann constant is $\sigma = 5.673\times10^{-8}$ W m^{-2} K^{-4}. It is assumed that the surrounds are radiating as perfect radiators. If $a_{surface}$ is the absorptivity of the surface, then

$$r_{surface} = 1 - a_{surface}$$

and, according to Kirchhoff's Law:

$$r_{surface} = 1 - \varepsilon_{surface}$$

Hence:

$$\varepsilon_{surface} = (T^4_{irt} - T^4_{surrounds})/(T^4_{surface} - T^4_{surrounds}). \tag{6.5}$$

If the surrounds are imperfect radiators, then $\varepsilon_{surface}$ can only be estimated and then with least error if $T_{surface} >> T_{surrounds}$. If $T_{irt} = T_{surface}$, $\varepsilon_{surface} = 1$.

If a short wave irradiance source is suspended above a perfect radiator with a net radiometer placed close to the latter, the net radiometer will register the incident short wave irradiance. The short wave source may alter the temperature of the radiator surface but these may be corrected for or the measurements performed quickly. The short wave incident at the surface of the radiator should be totally absorbed so there should be virtually no incident short wave irradiance incident at the underside of the net radiometer.

6.4 Materials and methods

6.4.1 Preparation of radiator

A large truck radiator (0.710 mm by 0.481 mm) was spray painted with matt black paint (Sprayon industrial acrylic enamel flat black number 03725, Bedford Heights, Ohio, USA). At each of five locations 24-gauge copper-constantan thermocouple wire (Omega Engineering Inc., Stamford, CT, product number PR-T-24) was pushed through from the bottom of the radiator to the top. The 5-mm tip of each thermocouple was bent to form an "L" shape. The thermocouples were then soldered on to the radiator surface so as to be flush with the radiator's surface, each thermocouple being 50 mm away from the nearest thermocouple. The thermocouples were also sprayed with matt black paint. These procedures minimized the possibility of a temperature gradient occurring between the cavities of the radiator and thermocouples. A single thermocouple was used to measure the temperature of circulated water in the well of the heater stirrer and water bath (Haake Gebruder, Berlin, Germany, type FE number 67236 distributed by PolyScience Corp, Evanston, Illinois) to check constancy of temperature of the circulated water. The base of the radiator was affixed to styrofoam covered with a sheet that had been painted matt black. This ensured that radiative cooling from the radiator was mostly from the top-side and reduced the rapid reduction in temperature after the heater was switched off. Measurements were performed within two hours. Laboratory doors were closed to reduce the possibility of the long wave irradiance from the ceiling and walls from changing significantly.

All openings into the radiator were sealed with silicon sealant apart from an inlet and an outlet opening. The radiator was placed on a trolley positioned in the centre of the laboratory. The inlet opening of the radiator was connected to the inlet of a heater stirrer device with the radiator outlet connected to the outlet of the heater stirrer. Short hose connections were used to ensure rapid water circulation between heater stirrer and radiator. The temperature of the heater stirrer was increased to 70 °C with water being circulated in the radiator.

6.4.2 Long wave calibration of net radiometers

A single net radiometer was placed in a darkened room at a distance of between 55 and 70 mm from the surface of the radiator. Placement of the radiometer closer than 55 mm from the radiator caused too great a heating of the domes and more variable net irradiance values. Measurements corresponding to radiator temperatures exceeding 65 °C were discarded. After a 5 min equilibration period, the heater circuit of the heater stirrer was switched off but the water circulation continued. A Campbell Scientific 21X datalogger was used to perform slow (16.67 ms integration time) differential temperature measurements of the six thermocouples and differential net radiometer voltage measurements immediately after the heater was switched off. Measurements were performed every 0.4 s with the average and the standard deviation of these measurements over a one minute period being recorded. Measurements were continued for a period of about two hours at which time the water temperature had decreased to close to the ambient temperature. The surface temperature of the radiator was calculated as the average of the temperature measured using the five thermocouples.

When the net irradiance above the radiator was changing rapidly, particularly for rapidly decreasing surface temperatures, it was necessary to correct the measured voltages for the relatively long (typically 20 s) time constant of the net radiometer. No correction was applied to the surface temperature measurements.

In some cases, the procedure was repeated for the same net radiometer some days later, another net radiometer was chosen or another laboratory was used for the calibration. For some of the calibrations, half of the laboratory lights were left on and in other calibrations, the lights were switched off. In all cases, the air-conditioning in the laboratories was not altered. For a few of the net radiometers, the calibration was repeated three or four times but all radiometers were calibrated at least twice.

The long wave irradiance emitted from the radiator was calculated using Eq. 6.3 assuming that the radiator surface, with its' cavity-like matt-black structure, is a perfect radiator so that $\varepsilon_{surface}$ in Eq. 6.3 is unity. In later experiments, $\varepsilon_{surface}$ was calculated (Eq. 6.5). In another experiment, a 0.3 m by 0.3 m aluminium plate was placed metal to metal above the radiator. The plate (Ham 1990, p 95) was coated with a galvanized spray with a fraction of the spray coating being removed to obtain a plate emissivity of approximately 0.49 (as judged by the calculated emittance from the infrared thermometer measurements and actual plate temperatures). The radiator was heated to 85 °C and the aluminium plate inverted and allowed to cool with a net radiometer (serial number 92062) placed 40 mm above it.

Seven Radiation and Energy Balance Systems (Seattle, Washington) Q*6 net radiometers were used for the calibration tests. For each net radiometer, a plot of its' measured voltage on the x-axis *vs* the view factor F multiplied by the upward long wave irradiance calculated from the thermocouples embedded in the radiator (Eq. 6.3) on the y-axis was performed and the slope and intercept calculated (assuming that $\varepsilon_{surface} = 1$ due to the cavity-like structure of the radiator).

6.4.3 Short wave calibration of net radiometers

All six net radiometers were also calibrated outdoors, on a cloudless day, using the so-called "occult" techniques. We used an Eppley radiometer model 60 (serial number 8960) as the standard for solar irradiance.

6.4.4 Calibration of infrared thermometers (IRT's)

The procedures for the calibration of the eight infra red thermometers were similar. The thermometers were placed directly above the centre of the plate at a distance of 0.97 m from the plate in some cases and 0.4 m in others. Once the temperature of the plate had decreased from 80 °C to room temperature, ice was used to lower the temperature to less than 15 °C. Measurements were collected as the system equilibrated back to room temperature. For these calibrations, Everest Interscience Inc. infra red thermometer models 4000ALCS, 40004-A, 4004AL and 110 were used. Some calibrations were performed at least twice for certain net radiometers.

6.5 Results and discussion

6.5.1 Long wave calibration of net radiometers

The non-linear decrease in reference temperature $T_{surface}$ and the corresponding standard deviation in temperature for all five thermocouples is shown (**Fig. 6.1**). The initial rapid temperature decrease prevents rapid data collection without decreasing the one minute data output period. The linear regression is therefore biased towards the lower temperatures. Only data points for which the surface temperature was less than 65 °C were included in the regression analysis.

The calibration data from two net radiometers are shown (**Fig. 6.2**). There is a 10 % difference in the slopes of these two net radiometers (**Table 6.1**). The one calibration was performed in a laboratory in which half of the lights were switched off, the net radiometer being placed in the darkened section of the laboratory. Extraneous radiation from outside the building was visible. In the other calibration, the laboratory lights were switched off and the room completely darkened. The intercept for both net radiometers is the value of the upward long wave irradiance for which the voltage from the net radiometer $V_{net} = 0$ mV and hence the net irradiance $R_{net} = 0$ W m^{-2}. In other words, the intercept also corresponds to the downward long wave irradiance:

$$L_d = F \cdot (L_u)_o. \qquad 6.6$$

where $(L_u)_o$ is the downward net irradiance for which $R_{net} = 0$ W m^{-2}. For these two net radiometers (Fig. 6.2), the intercepts were different, and consistently so for the two laboratories chosen. For a net radiometer placed above a radiator for which L_u using Eq. 6.3 is calculated, it is possible to separate the upward and downward long wave irradiance components of net irradiance.

The calibration statistics are shown (Table 6.1). The calibration statistics for two net radiometers placed next to each other were statistically different from those for which a single net radiometer was

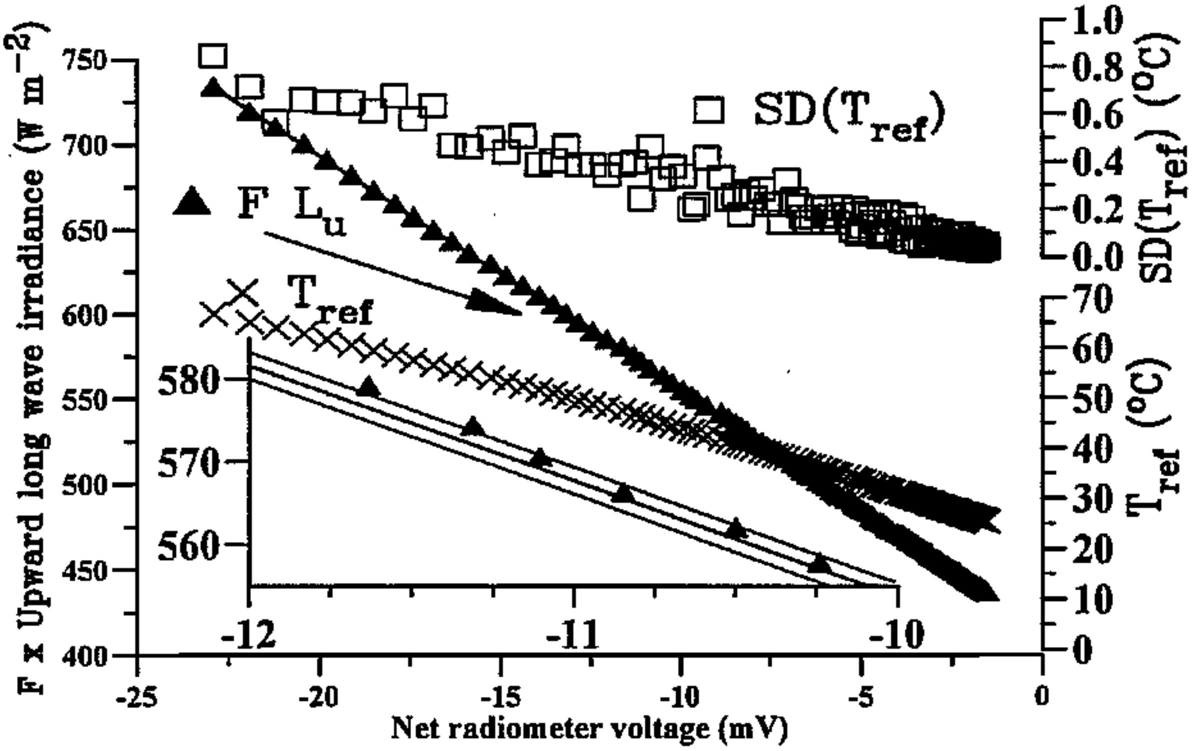

Fig. 6.1 A plot of the view factor F multiplied by the upward long wave irradiance (left hand y-axis, W m^{-2}), the reference temperature (bottom right-hand y-axis, °C) and the standard deviation of the reference temperature multiplied by 100 (top right hand y-axis, °C) as a function of the net radiometer voltage (mV) for net radiometer number 90217

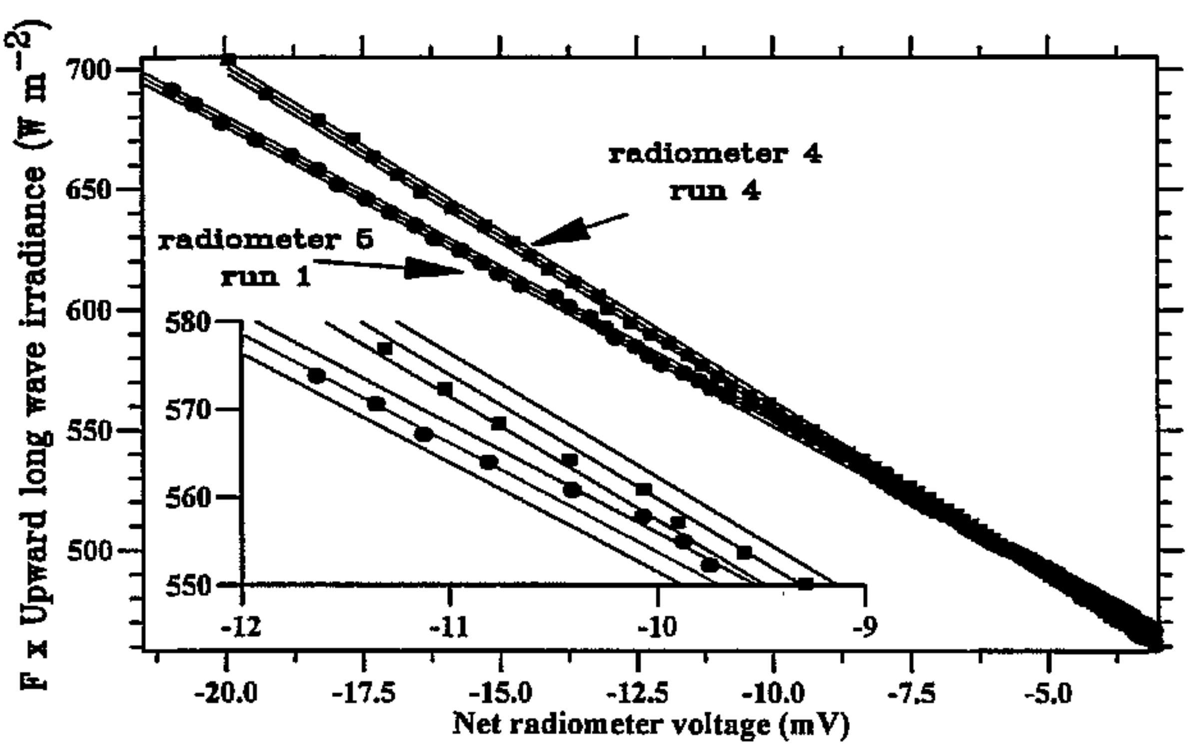

Fig. 6.2 A plot of the view factor F multiplied by the upward long wave irradiance (W m^{-2}) as a function of the net radiometer voltage (mV) for net radiometer numbers 92061 and 90226 (slope of -12.439 W m^{-2} mV^{-1}, r^2 = 0.9997 and -14.121 W m^{-2} mV^{-1}, r^2 = 0.9997 (Table 6.1))

Table 6.1 A comparison between net radiometer calibrations. The statistical parameters of the long wave calibrations are shown. Outdoor calibrations were performed using the short wave "occult" technique. All r^2 values exceeded 0.9993

Radio-meter no.	Calibration no.	S_{yx} ($W\ m^{-2}$)	Slope ($W\ m^{-2}\ mV^{-1}$)	Short wave calibration factor ($W\ m^{-2}\ mV^{-1}$)	
				Manufacturer's	Outdoor
1	1	0.83	-13.604	-13.70	-13.59
1	2	1.30	-13.563		
2	2	0.94	-13.878	-14.00	-14.84
2	3	0.81	-13.958		
3	3	0.80	-14.051		
4	2	0.25	-14.023	-14.10	-14.56
4	3	1.85	-14.098		
4	4	1.22	-14.121		
5	1	1.11	-12.439	-12.70	-13.82
5	2	1.05	-12.651		
5	3	0.57	-12.650		
5	4	1.08	-12.551		
6	1	0.95	-12.907	-12.90	-13.70

placed above the radiator and were rejected. We therefore always calibrated net radiometers individually.

6.5.2 Short wave calibration of net radiometers

For our net radiometer, the long wave calibration slopes agreed remarkably well with the manufacturers' calibration (Table 6.1) performed some two to three months previously using the "occult" technique in a chamber using a halogen lamp and a standard short wave pyranometer. Also shown (Table 6.1) are our outdoor short wave calibration slopes. The magnitude of these outdoor slopes were greater than both our long wave calibration slopes and the manufacturers short wave calibration slopes.

6.5.3 Calibration of infra red thermometers

The calibration relationship for the infra red thermometers (IRT's) showed a marked variation between the different sensors used (**Figs 6.3 and** 6.4). In the case of model 4000ALCS serial number 2001-1, the deviation between $T_{surface}$ of the radiator and T_{irt} decreased to -1.5 °C at $T_{surface}$ = 60 °C compared to about -0.2 °C for model 4000ALCS serial #2001-2 (second calibration). All but two of the IRT's exhibited a plateau as shown in the $T_{surface} - T_{irt}$ *vs* $T_{surface}$ curves (Figs 6.3 and 6.4). In one case, model 4000ALCS serial #2001-2 second calibration, the shape of $T_{surface} - T_{irt}$ *vs* $T_{surface}$ was parabolic with a maximum of 0.6 ° at 30 to 40 °C and a minimum of -0.4 °C at 70 °C. The hand held IRT model 110 serial #10152 had a near-linear $T_{surface} - T_{irt}$ vs $T_{surface}$ relationship (Fig. 6.5). For this IRT,

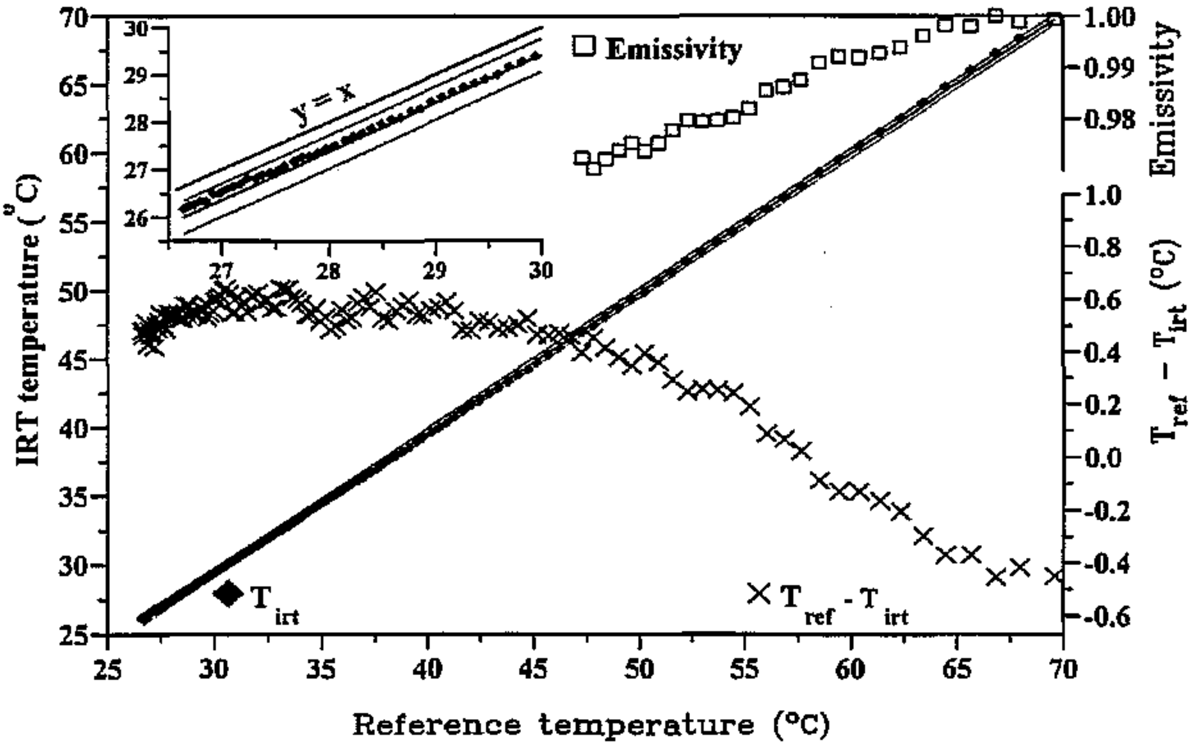

Fig. 6.3 A plot of the infra red thermometer (model 4000ALCS, number 2001-2) temperature (left hand y-axis, °C), the temperature difference between reference and infra red thermometer temperatures (bottom right hand y-axis, °C), and calculated emissivity of the radiator (top right hand y-axis, unitless) assuming that $T_{surface} >> T_{surrounds}$

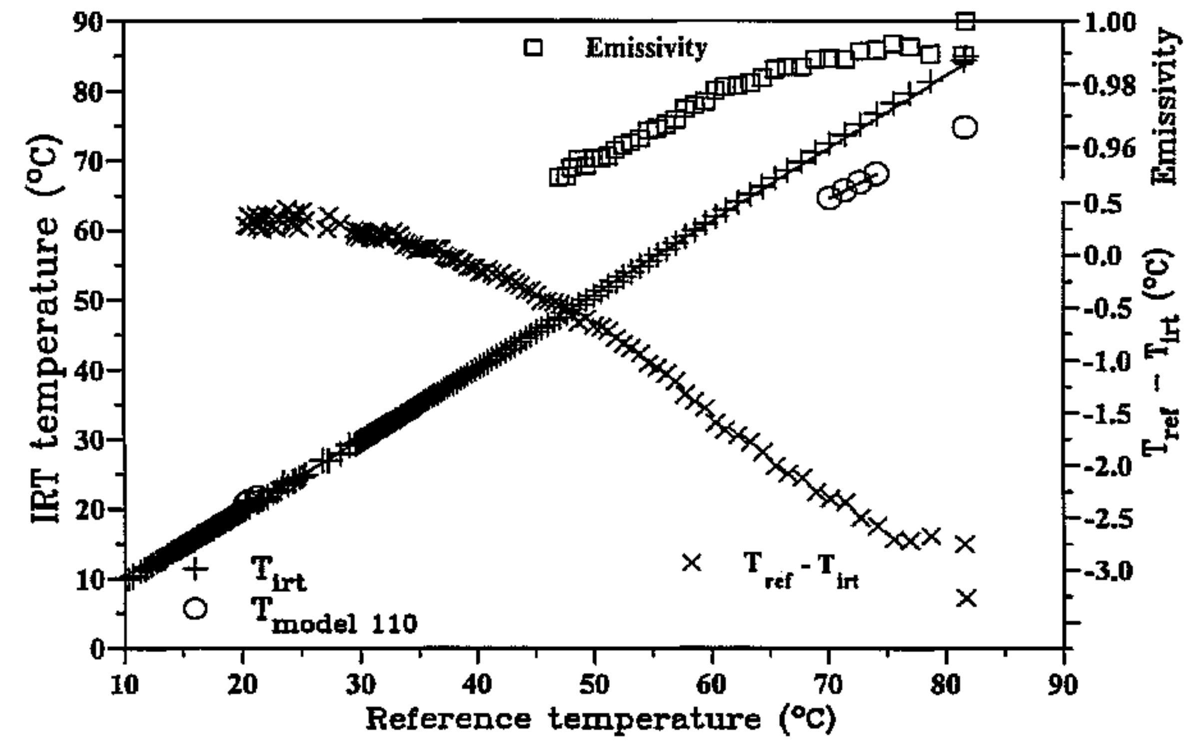

Fig. 6.4 A plot of the infra red thermometer (model 4000ALCS, number 20001-1) temperature (left hand y-axis, °C), the temperature difference between reference and infra red thermometer temperatures (bottom right hand y-axis, °C), and calculated emissivity of the radiator (top right hand y-axis, unitless) assuming that $T_{surface} >> T_{surrounds}$

$T_{surface} - T_{irt}$ was 0 °C at 20 °C increasing almost linearly to 6 °C at 70 °C.

The hand held infra red thermometer (model 110, serial number 10152) was calibrated twice for temperatures ranging between 15 and 70 °C, once with ten calibration points (Fig. 6.4) and once with nearly 1000 data points (Fig. 6.5). There was no significant difference in slope or intercept of the calibration relationship for the two calibrations (Table 6.2). This handheld model 110 infrared thermometer had the greatest error for all thermometers tested. In view of the differences between IRT's, it is important to calibrate such units prior to use and especially so for surface temperatures exceeding 35 °C.

6.5.4 Emissivity

A possible source of error in our calibration method for both infra-red thermometers and net radiometers is that the cavity emissivity may not be unity. Heinisch (1972) showed that a matt-black painted right-regular cylindrical cavity with a depth to aperture ratio of 5.0 has an emissivity greater than 0.999. Bedford (1972) showed that the ratio was 10.0 for spherical cavities. Our cavities were triangular shaped with a depth to aperture ratio of 5:1 in the horizontal plane and 20:1 in the perpendicular plane. Based on this, the assumption of an emissivity of unity is a good one. Using a pair of IRT's, one inverted and facing the radiator and another facing upwards, it was possible to estimate $\varepsilon_{surface}$ for the radiator. The upward facing IRT was used to measure $T_{surrounds}$ (Eq. 6.5) and this estimate was compared with the temperature estimate of $[L_d/(F\sigma)]^{1/4}$ calculated using Eq. 6.6 from net radiometer data. Although near unity, there is a non-linear increase in $\varepsilon_{surface}$ *vs* $T_{surface}$ (Figs 6.3 and 6.4). This calculation of $\varepsilon_{surface}$ assumes no error in T_{irt} at all temperatures. The non-linear shape would imply that the shape of $F \times$ the upward long wave irradiance (calculated using Eq. 6.3) *vs* net radiometer voltage would also be non-linear. No such gradual curvature in the net radiometer calibration relationships were observed for our temperature range. In another experiment, $\varepsilon_{surface}$ was estimated using

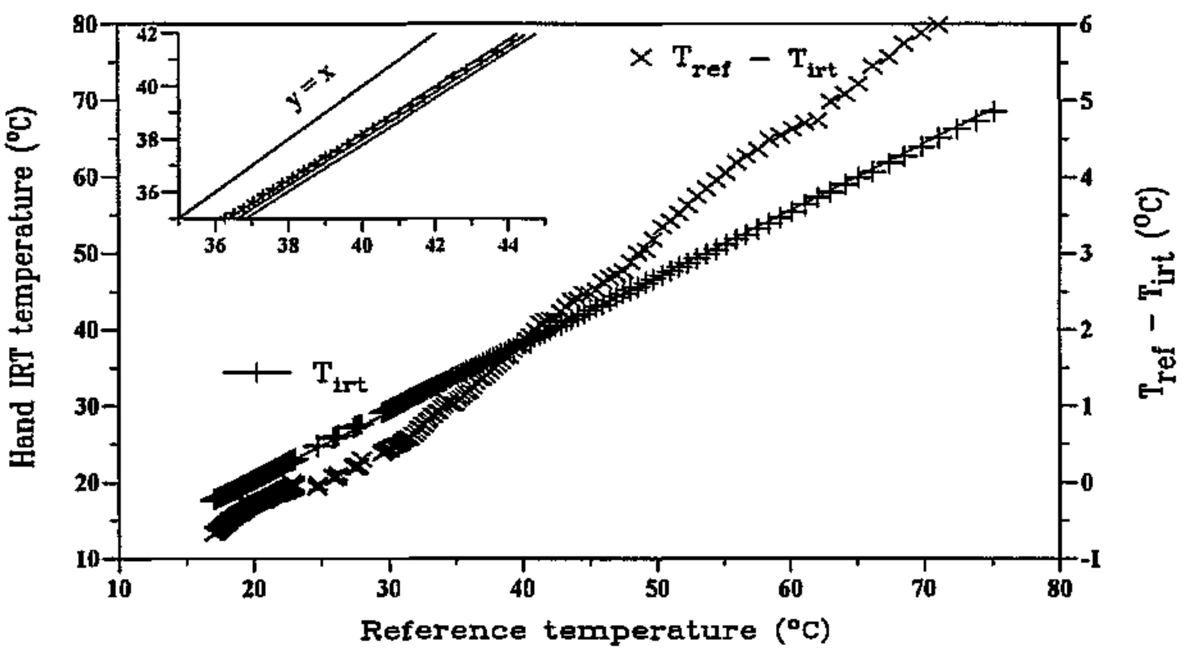

Fig. 6.5 A plot of the infra red thermometer (handheld model 110, number 10152) temperature (left hand y-axis, °C) and the temperature difference between reference and infra red thermometer temperatures (right hand y-axis, °C)

Table 6.2 The statistical parameters associated with the infrared thermometer calibrations. All r^2 values exceeded 0.9995

IRT	Calibra-tion no.	Intercept ($W\ m^{-2}$)	Slope ($W\ m^{-2}\ mV^{-1}$)	n	S_{yx} ($W\ m^{-2}$)
1	1	-1.1895	1.0415	237	0.291
1	2	-1.1868	1.0386	144	
1	3	-1.3486	1.0430	189	
1	4	-0.4424	1.0220	521	
2	1	-1.5002	1.0197	99	0.142
2	2	-1.1482	1.0186	131	0.133
3	1	-0.3799	0.9985	144	
3	2	-0.3532	0.9981	189	
3	3	0.2599	0.9840	521	
4	1	2.8885	0.8793	10 0	0.167
4	2	2.7761	0.8809	970	0.109
5	1	0.0015	0.9989	970	0.128
6	1	-1.1550	1.0420	970	0.107
7	1	-1.4763	1.0611	970	0.112

$T_{surrounds} = [L_d/(F\,\sigma)]^{1/4}$ where L_d is the y-intercept of a net radiometer long wave calibration.

For net radiometer serial number 92062, calibrated assuming that the radiator emissivity is unity at all temperatures, and placed above a cooling plate, the plot of $F\,\sigma\,T^4_{plate}$ as a function of the net irradiance above the plate is shown (Figs 6.2 and 6.3). The reciprocal of this relationship yields the plate emissivity ε_{plate}.

6.6 Conclusions

- 1. Using the radiator calibration technique, the net radiometer (long wave) calibration factors were reproducible.
- 2. Net radiometer (long wave) calibration factors were similar to the manufacturers short wave calibration factor obtained four months previously for new net radiometers.
- 3. Long wave calibrations over a wide irradiance range were possible.
- 4. Calibration of IRT's for a wide temperature range was possible. The calibration slope for the same IRT for different calibration runs is reasonably reproducible.
- 5. Most IRT's overestimated surface temperature for temperatures greater than 25 °C.
- 6. We recommend calibration of IRT's if surface temperatures greater than 35 °C are recorded.

Chapter 7

Comparisons of vineyard sensible heat measured using eddy correlation and Bowen ratio systems[15]

7.1 Abstract

The placement of an eddy correlation (EC) system, in a wide row system such as in a vineyard with limited fetch, is problematical. Sensible heat measurements in a 5-ha vineyard were obtained using two eddy correlation (EC) and four Bowen ration energy balance (BREB) systems. We compared EC and BREB measurements of sensible heat and evaporation. Sensible heat estimates from the two EC systems agreed with each other when the two EC systems were placed 1 m directly above adjacent N-S canopy rows 3 m apart. There were differences in EC sensible heat for EC systems placed directly above row and between row (above soil) positions. The EC sensible heat directly above the row was much greater than that at the between row position (1.5 m away). We attributed these differences to the lack of air mixing between the above row and between row positions. The standard deviation of the vertical wind speed at the between row position was also much greater than that at the above-canopy position. Our measurements demonstrate that sensible heat and the vertical turbulent intensity above the row compared to that between the canopy rows are different. These findings illustrate that due consideration should be given to the lateral placement of sensors for row crops for sites with limited fetch. At the 95 % level of significance, there was no statistical difference between BREB and EC sensible heat measurements when the EC systems were placed 1 m directly above adjacent N-S canopy rows. Our data suggests that the BREB sensible heat, due to the nature of the BREB calculation method, was very sensitive to changes in net irradiance. The EC sensible heat measurements were not sensitive to net irradiance since the EC technique is absolute and independent of net irradiance and soil heat flux density measurement.

7.2 Introduction

The usefulness of eddy correlation (EC) techniques for short-term measurements of the vertical transfer of sensible and latent heat in the lowest layers of the atmosphere is becoming recognized (Neumann and den Hartog 1985; Tanner *et al.* 1985, Tanner 1988, Dugas *et al.* 1991, Verma *et al.* 1992, Cellier and Olioso 1993). Hicks (1973) performed EC measurements of the eddy fluxes of momentum and of sensible heat over a vineyard with a fetch of 500 m by placing sensors at a height of 4.5 m above the soil surface. Dyer (1961) performed measurements, over a level pasture surface, at a height exceeding 3.5 m above surface. The EC measurements (Swinbank 1951, Dyer and Maher 1965) supposedly allow for absolute point measurements of sensible and latent heat flux density at a defined height above canopy. The Bowen ratio energy balance (BREB) technique (Tanner 1960) is a profile method involving measurements of mean air temperature and mean water vapour pressure at two heights above the canopy. The BREB technique also allows sensible and latent heat flux density to be determined. Two different types of BREB methods have been used. One involves an oscillating system in which two

15 Based on the paper in preparation by Savage, Heilman, McInnes and Gesch. Trade and company names are included for the benefit of the reader and do not imply endorsement or preferential treatment of the product by the authors, their organizations or their sponsors

sensors, one at each measurement level, are used for air temperature and water vapour pressure determinations (Gay and Greenberg 1985, Fritschen and Fritschen 1993). The other BREB method involves using two sensors for air temperature but one hygrometer, with air being pumped alternately from the one level and then from the other (Tanner *et al.* 1987, Cellier and Olioso 1993).

The calculation of sensible heat flux density using the EC method is based on the governing equation:

$$F_h = \rho\, c_p\, \overline{w'T'} \qquad 7.1$$

where ρ and c_p are respectively the density ($\approx$ 1.17 kg m^{-3} at 25 °C and 100 kPa) and specific heat capacity of air ($\approx$ 1056 J kg^{-1} K^{-1}) and where w' and T' are the vertical wind speed and the air temperature fluctuations and $\overline{w'T'}$ is the average covariance over a short period (usually less than an hour). The calculation of sensible heat flux density F_h using the BREB method is based on:

$$F_h = (I_{net} - F_s)/(1 + 1/\beta) \qquad 7.2$$

where I_{net} is the net irradiance at the canopy surface, F_s the soil heat flux density and β the Bowen ratio calculated using:

$$\beta = \gamma\,(\overline{T}_2 - \overline{T}_1)/(\overline{e}_2 - \overline{e}_1) \qquad 7.3$$

where γ ($\approx$ 66 Pa K^{-1}) is the psychrometric constant, $\overline{T}_2$, $\overline{e}_2$ and $\overline{T}_1$, $\overline{e}_1$ are the time-averaged air temperature (K) and water vapour pressures (Pa) at profile heights z_2 and z_1 above the canopy surface, respectively.

Few comparisons have been made between EC and BREB methods of flux density determination for an aerodynamically rough surface such as in a vineyard. In our study in a vineyard, with limited fetch, measurements from two EC systems (Tanner *et al.* 1985) were compared with that from four oscillating-type BREB systems (Gay and Greenberg 1985). We also wished to measure the EC sensible heat flux density, for systems placed at the row and between row positions, to ascertain if different lateral placements result in a change in sensible heat.

7.3 Materials and methods

All measurements were performed in the Delaney Vineyards in Lamesa, Dawson County in north Texas, USA at an altitude of 913 m, latitude of 33° 30' N and longitude of 102° W. The vineyard configuration was a vertical bilateral cordon with the cordon wire at 1.0 m above the soil surface, and catch wires at 1.25 and 1.5 m above the soil surface. The distance between rows was 3 m. The bare interrow was ploughed a few days before measurements were performed. A Campbell Scientific (Logan, Utah, USA) CA27 sonic anemometer and fine wire temperature system (serial number 1) was always placed at a height of 1 m and directly above the roughly 1.6 m high canopy row (measured relative to the position of the fine-wire thermocouple) with the thermocouple arm of the EC systems pointing into the predominantly southern winds. The placement height of EC system number 1 above soil surface was therefore 2.6 m. The other system (number 2) was either placed at the same height (1.0 m above an adjacent canopy row) or placed between rows 1.0 or 2.6 m directly above bare soil. Both EC systems were nearly 75 m from the south edge of the vineyard and 60 m from the east edge. The two EC systems were usually situated directly above a canopy row mid-way between two BREB systems pairs, about 30 m from each BREB pair. The two EC systems were 3 m apart. The predominant wind direction was from the south and the canopy rows ran from 10° east of south to 10° west of north.

Biltoft and Gaynor (1987) compared two types of sonic anemometers and fast response thermometers, finding good correspondence under a wide range of field conditions. The instruments they used provided precise vertical turbulence and flux measurements but they did suggest some uneasiness concerning the thermal time constant of their CA27 sonic anemometer (based on the initial design by Campbell and Unsworth 1979). For each of our systems, fluctuations in wind speed w' were measured using a CA27 sonic anemometer and the air temperature fluctuation T' obtained using a Model 127 fine wire (12.5 μm diameter) chromel-constantan thermocouple (both sensors available from Campbell Scientific). The Model 127 thermocouple design only allows a temperature difference relative to the temperature of the metal base to be measured. We modified the reference junction of the 127 thermocouple, inside the metal base, by applying additional insulation to increase the thermal time constant (reported by Tanner (1984) to be 20 min). The vertical metal arm of the sonic anemometer, housing the reference junction, was also heavily insulated. The need for insulating the metal base housing the reference thermocouple or for performing averages over sub-hourly periods is demonstrated by writing the fluctuation in the measured temperature difference as $(T - T_{arm})'$ where T is the temperature of the fine wire thermocouple and T_{arm} is the reference temperature inside the metal arm and where the $'$ shows a fluctuation. Writing the fluctuation in the temperature difference as the instantaneous value minus the mean, we get:

$$(T - T_{arm})' = T - T_{arm} - (\overline{T} - \overline{T}_{arm}) \qquad 7.4$$

where the overbar indicates the average over the sub-hourly time interval chosen. Hence

$$(T - T_{arm})' = T - \overline{T} - (T_{arm} - \overline{T}_{arm}). \qquad 7.5$$

The right-hand side of this equation is approximately $T - \overline{T}$ or T' only if $T_{arm} - \overline{T}_{arm}$ is sufficiently small. This can only be the case for a constant reference thermocouple temperature.

A Campbell Scientific 21X datalogger was programmed and used to gather all the eddy correlation data and to determine $\overline{w'T'}$. A 12-minute averaging period was used for final calculations. Measurements were performed every 0.2 s (corresponding to a frequency of 5 Hz). Use of a 12-min averaging period, instead of a longer period avoided the Campbell datalogger computation error (Tanner and Greene 1989) that can affect the standard deviation of the temperature difference measurements. The two EC systems were first compared by examining measurements of sensible heat flux density performed 1 m directly above the canopy, for adjacent rows (3 m apart). Frequency response corrections to our EC measurements, described by Moore (1986), were small and not routinely performed. No corrections for the shadowing effect of the sonic anemometer (Massman *et al.* 1990) were performed since Biltoft and Gaynor (1987) found no shadow effects for the CA27 sonic anemometer. We did not correct for air density fluctuations as these corrections were regarded as small compared to the spatial variation of sensible heat in the horizontal. Furthermore, the corrections would have been similar for both EC systems we used. Jacobs *et al.* (1992) suggested that during the daytime, weak inversion conditions within the canopy may prevent eddies from above the canopy from penetrating into the canopy. These weak inversion conditions did not occur in our experiment partly due to the wide interrow and interplant spacing.

Full details of the BREB surface energy balance measurements used here are discussed by Heilman *et al.* (1994). Surface energy balance was measured by the Bowen ratio method (Tanner 1960) using four independent systems (Gay and Greenberg 1985). Each BREB system contained two exchanging ceramic wick wet bulb and dry bulb psychrometers separated by a vertical distance of 1 m, and a net radiometer (Model Q*6, Radiation Energy Balance System, REBS, Seattle, WA). Two of the systems used six soil heat flux plates (Model HFT-1, REBS) per system wired in series, while the other two used three model HFT-1 plates wired in series. Masts were positioned 10 m from the north edge of the vineyard. The bottom psychrometer on each mast was 2.6 m above soil surface, 1.0 m above the plants. This configuration produced a fetch-to-height ratio of 73:1 for the prevailing southerly winds, which was greater than the minimum of 20:1 for Bowen ratio measurements found by Heilman *et al.* (1989). Wind direction was measured using a model 12005 wind vane (R M Young, Traverse City, Michigan).

Air temperatures were measured during a 3-min period during which psychrometers exchanged and equilibrated with the environment. This procedure eliminated sensor bias and allowed the Bowen ratio to be determined every 12 min. Net radiometers were mounted 3.2 m above the soil surface. Soil heat flux was determined using the combination method (Kimball and Jackson 1979). Heat flux plates were placed 0.05 m below the soil surface, at various positions (Heilman *et al.* 1994) and the change in heat content above the plates was determined from measurements of soil temperature in the 0 to 0.05 m layer, and an estimate of the heat capacity (De Vries 1963).

7.4 Results and discussion

The comparison of the correlation between vertical wind speed fluctuation and air temperature fluctuation for the two EC systems, placed directly 1 m above adjacent (3 m apart) canopy rows, is shown (**Fig. 7.1**). The systems were 2.6 m above the soil surface. The negative correlations correspond to sensible heat being directed from atmosphere to canopy surface in the early morning or late afternoon. The centroid point for the data of Fig. 7.1 is (0.355, 0.329). The highest correlation occurred

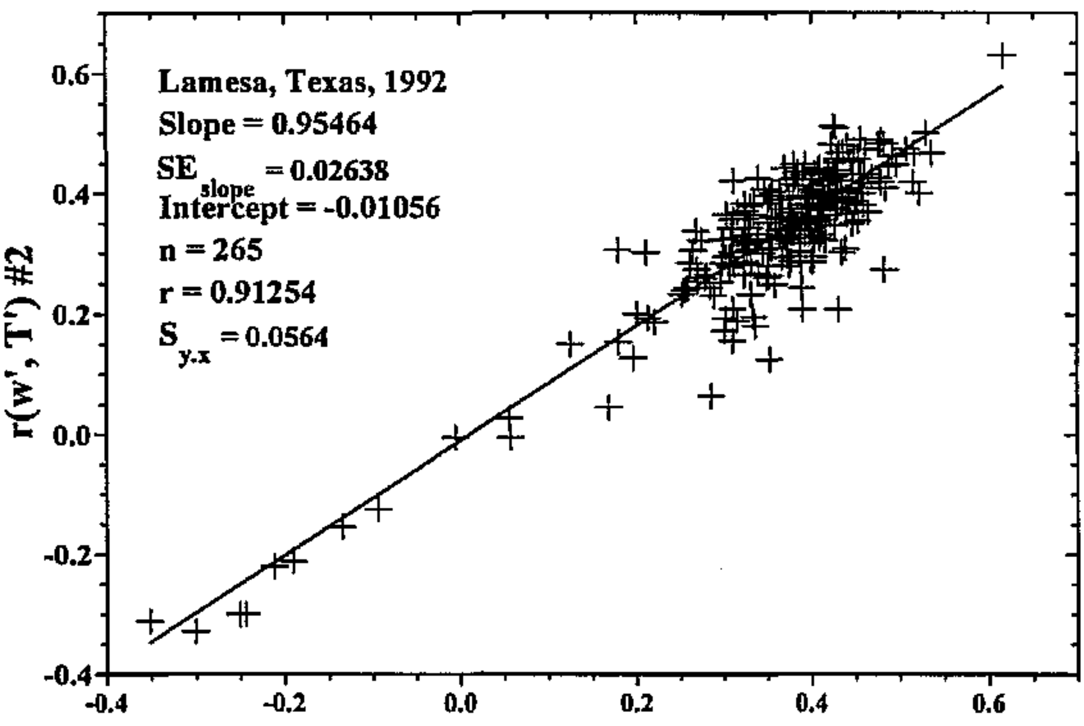

Fig. 7.1 Comparison of the correlation of vertical wind speed and air temperature fluctuations measured using two EC systems placed 1 m above the canopy row, for adjacent rows for Days 150 to 159, 1992 (northern hemisphere)

on day (day) 151 with a correlation exceeding 0.6. This occurred at Central Standard Time (CST) 12h36 and 12h48 with southerly winds down the canopy rows.

A typical diurnal variation in eddy correlation sensible heat flux density for Day 154, 1992 is shown in **Fig. 7.2**. It is evident, from the sudden in-phase increase or decrease in the sensible heat, that both EC systems responded well to the same stimulus. The correspondence was good for days with a low and high sensible heat (data not shown). Both systems detected the sign change of the sensible heat flux density on Day 154 at about 18h30 (Fig. 7.2). The data for 31 May 1992 to 7 June (Day 152 to 159 inclusive), for which the two systems were 1 m directly above canopy, show good agreement (Fig. 7.3). For EC sensible heat flux densities greater than 75 W m^{-2}, the agreement is however more variable. At the 95 % level of significance, there is no difference in the measurements from the two EC systems with the 95 % slope confidence interval being between 0.941 and 1.021.

The temporal comparisons between the average sensible heat flux density from the four BREB systems with that from EC system #1 is reasonable (**Fig. 7.4**) even on days with lower sensible heat values (Day 159). The reasonably good agreement for all BREB and EC data is shown (**Fig. 7.5**). The 95 % slope confidence interval is between 0.886 and 0.962. Close to the canopy, one might expect an underestimation in EC sensible heat measurements compared to BREB values, because of the higher eddy frequencies present in the eddy structure due to the smaller eddies. At a placement height of 1 m directly above the canopy row the EC sensible heat measurements, if anything, were larger than BREB values (slope of 0.924, Fig. 7.5). There was therefore no indication from these comparisons that the placement height of the EC sensors was too close to the canopy. Also, the separation distance of 30 m between the EC systems and each BREB system pair probably contributed to some variability between the two data sets. Dyer and Hicks (1972) showed that the variation in sensible heat flux in the horizontal is less than 10 % for a uniform site.

We compared latent heat flux density calculated from the EC sensible heat, net irradiance and the soil heat flux density (using the equation energy balance equation $L_v F_w = I_{net} - F_s - F_h$) with the latent heat calculated from the BREB system (using the BREB equation $L_v F_w = (I_{net} - F_s)/(1 + \beta)$). This regression was much improved (**Fig. 7.6**) compared to that of the measured sensible heat values of Fig. 7.5 due to the auto-selfcorrelation nature of the data. In both EC and BREB expressions for the calculation of the latent heat, the net irradiance I_{net} was the dominant term. The 95 % slope confidence interval for the regression line of (Fig. 7.6) is between 0.966 and 1.010.

Some energy balance terms, integrated over the day for daylight hours, are shown in **Table 7.1**. There was even better agreement between measured EC fluxes with that obtained using the BREB method for daylight totals, compared to the 12-minute averages (Figs 7.5 and 7.6).

The BREB sensible heat was very sensitive to the net irradiance (**Figs 7.7 and 7.8**). The EC sensible heat values were much less sensitive to net irradiance. This accounts for some variability in the data comparisons (Fig. 7.5). As a corollary to this: if the net irradiance (and soil heat flux density) measurements are in error, then the BREB sensible and latent heat flux density estimates will also have error. This was not so for the EC measurements of sensible heat since the technique is absolute and therefore independent of F_s and I_{net} measurement errors.

The assumption implicit in the use of the BREB technique is that of Similarity of the exchange coefficients for latent and sensible heat flux density. Since the EC and BREB data show reasonable agreement, the assumption of Similarity is a valid one for the time period of the experiment.

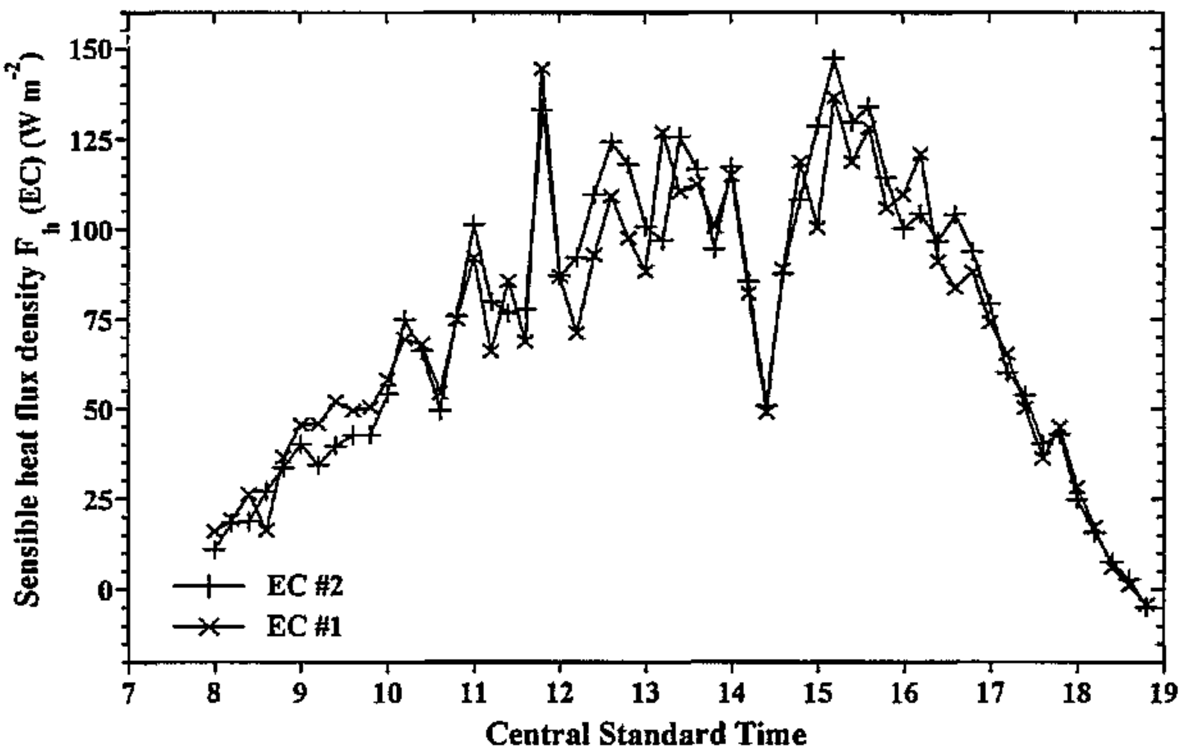

Fig. 7.2 The diurnal variation in the EC sensible heat flux density (W m^{-2}) for Day 154, 1992 for the two EC systems placed 1 m above the canopy row, for adjacent rows

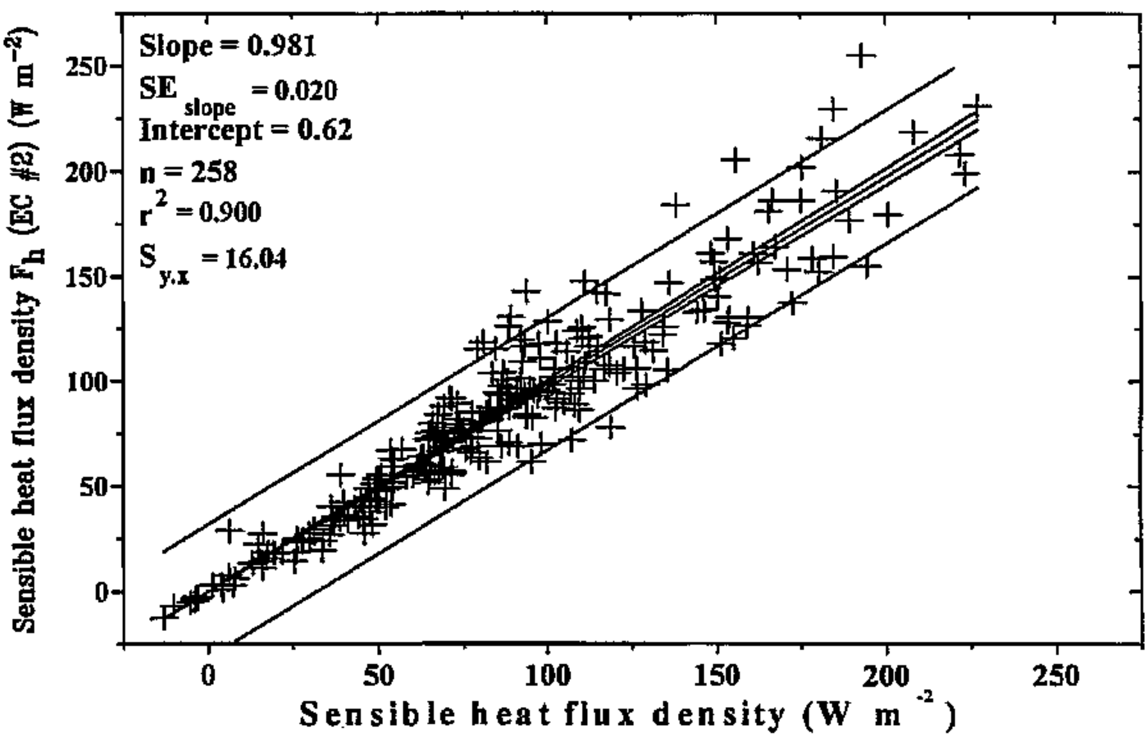

Fig. 7.3 Regression of the #1 EC sensible heat flux density against that average measured using system #2 for Days 151 and 156 to 159, 1992., the systems being placed 1 m above the canopy rows for adjacent rows. The wide limits are the 95 % confidence limits for an estimated individual y value and the narrower limits are the 95 % confidence limits for the population mean. Also shown is the regression line

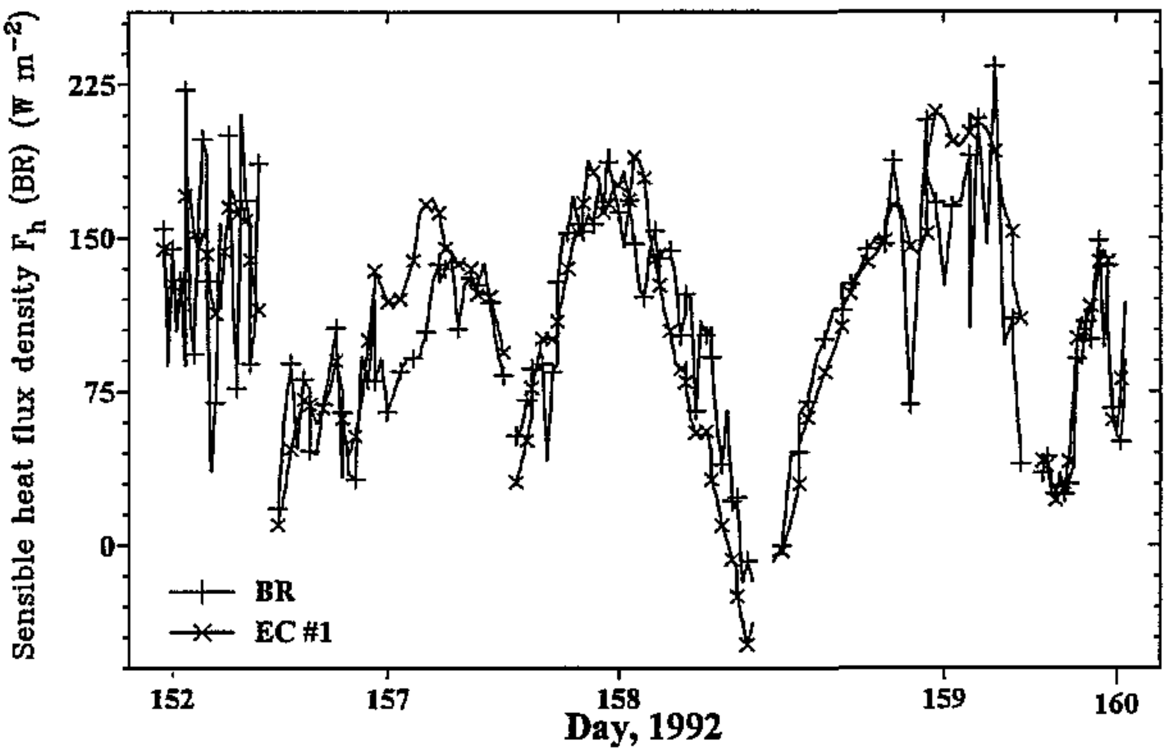

Fig. 7.4 Diurnal variation in EC sensible heat flux density for EC system #1 and the average of the four BR systems for Days 151 and 156 to 159, 1992

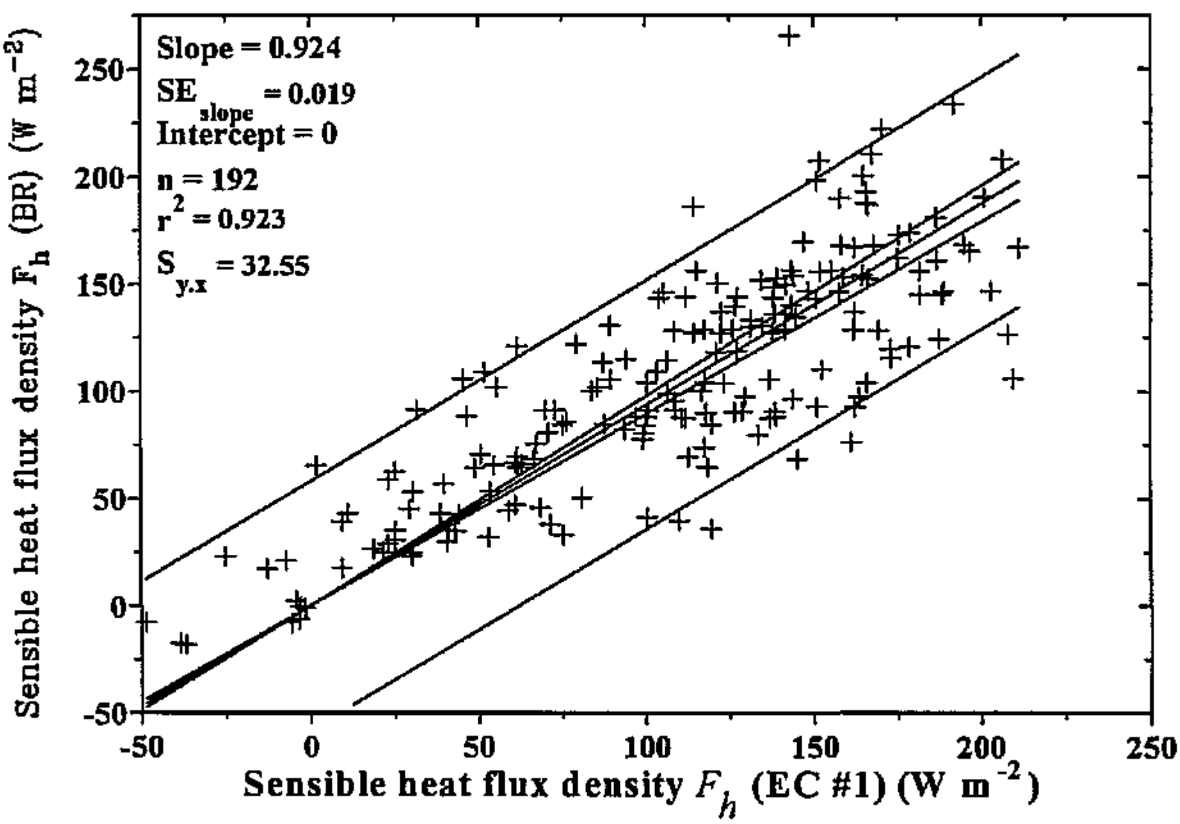

Fig. 7.5 Regression of the #1 EC sensible heat flux density against that measured using the four BR systems for Days 151 and 156 to 159, 1992

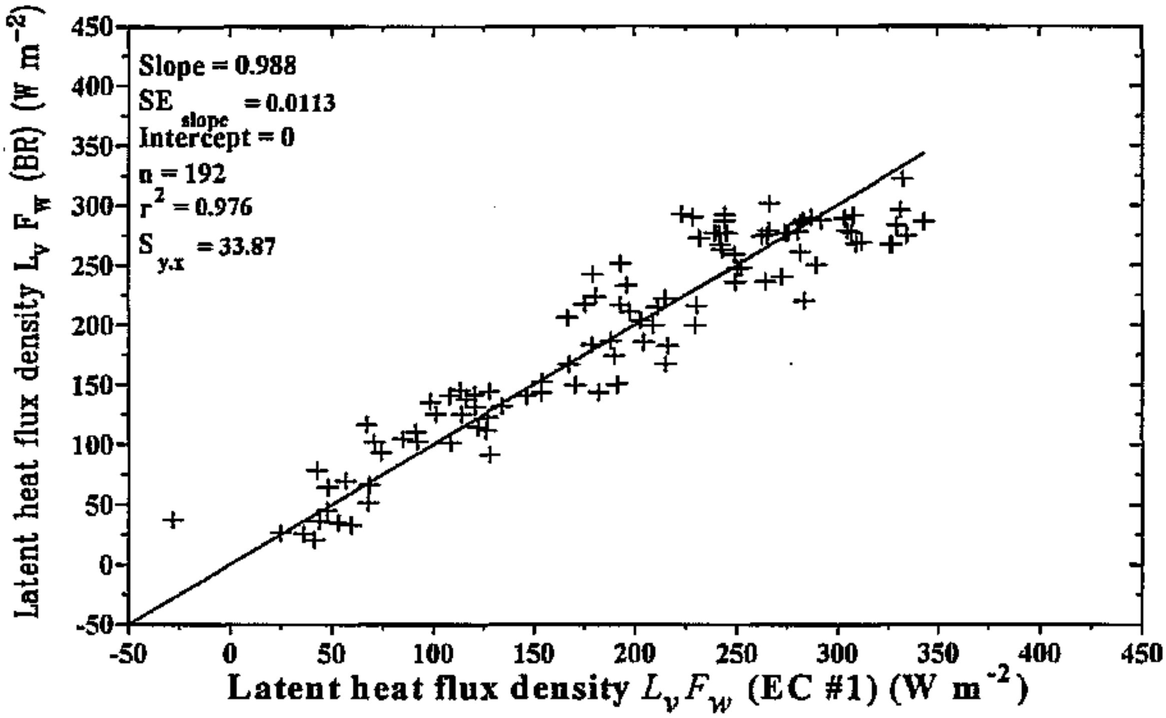

Fig. 7.6 Regression of the #1 calculated EC latent heat against that measured using the four BR systems for Days 151 and 156 to 159, 1992

Table 7.1 Total daily integrated values for eddy correlation (EC) and flux densities of Bowen ratio (BR) sensible heat F_h and latent heat $L_v F_w$, soil heat F_s, net irradiance I_{net}, solar irradiance I_s and rainfall for Days 151 to 159, 1992

Integrated value	Unit	Day, 1992					
		151	152	156	157	158	159
F_h (EC)	MJ m^{-2}		3.43	3.08	3.95	3.57	2.91
F_h (BR)	MJ m^{-2}		3.31	2.66	4.36	3.53	3.37
$L_v F_w$ (EC)	MJ m^{-2}		6.74	7.57	8.24	7.18	10.59
$L_v F_w$ (BR)	MJ m^{-2}		6.86	8.27	7.83	7.22	10.13
F_s	MJ m^{-2}		3.15	4.51	4.98	1.74	3.15
I_{net}	MJ m^{-2}		13.32	15.44	17.12	12.49	16.64
I_s	MJ m^{-2}			22.80	24.84	16.90	21.67
Rainfall	mm	8.1	0.3	0.0	0.0	8.6	7.1

The EC technique did not appear to underestimate the sensible heat flux as found by Tanner *et al.* (1985), Dugas *et al.* (1991) and Cellier and Olioso (1993). If anything, from the regression analysis (Fig. 7.5), the EC sensible heat flux density was larger than that calculated using the BREB technique. However, there is evidence suggesting that the early morning EC sensible heat flux densities were smaller than the corresponding BREB values (Fig. 7.8). These early morning differences could be due to a temperature effect on the sonic anemometer or they could be due to the influence of the lagged soil heat flux density values affecting the BREB sensible heat calculation (Eq. 7.2). Also, there were times

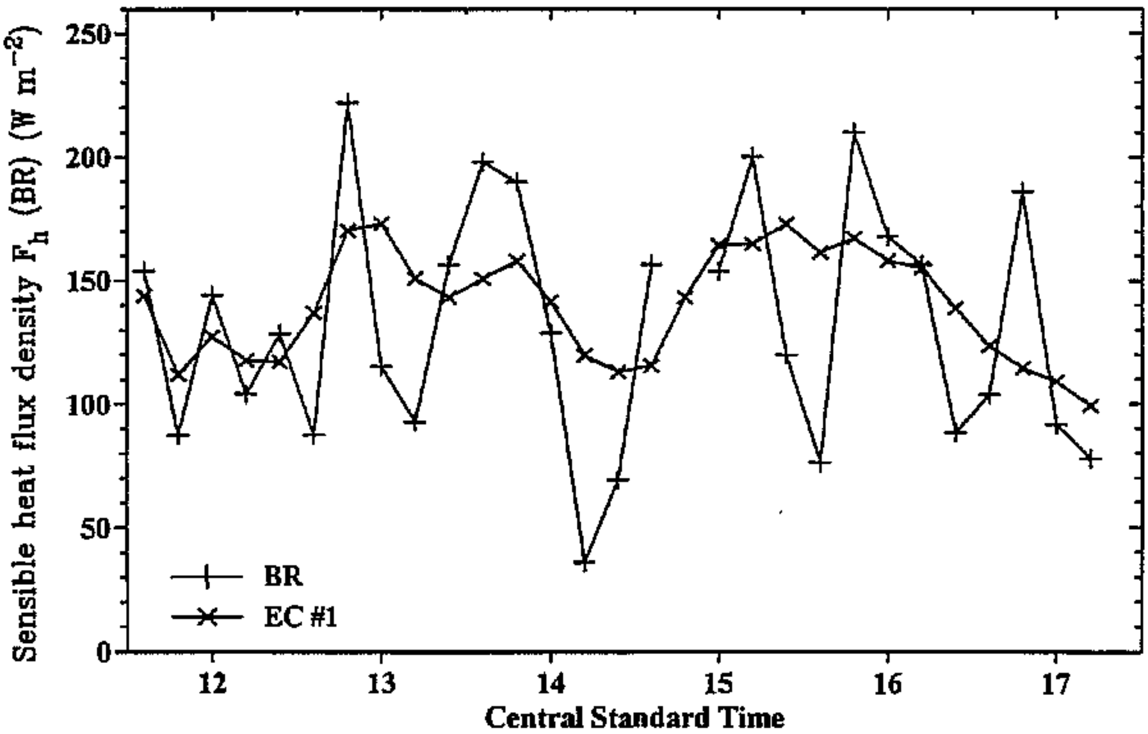

Fig. 7.7 The variation in sensible heat flux density for EC system #1 and the four BR systems for Day 152, 1992. The BR measurements are sensitive to changes in net irradiance whereas the EC measurements are less directly affected

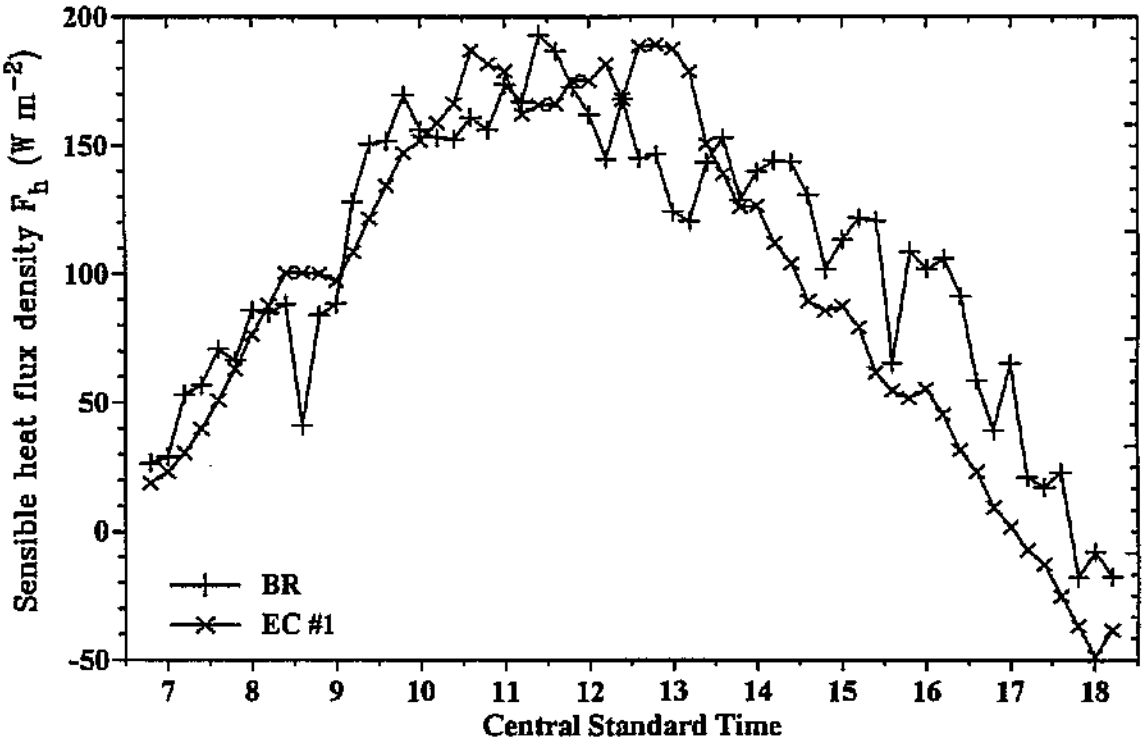

Fig. 7.8 The variation in sensible heat flux density for Day 157, 1992 for EC system #1 and the four BR systems. Of note is that the EC estimates of the sensible heat flux density are smaller than the BR values in the mid-afternoon to late-afternoon hours

when the afternoon EC sensible heat flux density values were less than that measured using the four BREB systems (Fig. 7.8) but on other days, for example Day 158, the reverse was true (Fig. 7.9).

Up to now, sensible heat comparisons have been for the case where the EC systems were placed directly above the canopy row. The sensible heat flux density for both EC systems for Day 156 and 157 is shown (Fig. 7.10). At around 12h30 CST, indicated by the large vertical arrow, EC system #2 was moved from being directly above a row position to the interrow but kept at 1 m above the soil surface. Movement of the system to the between row position significantly increased the sensible heat flux density (Fig. 7.10). Similarly, for Day 157, 12h30 CST, indicated by the second large vertical arrow, EC system #2 was moved to the between row position but kept at the same height (2.6 m above soil surface). Movement of the system to the between row position also significantly increased the sensible heat flux density (Fig. 7.10). The wind direction, indicated by a clockwise rotation from the vertical, is shown near the bottom of Fig. 7.10. The EC sensible heat flux density measurements on these two days, prior to 12h30 CST, were correlated to the BREB measurements. The EC measurements after 12h30, whether at a height of 2.6 m or 1.0 m above the soil surface, at the between row position, were significantly greater than the BREB measurements. Clearly then in our vineyard of limited fetch, the placement of the EC system above row or between row positions resulted in very different estimates of sensible heat. Since the measurements are not the same (Fig. 7.10), we conclude that there is limited mixing of air between above row and between row positions. In an experiment above a relatively smooth grassland surface, we show (Chapter 8) that the increase in measured sensible heat as one moves away from a surface is due to the scale of turbulence (eddy size) and not due to acoustic reflections from the surface.

We used the standard deviation in the vertical wind speed as a measure of vertical turbulent intensity. Evidence for differences in the vertical turbulent intensity above the row and between rows is

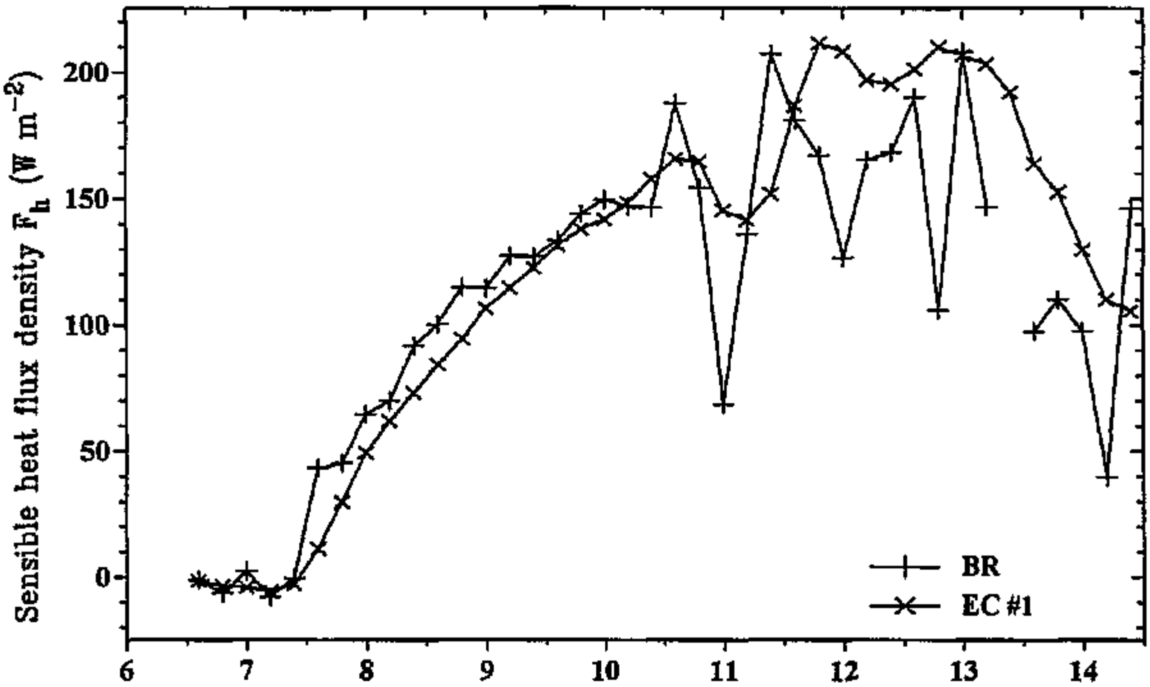

Fig. 7.9 The variation in sensible heat flux density for Day 158, 1992 for EC system #1 and the four BR systems. Of note is that the BR ratio estimates of the sensible heat flux density are greater than the EC values in the early to mid-morning hours

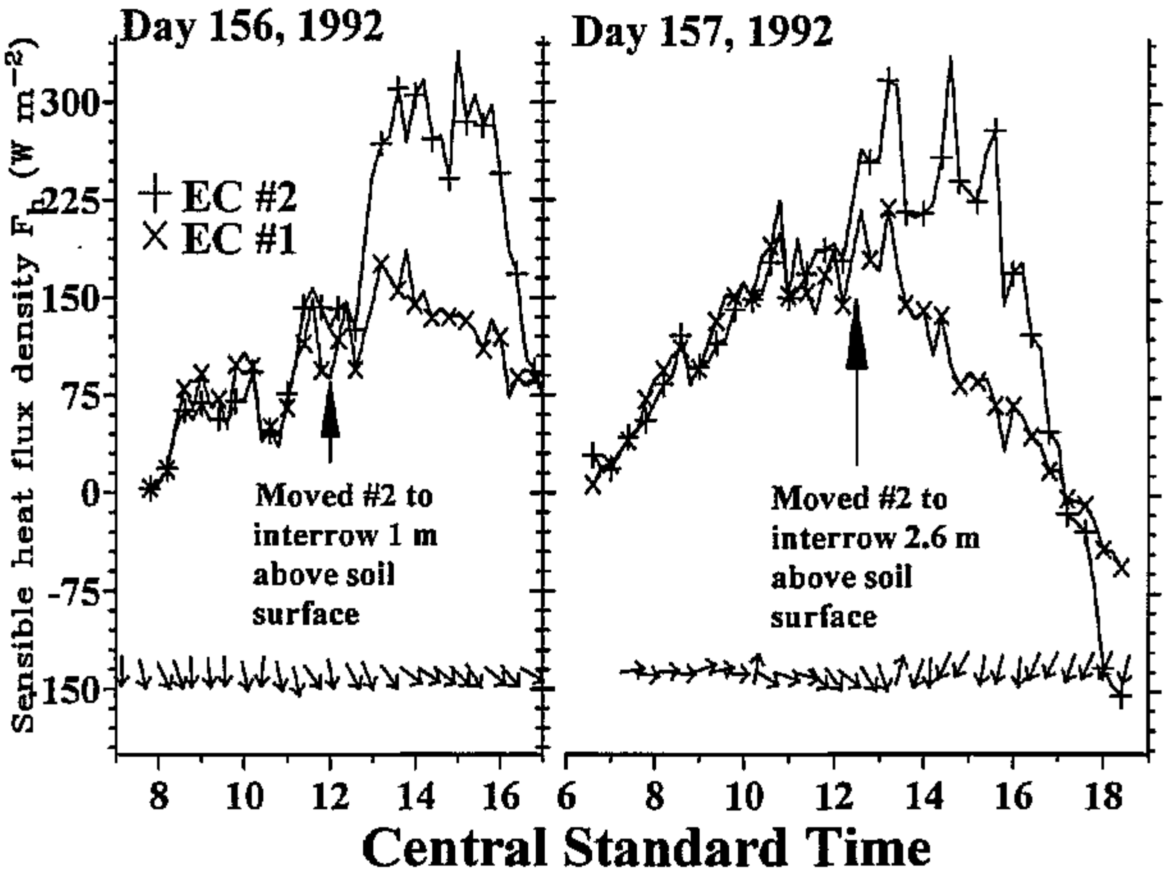

Fig. 7.10 The diurnal variation in the sensible heat flux density F_h (W m^{-2}) for EC system #1 placed 1 m above the canopy row on Days 156 and 157. On Day 156, EC system #2 was placed 1 m above the canopy row prior to 12h15 CST and then placed 1 m above the soil surface but at the between row position at 12h15 CST. On Day 157, EC system #2 was 1 m above the canopy row prior to 12h30 CST and then placed 2.6 m above the soil surface but at the interrow position at 12h30 CST. The wind direction (clockwise from the vertical) is shown near the bottom of both figures

shown in **Fig. 7.11**. The standard deviation in the vertical wind speed between the above canopy row and between row positions differ markedly. Interestingly enough the peaks and troughs in the standard deviation of the vertical wind speed, after the repositioning of system #2 (indicated by the vertical arrow), occur at the same time on both days. We have used vertical times to indicate the in-phase variation for the two positions (Fig. 7.11). During the afternoon period, the average standard deviation on Day 157 was about 0.5 m s^{-1} for system #1 (above the row) and 1.4 m s^{-1} for system #2 (between rows). The diurnal variation in the standard deviation of the air temperature was different on Day 156 for the above row and between row positions (**Fig. 7.12**). The differences were not of the same magnitude as the vertical wind speeds. On Day 157 where both EC systems were 2.6 m above the soil surface (but one at the above row and one at the between row positions), there was no difference in the standard deviation of the air temperature.

We conclude that the sensible heat and the vertical turbulent intensity above the row compared to that between the canopy rows are different. These findings illustrate the importance of the lateral placement of sensors above row crops in cases where fetch is limited.

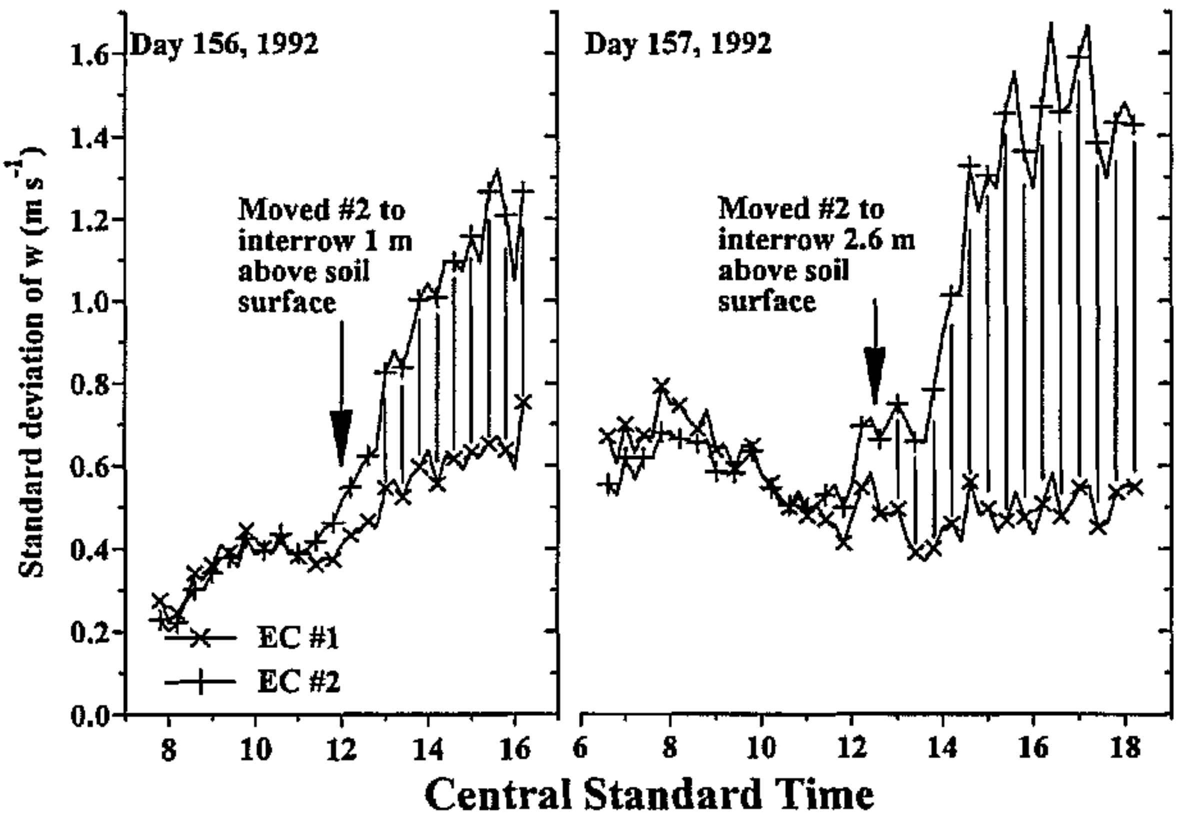

Fig. 7.11 The diurnal variation in the standard deviation in vertical wind speed (m s^{-1}). The placement of the two EC systems is described in the caption of Fig. 7.10. The vertical lines after the arrow are used to indicate the in-phase variation at the two positions

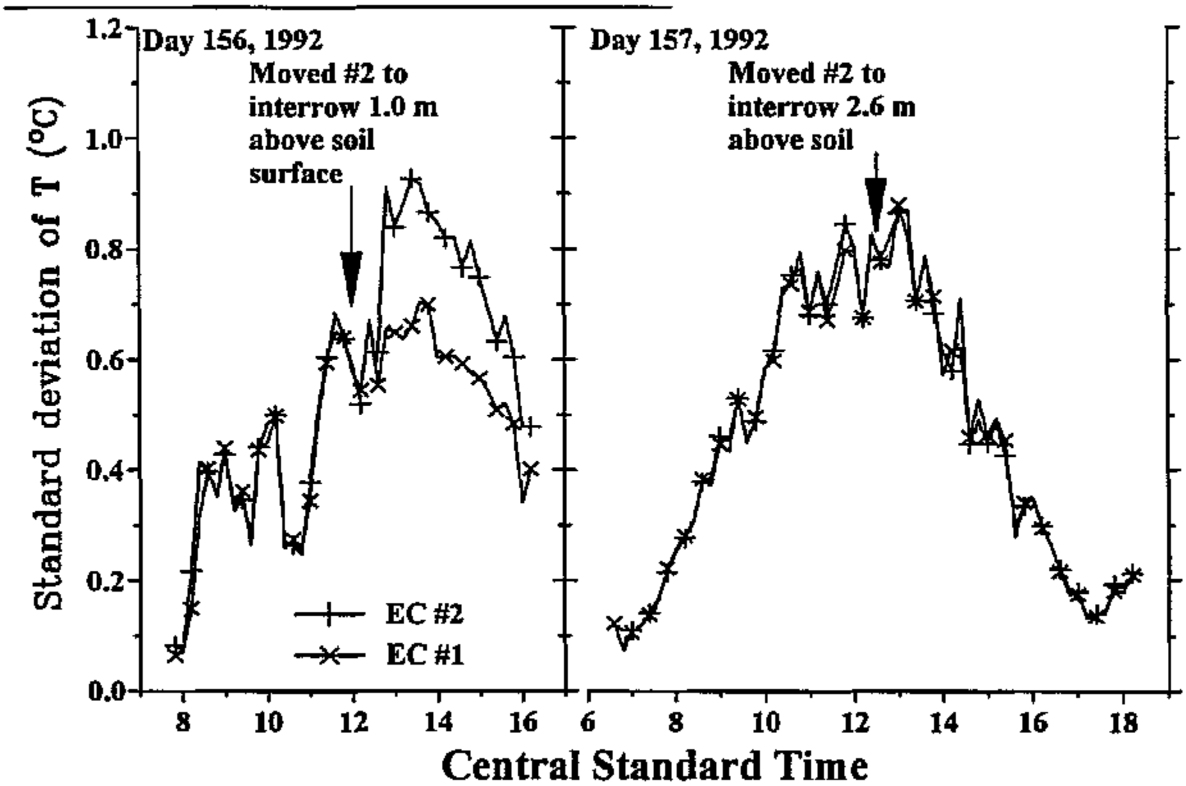

Fig. 7.12 The diurnal variation in the standard deviation in air temperature (°C). The placement of the two EC systems is described in the caption of Fig. 7.10

7.5 Conclusion

Sensible heat flux density estimates from two eddy correlation systems (EC) compared favourably when the sensors were placed 1 m above adjacent rows in a vineyard. Good sensible heat flux density comparisons, although more variable, were obtained between two EC systems placed directly above a row and four Bowen ratio systems placed 30 m apart. The EC estimates of sensible heat were relatively independent of net irradiance compared to the BREB measurements thereof. Real time measurements of sensible heat flux density were shown to be possible in a vineyard using the EC technique. Large differences in EC sensible heat were measured between above canopy row and between row positions. These measurements demonstrate the lack of mixing between the two canopy positions. Sensible heat and the standard deviation of the vertical wind speed were significantly greater at the between row position compared to the above-canopy row position. Care is needed in the lateral placement of sensors above row crops for sites with limited fetch.

Chapter 8

Placement height[15] and "footprints"[16] of eddy correlation sensors above a short turfgrass surface

8.1 Abstract

Variation in measured sensible heat flux density F_h with sensor height above short turfgrass during mainly unstable conditions was investigated using the eddy correlation (EC) technique. Our data showed that EC-measured sensible F_h at 0.25 and 0.38 m above the turfgrass were 15 and 10 % lower, respectively, than that at the 1.00-m height. There was no statistical difference in the EC-measured F_h at 0.50, 1.00 and 1.25 m. These placement heights corresponded to fetch-to-height ratios from 520:1 to 95:1. Calculations based on fetch showed that the lowest four heights were within the equilibrium layer whereas the heights at or greater than 1.25 m were above the equilibrium layer. The greater F_h measurements above the 1.25-m height, compared to the lower heights, were probably from advected F_h from nearby tar roads and buildings. Measurements of atmospheric stability were obtained by calculating the ratio of height z above surface to the Monin-Obukhov length. Most measurements were obtained under unstable conditions when mixed convection prevailed. Our measurements show that it is possible for EC sensors to be placed as low as 0.50 m above the surface, during unstable periods, without significant difference from the F_h measurements at a height of 1.00 m. Data were obtained with a pan filled with soil placed 0.27 m below the fine wire thermocouple of an EC system placed 1.00 m above surface. These data demonstrated that the reduction in the sensible heat was not due to acoustic reflections from that surface. Possibly, the reduction was due to small-sized eddies near the surface being contained between the sonic separation distance. An analysis of "footprints" shows that, at least 90 % of the measured F_h at a height of 0.5 m was from our experimental site, decreasing to less than 70 % at the 1.5-m height. Calculations showed that the fetch requirement for micrometeorological measurements above a forest canopy was more stringent than for grassland canopy. Sensor placement at the 0.5-m height would result in little reduction, as did occur at heights less than 0.50 m, in the covariance between vertical wind speed fluctuation and air temperature fluctuation due to small-sized eddies being contained between the separation distance of the sonic anemometer transducers. We speculate that measurements closer than 0.5 m to the surface differed from those at 1.00 m due to small-sized eddies near the surface being contained between the sonic separation distance and therefore not completely detected by the sonic anemometer.

8.2 Introduction

For certain chemically active substances, scalar flux measurements should be made as close to the surface as possible (Fitzjarrald and Lenschow 1983, Kristensen and Fitzjarrald 1984). Not much attention has been devoted to how close to vegetated surfaces eddy correlation (EC) sensors (Swinbank 1951) may be placed without the measured scalar flux being significantly different from that further from the surface, but still within the equilibrium boundary layer. In the present study, we only consider the flux of sensible heat (F_h) at various heights above the canopy surface.

15 Based on the paper by Savage, McInnes and Heilman (1995)

16 Based on the paper by Savage, McInnes and Heilman (1996)

Fetch considerations aside (Heilman *et al.* 1989), EC sonic anemometer measurements of vertical wind speed fluctuation should ideally be at a height that allows even small-sized eddies between the anemometer transducer to be sensed. If sensor height is too close to the plant canopy surface, small-sized eddies may not be sensed and possible sonic reflections from vegetation may affect measurements. Presumably, small-sized eddies between the separation distance of the sonic anemometer will result in spectral attenuation of the eddy structures and an underestimation in F_h. On the other hand, any sonic reflections from the vegetation would be detected by the sensor but not discriminated from the nonreflected fluctuations by the sensor and would, in all likelihood, increase the measured F_h.

Kaimal (1975) showed theoretically that the minimum operating height of the sonic anemometer above plant canopy in an unstable surface layer is 6 π multiplied by the spatial resolution of the sonic anemometer to avoid spectral attenuation from spatial averaging between the anemometer transducers. These recommendations have been used by some workers (for e.g., Kizer and Elliott 1991). Kaimal (1991, pers. comm.) however suggested that measurements, under unstable conditions, at a height of 1 m above plant canopy should be sufficiently valid without making any corrections for spectral attenuation from spatial averaging. There appears to have been some hesitation by researchers in placing their EC systems at heights approaching 1 m or closer above canopy.

Our goal was to compare EC sensible heat measured at various placement heights above short turfgrass and determine the fraction of these measurements, at each height, emanating from within the adjacent upwind area.

Fast response sensors (Swinbank 1951, Campbell and Unsworth 1979) allow eddy correlation (EC) determination of sensible heat flux density F_h, independent of the other terms of the surface energy balance, from the covariance of vertical wind speed fluctuation w' and the air temperature fluctuation T':

$$F_h = \rho\, c_p\, \overline{w'T'} \qquad 8.1$$

where ρ is the density of air (taken to be 1.17 kg m^{-3}, appropriate for a standard temperature of 25 °C and a atmospheric pressure of 100 kPa), c_p is the specific heat capacity of dry air (1056 J kg^{-1} K^{-1}) and the overbar shows a time average.

Heilman *et al.* (1989) investigated the fetch requirements of their Bowen ratio sensors by placement at various heights. Dyer (1961) and Dyer and Pruitt (1962) used a placement height of 4 m over an irrigated field for fetch distances of 190 m. Verma *et al.* (1992) placed their EC sensors at 3.5-m (3-D sonic anemometer) and 2.5-m (1-D sonic anemometer) heights above a peat surface for a site with at least 250 to 300 m of fetch. However, placement heights of several metres require large fetch distances to ensure adequate adjustment of the turbulent boundary layer and horizontal equilibrium of the measured vertical fluxes. Hicks *et al.* (1975) used various placement heights above a pine forest.

Ideally, measurements should be in that portion of the boundary layer that is in equilibrium with the surface. The equilibrium sublayer is defined as the region where the momentum flux density is within 10 % of that at the surface (Brutsaert 1982). As Brutsaert (1982) pointed out, this definition has led to formulations of minimum fetch-to-height ratios to ensure that Bowen ratio measurements are made in the equilibrium layer - ratios varying from 10:1 (Panofsky and Townsend 1964) to 200:1 (Dyer 1965) although 100:1 has been considered adequate for most measurements (Rosenberg *et al.* 1983).

Heilman *et al.* (1989) obtained adequate Bowen ratio measurements for ratios as low as 20:1.

To avoid spectral attenuation from spatial averaging between the anemometer transducers, the minimum operating height of the sonic anemometer above plant canopy in an unstable surface layer is 6π multiplied by the spatial resolution of the sonic anemometer (Kaimal 1975). These recommendations have been used by some workers (for e.g., Kizer and Elliott 1991). Kristensen and Fitzjarrald (1984) found no statistical difference between their measurements of F_h for five heights varying between 1.46 and 8.45 m for a 1-km upwind fetch consisting of patchy grass, 0.8-m tall. Similarly, Haugen *et al.* (1971) found sensible heat measurements at 5.66 and 22.6 m agreed to within ± 20 % for a site with a fetch of 500 m in all directions and no obstructions for tens of kilometres.

In spite of the theory presented by Kaimal (1975), he suggested (1991, pers. comm.) however that measurements, under unstable conditions, at a height of 1 m above plant canopy should be sufficiently valid without making any corrections for spectral attenuation from spatial averaging. To assess how close to canopy surfaces measurements may be obtained, we performed eddy correlation measurements using four systems placed at eight different heights above a short grassland surface of limited fetch (less than 200 m) with measurements at or below 2 m. We investigated the effect of placement height on measurements of F_h and using these measurements calculated, for different placement heights, for grassland and forest canopies, the fraction of sensible heat emanating from within an adjacent upwind area - the footprints of the measurements.

8.3 Materials and methods

Measurements were performed outside the Agricultural Engineering Workshop at Texas A & M University, College Station, TX, USA (altitude of 100 m, latitude 30° 30 ′ N and longitude of 96° W). The research area (**Fig. 8.1**) was a 1.6-ha short and flat bermudagrass (*Cynodon dactylon* L.) surface on a Boonville soil series (fine, montmorillonitic, thermic Mollic Albaqualfs). Measurements were obtained between 18 August and 13 October (Days 231 to 287, 1992).

Sensible heat flux density F_h was determined using four EC systems. Fluctuations in vertical wind speed w' and the air temperature T' were measured initially every 0.1 s but later every 0.2 s using a CA27 sonic anemometer (Campbell and Unsworth 1979) equipped with a fine wire (12.5-µm diameter) chromel-constantan thermocouple (Campbell Scientific, Logan, Utah, USA).

The thermocouple allowed a temperature difference measurement but not an absolute temperature measurement. Alterations to the sensors included insulating the reference thermojunction of the thermocouple and the metal arm containing the reference junction with pipe insulation material. We used extra insulation to increase the time constant of the reference junction to temperature change. This ensured a more stable reference junction temperature during our 12-min averaging period. Signals from two EC systems were measured with a 21X datalogger and signals from the other two systems using a CR7X datalogger (Campbell Scientific). These commonly-used dataloggers have the limitation that a measurement frequency greater than 5 Hz is not possible without loss of data. The CR7X datalogger was also used to gather the wind speed, wind direction, net irradiance and air temperature data. Data collection priority was always given to the EC data. Real-time measurements of F_h were possible by programming the datalogger to calculate F_h every 12 min.

This choice of averaging period was based on the work of Kaimal (1969), who found that a 15-min averaging period was sufficient for sensible heat measurements, and Kaimal and Gaynor (1991) who

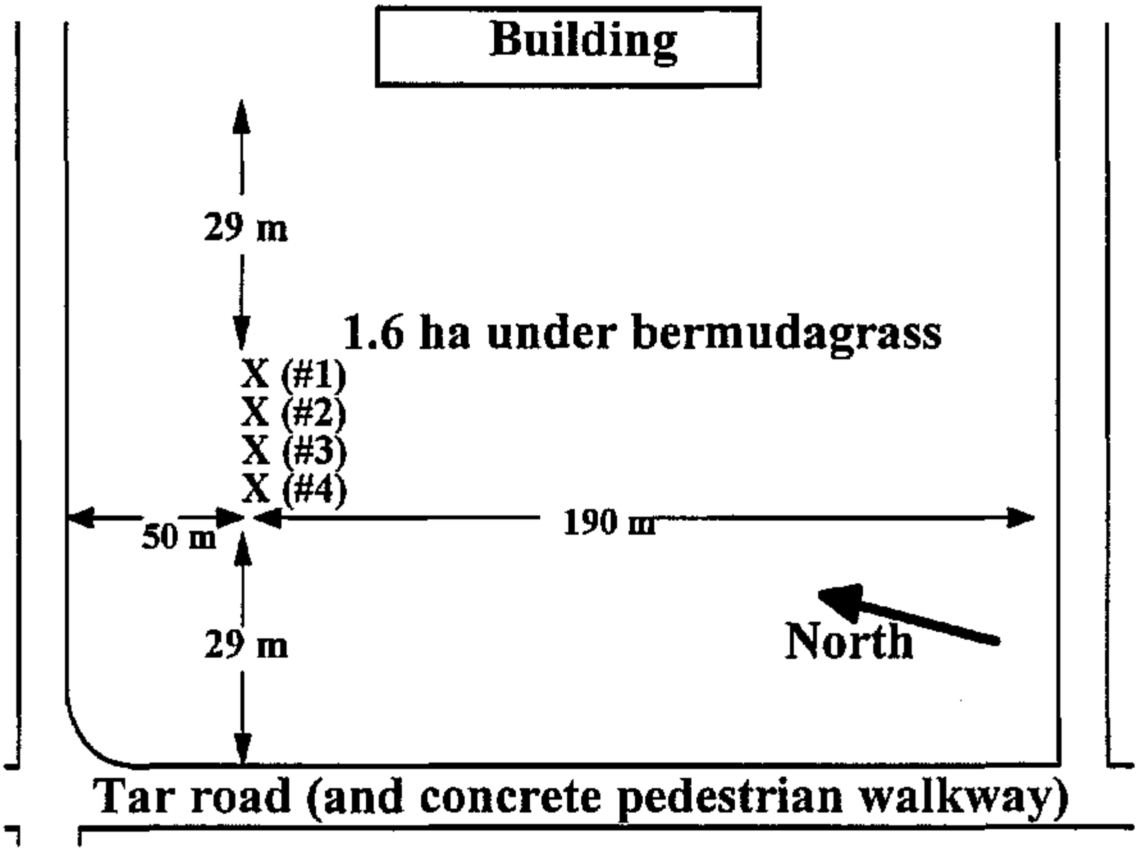

Fig. 8.1. A diagram (in plan view and not to scale) of the experimental site. The positions of the four EC systems are indicated by X's, each system 3 m from the next. EC system #1 was always positioned at 1.00 m above the turfgrass surface

used 10-min averaging periods. The datalogger program enabled the determination of $\overline{w'T'}$ and other parameters such as $\overline{w}$, $\overline{T}$ and the standard deviations of these quantities. To minimize datalogger program execution time, we used fast and single-ended voltage measurements.

According to Kanemasu *et al.* (1979), much of the transport of sensible heat energy is associated with normalized frequencies, $f = nz/\overline{u}$, between 0.001 and 2 where n is the cyclical frequency, z the sensor placement height above the canopy and $\overline{u}$ the mean horizontal wind speed. Assuming that the normalized frequencies of importance are bounded by these limits (0.001 and 2), the averaging period used must under ideal conditions respond to normalized frequencies less than 0.001 and the datalogger measurement frequency must respond to high frequency eddies at normalized frequencies greater than 2. Measurement systems should therefore be fast enough to respond to fluctuations of at least 2 $\overline{u}/z$. The choice of sampling rate is to insure that the highest frequency of interest is included in the statistics (Kaimal 1975). Based on sampling theory, he argued that the sampling rate should be at least twice the highest frequency of physical significance. The high frequency requirement for flux density measurements is $f = 3$ corresponding to a cyclic frequency $m = 3\,\overline{u}/z$ in the data. Even at this rate, there will be some underestimation in sensible heat because of aliasing. Ideally, the measurement sampling rate should be varied according to the mean horizontal wind speed and sensor placement height. This procedure is not practical. A frequency of greater than 5 Hz was not possible with our equipment. Other workers using the identical equipment presumably faced similar problems. Furthermore, many commercially available sonic anemometer systems do not allow sampling rates greater than 10 Hz (varying from 5 to 20 Hz for the units that we are aware of). It appears that a sampling rate greater than 10 Hz is not possible for analogue measurements. However, some digital measurement systems may allow measurement frequencies greater than 10 Hz.

In our preliminary measurements, not reported here, a datalogger measurement frequency of 10 Hz was employed. However datalogger overrun occurred with the possibility of data loss during measurement periods with an even greater possibility whenever data was transferred to final storage every 12 minutes. These commonly-used dataloggers have this limitation - measurement frequencies greater than 5 Hz are not possible without loss of data if two eddy correlation systems are connected to one datalogger. However, preliminary comparisons of sensible heat, using two eddy correlation systems at the same height with one system operating at 5 Hz on one datalogger and another system at 10 Hz, were not statistically different (data not shown) for our site and conditions.

One sonic anemometer-fine wire temperature system (system #1) was positioned at a height of 1.00 m above the turfgrass surface. The other three systems (#2, #3 and #4) were placed at a height of 0.25, 0.375, 0.50, 1.00, 1.25, 1.50, 1.75 or 2.00 m. These systems were kept at each of these heights until there were sufficient data to compare with measurements of F_h from system #1 at the 1.00-m height. Initial measurement comparisons were performed with all systems at the 1.00-m height.

In a separate experiment to assess the importance of sonic reflections (from a 0.22 m by 0.22 m metal pan placed 0.27 m directly beneath the fine wire thermocouple) on our measurements, EC systems #1 and #2 were placed at a height of 1.00 m above the turfgrass (**Fig. 8.2**). Air temperature 1 m above the turfgrass was measured as the average from five non-aspirated 50-µm diameter copper-constantan thermocouples. Wind speed was measured at 0.25, 0.50, 1.00, 1.25 and 1.50 m heights above the turfgrass using model 12102 DC three-cup anemometers (R.M. Young, Traverse

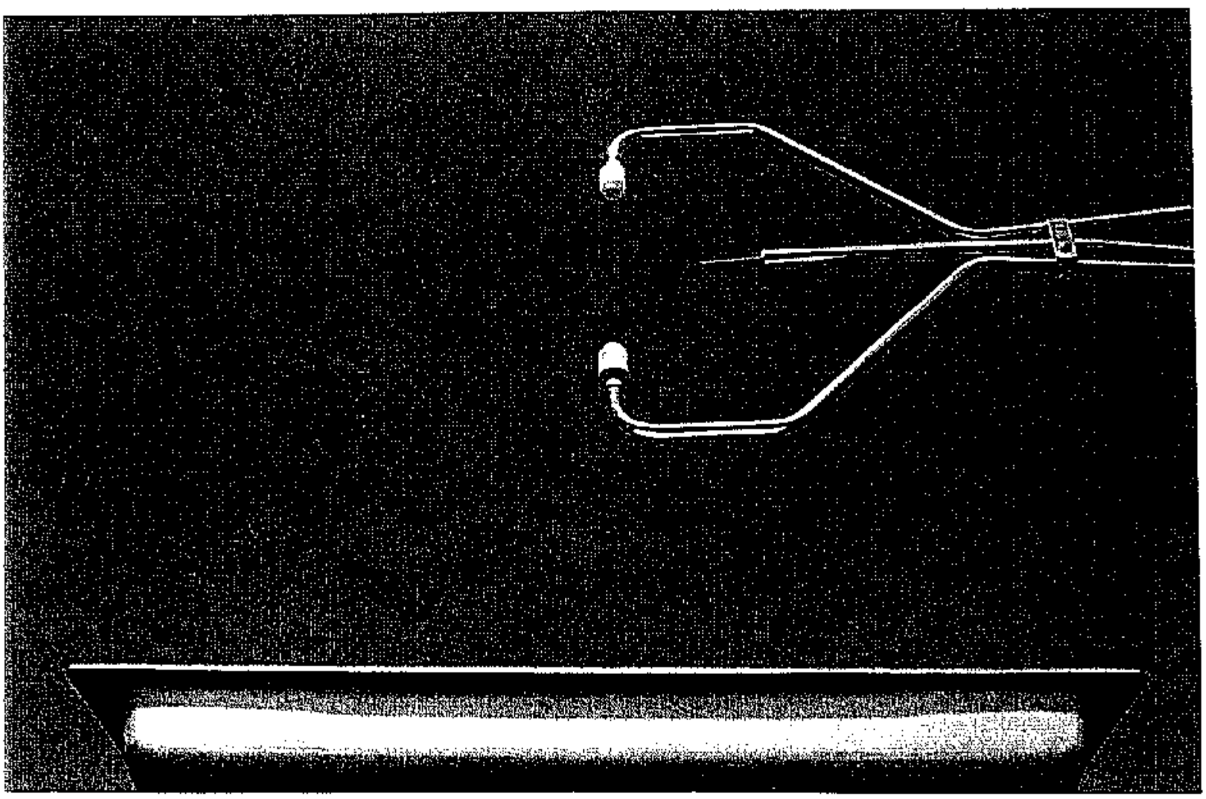

Fig. 8.2 A photograph showing the placement of a pan containing soil beneath an EC system to encourage acoustic reflections

City, Michigan). For each 12-minute period, friction velocity (u_*) was determined from the slope of the plot of $\bar{u}$ (average wind speed for the 12-min period) *vs* ln $(z - d)$ where z is the height and d is the zero-plane displacement. Wind direction was measured using a model 12005 wind vane (R.M. Young). These measurements were at 2 m above the turfgrass surface.

The CR7X datalogger was also used to gather the air temperature, net irradiance, wind speed and wind direction data. Data collection priority was always given to the EC data. Real-time measurements of F_h were possible by programming the datalogger to calculate F_h every 12 min.

Atmospheric stability was evaluated as the ratio of $z/\mathcal{L}$, where $\mathcal{L}$ is the Monin-Obukhov length (m), defined as:

$$\mathcal{L} = -u_*^{\ 3}/[k\,(g/T)\cdot F_h/(\rho\, c_p)] \qquad 8.2$$

where u_* is the friction velocity (m s^{-1}), k von Karman's constant ($\approx$ 0.41), g the acceleration due to gravity (9.795 m s^{-2}), and T the air temperature (K). Net irradiance was measured with a model Q*6 net radiometer (Radiation and Energy Balance Systems, Seattle, WA) at 1-s intervals and averaged over a 12-min period.

8.4 Results and discussion

During the study, winds were predominantly from the south with a uniform fetch distance of at least 190 m (Fig. 8.1). Sensible heat measurements for which the wind direction was between SW and ESE were only used for analysis. The thickness of the internal boundary layer ($\delta_{boundary}$) at the locations of the EC measurements was calculated using the Munro and Oke (1975) equation

$$\delta_{boundary} = x^{0.8}\, z_o^{\ 0.2} \qquad 8.3$$

where x is fetch, ($\approx$ 190 m) and z_o is the roughness length for momentum transport. For these values, $\delta_{boundary}$ varied between 18 and 21 m for z_o estimated as 13 % of canopy height. The height of the turfgrass was between 0.005 and 0.02 m. All sensor heights were measured relative to the plant canopy. Since a rough-to-smooth transition existed at our site, the lowest 5 % of the boundary layer was assumed to be in equilibrium with the surface (Brutsaert 1982, page 166). For a smooth-to-rough transition, the lowest 10 % of the boundary layer is assumed to be in equilibrium with the surface (Brutsaert 1982, page 166). For our site

$$\delta_{equilibrium} = 0.05 \times \delta_{boundary} \qquad 8.4$$

with $\delta_{equilibrium}$ varying between about 0.90 and 1.05 m. The calculated thickness of the internal boundary layer at the measurement site, using the Munro and Oke (1975) equation, was therefore between 0.90 and 1.05 m. It is therefore likely that measurements at or below 1.00 m were within the equilibrium layer while measurements above 1.00 m were above the equilibrium layer. Stability during the period of measurements was assessed by examining the ratio of height above canopy z (m) to the Monin-Obukhov length $\mathcal{L}$ (m). The length $\mathcal{L}$ was calculated from u_* determined from the wind profile measurements, the air temperature at 1 m and the F_h (Fig. 8.3) measured at 1.00 m using EC system 1. Under unstable conditions, free and mixed convection dominates. The magnitude of $\mathcal{L}$ for unstable conditions can be interpreted as the height above the zero plane displacement at which free convection becomes the dominant transfer mechanism. For unstable conditions and for a short grassland surface, free convection dominates when $z/\mathcal{L} < -1$ and mixed convection dominates when $-1 < z/\mathcal{L} < -0.01$. During the study, $z/\mathcal{L}$ varied between about −0.2 to −0.01 during the day and from about −0.01 to 0.02

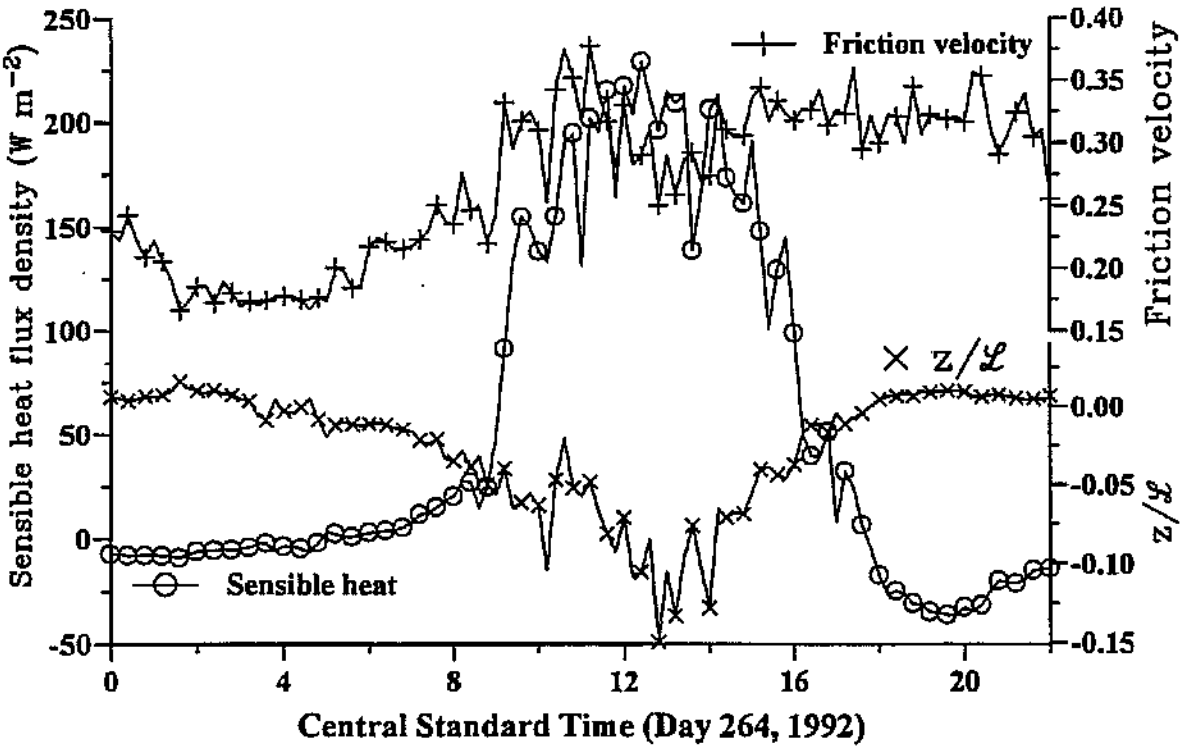

Fig. 8.3 The variation in the friction velocity and the ratio of sensor height z (= 1.00 m for system 1 used here) to the Monin-Obukhov length $\mathscr{L}$ and F_h for Day 264, 1992

during the night. Typical data are shown (Fig. 8.3). During these periods, friction velocity u_* varied between 0.15 and 0.38 m s^{-1}. Throughout the experiment, unstable conditions ($z/L < -0.01$) occurred during daylight hours when mixed convection dominated but tended towards free convection during the noon hours (Fig. 8.3). Neutral conditions ($-0.01 < z/L < 0.01$) occurred close to sunrise or sunset and stable conditions ($0.01 < z/L < 0.02$) occurred during the night. The z/L ratio was used to calculate the stability-corrected footprints.

A three-dimensional plot of $3\,\bar{u}/z$ (Hz), the high frequency requirement for flux density measurement corresponding to a normalized frequency $f = 3$, as a function of local time and height above grass canopy surface (Fig. 8.4) shows that the normalized frequency $3\,\bar{u}/z$ increases with height and increases progressively from morning periods from about 3 to 40 Hz in the late afternoon. Assuming a sampling time of 0.1 s (corresponding to a sampling rate of 10 Hz), it therefore seems that it would not be possible to obtain good correspondence between sensible heat measurements as a function of height, using a single 10 Hz sampling rate for all heights. However, a 10 Hz sampling rate must have allowed most of the frequencies to be included in the statistics. This statement is supported by the fact that, as we will show, reasonable EC sensible heat comparisons as close as 0.5 m from the surface, were possible.

In view of our aim of performing measurements close to the surface and in the light of Kaimal's (1991, pers. comm.) comments, we chose 1.00 m as a standard height above canopy. Before comparing measurements of sensible heat at the various heights, it was therefore important to first compare measurements from all EC systems at 1.00 m. There were no statistical differences in sensible heat flux density measurements from all EC systems at 1.00 m above surface. The 95 % slope confidence interval, for each system, contained the slope value of unity. Therefore, for the rest of the study, measurements from systems 2, 3 and 4 were treated as three independent measurements at the chosen

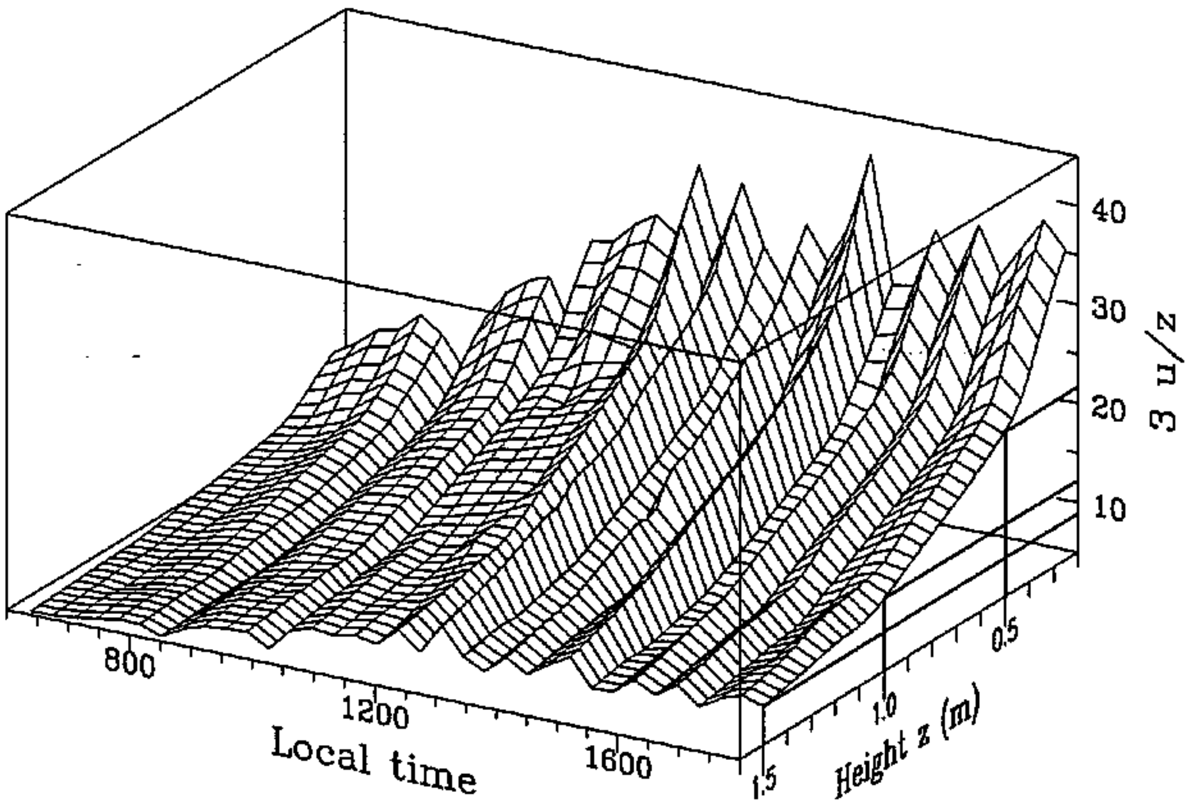

Fig. 8.4 A three-dimensional representation of three times the ratio of horizontal wind speed to placement height u/z, corresponding to the high frequency requirement for flux density measurement, as a function of local time and placement height for Day 249

height. These measurements were compared with the F_h measurements from system 1 at 1.00 m above surface.

Typical diurnal F_h measurements are shown (**Fig. 8.5**) for EC system 1 at 1.00 m and 2 and 3 both at 0.38 m. Of particular note is the underestimation in F_h at the 0.38-m height compared to 1.00 m. Measurements such as these were used to determine the dependence of the F_h flux density measurements on placement height. For the case shown (Fig. 8.5), measurements during the night were possible. For the duration of the study, the midday net irradiance did not exceed 600 W m^{-2}.

Sensible heat flux density measurements from all EC systems 1.00 m above surface were compared and no differences were found. The unsystematic root mean square error was a small fraction of the total root mean square error for each EC system (**Table 8.1**, first three data columns). The 95 % slope confidence interval, for each system, contains the slope value of unity. Therefore, for the rest of the study, measurements from systems #2, #3 and #4 were treated as three independent measurements at the chosen height.

Measurement comparisons between EC system #1 at 1.00 m and the other systems at 0.25 m, 0.38 m, 0.50 m and 1.00 m above turfgrass are shown in **Fig. 8.6**. Of particular note is the gradual increase in the slope from 0.8636 for the F_h measurements from system #1 at 1.00 m (x-axis) and the other systems at 0.25 m (y-axis) measurement comparisons (**Fig. 8.6a**) to 0.9126 at 0.38 m (**Fig. 8.6b**), 1.0245 at 0.50 m (**Fig. 8.6c**) and 1.0076 at 1.00 m (**Fig. 8.6d**).

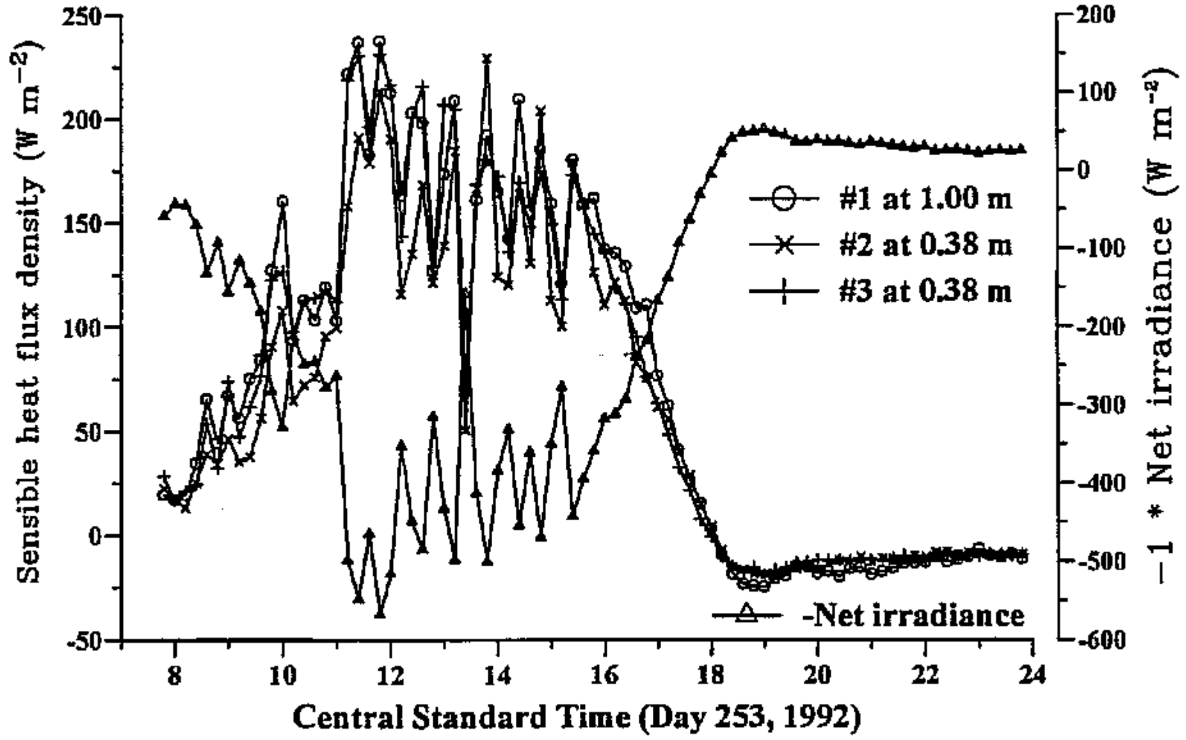

Fig. 8.5 Typical diurnal EC F_h measurements on Day 253, 1992. System 1 was at 1.00 m above the grassland surface 2 and 3 were both at 0.38 m. Also shown is the negative of the net irradiance (right-hand y-axis)

The slope of the curves of F_h at a known height, *vs* that measured at a height of 1.00 m using EC system #1 (Fig. 8.6), as a function of height above turfgrass is shown (**Fig. 8.7**). The bars above and below each datum point show the 95 % confidence limit in the slope. Statistically, there is a difference among the slopes at each of the 0.25-m, 0.38-m and 0.50-m heights (at the 95 % level of significance). There is also a difference among the slopes at 0.50, 1.75 and 2.00-m heights (Fig. 8.2). Slope of the ratio of F_h at height z over that at 1.00 m *vs* the height z above turfgrass relationships show three distinct regions (Fig. 8.7): (a) increasing slope between 0.25 and 0.50 m; (b) plateau region of constant slope between 0.50 and 1.25 m; (c) increasing slope (although not statistically significant) between 1.25 and 1.75 m. Root mean square errors (**Table 8.2**) show a decrease in the systematic mean square error (associated with a slope value different from unity) with height up to 1.00 m and then an increase in this error component above the 1.00-m height up to a height of 1.75 m.

The significance of the plateau region of Fig. 8.7 is that measurements at 0.50 m above the turfgrass were no different from measurements at between 1.00 and 1.25 m (Table 8.2). For heights less than 0.50 m, there was a sudden reduction in the slope by nearly 10 % (at 0.38 m) and 15 % (at 0.25 m) (Fig. 8.7). The generally increasing slope region between placement heights of 1.00 and 2.00 m deserves comment. The experimental site was surrounded by asphalt roads on three sides with buildings to the southeast and southwest (Fig. 8.1), the predominant wind direction being from the south. Wind from a generally southerly direction would flow between two nearby buildings and across the asphalt roads and advect hot air to the experimental site. It was uncertain whether the EC values at either 0.50 or 1.00 m were actually measures of the true sensible heat flux destiny at the site. However, we did obtain 543 12-minute comparisons between EC sensible heat at 1.00 m and that using an independent surface temperature method of determining sensible heat Section 5. The surface

Table 8.1 First three data columns: associated statistical parameters for the linear regression of F_h at 1.00 m measured using systems #2 and #3 compared with that measured 1.00 m at using system #1; last data column: associated statistical parameters for the linear regression of F_h at 1.00 m measured using systems #2 placed at 1.00 m but with a pan placed 0.27 m beneath the fine wire thermocouple compared with that measured at 1.00 m using system #1

	#2 (y) *vs* #1 (x) both at 1 m	#3 (y) *vs* #1 (x) both at 1 m	#2 and #3 (y) *vs* #1 (x) both at 1 m	#2 with pan placed 0.27 m beneath fine wire thermocouple (y) *vs* #1 (x) both at 1 m
n	155	82	237	496
Intercept (W m^{-2})	2.21	2.71	2.57	2.65
SE intercept (W m^{-2})	2.82	3.43	2.14	0.85
t value for zero intercept[a]	0.7823	0.7889	1.2024	3.1297[b]
Slope	1.0065	1.0150	1.0076	1.0032
SE slope	0.0190	0.0267	0.0151	0.0099
Slope confidence interval	(0.9690, 1.0441)	(0.9617, 1.0682)	(0.9779, 1.0374)	(0.9837, 1.0227)
t value for unit slope[a]	0.3428	0.5591	0.5049	0.3236
$S_{y \cdot x}$ (W m^{-2})	17.97	20.21	18.67	16.77
r^2	0.9483	0.9474	0.9498	0.9540
t value[c]	36.96	26.48	46.51	70.74
RMSE$_{\text{unsystematic}}$[d]	17.855	19.966	18.595	16.736
RMSE$_{\text{systematic}}$	3.079	4.345	3.510	2.783
RMSE$_{\text{total}}$	18.118	20.433	18.923	16.966

[a]Null hypothesis is that slope is 1 and intercept is 0; [b]Statistical significance at the 95 % level of significance; [c]$t = r\,[(n-2)/(1-r^2)]^{0.5}$;

[d]$MSE_{total} = MSE_{systematic} + MSE_{unsystematic}$; $MSE_{systematic} = \sum_{i=1}^{n} (\hat{y}_i - x_i)^2/n$; $MSE_{unsystematic} = \sum_{i=1}^{n} (y_i - \hat{y}_i)^2/n$

temperature sensible heat was about 0.96 of that measured using the EC technique at the 1.00 height, indicating that the 1.00-m height EC sensible heat adequately represented the true sensible heat at the site. There was however no statistical difference in measured sensible heat between the 1.25 and 2.00 m placement heights.

Koprov and Sokolov (1973) showed that sonic anemometer and thermocouple sensor separation can cause a discrepancy between measured and actual F_h values. It is not possible however to use their empirical relationship to correct for sensor separation as the closest separation between their sensors was 100 mm compared to the 20 mm in our case. Furthermore, the ratio of sensor separation distance to placement height for all our measurements was less than or equal to 0.01. This was considerably less than the 0.2 minimum value recommended by Koprov and Sokolov (1973) for application of their corrective empirical relationship.

The reason for the large reduction in the slope for heights less than 0.5 m (Fig. 8.7) was further

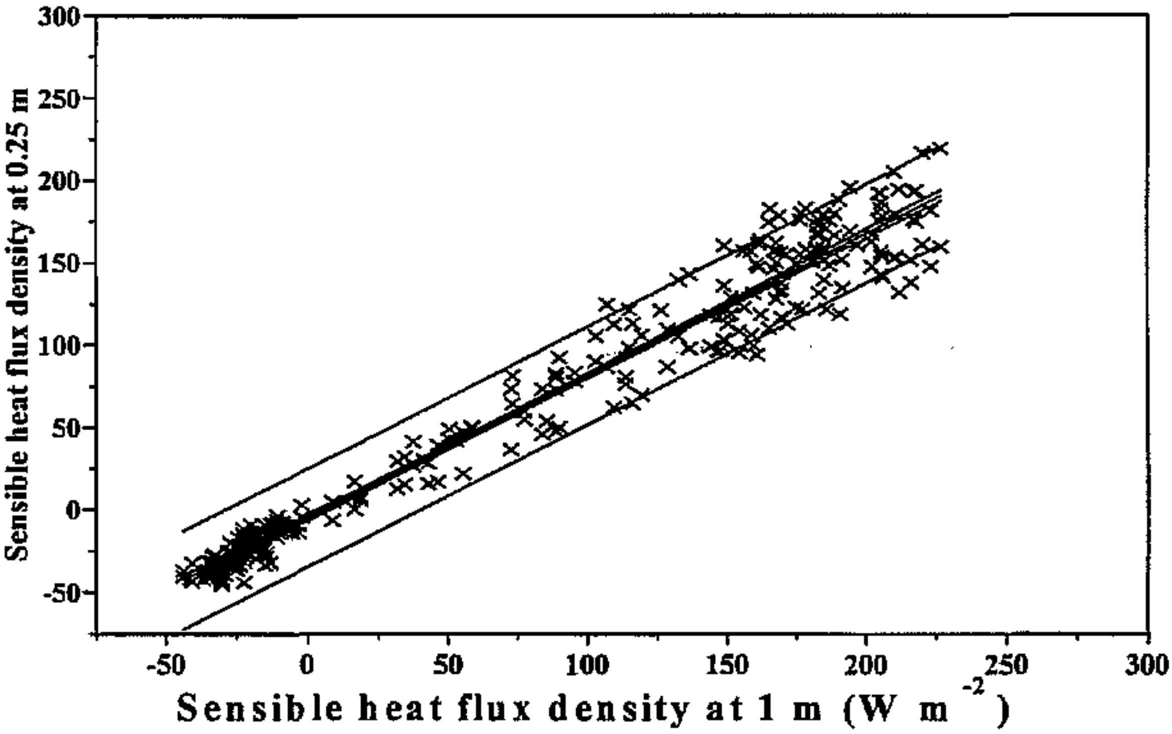

Fig. 8.6a Measurement comparisons between EC system #1 at 1.00 m and the other systems at 0.25 m (Days 241 to 242) above the surface. The wide 95 % confidence belts are for an estimated single y value and the narrower limits are for the population mean

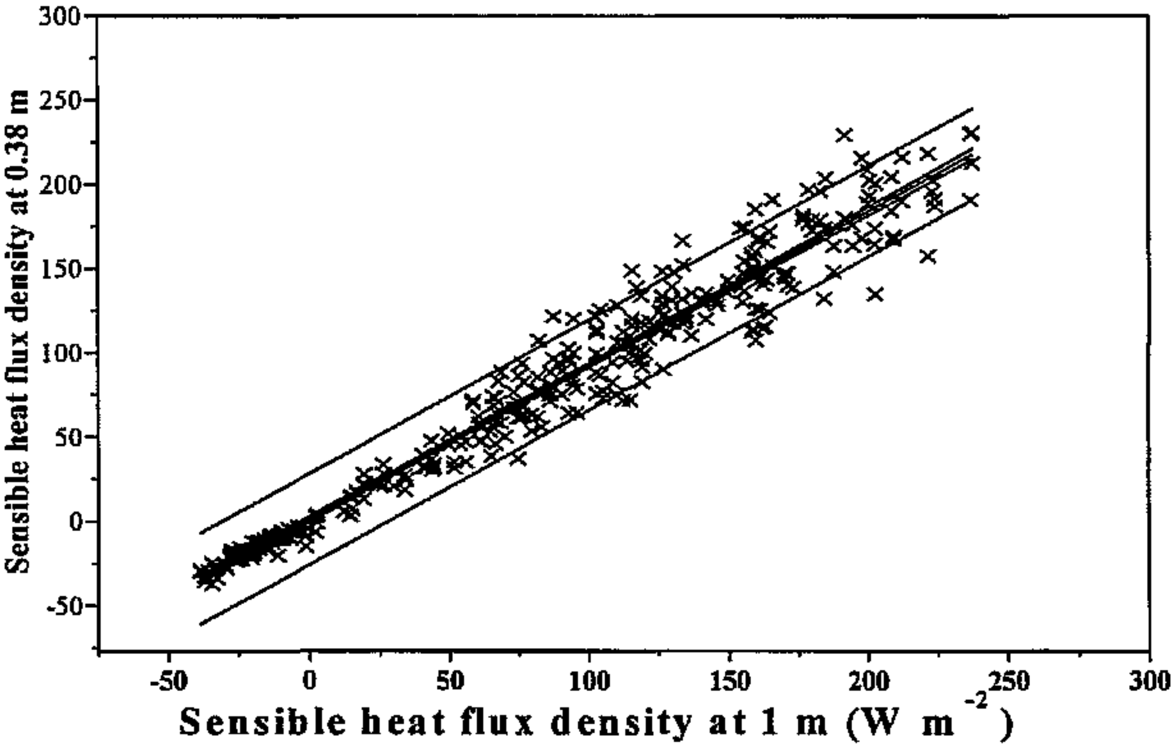

Fig. 8.6b Measurement comparisons between EC system #1 at 1.00 m and the other systems at 0.38 m (Days 247 to 254) above the surface. The wide 95 % confidence belts are for an estimated single y value and the narrower limits are for the population mean

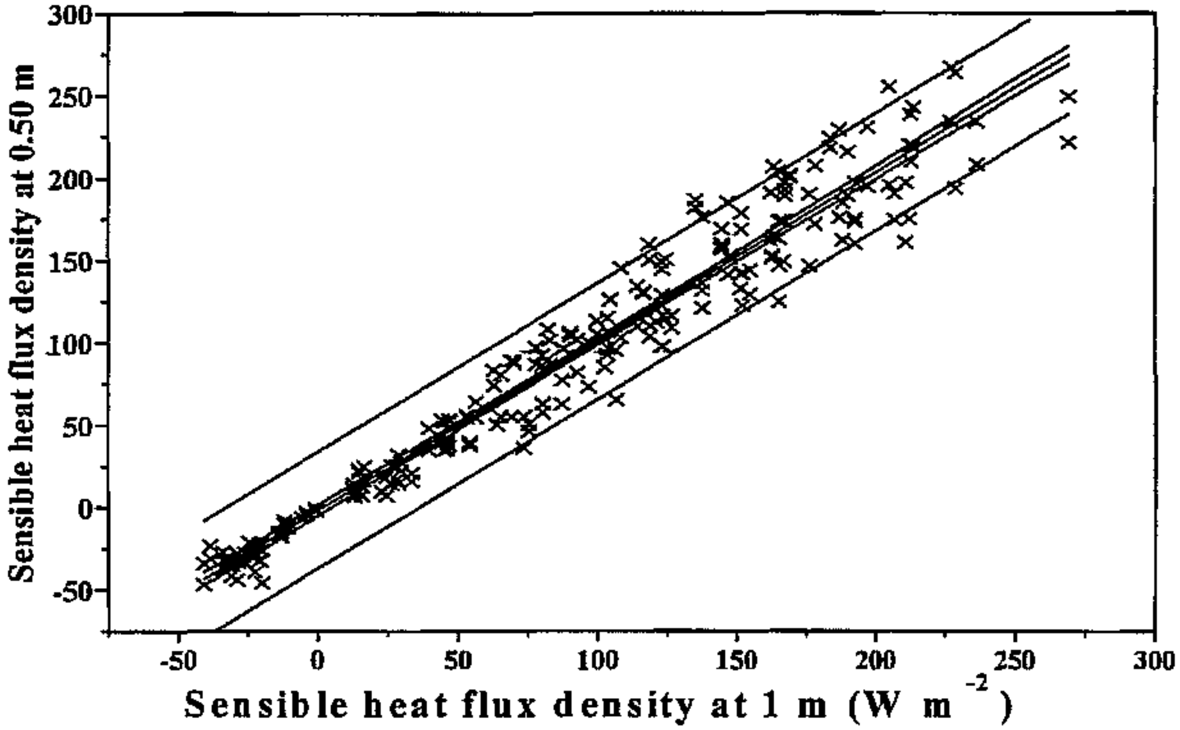

Fig. 8.6c Measurement comparisons between EC system #1 at 1.00 m and the other systems at 0.50 m (Days 233 to 235) above the surface. The wide 95 % confidence belts are for an estimated single y value and the narrower limits are for the population mean

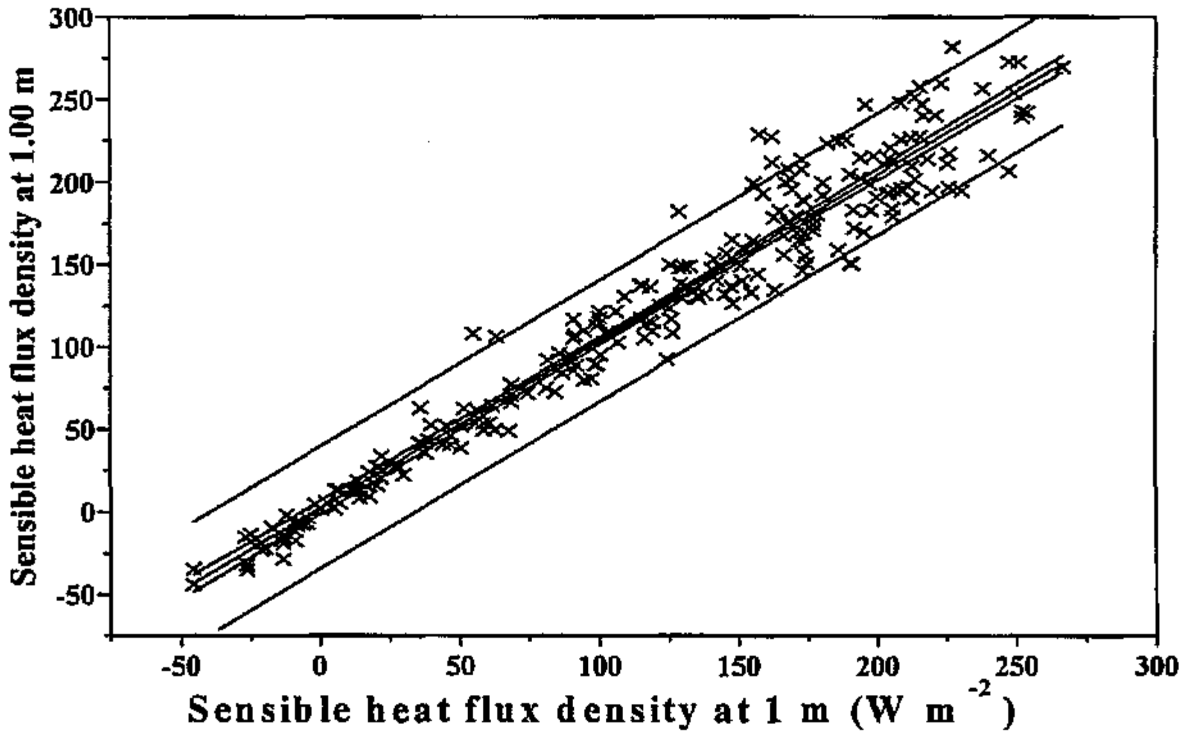

Fig. 8.6d Measurement comparisons between EC system #1 at 1.00 m and the other systems at 1.00 m (Days 231, 232, 259 to 262) above the surface. The wide 95 % confidence belts are for an estimated single y value and the narrower limits are for the population mean

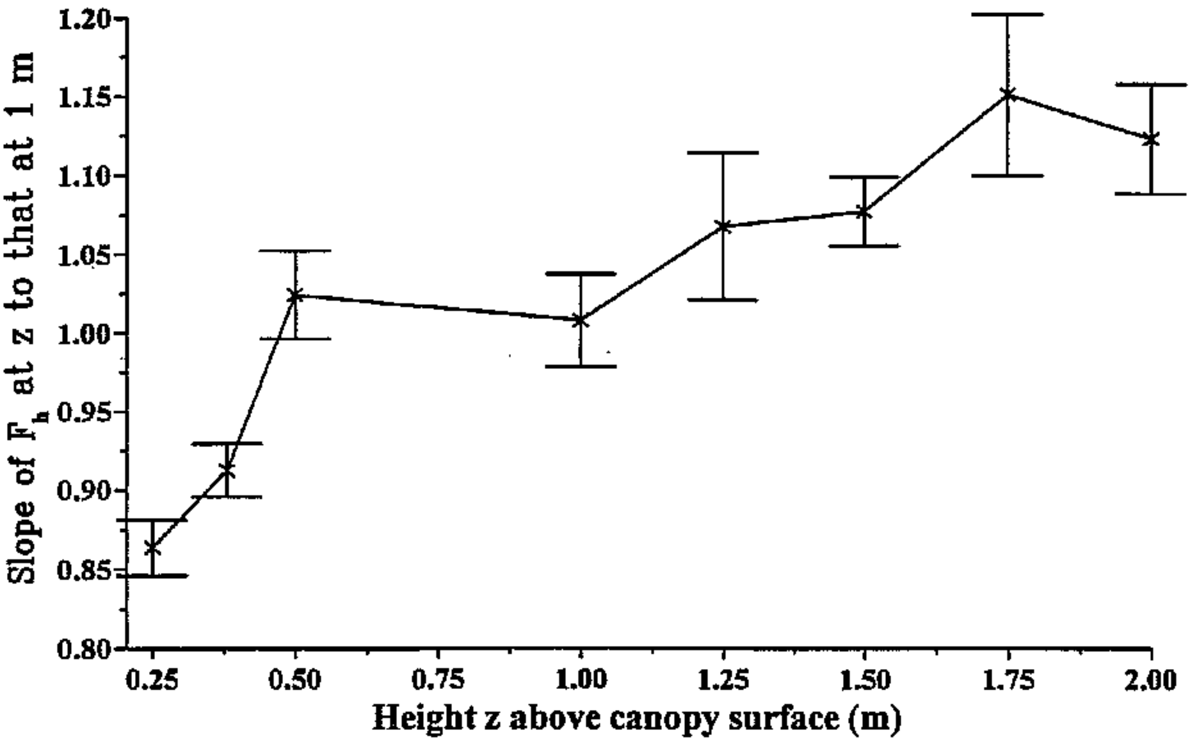

Fig. 8.7 The variation of the slope of the relationship sensible heat flux density measured at height z as a function of that at height 1.00 m. The bars above and below each datum point show the 95 % confidence limit of the slopes measured at 1.00 m using system #1

investigated. We wished to determine if the reduction could be attributed to sonic reflections from the underlying vegetated surfaces. The reduction could also be due to small-sized eddies, contained between the upper and lower arms of the sonic anemometer (100-mm separation), causing a reduction in the covariance between the vertical wind speed fluctuation and the air temperature fluctuation. Sensible heat flux density measurements with and without the metal pan 0.27 m beneath the fine-wire thermocouple were obtained for a week using EC system #1 and #2. Typical diurnal measurements with the pan in position at 12h00 (**Fig. 8.8**) show no differences in sensible heat after the pan was in place. A statistical comparison between the measurements showed no significant difference (Table 8.1, last column of data). There was therefore no evidence for sonic reflections from the pan affecting our F_h measurements. Eddies were presumably able to envelope the square pan. This envelopment would not alter the covariance between the vertical wind speed fluctuation and air temperature. Therefore, we speculate that measurements close to the canopy surface differ from those at 1.00 m due to small-sized eddies near the surface being contained between the sonic separation distance. These eddies would not be correctly measured by the sonic anemometer. At a measurement height z above the canopy surface, under neutral conditions, the mean eddy diameter, given by the mixing length l, is typically $k\,(z-d)$ where $k = 0.41$ is von Karman's constant (Thom 1975). Therefore for a grassland surface (with $d << z$) for a placement height $z = 1.00$ m, l is 0.41 m. The mean eddy size, l, in the vertical direction is greater than $k\,(z-d)$ under unstable conditions (Thom 1975). Eddies with typical diameters of 0.41 m were presumably able to envelope the square metal pan, filled with soil, of dimension 0.22 m This envelopment would not alter the actual sensible heat. Therefore, measurements close to the canopy surface differ from those at 1.00 m due to small-sized eddies near the surface being contained between the sonic separation distance. In order to conclusively demonstrate that the reduction in sensible heat near the surface is due to a loss of small-sized eddies, one would need to show that there is a loss of the

Table 8.2 Associated statistical parameters for the linear regression of F_h at various heights z (m) measured using systems #2, #3 and #4 compared with that measured at 1.00 m using system #1

	Sensible heat measurements at height z in metres (y) *vs* F_h for #1 at 1.00 m (x)						
	$z = 0.25$	$z = 0.38$	$z = 0.50$	$z = 1.25$	$z = 1.50$	$z = 1.75$	$z = 2.00$
n	327	412	246	103	308	63	223
Intercept (W m^{-2})	-4.98[b]	1.41	-1.62	6.73[b]	2.04	3.92	1.89
SE intercept (W m^{-2})	1.04	0.89	1.65	3.01	1.24	2.92	2.50
t value for zero intercept[a]	-4.7751[b]	1.5943	-0.9807	2.2344[b]	1.6432	1.3416	0.7534
Slope	0.8636[b]	0.9126[b]	1.0245	1.0673[b]	1.0771[b]	1.1505[b]	1.1226[b]
SE slope	0.0089	0.0086	0.0142	0.0235	0.0111	0.0256	0.0176
Slope confidence interval	(0.8460, 0.8811)	(0.8957, 0.9295)	(0.9966, 1.0524)	(1.0210, 1.1136)	(1.0553, 1.0988)	(1.0993, 1.2016)	(1.0879, 1.1572)
t value for unit slope[a]	-15.3116[b]	-10.1858[b]	1.7288	2.8646[b]	6.9711[b]	5.8800[b]	6.9681[b]
$S_{y \cdot x}$ (W m^{-2})	15.12	13.66	17.92	20.01	17.54	16.61	22.16
r^2	0.9666	0.9650	0.9554	0.9533	0.9688	0.9707	0.9485
t value[c]	96.98	106.32	72.30	45.41	97.44	44.95	63.83
$RMSE_{unsystematic}$	15.072	13.629	17.846	19.813	17.487	16.347	22.060
$RMSE_{systematic}$	19.346	8.183	2.024	14.417	9.987	20.111	19.004
$RMSE_{total}$	24.524	15.897	17.960	24.503	27.474	25.917	29.117

[a]Null hypothesis is that slope is 1 and intercept is 0

[b]Statistical significance at the 95 % level of significance

high frequency contribution in the cospectral estimates of sensible heat. Typically, measurements at a sampling rate at 20 Hz would be required. These rates were not possible with our equipment.

Since EC F_h measurements are absolute, requiring one measurement height only, the EC technique appears to have some advantages compared to the Bowen ratio (BREB) technique. The BREB technique requires measurements at two heights maintained sufficiently far apart for the sensors to detect differences in air temperature and water vapour pressure between the two levels. Given that the lower measurement level is at 0.50 m above the canopy, the upper level would be at least 1.00 m above a canopy similar to ours and usually at a height of 1.50 m. The EC measurements at the 0.5-m above canopy height would be less affected under limited fetch conditions than BREB measurements at 0.50 and 1.50 m, say. For our sonic anemometers, the minimum operating height of 6 π multiplied by sensor pathlength, for unstable conditions Kaimal (1975) would be equal to 1.8 m. Clearly then, adequate EC measurements of F_h are possible at heights much lower than previously thought. This fact has considerable importance for short-canopy situations where fetch may be limited.

If lower placement heights are also possible for other surfaces, the implication is that the fetch requirement for EC sensors is not as severe as was previously thought. For the less conservative fetch to placement height ratio of 20:1 found by Heilman *et al.* (1989), a Bowen ratio system would require a minimum fetch of 20 × 1.50 m = 30 m. The EC system, from our data, could be placed at a height above canopy of 0.50 m where the minimum fetch was 190 m.

Traditionally, the ratio of height z above the zero plane displacement d to the uniform upwind fetch

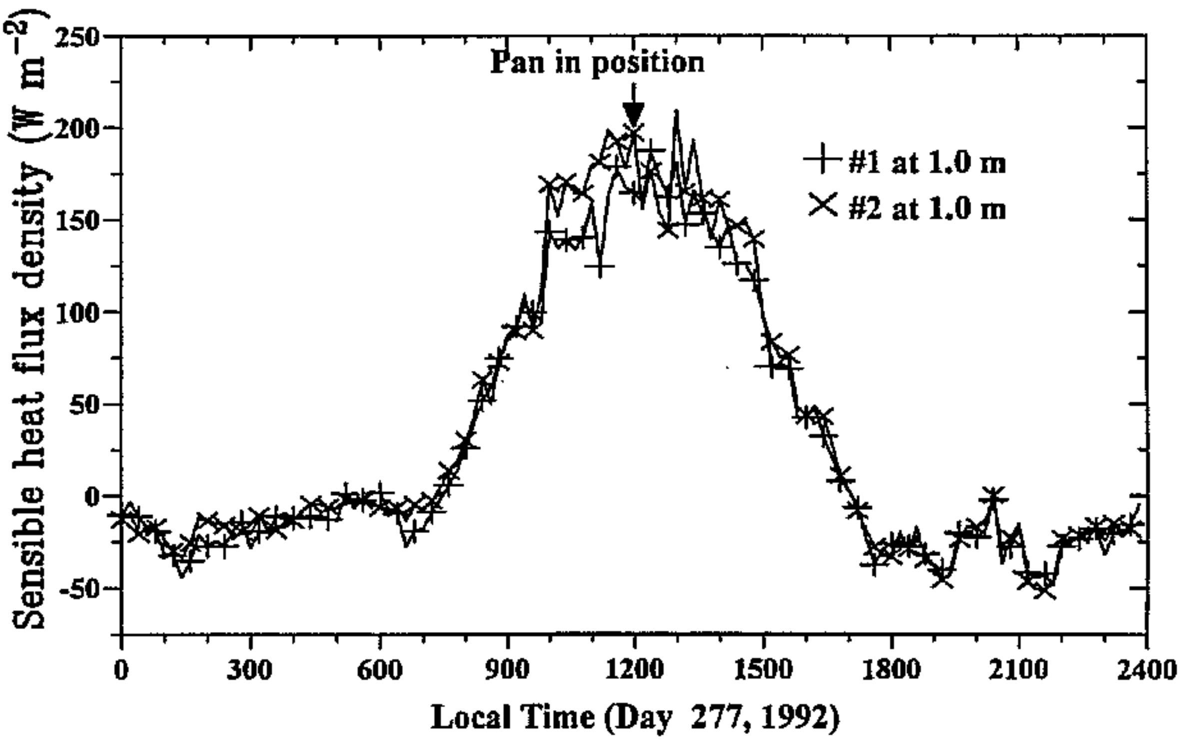

Fig. 8.8 The diurnal variation on Day 277, 1992 for system 1 placed at 1.00 m above the canopy and 2 also at 1.00 m above the grassland surface but with a metal pan located 0.27 m beneath the fine wire thermocouple. The arrow shows the time at which the pan was placed beneath system 2 (and kept in position for the rest of the Day 277)

distance x has been set to, say, 1:100 and then $(z-d)$ calculated from the known fetch x. This is a simplistic approach. A much-improved approach is to use an approximate analytical solution to the two dimensional diffusion equation for idealized surface boundary conditions (Philip 1959, Wilson 1982).

Under neutral conditions the fraction f of the measured F_h at a height z, that can be expected to emanate from within the adjacent upwind area a horizontal distance x from the measurement point is described by the relation:

$$f = \exp\left[-U(z-d)/(k\,u_*\,x)\right] \qquad 8.5$$

where U is the horizontal wind speed and k is von Karman's constant (Gash 1986, Lecleric and Thurtell 1990, Schuepp *et al.* 1990). The fraction f, also referred to in the literature as the cumulative footprint prediction, is shown (**Fig. 8.9**) on the z-axis as a function of local time on the x-axis (every 12 min between 09h48 to 17h12 local time for day 259, 1992), for various placement heights z (y-axis) for our grassland site. For these calculations we used the actual measured wind speeds averaged between 0.25 m and the measurement height, the friction velocity u_* calculated from our wind profile data, and a value of between 25 and 190 m for upwind distance x. A correction for stability was applied by replacing $(z-d)$ in Eq. 8.6 by $\Phi_m(z-d)$ where $\Phi_m = [1-16(z-d)/L]^{-0.25}$ is the dimensionless stability function for momentum transfer (Thom 1975) calculated using typical $(z-d)/L$ data depicted in Fig. 7.5. The fraction f exceeds 0.75 for $z > 1.00$ m for $x = 190$ m and $f > 0.94$ for $z = 0.50$ m. Of particular note, from the three dimensional plots (Fig. 8.8), is the large reduction in f with increase in placement height z from 0.25-m to 1.50 m. Also, the diurnal variation in f is more pronounced at 1.25 m than at the 0.25 m placement height. The fraction is shown in **Table 8.3** for two days (at midday) for

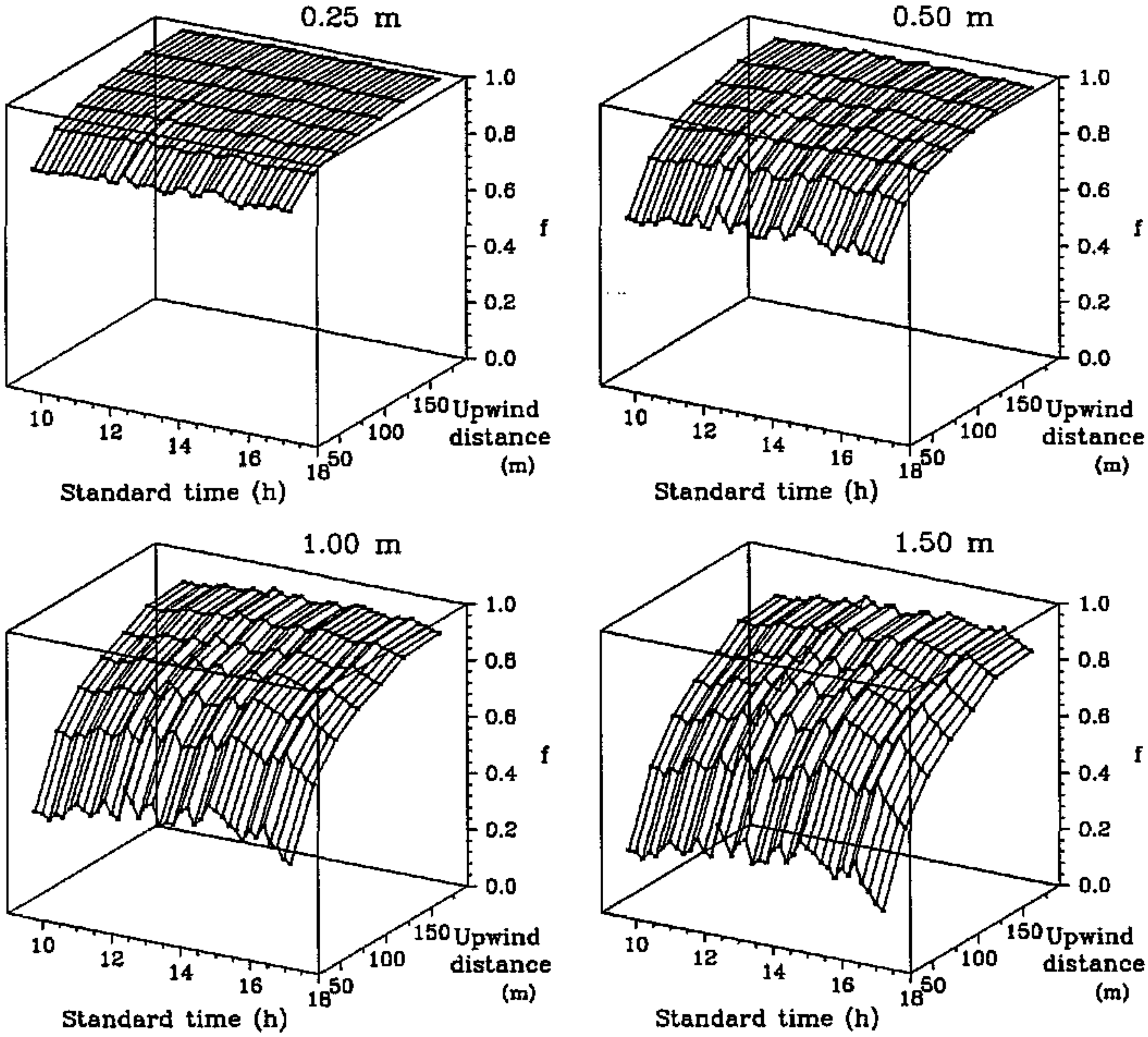

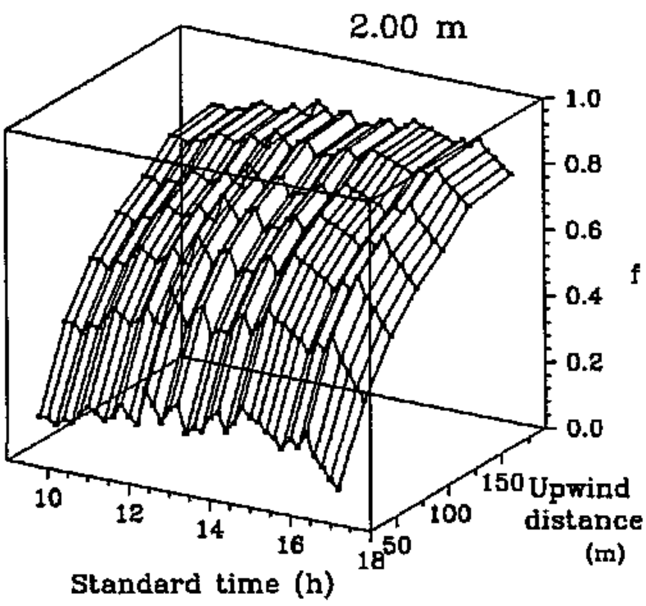

Fig. 8.9 Three dimensional representation of the diurnal variation for our grassland canopy in the cumulative footprint prediction, describing the fraction of sensible heat that can be expected to emanate from within the adjacent upwind area a horizontal distance x from the measurement point, for above-canopy placement heights between 0.25 and 2.00 m. The fraction f was corrected for stability

Table 8.3 Cumulative footprint prediction f (for a fetch of 190 m) as a function of placement height above the turfgrass surface, for two days at midday, with and without stability correction. Also shown is the position of the peak of the footprint x_{max} (m), horizontal wind speed U (m s^{-1}) and $z/\mathcal{L}$

Placement height	f	f (stability corrected)	x_{max}	x_{max} (stability corrected)	U	$z/\mathcal{L}$
Day 259, CST 12h00 ($u_* = 0.19$ m s^{-1})						
0.25	0.97	0.96	6.6	5.5	2.18	-0.07
0.50	0.91	0.93	16.0	10.2	2.59	-0.13
1.00	0.83	0.87	36.0	18.0	2.89	-0.26
1.25	0.74	0.83	58.4	24.9	3.12	-0.33
1.50	0.66	0.79	79.3	31.2	3.17	-0.40
Day 263, CST 12h00 ($u_* = 0.245$ m s^{-1})						
0.25	0.97	0.96	5.5	4.7	2.25	-0.06
0.50	0.92	0.93	13.9	8.6	2.78	-0.12
1.00	0.85	0.88	32.0	15.3	3.17	-0.24
1.25	0.77	0.84	51.0	21.1	3.36	-0.30
1.50	0.69	0.81	70.8	26.5	3.49	-0.36

various placement heights z, for the measured wind speed U at the different heights and a value of 190 m for x. The fraction exceeds 0.8 for $z > 1.0$ m but if corrections for stability are applied (Schuepp *et al.* 1990), the fraction is greater than 0.87. The position of the peak of the footprint, x_{max}, is calculated using:

$$x_{max} = U\,(z-d)/[\,2\,u_*\,k\,]. \tag{8.6}$$

This position describes the downwind distance to which the measurement is most sensitive (Schuepp *et al.* 1990). The x_{max} position is less than 36 m for $z \leq 1.0$ m but less than 18 m if stability corrections are applied. The stability corrections markedly reduce x_{max} for the $z = 1.25$ and 1.5 m placement heights. Since we found no statistical difference between F_h measurements between the 0.5 and 1.0 m placement heights, the advantages of the lower placement height of 0.5 m is the larger f fraction and a smaller x_{max} (Table 8.3).

The three-dimensional graphs (Fig. 8.9) may be used to determine the correct siting of an automatic weather station. Accepting a f-value of at least 0.70 and a sensor placement height at or below 2.00 m, the minimum fetch requirement is in excess 100 m for unstable conditions. A fetch of 125 m to 150 m would be more desirable, resulting in a f-value approaching 0.8 except in the early morning and late afternoon times when f may be less than 0.65.

It is possible to extrapolate our measurements to forest canopies. For this, a value for u_* for forests is required. We chose a value of 1 m s^{-1}, a value greater than that measured for our grassland site and greater than the typical value of 0.46 m s^{-1} used by Monteith and Unsworth (1990) for a tall crop. We used the logarithmic wind profile equation to estimate U where U is the average wind speed between height $z = d + z_o$ and z above the soil surface:

$$U = \int u\, dz / \int dz.$$

The horizontal wind speed u was obtained from the wind profile equation:

$$u = (u_* / k) \ln [(z - d)/z_o]$$

where $d \approx 2/3h$ and $z_o \approx 1/10\, h$ where h is the canopy height. We chose a canopy height of 20 m. To correct the calculation of f for stability, we recalculated the Monin-Obukhov length L for a friction velocity $u_* = 1$ m s^{-1} allowing for a diurnal variation in L based on the $z/$L values shown in Fig. 8.5 The results of these calculations are shown (**Fig. 8.10**). Compared with the three dimensional plots for the grassland surface (Fig. 8.8), the fraction f for a forest canopy had little diurnal variation. However, there was a rapid reduction in f with a decrease in the upwind distance x = 25 to 190 m for all placement heights z = 0.25 to 2.00 m. The significance of these results is that the fetch requirement for above-forest canopy micrometeorological measurements are necessarily more stringent than those for measurements above grassland canopies at all placement heights between 0.25 and 1.50 m. Also, for a given fetch distance, there may be little advantage in using a low placement height for a forest canopy (f varying between 0.69 and 0.80 for a fetch of 190 m compared to between 0.75 an 0.98 for a grassland canopy with the same fetch).

There is another problem that needs to be considered with above-forest canopy micrometeorological measurements. Due to the aerodynamically rough nature of forest canopies (compared to a grassland surface), profile measurements such as is used with the Bowen ratio technique, would require a much larger distance between the lower and upper placement heights for the water vapour and air temperature differentials to be measurably large. Typically, one would use 0.50 and 2.00 m or even 0.50 and 2.50 m placement heights. These placement heights would impose greater fetch limitations on the measurements (Fig. 8.10).

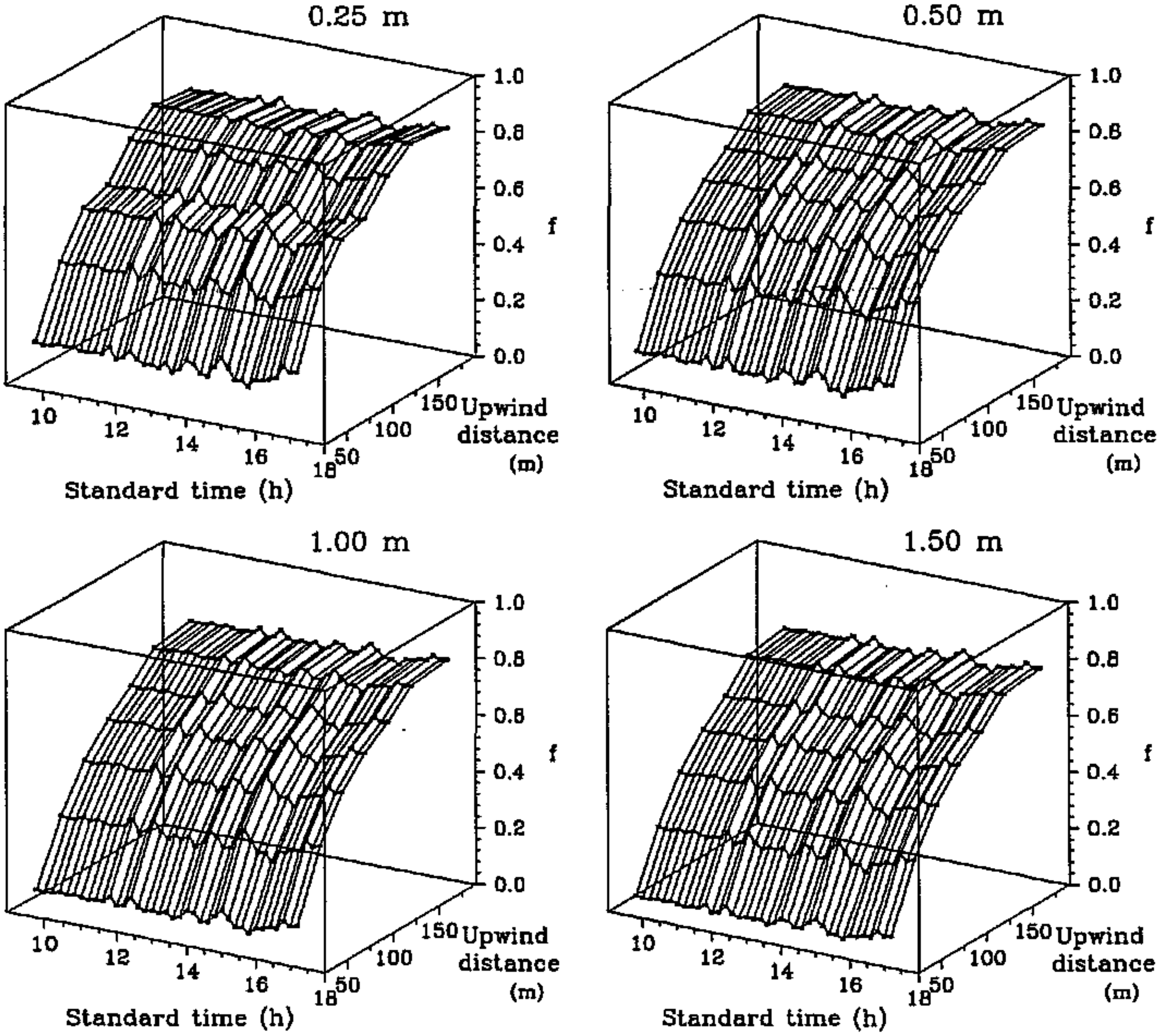

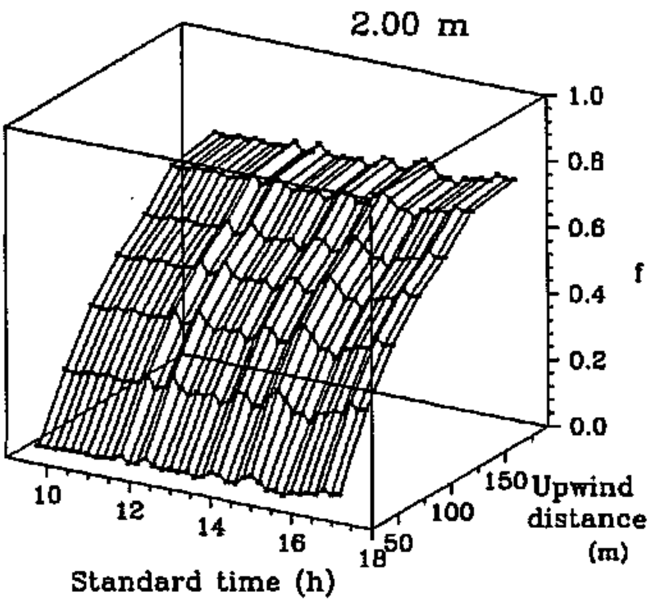

Fig. 8.10 Three dimensional representation of the diurnal variation for a forest canopy in the calculated footprint prediction for above-canopy placement heights 0.25 to 2.00 m. The fraction *f*, was corrected for stability

8.5 Conclusions

No significant differences between sensible heat (F_h) measurements with sensors placed at the 0.50, 1.00 and 1.25 m heights were found to occur. Below 0.50 m, there was a significant reduction in F_h. At heights greater than 1.50 m above canopy there was a significant increase in F_h compared to that measured at the 1.00-m height above canopy but measurements between 1.25 and 2.00 m were not significantly different. We speculate that placement of the sensors at heights less than 0.50 m caused a reduction in the covariance between the vertical wind speed fluctuation and the air temperature fluctuation presumably due to a larger fraction of eddies of small size occurring between the separation distance of the sonic anemometer transducers. The reduction was not due to acoustic reflections from the surface. Footprint calculations showed that at least 90 % of the measured F_h at the 0.5-m height was from our experimental site. Footprint calculations showed that the fetch requirement for micrometeorological measurements above forest canopies is more stringent than above grassland canopies. Placement height to fetch ratio calculations to determine sensor placement height is too simplistic an approach. Footprint calculations should be routinely performed.

8.6 Acknowledgements

Texas A & M University and the United States Council for the International Exchange of Scholars for a Fulbright grant is gratefully acknowledged. Use of two of the EC systems from Dr W.A. Dugas, Blackland Research Centre, Texas Agricultural Experiment Station, Temple, Texas is gratefully acknowledged. This chapter is based on two published papers. The comments from anonymous reviewers are gratefully acknowledged.

Chapter 9

Seasonal comparisons of total evaporation in a Drakensberg catchment

9.1 Abstract

Evaporative water loss is often the largest component of the hydrological cycle and yet is often calculated as the remainder term of the soil water mass balance. Quantifying the total evaporative loss is difficult but necessary for an informed, objective long term management plan of catchment areas, the most significant of which are within the Drakensberg mountain range. Determination of total evaporation from a catchment in Cathedral Peak, a fire climax grassland, was carried out over three years (March 1990 to March 1993) using the Bowen Ratio Energy Balance technique. Two identical Bowen ratio systems at the site showed good agreement between each other and the more absolute lysimetric technique ($p < 0.08$). The seasonal trend in latent heat density (evaporation) over the period is discussed. Equilibrium evaporation was a good estimate of summer evaporation amounts but the method was unreliable during the drier winter periods, overestimating the Bowen ratio evaporation. An automatic data exclusion procedure was used to replace evaporation values associated with the Bowen ratio approaching −1. Data values that were identified as requiring exclusion were replaced by equilibrium evaporation, usually at early morning and late afternoon times. The 20 min values were totalled for the day and then totalled to form monthly and annual totals. The 1992 annual total showed that during this particularly dry year, measured evaporation exceeded the annual rainfall. Daily total evaporation typically decreased from a summer maximum of 17 MJ m^{-2} (7 mm) to a winter season minimum close to zero. In 1992, the one Bowen ratio system was moved to a riparian location and the other remained upslope. For January 1992, the measured daily total evaporation at the riparian location was about 30 % greater than that upslope and greater than that upslope on two out of three days. Measured 20 min air temperature profile differences (δT) were smaller for the upslope location compared with the riparian location, the measured water vapour pressure profile differences greater, the soil heat flux density smaller and the radiant density smaller. Apart for the smaller soil heat flux, these differences all contributed to a greater daily total evaporation for the riparian location compared with that upslope. The daily total energy balance components, for each day of January 1992, for the riparian and upslope locations were statistically different at the 5 % level of significance. Net radiant density, latent heat and soil heat density were greater for the riparian location compared with that upslope but the sensible heat density was significantly smaller. The least significant difference was in the sensible heat component. Over the study period, peak summer evaporation rates appeared independent of rainfall or soil water content, but were related to the time between burn events. The winter season evaporation rate varied little between one year old, two years old and burnt canopies. The total evaporation for 39 months was 3330.7 mm, compared with a rainfall total of 3618.4 mm and a total net radiant density of 12470.82 MJ m^{-2}. The Bowen ratio energy balance method was shown to be suitable for long term monitoring of daily total evaporation and capable of detecting the effects of management fires.

9.2 Introduction

One of the most important factors affecting water supply from any catchment is the evaporative loss from the vegetative community, which in the Drakensberg is a fire-determined climax grassland.

The loss of water in the gaseous phase may be estimated by measuring, *inter alia*, the flux of water vapour, in various parts of the soil-plant-atmosphere system, by various means.

The flux density of an entity above and away from an exchanging surface is dependent on the gradient of that entity. With the Bowen Ratio Energy Balance micrometeorological method (BREB), the flux density of water vapour, (the latent heat flux density), from the surface is estimated with the sensible heat flux density. These two heat flux densities are obtained simultaneously by measuring both the water vapour pressure difference and the air temperature difference between the same two vertical heights above the canopy or soil, the net irradiance and the soil heat flux density.

The BREB method is one employed for the quantification of evaporation over various surfaces, from open water, to crop land to forest. Besides the measurement of how much water is lost from a surface, the Bowen ratio, by virtue of its formulation, provides additional valuable information about the distribution or partitioning of available energy at the surface (Suomi and Tanner 1958; Tanner 1960).

Energy available at the earth's surface is consumed mainly as sensible heat F_h (the temperature change with no phase change of water) or latent heat $L_v F_w$ (the phase change of water with no temperature change). Bowen (1926) realised the relative significance of these terms, and considered the ratio $F_h/L_v F_w$, now more commonly known as the Bowen ratio (β). The Bowen ratio has traditionally been employed as a research tool over flat and only moderately hilly, extensive crop surfaces to determine crop responses to various treatments, most commonly different weather conditions causing different atmospheric demands and water stresses (Garratt 1984). The Bowen ratio is also commonly tested and used over uniform agricultural crops but less often over natural grasslands such as in this work (Tanner 1960; Webb 1960; Fritschen 1965; Tanner and Fuchs 1969; Lourens and Pruitt 1971; Perrier *et al.* 1972; Verma *et al.* 1978; Tanner 1988). Henrici (1943) appears to have been the only worker to have attempted evaporation measurements in these catchments, and these were entirely plant based.

In the BREB method there are, apart from measurement of the soil heat flux density and the net irradiance above the surface (but detecting reflected solar irradiance and long wave irradiance from the surface), no surface-based measurements of any kind. The problems associated with measuring or obtaining resistances, surface temperature, and saturation water vapour pressure as a function of surface temperature are therefore avoided.

The use of the BREB method on a 22° slope has been verified by Nie *et al.* (1992), and comparisons made against an adjacent weighing lysimeter at the site verified the accuracy of the method (Chapter 5).

The aim of this research is to use the Bowen ratio energy balance technique to collect accurate and reliable evaporation measurements on a long term basis to enable seasonal and site comparisons of total evaporation, and an evaluation of the management practice of catchment burning.

9.3 Materials and methods

The research location was Catchment VI of the Cathedral Peak Forestry Research Station, in the foothills of the Drakensberg, Natal, South Africa at 29.00°S, 29.25°E, at an altitude 1935 m and with a predominantly north-facing aspect and average slope of 0.27 (about 15°). It is 0.677 km^2 (68 ha) in area and varies in altitude from 1847 to 2076 m (Schulze 1975). Two locations were used in the catchment - an upslope site at which two Bowen ratio systems were employed for simultaneous measurement comparisons and a location within a riparian zone. All measurements were performed in Catchment VI.

Initially two independent (separate) Bowen ratio systems were placed at the same site to later compare the measurements at different sites. For the period March 1990 to October 1991, the results presented are therefore those from the equipment that remained permanently in the open grassland (upslope) site following which the one system (UNP) was moved to the riparian zone.

The sensors at the ends of the supporting arms were placed 1 m apart. To measure the dewpoint T_{dp} (°C) of air drawn in from 0.8 m and 1.8 m above ground, a single cooled dewpoint hygrometer was employed with a switching device to alternate the air flow. The air temperature at 0.8 m and the air temperature difference between 0.8 and 1.8 m was measured using two unshielded type E thermocouples each with a parallel combination of 76 μm diameter thermocouples. An independent net radiometer and set of two soil heat flux plates and four soil temperature thermocouples were used to calculate the remainder of the components in the energy balance. All sensors were connected to a Campbell Scientific Inc. (Logan, Utah) 21X datalogger. At the upslope site, data from an adjacent weighing lysimeter data enabled the surface latent heat flux density to be measured directly for absolute verification of the calculated fluxes.

9.4 Results and discussion

9.4.1 Diurnal trends of the measured and calculated variables

Diurnal trends of the fluxes of latent and sensible heat for several typical summer days are presented (**Fig. 9.1**). The periods for which data were rejected are shown at the top by the vertical bars - periods for which the measured air temperature difference δT between the measurement heights was outside the range defined by the left and right limits (Chapter 3, Eq. 3.32). The corresponding net irradiance and Bowen ratio values are presented in **Fig. 9.2**, and the diurnal trends in the air temperature and WVP profile differences for the same days in **Fig. 9.3**.

On cloudless days, the large constant radiation load results in high and constant evaporative fluxes compared with cloudy days. Both the air temperature and WVP differences are larger and more constant on these high evaporative flux days: the former difference due to convective cooling of the warm surface, and the latter due to the greater energy available to evaporate water. On days with high evaporative demand, the Bowen ratio is small and stable with time (Fig. 9.2, right-hand axis). The small Bowen ratio values result from larger δe values, while δT remains small, as opposed to days with variable cloud cover, and/or rain, when the differences vary greatly within and between measuring periods.

9.4.2 Verification against an independent measuring system

To verify the evaporative losses measured with the BREB systems, comparison against a more absolute method was necessary. The 20 min evaporative water losses measured from the adjacent weighing lysimeter used for this purpose (**Fig. 9.4**), tracked very well with the Bowen ratio evaporation values. Data during the early morning has been manually rejected, and it is evident there are several midmorning data points leading up to the first value plotted each day missing. Subsequently, all rejections were automated using the LE_CALC software programme by Metelerkamp and Savage (unpublished). The net irradiance and Bowen ratio levels for these days are presented in **Fig. 9.5**.

The same four days were used for the comparison of 20 min BREB *vs* lysimeter evaporation (**Fig. 9.6**), the linear regression statistics for which are presented in **Table 9.1**.

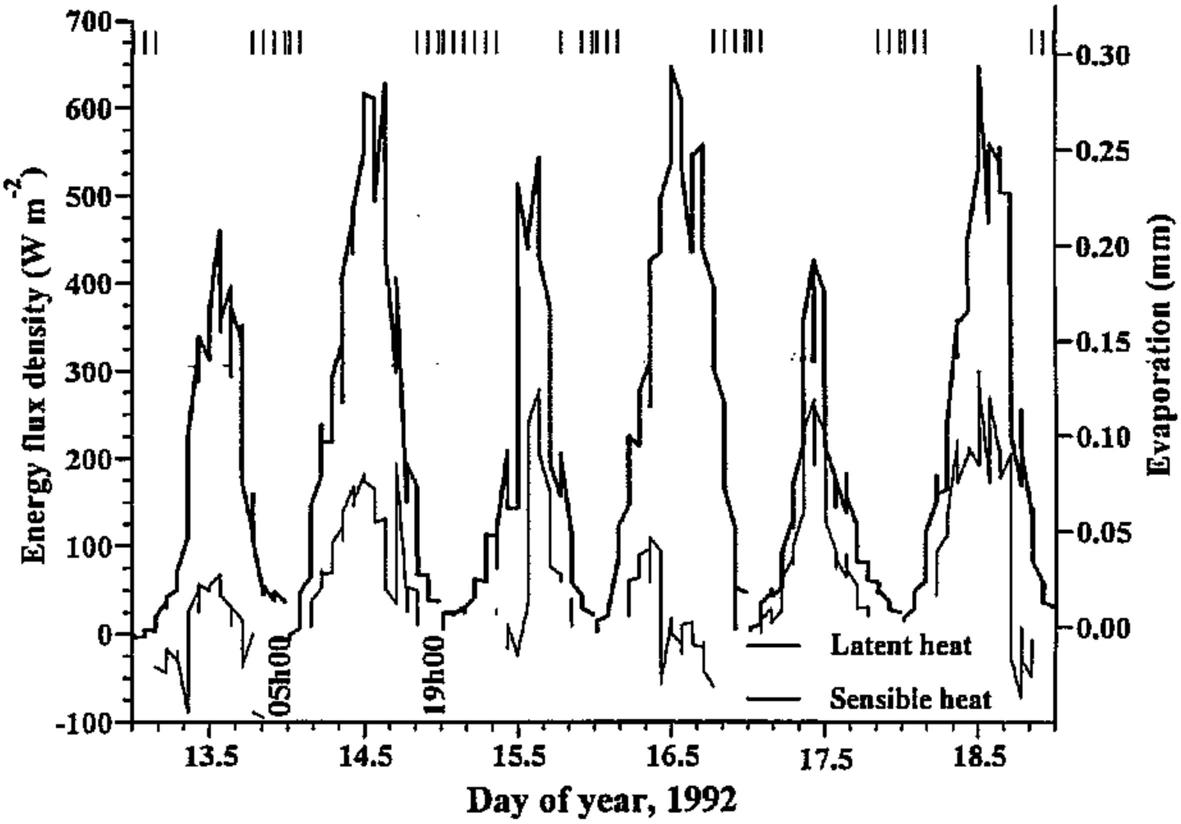

Fig. 9.1 Typical diurnal trends of latent heat flux density and sensible heat flux density for Catchment VI at Cathedral Peak, for the UNP Bowen ratio system located within the riparian zone

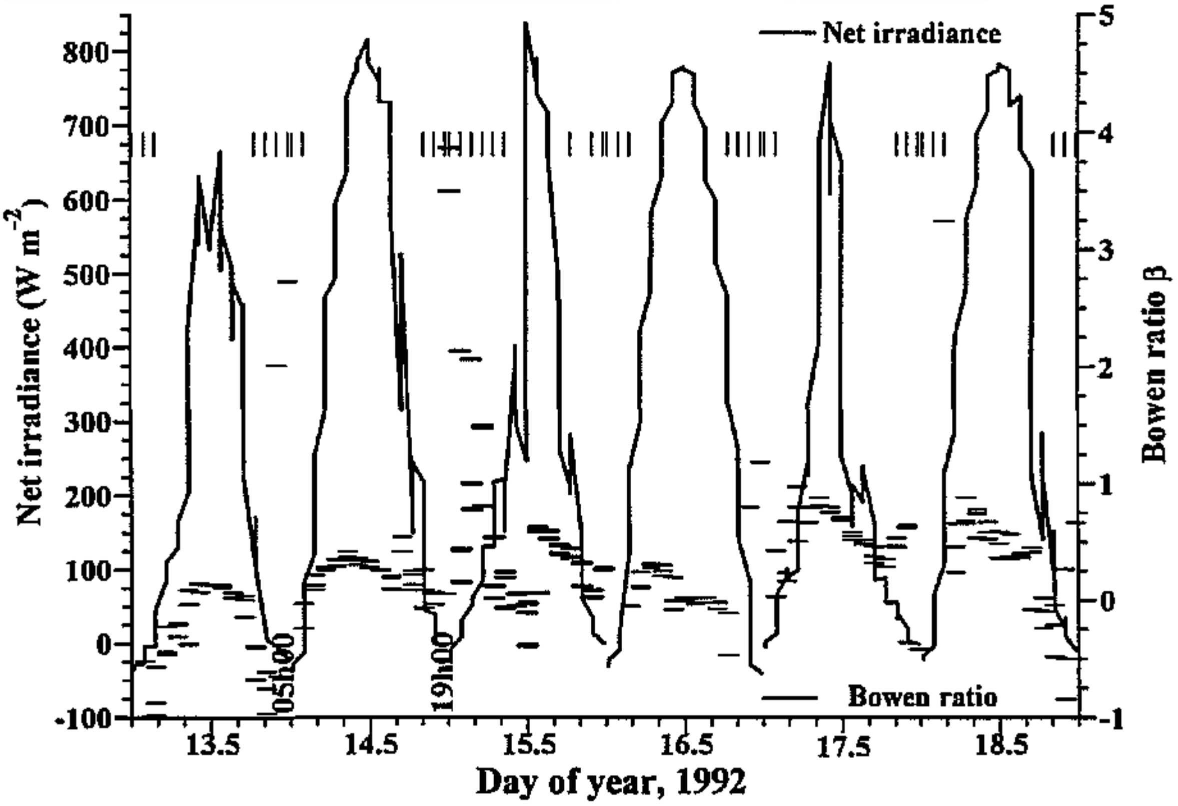

Fig. 9.2 Typical diurnal trends in net irradiance with the Bowen ratio β indicated by a short horizontal bar. The periods for which data were rejected are shown by the vertical bars

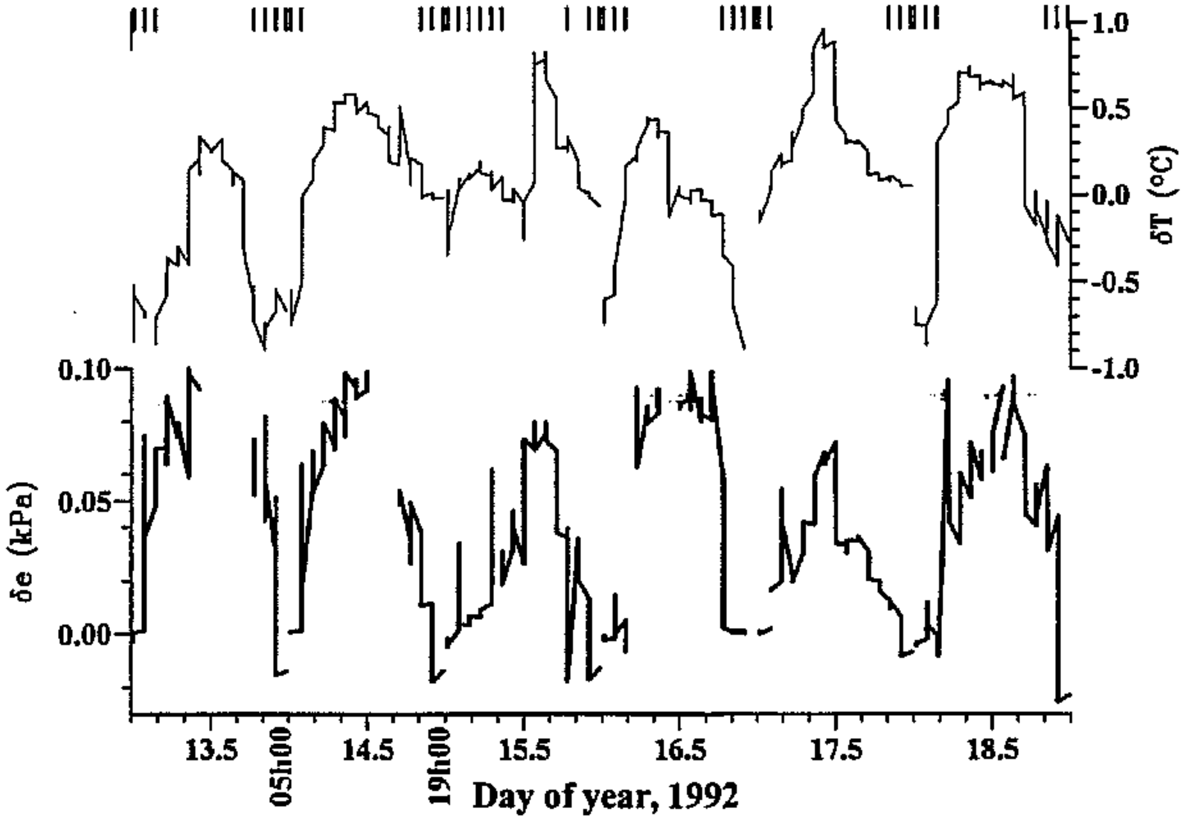

Fig. 9.3 Typical trends in profile differences in air temperature (δT) and water vapour pressure (δe) between the two Bowen ratio measurement heights

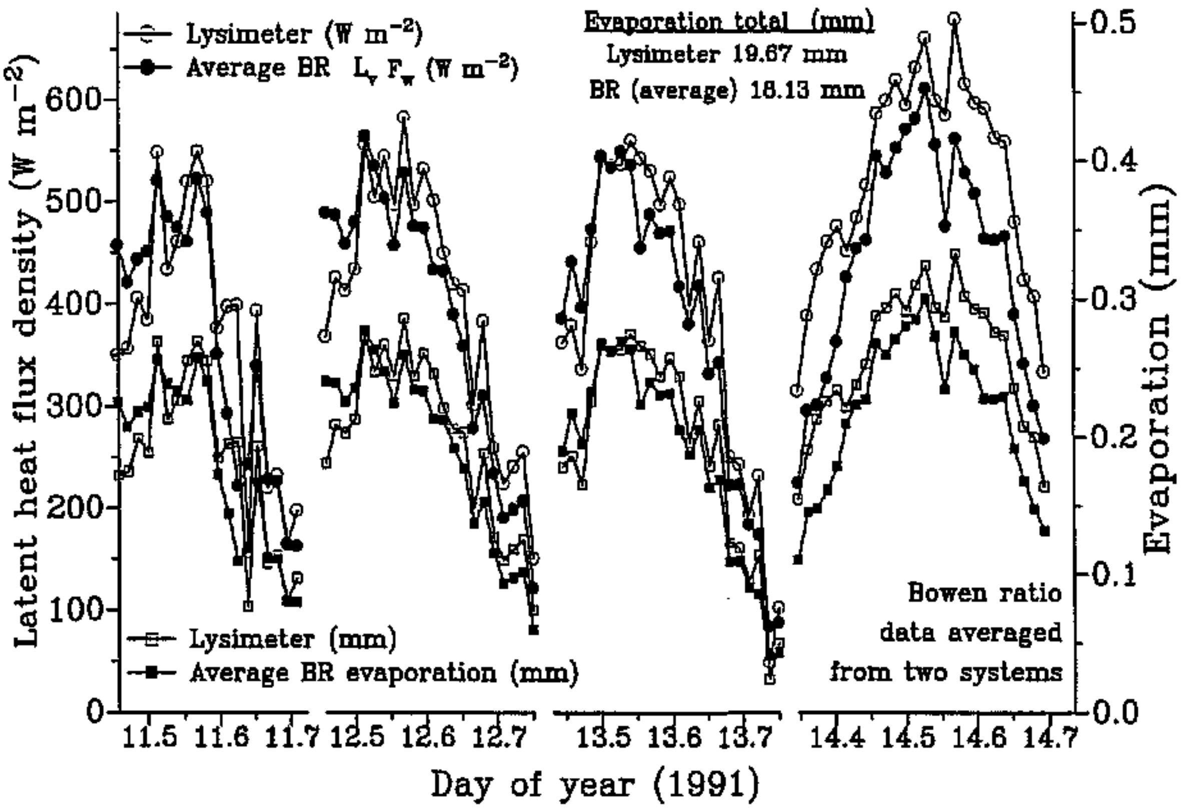

Fig. 9.4 Comparison of 20 min lysimeter and Bowen ratio evaporation for the upslope site. The BREB evaporation from the two systems was averaged. There was very good agreement between lysimeter and Bowen ratio (average) evaporation total for this four day period

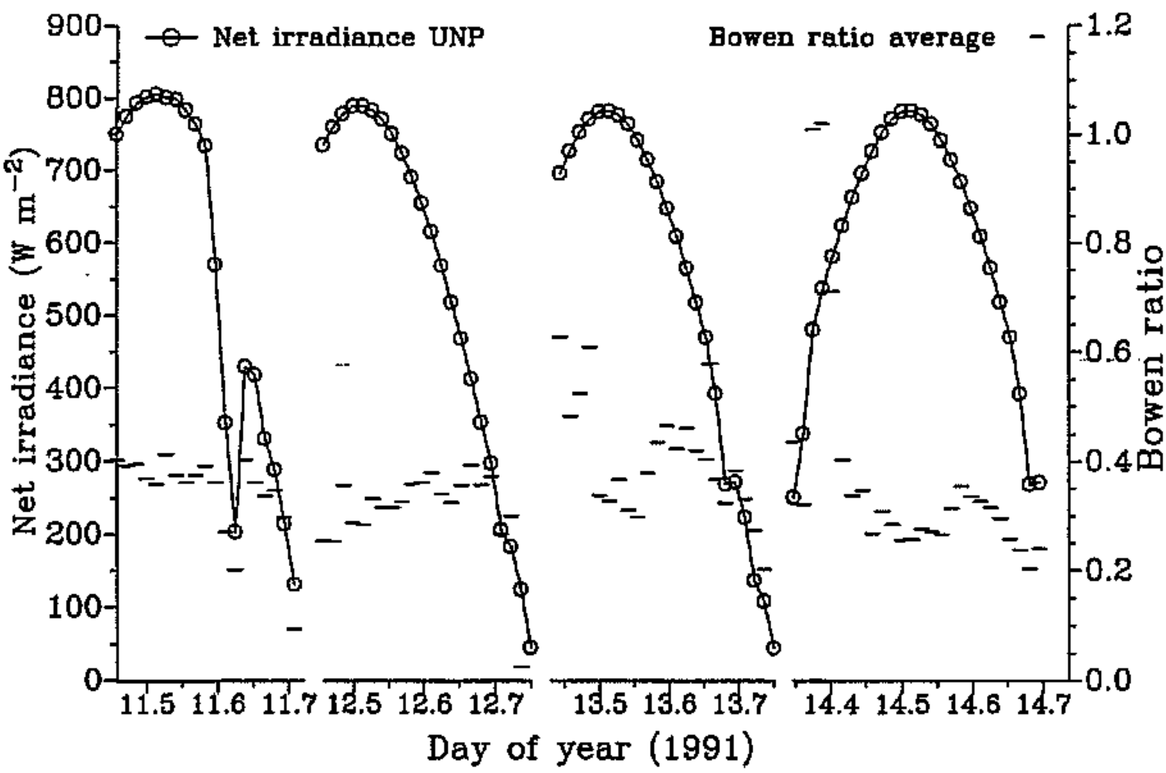

Fig. 9.5 Diurnal trends of net irradiance and the Bowen ratio (averaged for the two systems) for the days in Fig. 9.4

Since the overall time scale of much hydrological research is based on daily totals, further comparisons between BREB- and lysimeter-determined evaporation were based on daily totals (**Table 9.2**). Since lysimetric evaporation is often regarded as the standard for evaporation measurements, the good agreement between the two verifies the accuracy and integrity of the BREB method.

9.4.3 Inter-comparison between the UNP and CSIR Bowen Ratio systems

The data from two adjacent Bowen ratio systems were compared continuously for the years 1990 and 1991 until the UNP Bowen ratio system was moved to a riparian zone in the same catchment on the 2nd October 1991.

Several days from January 1991 were chosen to show typical conditions — high radiation load in the morning, with commensurately high evaporative flux conditions, and periods of cloud in the afternoon when less than optimum conditions exist for measurements with the BREB method.

The upper and lower air temperatures for the two Bowen ratio systems, and therefore δT, tracked well (see **Fig. 9.7**). The upper and lower WVP and δe occasionally deviated due to the hygrometer mirror becoming dirty and/or inadequate damping of the bias. One-off problems also occurred. For example, at one stage a leak in the air intake pipe was found and rectified. Once all of these problems had been solved, inter-comparisons between the two systems improved (see **Fig. 9.8**). Since the Bowen ratio is the product of the psychrometric constant γ and the ratio of the above profile differences, the agreement between two Bowen ratios measured was directly affected by the correlations of the two differences.

A weekly check between the two systems was made on the comparison of many variables

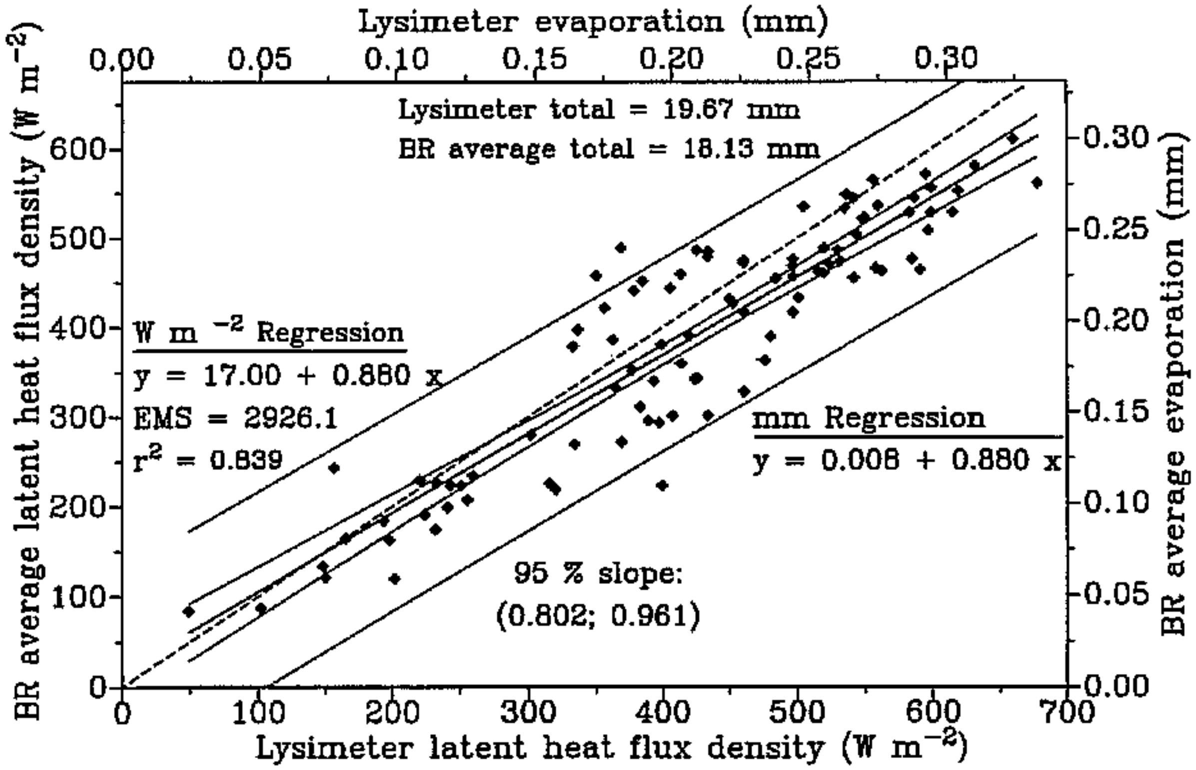

Fig. 9.6 Comparison of 20 minute evaporation data averaged from two Bowen ratio systems and from the lysimeter for Day 11 to 14, 1991. The dotted line is the 1:1 line. The confidence limits for the population mean and the confidence limits of a single predicted value and the regression line are also shown. Each point is a 20 min value (W m $^{-2}$) or a total (mm)

Table 9.1 Linear regression statistics of comparisons between 20 minute Bowen ratio evaporation estimates against the independent lysimeter evaporation estimates for Day 11 to 14, 1991 (Fig. 9.6) for the upslope site

Regression statistic	mm totals	W m $^{-2}$ totals
Slope	0.880	0.880
SE_{slope}	0.04	0.04
Slope + $t\,SE_{slope}$	0.961	0.961
Slope − $t\,SE_{slope}$	0.802	0.802
Intercept	0.008 mm	17.00 W m $^{-2}$
r	0.916	0.916

Table 9.2 Comparison of daily BREB (averaged from the two systems) and lysimeter evaporation totals

Day (1991)	Daily total evaporation				% difference
	(MJ m $^{-2}$)		(mm day $^{-1}$)		
	Lysimeter	BREB	Lysimeter	BREB	
11	8.72	8.49	3.57	3.48	-2.52
12	10.74	10.33	4.40	4.23	-3.86
13	11.22	10.78	4.59	4.42	-3.70

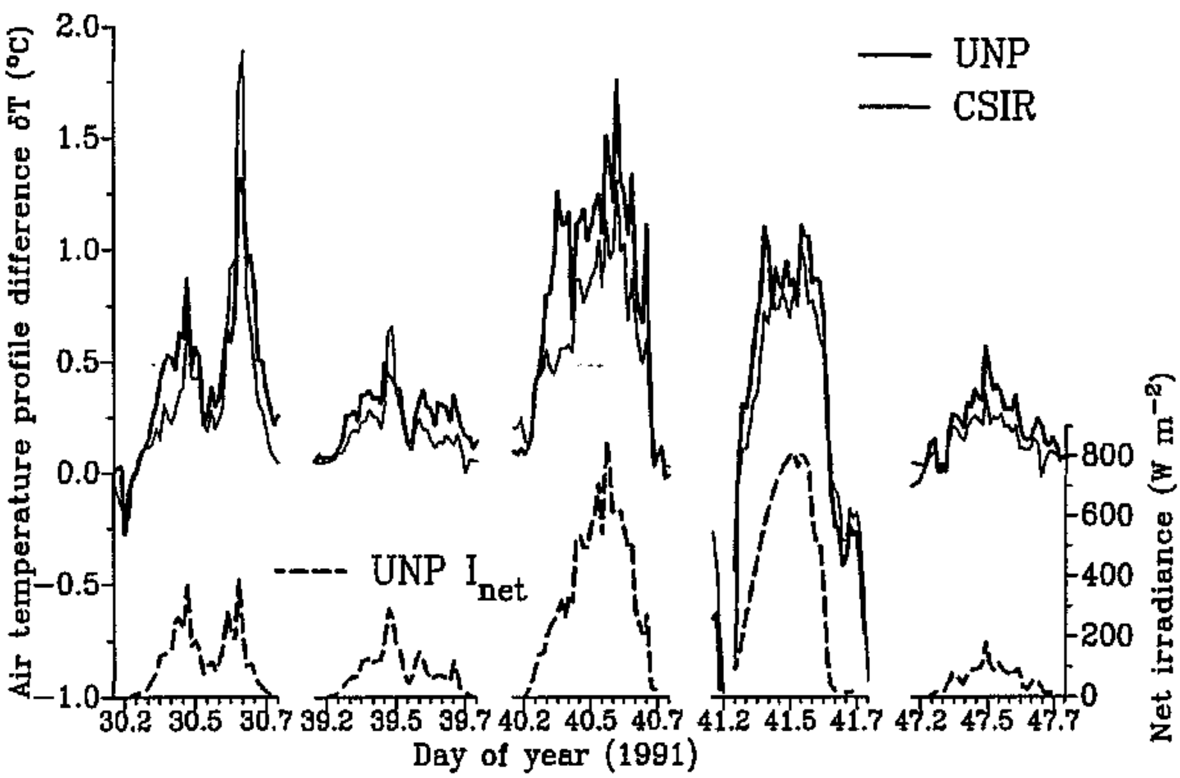

Fig. 9.7 Typical diurnal trends showing the good agreement of air temperature difference δT between the two measurement heights of the two systems (05h00 to 19h00; January 1991 accepted data). Both systems were on an upslope in Catchment VI. Each minor tick mark on the x axis corresponds to 1 h

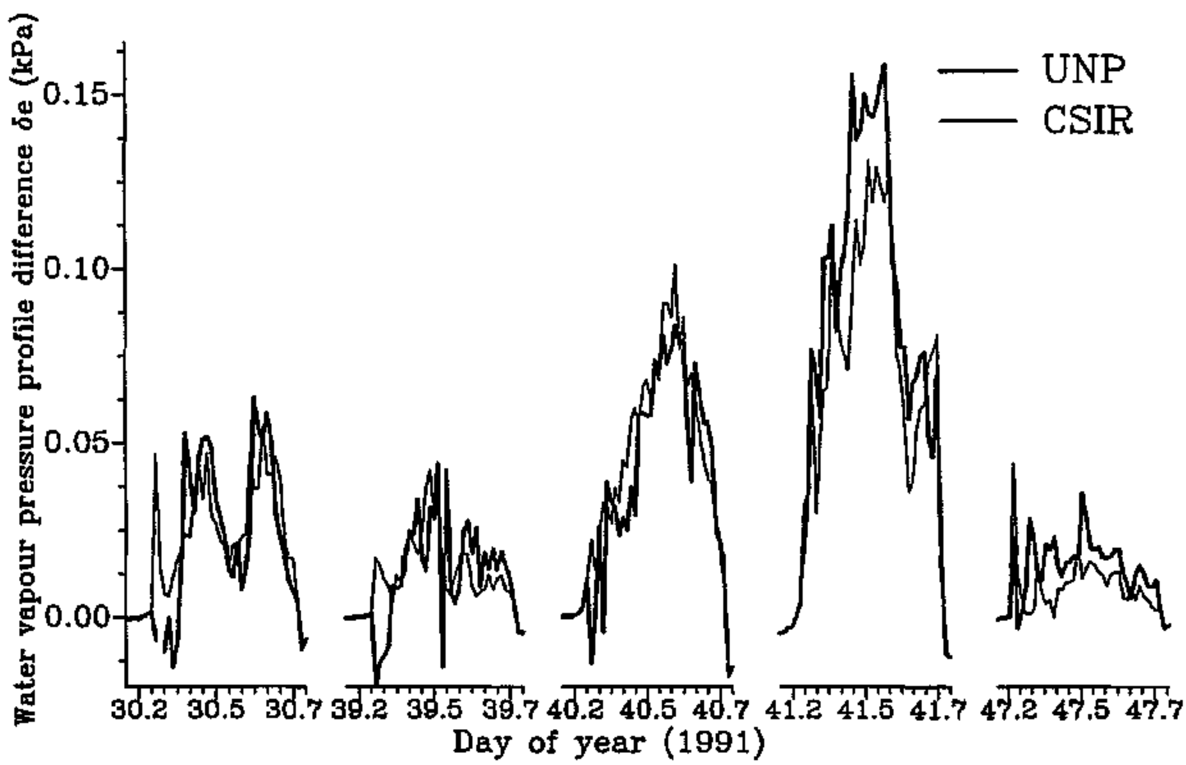

Fig. 9.8 Typical diurnal trends showing the WVP difference δe between the two measurement heights for both Bowen ratio systems (05h00 to 19h00; January 1991 accepted data). Both systems were on an upslope in Catchment VI

measured, especially the WVP and air temperatures and the respective differences. By its nature, WVP is extremely difficult to measure continuously and accurately. Thus almost weekly maintenance was required to keep the two systems measuring similar δe's and δT's when the systems were at the same site. Eventually, from experience, the ability to accurately and consistently measure the differences was achieved. The Bowen ratio systems could then be moved apart and used individually with confidence. The results from the two individual systems at two different sites could be then compared.

The CSIR net radiometer always gave a slightly higher net irradiance than did the UNP sensor. This was due ostensibly to a small constant calibration error in one or both of the instruments (**Fig. 9.9**, **Table 9.3**), if both net radiometers were exposed similarly. Using a paired t comparison, the daily total radiant density CSIR values for 1990 and 1991 were 5 % greater than the corresponding UNP daily totals. The agreement between the overall soil heat flux density (**Fig. 9.10**) of the two systems is adequate.

The calculated 20 min latent and sensible heat flux densities tracked adequately during the day (see **Figs 9.11** and **9.12**). During comparison, better (and worse) agreements than that presented were obtained. Daily total comparisons showed much better agreement.

Having the two Bowen ratio systems next to each other allowed the development of any problems to be detected, while experience was being gained in the data collecting procedure. Early in the project, for example, poor WVP comparisons led to the routine maintenance procedures of hygrometer mirror cleaning and bias setting, which was subsequently carried out weekly.

9.4.4 Inter-comparison between sites

After the UNP Bowen ratio system was moved to the riparian zone of catchment VI, the normal

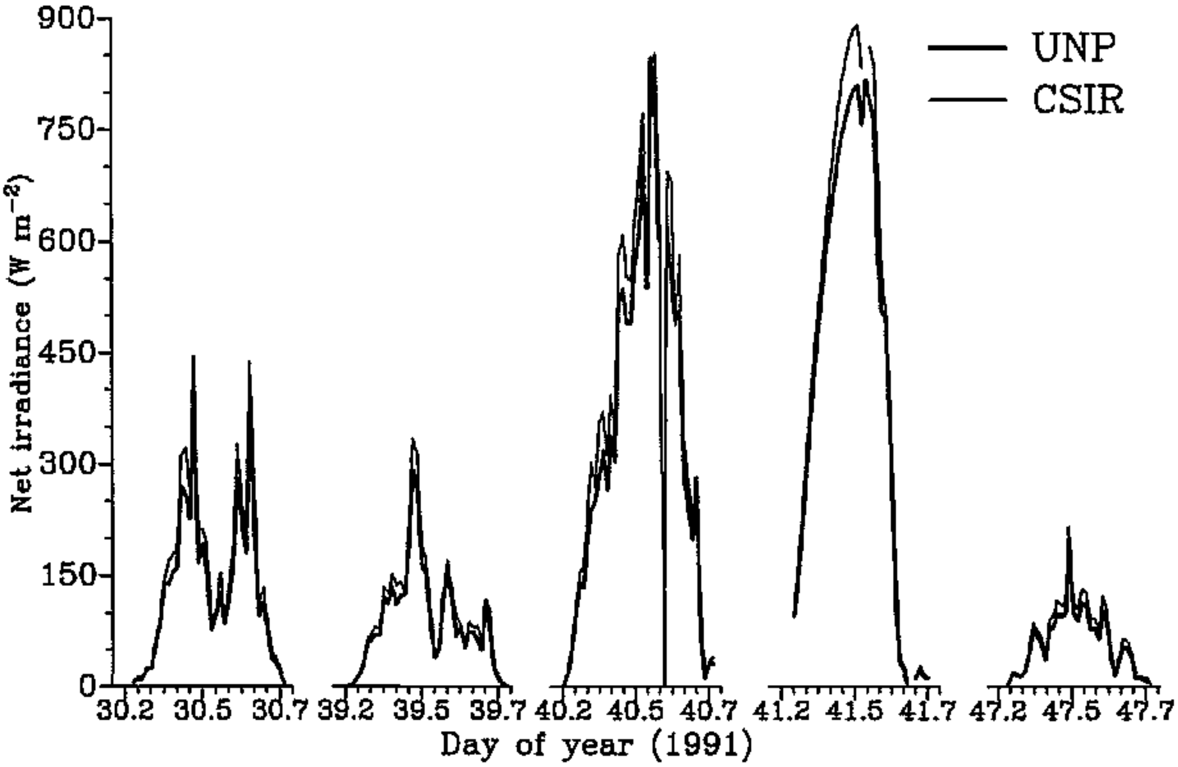

Fig. 9.9 Typical diurnal trends in net irradiance I_{net} for the two systems (05h00 to 19h00; January 1991 accepted data). Both systems were on an upslope in Catchment VI

Table 9.3 Paired two-sample *t*-test for means for daily total values of net radiant density for the two Bowen ratio systems for 1990 (Day 74 to 275, 289 to 333) and 1991 (Day 2 to 87, 114 to 141, 163 to 265). The radiometers were both at the upslope location for the entire period. The comparative difference were all significant at the 1 % level of significance with the UNP net radiant density 5 % lower than that measured using the CSIR net radiometer at the same site

	Paired statistics	UNP I_{net}	CSIR I_{net}
Mean (MJ m^{-2})		9.532	9.992
Variance (MJ)^2 m^{-4}		16.327	21.716
Observations		398	398
Percentage difference between the two means	-4.60		
Pearson correlation	0.9382		
Pooled variance (MJ)^2 m^{-4}	19.022		
Hypothesized mean difference	0		
Degrees of freedom	397		
t	-5.575		
100×$p(t \le t_{0.05})$ one-tail	0.00		
t (5 %) Critical one-tail	1.6487		

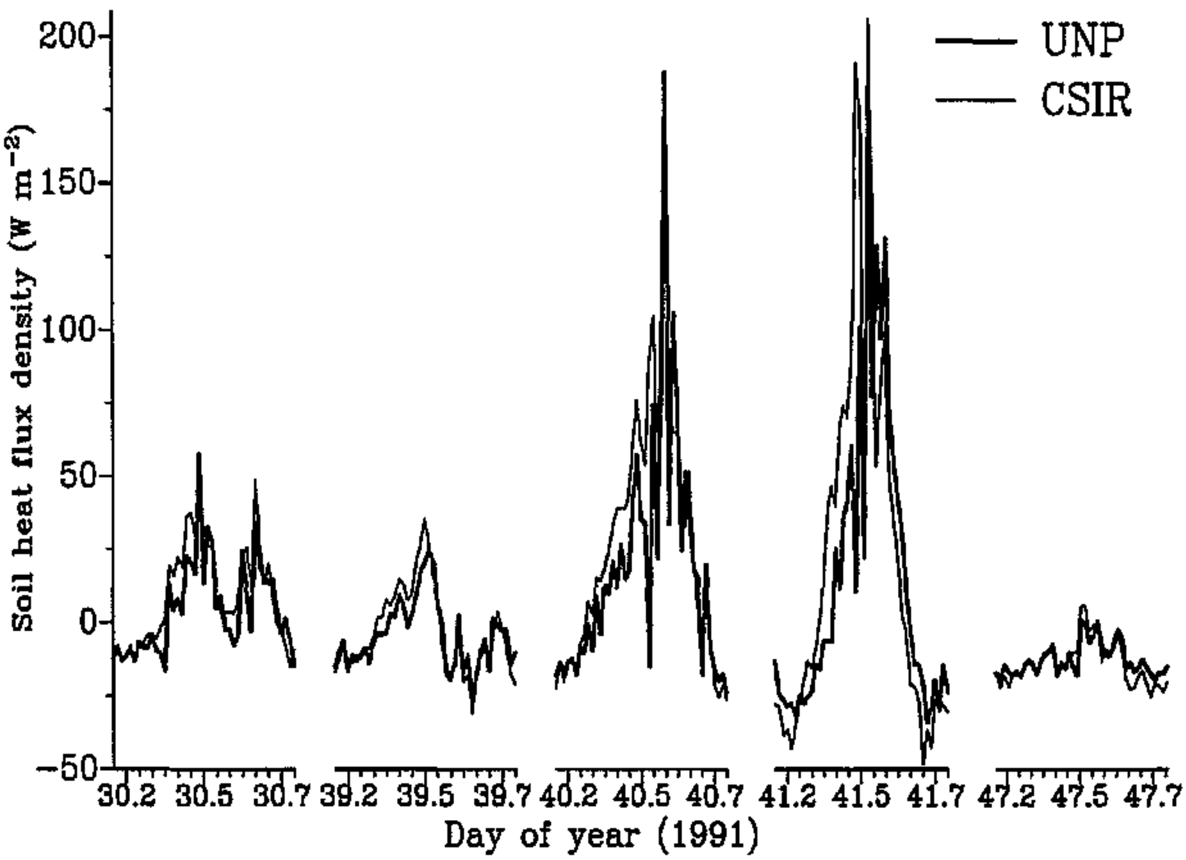

Fig. 9.10 Typical diurnal trends in overall soil heat flux F_s for the two systems (05h00 to 19h00; January 1991 accepted data). Both systems were located on an upslope in Catchment VI

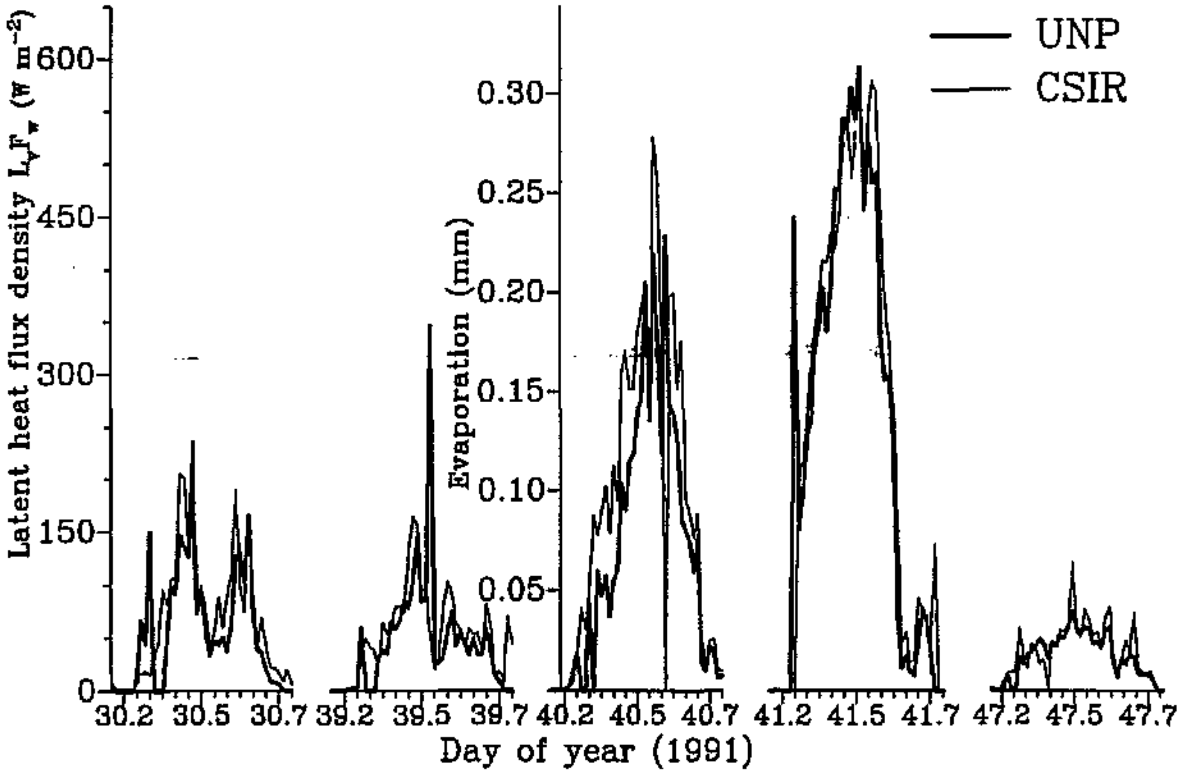

Fig. 9.11 Typical diurnal trends in calculated latent heat flux density $L_v F_w$ for both Bowen ratio systems (05h00 to 19h00; January 1991 accepted data). Both systems were located on an upslope in Catchment VI

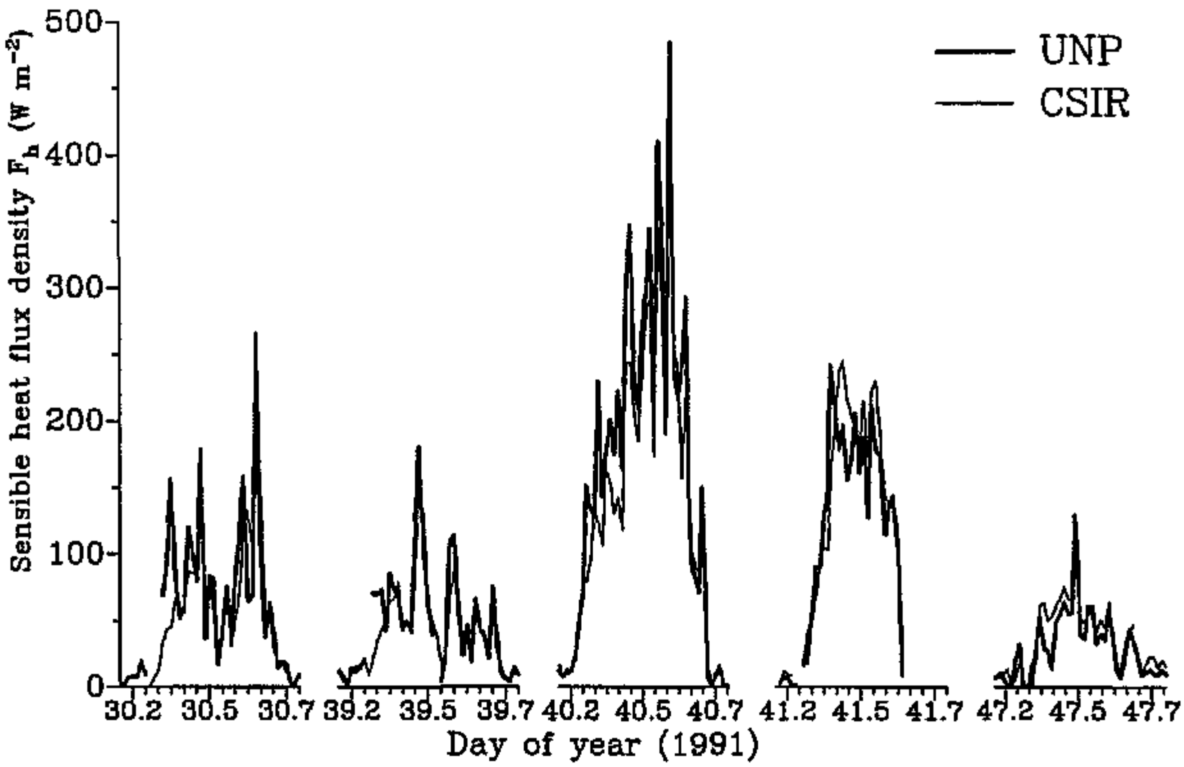

Fig. 9.12 Typical diurnal trends in calculated sensible heat flux density F_h for both Bowen ratio systems (05h00 to 19h00; January 1991 accepted data). Both systems were located on an upslope in Catchment VI

procedures were continued. Comparison of simultaneously measured 20 min flux and daily total densities from January 1992 for the two sites allowed for a measurement comparison of evaporation from the two sites. It should however be noted that the air flowing across the riparian zone flowed upslope - during the daytime at the upslope location, the winds were from the north and from the riparian zone.

The WVP and air temperature profile difference were compared (Figs 9.13, 9.14 and 9.15), as was the net irradiance and the Bowen ratio (Figs 9.16 and 9.17). The Bowen ratios showed some scatter between the sites (Fig. 9.17), with the net irradiance measurements agreeing for the periods shown in Fig. 9.16. This result was surprising considering the different vegetation types at the two sites. The net irradiance differences did however increase from about the middle of January 1992.

The soil heat flux component, was markedly different between the two sites with poor comparisons (Figs 9.18 and 9.19). For this time, the soil heat flux density was generally greater for the riparian than for the north facing upslope site (Fig. 9.19). Most of the soil heat term is contributed by the stored heat component. The comparison between the plate components of the two systems when plotted against one another (data not shown) exhibited an interesting cyclical nature. The CSIR plates (upslope) yielded lower values than the UNP plates (riparian location) in the morning with greater values after midday. This was clear when the data was being displayed in a graph on the computer's monitor. This shows a distinct lag between the sensors, perhaps due to the different radiation loads on the different slopes. Another possible reason could be that the riparian zone soils are wetter, resulting in a lagged

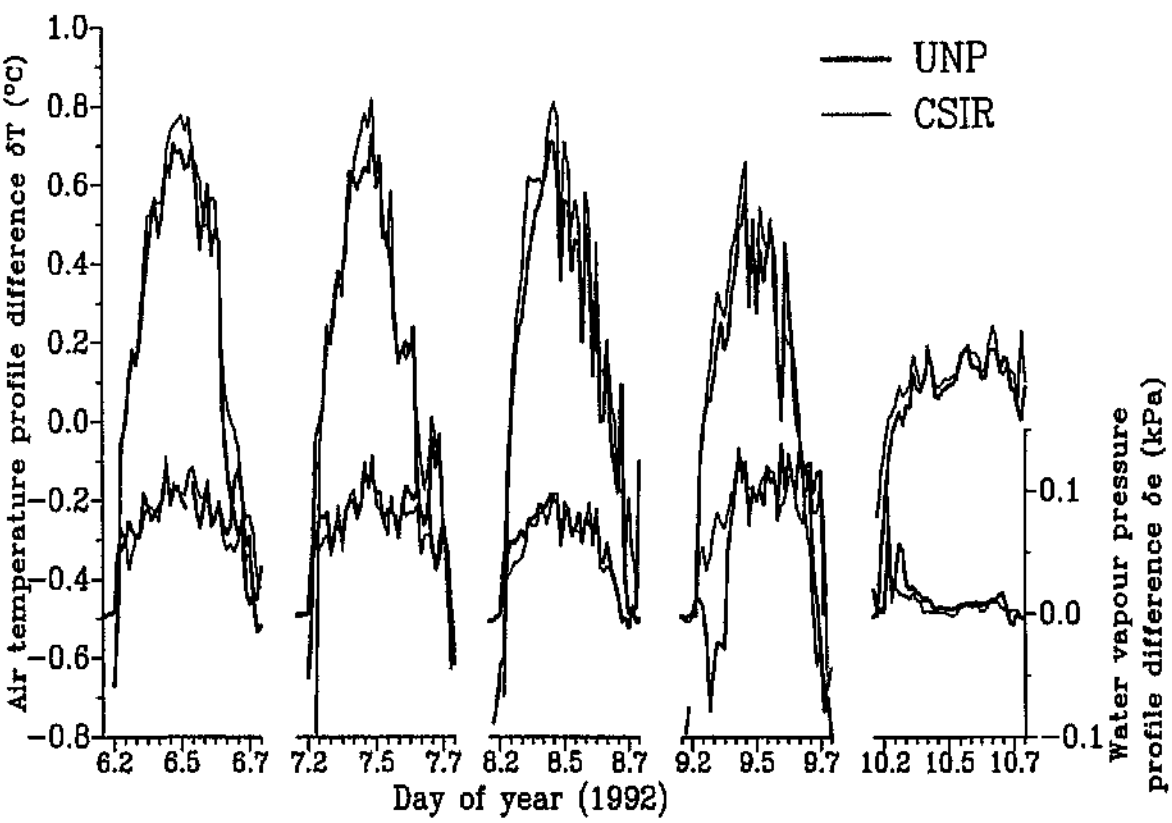

Fig. 9.13 Typical diurnal trends showing the good agreement of air temperature δT (top pair of curves) and the WVP differences δe (bottom pair of curves) for the two Bowen ratio systems (05h00 to 19h00; January 1992 accepted data). The UNP system was located in a riparian zone and the CSIR system upslope in Catchment VI

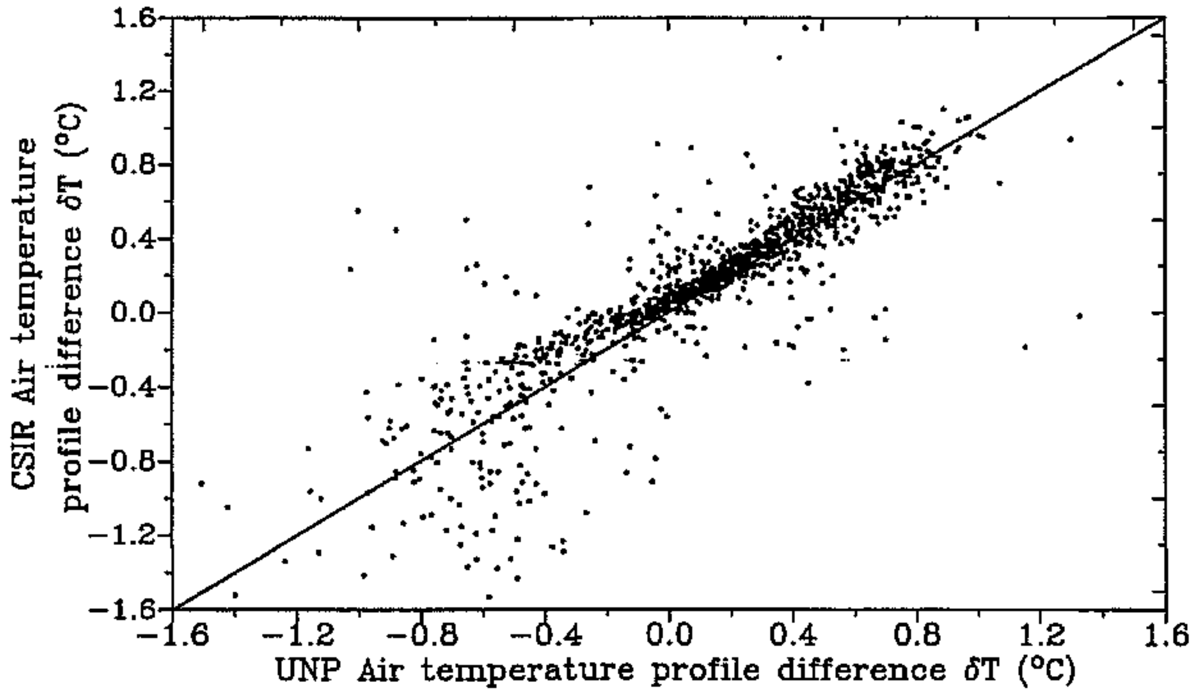

Fig. 9.14 Comparison between air temperature difference δT measured with the UNP system (abscissa) and the CSIR system (ordinate) showing agreement for most times at the two sites (05h00 to 19h00; January 1992 accepted data). The solid line is shown for convenience. Each point is for a 20 min period. The UNP system was in a riparian zone and the CSIR system upslope, both in Catchment VI

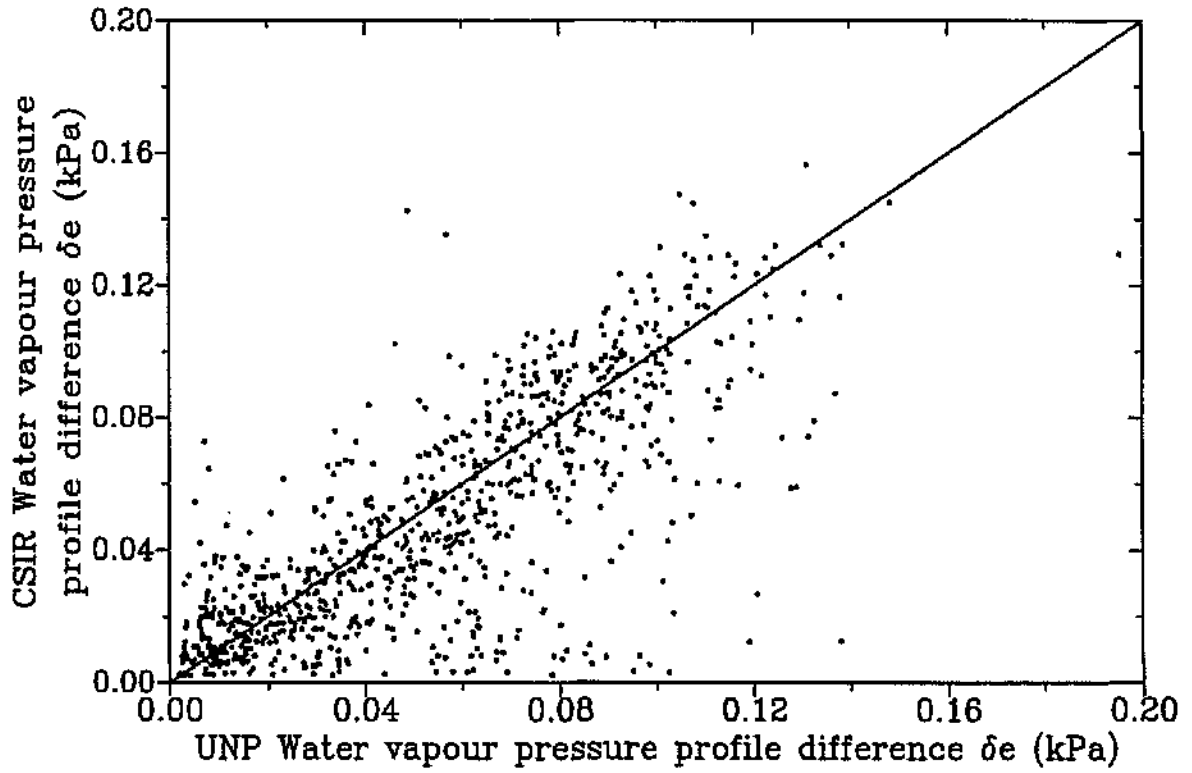

Fig. 9.15 Comparison between WVP difference δe measured with the UNP system (abscissa) and the CSIR (ordinate) for the two sites (January 1992 accepted data). The UNP system was located in a riparian zone and the CSIR system upslope, both in Catchment VI

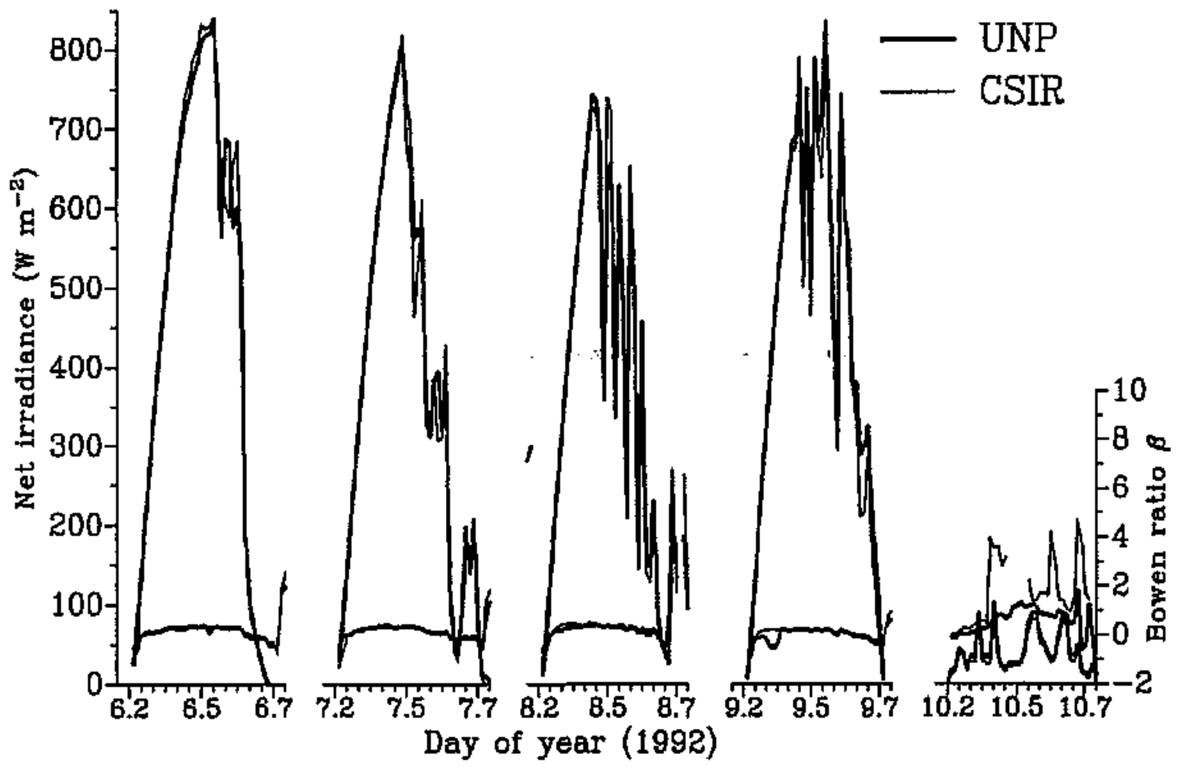

Fig. 9.16 Typical diurnal trends in net irradiance I_{net} (upper pair of curves) and the Bowen ratio β (lower pair of curves) at the two sites (05h00 to 19h00; January 1992 accepted data). The UNP system was in a riparian zone and the CSIR system upslope, both in Catchment VI

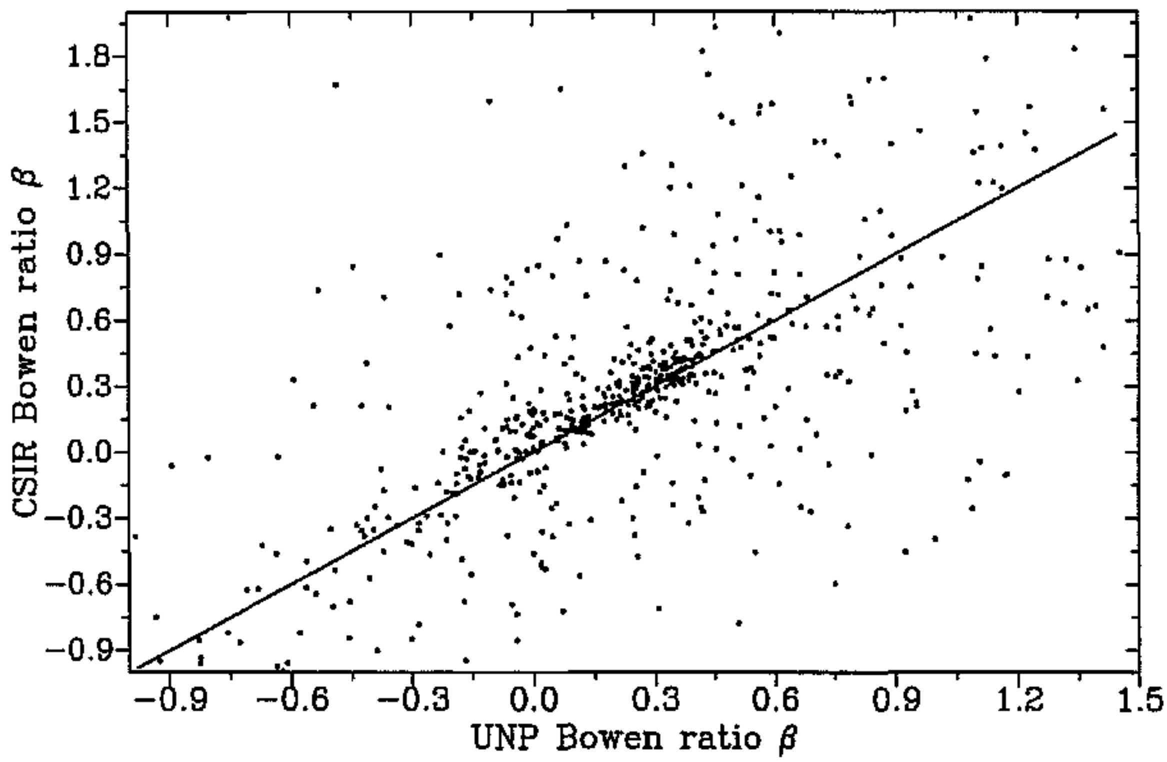

Fig. 9.17 Comparison between Bowen ratio β measured with the UNP system (abscissa) and the CSIR system (ordinate) at the two sites (all of January 1992 accepted data). The UNP system was in a riparian zone and the CSIR system upslope, both in Catchment VI

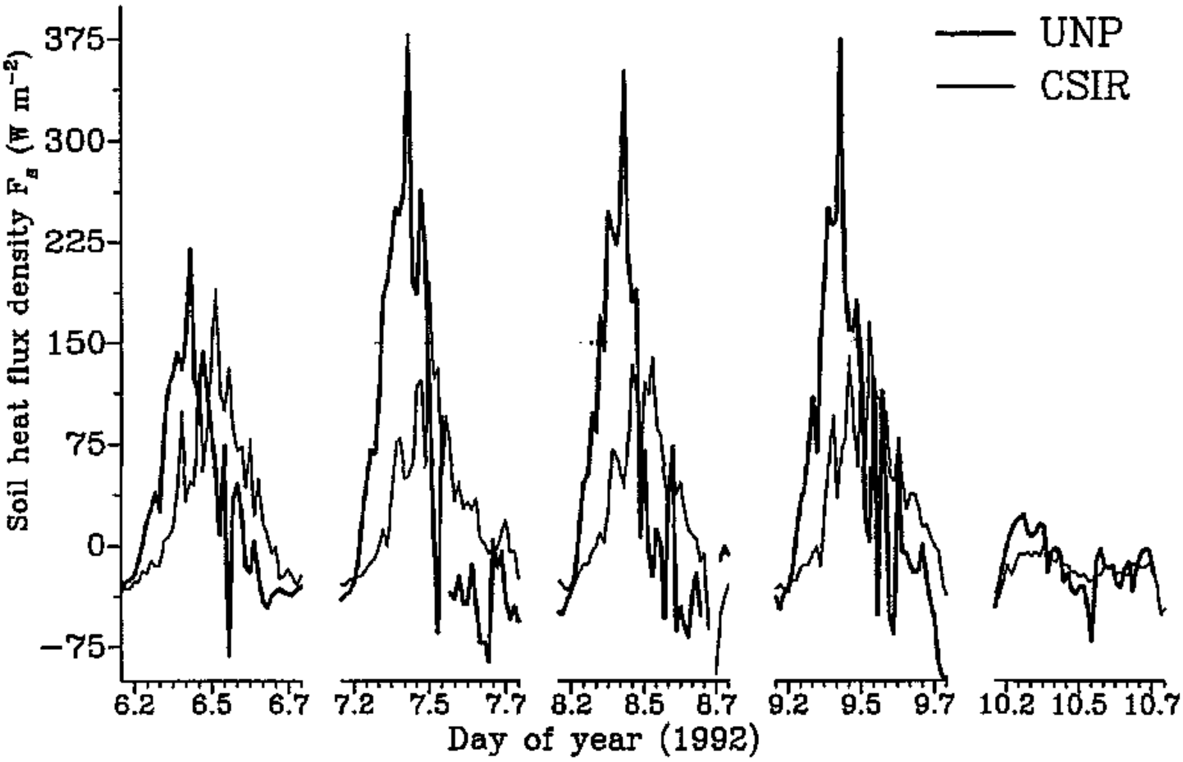

Fig. 9.18 Typical diurnal trends in overall soil heat flux density F_s, the sum of the plate measured soil heat flux density component F_{plate} and the stored heat flux component F_{stored} at the two sites (January 1992 accepted data). The UNP system was in a riparian zone and the CSIR system upslope, both in Catchment VI

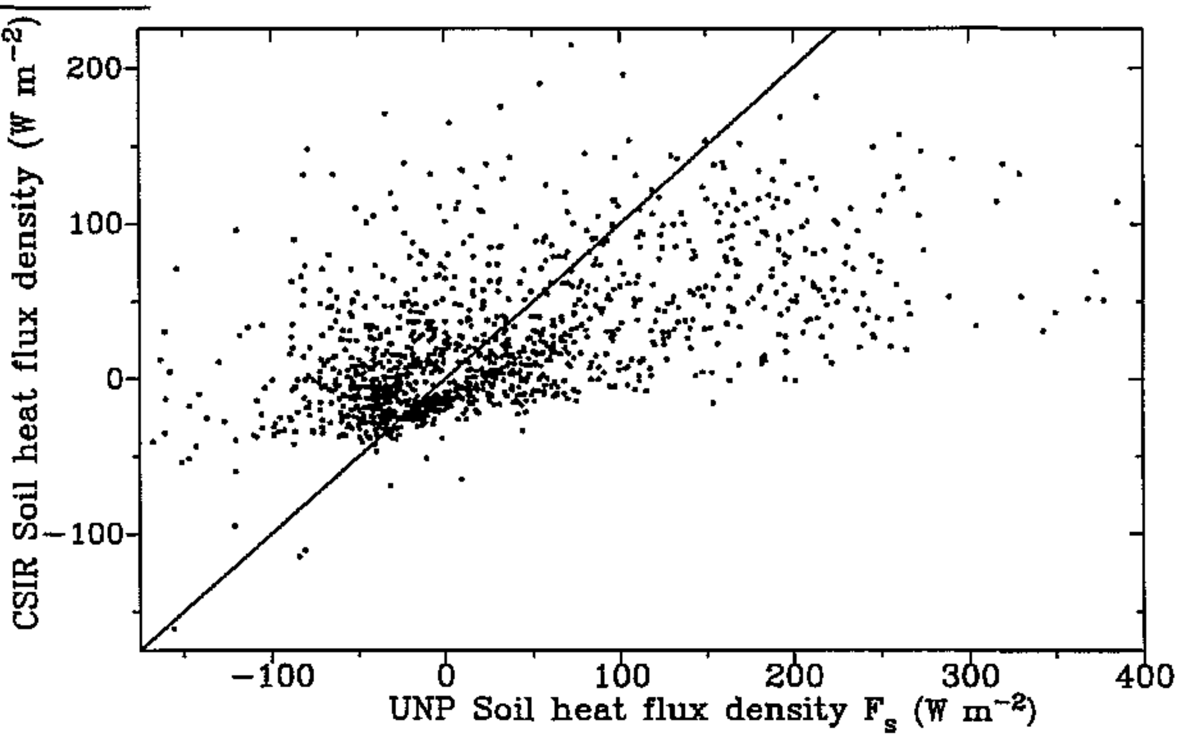

Fig. 9.19 Comparison between soil heat flux F_s measured with the UNP system (abscissa) and the CSIR system (ordinate) at the two sites (January 1992 accepted data). The UNP system was in a riparian zone and the CSIR system upslope, both in Catchment VI

exchange of energy due to the high specific heat capacity of water. No such pattern was observed in the stored heat component, which shows that the radiative load difference is probably overshadowed by the soil water content lagging.

The 20 minute $L_v F_w$ and F_h values (Figs 9.20 to 9.22) are not very different in relative amounts. Nevertheless, the inconsistency of the curves suggests that the sites are different. The data suggest (Fig. 9.20) that the evaporation at the upslope site is a maximum and greater before noon when compared to the time of maximum evaporation for the riparian zone. In the afternoon, the riparian zone evaporation appeared to exceed that upslope. This could be due to the north facing upslope resulting in a before-noon $L_v F_w$ maximum. Also, the influence of the lagged effect of water heating at the riparian zone could delay the time of maximum evaporation for the riparian location.

The 20 min values are difficult to compare and need to be totalled for each day to perform a water balance (and daily energy balance) comparison between the two sites. The 20 min data were totalled for the period 05h00 to 19h00 with the excluded 20 min values replaced by equilibrium evaporation.

For January 1992, the evaporation from the riparian location was more than 29 % greater than the upslope evaporation (Fig. 9.23). The top curve of Fig. 9.23 shows that the total solar radiant density

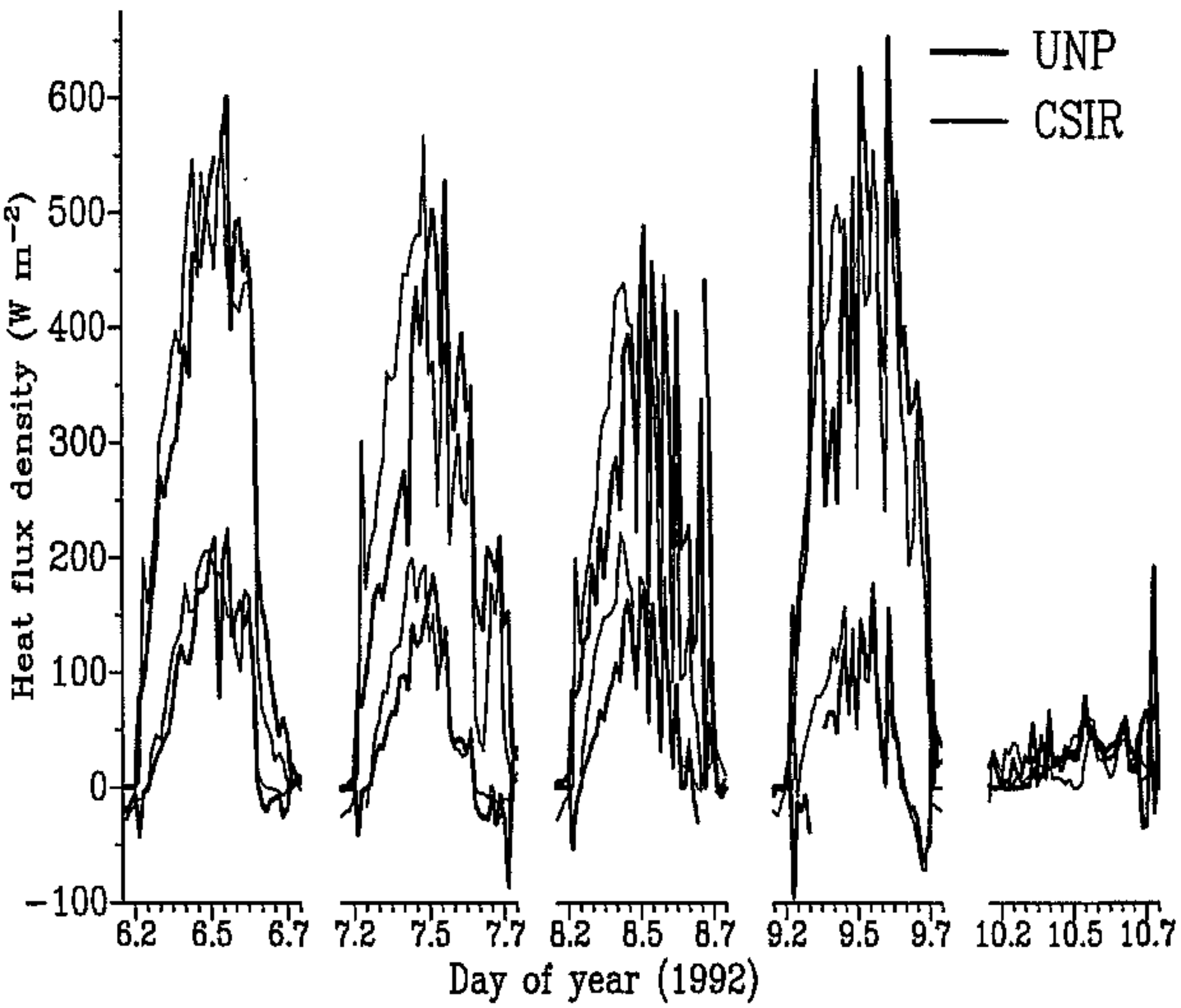

Fig. 9.20 Typical diurnal trends in calculated sensible (F_h, bottom pair of curves) and latent heat fluxes ($L_v F_w$, top pair of curves) at the two sites (05h00 to 19h00; January 1991 accepted data). The UNP system was in a riparian zone and the CSIR system upslope, both in Catchment VI

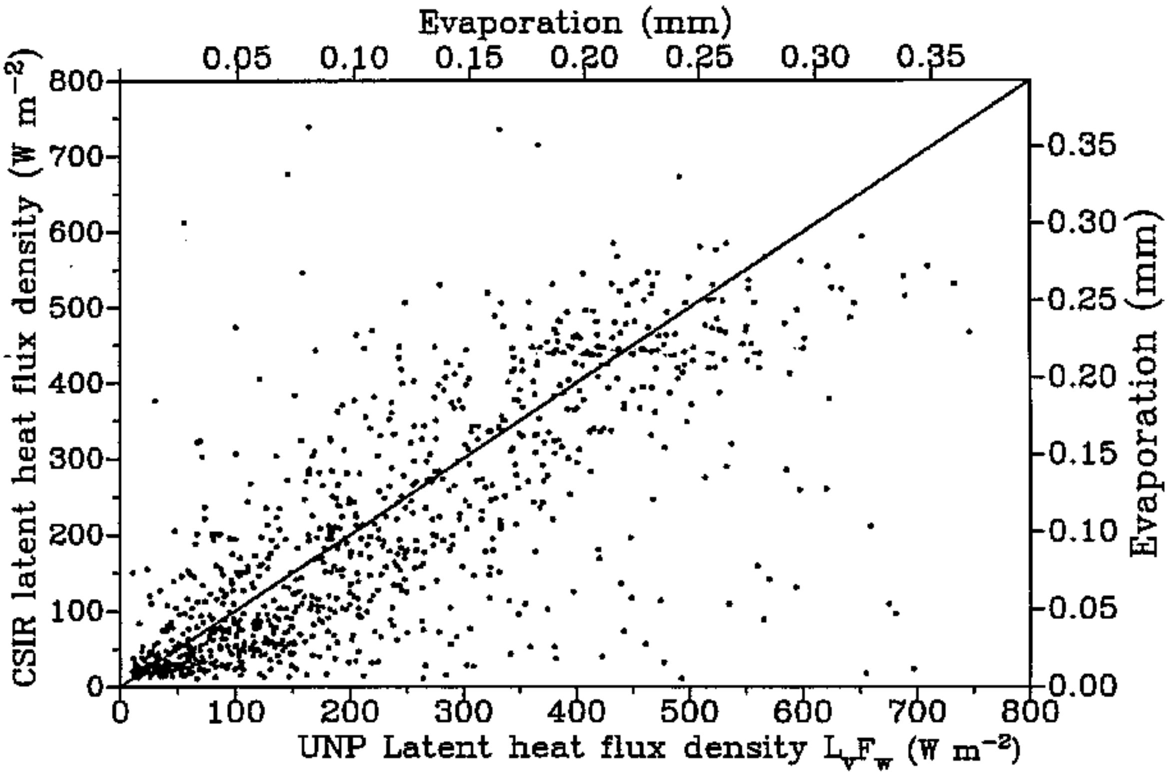

Fig. 9.21 Comparison between latent heat flux density $L_v F_w$ measured with the UNP system (abscissa) and the CSIR system (ordinate) (January 1992 accepted data). The UNP system was in a riparian zone and the CSIR system upslope, both in Catchment VI

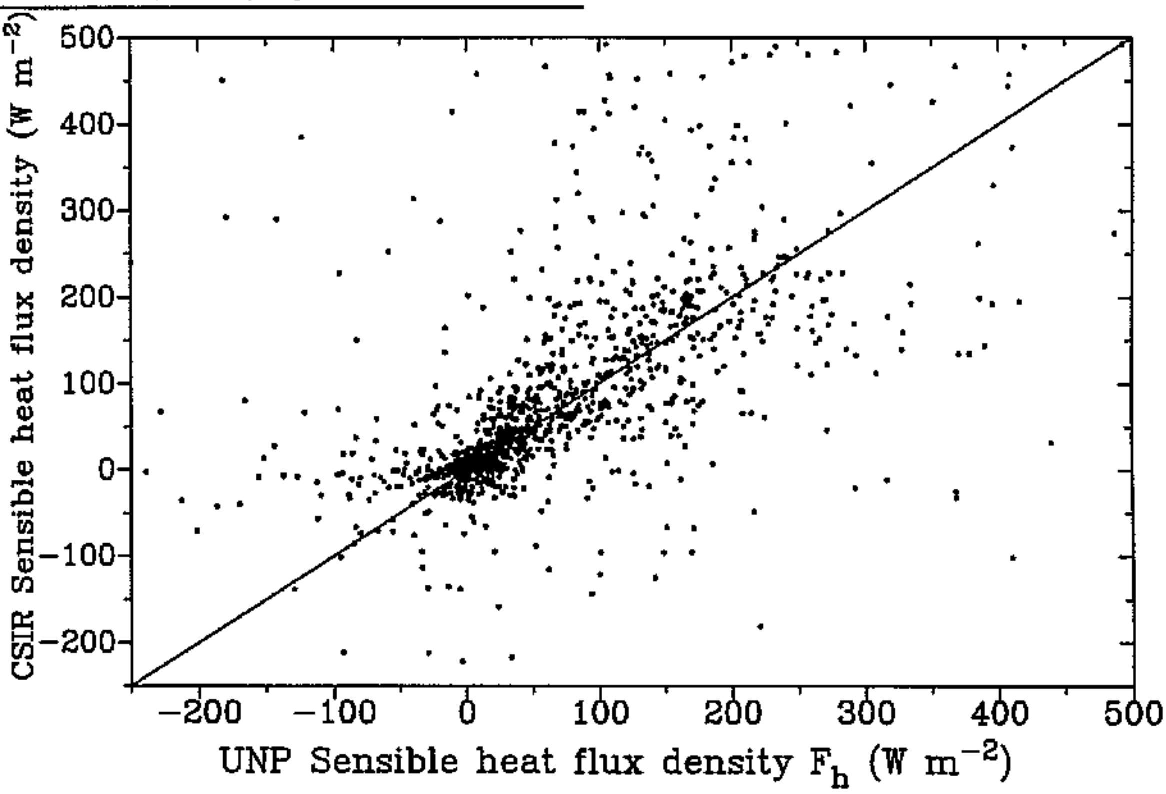

Fig. 9.22 Comparison between sensible heat flux density F_h measured with the UNP system (abscissa) and the CSIR system (ordinate) at the two sites (January 1992 accepted data). The UNP system was in a riparian zone and the CSIR system upslope, both in Catchment VI

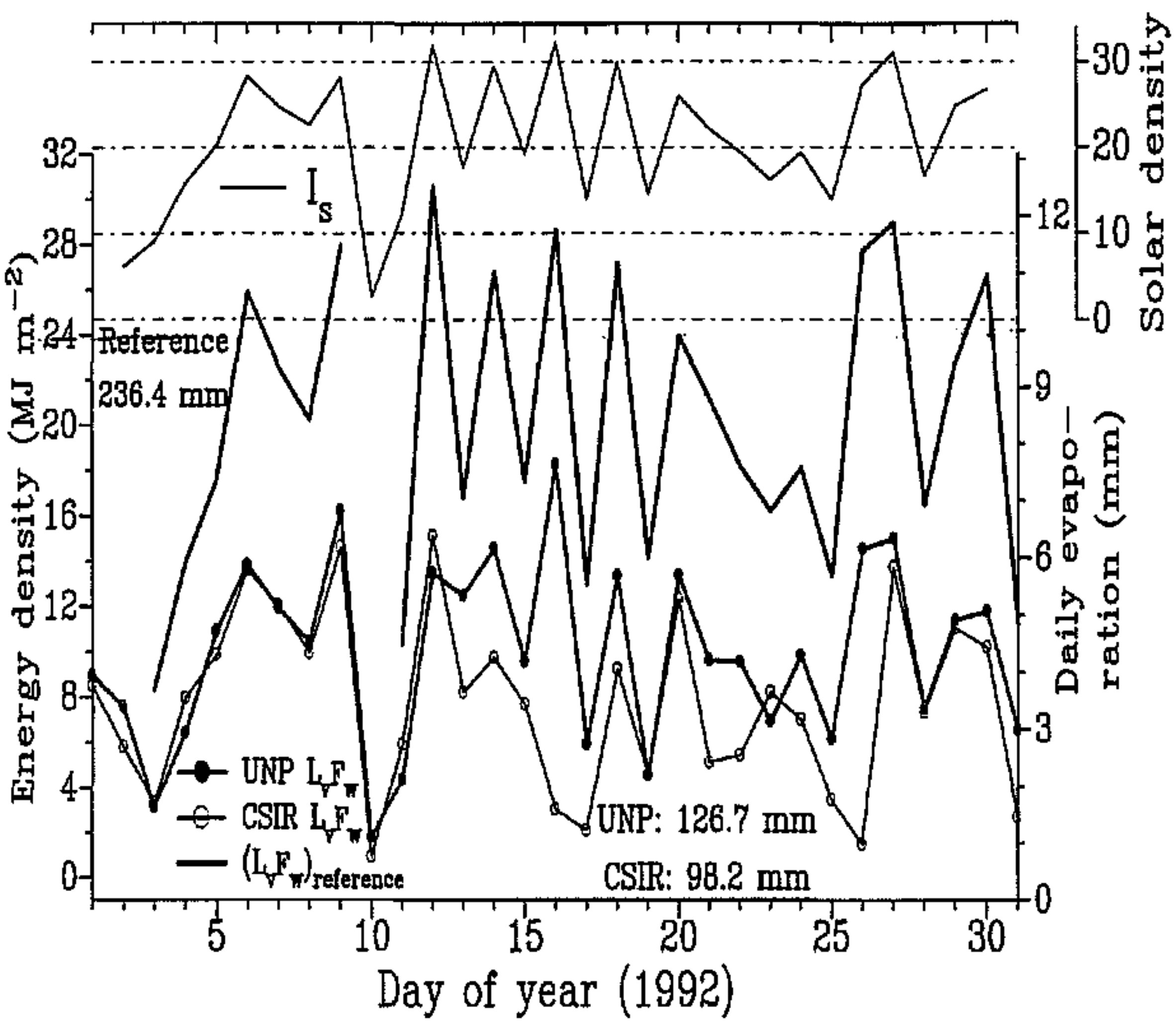

Fig. 9.23 Comparison of daily evaporation totals calculated with the two Bowen ratio systems (for two sites (January 1992) and reference evaporation. The UNP system was in a riparian zone (total of 126.7 mm) and the CSIR system upslope (total of 98.2 mm), both in Catchment VI

(MJ m^{-2}) drives the evaporation process for both locations. The totals calculated for the two sites for January 1992 (Fig. 9.23) are 126.7 mm for the riparian location and 98.2 mm for the upslope location.

The daily total energy balance components for the riparian and upslope locations are shown (Fig. 9.24). All energy balance components, totalled for each day of January 1992, were determined to be statistically different, using a paired-*t*-test (Table 9.4), at the 5 % level of significance. A paired *t*-test is appropriate since each daily total measurement pair were obtained at the same time. The null hypothesis of this statistical test is that the average difference between each measurement pair is zero. The least significant difference was in the sensible heat component. The net radiant density, latent heat and soil heat densities are all greater for the riparian location compared with that upslope. The differences in net radiant density between the two locations does not take into account the slight differences in the measured net radiant density at the same site during 1990 and 1991 (Table 9.3). If these differences were taken into account, the differences in net radiant density and latent heat density between the upslope and riparian locations shown in Table 9.4 would be even greater than the 29 %

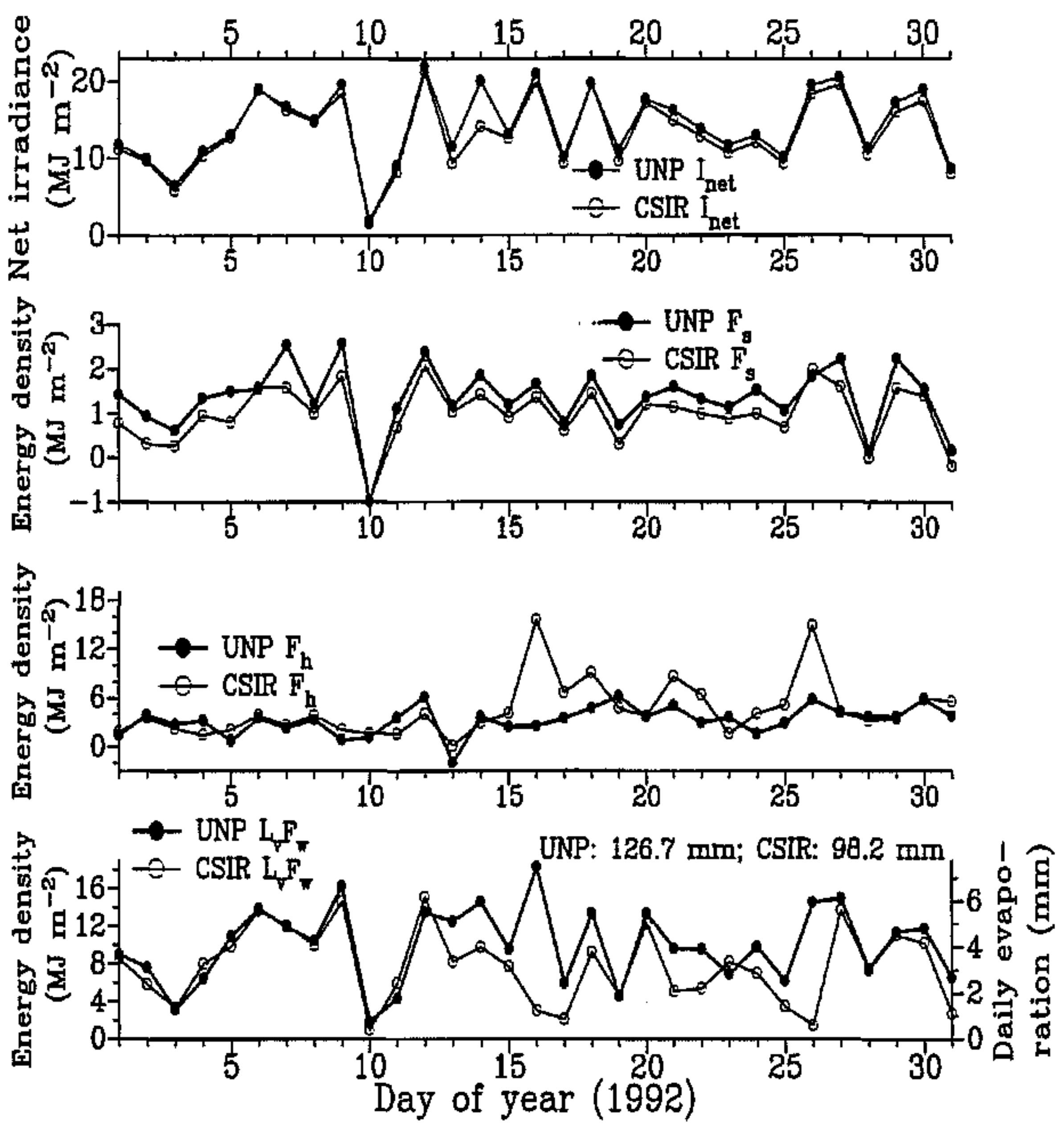

Fig. 9.24 The daily energy densities of the energy balance components for both upslope (CSIR system) and riparian locations (UNP system) for January 1992

shown. If this underestimation of 4.6 % (Table 9.3) were included, evaporation for the riparian location would be at least 30 % greater than that upslope (Table 9.4). This large difference exceeds the differences between measurements when the two Bowen ratio systems were upslope.

The values for evaporation in Fig. 9.24 clearly show the greater evaporation for the riparian site compared with that upslope. The evaporation for the riparian location was greater than that upslope two out of every three days on average. The data of Figs 9.14, 9.15 and 9.24 show three possible reasons for the increased evaporation for the riparian location compared with upslope, the first tow of which are associated with the generally wetter surface conditions of the riparian site:

1. the measured air temperature profile differences (δT) were generally smaller for the upslope (CSIR

Table 9.4 Paired two-sample t-test for means for net radiant density, latent heat density, sensible heat density and soil heat density for the January daily totals for the two Bowen ratio systems (UNP system in the riparian zone, CSIR system upslope). The comparative differences were all significant at the 5 % level of significance and in most cases the 1 % level

	UNP I_{net}	CSIR I_{net}	UNP $L_v F_w$	CSIR $L_v F_w$	UNP F_h	CSIR F_h	UNP F_s	CSIR F_s
Mean (MJ m^{-2})	14.208	13.241	9.990	7.743	3.227	4.532	1.333	0.966
Mean (mm)			4.09	3.17				
Percentage difference between the two means (relative to upslope site)	7.31		29.02		-28.80		38.06	
Variance $(MJ)^2$ m^{-4}	23.892	22.715	16.436	15.892	3.047	12.303	0.553	0.437
Variance (mm^2)			2.76	2.67				
Observations	31	31	31	31	31	31	31	31
Pearson correlation	0.977		0.577		0.440		0.945	
Pooled variance $(MJ)^2$ m^{-4}	23.304		16.164		7.675		0.495	
Pooled variance (mm^2)			2.72					
Hypothesized mean difference	0		0		0		0	
Degrees of freedom	30		30		30		30	
t	5.205		3.381		-2.303		8.279	
$100 \times p(t \leq t_{0.05})$ one-tail	0.001		0.101		1.419		0.000	
t (5 %) Critical one-tail	1.697		1.697		1.697		1.697	

system) location (Fig. 9.14);

2. the measured water vapour pressure profile differences (δe) were generally greater for the upslope (CSIR system) location (Fig. 9.15);

3. a greater net radiant density for the riparian location than that upslope (Fig. 9.24).

These three reasons all operate to increase evaporation for the riparian location (Fig. 12.23): for the first two reasons, the Bowen ratio $\beta = \gamma\, \delta T / \delta e$ is generally smaller upslope and therefore, in combination with the third reason, $L_v F_w = (I_{net} - F_s)/(1 - \beta)$ is generally smaller upslope than in the riparian location. However, offsetting these three reasons is the generally reduced soil heat flux density upslope that increased evaporation compared with the riparian location (Fig. 9.19).

Greater evaporation for the riparian location results in a generally reduced sensible heat from the riparian location compared with the upslope location. The differences in soil heat, particularly the stored soil heat flux density, between the two locations does however play a significant role in decreasing this difference.

9.4.5 Seasonal comparisons

Comparisons between the two independent Bowen ratio systems before moving one system, and between these and the lysimetrically determined evaporation have verified the accuracy and integrity of the systems (Chapter 5; Fig. 9.11). The seasonal comparisons were made over the open grassland site that had a fetch of some 125 m and is thus considered representative of the catchment as a whole. Measurements commenced in autumn 1990 and continued to autumn 1993. The variation in evaporation and net radiant density for each day of 1991 is shown (Fig. 9.25).

The daily total evaporation for 1992 is shown (Fig. 9.25) with the net energy density (MJ m^{-2}). The rainfall total was 973.4 mm and the total evaporation was 1311.4 mm.

Our initial comparisons in this project involved the use of equilibrium evaporation as a simplified method of calculating total evaporation. These initial experiments were conducted in a wet year. The variation in the Bowen ratio evaporation, taken as the average between the riparian and upslope evaporation measurements, with the calculated equilibrium evaporation (Section 5.5.4) is shown for two periods during 1992 (Fig. 9.26a, b). The equilibrium evaporation estimate may be valid for long periods when the canopy is wet. During winter however, the method may be a poor estimator of evaporation (Fig. 9.26b).

Monthly total rainfall levels for the catchment (Figs 9.27 to 9.30), compared with the 51-year mean monthly rainfall illustrate the relatively dry years through which the measurements have been made. The lowest rainfall in recent times was recorded during 1992 (Everson 1993). Of particular note during

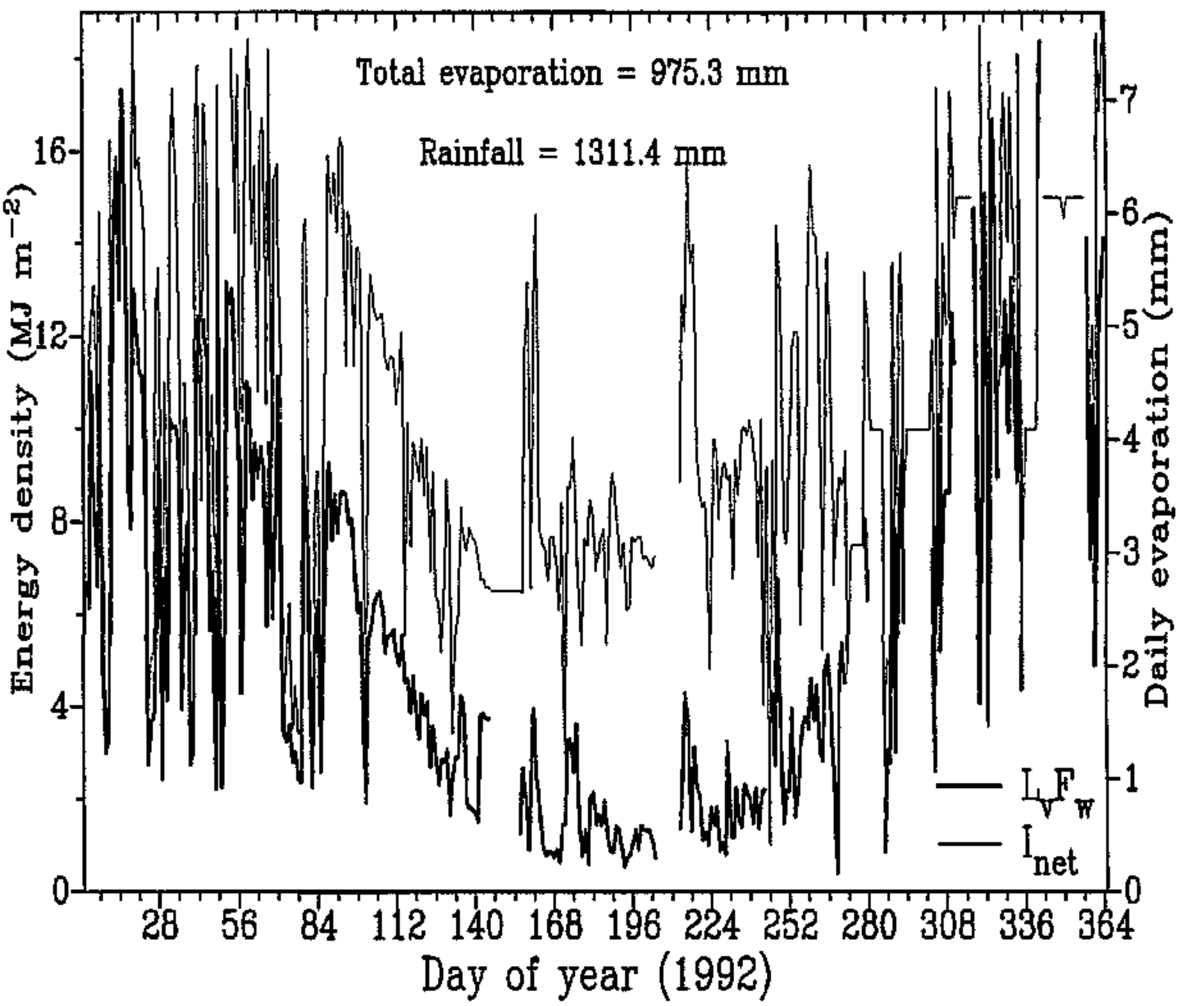

Fig. 9.25 The daily variation in latent heat and net energy density for 1992. The measurements are an average of the measurements collected at the riparian and upslope locations

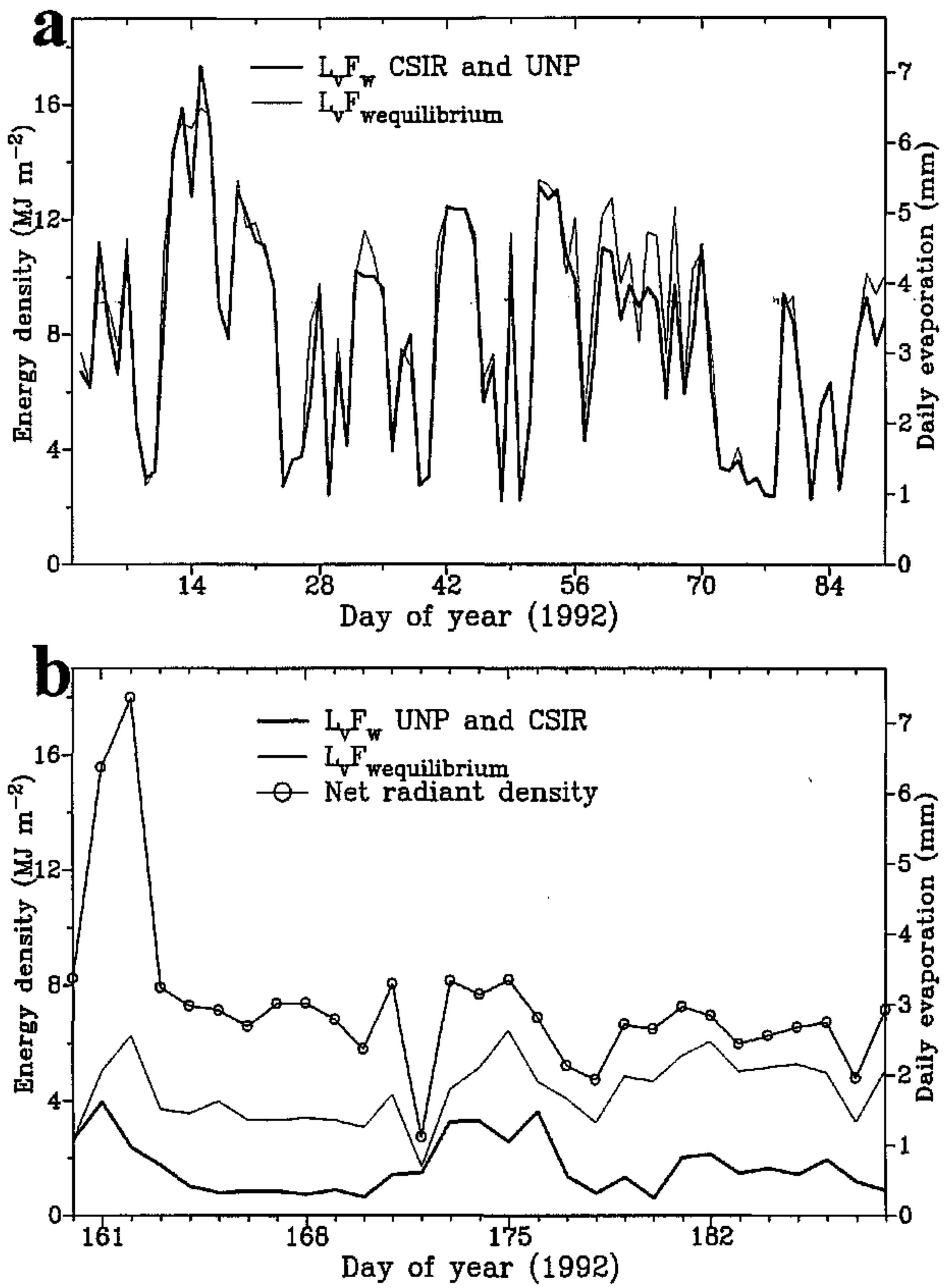

Fig. 9.26a Comparison between daily total energy density for latent heat estimated using the Bowen ratio technique and the equilibrium evaporation for the first 90 days of 1992. The values were estimated by averaging measurements for both riparian and upslope locations. The net radiant density is shown - this value is crucial for the calculation of equilibrium evaporation (Chapter 5)

b As in 9.26a except that a period during the middle of the year (drier) was chosen, showing the comparatively poor agreement between equilibrium and Bowen ratio measurements for this time of year

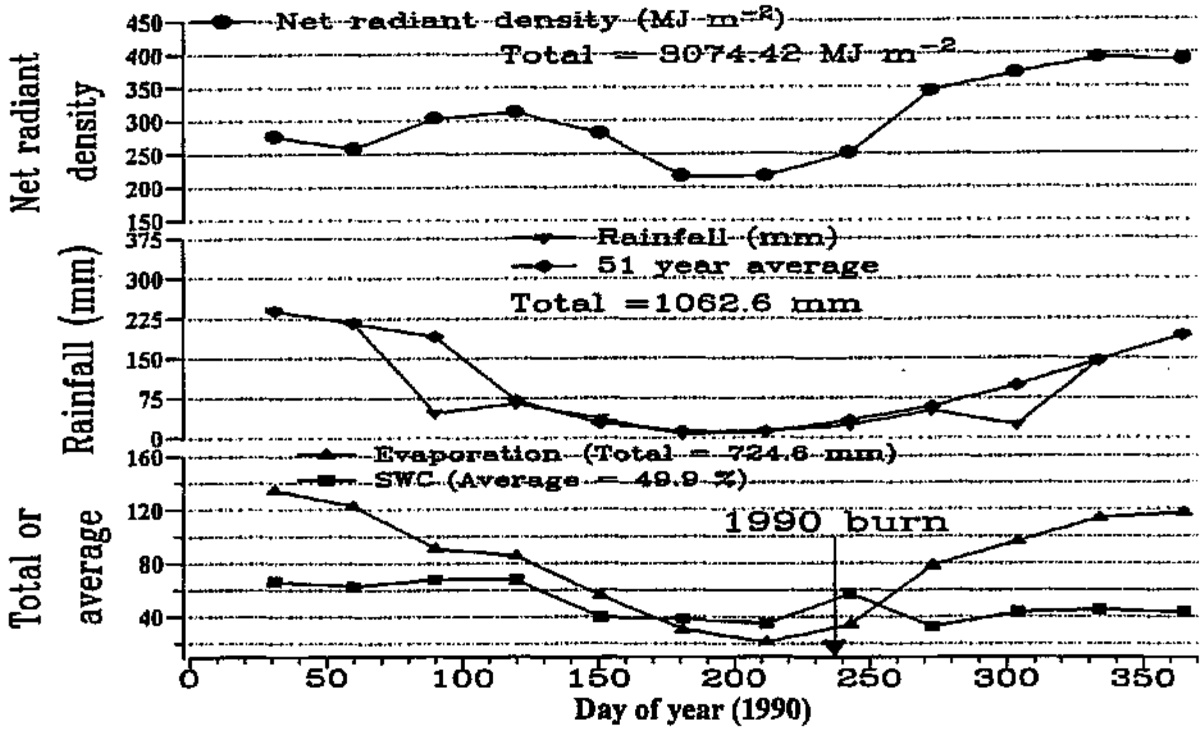

Fig. 9.27 The variation in some components of the energy and water balance of Catchment VI as a function of time. The soil water content (%) was the value at month-end. Occasionally, in particular before March, the data was patched from the long-term mean values available. The totals for the various components are also shown as is the date of the 1990 burn (Day 237)

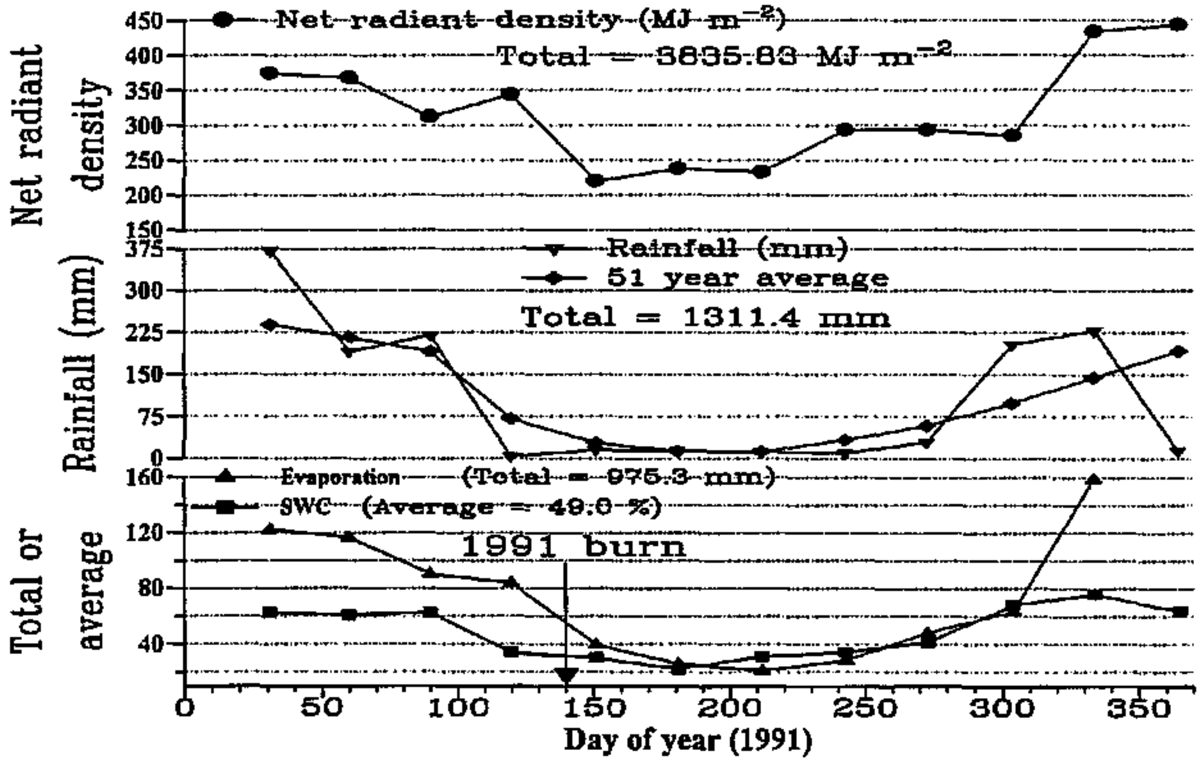

Fig. 9.28 The variation in some components of the energy and water balance of Catchment VI as a function of time. The soil water content (%) was the value at month-end. Occasionally, the data was patched from the long-term mean values available. The totals for the various components are also shown as is the date of the burn (Day 140)

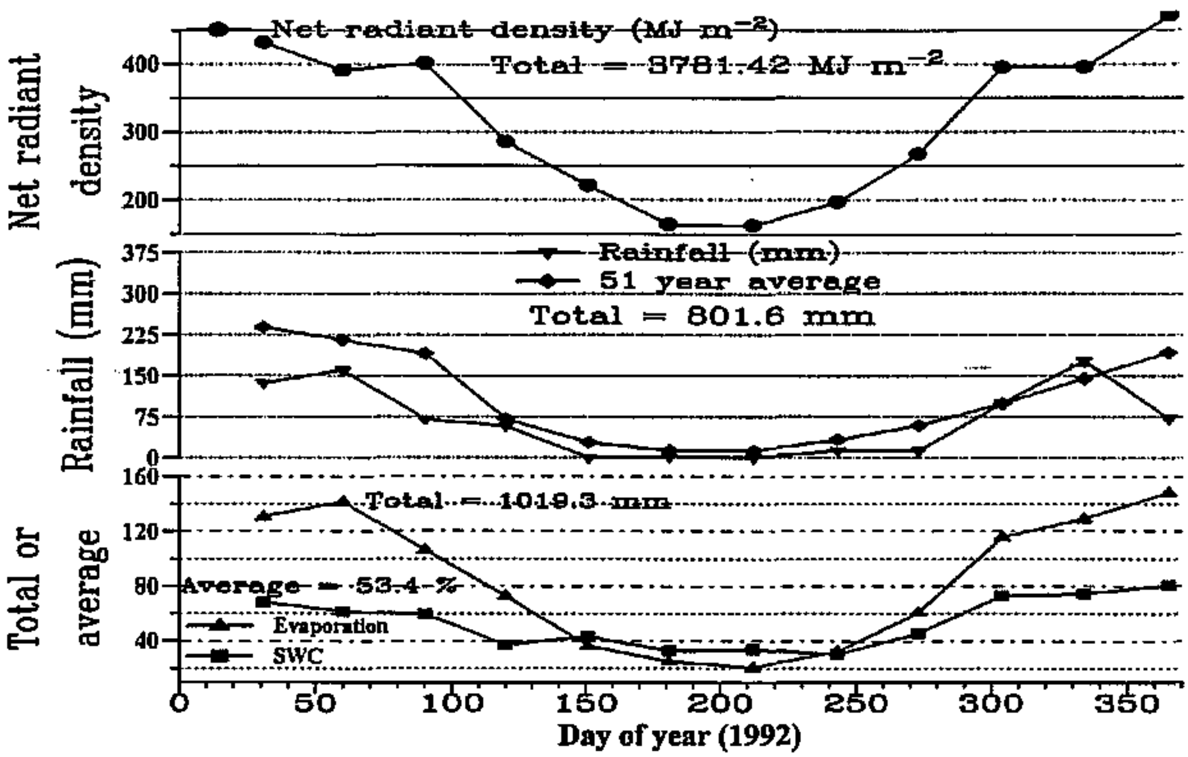

Fig. 9.29 The variation in some components of the energy and water balance of Catchment VI as a function of time. The soil water content (%) was the value at month-end. The Bowen ratio evaporation of the upslope and riparian locations were averaged. Occasionally, the data was patched from the long-term mean values available. The totals for the various components are also shown

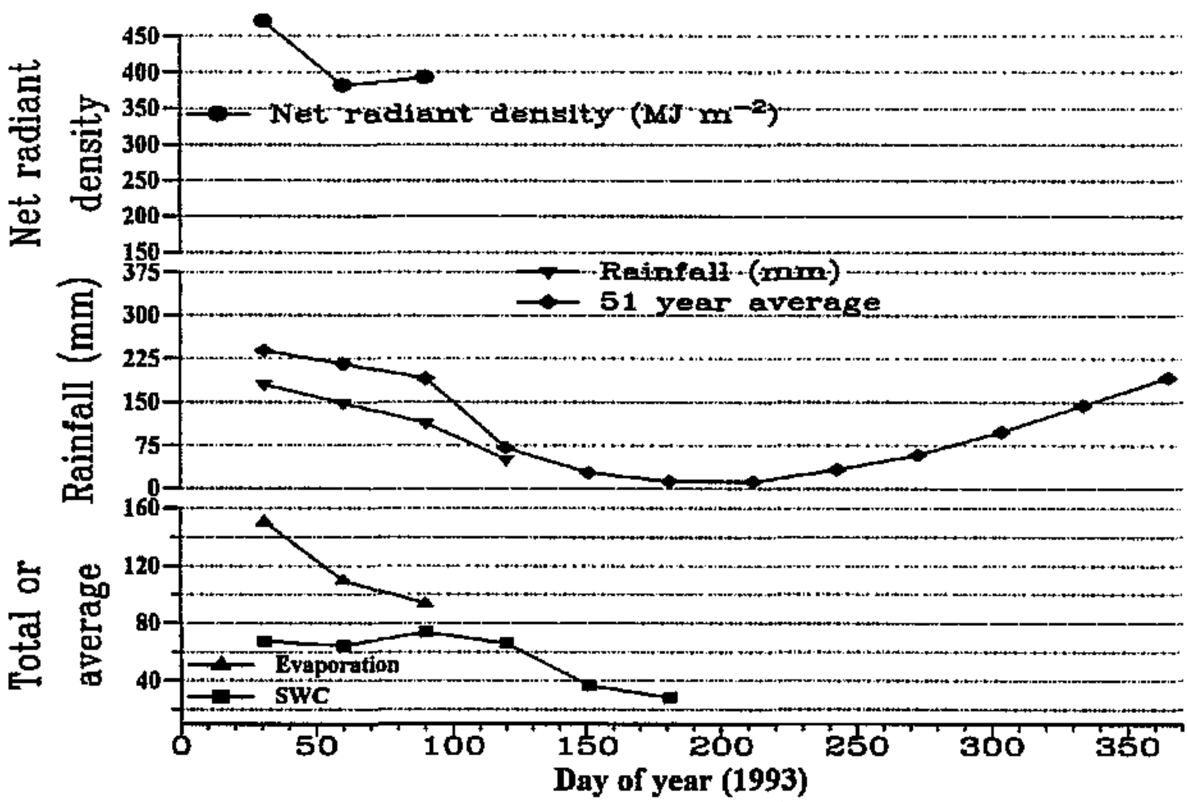

Fig. 9.30 The variation in some components of the energy and water balance of Catchment VI as a function of time. The soil water content (%) was the value at month-end. Occasionally, the data was patched from the long-term mean values available. The totals for the various components are also shown

1992 is that the total annual rainfall was less than the measured (averaged between riparian and upslope locations) Bowen ratio evaporation (Fig. 9.29). The rainfall for 1993 was also low up to the end of the work. Missing data during the summer of 1990 was patched from long-term or other available data. The temporal variation in monthly evaporation, rainfall and net radiant density is shown in Fig. 9.31. The monthly evaporation, net radiant density and rainfall lows and highs are reasonably synchronised. Of note though is that the low rainfall in December 1991 resulted in decreased evaporation in January 1992.

Having observed the rainfall variations, one would expect the evaporation levels to follow some similar related pattern. As Everson (1993) noted, this does not seem to hold during these dry years (Figs 9.27 to 9.30). Everson (1993) suggested that evaporation from these catchments during these dry years might be independent of rainfall to which Figs 9.27 to 9.30 attest. Certainly, for 1993, the year with the greatest evaporation, the lowest rainfall was measured.

Following the spring burn of 1990 (Fig. 9.27) the evaporation rate did not attain the high levels of the 1992 spring, yet maintained its consistent summer rate for longer than was the case after the high levels of 1992's spring.

The wildfire of autumn 1991 upset the biennial spring burning management regime applied to this catchment. It also resulted in lower winter evaporation levels than the previous year (Fig. 9.31, comparing evaporation for May to September in 1990 and 1992) when the trash level (from two unburnt growth seasons) was high and could have impeded soil evaporation considerably (Metelerkamp *et al.*, 1993). However, it was not as low as the 1992 winter levels (with only a single season's trash load). The burn had the unique result, when compared with the previous and subsequent years, that the evaporation rate took longer to increase in spring. Unfortunately, due to missing data for spring 1991, any conclusions as to the effect of this wildfire have to drawn from inferences made by looking at the levels of the start of the 1992 data, and the pattern at this time during the previous year. The levels at the beginning of 1992 suggest that there was a complete, albeit delayed spring recovery. The lower and late rains of that spring could, however, have been entirely responsible for this delay. If this were the case, the autumn fire would have only aggravated any effect the late rains may have had.

By summer 1992, no burn had occurred for more than 12 months, and high evaporation rates were measured. At this time, the canopy's biomass would have been at its greatest.

The late 1992 spring and subsequently low summer rainfall patterns were similar to those of the previous season. Since the summer evaporation rates were similar, and the rainfall slightly lower during 1992, the high rates can only be attributed to the greater biomass (due to the lack of fire for more than one season).

The soil water content levels for the period (data not shown) followed similar trends for each year, and were not obviously linked to rainfall levels. The soil water content was only slightly influenced by the evaporation.

The cumulative totals of net radiant density, rainfall and Bowen ratio evaporation are shown (Fig. 9.32). More than 90 % of the total rainfall for the 39-month period was measured as evaporation. Concerning the energy balance, the latent heat component totalled nearly 65 % (8126.91 MJ m^{-2}) of the net radiant density (12470.82 MJ m^{-2}). Evaporation is a therefore a significant part of the water and energy balances for this fire-determined climax grassland.

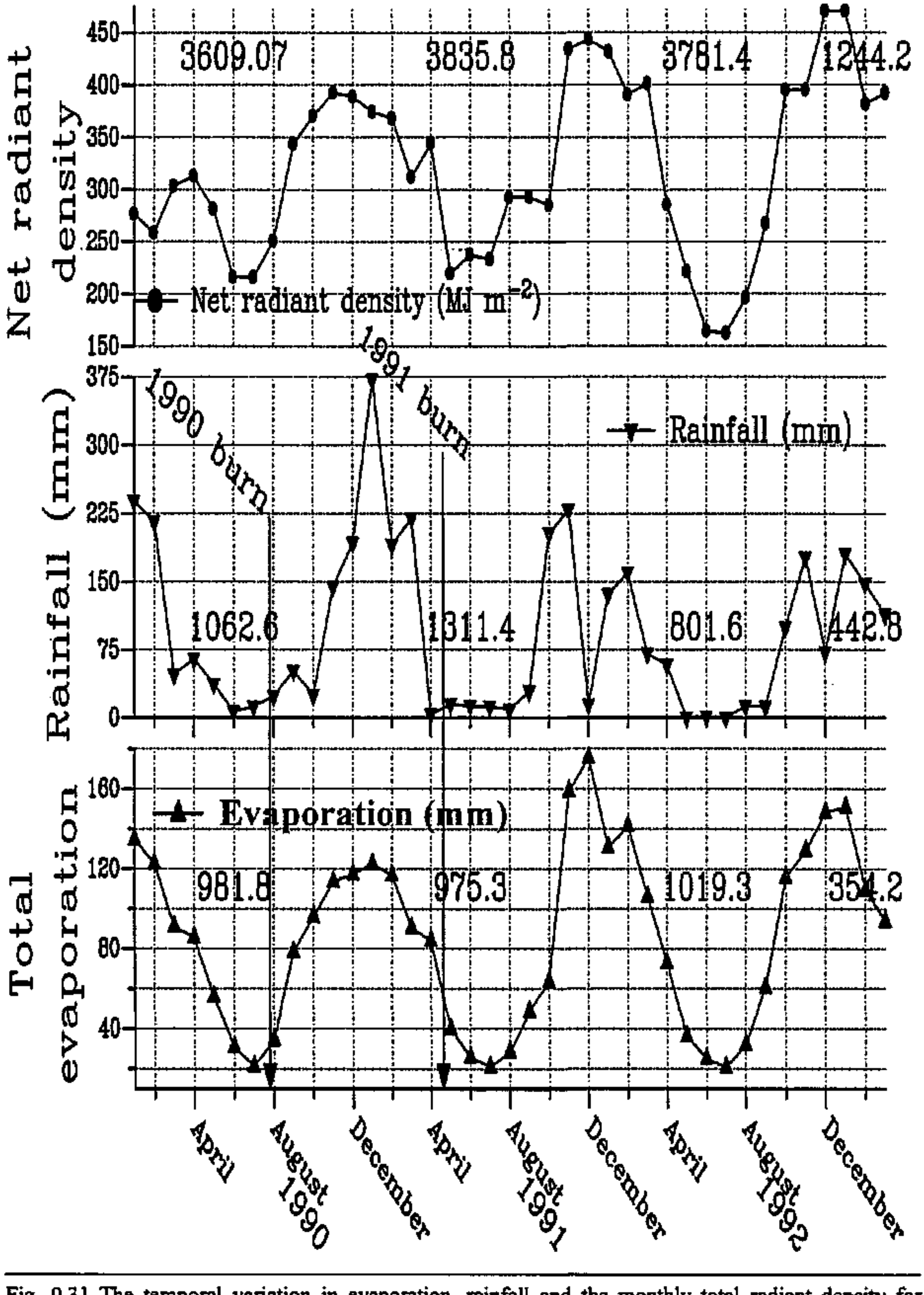

Fig. 9.31 The temporal variation in evaporation, rainfall and the monthly total radiant density for Catchment VI for the January 1990 to March 1993 period. Occasionally, in particular before March 1990, the data was patched from the long-term mean values available

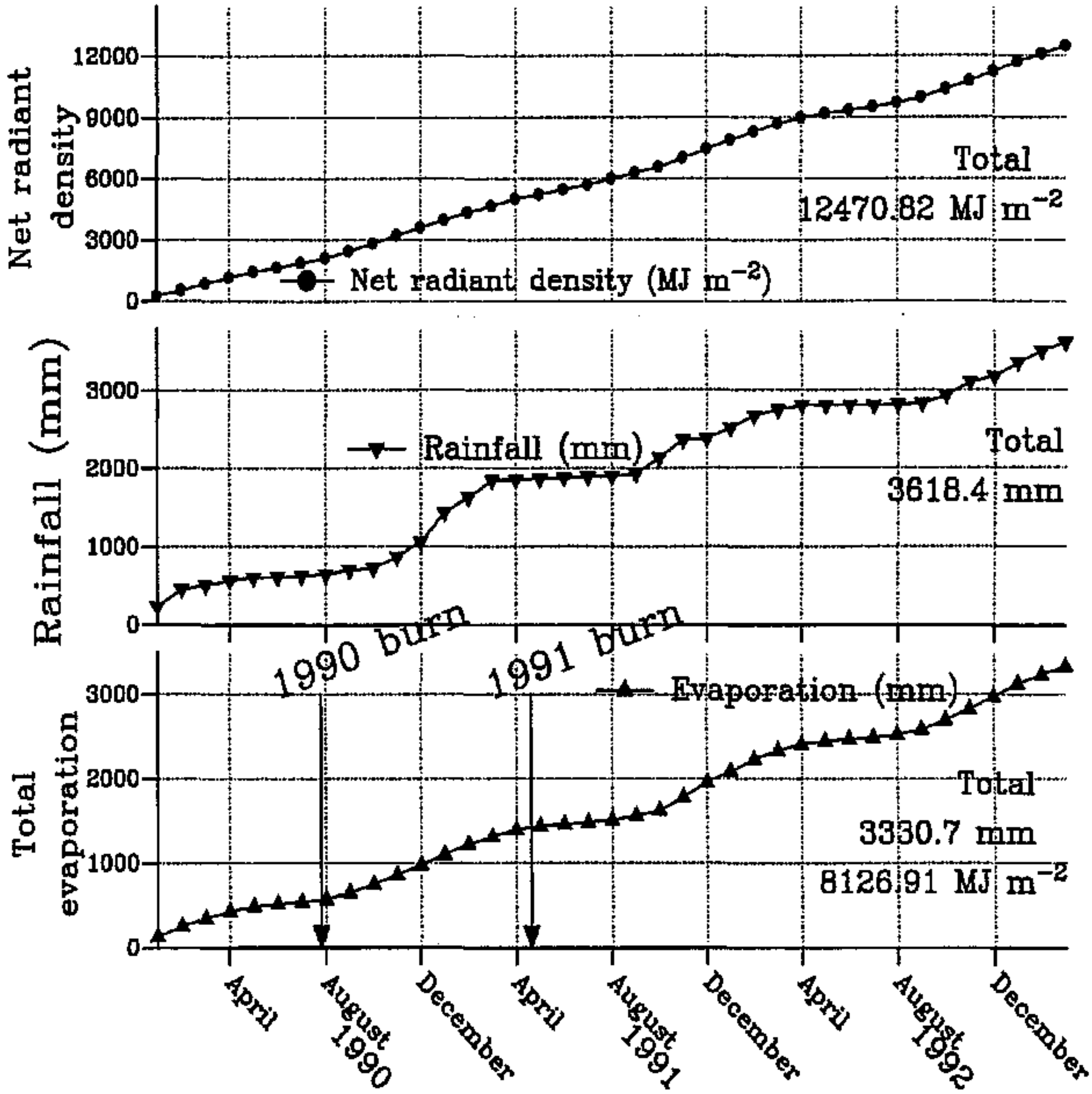

Fig. 9.32 The cumulative totals of evaporation, rainfall and the monthly total radiant density for Catchment VI for the 39 month period (January 1990 to March 1993). Occasionally, in particular before March 1990, the data was patched from the long-term mean values available

The calculation of hourly or sub-hourly Penman-Monteith evaporation for modelling purposes requires the available energy flux density $I_{net} - F_s$ in addition to other values for aerodynamic resistance r_a, r_c, and r_i, water vapour pressure deficit and temperature dependent constants Δ, γ and c_p (Eqs 2.10 and 2.11). However, under high rainfall and humid conditions, usually during summer months when evaporation is greatest, one may calculate equilibrium evaporation (Eq. 2.13) from air temperature and $I_{net} - F_s$. Often, $I_{net} - F_s$ data are unavailable, but there is a correlation with solar irradiance I_s from an automatic weather station. The regression for January 1992 had a slope of about 0.552 and an intercept 26.85 W m^{-2} (Fig. 9.33). This regression suggests that $I_{net} - F_s$ could be calculated from measured solar irradiance I_s. Part of the scatter in this plot could be due to the differing time constants of the various sensors used to gather the data, particularly the lag in the F_s data.

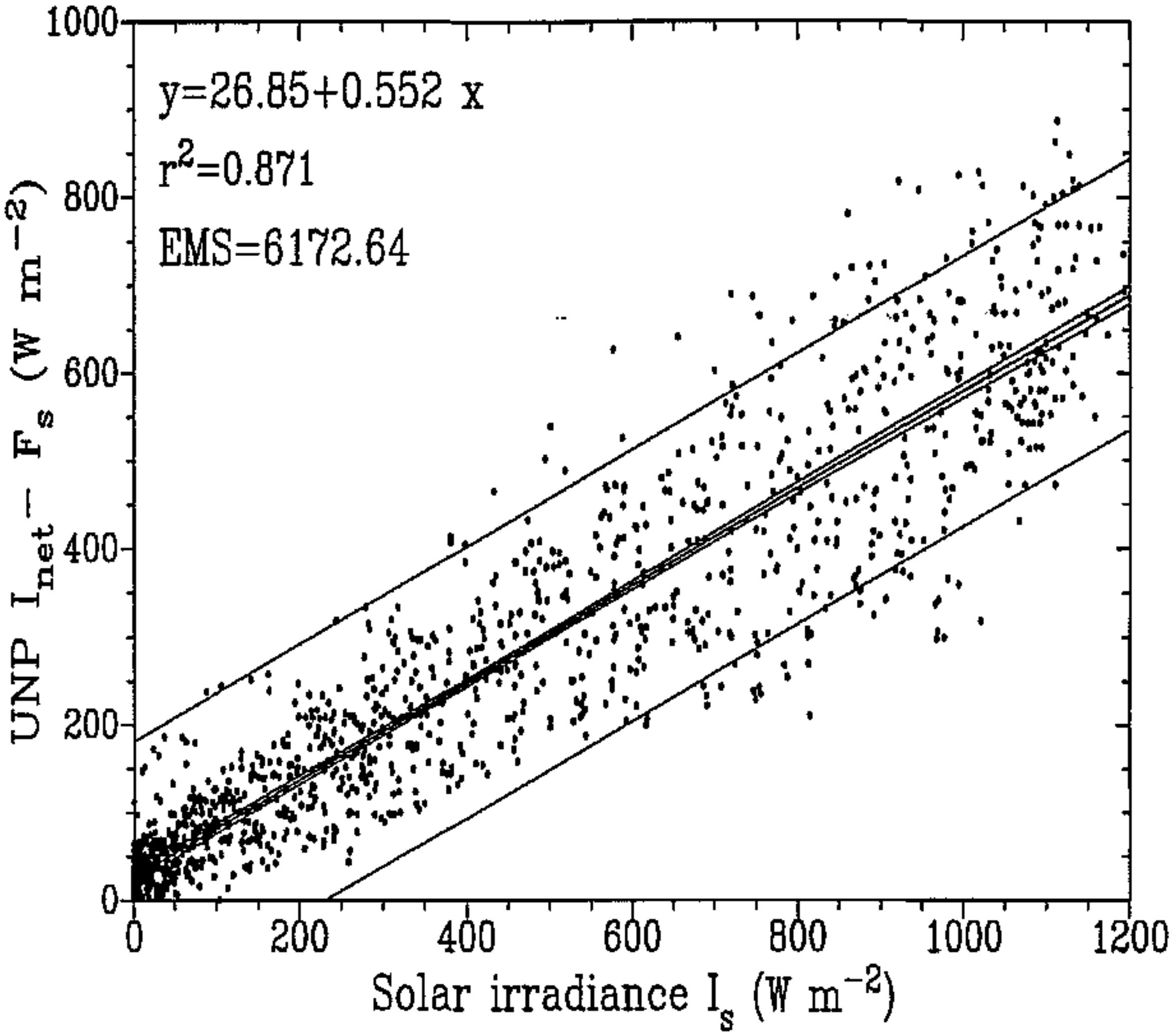

Fig. 9.33 Solar irradiance as a function of net irradiance less the soil heat flux density for Catchment VI for January 1992 - data is for the time period 05h00 to 19h00 only. Most of the data points below the regression line occurred under high radiation conditions (solar irradiance greater than 900 W m^{-2}). Each point is a 20 min value

9.5 Conclusion

We have shown that it is possible to measure evaporation continuously using the Bowen ratio technique in Catchment VI. Winter total evaporation rates varied very little whether the canopy was one year old, two years old or even completely burnt. Equilibrium evaporation, dependent on the ratio between the difference between net irradiance and soil heat flux density and $(1 + \beta)$, is not a good indicator of Bowen ratio evaporation in winter. It may however be a reasonable predictor for the summer months for this catchment.

The evaporation for the riparian location, for the month of January 1992, was about 30 % greater than that upslope. Apart from the soil heat, each term of the Bowen ratio equation used to calculate the evaporation contributed to greater evaporation values at the riparian location. The term that showed the most marked difference between the two sites was the soil heat flux, which decreased evaporation for the riparian location compared with that upslope.

The total net radiant density for the 39-month period was 12470.82 MJ m^{-2}. Evaporation (latent heat) is a significant fraction of both the energy and water balance. It represented more than 65 % of the net radiant density over the 39-month period and more than 90 % of the rainfall over the same period. The total evaporation was 3330.7 mm and the rainfall was 3618.4 mm.

References

1. Abdel-Aziz, M., Taylor, S. A., and Ashcroft, G. L., 1964. Influence of advected energy on transpiration. Agron. J., 56: 139-142.
2. Angus, D. E., and Watts, P. J., 1984. Evapotranspiration - how good is the Bowen ratio method? Agric. Water Mgt., 8: 133-150.
3. Anon., 1991. CSI Bowen Ratio Instrumentation Instruction Manual. Revision 4/91.
4. Arya, S. P., 1988. Introduction to Micrometeorology. Academic Press, London.
5. Barber, R., and Brown, M. E., 1978. Calibration methods and standards for infrared thermometers. Instr. Soc. Am. Trans., 17(3): 63-69.
6. Bedford, R. E., 1972. Effective emissivities of blackbodies - a review. In H. H. Plumb (ed). Temperature - its measurement and control in science and industry 4(1): 425-434. Instrument Society America, Pittsburg, Pa.
7. Bertela, M., 1989. Inconsistent surface flux partioning by the Bowen ratio method. Boundary-Layer Meteorol., 49: 149-167.
8. Biltoft, C. A., and Gaynor, J., 1987. Comparison of two types of sonic anemometers and fast response thermometers. Sixth Symposium on Meteorology Observations and Instrumentation. 173-176.
9. Black, T. A., 1973. Evaporation from Douglas-fir stands exposed to soil water deficits. Water Resour. Res., 15: 164-170.
10. Blad, B. L., and Rosenberg, N. J., 1974. Lysimetric calibration of Bowen ratio energy balance method for evapotranspiration estimation in Central Great Plains. J. Appl. Meteorol., 13: 227-237.
11. Blad, B. L., Verma, S. B., and Rosenberg, N. J., 1977. Turbulent exchange coefficients for sensible heat and water vapour under advective conditions. J. Appl. Meteorol., 330-339.
12. Bowen, I. S., 1926. The ratio of heat losses by conduction and by evaporation from any water surface. Phys. Rev., 27: 779-787.
13. Brakke, T. W., Verma, S. B., and Rosenberg, N. J., 1978. Local and regional components of sensible heat advection. J. Appl. Meteorol., 17: 955-963.
14. Brooks, F. A., 1961. Need for measuring horizontal gradients in determining vertical eddy transfers of heat and moisture. J. Meteorol., 18: 589-596.
15. Brutsaert, W. H., 1982. Evaporation into the atmosphere. Reidel, Dordrecht, Holland. pp. 299.
16. Byers, H.R., 1974. General Meteorology, 4th ed., pp. 74-77. McGraw-Hill Book Company, New York.
17. Campbell, A. P., 1973. The effect of stability on evapotranspiration rates measured by the energy balance method. 11: 261-267.
18. Campbell, G. S. and Unsworth, M. H., 1979. An inexpensive sonic anemometer for eddy correlation. J. App. Meteorol., 18: 1072-1077.
19. Cellier, P., and Olioso, A., 1993. A simple system for automated Bowen ratio measurement. Agric. For. Meteorol., 66: 81-92.
20. Corsin, S., 1974. Limitations of gradient models in random walks in turbulence. Adv. Geophys., 18A: 25-60.
21. Cummings, 1925. Phys. Rev., 25: 721., and J. Elect. 46: 491. (Cited by I.S. Bowen).
22. Denmead, O. T., 1984. The measurement of evaporation by meteorological methods. In Sharma, M. L. (Ed.) Evapotransipration from plant communities. Elsevier, Amsterdam.
23. Denmead, O. T., and McIlroy, C. L., 1970. Measurements of non-potential evaporation from wheat. Agric. Meteorol., 7: 285-302.
24. Denmead, O. T., and Bradley, E. F., 1985. Flux-gradient relationships in a forest canopy. In: Hutchinson, B.A., and Hicks, B. B., (Eds) The Forest-Atmosphere Interaction. Reidel,

Dordrecht.

25. De Vries, C. A., 1963. Thermal properties of soils. In W. R. van Wijk (Editor), Physics of the Plant Environment. John Wiley & Sons, New York, NY pp. 210-235.

26. Duell, L. F. W., and Nork, D. M., 1985. Comparison of three micrometeorological methods to calculate evapotranspiration in Owen's Valley California. 161-165.

27. Dugas, W. A., Fritschen, L. J., Gay, L. W., Held, A. A., Matthias, A. D., Reicosky, D. C., Steduto, P., and Steiner, J. L., 1991. Bowen ratio, eddy correlation, and portable chamber measurements of sensible and latent heat flux over irrigated spring wheat. Agric. For. Meteorol., 56: 1-20.

28. Dyer, A. J., 1961. Measurements of evaporation and heat transfer in the lower atmosphere by an automatic eddy correlation technique. Quart. J. R. Meteorol. Soc., 87: 401-412.

29. Dyer, A. J., 1963. The adjustment of profiles and eddy fluxes. Quart. J. R. Meteorol. Soc., 98: 276-280.

30. Dyer, A. J., 1965. Discussion on change of terrain roughness and the wind profile by H.A. Panofsky and A.A. Townsend. Q.J.R. Meteorol. Soc., 91: 241.

31. Dyer, A. J., 1967. The turbulent transport of heat and water vapour. Quart. J. R. Meteorol. Soc., 93: 501-509.

32. Dyer, A. J., 1974. A review of flux-profile relationships. Boundary-Layer Meteorol., 7: 363-372.

33. Dyer, A. J. and Crawford, T. V. 1965. Observations of the modification of the microclimate at a leading edge. Quart. J. R. Met. Soc., 91: 345-348.

34. Dyer, A. J. and Hicks, B. B., 1972. The spatial variability of eddy fluxes in the constant flux layer. Quart. J. R. Meteorol. Soc., 98: 206-212.

35. Dyer, A. J., and Maher, E. J., 1965. Automatic eddy-flux measurement with the evapotron. J. Appl. Meteorol., 4: 622-625.

36. Dyer, A. J., and Pruitt, W. O., 1962. Eddy flux measurements over a small irrigated area. J. App. Meteorol., 1: 471-473.

37. Everson, C. S., 1993. Proposed model structure to simulate evaporation from a grassland catchment. Workshop on the field water balance in the modelling of cropping systems. University of Pretoria, South Africa.

38. Elliot, W. P., 1958. The growth of the atmospheric internal boundary layer. Trans. Amer. Geophys. Un., 39: 1048-1054.

39. Fitzjarrald, D. R., and Lenschow, D. H., 1983. Mean concentration and flux profiles for chemically reactive species in the atmospheric surface layer. Atmos. Environ., 17: 2505-2512.

40. Fritschen, L. J., 1965. Accuracy of evapotranspiration rate of field crops determined by the Bowen ratio method. Bull. Intern. Assoc. Sci. Hydrol., 10: 38-48.

41. Fritschen, L. J., and Fritschen, C., 1993. Surface energy balance system. 4th Symposium Global Change Studies, 73rd AMS Annual Meeting, Anaheim, CA, USA.

42. Fritschen, L. J., and Gay, L. W., 1979. Environmental Instrumentation. Springer-Verlag, London.

43. Fritschen, L. J., Gay, L. W., and Simpson, R., 1985. Eddy diffusivity and instrument in relation to plant height. In: Hutchinson, B. A., and Hichs, B. B. (Eds.), The Forest-Atmosphere Interaction. pp. 583-590, D Riedel Publishing Company, Dordrecht, Holland.

44. Fuchs, M., and Tanner, C. B., 1970. Error analysis of Bowen ratio measured by differential psychrometry. Agric. Meteorol., 7: 329-334.

45. Garrat, J. R., 1978. Flux profile relations above tall vegetation. Quart. J. R. Meteorol. Soc., 104: 199-211.

46. Garrat, J. R., 1984. The measurement of evaporation by meteorological methods. In Sharma, M.L. (Ed.) Evapotransipration from plant communities. Elsevier, Amsterdam.

47. Gash, J. H., 1986. A note on estimating the effect of a limited fetch on micrometeorological evaporation measurements. Boundary-Layer Meteorol., 35: 409-413.

48. Gay, L. W., and Greenberg, R. J., 1985. The AZET battery-powered Bowen ratio system. Proceedings of 17th Conference. Agric. For. Meteorol., 7: 329-334.

49. Grip, H., Halldin, S., Jansson, P. E., and Perttu, K., 1979. Discrepancy between energy and water balance estimates of evapotranspiration. In Halldins (Ed.) Comparison of Forest Water and Energy Exchange Models. Elsevier, Amsterdam.

50. Ham, J. M., 1990. Soil water evaporation and transpiration from a row crop at partial cover. Ph. D. Diss, Texas A & M University, College Station, USA. pp. 109.

51. Hanks, R. J., Allen, L. H., and Gardner, R. H., 1971. Advection and evapotranspiration in wide-row sorghum in the Central Great Plains. Agron. J. 63:520-527

52. Haugen, D. A., Kaimal, J. C., and Bradley, E. F., 1971. An experimental study of Reynolds stress and heat flux in the atmospheric surface layer. Quart. J. R. Meteorol. Soc., 97: 168-180.

53. ~~Heilman, J. L., and Brittin, C. L., 1989. Water use by shrubs as affected by~~ energy exchange with building walls. Agric. For. Meteorol., 48: 345-357.

54. Heilman, J. L., Brittin, C. L., and Neale, C. M. U., 1989. Fetch requirements for Bowen ratio measurements of latent heat and sensible heat fluxes. Agric. For. Meteorol., 44: 261-273.

55. Heilman, J. L., McInnes, K. L., Savage, M. J., Gesch, R. W., and Lascano, R. J., 1994. Soil and canopy energy balance in a west Texas vineyard. Agric. For. Meteorol., 71: 99-114.

56. Heilman, J.L., K.J. McInnes, R.W. Gesch, R.J. Lascano, and M.J. Savage, 1996. Effects of trellising on the energy balance of a vineyard. Agricultural and Forest Meteorology 81: 79-93.

57. Heinisch, R. P., 1972. The emittance of blackbody cavities. In H. H. Plumb (ed). Temperature - its measurement and control in science and industry 4(1): 435-447. Instrument Society America, Pittsburg, Pa.

58. Henrici, M., 1943. Transpiration of grasses in the sour mountain grassveld of the Drakensberg in comparison with the water loss of indigenous forests. S. Afr. J. Sci., 39: 155-163.

59. Hicks, B. B., 1973. Eddy fluxes over a vineyard. Agric. Meteorol,. 12: 203-215.

60. Hicks, B. B., Hyson, P., and Moore, C. J., 1975. A study of eddy fluxes over a forest. J. Appl. Meteorol., 14: 58-66.

61. Idso, S. B., 1971. A simple technique for the calibration of long-wave radiation probes. Agric. Meteorol., 8: 235-243.

62. Idso S. B., 1974. The calibration and use of net radiometers. Adv. Agron., 26: 261-275.

63. Idso, S. B., and Jackson, R. D., 1969. Thermal radiation from the atmosphere. J. Geophys. Res., 74: 5397-5403.

64. Jackson, R. D., 1982. Canopy temperature and crop water stress. Adv. in Irrig., 1: 43-85.

65. Jacobs, A. F. G., van Boxel, J. H., and Shaw, R. H., 1992. The dependence of canopy layer turbulence on within-canopy thermal stratification. Agric. For. Meteorol., 58: 247-256.

66. Kaimal, J. C., 1969. Measurement of momentum and heat flux variations in the surface of the boundary layer. Radio Sci., 4: 1147-1153.

67. Kaimal, J. C., 1975. Sensors and techniques for direct measurement of turbulent fluxes and profiles in the atmospheric surface layer. Atmos. Tech., 7: 7-14.

68. Kaimal, J. C. and Gaynor, J. E., 1991. Another look at sonic thermometry. Boundary-Layer Meteorol. 56: 401-410.

69. Kanemasu, E. T., Asrar, G., Nie, D., Watts, D., Fritschen, L., Gay, L., Weaver, H., Stannard, D., Tanner, B., Tanner. M., and Greene, J., 1987. Inter- and intra-sensor comparisons among Bowen ratio and eddy correlation instruments. International Symposium on Flow and Transport in the Natural Environment: Advances and Applications. Poster Abstract. pp. 11.

70. Kanemasu, E. T., Wesley, M. L., Hicks, B. B. and Heilman, J. L., 1979. Techniques for calculating energy and mass fluxes. In Barfield, B. J. and Gerber, J. F. (Eds), Modification of the Aerial Environment of Plants. Kansas State University, Manhattan, USA, p. 156.

71. Kaye, G. W., and Laby, J. H., 1986. Table of Physical and Chemical Constants. 15th rev. ed. Longmans, London.

72. Kimball, B. A., and Jackson, R. D., 1979. Soil heat flux. In B. J. Barfield and J. F. Gerber (Editors), Modification of the Aerial Environment of Plants. ASAE Monogram No. 2,

American Society Agricultural Engineering. St. Joseph, MI, pp. 211-229.

73. Kizer, M. A., and Elliott, R. L., 1991. Eddy correlation systems for measuring evapotranspiration. Trans. Am. Soc. Agric. Eng., 34: 387-392.

74. Kizer, M. A., Elliott, R. L., and Stone, J. F., 1990. Hourly ET model calibration with eddy flux and eddy balance data. J. Irrig. Drain., 116: 172-181.

75. Kopov, B. M., and Sokolov, D. Y., 1973. Spatial correlation functions of velocity and temperature components in the surface layer of the atmosphere. Atmos. Oceanic Phys., 9: 178-182.

76. Kristensen, L., and Fitzjarrald, D. R., 1984. The effect of line averaging on scalar flux measurements with a sonic anemometer near the surface. J. Atmos. Oceanic Tech., 1: 138-146.

77. Lang, A. R. G., 1973. Measurement of evapotranspiration in the presence of advection-energy balance. Agric. Meteorol., 12: 75-81.

78. Lang, A. R. G, McNaughton, K. G., Fazu, C., Bradley E. F., and Ohtaki. H., 1983. Inequality of eddy transfer coefficients for vertical transport of sensible and latent heats during advection. Boundary-Layer Meteorol., 25: 25-41

79. Leclerc, M. Y., and Thurtell, G. W., 1990. Footprint prediction of scalar fluxes using a Markovian analysis. Boundary-Layer Meteorol., 52: 247-258.

80. Lettau, H. H., 1959. Computation of heat budget constituents of the earth/air interface. Exploring the Atmosphere's First Mile.Vol. 1. Pergamon Press, New york. pp. 305-327.

81. Lindroth, A., and Halldin, S., 1990. Gradient measurements with fixed and reversing temperature and humidity sensors above a thin forest. Agric. For. Meteorol., 53: 81-103.

82. List, R. J., 1951. Smithsonian Meteorological Tables, 6th revised ed. Smithsonian Institution Press, Washington, DC.

83. Lourens, F. J., and Pruitt, W. O., 1971. Energy balance and water use of rice grown in the Central Valley of California. Agon. J. 63:827-832

84. Lorentz, D., 1968. Temperature measurements of natural surfaces using infrared radiometers. Appl. Opt. 7: 1705-1710.

85. Massman, W. J., Fox, D. G., Zeller, K. F., and Lukens, D., 1990. Verifying eddy correlation measurements of dry deposition: a study of the energy balance components of the Pawnee grasslands. USDA Forest Sci., 1-15.

86. McBean, G. A., and Miyake, G., 1972. Instrument requirements for eddy correlation measurements. J. Appl. Meteorol., 11: 1078-1085.

87. McInnes, K. J., Heilman, J. L., and Savage, M. J., 1994. Aerodynamic conductances along a bare ridge-furrow tilled soil surface. Agric. For. Meteorol., 68: 119-131.

88. Metelerkamp, B. R., 1992. Measuring the loss. Natal University Focus on Water 3: 19.

89. Metelerkamp, B. R., 1993. M. Sc. Agric. The use of the Bowen Ratio energy balance method for the determination of total evaporation over a grassed surface. Department of Agronomy. University of Natal. Pietermaritzburg, South Africa. Pp. 153.

90. Metelerkamp, B. R., Savage, M. J., and Everson, C. S., 1993. Seasonal comparisons of evaporative flux density in a Drakensberg catchment under a biennial veld burning regime. In S. A. Lorentz, S. W. Kienzle and M. C. Dent (eds). Proceedings of the Sixth South African National Hydrological Symposium, Vol. 1: 35-42.

91. Monnik, K. A. and M. J. Savage, 1993. Eddy correlation estimate of total evaporation over maize. Abstracts of the Tenth Annual Conference of the South African Society of Atmospheric Sciences. P 41.

92. Monnik, K. A., and Savage, M. J., 1994. Eddy correlation estimate of total evaporation over maize. Southern African Society for Crop Production, Cedara, Natal. P. 46.

93. Monnik, K. A., Savage, M. J., and Everson, C. S., 1995. Comparison of eddy correlation estimates of evaporation with Bowen ratio and equilibrium evaporation. Proceedings of the Southern African Irrigation Symposium, 167-171.

94. Monin, A. S., and Obukhov, A. M., 1954. Basic laws of turbulebt mixing in the ground layer of the atmosphere. Tr. Goefiz. Instit. Akad. Nauk. SSSR, 24(151): 163-187.

95. Monteith, J. L., 1963. Gas exchange in plant communities. In Evans, L. J. (Ed.) Enviornmental Control of Plant Growth. Academic Press, New York. pp. 95-112.

96. Monteith, J.L. 1965, Evaporation and environment. In G. E. Fogg (ed.) *The State and Movement of Water in Living Organisms*, Sympos. Soc. Exper. Biol. vol 19, Academic Press, New York, pp 205-234.

97. Monteith, J. L., and Unsworth, M. H., 1990. Principles of Environmental Physics. 2nd Edition. Edward Arnold, London.

98. Moore, C. J., 1986. Frequency response corrections for eddy correlation systems. Boundary-Layer Meteorol., 37: 17-35.

99. Morton, F. I., 1971. Catchment evaporation and potential evaporation - further development of a climatologic relationship. J Hydrol. 12: 81-99.

100. Motha, R. P., Verma, S. B., and Rosenberg, N. J., 1979a. Turbulence spectra above a vegetated surface under conditions of sensible heat advection. J. Climate Appl. Meteorol., 18: 317-323.

101. Motha, R. P., Verma, S. B., and Rosenberg, N. J., 1979b. Exchange coefficients under sensible heat advection determined by eddy correlation. Agric. Meteorol., 20: 273-280.

102. Mottram, R., de Jager, J. M., and Savage, M. J., 1991. Telecommunications networking of weather data for use in agricultural systems. Water SA., 17(4): 243-247.

103. Munro, D. S., and Oke, T. R., 1975. Aerodynamic boundary-layer adjustment over a crop in neutral stability. Boundary-Layer Meteorol., 9: 53-61.

104. Munro, D. S., 1985. Internal consistency of the Bowen ratio approach to flux estimation over forested wetland. In Hutchinson, B. A., and Hick. B. B. (Eds.), The Forest-Atmosphere Interaction. D Reidel Publishing Company, Dordrecht, Holland. pp. 395-404.

105. Neumann, H. H., and den Hartog, G., 1985. Eddy correlation measurements of atmospheric fluxes of ozone, sulphur and particles during the Champaign intercomparison study. J. Geophys. Res., 90: 2079-2110.

106. Nie, D., Flitcroft, I. E., and Kanemasu, E. T., 1992. Performance of Bowen ratio systems on a slope. Agric. For. Meteorol., 59: 165-181.

107. Obukhov, A. M., 1946. Turbulence in the atmosphere with non-uniform temperature. Trudy Instit. Teoret. Goefiz. AN-SSSR No. 1 (English Translation (1971) Boundary-Layer Meteorol. 2: 7-29.

108. Ohmura, A., 1982. Objective criteria for rejecting data for Bowen ratio flux calcuations. J. Appl. Meteorol., 21: 595-598.

109. Oke, T. R., 1970. Turbulent transport near the ground in stable conditions. J. Climate Appl. Meteorol., 9: 778.

110. Oke, T. R., 1978. Boundary Layer Climates. Metheun, New York.

111. Oke, T. R., 1987. Boundary Layer Climates, 2 nd ed. Routledge, London.

112. Panofsky, H. A., 1965. Reanalysis of Swinbank's Kerang observation. Flux of heat and momentum in the planetary boundary layer. Department. of Meteorology. Republican Pennsylvania State University. pp. 67-76.

113. Panofsky, H. A., and Dutton, J. A., 1984. Atmospheric turbulence. Models and Methods for Engineering Applications. Wiley, NY.

114. Panofsky, H. A., and Townsend, A. A., 1964. Change of terrain roughness and the wind profile. Quart. J. R. Meteorol. Soc., 91: 147-155.

115. Pasquill, F., 1949. Eddy diffusion of water vapour and heat near the ground. Proc. Roy. Soc., London. A198: 116-140.

116. Pasquill, F., 1972. Some aspects of boundary-layer description. Quart. J. R. Meteorol. Soc., 98: 469-475.

117. Philip, J. R., 1959. The theory of local advection: 1. J. Meteorol., 16: 535-547.

118. Penman, H. L., 1948. Natural evaporation from open water, bare soil and grass. Proc. Roy. Soc. London A 193:120-146

119. Perrier, E. R., Robertson, J. M., Millington, R. J., and Peters, D. B., 1971. Spatial and temporal variation of wind above and within a soybean canopy. Agric. Meteorol. 10:421-442

120. Priestley, C. H. B., 1959. Turbulent Transfer in the Lower Atmosphere. University of Chicago Press, Chicago.

121. Priestley, C. H. B., and Taylor, R. J., 1972. On the assessment of surface heat flux and evaporation using large-scale parameters. Monthly Weather Rev., 100: 81-92.

122. Pruitt, W.O., and Aston, M. J., 1963. Atmospheric and surface factors affecting evapotranspiration. In Investigation of energy and mass transfers near the ground including the influences of the soil-plant-atmosphere system. Univ. Calif. (Davis), Depts. of Agric. Engr. and Irrigation. Final Rpt. USAEPG Contract No. DA-36-039-SC-80334.

123. Pruitt, W. O., and Swann, B. D., 1987. Bowen ratio and Penman Australian Californian tests. 21st Century Irrigation Systems, 14-159.

124. Pruitt, W. O., Swann, B. D., Held, A., Sutton, B., Matista, A., and Hsiao, T. C., 1987. Evaluation of Bowen ratio and Penman evapotranspiration equations; Studies in New South Wales Australia and California USA In: James, L. G and English, M. J. (Eds.) Irrigation systems for the 21st century. A.S.C.E, New York.

125. Rao, K. J., Wyngaad, J. C., and Cote, A. R., 1974. Local advection of temperature, momentum, sensible and latent heat in micrometeorology. Boundary-Layer Meteorol. 7:331-348

126. Raupach, M. R., and Legg, B. J., 1984. The uses and limitations of flux-gradient relationships in micrometeorology. In Sharma, M. L. (Ed.) Evapotransipration from Plant Communities. Elsevier, Amsterdam.

127. Revfeim, K. J. A., and Jordan, R. B., 1976. Precision of evaporation measurement using the Bowen ratio. Boundary-Layer Meteorol., 10: 97-111.

128. Rider, N. E., 1954. Eddy diffusion of momentum, water vapour, and heat near the ground. Phil. Trans, Royal Soc. Series A., 246: 481-501.

129. Rider, N. E., and Robinson, G. D., 1951. A study of the transfer of heat and water vapour above a surface of short grass. Quart. J. Roy. Meteorol. Soc., 77: 375-401.

130. Ripley, E. A., and Redman, R. E., 1976. Grassland. In Monteith, J. L. (Ed.) Vegetation and the atmosphere. Vol. 1. Principles. Acad. Press. London pp. 349-398.

131. Rosenberg, N. J., 1969. Seasonal patterns in evapotranspiration by irrigated alfalfa in Central Great Plains. Agron. J., 61: 879-886.

132. Rosenberg, N. J., 1974. Microclimate: the Biological Environment (Second edition). Wiley and Sons, New York.

133. Rosenberg, N. J., Blad, B. L., and Verma, S. B., 1983. Microclimate: the Biological Environment (2 nd edition). Wiley and Sons, New York.

134. Sadler, E. J., and van Bavel, C. H. M., 1982. A simple method to calibrate an infrared thermometer. Agron. J., 74: 1096-1098.

135. Salisbury, F. B., and Savage, M. J., 1995. Energy transfer. *In* F.B. Salisbury (ed) Units, Symbols and Terminology for Plant Physiology: A Reference for Presentation of Research Results in the Plant Sciences, Chapter 7, 65-71. Oxford University Press, Oxford.

136. Savage, M. J., 1979. Use of the international system of units in the plant sciences. HortScience, 14: 492-495.

137. Savage, M. J., 1980. An inexpensive resistance thermometer for air temperature, soil temperature and relative humidity measurements. Agrochemophysica, 12: 1-3.

138. Savage, M. J., 1988. Radiation measurement in environmental plant physiology. S. Afr. J. Sci., 84: 836-843.

139. Savage, M. J., 1995. Basic thermodynamic quantities. *In* F.B. Salisbury (ed) Units, Symbols and Terminology for Plant Physiology: A Reference for Presentation of Research Results in the Plant Sciences, Chapter 4, 45-54. Oxford University Press, Oxford.

140. Savage, M. J., Campbell, G. S., and Heilman, J. L., 1993. Calibration of net radiometers and infra red thermometers. Abstracts of the Tenth Annual Conference of the South African Society of Atmospheric Sciences, pp. 45.

141. Savage, M. J., Everson, C. S. and, Metelerkamp, B. R.,1995. Evaporation measurement comparisons and advective influences using Bowen ratio, lysimetric and eddy correlation methods. Proceedings of the Southern African Irrigation Symposium, 160-166.

142. Savage, M. J. and Heilman, J. L., 1993a. Aerodynamic measurement of evaporation. *In* S.A. Lorentz, S.W. Kienzle and M.C. Dent (eds). Proceedings of the Sixth South African National Hydrological Symposium, Volume 1: 63-70.

143. Savage, M. J. and Heilman, J. L., 1993b. Field use aspects and laboratory calibration of net radiometers and infra-red thermometers. South African Society of Atmospheric Sciences, Midrand, Transvaal.

144. Savage, M. J., Heilman, J. L., and McInnes, K. J., 1993. Comparison between a surface temperature and eddy correlation method for sensible heat transfer above a grassland surface. Abstracts of the Tenth Annual Conference of the South African Society of Atmospheric Sciences, P. 41.

145. Savage, M.J., Heilman, J. L., McInnes, K. J., and Gesch, R. W., 1993. Evaporation and micrometeorological measurements in a vineyard using the eddy correlation technique. Supplement to Journal of the South African Society for Horticultural Sciences, 3: 20.

146. Savage, M.J., Heilman, J. L., McInnes, K. J., and Gesch, R. W., 1992. Evaporation and turbulence measurements in a vineyard. Abstracts of the 84 th Agronomy Meetings, Minneapolis, Minnesota, P. 22.

147. Savage, M.J., Heilman, J. L., McInnes, K. J., and Gesch, R. W., 1995a. Placement height of eddy correlation sensors above a short grassland surface. Agric. For. Meteorol., 74: 195-204.

148. Savage, M. J., Heilman, J. L., and McInnes, K. J., 1995b. The "footprints" of eddy correlation sensible heat flux density, and other micrometeorological measurements. South African Journal of Science 92, 137-142.

149. Savage, M. J., Metelerkamp, B. R., Everson, C. S.,1994. A back-calculation method for determining all terms of the Penman Monteith equation using Bowen Ratio measurements I: Theory and application. Southern African Society for Crop Production, Cedara, Natal. P. 58.

150. Schuepp, P. H., Leclerc, M. Y., Macpherson, J.I . and Desjardins, R. L., 1990. Footprint prediction of scalar fluxes from analytical solutions of the diffusion equation. Boundary-Layer Meteorol., 50: 355-373.

151. Schulze R. E., 1975. Catchment evaporation in the Natal Drakensberg. Unpublished M.Sc. thesis. University of Natal, Pietermaritzburg

152. Sellers, W. D., 1965. Physical Climatology. Univ. of Chicago Press, Chicago. pp. 272.

153. Selirio, I. S., 1975. Study of variation of apparent Bowen ratio with height above a cornfield. Ph. D. Thesis, University of Guelph. pp. 77. (Available from National Library Ottawa, Canada).

154. Sharma, M. L., 1987. Estimating evapotranspiration. Adv. Irrig., 4: 213-281.

155. Sinclair, T. R., Allen, L. H., and Lemon, E. R., 1975. An analysis of errors in the calculation of energy flux densities above vegetation by a Bowen-ratio profile method. Boundary-Layer Meteorol., 8: 129-139.

156. Slayter, R. O., 1967. Plant-water Relationships. Academic Press, London.

157. Slayter, R. O., and McIlroy, I. C., 1967. Practical Micrometeorology. CSIRO, Melbourne, Australia.

158. Smith, M., 1991. Report on the expert consultation on procedures for revision of FAO guidelines for crop water requirements. Food and Agriculture Organization of the United Nations, Rome, Italy.

159. Spittlehouse, D. L., and Black, T. A., 1980. Evaluation of the Bowen ratio - energy balance method for determing forest evapotranspiration. Atmosphere-Ocean, 18: 98-116.

160. Suomi, V. E., and Tanner, C. B., 1958. Evapotranspiration from a heat-budget measurements over a field crop. Trans. Am. Geophys. Union 39:298-304

161. Swinbank, W. C., 1951. The measurement of vertical transfer of heat and water vapor by eddies in the lower atmosphere. J. Meteorol., 8(3): 135-145.

162. Swinbank, W. C., and Dyer, A. J., 1967. An experimental study in micrometeorology. Quart. J. Roy. Meteorol. Soc., 93: 494-500.

163. Tanner, B. D., 1988. Use requirements for Bowen ratio and eddy correlation determination of evapotranspiration. Irrig. Drain. Div., 1-12.

164. Tanner, B. D., 1984. Measurements with a portable eddy correlation system. International Symposium-Dr Franz Sauberer. October: 23-25.

165. Tanner, B. D. and Greene, J. P., 1989. Measurements of sensible heat and water vapor fluxes using eddy correlation methods. Final Report to U.S. Army Dugway Proving Grounds Dugway, UT, Contract No. DAAD09-87-D-0038.

166. Tanner, B. D., Greene, J. P., and Bingham, G. E., 1987. A Bowen ratio design for long term measurements. Am. Soc. Agric. Eng. Tech. Paper no. 87-2503, American Society Agricultural Engineers St. Joseph, MI.

167. Tanner, B. D., Tanner, G. S., and Dugas, W. A., 1985. Evaluation of an operational eddy correlation system for evapotranspiration measurements. Amer. Soc. Agric. Eng. 1-14.

168. Tanner, C. B., 1960. Energy balance approach to evapotranspiration from crops. Soil Sci. Proc. of Amer., 24: 1-9.

169. Tanner, C. B., and Fuchs, M., 1969. Error analysis of Bowen ratio measured by differential psychrometry. Agric. Meteorol., 7: 329-334.

170. Tanner, C. B., 1963. Basic instrumentation and measurements for plant environmental and micrometeorology. Soil Bulletin, 6: 1-32.

171. Tanner, C. B., 1960. A simple aero-heat budget method for determining daily evapotranspiration. International Congress of Soil Science, 203-208.

172. Tanner, B. D., Tanner, G. S., Dugas, W. A., and Bland, B. L., 1985. Evaluation of an operational eddy correlation system for evapotranspiration measurements. Amer. Soc. Agric. Eng.

173. Tanner, C. B., and Pelton, W. L., 1960. Potential evapotranspiration by the approximate energy balance method of Penman. J. Geophys. Res., 65: 3391-3399.

174. Tanner, B. D., Tanner, G. S., Dugas, W. A., Campbell, E. C. and Bland, B. L., 1985. Evaluation of an operational eddy correlation system for evapotranspiration measurements. Trans. Amer. Soc. Agric. Eng., 1-14.

175. Tennekes, H., and Lumley, J. L., 1972. A first course in turbulence. MIT Press, Cambridge, Mass., USA.

176. Thom, A. S., 1972. Momentum, mass and heat exchange of vegetation. Quart. J. Roy. Meteorol. Soc., 98: 124-134.

177. Thom, A. S., 1975. Momentum, mass and heat exchange in plant communities. In Monteith, J.L. (Ed.) Vegetation and the atmosphere. Vol. 1. Principles. Acad. Press. London pp. 57-109.

178. Unwin, D. M., 1980. Microclimate Measurement for Ecologists. Academic Press.

179. van Bavel, C. H. M., 1967. Changes in canopy resistance to water loss from alfalfa induced by soil water depletion. Agric. Meteorol., 4: 165-176.

180. Verma, S. B., Rosenberg, N. J., and Blad, B. L., 1978. Turbulent exchange coefficients for sensible heat and water vapour under advective conditions. J. Appl. Meteorol., 17: 330-338.

181. Verma, S. B., Ullman, F. G., Billesbach, D., Clement, R. J., and Kim, J., 1992. Eddy correlation measurements of methane flux in a northern peatland ecosystem. Boundary-Layer Meteorol., 58: 289-304.

182. Warhaft, Z., 1976. Heat and moisture in the stratified boundary layer. Quart. J. Roy. Meteorol. Soc. 102:703-704.

183. Weast, R. C., 1989. CRC Handbbok of Chemistry and Physics. CRC Press Inc. Florida, USA.

184. Webb, E. K., 1960. On estimating evaporation with fluctuating Bowen ratio. J. Geophys. Res. 65: 3415-3417.

185. Webb, E. K., 1965. Aerial microclimates In Meteorological Monographs, 6(28): Agric. Meteorol. American Meteorological Society.

186. Webb, E. K., 1970. Profile relationships: the log-linear range and extension to strong stability. Quart. J. Roy. Meteorol. Soc., 96: 67-90.

187. Wilson, J. D., 1982. An approximate analytical solution for the diffusion equation for short-range dispersion from a continous ground-level source. Boundary-Layer Meteorol. 23: 85-103.

188. Yeh, G. T., and Brutsaert, W. H., 1971. A solution for simultaneous turbulent heat and vapour transfer between a water surface and the atmosphere. Boundary-Layer Meteorol., 2: 64-82.

Bowen ratio br1old.dld/br2new.dld: 16/6/1997

The sample Bowen ratio program supplied by Campbell Scientific may not function with the newer 21X dataloggers with PROM's OSX 1.1 and OSX 2.1. The change involves the intermediate processing disable flag (flag 9). The program listed here will work with both old and new dataloggers.

Important note: 1. In order to continuously check the validity of the dewpoint temperature measurements, a 207 relative humidity sensor must be connected; 2. mirror cleanliness and bias must be checked weekly; 3. most of the problems with data loss have been due to flat batteries, accidental switching off of the battery supply (by bumping) or the fuse problem; 4. on occasion, the incorrect day of year has been entered in to the data logger when there has been a power interruption; 5. when there is a power interruption, memory must be repartitioned using the *A option; 6. comparisons between the net radiometer and a standard net radiometer are crucial and should be performed quarterly.

Times for 21X. Table 1: 590 ms; total time for standard deviations = 155 ms; time TC temp (SE)/ms = 40 + 23.2 * Rep; time TC temp (DIFF)/ms = 39.2 + 42.7 * Rep; time full bridge/ms = 41.8 + 73 * Rep; time standard deviation/ms = 2.5 + 17.7 * Rep

Flag Usage. Set flag 6 to initiate program by switching on pump: press *6 A D 6 The response to setting the flag may not be immediate.; Set flag 7 to terminate program by switching on pump: press *7 A D 7 May not be an immediate response to setting this flag.

Mirror and pump on/off routine. Input location 29 is for minutes into day for switch on time; 30 is for minutes into day for switch off time; 31 is for current time (minutes into day). Press *A 31 A *0 to repartition input memory allocation from default of 28 input locations to 31 input locations.

```
;{21X}
;Program: 17 Apr 1995
;Flags Used in Program:
;1 High to disable averaging while the mirror stabilizes.
;2 Active air intake: High - Upper, Low - Lower.
;3 Battery subroutine: High - Pump and Mirror are off.
;4 Set high to output data up to current time and disable
; processing. Set low to resume processing.
;5 Used by the program when the operator disables the station.
;6 Set high to turn on the pump and mirror.
;7 Set high to turn off the pump and mirror.
;8 Set high at the end of a 15 minute interval. Used to average
; soil temperature during the last five minutes of a 20 minute
; interval.
*Table 1 Program
 01: 1.0    Execution Interval (seconds)
;Measure panel temperature, air temperature, and
;cooled mirror PRT.
1: Internal Temperature (P17)
 1: 1     Loc [ Pan_Temp ]
2: Thermocouple Temp (SE) (P13)
 1: 1     Reps
 2: 1     5 mV Slow Range
 3: 8     In Chan
 4: 2     Type E (Chromel-Constantan)
 5: 1     Ref Temp Loc [ Pan_Temp ]
 6: 3     Loc [ Low_TC  ]
 7: 1     Mult
 8: 0     Offset
3: Thermocouple Temp (DIFF) (P14)
 1: 1     Reps
 2: 1     5 mV Slow Range
 3: 4     In Chan
 4: 2     Type E (Chromel-Constantan)
 5: 3     Ref Temp Loc [ Low_TC  ]
 6: 2     Loc [ Upp_TC  ]
 7: 1     Mult
 8: 0     Offset
4: Full Bridge (P6)
 1: 1     Reps
 2: 1     5 mV Slow Range
 3: 2     In Chan
 4: 1     Excite all reps w/Exchan 1
 5: 5000  mV Excitation
 6: 8     Loc [ Dew_Point ]
 7: 0.001  Mult
 8: 0.00498  Offset
;Calculate temperature gradient, dew point
;temperature, and vapor pressure.
5: Z=X-Y (P35)
 1: 3     X Loc [ Low_TC  ]
 2: 2     Y Loc [ Upp_TC  ]
 3: 4     Z Loc [ Del_T  ]
6: BR Transform Rf[X/(1-X)] (P59)
 1: 1     Reps
 2: 8     Loc [ Dew_Point ]
 3: 200   Mult (Rf)
7: Temperature RTD (P16)
 1: 1     Reps
 2: 8     R/RO Loc [ Dew_Point ]
 3: 8     Loc [ Dew_Point ]
 4: 1     Mult
 5: 0     Offset
8: Saturation Vapor Pressure (P56)
 1: 8     Temperature Loc [ Dew_Point ]
 2: 9     Loc [ Vap_Press ]
;Output Processing
9: If Flag/Port (P91)
 1: 15    Do if Flag 5 is High
 2: 0     Go to end of Program Table
10: If time is (P92)
 1: 0     Minutes into a
 2: 20    Minute Interval
 3: 10    Set Output Flag High
11: Set Active Storage Area (P80)
 1: 1     Final Storage
 2: 110   Array ID or Loc [ _________ ]
;User can set flag 4, to output data up to the current
;time and disable further output processing while
;working on the system.
12: If Flag/Port (P91)
 1: 14    Do if Flag 4 is High
 2: 30    Then Do
13: Do (P86)
 1: 10    Set Output Flag High
14: Set Active Storage Area (P80)
 1: 1     Final Storage
 2: 112   Array ID or Loc [ _________ ]
15: Do (P86)
 1: 15    Set Flag 5 High
16: End (P95)
17: Real Time (P77)
 1: 110   Day,Hour/Minute
18: Sample (P70)
 1: 1     Reps
 2: 1     Loc [ Pan_Temp ]
19: Average (P71)
 1: 2     Reps
 2: 3     Loc [ Low_TC  ]
20: If Flag/Port (P91)
 1: 12    Do if Flag 2 is High
 2: 30    Then Do
21: Do (P86)
 1: 19    Set Flag 9 High
22: Else (P94)
23: If Flag/Port (P91)
 1: 11    Do if Flag 1 is High
 2: 19    Set Flag 9 High
24: End (P95)
25: Average (P71)
 1: 2     Reps
 2: 8     Loc [ Dew_Point ]
26: Do (P86)
 1: 29    Set Flag 9 Low
27: If Flag/Port (P91)
 1: 22    Do if Flag 2 is Low
 2: 30    Then Do
28: Do (P86)
 1: 19    Set Flag 9 High
29: Else (P94)
30: If Flag/Port (P91)
 1: 11    Do if Flag 1 is High
 2: 19    Set Flag 9 High
31: End (P95)
32: Average (P71)
 1: 2     Reps
 2: 8     Loc [ Dew_Point ]
*Table 2 Program
 01: 10.0   Execution Interval (seconds)
;Time the cooled mirrors settling time.
1: Time (P18)
 1: 0     Tenths of seconds into current minute (maximum 600)
 2: 400   Mod/By
 3: 11    Loc [ s_into_m ]
2: IF (X<=>F) (P89)
 1: 11    X Loc [ s_into_m ]
 2: 4     <
 3: 100   F
 4: 21    Set Flag 1 Low
;Check for system disable or re-enable.
3: If Flag/Port (P91)
 1: 15    Do if Flag 5 is High
 2: 30    Then Do
4: If Flag/Port (P91)
 1: 24    Do if Flag 4 is Low
 2: 1     Call Subroutine 1
5: End (P95)
;Switch the cooled mirror intake every two minutes.
6: If time is (P92)
 1: 0     Minutes into a
 2: 2     Minute Interval
 3: 30    Then Do
7: Do (P86)
 1: 11    Set Flag 1 High
8: If time is (P92)
 1: 0     Minutes into a
 2: 4     Minute Interval
 3: 30    Then Do
9: Set Port (P20)
 1: 1     Set High
 2: 2     Port Number
10: Do (P86)
 1: 12    Set Flag 2 High
11: Else (P94)
12: Set Port (P20)
 1: 1     Set High
 2: 1     Port Number
13: Do (P86)
 1: 22    Set Flag 2 Low
14: End (P95)
15: Excitation with Delay (P22)
 1: 1     Ex Chan
 2: 0     Delay w/Ex (units = 0.01 sec)
 3: 2     Delay After Ex (units = 0.01 sec)
 4: 0     mV Excitation
16: Set Port (P20)
 1: 0     Set Low
 2: 1     Port Number
17: Set Port (P20)
 1: 0     Set Low
 2: 2     Port Number
18: End (P95)
;Measure the battery voltage, net radiation, soil
;temperature, soil heat flux, wind speed, and
;wind direction.
19: Batt Voltage (P10)
 1: 10    Loc [ Battery  ]
20: Volt (Diff) (P2)
 1: 1     Reps
 2: 3     50 mV Slow Range
 3: 1     In Chan
 4: 15    Loc [ Inet     ]
 5: 1     Mult
 6: 0     Offset
21: IF (X<=>F) (P89)
 1: 15    X Loc [ Inet     ]
 2: 3     >=
 3: 0     F
 4: 30    Then Do
;Apply the positive multiplier and wind correction.
22: Do (P86)
 1: 3     Call Subroutine 3
23: Else (P94)
;Apply the negative multiplier and wind correction.
24: Do (P86)
 1: 4     Call Subroutine 4
25: End (P95)
26: Volts (SE) (P1)
 1: 2     Reps
 2: 2     15 mV Slow Range
 3: 9     In Chan
 4: 16    Loc [ SHF1    ]
 5: 1     Mult
 6: 0     Offset
27: Thermocouple Temp (DIFF) (P14)
 1: 1     Reps
 2: 1     5 mV Slow Range
 3: 3     In Chan
 4: 2     Type E (Chromel-Constantan)
 5: 1     Ref Temp Loc [ Pan_Temp ]
 6: 20    Loc [ Tsoil   ]
 7: 1     Mult
 8: 0     Offset
28: Z=X*F (P37)
 1: 16    X Loc [ SHF1    ]
 2: 1     F
 3: 16    Z Loc [ SHF1    ]
29: Z=X*F (P37)
 1: 17    X Loc [ SHF2    ]
 2: 1     F
 3: 17    Z Loc [ SHF2    ]
30: Pulse (P3)
 1: 1     Reps
```

```
2: 1      Pulse Input Chan
3: 21     Low Level AC, Output Hz
4: 5      Loc [ Wnd_Spd  ]
5: 0.75   Mult
6: 0.2    Offset
31: AC Half Bridge (P5)
 1: 1     Reps
 2: 5     5000 mV Slow Range
 3: 11    In Chan
 4: 2     Excite all reps w/Exchan 2
 5: 5000  mV Excitation
 6: 6     Loc [ Win_Dir  ]
 7: 355   Mult
 8: 0     Offset
;Soil temperature is only averaged over the last five
;minutes of the output interval in order to have the
;change in temperature during the interval. An average
;rather than a sample is used to avoid perturbation by
;an anomalous reading.
32: If time is (P92)
 1: 15    Minutes into a
 2: 20    Minute Interval
 3: 18    Set Flag 8 High
33: If Flag/Port (P91)
 1: 18    Do if Flag 8 is High
 2: 30    Then Do
34: Z=X+Y (P33)
 1: 20    X Loc [ Tsoil   ]
 2: 21    Y Loc [ Ts_tot  ]
 3: 21    Z Loc [ Ts_tot  ]
35: Z=Z+1 (P32)
 1: 22    Z Loc [ num_smpls ]
36: End (P95)
;Output average net radiation and heat flux, average soil
;temperature for the last five minutes, the change in soil
;temperature, wind speed, wind direction, and standard
;deviation of wind direction.
37: If time is (P92)
 1: 0     Minutes into a
 2: 20    Minute Interval
 3: 30    Then Do
38: Z=X/Y (P38)
 1: 21    X Loc [ Ts_tot  ]
 2: 22    Y Loc [ num_smpls ]
 3: 24    Z Loc [ avg_Ts  ]
39: Z=X-Y (P35)
 1: 24    X Loc [ avg_Ts  ]
 2: 23    Y Loc [ prev_avg ]
 3: 25    Z Loc [ Del_Ts  ]
40: Z=X (P31)
 1: 24    X Loc [ avg_Ts  ]
 2: 23    Z Loc [ prev_avg ]
41: Z=F (P30)
 1: 0     F
 2: 21    Z Loc [ Ts_tot  ]
42: Z=F (P30)
 1: 0     F
 2: 22    Z Loc [ num_smpls ]
43: Do (P86)
 1: 28    Set Flag 8 Low
44: Do (P86)
 1: 10    Set Output Flag High
45: Set Active Storage Area (P80)
 1: 1     Final Storage
 2: 237   Array ID or Loc [ ________ ]
46: End (P95)
47: Real Time (P77)
 1: 110   Day,Hour/Minute
48: Average (P71)
 1: 3     Reps
 2: 15    Loc [ Inet      ]
49: Sample (P70)
 1: 2     Reps
 2: 24    Loc [ avg_Ts  ]
50: Wind Vector (P69)
 1: 1     Reps
 2: 30    Samples per Sub-Interval
 3: 00    Polar Sensor/(S, D1, SD1)
 4: 5     Wind Speed/East Loc [ Wnd_Spd ]
 5: 6     Wind Direction/North Loc [ Win_Dir ]
;Insert addition measurement/output programming here.
51: Do (P86)
 1: 2     Call Subroutine 2
*Table 3 Subroutines
;Subroutine 1, output the time that the processing is re-enabled.
1: Beginning of Subroutine (P85)
 1: 1     Subroutine 1
2: Do (P86)
 1: 25    Set Flag 5 Low
3: Do (P86)
 1: 10    Set Output Flag High
4: Set Active Storage Area (P80)
 1: 1     Final Storage
 2: 303   Array ID or Loc [ ________ ]
5: Real Time (P77)
 1: 110   Day,Hour/Minute
6: End (P95)
;Subroutine 2, power the pump and cooled mirror in
;response to a user flag. Turn the pump and cooled
;mirror off if the battery is <11.25 volts and switch it on
;again if >12 volts. Also turns off pump at 1140 min
(19h00) and on at 300 min (05h00)
7: Beginning of Subroutine (P85)
 1: 2     Subroutine 2
8: P30 Z = F
01: 300 F
02: 29 Z Loc :
9: P30 Z = F
01: 1140 F
02: 30 Z Loc :
10: P18 Time
01: 1 Minutes into current day (maximum 1440)
02: 0 Mod/by
03: 31 Loc :
11: P88 If X < = > Y
01: 29 X Loc
02: 1 =
03: 31 Y Loc
04: 16 Set flag 6
12: Set Port (P20)
 1: 16    Set According to Flag 6
 2: 3     Port Number
13: Do (P86)
 1: 26    Set Flag 6 Low
14: P88 If X < = > Y
01: 30 X Loc
02: 1 =
03: 31 Y Loc
04: 17 Set flag 7
15: Set Port (P20)
 1: 17    Set According to Flag 7
 2: 4     Port Number
16: Do (P86)
 1: 27    Set Flag 7 Low
17: IF (X<=>F) (P89)
 1: 10    X Loc [ Battery  ]
 2: 4     <
 3: 11.25 F
 4: 30    Then Do
18: If Flag/Port (P91)
 1: 23    Do if Flag 3 is Low
 2: 30    Then Do
19: Set Port (P20)
 1: 1     Set High
 2: 4     Port Number
20: Excitation with Delay (P22)
 1: 4     Ex Chan
 2: 0     Delay w/Ex (units = 0.01 sec)
 3: 1     Delay After Ex (units = 0.01 sec)
 4: 0     mV Excitation
21: Set Port (P20)
 1: 0     Set Low
 2: 4     Port Number
22: Do (P86)
 1: 13    Set Flag 3 High
23: Do (P86)
 1: 10    Set Output Flag High
24: Set Active Storage Area (P80)
 1: 1     Final Storage
 2: 317   Array ID or Loc [ ________ ]
25: Real Time (P77)
 1: 1220  Year, Day (current day at midnight),
Hour/Minute (24h00 at midnight)
26: Sample (P70)
 1: 1     Reps
 2: 10    Loc [ Battery  ]
27: End (P95)
28: Else (P94)
29: If Flag/Port (P91)
 1: 13    Do if Flag 3 is High
 2: 30    Then Do
30: IF (X<=>F) (P89)
 1: 10    X Loc [ Battery  ]
 2: 3     >=
 3: 12    F
 4: 30    Then Do
31: Set Port (P20)
 1: 1     Set High
 2: 3     Port Number
32: Excitation with Delay (P22)
 1: 4     Ex Chan
 2: 0     Delay w/Ex (units = 0.01 sec)
 3: 1     Delay After Ex (units = 0.01 sec)
 4: 0     mV Excitation
33: Set Port (P20)
 1: 0     Set Low
 2: 3     Port Number
34: Do (P86)
 1: 23    Set Flag 3 Low
35: Do (P86)
 1: 10    Set Output Flag High
36: Set Active Storage Area (P80)
 1: 1     Final Storage
 2: 328   Array ID or Loc [ ________ ]
37: Real Time (P77)
 1: 110   Day,Hour/Minute
38: Sample (P70)
 1: 1     Reps
 2: 10    Loc [ Battery  ]
39: End (P95)
40: End (P95)
41: End (P95)
42: End (P95)
;Apply the positive calibration and wind speed
;corrections to the measured net radiation.
43: Beginning of Subroutine (P85)
 1: 3     Subroutine 3
44: Z=X*F (P37)
 1: 5     X Loc [ Wnd_Spd  ]
 2: 0.2   F
 3: 14    Z Loc [ C       ]
45: Z=X*F (P37)
 1: 14    X Loc [ C       ]
 2: 0.066 F
 3: 12    Z Loc [ A       ]
46: Z=X+F (P34)
 1: 14    X Loc [ C       ]
 2: 0.066 F
 3: 13    Z Loc [ B       ]
47: Z=X/Y (P38)
 1: 12    X Loc [ A       ]
 2: 13    Y Loc [ B       ]
 3: 7     Z Loc [ Corr_Fact ]
48: Z=Z+1 (P32)
 1: 7     Z Loc [ Corr_Fact ]
49: Z=X*F (P37)
 1: 15    X Loc [ Inet    ]
 2: 1     F
 3: 15    Z Loc [ Inet    ]
50: Z=X*Y (P36)
 1: 15    X Loc [ Inet    ]
 2: 7     Y Loc [ Corr_Fact ]
 3: 15    Z Loc [ Inet    ]
51: End (P95)
;Apply the negative calibration and wind speed
;correction to the measured net radiation.
52: Beginning of Subroutine (P85)
 1: 4     Subroutine 4
53: Z=X*F (P37)
 1: 5     X Loc [ Wnd_Spd  ]
 2: 0.00174 F
 3: 12    Z Loc [ A       ]
54: Z=X+F (P34)
 1: 12    X Loc [ A       ]
 2: 0.99755 F
 3: 7     Z Loc [ Corr_Fact ]
55: Z=X*F (P37)
 1: 15    X Loc [ Inet    ]
 2: 1     F
 3: 15    Z Loc [ Inet    ]
56: Z=X*Y (P36)
 1: 15    X Loc [ Inet    ]
 2: 7     Y Loc [ Corr_Fact ]
 3: 15    Z Loc [ Inet    ]
57: End (P95)

End Program

-Input Locations-
1 Pan_Temp  1 3 1
2 Upp_TC    1 1 1
3 Low_TC    1 3 1
4 Del_T     1 2 1
5 Wnd_Spd   0 3 1
```

6 Win_Dir 0 1 1
7 Corr_Fact 0 3 3
8 Dew_Point 1 5 3
9 Vap_Press 1 2 1
10 Battery 1 4 1
11 s_into_m 1 1 1
12 A 0 2 2
13 B 0 1 1
14 C 0 2 1
15 Inet 0 8 4
16 SHF1 5 2 2
17 SHF2 17 2 2
18 ________ 0 0 0
19 ________ 0 0 0
20 Tsoil 1 1 1
21 Ts_tot 1 2 2
22 num_smpls 1 2 2
23 prev_avg 1 1 1
24 avg_Ts 1 3 1
25 Del_Ts 1 2 1
26 ________ 0 0 0
27 ________ 0 0 0
28 ________ 0 0 0

Flag usage

To initiate program, set flags: set flag 6 high to turn on pump and mirror by pressing *6 A D 6 Response to setting the flag may not be immediate.
To switch system off, set flag 7 high to turn off pump and mirror by pressing *6 A D 7 Response to setting this flag may not be immediate.
Flag 4 is set high to output to current time and disable data processing and set low to resume. Press *6 A D 4 to set high to disable and low to resume.
Flag 1: High to disable averaging while mirror stabilizes; Flag 2: Active air intake high for upper and low for lower; Flag 3: Battery subroutine high for pump and mirror off; Flag 4: Set high to output to current time and disable processing and set low to resume; Flag 5: Used by program during user disable; Flag 6: Pulse high to turn on pump and mirror; Flag 7: Pulse high to turn off pump and mirror; Flag 8: High at the end of intervals while soil temperature is averaged; Flag 9: intermediate processing flag

Some 21X processing instructions

30: Z = F; 31: Z = X; 32: Z = Z + 1; 33: Z = X + Y; 34: Z = X + F; 35: Z = X - Y; 36: Z = X * Y; 37: Z = X * F; 38: Z = X/Y; 40: Z = ln X

Sensor connections for 21X:

Analogue
1 H Rnet + red
1 L Rnet - black
2 H Cooled mirror PRT green
2 L Cooled mirror PRT white
2 G Cooled mirror PRT black
3 H Soil temp TC chromel purple
3 L Soil temp TC constantan red
4 H Upper 0.003 TC chromel purple
4 L Lower 0.003 TC chromel purple
4 G Air temp TC's constantan red
5 H Soil flux plate #1 high red
5 L Soil flux plate #2 high red
5 G Soil flux plates ground black
For BRUNP
6 H Advection TC 1 copper red
6 L Advection TC 2 copper red
6 G Advection TC 1, 2 blue
7 H Advection TC 3 copper red
7 G Advection TC 3 blue
For BRCSIR
6 H 207 Temp red
6 L 207 RH white
6 G green
Excitation
1 Cooled mirror excitation red
2 Switched analogue out for 207 RH probe black
Control ports
1 Pulse for lower air intake green
2 Pulse for upper air intake white
3 Pulse to turn on power to mirror/ pump (flag 6) black
4 Pulse to turn off power to mirror/ pump (flag 7) red
G Ground wire clear
Pulse ports
1 2 3 Wind anemometer

The 207 relative humidity sensor wiring

Note: never apply a DC voltage to this sensor. Sensor will be polarized causing irreparable damage. Only AC voltages with of at least 20 Hz with a zero DC component should be used. Sustained operation on DC voltage or AC voltage with a DC component may result in a calibration shift.

When unit was supplied, red: T on ch S1; white: RH on ch S2; clear: ground; black: excit 1 (switched analogue out)

Wiring of first 207 probe purchased was extended with colour code changed: Red is now red; white is white; clear is now green (was orange but changed it); black is black. Wiring of second 207 probe purchased was red H, white L, purple G, black EX. This wire was extended with colour code changed: Red is now red; white is white; purple is now green; black is black. Datalogger instruction P11 is used to measure temperature and P12 for relative humidity for 207 probe. Instruction P11 provides AC excitation, makes a single ended voltage measurement and calculates temperature using a fifth order polynomial (multiplier of 1 and offset 0 if °C units are used). Instruction P12 provides AC excitation, makes a single ended voltage measurement, calculates relative humidity using a fifth order polynomial (multiplier of 1 and offset of 0 if relative humidity/% is to be displayed) and then performs required temperature compensation. The sensor must be grounded; nonsense data is collected otherwise.

Analogue
7 H 207 Temp red
7 L 207 RH white
7 G green/orange or purple
Excitation
1 Switched analogue out : ~~black~~

Instructions for save/load program from tape

Load from tape: *D 4A Monitor/ear connector of SC93A must be in EAR position of tape recorder and power to power socket of tape. Tape must be on play, not play/record. It seems that the new 21X cannot load programs from tape
Store on tape: *D 3A For Philips recorder, monitor/ear connector of SC93A in EAR position, power connector in power socket of tape and third connector in MIC position. For Tandy recorder, monitor/ear connector of SC93A in AUX position, power to power socket of tape and third connector in MIC position. Tape must be on play/record, not play

Modes

Modes to be set prior to unattended logging: Output option: *4 11 2 (for tape and printer on and 9600 baud); Set/display time option: *5 yy A ddd A hhmm A; Display/alter input storage: *6 Panel temperature; 2 T_{upp}; 3 T_{low}; 4 $T_{lower} - T_{upper}$;
For BRUNP only 5 Windspeed W of UNP BR system at 0,8 m; 6 Windspeed 4 m N of UNP logger at 2 m; 7 Windspeed W of UNP logger at 1,8 m;
For BRCSIR only 6 T_{107}; 7 e_{207}/kPa;
For both logger systems: 8 T_{dp}; 9 e (kPa); 10 Battery voltage; 11 s into min; 15 I_{net} (W m^{-2}); 16 F_s #1; 17 F_s #2; 20 T_s; 21 T_s integrated (5 min period); 22 No. of samples for T_s integration; 23 Previous T_s average; 24 Average T_s; 25 ΔT_s; 29 minutes on; 30 minutes off; 31 time of day (minutes)
For BRUNP only for part of 1990 26 27 28 TC 2, 4, 6 m (respectively) N of UNP logger at a height of 2 m (all TC's in UNP shields)
Display output storage: *7
Output storage can only be sensibly viewed 20 min after sensors have been connected to datalogger
1 110; 2 Day of year; 3 hhmm; 4 Sample panel temperature; 5 T_{low}; 6 Average $T_{low} - T_{upp}$; 7 Average $T_{dp\,low}$; 8 Average e_{low}; 9 Average $T_{dp\,upp}$; 10 Average e_{upp}
1 237; 2 Day of year; 3 hhmm; 4 Average I_{net}; 5 Average F_s #1; 6 Average F_s #2; 7 Average T_s (last 2 min); 8 Change in T_s from previous value;
For BRUNP 9 Windspeed W of UNP BR system at 0,8 m; 10 Windspeed 4 m N of UNP BR system at 2 m; 11 Windspeed W of UNP BR system at 1,8 m; 12 13 14 Advection TC 2 m, 4 m and 6 m from UNP Bowen ratio system respectively (at a height of 2 m)
For BRCSIR 11 T_{107}; 12 e_{207}/kPa
Data transfer to tape: *8
1. To check data transfer prior to unattended operation, press *8 3A 3A Tape should advance automatically.
2. To transfer part of memory ring, press *8 A 1 A A 3 A Format will be comma delineated ASCII.
Data transfer to computer: *9
1. To transfer part of the memory ring, press *9 A 1 A A 3 A The format for these data will be printable ASCII, not comma delineated ASCII

Tape checks

1. Power to power; EAR/MONITOR of SC93A to AUX; third connector to MIC;
2. Press *8 3A 3A to check and transfer last stored data to tape.

System operation

Air is drawn from both heights (flow rate of 0.4 l min^{-1}) with 2 l mixing chambers to yield a 5 min time constant. Every 2 min air being drawn through cooled mirror is switched from one height to the other. About 40 s is used for mirror stabilization on new T_{dp} and 1 min 20 s for measurements for an individual level for each 2 min cycle. T_{dp} is measured every 1 s and e averaged every 20 min.

Sensor accuracy

Resolution of T_{dp} is within 0.003 °C and stability within 0.05 °C yielding resolution in e of within 10 Pa. Datalogger resolution in T is 0.006 °C. Radiation error minimized by measuring $T_{low} - T_{upp}$ with neither sensor shielded.

Instrumentation details

1. Soil heat flux plates placed at a depth of 80 mm; 2. Soil temperature probes placed at a depth of 20 and 60 mm; 3. Windspeed measured at a height of 2 m; 4. Upper Bowen ratio arm height to not exceed 0.01 of the uniform upwind fetch; 5. Lower Bowen ratio arm to be placed above canopy; 6. Change air intake filters every 1 to 2 weeks. Only one filter is necessary. *Do not touch filters. use tweezers.* Filters have a blue separator which should not be used. Use white filter only. Filter consists of two layers. First layer (has a coarse and fibrous look) filters out particulate matter. Second layer filters out liquid water and appears shiny (manufactured from teflon). Shiny side should be on pump side and coarse side exposed to atmosphere. If flow rates do not set properly, blue separator should be removed as it is not allowing a sufficient flow of air; 7. Clean TC's frequently (cobwebs). Contamination of one thermojunction and not the other can cause errors; 8. Radiometer at a height of 1 m. Clean net radiometer domes of net radiometer with hair brush and distilled water frequently. Always replace both domes when replacing domes; Check colour of desiccant monthly but more often in rainy season; 9. Anemometer details in order of input storage location, output storage position, Casella serial number, position and calibration equation where W is in m s^{-1} and C is the average counts per 10 s:
1, 9, 558, W of UNP logger at 0,8 m; W = 0,19 + 6*C*0,03791
2, 10, 572, 4 m N of UNP logger at 2 m, W = 0,14 + 6*C*0,03726;
3, 11, 2141, W of UNP logger at 1,8 m, W = 0,1 + 6*C*0,02552
10. Clean mirror and adjust bias every 1 to 2 weeks; 11 Check the water vapour pressure of the 207 RH probe (input location 7) with that of the Bowen ratio system (input location 9); 12 Check the air temperature of the 207 RH probe (input location 6) with that of the Bowen ratio system (input locations 2 and 3).
Optical bias adjustment is normally preceded by cleaning of mirror.

3.4. Mirror Contamination
The DEW-10 uses a "submicron" filter to remove particular contaminants below 1 µm. Some contaminants on a molecular scale, particularly salts, may still be carried into the measurement cavity causing gradual contamination of mirror.
As mirror accumulates contaminants, reflectance decreases causing system to have a thinner layer of dew. Over a broad range of decrease in mirror reflectance there is a little influence over system accuracy. If contaminated mirror is not cleaned, system will fail to control at dew point.
Another effect caused by certain soluble contaminants is lowering of saturation vapour pressure. This slightly increases mirror temperature with respect to true dew point in order to maintain equilibrium with water vapour pressure of sampled atmosphere.
The mirror must be cleaned periodically to maintain system's stated accuracy. Cleaning of mirror surface is simple, does not deteriorate surface and maintains system at its specified accuracy over its life. DEW-10 has a built-in capability to check mirror reflectance. When mirror reflectance test is activated system gives the "acceptable" answer whenever decrease in reflectance is < 10 %. This percentage decrease is, by a safe margin, less than what would cause a deterioration in measurement accuracy. When mirror reflectance has decreased by > 10 % then system gives "unacceptable" and should be cleaned for accurate T_{dp} measurements.

4.4.1 Manual Mirror Contamination Test
Wait at least 120 s between turning off cooler and adjusting - essential for evapouration from mirror.
Manual mirror reflectance test requires a single pole momentary action normally open switch with LED across it. Switch and LED combination should be connected to terminals 16 and 1 of PCB #1 board. Test consists of depressing switch for a period of 120 s, releasing it and observing if LED turns on. If light turns on for at least a few seconds, mirror reflectance is acceptable. If light does not turn on when switch is released, clean mirror or replace unit.

5.2 Mirror Cleaning and Bias Adjustment
Adjustment of optical bias determines dew layer thickness on which system reaches its control point. Proper adjustment of this bias is essential; system will not control on excessively thick dew layer whereas controlling on a thin layer requires more frequent mirror cleaning.
1. Locate PCB #1 board and be certain power is applied to unit.
2. Shut off thermoelectric cooler by sliding switch SW1 towards nearest edge of the card.

3. Remove sensor system from its housing to gain access to mirror by a pulling and twisting motion.
4. Clean mirror in the measurement cavity using a cotton swab and a mixture of 40 % methanol and 60 % water. Remove excess cleaning fluid with a clean dry swab.
5. Return sensor shield; this will block ambient light from entering mirror cavity which is important for next step.
6. Using a screwdriver, turn potentiometer R34, located on top edge of PCB #1, CCW until red LED located near by extinguishes. Turn it CW slowly until same light just comes on. Wait at least 120 s between turning off cooler and before adjusting - essential for evapouration from mirror.
7. Return switch RSW1 to normal operating position. With two extra steps, the period between mirror cleaning can be extended:
8. Allow system to return to normal operation for 8 to 24 h.
9. Repeat steps 2 and 6 above and return SW1 to operate position.

For the newer Bowen ratio system, the procedure for testing for mirror cleanliness and setting of bias is as follows: 1. Press *6 A D 4 to disable output. ONE HAS TO REMEMBER TO THEN PRESS *6 A D 4 TO ENABLE OUTPUT WHEN THESE PROCEDURES ARE COMPLETED; 2. Press *6 8 A to display the dewpoint temperature; 3. Slide switch SW1 down. The red light should be off; 4. Wait 120 s until the dewpoint increases to the ambient temperature; 5. Switch the switch to the middle position. The red LED light should come on. If it does not, the mirror needs to be cleaned; 6. To set the mirror bias, slide the switch SW1 upwards. Wait 120 s for the dewpoint to increase to the ambient temperature. The light should come on. If not, turn potentiometer R34 CW until the red light just comes on. Then switch the switch to the middle position. If the light did come on, turn the potentiometer CCW until the light goes off and then *slowly CW until the light comes on. Then* switch the switch to the middle position.

Battery details

Use a 20 W solar panel and 70 A h battery capable of providing a continuous current of 300 to 350 mA.

What to do if the 21X power fails

1. Make a note in diary that power failed. Try and establish the cause of power dip and note this in diary as well; 2. Power up the datalogger; 3. Set the date and time by pressing *5 A 90 A 278 A 0927 A *0 to set the year at 1990, the day of year 278 (corresponding to 5 October) and a time of day of 09h27); 4. Download the datalogger program using a personal computer; 5. Alternatively, type in Bowen ratio program tables 1, 2 and 3 shown on the card. To type in program table 1, type *1 A 1 A {78 A 1 A} 13 A 1 A 1 A etc. and then *0 to compile it. The braces obviously cannot be typed and are used to indicate that the contents are only used for the UNP system. In a similar manner, type in table 2 and 3; 6. If the pump and mirror are being switched off at night and on in the early morning, repartition the memory. Press *A 31 A *0 to allow for 31 input storage memory allocations; 7. If the program has been typed in manually (as opposed to downloaded using a computer), set the enable final storage mode (*4 mode) by pressing *4 A 11 A 2 A *to set the tape and printer/computer on* (11) and the baud rate at 9600 (2); 8. To initiate the Bowen ratio program, press *6 A D 6 This will set flag 6 and start the pump; 9. Check the values of the input storage locations by pressing *7 A A A A A A etc. and examining these against the card.

Computation details using Split

Order of data after pass 1 (using bowmspa1 or bowceps1) is: 1 day of year; 2 time; 3 average $T_{low} - T_{upp}$; 4 e_{low}; 5 e_{upp}; 6 I_{net}; 7 average F_s #1; 8 average F_s #2; 9 change in T_s from previous value; 10 11 12 windspeed
Order of data after pass 2 (using bowenps2) is: 1 day of year; 2 time; 3 I_{net}; 4 F_s (plate + that above the plate); 5 Bowen ratio; 6 $L_v F_w$;
7 F_h; 8 F_s at 80 mm; 9 F_s stored above plate; 10 11 12 Windspeed 1, 2, 3; 13 14 15 Air temperature 1, 2, 3; Standard deviations

File name convention

For raw data: ddmmbynm.prn where dd is day of month, mm month of year, b Bowen ratio data, y is 0 for 1990, 1 for 1991, etc., n file number to be transferred, and m for Bowen ratio system of MJS (c for Colin's data). Date used is date data was captured from datalogger or tape recorder. 1103b01m.prn where 0 is for 1990 and 1 first file to be transferred. Psychrometer files are named: 1103p01m.prn and lysimeter files 1103l01c.prn. If Split is used for any of these files (≥ 1 passages), file name convention is: iiifffbm.ps1 where b is for Bowen ratio, m for Bowen ratio system of MJS (c for Colin's) and ps1 for SPLIT (pass 1); iii is first day of year of data and fff last DOY. Following final Split, file name convention is: dddeeebm.ps2 where ddd is initial DOY of data, eee final DOY, b for Bowen ratio data and y year.

Day of year conversion

Non-leap year 31 Jan: 31; 28 Feb: 59; 31 Mar: 90; 30 Apr: 120; 31 May: 151; 30 June: 181; 31 July: 212; 31 Aug: 243; 30 Sep: 273; 31 Oct: 304; 30 Nov: 334
Leap year 31 Jan: 31; 29 Feb: 60; 31 Mar: 91; 30 Apr: 121; 31 May: 152; 30 June: 182; 31 July: 213; 31 Aug: 244; 30 Sep: 274; 31 Oct: 305; 30 Nov: 335

Equipment/materials checklist

Tape measure; silica gel; net radiometer domes; filters; TC's; methanol; cotton buds; small screw driver, soldering iron; solder; toolbox; Bowen ratio card; spare tapes (2 C60's and 2 C90's for CR7X, 21X's); computer; boot up disks; spare disks; keys for gate; spare batteries; generator, petrol; Assmann hygrometer; distilled water; manual for mirror; hair brush and water for cleaning net radiometer domes

History and site details (Cathedral Peak)

Mirrors first cleaned on 20/6/90 (DOY 171). Bias adjusted; readjusted a week later
Net radiometer (UNP): blown over between 13 and 20/6/90 (DOY 164 and 171). Reinflated dome, replaced silica gel and moved both radiometers away from shadows. CSIR's mirror cleaned on 16/7/90 (DOY 197) and bias of both systems adjusted. Replaced domes of CSIR's net radiometer.
Canopy height at 20/6/1990 (DOY 164): 0,4 m
Bowen ratio arms were 1,0 and 1,8 m before 19/6/1990 (DOY 170). Heights for UNP system altered to 0,7 and 1,5 m on 19/6/90.
Advection TC's (UNP) connected 10/4/90 (DOY 100). Changed the lead wires of TC2 and TC3 around on 19/6/90 (DOY 163).
Anemometers (UNP) connected 10/4/90 (DOY 100)
CSIR's Bowen ratio mirror was recleaned on 16 July 1990 (DOY 197) and bias adjusted. The UNP mirror was found to be clean and the bias was adjusted.
Fetch BR systems are 51 m from road with about 26 m of uniform fetch below the road. The riparian zone is about 145 m from the road.
Burning dates: 30/8/90 DOY 243?)
Eddy correlation with Bowen ratio comparison: 6 and 8 November 1990. On 6 Nov, it was extremely windy but reasonably cloudless; on 8 November, calm and somewhat cloudless. Main problem for both days was that the low side of the sonic anemometer was not connected to low side of the fine wire thermocouple.
21X serial numbers of the old loggers: BRUNP S/N 6520 (proms 391B, 392E *A 60 72 19160 142 *B 20294 33080 9722.0 59355), BRCSIR S/N 5600 (proms 391B 392E *A 31 64 19234 *B 10643 33080 97220 36855); 21X lysimeter logger LYCSIR S/N 6587 (proms 574/2 575/2 576/2 *A 70 100 19084 68 *B 5967.0 65053 45425 52177); UNPPSY7X logger S/N 15697 (prom 405B sig 21136 prom 406D sig 15318 prom 408E sig 45679 I/O 357 sig 12196) *A 160 64 *B 17802 21136 15318 45679 1100; 21X serial numbers of the new UNP loggers: S/N 8068 (proms 6145, 6146, 6147) and S/N 8066 (proms 6145, 6146, 6147) are the latest type of 21X (standard deviation instruction P52 replaced by P92) received 24/9/1990
Changed PROM's of UNP 21X data loggers on 23/9/1991: serial number 8539 top left chip changed to 6146, top right 6145, bottom right 6070 with the result that logger can download program to tape; serial number 6520 top left chip kept 392E, top right 391B, bottom right 401F has the old PROM's with the result that logger can still download program to tape; serial number 8512 top left chip changed from 6363 to 6146, top right kept chip 6145, bottom right changed from 6147 to 6070 with the result that logger can download program to tape.

History and site details (UNP metsite upper)

Mirrors first cleaned on 12/7/94 (DOY 193). Bias adjusted; readjusted a week later
Replaced pump of BR2NEW.DLD end June 1994. Replaced pump of BR1OLD.DLD 13 July 1994. Entered in new active storage areas on 12 July 1994. Definitions 114 for br1old.dld for table 1 for 1994; 214 for br1old.dld for table 2 for 1994; 314 for br1old.dld for table 3 for 1994; 124 for br2new.dld table 1 for 1994; 224 for br2new.dld for table 2 for 1994; 324 for br2new.dld for table 3 for 1994; 134 br3co2.dld for table 1 for 1994; 234 for br3co2.dld for table 2 for 1994; 334 for br3co2.dld for table 3 for 1994; 144 for ec*.dld for table 1 for 1994; 154 for 3dlower.dld for 1994; 164 for 3dupper.dld for 1994; 174 for irt*.dld for table 1 for 1994

Use of storage modules

Data
The SM192 and the SM716 are identical except for their storage capacity which is 192 896 bytes (six 32k RAM chips), and 716672 bytes (16 extra chips) respectively. Up to eight datalogger programs may be stored on the SO.
To manually dump all data in a data logger to a storage module, use the necessary 9-pin connectors and type the following at the datalogger:
*9 30 A (for SM192/716 storage modules - 31 for a filemark)
1 A (start of dump); A (end of dump); 3 A (to start dumping).
To dump only the new data logger data, the pointer corresponding to the start of dumping has to have been previously recorded. If this pointer is say 45456, then typing *9 30 A 45457 A 3 A will transfer only the new data.
To routinely dump data to a SO permanently connected to a datalogger, ensure that there is a P96 command with a 30 option (for the SM192/716 SMs).
Programs
Use the *D mode with option 71 (for store/load/clear program from storage module):
1z to STORE program from logger to SO
2z to LOAD program from SO to logger
3z to clear program from SO
where z is a any number from 1 to 8 representing program #1 to #8. So, for example, *DA 71A 24 will transfer program 4 in SO to logger; *DA 71A 17 will transfer program 7 in logger to SO; *DA 71A 38 will clear program 8 of the SO.
Pre-17 July 1994
Order of dld programs in the storage modules: 1. 3l240594.dld (3D lower); 2. 3u240594.dld (3D upper); 3. tsurf.dld (IRT's); 4. b1r2505.dld (Bowen ratio, system on the left - newer BR system); 5. b2r2405.dld (Bowen ratio, system on the right - old Cath Peak system); 6. 210grpc.dld (AMET 210 group project on the met site data collection). All of these files, in this order were placed on the largest storage module on 14 June 1994. This storage module was connected to the second Bowen ratio system - this should be checked.
Post-17 July 1994
Order of dld programs in the storage modules:
1. BR1OLD.DLD; 2. BR2NEW.DLD; 3. 3DLOWER.DLD; 4. 3DUPPER.DLD; 5. IRT.DLD
M J Savage 13 July 1994 c:\campbell\pc208\bowen.chp boweno.wp c:\typeset\&campbel.sty

Eddy correlation system

Cautions

1. Sonic anemometer can be permanently damaged if tubes get wet;
2. the 100 mm path length of sonic anemometers allow sensor placement height at $6\pi 0.1 = 1.9$ m above canopy; 3. limitation in height is due to effect of acoustic reflections off of vegetation and the fact that only one eddy must be sensed; 4. theory requires that the mean vertical wind speed is 0 m s^{-1} over the averaging time period. Is this assumption correct?

Theory

To convert $\overline{w'T'}$ to sensible heat flux density F_h in W m^{-2}: $F_h = c_p D_a \overline{w'T'}$ where c_p = specific heat capacity of air at constant pressure (= 1.010 J g^{-1} K^{-1}) and D_a = air density (g m^{-3}).

Comment on the P62 covariance instruction

It can be shown that $\overline{w'T'} = \overline{wT} - \overline{w}\,\overline{T}$.
However, the covariance between w and T is defined as cov $(w, T) = \overline{wT} - \overline{w}\,\overline{T}$, which must also equal to $\overline{w'T'}$.

System operation

Sonic anemometer (CA27) and fine-wire chromel-constantan 127 TC are monitored every 0.1 s. Covariance instruction P62 is then performed on first 2000 data points (corresponds to time interval of 200 s) and these 200 s data are averaged 3 times in 10 min period and sent to output storage. This can be altered for convenience.

Distribution of atmospheric frequency and fluid transport

Tanner (1988) states that distibution of atmospheric frequencies important to scalar transport is a function of mean horizontal wind speed u, measurement height z and atmospheric stability. From several studies, range of interest is defined by: $10^{-3} < fz/u < 10$ where f is frequency. For a given z and u, upper frequency dictates sensor response and lower frequency the averaging time needed to include longer time periods. For z = 1 m, $10^{-3}\,u < f < 10\,u$.

Sensor accuracy

Apart from calibration factors provided for the sensors, no manufacturers information was supplied with regard to sensor accuracy. An absolute measure of wind speed and air temperature is not required for the calculation of sensible heat flux density. The TC response is quoted as 30 Hz.

Instrumentation details

Main advantage of eddy correlation instrumentation is that placement height of sensors can be much lower than Bowen ratio instrumentation. However, Kaimal (1975) showed that the minimum operating height is $6\pi d$ where d is the spatial resolution of the sonic anemometer. Limiting factor is loss of response to eddies dimensionally smaller than sonic pathlength (100 mm) (Tanner, 1988). Measurement height should therefore exceed 2 m

Sonic anemometer

Primary limitation in measurement height is the effect of acoustic reflections off of vegetation. The device experiences offset drift with temperature changes because of transducers, precluding its use for absolute wind speed measurements. The calibration factor for the sensor is 1 m s^{-1} V^{-1} and the resolution is 1 mm s^{-1} (equivalent to 1 mV). Sensors can sustain permanent damage if wetted. Sensor current drain is 4 mA from a 12 V battery. A 100 mm path length limits measurement to heights exceeding 2 m. However, Kaimal (1991, personal communication) claims that it is possible to place the sonic anemometer 1 m above the canopy surface for which sensibel heat flux density measurements are required without having to apply any corrections to the data. Alignment errors of vertical anemometer or vertical placement over flat but sloping surfaces causes fluctuations in horizontal wind speed to appear larger than normal fluctuations in measured vertical wind speed.

Fine wire thermocouple

Temperature fluctuations are measured with a 13 µm type E TC (with a frequency response greater than 30 Hz). The TC is referenced to temperature inside base mount of sonic anemometer. Thermal time constant is about 20 minutes for reference junction. Shifts in reference temperature during 10 min averaging period affect measurement of F_h for sonic anemometer. Base mount can be insulated to increase time constant. Absolute air temperature is not measured. The TC plugs into a shaft on anemometer for easy field replacement. Junction is 20 to 30 mm from sonic path. Circuitry on sonic anemometer amplifies output signal of the TC to 0.004 °C mV^{-1}.
In the Lamesa experiment, the fine wire thermocouple on the serial number 1149 of the sonic anemometer sometimes did not appear to make contact and the value of 289 or thereabouts was noted for the temperature fluctuation. It appeared as if the wire inside the thermocouple shaft had become twisted. On one of the days, the temperature fluctuation was reasonable but then indicated 289 for no apparent reason. Some patience and care was required when the thermocouple end was twisted while plugged in while the temperature fluctuation was noted. When the fluctuation decreased from 289 to a variable value, this was a sign that the unit was functioning satisfactorily.

Simple check program for fine wire thermocouple

There are a number of checks that one should perform on the sensors. At the back of the sonic anemometer arm there is a green military connector. Connect a wire between the A position of the connector and 1H of the 21X. Connect another wire between the H position of the military connector and 1L of the 21X.

```
*    1      Table 1 Programs
 01: 0.2     s Execution Interval
01:  P17     Panel Temperature
 01: 1       Loc :
02:  P14     Thermocouple Temp (DIFF)
 01: 1       Rep
 02: 11      5 mV fast Range
 03: 1       IN Chan
 04: 2       Type E (Chromel-Constantan)
 05: 1       Ref Temp Loc
 06: 2       Loc :
 07: 1       Mult
 08: 0.0000  Offset
03:  P       End Table 1
```

Press *0 to compile and *6 A A to view the actual temperature of the fine wire thermocouple (not the temperature fluctuations). When placed in a laboratory, the temperature of the fine wire thermocouple should be fairly close to the datalogger panel temperature. A fine wire thermocouple temperature of -99999 indicates a disconectivity which would imply a damaged thermocouple or a loose wire.

System checks

There are two tests that one may perform to determine if the temperature signal is getting through to the white electronic box and in turn to the datalogger:
1 (a) CARE IS NECESSARY IN ALL OF THESE CHECKS AS THE FINE WIRE THEMOCOUPLE CAN EASILY BE DAMAGED. The first check involves checking the actual thermojunction and that the wiring is correct. At the fine wire thermocouple, there are three thermojunctions. The main thermojunction (call it junction 2) is formed by the connection of the thin chromel wire and the thin constantan wire. There are two other thermojunctions: one formed by the connection between the thin chromel wire and the thicker chromel wire (call it junction 1) and yet a third thermojunction formed by the connection between the thin chromel wire and the thick chromel wire (call it junction 3). Any temperature changes near junction 2 will cause major changes in the milivoltage signal viewed on the 21X LCD (refer to it as TEST 1). Any temperature changes near junctions 1 and 3, because the wires making up these junctions are of similar wires (thin chromel and thick chromel wires in the case of junction 1 and thin constantan and thick constantan wires in the case of junction 3), should not cause large changes in the milivoltage signal viewed at the datalogger. If temperature changes near junctions 1 and 3 do cause large changes in the millivoltage signal, then there is a problem with the thermojunction wiring. These tests as referred to as TESTS 2 AND TESTS 3. The temperature changes can be created by using a very small heated needle that can be held close to BUT NEVER TOUCH each of the thermojunctions in turn. If the temperature increases near junction 1, 2 and 3, in turn, only cause major increases in the temperature signal occurs in the case of thermojunction 2.
NOTE ON HEATING: I used a syringe for the small needle. In order to standardize things, I always heated the tip of the needle for exactly 5 s and then waited 10 s before placing near a thermojunction. For junction 2, I always held the needle about 7 mm below the junction with the needle axis being parallel to the thick metal axis of the metal arm of the temperature sensor. For junction 1, I also held the needle about 7 mm below the junction but with the needle axis perpendicular to the metal axis of the temperature sensor. For heating of junction 2, I observed a more than 10 K temperature increase. For junctions 1 and 3, the increase was less than 2 K.
(b) One may check the wiring between the military type connector at the metal arm of the sonic anemometer/temperature sensor. Firstly remove the fine wire thermocouple. Next, remove the four screws at the back of the sonic anemometer base. Pry the military connector away from its' seal (carefully). Carefully pull the wiring out to expose the wires at the other end of the military connector. Locate the wire corresponding to the label A (a black wire). Now measure the electrical resistance (with a multimeter) between the gold pin at the temperature sensor end and connection point A of the military connector end. The resistance should be a couple of ohms. Obviously a large resistance means that there is an open circuit between the two. Refer to this as TEST 4. Similarly, measure the electrical resistance between the socket (right near the gold pin) at the temperature sensor end (with the sensor removed) and point H of the military connector. Again, the resistance should be a few ohms. If not, there is an open circuit. Refer to this as TEST 5.
The next check involves opening up the white electronic box. Locate in the middle electronic circuitry the H10 strip and position 5. In some cases the strip may be labelled H10 but not in others. The numbering of the positions may be figured as follows: hold the box with the two grey cable wires toward your body.

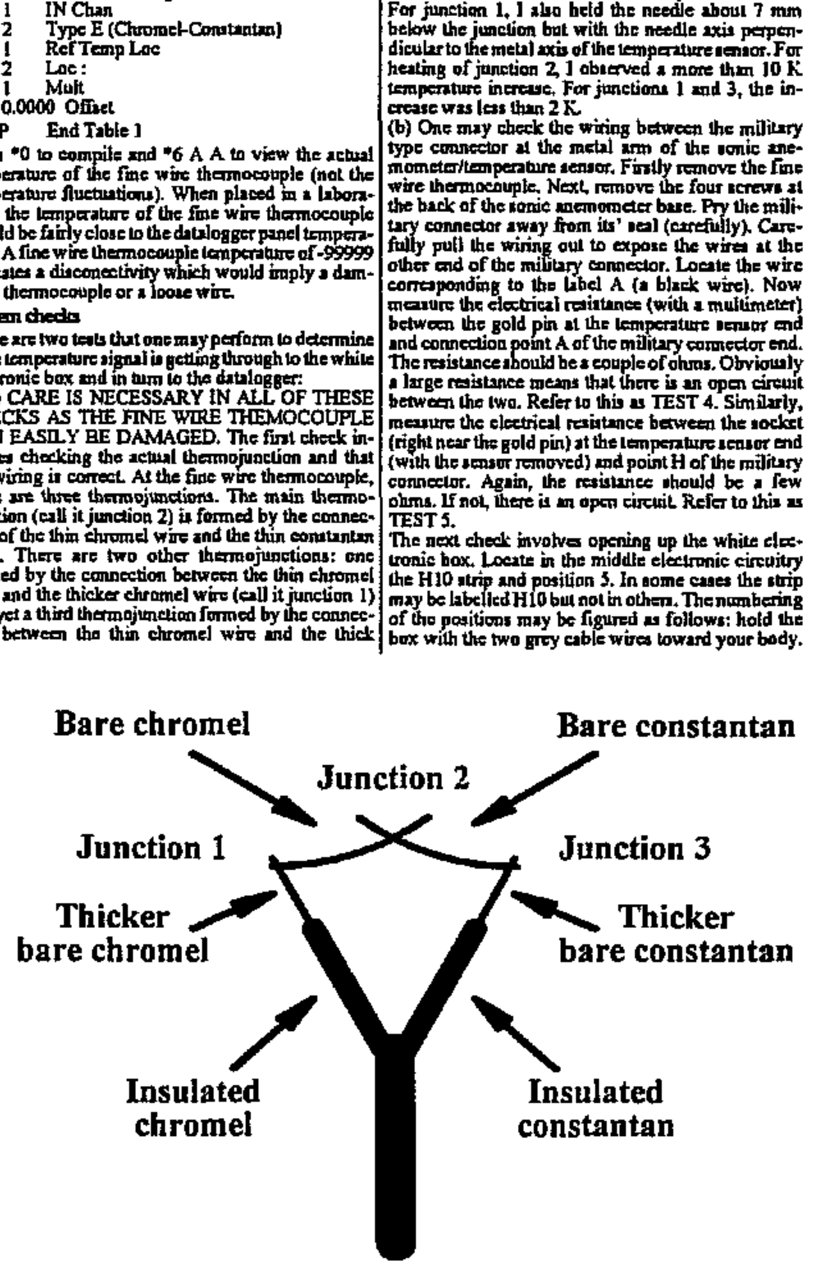

Diagrammatic representation (not to scale) of the Campbell Scientific CA27 fine-wire chromel-constantan thermocouple used as part of the eddy correlation system for the measurement of air temperature fluctuations

The first H10 position nearest your body is position 1 and the furtherest is 5. The electrical resistance between the gold pin at the thermometer end (with the thermocouple removed) and pin 5 of the H10 board should be very low. Refer to this as TEST 6. The electrical resistance between the socket at the thermometer end (with the thermocouple removed) and pin 4 of the H10 board should also be very low. Refer to this as TEST 7.

1 (b) To check the sonic anemometer, get a 20 liter drum and wrap sound absorbing material around the inside. Place the anemometer in the drum and seal the open end with cloth and towel material to absorb the sonic signal. At the logger, view the signal from the anemometer (input location number 1). The signal should be less than 30 mV. Much larger than 200 mV is cause for concern. Refer to this as TEST 8.

It is possible to test the sign of the sensible heat flux density using an eddy correlation system. Using a hot air blower (- a hair dryer works fine), blow upwards to the top sensor (TEST 9). At some distance from the sensor I measured -300 W m^{-2} for the sensible heat flux density. Blowing downwards, I measured 300 W m^{-2} sensible heat (TEST 10).

2. It may be better that the reference thermocouple of the fine wire temperature sensor is at the datalogger and not at the reference in the base of the sonic anemometer. This would mean rewiring the sensor. In the meantime, it may be best to improve the insulation on the reference thermojunction. Remove the four screws at the base of the sonic anemometer arm. Carefully remove the wiring (two thick grey wires and a number of thinner red and black wires). Follow the one set of red and black wires until there is a foam rubber insulation covering tied with two cable ties. Cut the ties and remove the insulation. Replace the insulation with insulation of the same type but double the thickness. Get another set of cable ties to replace those that were cut off.

3. Construct, from perspex, a protective cover for the sonic anemometer. The perspex would need to be roughly the same shape as the anemometer with two small screws to keep the unit attached to the anemometer.

Data logger program

Program: eddygsc.dld 23 March 1992 for eddy correlation for sensible heat flux density only. No other sensors other than a sonic anemometer and a fine wire thermocouple have been allowed for.

The factor of 1200 = $\rho\, c_p$ where ρ is the density of air (kg m^{-3}) and c_p is the specific heat capacity of air (J kg^{-1} K^{-1}) may need to be altered for air temperature, water vapour pressure and atmospheric pressure:

ρ=2934.7773 /[8.31451 (T_a+273.15)+0.28362157h)]

where T_a is the average air temperature in °C and h is the altitude in m

and

c_p = 1.0047226 + 1.148254 × e/P

where e is an average water vapour pressure (in kPa) and P is the atmospheric pressure (kPa). If in doubt, use T_a = 25 °C and e/P = 0.01.

For Texas, T_a = 25 °C, e/P = 0.01 and h = 100 m so that ρ = 1.17 kg m^{-3} and c_p = 1016.21 J kg^{-1} K^{-1} so that $\rho\, c_p$ = 1188.97 J m^{-3} K^{-1} which is equivalent to $\sqrt{0.001 \times 0.004\ \rho\, c_p} = 0.06896$.

For an altitude of 700 m, $\rho\, c_p$ = 1113.85 J m^{-3} K^{-1} or $\sqrt{0.001 \times 0.004\ \rho\, c_p} = 0.06675$.

Table 1. The numer of samples per average for two, three or four averages is dependent on the execution time and the If time interval.

Execution time (s)	"If time" time interval (min)	Sample/average for 3 averages	Sample/average for 2 averages	Sample/average for 4 averages
0.1	5	1000	1500	750
0.1	10	2000	3000	1500
0.1	20	4000	6000	3000
0.1	30	6000	9000	4500
0.2	5	500	750	375
0.2	10	1000	1500	750
0.2	20	2000	3000	1500
0.2	30	3000	4500	2250

Flag Usage:
Input Channel Usage:
1 H: sonic anemometer sensor
1 L: temperature sensor
Excitation Channel Usage:
Continuous Analog Output Usage:
Control Port Usage:
Pulse Input Channel Usage:
Output Array Definitions:

```
*    1     Table 1 Programs
 01: 0.2   s Execution Interval
01: P1      Volt (SE)
 01: 2      Reps
 02: 15     5000 mV fast Range
 03: 1      IN Chan
 04: 1      Loc :
 05: 0.069  Mult 0.001 m/(s mV); 0.004 K/mV; 1200
= ρ cp
        Multiplier is the square root of 0.001 * 0.004
* 1200 to yield Fh in W m^-2
 06: 0.0000  Offset
02: P92     If time is
 01: 0      minutes into a
 02: 5      minute interval
 03: 10     Set flag 0 (output)
03: P62     CV/CR (OSX-0)
 01: 2      No. of Input Values
 02: 2      No. of Means
 03: 00     No. of Variances
 04: 00     No. of Std. Dev.
 05: 1      No. of Covariances
 06: 00     No. of Correlations
 07: 0.0000 Samples per Average; Make this 500 for
three subinterval averages, 750 for two averages and
375 for four averages during the If time 5 min interval.
 08: 1      First Sample Loc
 09: 3      Loc :
04: P77     Real Time
 01: 110    Day,Hour-Minute
05: P70     Sample
 01: 3      Reps
 02: 3      Loc
06: P71     Average
 01: 3      Reps
 02: 6      Loc
07: P       End Table 1
```

Sensor connections for 21X for two eddy correlation systems

Analogue (single-ended measurements)

1 H Sonic anemometer CA27 number one (serial number 1147)	green
1 L Fine wire 127 TC	white
1 ground	black
2 H Sonic anemometer CA27 number one (serial number 1149)	green
2 L Fine wire 127 TC	white
2 ground	black
4 H Net radiometer +	red
4 L Net radiometer -	black
5 H Soil temperature TC chromel	purple
5 L Soil temperature TC constantan	red
6 H Soil flux plate #1 high	red
6 L Soil flux plate #2 high	red
6 G Soil flux plates ground	black
7 H 207 Temp	red
7 L 207 RH	white
7 G	green/orange or purple
8 H	red
8 L	red
8 G	blue
9 H	red
9 G	blue

Pulse ports

1 2 3 Wind anemometer

Excitation

1 Switched analogue out for 207 RH probe black

CA27 sonic anemometer and TC connections

Power cable

Red 7 to 12 V unregulated power supply; black power supply ground

signal cable green wind signal; white temperature signal; black signal ground; clear shield

KH20 Krypton hygrometer connections

Red 12 VDC; black power ground; white signal (0 to 5.2 VDC); black signal ground; clear shield

Day of year conversion

Non-leap year 31 Jan: 31; 28 Feb: 59; 31 Mar: 90; 30 Apr: 120; 31 May: 151; 30 June: 181; 31 July: 212; 31 Aug: 243; 30 Sep: 273; 31 Oct: 304; 30 Nov: 334

Leap year 31 Jan: 31; 29 Feb: 60; 31 Mar: 91; 30 Apr: 121; 31 May: 152; 30 June: 182; 31 July: 213; 31 Aug: 244; 30 Sep: 274; 31 Oct: 305; 30 Nov: 335

M J Savage c:\campbell\docuprog\eddytamu.txt
c:\campbell\docuprog\eddytamu.chp
4 June 1992